

Volume I

Final Technical Report

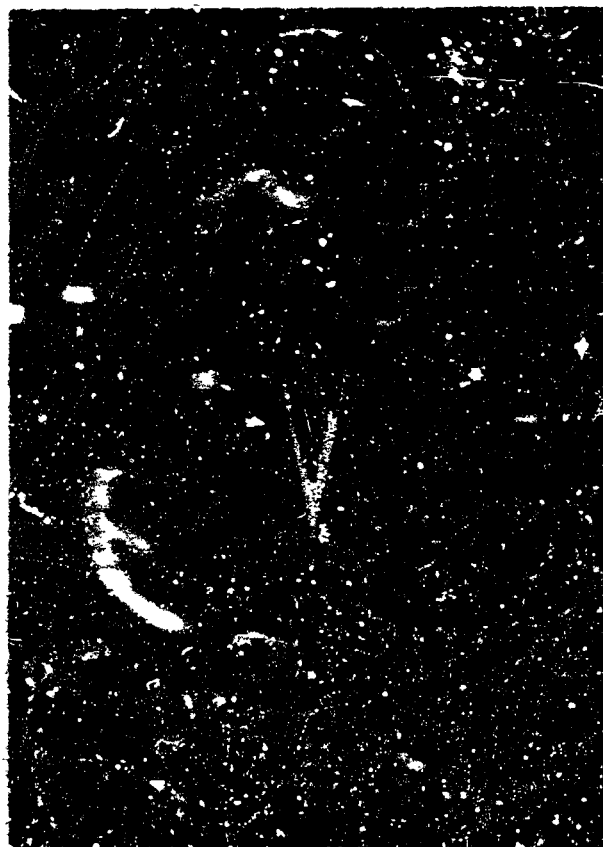
October 1973

Space Shuttle Solid Rocket Booster Recovery System Definition

100-13379

100-13379

(NASA-CR-129100) SPACE SHUTTLE SOLID
ROCKET BOOSTER RECOVERY SYSTEM DEFINITION,
VOLUME I FINAL TECHNICAL REPORT (PART I)
MAY 1973 323 P HC \$15.75 GPO 42-220
MAIL STOP 2011



MARTIN MARBLE

MCR-73-247
NAS8-29622

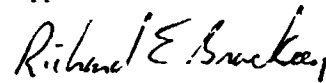
Final
Technical
Report

October 1973

Volume I

SPACE SHUTTLE
SOLID ROCKET BOOSTER
RECOVERY SYSTEM
DEFINITION

Approved



Richard E. Brackeen
Program Manager
Shuttle Booster Programs

MARTIN MARIETTA CORPORATION
DENVER DIVISION
P.O. Box 179
Denver, Colorado 80201

FOREWORD

This report is submitted in three volumes to the National Aeronautics and Space Administration, Marshall Space Flight Center, in partial fulfillment of the requirements of Contract NAS8-29622.

The objective of this contractual effort has been to define performance requirements, preliminary designs, and development program plans for an airborne recovery system for the Space Shuttle Solid Rocket Booster, with minimum total program costs being the primary selection criterion.

Volume I, entitled *Technical Report, Space Shuttle Solid Rocket Booster Recovery System Definition*, contains the results of all analyses performed during the study term to define the performance requirements, preliminary designs, and development program plans for the SRB Recovery Subsystem.

Volumes II and III contain user's instructions for two computer programs developed in support of the contract technical studies. Volume II is entitled *Solid Rocket Booster Water Impact Monte Carlo Computer Program* and Volume III is entitled *Solid Rocket Booster Water Impact Monte Carlo Computer Program*.

CONTENTS

	Page
FOREWORD	ii
SUMMARY	xiii
INTRODUCTION	1-1 thru 1-3
2.0 AIRBORNE SYSTEM ANALYSIS	2-1
2.1 Terminal Deceleration and Descent (TD&D)	2-1
2.1.1 Parachute Design Considerations	2-2
2.1.2 Recovery System Baseline Design	2-3
2.1.3 Parachute Parametrics	2-8
2.1.4 Hybrid System Performance Trends	2-11
2.1.5 Point Mass Simulation Analyses	2-14
2.1.6 Parachute Dynamic Analysis	2-19
2.1.7 Parachute Attenuation of Slapdown Loads	2-22
2.2 Initial Deceleration and Stabilization	2-28
2.2.1 SRB Configuration	2-28
2.2.2 6 DOF Reentry Analysis	2-33 thru 2-47
3.0 SRB IMPACT LOADS ANALYSIS (INCREMENT II)	3-1
3.1 Computer Program to Translate Slapdown Pressure Distributions to Concentrated Normal Loads	3-1
3.1.1 General Description	3-1
3.1.2 Program Inputs	3-1
3.1.3 Program Outputs	3-4
3.2 Water Impact Failure Criteria	3-4
3.2.1 Failure Criteria	3-4
3.2.2 Design Allowables	3-9
3.3 Structural Response of 120-in. Drop Test Specimen	3-13
3.3.1 Tabulation of Drop Test Results	3-14
3.3.2 Plots of Drop Test Results	3-21
3.3.3 Conclusions	3-29
3.4 Monolithic Versus Segmented Joint Case Design	3-29
3.4.1 Subscale Model Test Specimens and Loading Conditions	3-29
3.4.2 Subscale Test Results Extrapolated to Yield Strength	3-33

3.4.3	Subscale Yield Allowables Ratioed to 142-in. Diameter	3-33
3.4.4	Allowables Converted to Hoop Bending Moments	3-37
3.4.5	Conclusions	3-40
4.0	WATER IMPACT REQUIREMENTS DEFINITION	4-1
4.1	Attrition	4-1
4.1.1	Environmental Parameters	4-1
4.1.2	TD&D Parameters	4-6
4.1.3	Monte Carlo Computer Model	4-9
4.1.4	Water Entry Conditions	4-13
4.2	Water Impact Loads Analysis	4-18
4.2.1	Critical Impact Loading Conditions	4-19
4.2.2	Impact Conditions Using Monte Carlo Analyses	4-21
4.2.3	Scale Test Models	4-22
4.2.4	Aft End Configuration Effects	4-23
4.2.5	Attached Parachute Effects on Slapdown Loads	4-26
4.2.6	Sea State Effects on Slapdown Loads	4-27
4.2.7	Aft End Loads	4-29
4.2.8	SRB Case and Forward Skirt Loads	4-31
4.2.9	Loads Summary	4-34
4.3	Component Strength Analysis	4-35
4.3.1	Forward Skirt	4-38
4.3.2	Aft Skirt	4-41
4.3.3	Aft Dome	4-41
4.3.4	Nozzle and Extension	4-45
4.3.5	Case Center Segments	4-45
4.3.6	SRB Strength Analysis Uncertainties	4-46
		thru
		4-60
5.0	PRELIMINARY DESIGN CONCEPTS AND CONSIDERATIONS	5-1
5.1	Baseline System Selection and Rationale	5-1
5.2	Baseline Sequence of Events	5-2
5.3	Baseline General Arrangement	5-2
5.4	Alternative Concepts	5-8
5.4.1	Drogue	5-8
5.4.2	Pilot Chute Deployment	5-9
5.4.3	Multiple Parachutes	5-12
5.4.4	Hybrid Recovery System	5-12
5.5	Recovery System Weights	5-14
5.6	Flotation	5-14
5.6.1	Basic Flotation Characteristics	5-15
5.6.2	Thermal Effects on Flotation	5-19
5.7	Recovery Environmental Analysis	5-30
		thru
		5-32

6.0	CONCEPT EVALUATION AND SELECTION	6-1
6.1	Approach	6-1
6.2	Parametric Cost Trades	6-3
	6.2.1 Cost Analysis Methodology	6-4
	6.2.2 Programmatic Parametrics	6-6
	6.2.3 Structural Component Cost/Failure Parametrics	6-10
	6.2.4 Recovery SRB System Cost Parametrics	6-21
	6.2.5 Hybrid Retrorocket/Parachute Costs	6-27
	6.2.6 Total SRB Program Parameter Cost Results	6-36
6.3	Point Designs Cost Estimates	6-36
6.4	Baseline Recovery System Selection Considerations	6-45
		thru
		6-49
7.0	RECOVERY SYSTEM PROGRAM PLANS	7-1
7.1	DEVELOPMENT TEST PLAN	7-1
	7.1.1 Decelerator Development	7-12
	7.1.2 Avionics Systems	7-17
	7.1.3 Interface Tests	7-18
7.2	Qualification Test Plan	7-19
	7.2.1 Component Qualification	7-20
	7.2.2 System Qualification	7-22
	7.2.3 Maintainability Demonstration	7-24
	7.2.4 DDT&E Flight Test	7-24
7.3	Manufacturing Plan	7-26
	7.3.1 Fabrication	7-30
7.4	Operations Plan	7-31
	7.4.1 Assembly and Checkout	7-31
	7.4.2 Launch	7-31
	7.4.3 Refurbish and Repair	7-31
7.5	Logistics Plan	7-36
	7.5.1 Logistics Support Considerations	7-45
	7.5.2 Spares and Supply Support	7-49
7.6	Facilities Plan	7-50
	7.6.1 Test Facilities	7-51
	7.6.2 Refurbish and Repair Facility	7-51
	7.6.3 Storage	7-55
		thru
		7-57
8.0	CONCLUSIONS AND RECOMMENDATIONS	8-1
8.1	Conclusions	8-1
8.2	Recommendations	8-3
		and
		8-4

Figure

1	Mission Profile Defines Recovery System Requirements in Reverse Sequence	xiv
2	High α Reentry with Dispersions Meets ID&S Requirement	xvi
3	Longitudinal cg Location Determines Maximum and Deployment q	xvi
4	Critical Loads Vary During Impact Sequence	xviii
5	Impact Parameter Probability Distributions Determined by Monte Carlo Analysis	xx
6	Baseline Recovery System Sequence	xxii
7	Optimum Descent Velocity Is 125 fps	xxv
2.1-1	Ribbon Parachutes for SRB Recovery	2-4
2.1-2	SRB Recovery Mission Profile	2-6
2.1-3	Baseline Recovery System within the State of the Art	2-7
2.1-4	Canopy Diameter and Cluster Size, Primary Dependent Variables	2-9
2.1-5	Drogue May Not Be Necessary	2-12
2.1-6	Hybrid System May Reduce Recovery System Weight	2-13
2.1-7	Hybrid System Performance Best for Low Impact Velocities	2-15
2.1-8	Main Parachute Loads Reduced by Increasing Drogue Size	2-17
2.1-9	Single Parachute Experiences Lower Opening Load	2-18
2.1-10	Lower Reefing Efficiency Reduces Altitude Loss During Deployment	2-18
2.1-11	Successful Pilot Deployment from High α Reentry	2-21
2.1-12	Initial and Disreefing Are Balanced	2-21
2.1-13	Parachute Elasticity Effects Are Minimal	2-21
2.1-14	Deployment Altitude-Dynamic Pressure Histories	2-23
2.1-15	SRB Attitude Transition Accomplished in Three Seconds	2-23
2.1-16	Parachute Reduces SRB Nose Velocity During Slapdown	2-25
2.1-17	Parachute Continues Descent During Slapdown	2-26
2.1-18	Parachute Retards SRB Attitude History During Slapdown	2-27
2.2-1	SRB Baseline Configuration	2-29
2.2-2	Longitudinal CG Location Is Most Sensitive to Nozzle Extension Jettison	2-31
2.2-3	Supersonic Aerodynamic Uncertainties Are Not Critical	2-34
2.2-4	Subsonic Aerodynamic Uncertainties Define Maximum Reentry Dispersions	2-35

2.2-5	SRB Baseline Reentry Trajectory	2-38
2.2-6	High α Trim Produces Maximum Total Drag	2-38
2.2-7	Dynamic Pressure Buildup Provides Damping Force	2-39
2.2-8	SRB Experiences Large Attitude Rates at Max q	2-40
2.2-9	Longitudinal CG Location Determines Maximum and Deployment q	2-42
2.2-10	Maximum Dynamic Pressure Insensitive to Most Dispersions	2-42
2.2-11	Roll Rates at Deployment Altitudes Correlated to Conditions at Maximum Dynamic Pressure	2-45
2.2-12	Parachute Deployment Will Require Active Altitude Sensing Device	2-46
2.2-13	High α Reentry with Dispersions Meets ID&S Requirements	2-46
3.1-1	Normalized Keel Slapdown Pressure Distribution and Wetted Angle Curves	3-2
3.1-2	Normalized Radial Slapdown Pressure Distribution Curves	3-3
3.3-1	120-in. Drop Instrumentation Locations	3-13
3.3-2	120-in. Drop Maximum Diameter Deflection	3-22
3.3-3	120-in. Drop Maximum Hoop Bending Stresses	3-23
3.3-4	Slapdown Longitudinal and Circumferential Load Distribution	3-24
3.3-5	Average Running Hoop Moment for 6900 N/m ² (1 psi) Pressure	3-25
3.3-6	Maximum Hoop Bending Stress for Static Hoop Moments	3-26
3.3-7	Comparison of Static and Drop Test Deflections	3-27
3.3-8	Comparison of Static and Drop Test Hoop Stresses	3-28
3.4-1	Three Subscale Models Static Tested	3-30
3.4-2	Five Loading Conditions Applied to 13- and 31-in. Monolithic Specimens	3-31
3.4-3	Three Loading Conditions Evaluated for the 120-in. Specimen	3-32
3.4-4	13-in. Case Center Segment Yield Strength Extrapolated from Static Test Results	3-34
3.4-5	31-in. Case Center Segment Yield Strength Extrapolated from Static Test Results	3-35
3.4-6	120-in. Case Center Segment Yield Strength Extrapolated from Static Test Results	3-36
3.4-7	142-in. Case Hoop Bending Strength Determined for Monolithic Case	3-38
3.4-8	142-in. Case Hoop Bending Strength for Monolithic and Segmented Case Design	3-39

3.4-9	142-in. Segmented Design Appreciably Stronger Than Monolithic Design for a Given Value of MEOP	3-40
4.1-1	Impact Related Variables Defined by Environmental and State Vector Uncertainties	4-2
4.1-2	Water Mass Velocity	4-4
4.1-3	Water Mass Direction	4-4
4.1-4	Wave Direction	4-4
4.1-5	Water Current Velocity	4-4
4.1-6	Water Current Direction	4-5
4.1-7	One Kilometer Wind Velocity Distribution	4-7
4.1-8	Parachute Hang Angle	4-8
4.1-9	Terminal Descent Velocity	4-8
4.1-10	Monte Carlo Analysis Macrologic	4-10
4.1-11	Independent Random Numbers Generate Impact Conditions	4-11
4.1-12	SRB Components Loads Determined from Impact Conditions	4-12
4.1-13	Damage Assessment Compares Impact Loads with Randomly Selected Component Strengths	4-14
4.1-14	Cumulative Probability of Vertical Impact Velocity	4-15
4.1-15	Cumulative Probability of Horizontal Impact Velocity	4-16
4.1-16	Cumulative Probability of Impact Angle	4-17
4.2-1	Critical Loads Vary During Impact Sequence	4-20
4.2-2	Monte Carlo Analysis Predicts High V_H and Low Impact θ	4-21
4.2-3	Fronde Scaling Relationships Used on Test Models	4-22
4.2-4	SRB Aft End Baseline Configuration	4-24
4.2-5	Minimum V_H for Collapse Pressure on Aft Skirt	4-25
4.2-6	Sea State 5 Wave Conditions	4-27
4.2-7	Aft End Peak Loading Highly Sensitive to Impact Conditions	4-30
4.2-8	Critical SRB Case and Forward Skirt Loads Occur at Slapdown	4-32
4.2-9	Slapdown Pressure Peak Moves Forward and Increases with Time	4-34
4.3-1	All Major Structural Elements Included in the Monte Carlo Analysis	4-36
4.3-2	Statistical Strength Distributions Applied to Each Structural Element	4-37
4.3-3	Forward Skirt: Preliminary Design Curves Used for Stringer and Frame Capabilities	4-39
4.3-4	Forward Skirt: Baseline Frame Design Inadequate for Slapdown Pressure Loads	4-40
4.3-5	Aft Skirt Structural Baseline	4-42
4.3-6	Aft Skirt: Adequate for Burst Pressure Loads	4-43

4.3-7	Aft Dome Strength Capability Based on Analytical Results	4-44
4.3-8	Aft Dome Probability of Failure High without Increase Structural Strength	4-46
4.3-9	Aft Dome Protector Baffle Concept	4-47
4.3-10	Nozzle and Extension Design Strength Requirements	4-48
4.3-11	Gimbal Joint Design Strength Requirement Reduced by Jettisoning Extension	4-49
4.3-12	Case Center Segments: Strength Capability Based on 120-inch Case Static Tests	4-51
4.3-13	120-inch Case Center Segment Yield Strength Extrapolated from Static Test Results	4-52
4.3-14	Center Segment Strength Increase Factors Used to Adjust Test Results to 142-inch Case	4-54
4.3-15	Center Segment Hoop Bending Strength Determined from Static Test Results	4-55
4.3-16	Slapdown Hoop Moments Averaged for Strength Comparisons	4-57
4.3-17	Center Segment Probability of Failure Sensitive to MEOP	4-58
5.2-1	Deployment Sequence	5-3
5.3-1	Recovery System Packaging Concept and Design Details	5-5
5.3-2	Possible Universal Joint Attachment	5-7
5.4-1	Concept More Complex If Drogue Needed	5-10
5.4-2	Alternative Concepts for Pilot Deployment Feasible	5-11
5.4-3	Hybrid System Sequence Same As All-Parachute System To Retrofire	5-13
5.6-1	Typical Impact Sequence Leads To Vertical Flotation	5-16
5.6-2	Flotation Height, a Function of Amount of Air Trapped	5-17
5.6-3	Small Effect of Steam Generation on Rebound Characteristics	5-20
5.6-4	SRB Case Temperature Profiles	5-22
5.6-5	Temperature Profiles Defined by Aero Heating	5-23
5.6-6	Increased Initial Water Film Thickness Drains More Rapidly from Flat Plate	5-25
5.6-7	Thick Water Film Retards Steam Generation	5-26
5.6-8	Predicted Steam Volumes Versus Time	5-29
5.7-1	Shock Attenuation Curve	5-31
6.1-1	Requirements and Configuration Evaluations Based on Total SRB Program Cost Analysis	6-2
6.2-1	SRB Total Program Costs Increase with Number of New SRBs	6-7

6.2-2	Attrition Rate and Refurbishment Times Determine Number of Subsystems Required	6-9
6.2-3	Average Number of Reuses per Unit Based on Refurbish- ment Time and Attrition Rate	6-9
6.2-4	Production Cost Tradeoffs	6-10
6.2-5	Structural Strengthening Decreases Forward Skirt Cost	6-12
6.2-6	Optimum Forward Skirt Design Independent of SRB Attrition Rate	6-15
6.2-7	Structural Strengthening Reduces Aft Dome Cost	6-16
6.2-8	Aft Skirt Baffle Minimizes Dome and Skirt Costs	6-18
6.2-9	Strengthening the SRM Case Increases Production Costs	6-19
6.2-10	Effect of MEOP on SRM Case Program Costs	6-20
6.2-11	Optimum SRB Component Costs Increase with Terminal Descent Velocity	6-22
6.2-12	Parachute Total Cost Is Primarily a Function of Diameter	6-23
6.2-13	Diameter Dependent Parachute Costs	6-25
6.2-14	Velocity Dependence of Parachute System DDT&E	6-26
6.2-15	Parachute Refurbishment Fraction Depends on Reuses	6-26
6.2-16	Parachute Manufacturing Costs Depend on Refurbishment Fraction	6-27
6.2-17	Manufacturing and Refurbishment Cost Trade Yields Optimum Refurbishment Fraction	6-29
6.2-18	Cost of All-Parachute Recovery System	6-30
6.2-19	Retrorocket Motor Costs for Hybrid System Correlate with Total Impulse	6-30
6.2-20	Retrorocket Motor DDT&E Costs	6-32
6.2-21	Retrorocket System Costs Nearly Linear with ΔV	6-33
6.2-22	Optimum Parachute Terminal Velocity for Hybrid System between 33 and 41 m/s	6-34
6.2-23	All-Parachute Systems Cost Less Than Hybrid Above 27.4 m/s (90 fps)	6-35
6.2-24	Pessimistic Parachute Costs Still Show All-Parachute System Cost Advantages	6-37
6.2-25	Optimum Descent Velocity Is 38 m/s (125 fps)	6-38
6.2-26	Reducing Number of Shuttle Flights Lowers Optimum Terminal Descent Velocity 3 m/s (10 fps)	

6.3-1	DDT&E Costs Are Sensitive to State of the Art Uncertainties	6-43
6.3-2	Optimal Terminal Descent Velocity Insensitive to Recovery System DDT&E Cost Uncertainty	6-44
7.0-1	SRB Recovery System Development Plan	7-3
7.0-2	SRB Recovery System Logic Network	7-5
7.1-1	SRB Recovery System Development Test Summary	7-9
7.1-2	SRB Recovery System Test Schedule	7-11
7.2-1	SRB Recovery Qualification Summary	7-23
7.3-1	SRB Recovery System Manufacturing and Refurbishment Flow Plan	7-28
7.3-2	Manufacturing Flow - Launch and Refurbishment	7-29
7.4-1	Recovery Subsystems Postassembly Functional Checkout	7-32
7.4-2	SRB Launch Site Operations	7-33
7.4-3	SRB Refurbishment Disassembly	7-35
7.4-4	Parachute System Refurbishment Functional Flow	7-37
7.4-5	Recovery System Avionics Refurbishment Functional Flow	7-39
7.4-6	Main Chute Attach Hardware Refurbishment Functional Flow	7-41
7.4-7	Nose Cone Structure Refurbishment Functional Flow	7-43
7.5-1	Logistics Requirements Tree SRB Recovery System	7-44
7.5-2	Refurbishment Planning Process	7-47
7.6-1	SRB Facilities Recovery System Subassembly Flow	7-51
7.6-2	Main Chute Refurbishment Work Plan	7-56
7.6-3	Parachute Processing Facilities	7-57

Table

1.	Parameters Considered in Attrition Analysis	xix
2.	Data Changes and Design Modifications	xxiii
2.2-1	Flotation Weight 9,513 kg Less Than Inert Weight.	2-30
2.2-2	Initial State Vector for Reentry Analysis	2-32
2.2-3	Staging Rates for Reentry Analysis.	2-32
2.2-4	Summary of Reentry Dispersion Results	2-43
2.2-5	Recovery Area Ellipse	2-47
3.2-1	Recommended Factors of Safety	3-5
3.3-1	120-in. Drop Peak Pressures	3-15
3.3-2	120-in. Drop Diameter Deflections (Roll Compensated)	3-17
3.3-3	120-in. Drop Maximum Stresses	3-19
4.1-1	One Kilometer Wind Statistics in SRB Recovery Zone.	4-5
4.1-2	TD&D Parameter Values Used in Attrition Analysis.	4-7
4.3-1	Structural Weight Increases Required to Achieve Low Failure Probability (1%).	4-59
5.5-1	Baseline Recovery System Weights.	5-14
5.6-1	Probable (Assumed) Wetting Conditions	5-28
5.7-1	SRB Environments Remain within Equipment Capabilities	5-31
6.2-1	Cost Analysis Terminology	6-3
6.2-2	Baseline System Cost Data	6-5
6.2-3	New Unit Requirements for Low Failure Probabilities	6-11
6.3-1	Single Parachute Recovery Subsystem Has Lowest DDT&E and Production Costs.	6-40
6.3-2	DDT&E Uncertainties Were Systematically Explored.	6-42
6.4-1	Cost-Optimum V_{TD} Is Insensitive to Design Approach and Cost Assumptions.	6-46
6.4-2	System Simplicity Improves Reliability.	6-49
6.4-3	Parachute Configuration Options - 38 m/s (125 fps) Terminal Descent Velocity	6-53
7.1-1	SRB Decelerator Development Test Summary.	7-13
7.2-1	SRB Recovery Component Qualification Test Requirements.	7-21
7.6-1	SRB Decelerator Development and Qualification Test Facility Requirements	7-54
7.6-2	Estimated Costs for Parachute Facility.	7-55

SUMMARY

A study has been conducted to define the requirements for a recovery system capable of providing water impact conditions for the Solid Rocket Booster (SRB) which would result in a high probability of SRB flotation, retrieval, and reuse. This study encompassed the flight phases of the SRB following a successful ascent and separation from the Shuttle External Tank to water impact. The groundrules applied to this study were:

- Total systems cost is the primary criterion for all trade decisions. These costs include development, vehicle performance, facilities, recurring hardware, and refurbishment costs.
- The recovery system was not designed to accommodate the recovery of SRBs from an aborted mission.
- Avionics and ignition systems have dual redundancy.
- SRB survivability with a major recovery system element failed (e.g., parachute or retrorocket) was considered only when it proved to be cost effective.
- The recovery system must not have significant impact on total Shuttle system safety or mission success probability.

The SRB baseline configuration, separation conditions, aerodynamic characteristics, water impact test data, and SRB motor case strength data were supplied by the NASA. A Monte Carlo statistical technique using random sampling of the probability distribution for the critical water impact parameters was used to determine the failure probability of each SRB component as functions of impact velocity and component strength capability.

We applied the best available SRB aerodynamic and water impact loads data to the analysis defining the recovery system requirements, minimizing subjective value judgments. Baseline design concepts were derived to satisfy these requirements and a minimum cost recovery system was established, assuming these data were complete and accurate. We then (1) identified concerns regarding the completeness, accuracy, and applicability of the data, (2) suggested methods for resolving these concerns, and (3) estimated the impact various data uncertainties could have on the recovery system design and program costs. Thus, the results of this study

provide the NASA with a minimum cost SRB recovery system for a specific set of input data, plus parametric results and alternatives that allow application of justified subjective value judgments, contingencies, and conservatism in selecting a recommended SRB recovery system.

The flight phases of particular interest to this study are illustrated in Figure 1. In sequential order, these phases are post-separation, coast, initial deceleration and stabilization (ID&S), terminal deceleration and descent (TD&D), water impact, and flotation. The recovery system requirements propagate in reverse order; i.e., acceptable water entry conditions define requirements for TD&D system design; TD&D deployment conditions set the requirements for the ID&S phase.

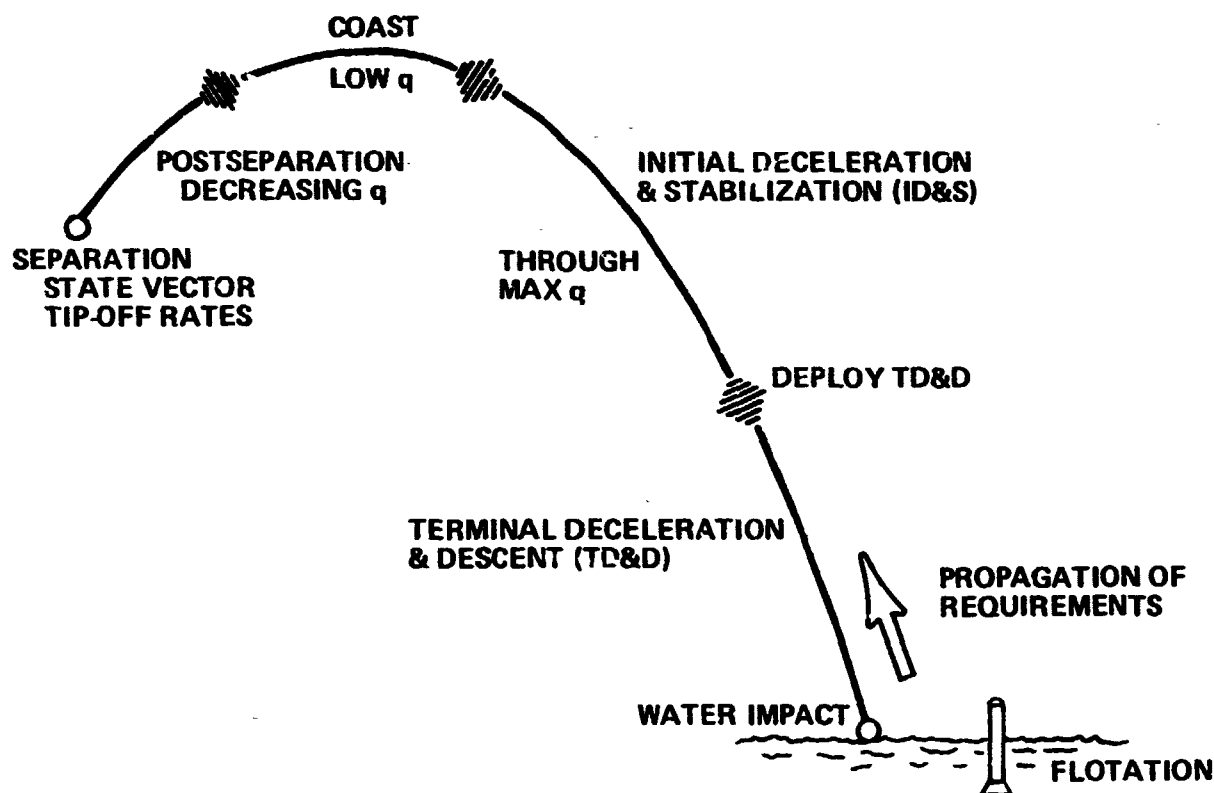


Figure 1 Mission Profile Defines Recovery System Requirements in Reverse Sequence

The TD&D phase studies have been parametric in nature to allow weight and cost tradeoffs for variations in chute size, type, number of chutes, use of a drogue versus direct deployment of the mains, acceleration history, and deployment altitude. Guidelines for low risk parachute design gathered from specialists in the parachute industry have been observed in formulating the conclusions of the study and selection of the baseline preliminary design concept. The results of this study phase indicate:

- Low risk design results from parachute diameter 41 m (135 ft) and cluster size of 3 or less, with a basic the-simpler-the-better philosophy;
- Ribbon parachutes are the most practical type for this application;
- A drogue chute is not required;
- Deployment altitude less than 3.0 km is feasible;
- A single reefing stage is sufficient;
- Hybrid systems (parachutes plus retrorockets) are more cost effective than a pure parachute system for impact velocities below 27.4 m/s (90 fps).

The deployment boundaries for the drogue and main parachute systems are presented in Figure 2. The nominal and dispersed entry trajectories of the SRB are also shown in this figure. These data indicate that the natural stability of the SRB will assure satisfactory deployment conditions for either a system employing a drogue or one using only main parachutes.

The aerodynamic data for the SRB indicates a very strong subsonic stable trim point at an angle of attack of 1.75 rad (100 deg) for the nominal cg location (57% body length). The trim angle of attack varies from 1.4 to 2 rad (80 to 115 deg) over a $\pm 4\%$ body length variation in the relative cg and cp locations. These data predict the SRB will trim in a high drag attitude over a substantial uncertainty in cg and/or cp location resulting in a dynamic pressure of less than 9600 N/m^2 (200 psf) at main parachute deployment altitude, as illustrated in Figure 3.

The SRB entry trajectory analysis also predicts that a roll rate up to 1.75 rad/s (100 deg/s) may be experienced at the time of parachute deployment. The occurrence of this continuous roll is a function of the roll attitude and rate at maximum dynamic pressure, and thus while not truly random in nature, cannot be avoided. Thus, recovery system design must accommodate deployment from a rolling body.

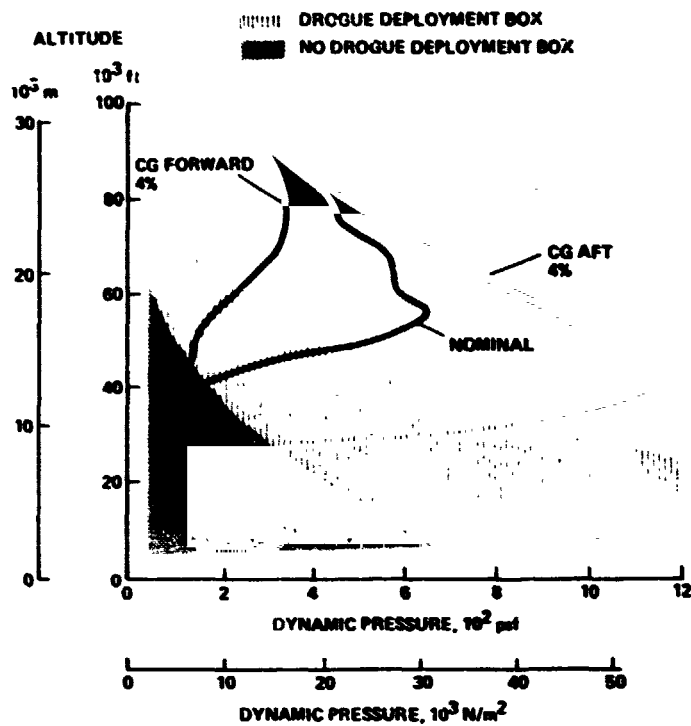


Figure 2 High α Reentry with Dispersions Meets ID&S Requirements

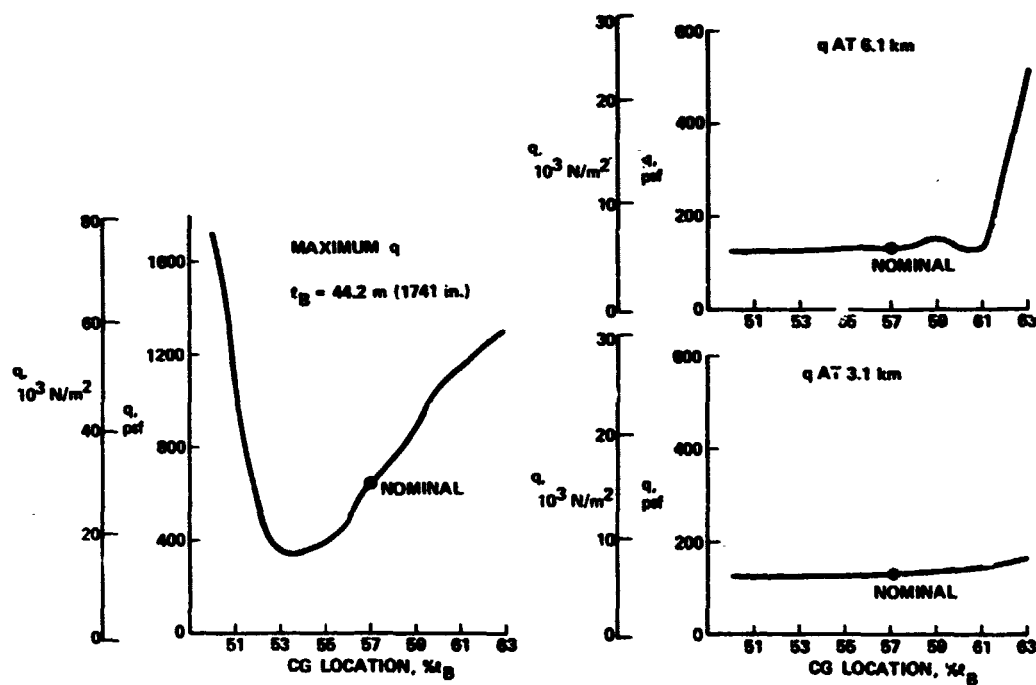


Figure 3 Longitudinal CG Location Determines Maximum and Deployment q

Increment II of the contract was added to aid in the definition of water impact loads and SRB strength analysis. These are summarized as follows:

- The computer program developed to translate slapdown pressure distributions to concentrated normal loads is being used to analyze the SRM case during slapdown.
- Failure criteria have been developed for use as design and analysis criteria for the SRB.
- Comparison of static stress and dynamic deflection test results have shown a dynamic amplification factor over the range of test data available. Thus, the knock-down factor applied to static loads has not been completely justified by test.
- Comparison between monolithic and segmented case designs shows that for equal weight, the strength of the 142-in. segmented case to withstand slapdown loads is 25% greater than the monolithic case.

The loads experienced by the SRB at water impact were based primarily on the results of the NASA drop tests on a 12.5-in. scale model and the 120-in. Titan III SRM. Figure 4 depicts the critical loads on the various components and indicates the impact conditions contributing to these loads. The aft end of the vehicle (skirt, nozzle, and dome) experience peak loads at water impact, and the loads increase significantly with increased vertical velocity. At combinations of high vertical and horizontal velocities, case loads also become critical because of peak accelerations. The forward skirt and the forward portion of the SRB case experience critical loading at initial slapdown. These values are sensitive to horizontal velocity and impact angle, but do not change significantly with vertical velocity. Maximum penetration depth is a function of vertical velocity but does not appear to be critical for this configuration. Secondary (rebound) slapdown loads may be critical to the forward skirt and case, and should be most severe for high vertical velocity and low horizontal velocity. Test results are inconclusive, but tend to show that initial slapdown is more critical than secondary slapdown.

The strength of the motor case was derived from results of the NASA static test on the 120-in. Titan III motor case. The strength of the other stage hardware components was estimated as a function of weight. Strength probability curves were generated for all of the components for use with the Monte Carlo statistical sampling techniques. The parameters considered in the analysis are listed

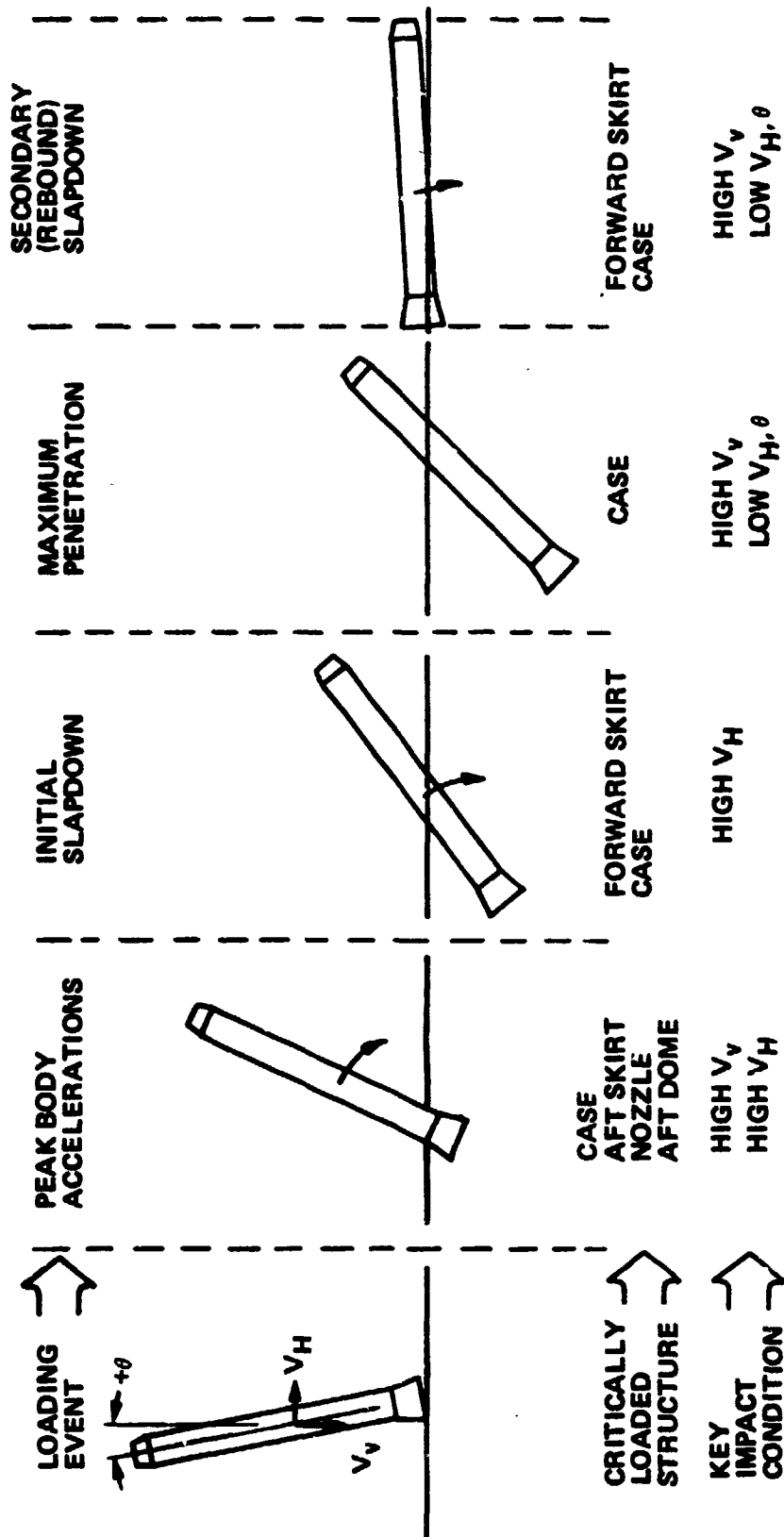


Figure 4 Critical Loads Vary During Impact Sequence

in Table 1. The parameters marked with an asterisk were deleted from the analysis, or combined with other parameters, after their effects were found to be negligible. The probability distribution of the significant water impact parameters--horizontal velocity V_H , vertical velocity V_V , and impact angle (θ)--are illustrated in Figure 5 for a nominal impact velocity of 30.5 m/s (100 fps).

Table 1 Parameters Considered in Attrition Analysis

SYMBOL	DEFINITION
θ_1^*	Hang angle-parachute ϵ to vertical
θ_2	Hang angle-SRB ϵ to parachute ϵ
ω_1^*	Parachute rotation rate about vertical
ω_2^*	SRB rotation rate about parachute ϵ
ψ_1^*	Parachute ϵ projected azimuth
ψ_2	SRB ϵ projected azimuth
V_{TD}	Mean terminal descent (design) velocity
V_{PT}^*	Parachute translation velocity due to lift
V_{PO}^*	Nozzle tangential velocity due to rotation
D_{VR}	Retromotor ΔV (if applicable)
θ_R	Retro thrust vector misalignment (to SRB ϵ)
V_W	Wind velocity
V_{WM}	Wave mass velocity
V_{CUR}	Current velocity
h	Wave height
ψ	Wave mass direction angle
θ_{WM}	Wave direction angle
θ_{CUR}	Current direction angle
*Effects negligible.	

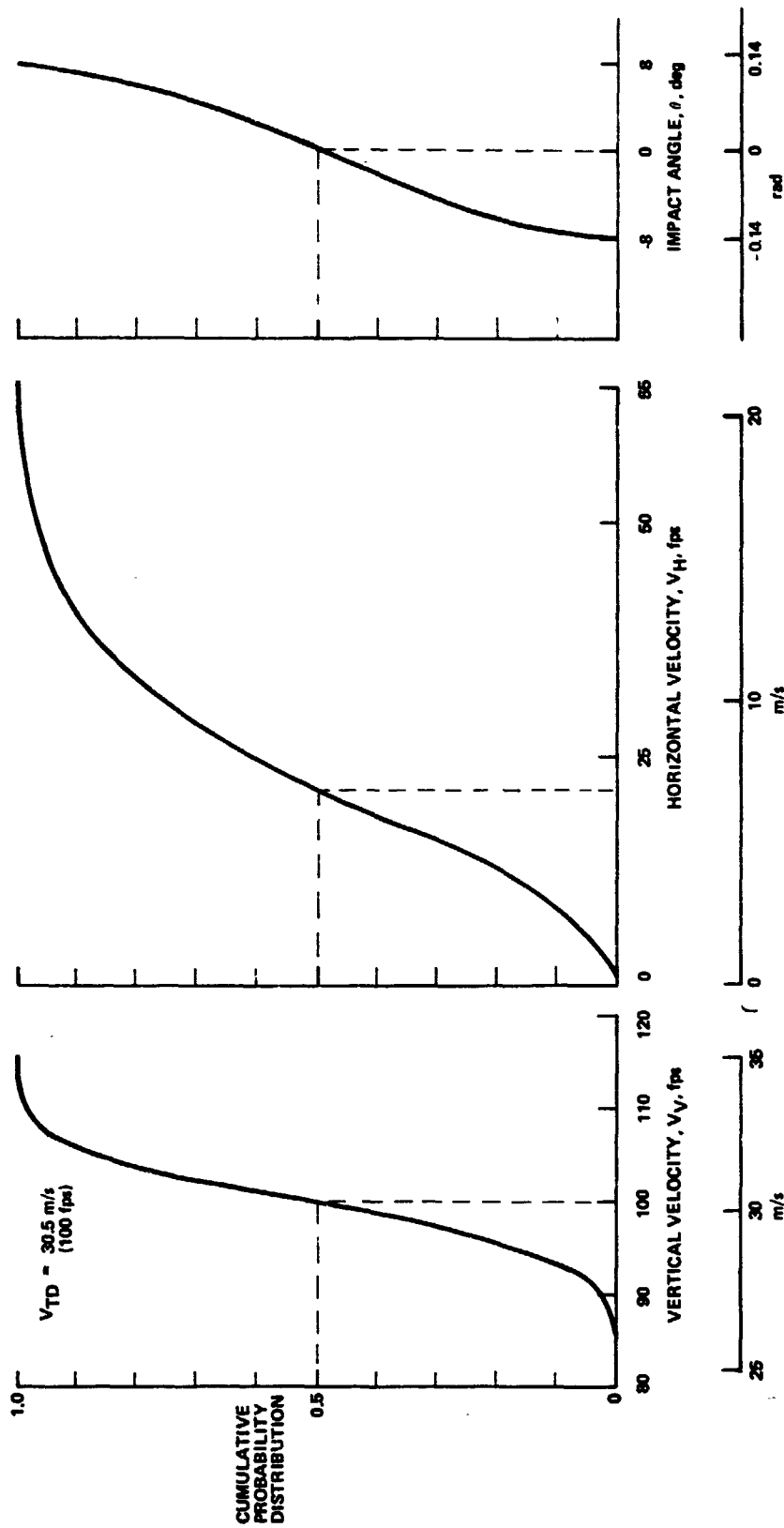


Figure 5. Impact Parameter Probability Distributions
Determined by Monte Carlo Analysis

Figure 5 Impact Parameter Probability Distributions Determined by Monte Carlo Analysis

While the primary objective of this study was to define requirements rather than develop a configuration, preliminary design concepts were derived for cost comparisons and planning purposes. The baseline concept was selected to reflect the three basic results that continued to prevail during the study:

- 1) The SRB trims in a high drag attitude during entry, thus eliminating the need for a drogue parachute;
- 2) Strengthening the stage hardware components to reduce damage probability is more cost effective than reducing impact velocity as long as extensive modification to the motor case itself is not involved;
- 3) The-simpler-the-better philosophy results in high reliability, low risk, and low cost.

The baseline recovery system design concept selected and a sequence of events are illustrated in Figure 6. The pertinent features of this configuration are a single 40.4 m (132 ft) diameter main parachute with a 7.6 m (25 ft) diameter pilot chute. The deployment sequence is initiated at about 2.3 km (7,500 ft) altitude by ejecting the nose cap, containing the pilot chute, with three small pyro-thrusters. After inflation, the pilot chute pulls off the portion of the nose cone frustum that contains the main chute. After main chute line stretch, the frustum strips away from the main parachute, allowing inflation to reefed condition of 30% of the total parachute drag area. The system is disreefed 6.4 seconds after initiation of deployment of the main parachute. The parachute loads are transmitted to the SRB through a swivel to allow for the expected roll of the SRB. The terminal velocity for this system is 38 m/s (125 fps). This impact velocity is higher than available test data simulates and may be approaching conditions that produce critical loads in the case, such as peak acceleration, hydrostatic pressure caused by increased depth of penetration, or secondary slapdown. Extrapolation of these data indicate that of these three loading conditions, peak acceleration is most critical and this load is not likely to cause case failure below 40 m/s (130 fps) vertical velocity.

Our baseline design isolates the SRM case aft dome from water impact loads by employing a baffle in the aft skirt and jettisoning the nozzle extension before water impact. This approach not only allows the case to be designed and optimized for ascent [if the impact velocity is below 40 m/s (130 fps)], but is considerably lighter than strengthening the aft dome.

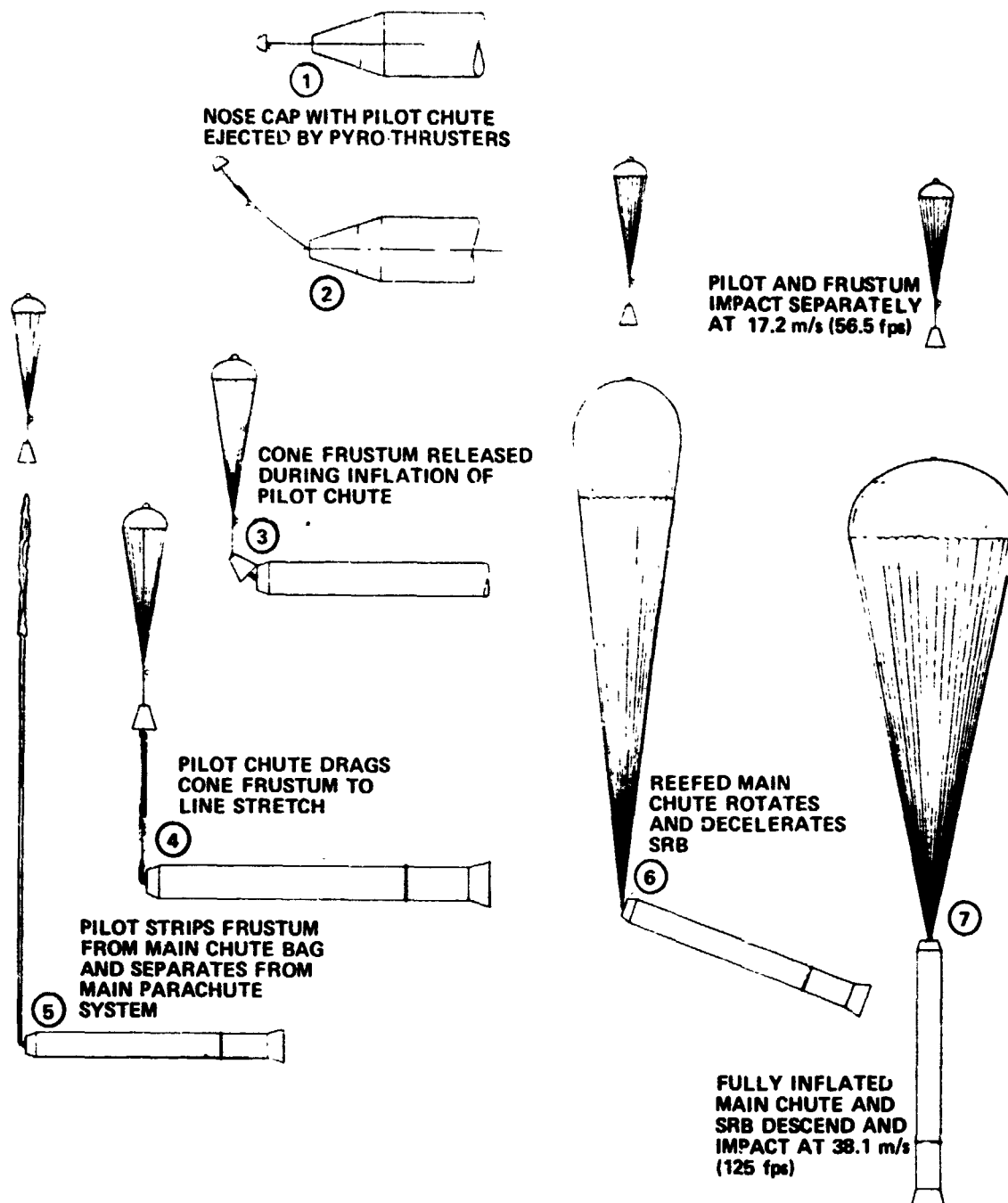


Figure 6 Deployment Sequence

The baseline design employs a swivel to accommodate the roll rate that may be present during deployment. This swivel serves two purposes: (1) prevents wrap-up of the suspension lines, and (2) allows the attach mechanism to align with the suspension lines to provide maximum strength.

The requirement for the swivel is somewhat weak and a less expensive alternative should be investigated. If a roll rate of 1.75 rad/s (100 deg/s) continued from the initiation of deployment to impact, about 11 complete revolutions of the SRB would result. It is possible the parachute suspension lines could accommodate this amount of wrapping. A universal joint to allow the attach mechanism to align with suspension lines to provide maximum strength during deployment may be an acceptable alternative to a swivel.

The selected concept should be capable of accommodating changes in requirements as additional data become available. Several approaches are possible, depending upon when the data become available and the nature of the changes in requirements. Table 2 lists some possible changes and probable recovery system design modifications in response to these changes.

Table 2 Baseline has Flexibility to Accommodate Future Design Requirement Changes

DESIGN REQUIREMENT CHANGE	MOST LIKELY DESIGN MODIFICATION TO MAINTAIN MINIMUM COST SYSTEM
MORE NOZZLE-FIRST TRIM RESULTING IN HIGHER DEPLOYMENT q	ADD STRAKES TO AFT SKIRT OR ADD DROGUE TO ACCOMMODATE HIGHER q DEPLOYMENT
UNPREDICTABLE OR TUMBLING ENTRY	ADD STRAKES OR FINS TO FORWARD SKIRT, FORCE NOZZLE-FIRST ENTRY AND ADD DROGUE
HIGHER IMPACT LOADS ON STRUCTURAL COMPONENTS	STRENGTHEN STRUCTURAL COMPONENTS
HIGHER IMPACT LOADS ON SRM CASE REQUIRING: V_{TD} 110 \leftrightarrow 125 fps	INCREASE MAIN PARACHUTE DIAMETER
V_{TD} 80 \leftrightarrow 115 fps	CHANGE TO CLUSTER OF THREE MAIN PARACHUTES
V_{TD} < 90 fps	ADD RETROROCKET TO SINGLE MAIN PARACHUTE DESIGN
20% SRB INERT WEIGHT GROWTH	INCREASE MAIN PARACHUTE DIAMETER

The results of these studies consistently lead to the conclusion that minimum costs occur if the SRB structural component failure probability is less than 1%. Figure 7 shows the total SRB program cost as a function of impact velocity, assuming components are designed for a 1% failure probability at each descent velocity. These data include DDT&E, new unit production, refurbishment, and performance costs. The minimum SRB program cost for a 445-flight program is \$1,387 million and occurs at an impact velocity of 38 m/s (125 fps). If the impact velocity is reduced to 24.4 m/s (80 fps), the total SRB program cost is shown on Fig. 7 to be \$1,417 million for a hybrid (parachute plus retrorocket) recovery system, or \$30 million more than the minimum cost system. These data show that using a pure parachute recovery system for a 24.4 m/s (80 fps) impact velocity would increase the cost of the recovery system by \$10 million over the hybrid system. This increment is within the uncertainty of DDT&E costs of the recovery system at the lower impact velocities, so if the reduced impact velocity is desired, additional trade studies must be conducted between the hybrid and pure parachute recovery system to define the most cost effective system.

If the total flight schedule is reduced to 225 flights, the minimum SRB program cost is \$840 million and occurs at an impact velocity of 36 m/s (118 fps). Based on the total cost and flight schedule, the cost per flight is estimated to be \$3.12 million for a 445-flight program and \$3.74 million for a 225-flight program. In considering only operational cost and flights, the cost per flight reduces to \$2.7 million for the 445-flight program and \$2.9 million for the smaller program.

These results were based on parametric cost data. In order to validate these trends, the costs of several recovery system point designs were also estimated. Analysis of these point designs support the selection of a high impact velocity for a minimum cost system and result in the same minimum total cost. The sensitivity to impact velocity, however, was less for the point designs than for the parametric costing studies. The parametric data show a cost increase of \$30 million in reducing impact velocity from 38 to 24.4 m/s (125 to 80 fps), while the point designs show this increase could be as low as \$6 million.

Program plans for development test, qualification test, manufacturing, operations, logistics, and facilities were generated to the depth required to support estimates in DDT&E and operational costs and refurbishment cycles.

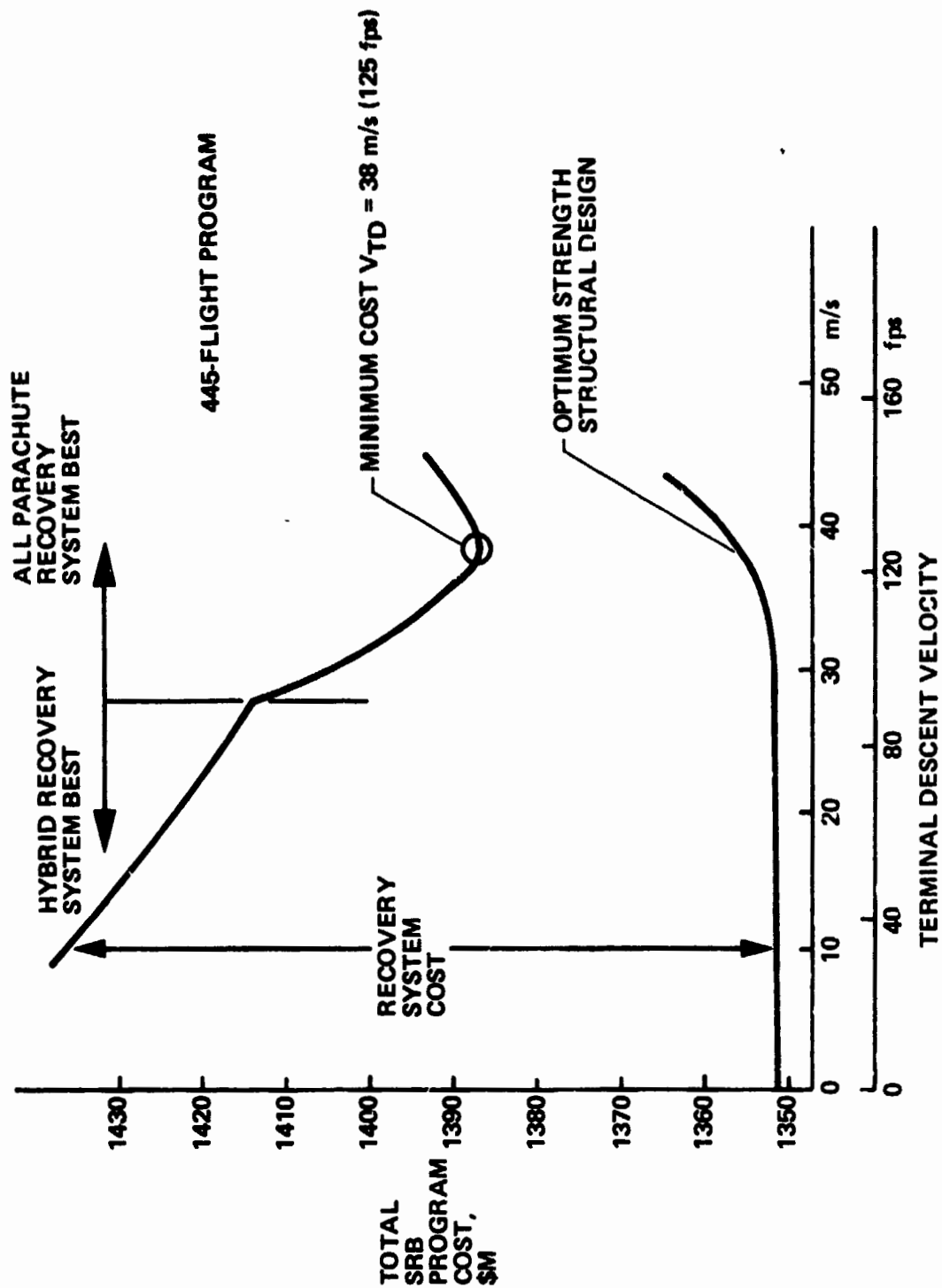


Figure 7 Optimum Descent Velocity Is 38 m/s (125 fps)

1.0 INTRODUCTION

One of the keys to achieving an economically feasible Space Shuttle system is the development of a cost-effective means of recovering and reusing the solid rocket boosters (SRB). Martin Marietta undertook the task of defining the requirements for such a recovery system under contract NAS8-29622 from NASA MSFC on March 2, 1973. This document constitutes the final report of this contract and presents the results of the study with our conclusions and recommendations for future action.

The primary objective of this study has been to define the requirements of the system that provide the most cost-effective means of recovering the SRB with a high probability of reuse. The single most important criterion used in this evaluation was lowest total program cost. The primary dependent variable affecting the cost tradeoff was terminal descent velocity, V_{TD} ; however, the effect of specified design conditions for SRB structural components was also considered. The minimum cost system is the one having the lowest combination of costs due to the recovery system, component damage or attrition, refurbishment, and the design and fabrication of certain SRB structural components to withstand water impact loads. The effects of impact velocity and design concept on DDT&E and facility costs were also included in considering total program costs.

The major emphasis of this study was placed on defining requirements, with secondary emphasis on generating preliminary design concepts. Those design concepts were carried only to the depth necessary to establish feasibility, perform major cost trades, and serve as a basis for preparing development and operational plans.

Our study approach was to use the NASA-supplied SRB baseline configuration, water impact, aerodynamic, and structural test data to develop a set of design requirements for the SRB recovery system from separation through water impact and flotation. Baseline design concepts were derived to satisfy these requirements and a minimum cost recovery system was established, assuming these data were complete and accurate. We then identified concerns regarding the completeness, accuracy, and applicability of the data, suggested methods for resolving these concerns, and estimated the impact that various data uncertainties could have on the recovery system design and program costs.

Accuracy limits of the aerodynamic data were estimated to assess the criticality of the design and to determine the dispersions that could be tolerated. The results of the water impact tests were extrapo-

lated to estimate loads at the higher impact velocities that our analysis predicts are required to achieve a minimum cost system. The two areas of data uncertainty that cause the greatest concern regarding the finality of our design concept are the SRB aerodynamic characteristics and the water impact loads. If the aerodynamic data is in error, the dynamic behavior of the SRB during entry will not be accurately predicted, thus invalidating the assumed recovery system deployment conditions. Erroneous extrapolation of the water impact loads data affects the accuracy with which the impact velocity for minimum cost can be selected. We feel additional testing and analysis is necessary to eliminate these uncertainties.

The recovery system requirements propagate in reverse order from the flight sequence. Acceptable water impact loads define the maximum impact velocity which in turn defines the Terminal Deceleration and Descent (TD&D) requirements for terminal velocity and attitude. The Initial Deceleration and Stabilization (ID&S) requirements are defined by the required deployment conditions of the TD&D phase. The results of the TD&D phase analysis, including parachute parametric data, and the ID&S phase entry dispersion studies are discussed in Section 2 of this report.

During the contract period, the performance of additional tasks was directed by the NASA and the contract was changed accordingly. These tasks were to:

- develop a FORTRAN computer program to relate impact pressure distribution to total loads and prepare these loads for STAGS program input;
- develop SRB failure criteria;
- resolve structural dynamic response uncertainties from 120-in. SRM model drop tests;
- compare structural capabilities for monolithic and segmented case designs.

The results of these analyses are presented in Section 3.

Section 4 discusses the water impact loads analysis and SRB component strength capability. We used a Monte Carlo technique to statistically combine the probability distributions of environmental parameters, water impact loads, and structural strength capability to define the failure probability of various SRB components. This analysis technique and the results obtained are also presented in Section 4.

The baseline design concept and promising alternatives are presented in Section 5 along with the rationale supporting the selections made. SRB flotation characteristics showing the results of a simplified thermal transient analysis are included in this section.

Section 6, entitled Concept Evaluation and Selection, contains parametric cost data and cost trades. This section includes the effects of reliability, refurbishment cycle time, new unit costs, refurbishment costs, component failure probability, component design strength, and maximum expected operating pressure (MEOP) of the SRM on total program costs as a function of impact velocity.

Preliminary plans for development and qualification testing, manufacturing, operations, logistics, and facilities have been generated and are presented in Section 7. These plans were used to support the cost analysis and provide a base for more detailed plans that will be required as the SRB recovery design matures.

The overall conclusions drawn as a result of this study are discussed in Section 8, which also presents our recommendations for future testing and analysis.

The airborne studies of the SRB reentry and recovery system concepts have been performed using a parametric approach. In a sense, the definition of recovery system requirements involved the simultaneous analysis of reentry dynamics, parachute trending analytics, the definition of water impact loads, and estimation of SRB strength. Even though these studies were performed on a concurrent schedule, the actual propagation of recovery system requirements flows from the water entry conditions back up the trajectory to SRB separation from the external tank. The acceptable water entry conditions determined from the attrition study set the requirement for the Terminal Deceleration and Descent (TD&D) system. The TD&D system in turn sets requirements on the Initial Deceleration and Stabilization (ID&S) system for acceptable deployment conditions, while both of these reentry phases impose environmental conditions on the recovery system design.

This section presents the results of parametric analyses of both the TD&D and ID&S mission phases of SRB recovery. The parachute trending data and 6 DOF two-body dynamics simulation results presented have been used to select and analyze the baseline recovery system. The 6 DOF reentry dispersion analysis has established a reentry corridor that satisfies the TD&D deployment requirements without the necessity of an ID&S system (i.e., the basic SRB high α reentry stability and drag are sufficient to produce conditions compatible with TD&D deployment). The expected levels of reentry environmental parameters (shock, vibration, acoustic, and temperature) are identified for use in component selection and/or design criteria.

2.1 TERMINAL DECELERATION AND DESCENT (TD&D)

Two concepts were identified for study at the onset of this contract: an all parachute system and the so-called hybrid (parachute and retromotors) system. The selection criteria for these two was mainly the desired terminal velocity. Beyond these two highly visible issues, this section will discuss many more selection trends that were not actively discussed until very recently.

The analytic analysis techniques for parachutes are just beginning to emerge from an industry that has traditionally relied mostly on build-and-test procedures to develop parachutes. Our approach has been to consult with the leading parachute experts, both within our Division, and at other companies, to define some parachute design guidelines based on current experience. But beyond this, the available analytic models have been used to develop parachute trending data via parametric techniques common to aerospace. The areas of most interest revealed through these parametrics have been refined using our point mass parachute simulation program. The baseline recovery system has been dynamically simulated in our two-body 6 DOF program to verify the concept feasibility. In addition, an assessment of possible slapdown load alleviation, resulting from not releasing the parachutes at water impact, has been made.

2.1.1 Parachute Design Considerations

The analytical modeling of the parachute system has not progressed to the point of system design without the aid of extensive development testing. While this situation seems to be improving rapidly, experience still plays an important roll in parachute design and performance estimation. Thus, to begin our parametric approach to TD&D concepts, we consulted our Viking Decelerator Project Staff, Pioneer Parachute Company, Goodyear Aerospace Corporation, and Sandia Laboratories to benefit from their parachute development ideas. These conversations along with an extensive literature search culminated in the following low risk parachute design guidelines.

1) Parachute nominal diameter(s) should be limited to 40 m (135 ft) for either single or clustered systems. If a cluster of parachutes is necessary, the size should be three to maximize the use of available operational and test experience.

2) Controlling the effective drag area growth to limit peak loads may be accomplished by two methods: (a) sequential deployment of multiple parachute systems, or (b) restricting the drag area buildup to discrete increments while the dynamic pressure diminishes (reefing). Reefing should be limited to two stages for clustered system, to minimize the nonuniformity in inflation loads of the individual parachutes resulting from reefing cutter timing uncertainties. Within these limits, it is preferred to increase the number of reefings before increasing the number of parachute systems. Controlling drag area growth through reefing has a higher total system reliability than multiple stages.

3) The Mach number design limits are established at 3.0 to avoid nylon aerodynamic heating, 1.5 for large diameter drogue parachutes, and 0.7 for the main parachutes. These are conservative values and only indicate that additional analysis is needed if these values are exceeded.

4) A pilot chute(s) is the optimum mechanism for extracting the large main parachute. The required mortar, tractor, catapult, and drogue gun mechanism sizes would impose a weight penalty on the system without a comparable improvement in reliability.

5) Only heavy duty ribbon parachutes qualify for the size and required strength of the SRB main parachutes. The high SRB weight combined with the terminal velocity requirements dictate large canopy diameters with high loading. In addition, a low opening load factor is desired to minimize parachute weight. The solid textile canopy parachutes (flat circular, conical, extended skirt, guide surface, and shaped gore) exhibit higher drag coefficients, but generally have higher opening shock loads than ribbon chutes and are not easy to refurbish. In addition, they do not meet the SRB loading or the relatively large diameter requirements. The annular, DGB, and cross parachutes designed and developed for planetary entry are advanced concepts and not designed for the high loads and large diameters required for SRB recovery. A comparison of heavy duty ribbon parachute characteristics is presented in Figure 2.1-1.

6) Where an equivalent single parachute will meet the above requirements, clusters should be avoided because of added system complexity, nonuniformity in opening and disreefing loads, and lower total system reliability. The single parachute will permit the use of a greater number of reefing stages and higher overall operational reliability.

2.1.2 Recovery System Baseline Design

The TD&D system baseline design developed during this study satisfies the water impact requirements developed from the SRB attrition analysis. The design did not precede the trending analyses of the following sections, but introducing the baseline should demonstrate the value of parametric trending data in system design work.

PARACHUTE FEATURES NEEDED FOR SRB RECOVERY:

- HIGH CANOPY LOADING
- LARGE CANOPY DIAMETERS
- CLUSTERED DEPLOYMENT OF LARGE DIAMETER CHUTES
- EASE OF REFURBISHMENT
- LOW OPENING LOAD FACTOR DESIRED
- GOOD DRAG TO WEIGHT EFFICIENCY
- OPERATIONAL DESIGN

RIBBON PARACHUTE CHARACTERISTICS							
TYPE	C_D	STABILITY	TEST & DESIGN DATA	FEASIBLE SIZE RANGE	EASE OF REFURBISHMENT	FEASIBLE LOADS RANGE	$C_D S_0$ WEIGHT
CONICAL	0.45-0.58	VERY GOOD	VERY GOOD	LARGE	GOOD	VERY HIGH	MEDIUM
FLAT CIRCULAR	0.50-0.70	GOOD	GOOD	LARGE	VERY GOOD	MEDIUM	HIGH
RING-SAIL	0.40-0.90	FAIR	VERY GOOD	LARGE	POOR	HIGH	MEDIUM
RING-SLOT	0.55-0.75	FAIR	GOOD	LARGE	POOR	HIGH	MEDIUM
VARIABLE POROSITY	0.50-0.60	VERY GOOD	POOR	LARGE	GOOD	VERY HIGH	MEDIUM
HEMISFLO	0.25-0.45	VERY GOOD	POOR	MEDIUM	GOOD	VERY HIGH	LOW
EQUIFLO	0.15-0.47	VERY GOOD	POOR	MEDIUM	GOOD	VERY HIGH	LOW

Figure 2.1-1 Ribbon Parachutes for SRB Recovery

The SRB recovery mission profile from SRB separation from the external tank through water impact is depicted in Figure 2.1-2. The baseline parachute system consists of one 40.2 m (132 ft), single reefed parachute, an extraction pilot parachute of 7.62 m (25 ft) diameter, and associated subsystems.

A complete discussion of the baseline system is presented in Section 5.0. Briefly, the pilot chute is packaged in the nose cap, which is ejected via thrusters to start the deployment sequence. The pilot chute is pulled from the nose cap at line stretch and begins inflating. As the pilot line tension increases, the cone frustum, containing the main parachute, is released and pulled away by the pilot parachute. The main parachute is stripped from the frustum, which remains attached to the pilot parachute for recovery, at line stretch and begins inflation. Following the single disreefing, the main parachute and SRB descend to a water impact at 38 m/s (125 fps).

The baseline system is within the low risk design guidelines established earlier. These guidelines should keep any parachute development within current state of the art. However, state of the art is difficult to precisely define for parachutes. Numerous design and development parameters are involved, all of which may not be satisfied. Figure 2.1-3 was taken from the *NASA Space Vehicle Design Criteria - Deployable Aerodynamic Decelerator System*, NASA SP-8066, June 1971. To this representation of current parachute design experience, we have added the baseline design point which is within the parachute experience base and meets SRB recovery requirements.

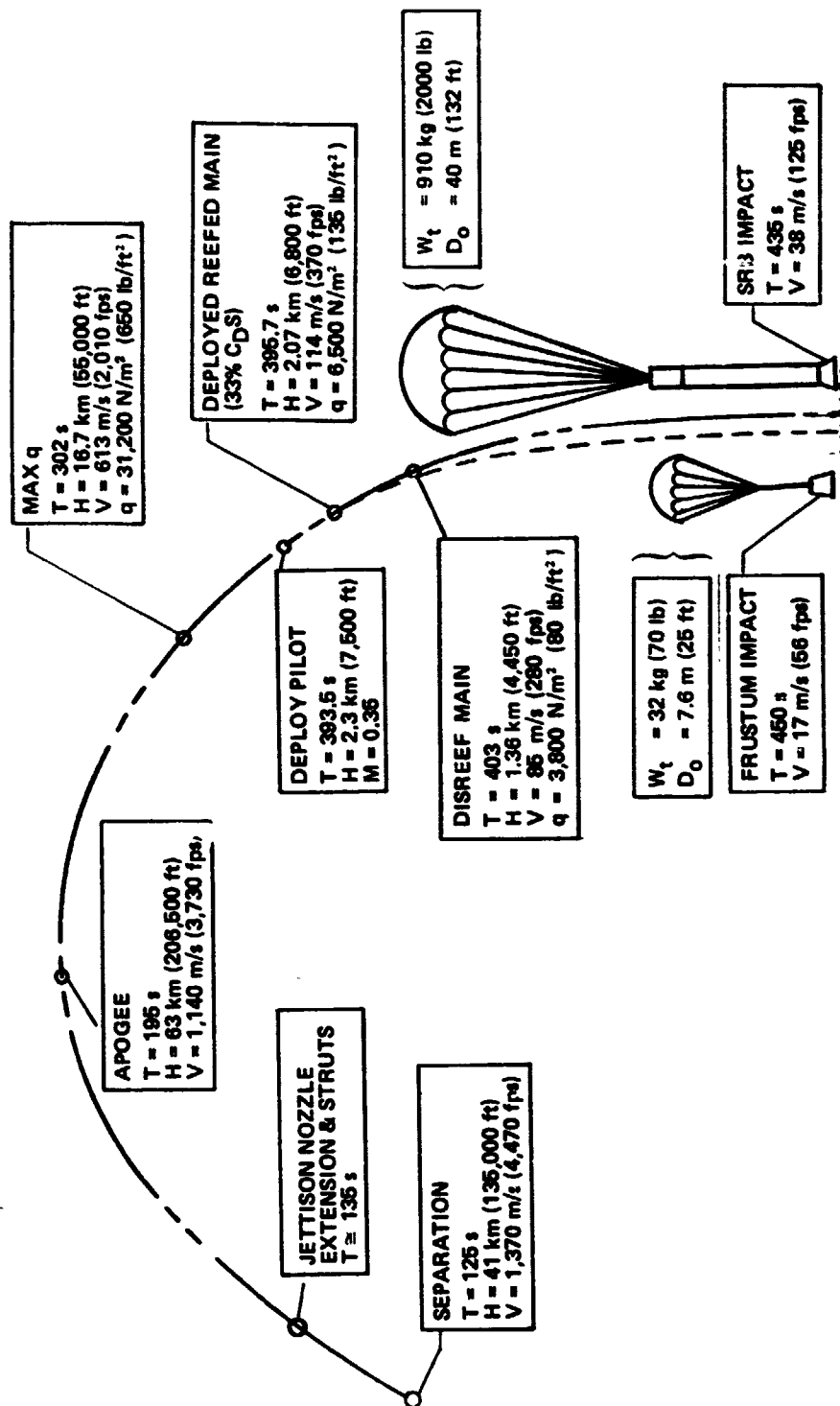
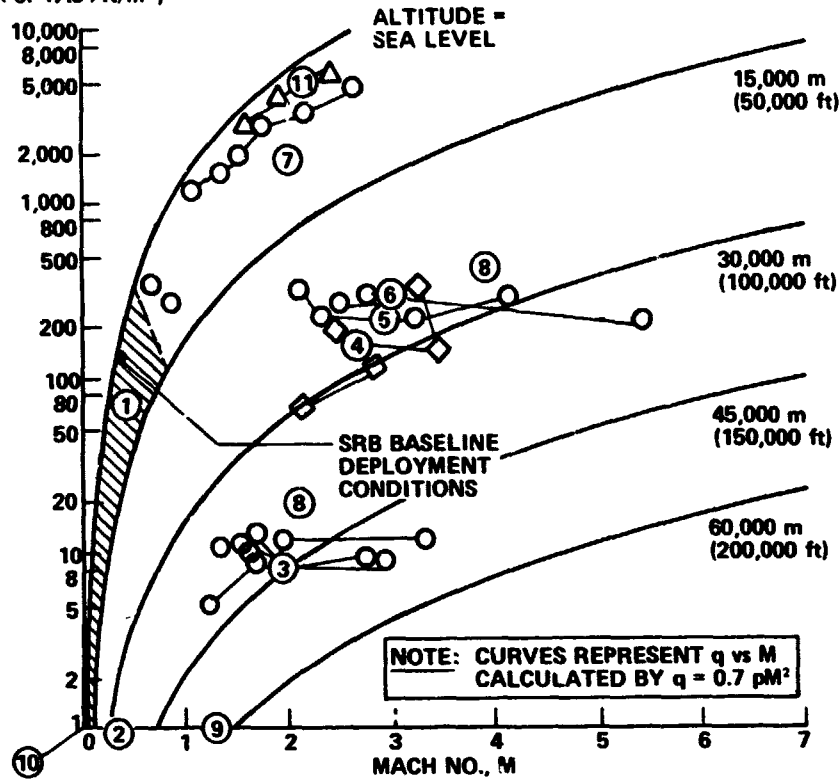


Figure 2.1-2 SRB Recovery Mission Profile

DYNAMIC PRESSURE,
q (psf or 47.88 N/m²)



GROUP	DECELERATOR TYPE	SIZE (DIAMETER)
1	CONVENTIONAL PARACHUTES GLIDING PARACHUTES DEPLOYABLE WINGS AERIAL-RECOVERY PARACHUTES	$D_o = 0.3 - 61 \text{ m (1 - 200 ft)}$ $D_o = 4.9 - 27 \text{ m (16 - 88 ft)}$ $b_w = 3.7 - 27.4 \text{ m (12 - 90 ft)}$ $D_o = 7.3 - 21.4 \text{ m (24 - 70 ft)}$
2	SOUNDING-ROCKET PARACHUTES	$D_o = 1.8 - 4.9 \text{ m (6 - 16 ft)}$
3	PLANETARY-ENTRY PARACHUTES	$D_o = 9.1 - 26 \text{ m (30 - 85 ft)}$
4	EXPERIMENTAL HEMISFLO AND HYPERFLO DROGUES	$D_o = 0.82 - 1.98 \text{ m (2.7 - 6.5 ft)}$
5	EXPERIMENTAL TEXTILE BALLUTES	$D_p = 0.61 - 1.52 \text{ m (2 - 5 ft)}$
6	EXPERIMENTAL PARASONIC DROGUES	$D_o = 1.22 \text{ m (4 ft)}$
7	HEMISFLO DROGUES	$D_o = 4.88 \text{ m (16 ft)}$
8	ALARR BALLUTES	$D_p = 0.61 \text{ m (2 ft)}$
9	SOUNDING-ROCKET BALLUTES	$D_p = 2.13 - 4.88 \text{ m (7 - 16 ft)}$
10	EXPERIMENTAL AID _s	$D_p = 11.28 \text{ m (37 ft)}$
11	CONICAL-RIBBON PARACHUTES	$D_o = 3.81 - 23.2 \text{ m (12.5 - 76 ft)}$

Figure 2.1-3 Baseline Recovery System within the State of the Art

2.1.3 Parachute Parametrics

The question asked most often about a parachute recovery system is, "How many and what size parachutes are required?" These are really two dependent variables that are determined by the terminal descent conditions desired. The terminal descent velocity (V_{TD}) and SRB weight allow for the selection of a unique parachute diameter for each cluster size being considered. The equilibrium flight relationship:

$$\begin{aligned} W_{SRB} &= q\eta NC_D A \\ &= \frac{1}{2}\rho V_{TD}^2 \eta NC_D \pi D_o^2 / 4 \end{aligned}$$

permits calculating the parachute nominal diameter (D_o) in terms of the terminal descent velocity (V_{TD}), cluster size (N) and cluster efficiency (η) as:

$$D_o \approx \sqrt{\frac{8 W_{SRB}}{\pi \rho V_{TD}^2 \eta NC_D}}$$

Figure 2.1-4 displays parachute diameter versus V_{TD} for cluster sizes of 1, 3, and 6. For a V_{TD} of 30 m/s (100 fps) the cluster size and diameters could be one 51.3-m (168-ft), three 31-m (103-ft), and six 20-m (65-ft) parachutes. For this example, we would not consider the 51.3-m (168-ft) parachute since it exceeds our low-risk design limit.

The use of a single parachute for recovery is generally conceded to be the most reliable system. However, if the design V_{TD} is less than 38 m/s (125 fps), a multichute cluster must be used for a low-risk design approach. The design guideline is to minimize the number of parachutes in the cluster. The plot on the right of Figure 2.1-4 shows the system weight effects of increasing cluster size for terminal descent velocities of 24 m/s (80 fps) and 46 m/s (150 fps). The solid line is a solution using the equations extracted from Goodyear Aerospace Corporation Report GER-15887, dated May 1, 1973.

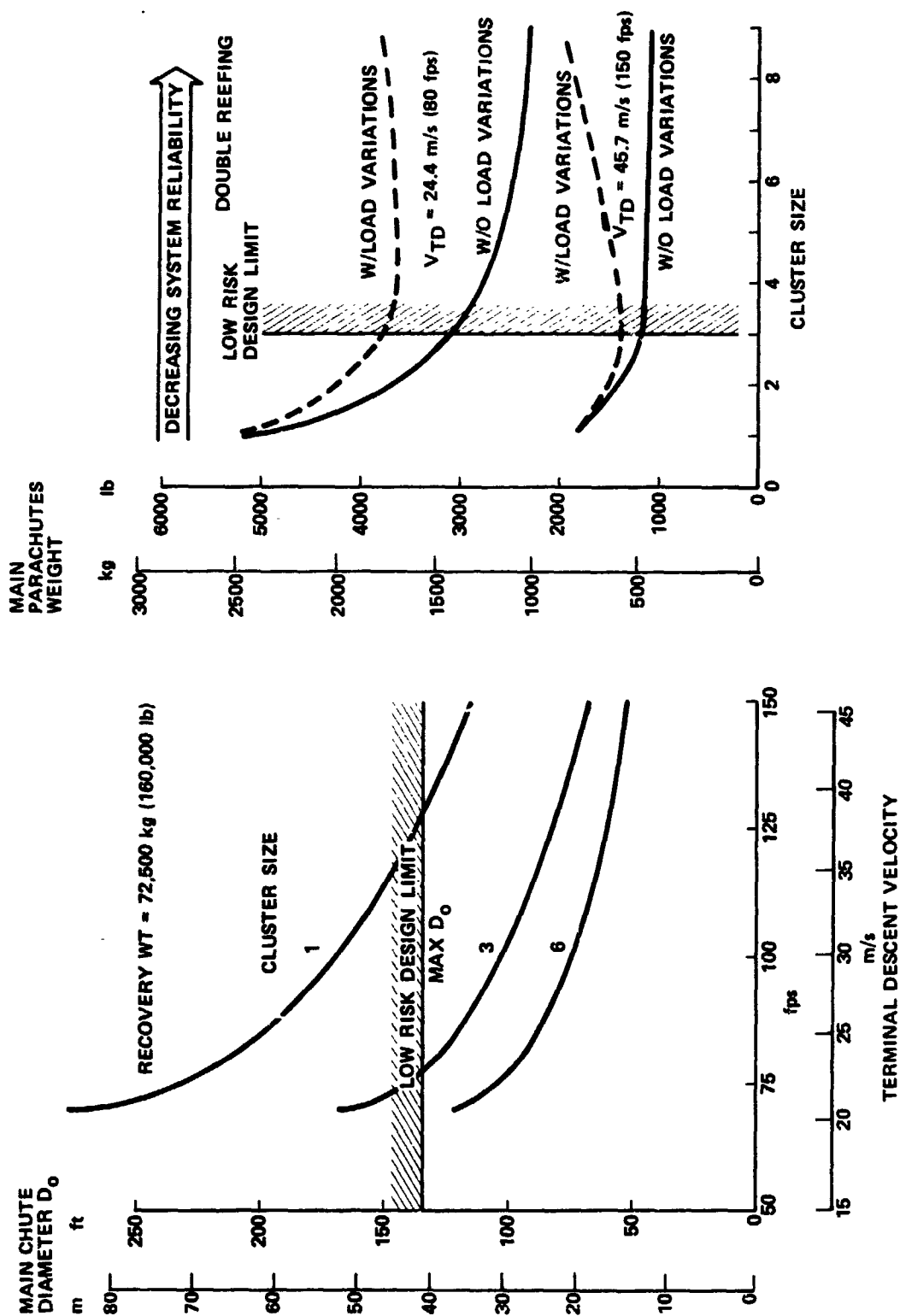


Figure 2.1-4 Canopy Diameter and Cluster Size, Primary Dependent Variables

$$W_p = 24.75 \times 10^{-5} * D_o * g * W_{SRB}$$

where W_p is the parachute weight, W_{SRB} is the total system weight, g is the deceleration load factor, and D_o = parachute diameter.

(For English system units the constant is 5.55×10^{-5} .) The dashed line, we feel, represents more realistically the trend with design increases to account for unequal load distribution between chutes and estimated cluster drag efficiency.

The general trend of either curve is decreasing system weight with increasing cluster size. Briefly, this can be thought of as a hoop stress condition wherein the larger the canopy diameter the greater the linear stress for a given load. The increasing stress results in heavier construction techniques, thus more parachute weight. It should be noted that this is not universally accepted by all parachute analysts. The NASA SP-8066 *Deployable Aerodynamic Decelerator Systems* document clearly states that the weight of a clustered parachute system is greater than that of an equivalent single parachute system. Therefore, weight is not the deciding factor between single and clustered parachute systems.

Variations in the canopy load on any single chute in a cluster can result from two primary sources: (1) unequal deployment and inflation times and (2) the reefing cutter time dispersions (especially the second disreefing). Our estimates of the load variation are: 20% for a cluster of three, and 50% for a cluster of six on the opening loads at second disreefing. Since we cannot predict which parachute must survive these dispersions, all the parachutes must be designed for maximum possible loads.

The parachute deployment opening load is approximated by:

$$g \approx q_D / \beta = q_D C_D S / W_{SRB}$$

where β is the ballistic coefficient and $C_D S$ the effective drag area. When the system has reached equilibrium flight conditions,

$$W_{SRB} \approx q_T C_D S.$$

It is from these force relationships that the loading may be approximated from the required reduction in dynamic pressure.

$$q_T = W_{SRB} / C_D S = q_D g^i,$$

where i is the number of stages.

Figure 2.1-5 was developed to demonstrate a performance trend for recovery systems with and without a first stage drogue. On the left are curves of constant deployment dynamic pressure (q_D) showing a weight optimum terminal dynamic pressure (q_T); e.g., the drogue should be released at this q_T and the main parachutes deployed, for each q_D . For instance, if the q_D is 28,700 N/m² (600 psf) then the drogue should be released at approximately 4,060 N/m² (85 psf).

The curves on the right are a comparison of one- and two-stage parachute systems; i.e., mains only versus mains plus drogue. The dashed lines are the drogue plus mains for optimum drogue q_T . The solid lines are a mains-only system deployed without a drogue. These curves show a crossover does exist such that below some q_D the system is lighter if the drogue is eliminated. It is also interesting to note the crossover, q_D , increases with increasing V_{TD} .

2.1.4 Hybrid System Performance Trends

Parametric trends have also been developed for the performance of an all parachute system versus a parachute plus retromotor hybrid system. The solid propellant retromotor system was assumed to add a nominal fixed weight of 226 kg (500 lb) in addition to the weights associated with total impulse. This weight is made up of 68 kg (150 lb) for subsystems, 90 kg (200 lb) of attachment hardware, and 68 kg (150 lb) for the motor case and ignition system. The retromotor weight will increase from the 226 kg (500 lb) minimum with increasing total impulse. Figure 2.1-6 shows the weight relationships of retromotor, parachutes, and combined hybrid system weight as a function of terminal parachute velocity and water impact velocity. The buckets of hybrid weight curves would be the optimum parachute terminal velocity for a particular impact velocity.

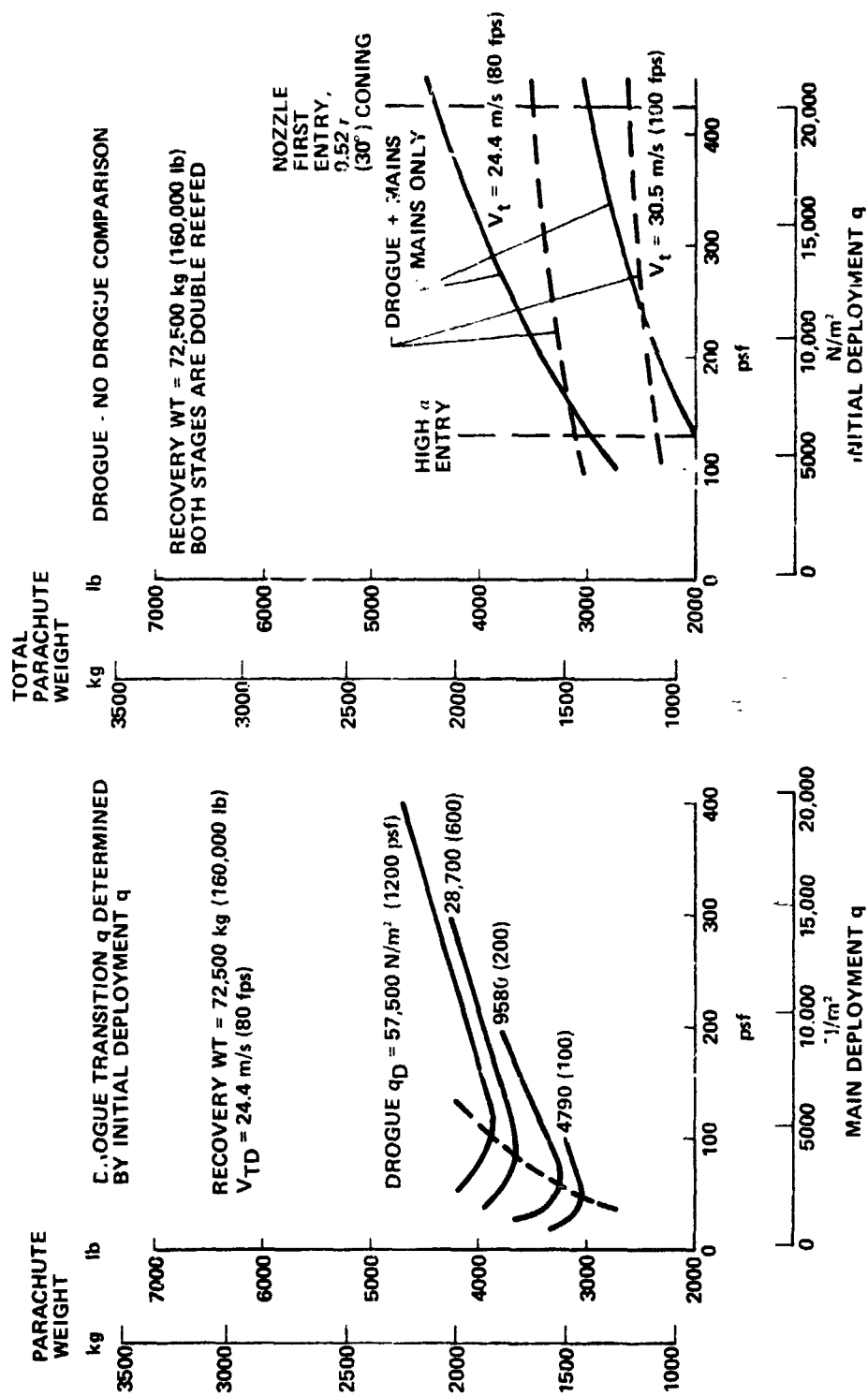


Figure 2.1-5 Drogue May Not Be Necessary

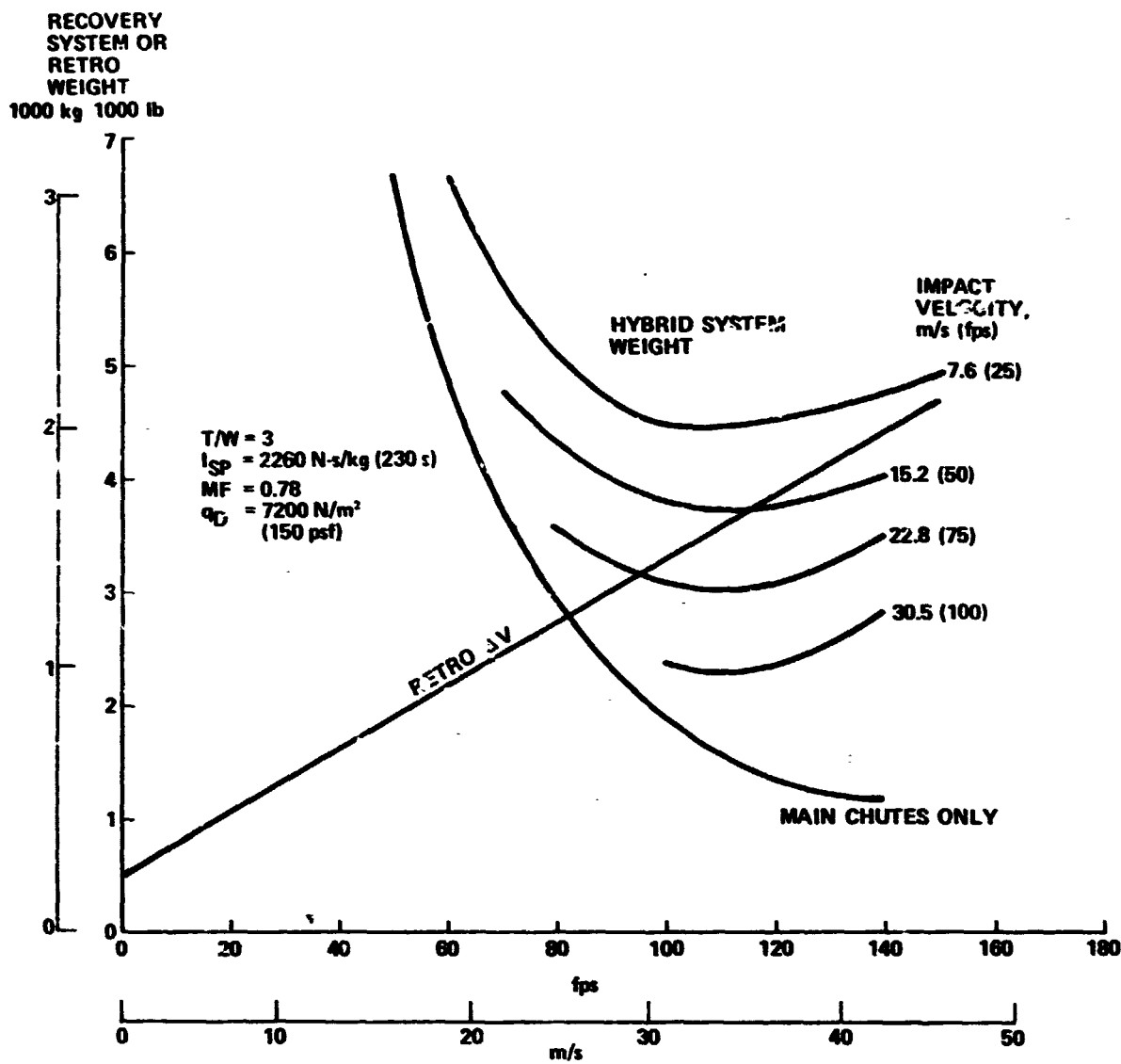


Figure 2.1-6 Hybrid System May Reduce Recovery System Weight

Comparing the system weight performance trend for hybrid versus all parachute systems yields the data of Figure 2.1-7. A system weight crossover exists at 25 m/s (83 fps), indicating the all-parachute system is lightest above 25 m/s (83 fps) and the hybrid system is lightest below 25 m/s (83 fps). The parachute low-risk design guideline of the three-parachute cluster of 41-m (135-ft) diameter is also shown to emphasize the potential advantage of hybrid systems below desired impact velocities of 25 m/s (83 fps).

2.1.5 Point Mass Simulation Analyses

The previous parametric data made some simplifying assumptions to allow a broad overview of parachute trends. Two basic assumptions were:

- 1) negligible bag strip and inflation times;
- 2) 100% reefing efficiency.

These parametric trends narrow the scope of the point mass simulations required to more fully analyze the parachute performance.

The point mass program is configured to solve for deployment sequence initial altitude, disreefing times, and reefing areas using input conditions for parachute load limits, SRB ballistic coefficients, and stage transition times. The disreefing times are based on achieving various efficiencies in dynamic pressure loss from the expression $q_T = q_D (1 - \xi + \xi/g)$ where g is the design

load limit and ξ is the efficiency of the disreefing. The reefing areas are constrained by parachute design load including an opening shock factor. Initially, the effective drag area was estimated using the expression $S = q_D/g$ which assumes a negligible inflation

time. This was found to be erroneous, especially for the longer inflation times caused by the relatively low velocities encountered with reefing the large diameter parachutes. The effective drag area is now determined by iterating until the design opening load is reached within specified limits. The parachute inflation times are calculated from the quadratic equations derived from the mean value inflation times given in the *Performance and Design Criteria for Deployable Aerodynamic Decelerators*, ASD-TR-61-579, December 1963. The point mass simulation affords a more detailed examination of those trends identified by our previous parametrics.

RECOVERY SYSTEM WEIGHT
1000 kg 1000 lb

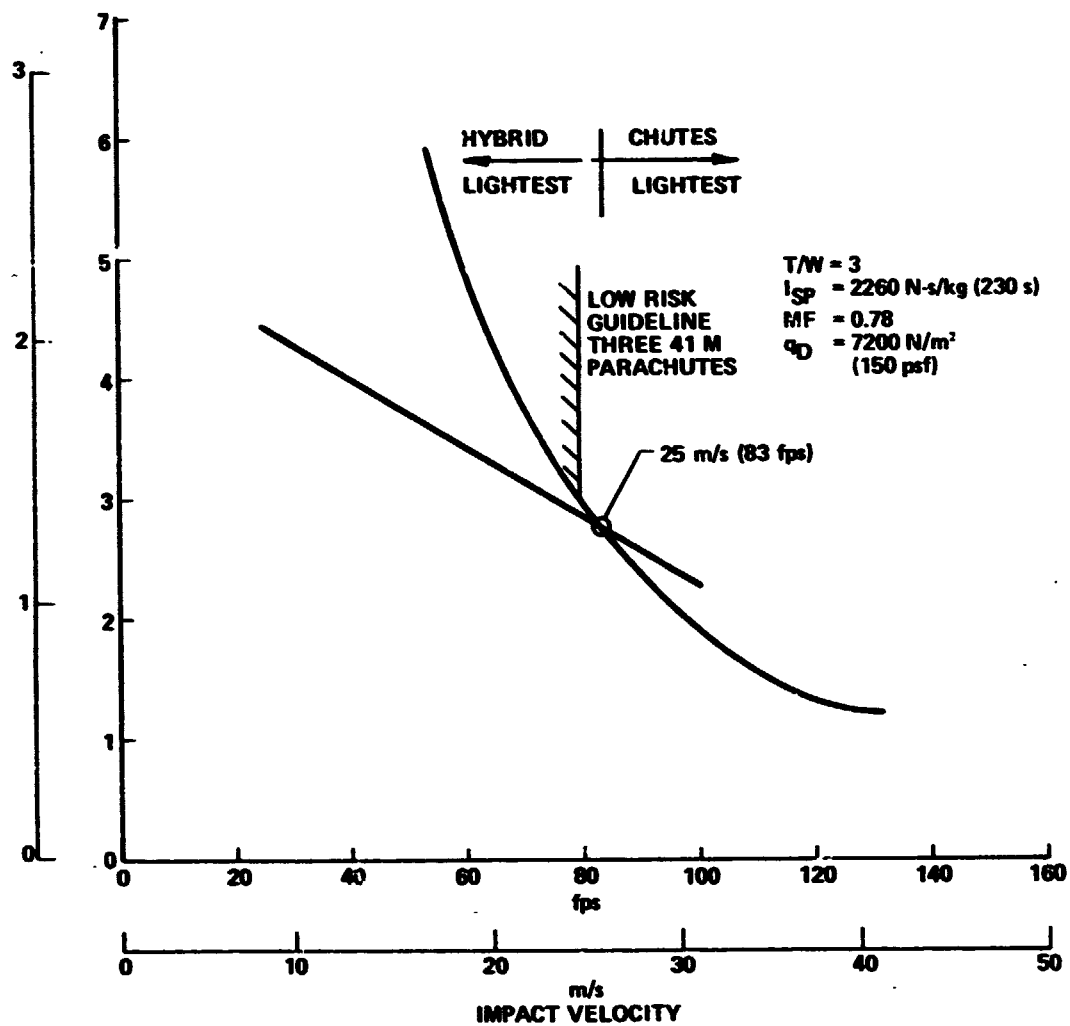


Figure 2.1-7 Hybrid System Performance Best for Low Impact Velocities

The main parachute system loading sensitivities generated using the point mass program are graphically presented in Figure 2.1-8 for double reefed parachutes deployed from the high α baseline reentry attitude. Varying the design load of the drogue stage (changing the nominal diameter for a given deployment q causes the load to change) results in a change in required load on the main parachute stage. Choosing a derived terminal velocity of 38 m/s (125 fps) and replotting these data reveals the trend shown in Figure 2.1-8. This figure shows the no-drogue/main-only system load (horizontal line), and the loading trend for adding a drogue. To reduce main parachute loads, the drogue would have to be at least 18 m (60 ft) diameter.

The importance of design load on the parachute system is directly reflected in parachute weight. The argument for a drogue in the system would revolve around absorbing a higher load in a smaller parachute, thereby reducing the load and weight of the larger main parachute. For our system, this approach has less merit since the drogue diameter required to reduce main parachute load is not considered small.

The actual load seen by a parachute can be controlled by reefing areas, reefing times, and the inherent inflation times associated with the parachute diameter and deployment velocity. The reefing time sequence and the inflation time have the effect of restricting the drag area buildup until q is reduced to a more desirable value. A single parachute system, having a correspondingly larger diameter than an equivalent cluster, will have a longer inflation time. This longer inflation time can be used to simplify the system by eliminating one reefing. Figure 2.1-9 shows the effect of number of reefings on opening and inflation loading. While the double reefed single parachute does achieve a lower loading, the reduction does not necessarily justify the additional complexity.

The point mass studies have also evaluated the reefing efficiency effects on parachute loads (or weight) and deployment altitude loss. The reefing efficiency is the percentage reduction of dynamic pressure achieved before a subsequent reefing or staging. Altitude loss is the altitude change during reefing from initiation to achieving the desired terminal velocity. Figure 2.1-10 shows that reducing the reefing efficiency from 95% (used for mid-term results) to the current baseline of 80% reduces the altitude loss by 214 m (700 ft) while increasing the weight approximately 45 kg (100 lb). However, the recovery system is not weight-critical, but minimizing the altitude loss helps expand the deployment box discussed in Section 2.2.

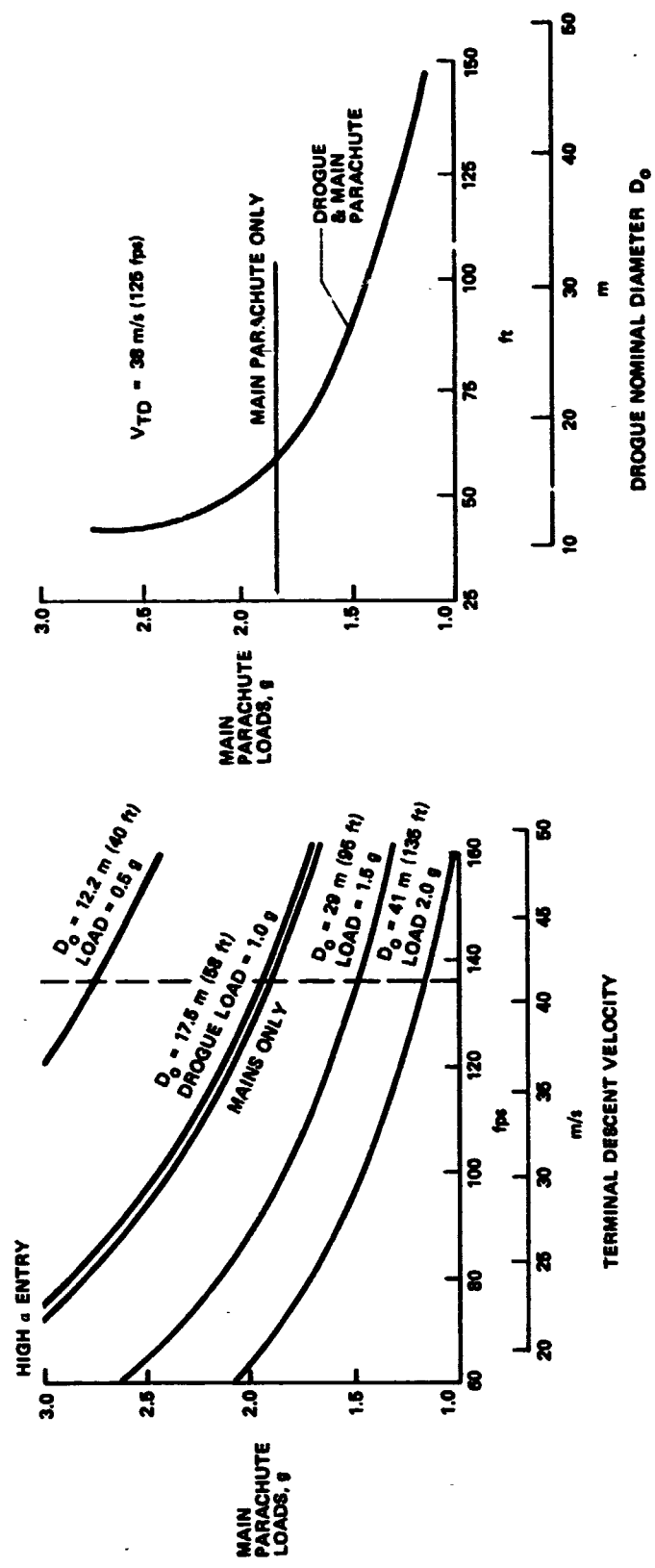


Figure 2.1-8 Main Parachute Loads Reduced by Increasing Drogue Size

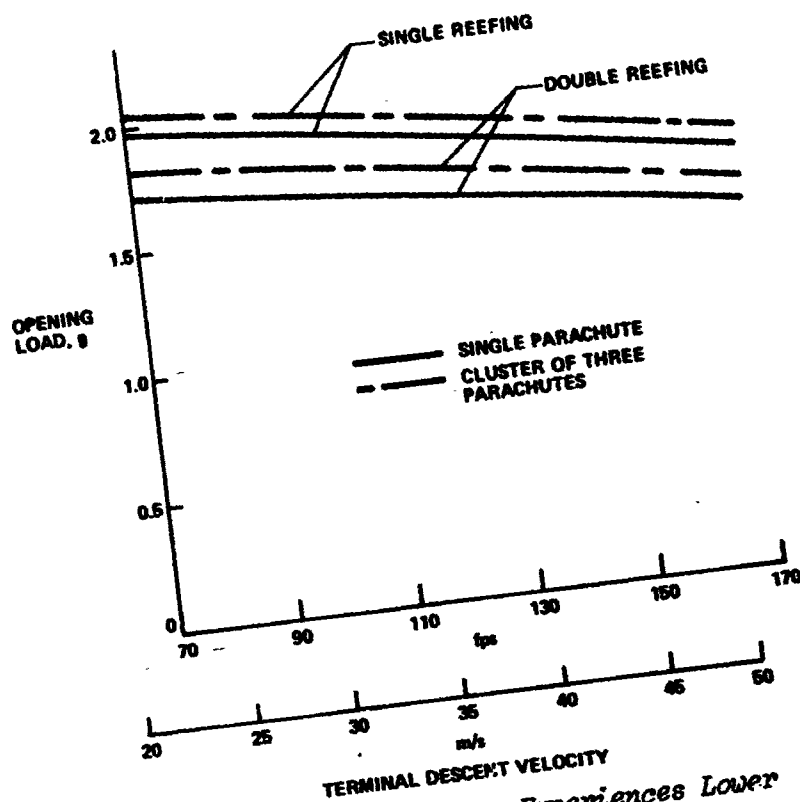


Figure 2.1-9 Single Parachute Experiences Lower

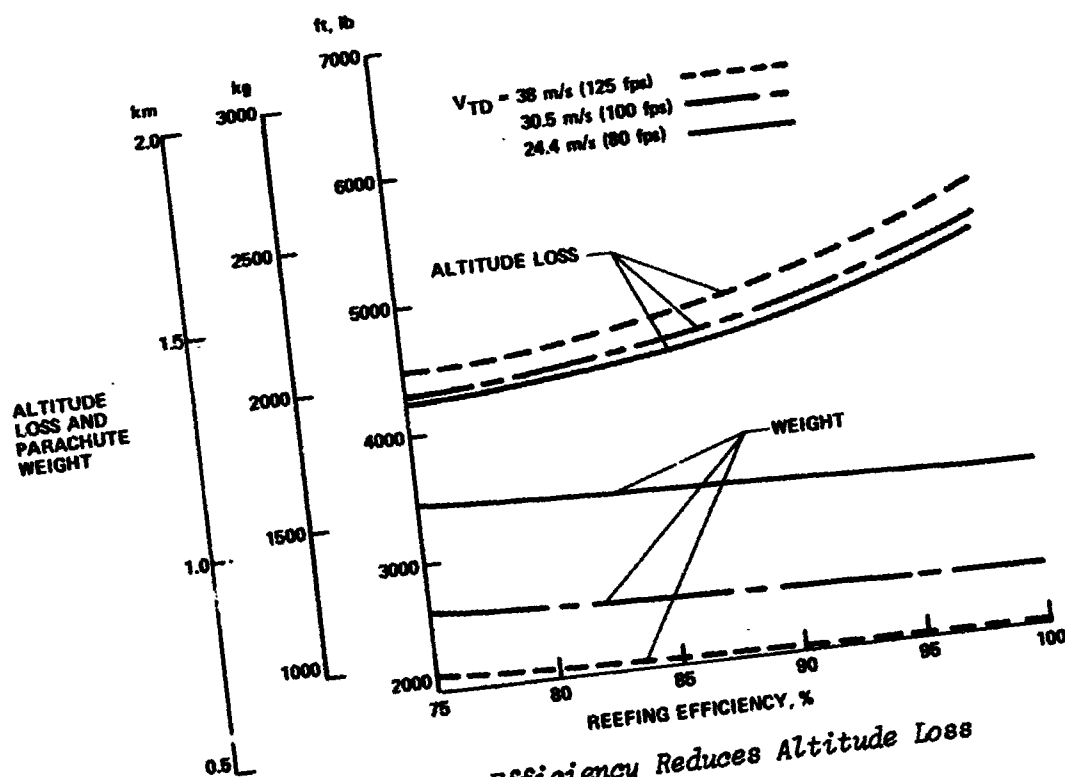


Figure 2.1-10 Lower Reefing Efficiency Reduces Altitude Loss During Deployment

A single reefing on the main parachute was chosen for its simplicity. The relationship of number of reefings, reefing efficiency, and parachute loadings should be examined in more detail by future studies. In addition, the principal concern for large diameter parachutes is the inflation characteristics. A detailed analysis will be necessary to balance the parachute porosity, reefing areas, and number of reefings to ensure uniform inflation characteristics.

2.1.6 Parachute Dynamic Analysis

A complete dynamic analysis of the baseline system was made to verify the design feasibility. The dynamic analysis was made using a two-body, 6 DOF parachute program developed for the NASA Viking 75 Project. The computer program results have been correlated and verified with the Viking ELDT parachute tests conducted at the WSMR. Our analysis simulated the recovery sequence from pilot chute deployment, actuated by separation thrusters, through SRB slapdown. The latter was simulated using hydrodynamic force histories obtained from NASA model drop tests.

The Viking decelerator dynamic simulation program has the following features:

- 1) Two-body analysis (Both the SRM and pilot or main parachutes have full 6 DOF.).
- 2) Bag stripping (the stretchout of risers, suspension lines, and canopy) and canopy inflation are simulated to determine snatch and opening shock forces for both the pilot and main parachutes.
- 3) The apparent and enclosed mass and their derivatives are considered for the main parachute.
- 4) The pilot/main parachute system modeled is one in which the pilot parachute, enclosed within the deployment bag, is ejected by a mortar device and, in turn, is used to extract the main parachutes.
- 5) The deployment of the parachute is simulated in considerable detail by separating the analysis into an inelastic phase and an elastic phase. The inelastic phase considers the changes in momentum and the bag stripping forces as the suspension lines and canopy are pulled from a deployment bag. At bag strip, the canopy and suspension lines are fully extended and inflation can occur. At this point, the elastic phase begins and treats the system as a two-body elastic coupled system.

The two-body simulation begins at 3.05-km (10,000-ft) altitude, before pilot parachute deployment, and simulates all events through water impact and primary slapdown. The ability to deploy the pilot and main parachutes into the free stream velocity from the high α attitude is a key to the current recovery system design. The analysis performed does not conclusively validate this concept, but the results definitely establish that the concept is feasible.

The pilot parachute motion after deployment is shown in Figure 2.1-11. The initial motion is along the SRB longitudinal axis resulting from the nose cap thrusters which impart a delta velocity of 3.05 m/s (10 fps). The motion continues outward until bag strip, 2.4 s, and the start of pilot parachute inflation, where the aerodynamic forces begin to carry the pilot up with the free stream velocity. Since the suspension and riser lengths are fixed, the motion after inflation describes an arc from the maximum outward distance upward toward the vertical trailing position. The wiggles in the arc are the results of elastic elongation from the opening shock load of the pilot. The effects of suspension line fish hooking caused by the aerodynamic loading on the suspension lines before pilot inflation are not currently simulated. However, the motion of the pilot does demonstrate that deployment normal to the free stream velocity is feasible.

The pilot suspension and riser lengths are designed for 5.5 hydraulic diameters which should be sufficient to avoid SRB wake interference effects during inflation. The motion history of Figure 2.1-11 shows the pilot chute has begun inflation before entering the region of probable SRB wake interference. The cone frustum containing the main parachutes is released as the pilot nears full inflation, which will allow the pilot to trail the SRB even further as the main parachutes are being deployed.

The main parachute loading and corresponding drag area buildup from opening and disreefing are presented in Figure 2.1-12. The peak opening load occurs very near the first drag area plateau, but the peak load from disreefing precedes the full open drag area. This results from the rapid decline in dynamic pressure during the long inflation time period. Figure 2.1-13 shows the comparison of parachutes loads from the 6 DOF and point mass simulations. The small perturbation differences in the dynamic analysis are mostly the elastic body effects of the parachute suspension lines. The spring constant was computed for nylon suspension lines at approximately 219,000 N/m (15,000 lb/ft) with approximately 10% critical damping. Actual damping values range from 5 to 10% of critical, but the system was relatively insensitive to damping within these bounds.

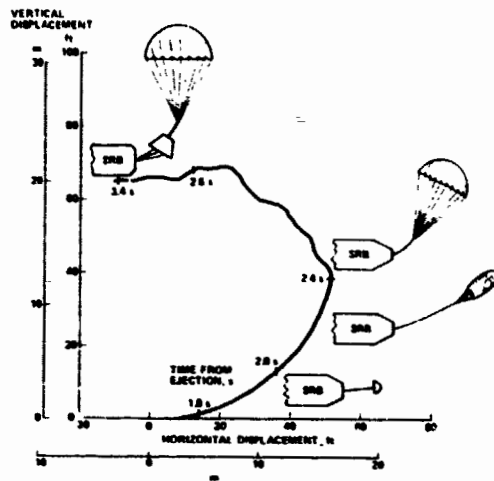


Figure 2.1-11 Successful Pilot Deployment from High α Reentry

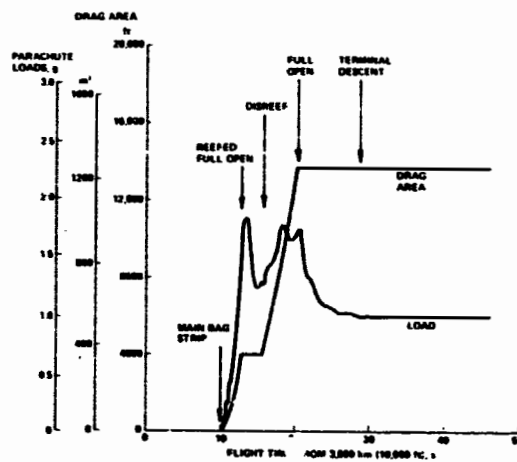


Figure 2.1-12 Initial and Disreefing Loads Are Balanced

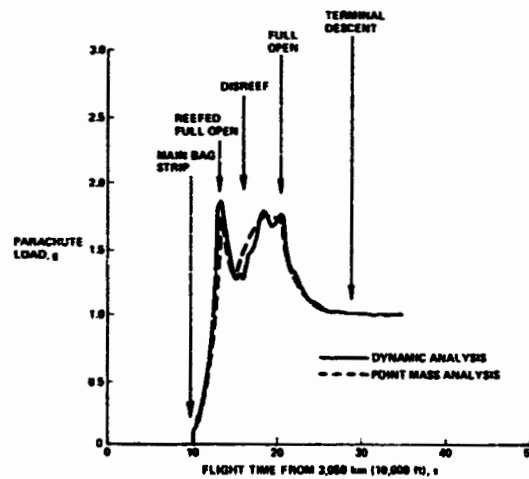


Figure 2.1-13 Parachute Elasticity Effects Are Minimal

The dynamic pressure and altitude histories are shown in Figure 2.1-14. Noted on the curves are main parachute events that correlate with the near step changes in q . Main parachute deployment begins at 1.8 km (6000 ft) followed by an altitude loss of 1.2 km (4000 ft) before achieving terminal dynamic pressure at approximately 0.6 km (2000 ft). The parachute and SRB then descend at 38 m/s (125 fps) to water impact.

The SRB altitude history is shown in Figure 2.1-15. Commencing with main parachute bag strip and the start of inflation, the SRB attitude is changed from broadside to vertical in approximately three seconds. The subsequent oscillations are damped to near zero in less than 15 seconds after bag strip.

2.1.7 Parachute Attenuation of Slapdown Loads

The Viking two-body 6 DOF dynamics program was modified to include slapdown hydrodynamic force and moment histories obtained from the NASA 12.5-inch model drop test telemetry and photographic coverage data. This was done to obtain an estimate of the benefits of retaining the parachute until after slapdown.

NASA water impact test data show that the initial water impact loads rotate the SRB during water entry causing the nose and forward section to accelerate and experience increased slapdown loads. The parachute performance characteristics (drag as a function of velocity, and elastic line elongation under load) will resist this acceleration, supplying some attenuation of the initial slapdown loads.

The hydrodynamic force and moment time histories derived from the test instrumentation were scaled and biased to produce an attitude history that agreed with the data provided by the NASA. Scaling adjustments were made by a successive approximation using the two-body 6-DOF program until the attitude history dynamics matched the NASA-supplied data. To assess the parachute attenuation of slapdown load, the same hydrodynamic force and moment histories were simulated with the parachute attached during slapdown.

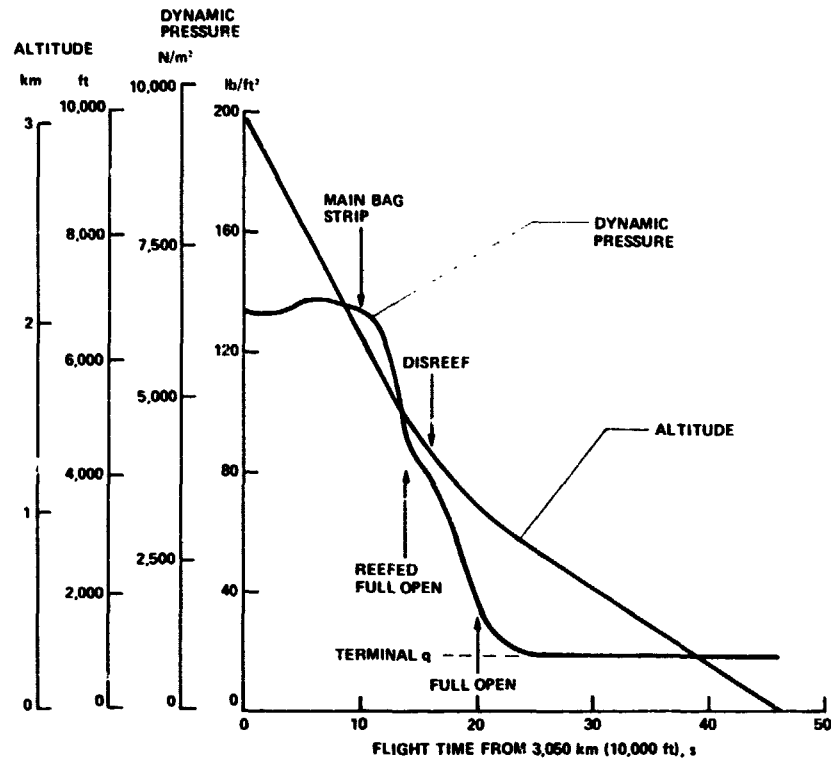


Figure 2.1-14 Deployment Altitude-Dynamic Pressure Histories

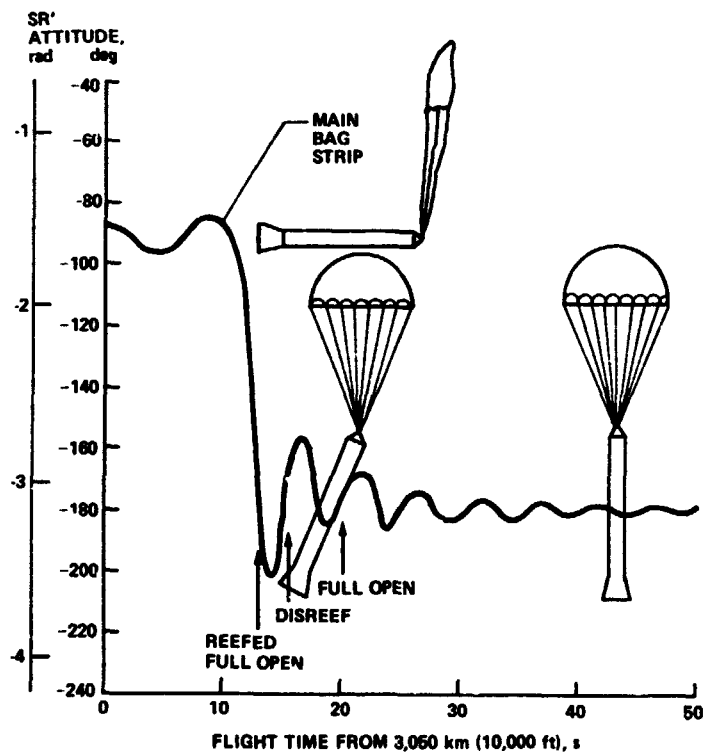


Figure 2.1-15 SRB Attitude Transition Accomplished in Three Seconds

The relative velocities for the SRB nose and cg obtained from the dynamics simulation with and without the parachute are shown in Figure 2.1-16. These velocities for the parachute-attached configuration are shown with the resulting parachute velocity and parachute pull force (line tension) in Figure 2.1-17. The parachute line tension reduces initially as the SRB decelerates from impact, after which the rotational moment increases the nose velocity, which increases the parachute retention force momentarily before the lines become slack. This secondary force acts normal to the SRB rotation, which appreciably reduces the rotational rate and associated slapdown loads.

The resulting attitude history is shown in Figure 2.1-18 (dashed lines). During the first second after water impact, the unrestrained SRB attitude changes by 1.05 rad (60 deg) compared to 0.87 rad (50 deg) for the restrained SRB. This difference increases rapidly from 1 sec to the respective slapdown events i.e., when the unrestrained SRB is nearly horizontal, the parachute restrained SRB is still 0.49 rad (28 deg) above the water.

The restraining effect of the parachute is actually over before the SRB experiences the full slapdown load. However, the key issue is that the parachute has restrained the angular acceleration during the critical initial penetration. Comparison of nose impact velocities for the two cases shows that the parachute will reduce nose impact velocity by 25%. If the peak slapdown loads are assumed to be a function of dynamic pressure, the loads would be 40% lower for the parachute attached condition.

While these results are encouraging, there are several limiting factors to this analysis. The results are for a specific set of impact conditions ($V_V = 21.4$ m/s, $V_H = 15.2$ m/s, $\theta = 0.17$ rad).

The force and moment histories would not be the same with and without a parachute attached. These test data were adjusted to agree with a visual attitude history.

In general, what is needed is more test data and a hydrodynamic simulation model with two-body capability. Test data giving trajectory information for high V_H conditions are scarce at the present, but additional test results, as they become available, will shed more light on this subject. If peak slapdown loads are a function of the slapdown velocity, and if the slapdown velocity increases with increasing horizontal impact velocity, it is possible that the effect of an attached parachute recovery system will indeed reduce peak slapdown on both the forward skirt and the SRM case.

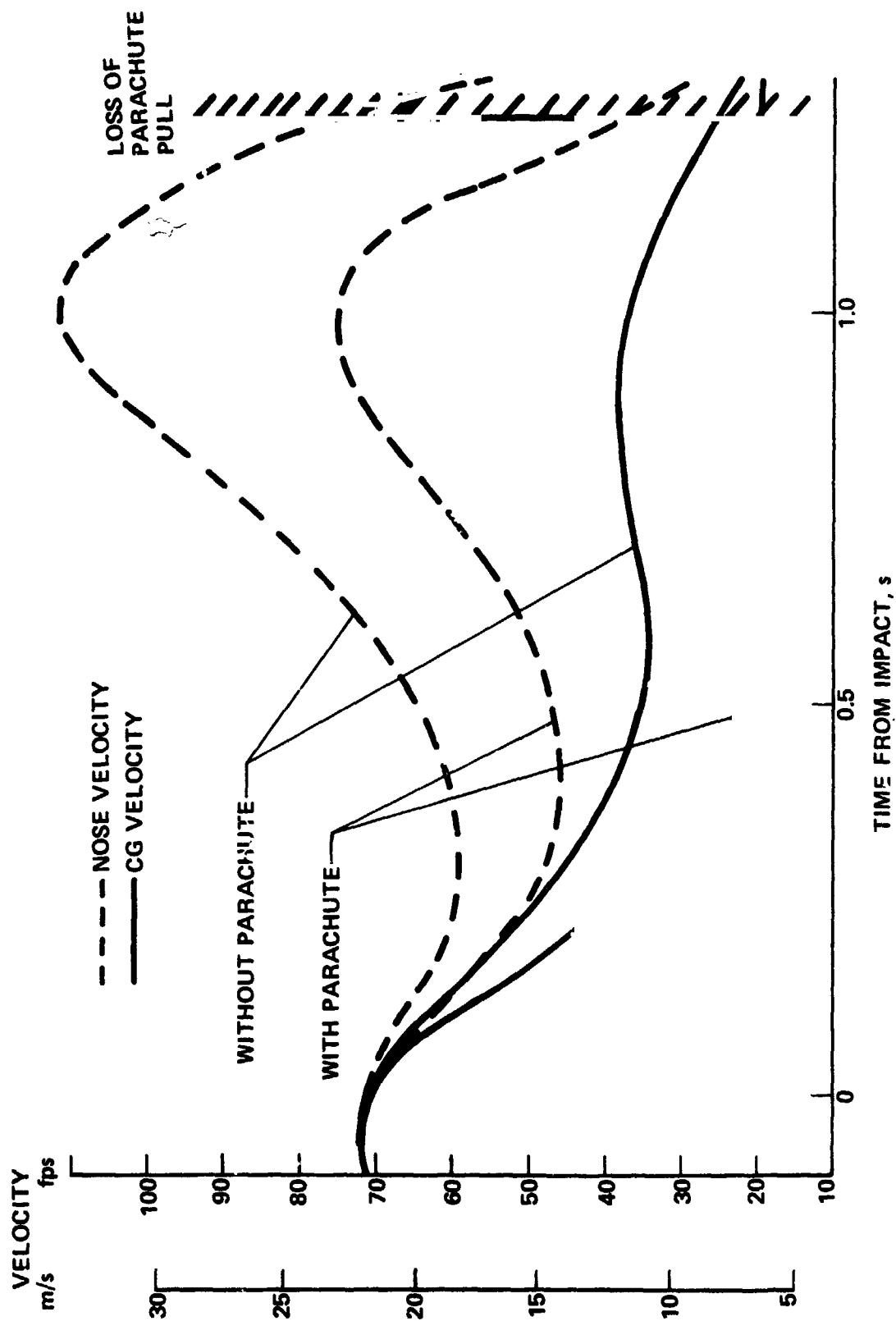


Figure 2.1-16 Parachute Reduces SRB Nose Velocity During Slapdown

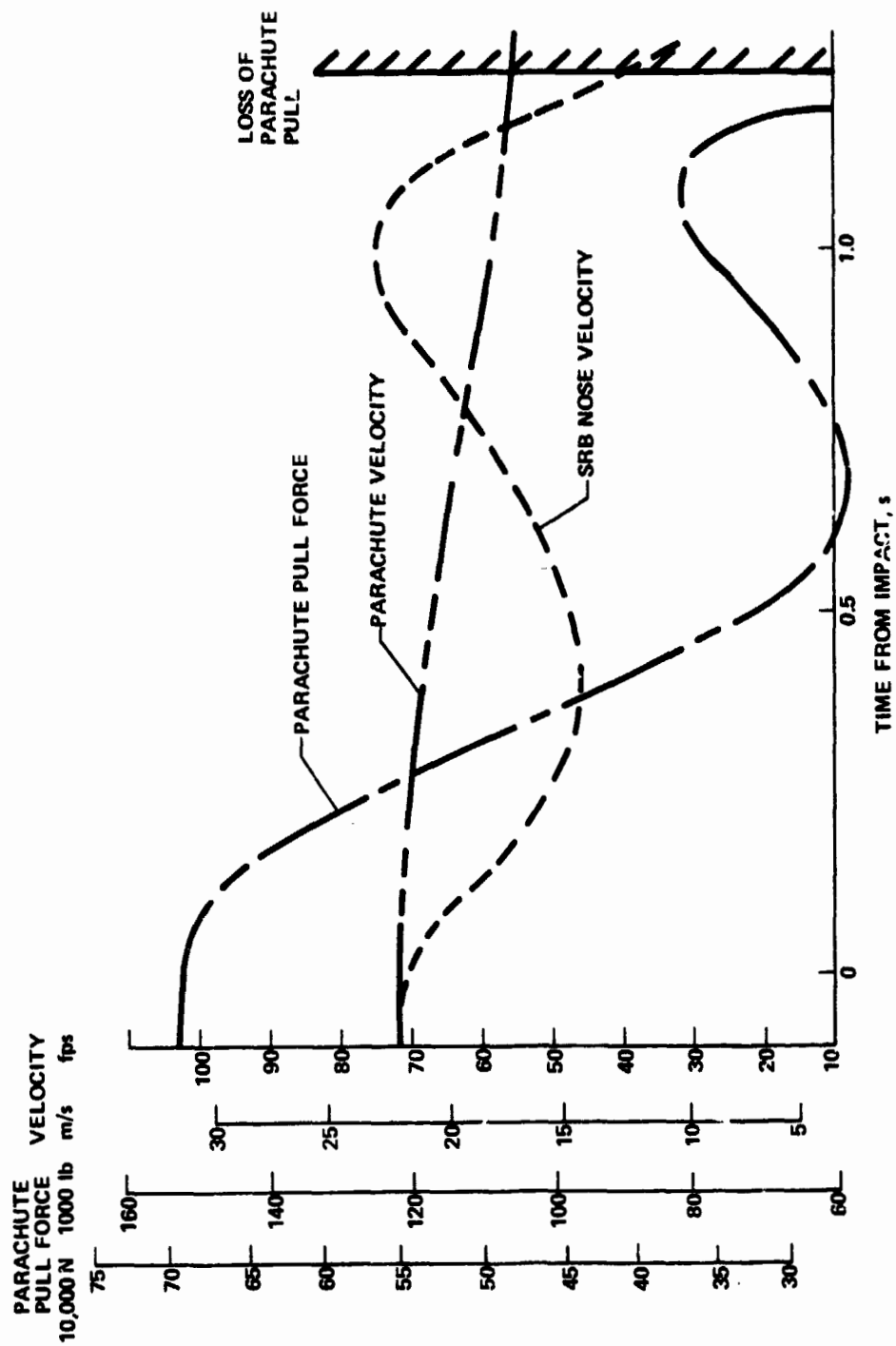


Figure 2.1-17 Parachute Continues Descent During Slapdown

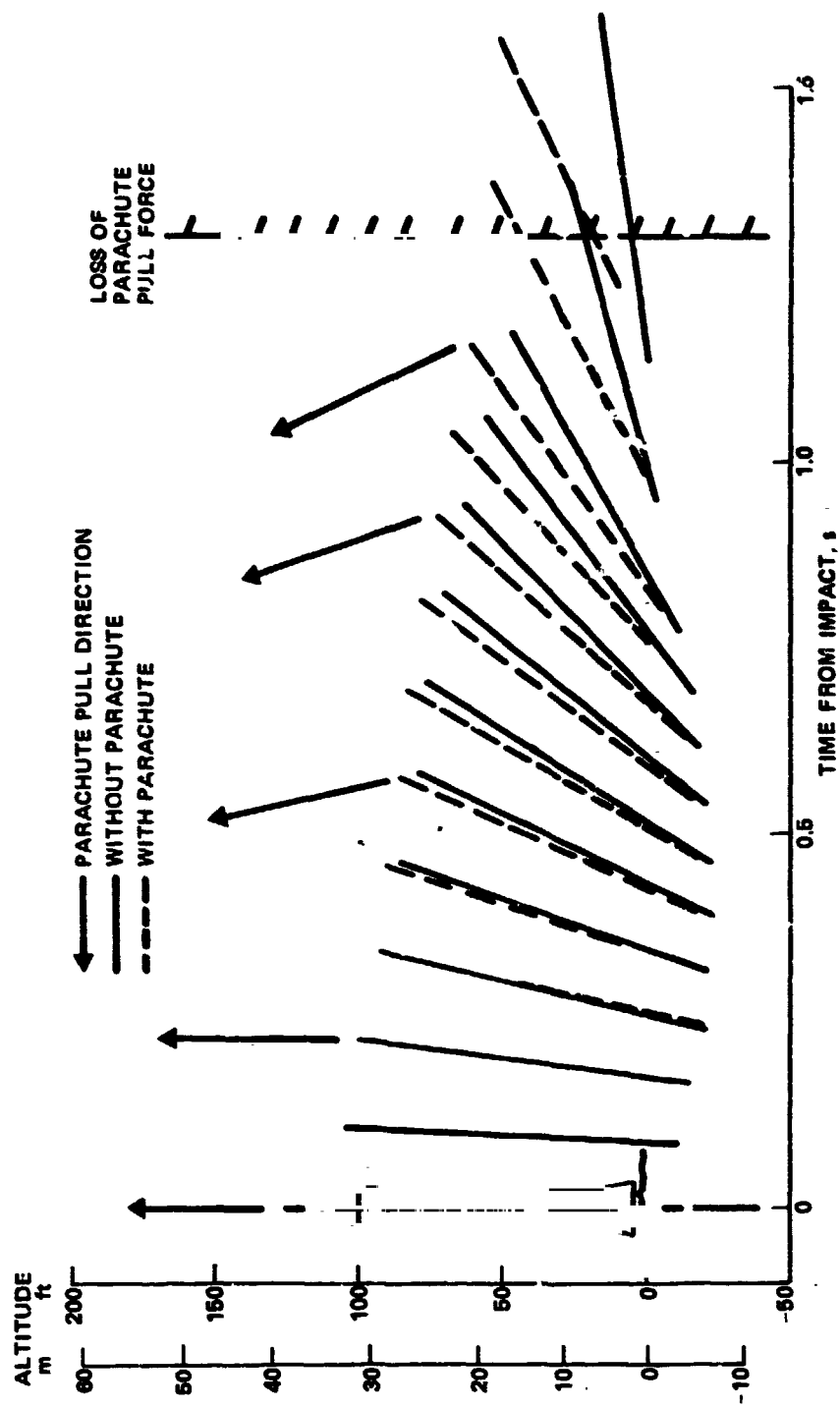


Figure 2.1-18 Parachute Retards SRB Attitude History During Slapdown

2.2 INITIAL DECELERATION AND STABILIZATION

The SRB reentry analysis performed is the most straightforward and input-data-dependent aspect of this study. The reentry analysis was performed using a 6 DOF trajectory simulation program incorporating the physical characteristics, initial state vector and staging rates, and aerodynamic characteristics provided by NASA. To determine the effect of uncertainties in any of these parameters on the reentry, each of the parameters was perturbed individually in the 6 DOF simulation. This technique of linear perturbation has wide use in the industry on similar problems.

Determination of the parameter uncertainties to be used for simulation was a major portion of the reentry analysis. In some cases, the uncertainty was provided by NASA, others were established from accepted industry experience, and for the aerodynamics a combination of analysis and experience was used to set a reasonable uncertainty.

The input data, both nominal and uncertainties, and 6 DOF simulation results are presented in this section.

2.2.1 SRB Configuration

The results of all analyses to be presented are based on configuration data provided by NASA. These data have been reviewed, evaluated, and, in some cases, independently derived to ensure completeness and accuracy before incorporation in the study. In all studies, NASA data were used to ensure consistency of results and compatible requirements definition.

During the contract performance period, two SRB configurations were examined in the reentry dynamics analysis. Because the second configuration represents the later SRB design evolution, all the reentry dispersion results have been normalized to this configuration.

2.2.1.1 Physical Characteristics

The baseline SRB is shown in Figure 2.2-1 along with a brief summary of the mass properties. This configuration differs with the first SRB studies in several areas: design MEOP is $6.2 \times 10^6 \text{ N/m}^2$ (900 psi), aft skirt flare is 0.26 rad (15 deg), and the aft skirt length is only 2.36 m (93 in.). Most important is the longitudinal center of gravity (X_{cg}) location

[illegible]

MASS PROPERTIES (METRIC)		MASS PROPERTIES	
INERT X.T	= 72.732 kg	INERT W.T	= 160.375 lb
CG: X	= 57.1% ℓ_B	CG: X	= 57.1% ℓ_B
Y	= 0.08 m	Y	= 3.2 in.
Z	= -0.05 m	Z	= -1.9 in.
I_{xx}	= $0.21 \times 10^6 \text{ kg}\cdot\text{m}^2$	I_{xx}	= $0.155 \times 10^6 \text{ slug}\cdot\text{ft}^2$
$I_{yy} = I_{zz}$	= $11.35 \times 10^6 \text{ kg}\cdot\text{m}^2$	$I_{yy} = I_{zz}$	= $8.375 \times 10^6 \text{ slug}\cdot\text{ft}^2$

Table 2.2-1 presents a weight breakdown by recovery phase for the baseline SRB. The inert weight column represents the SRB at burnout, but before firing of the staging motors. The inert weight was used for reentry dynamic studies to maintain consistency with concurrent work at the MSFC labs. The postseparation column reflects the firing of staging motors, burning of case and nozzle insulation, and jettison of nozzle extension and attachment structure. The column labeled "flotation" reflects the deployment of the recovery system and jettison of nose cap and frustum.

Table 2.2.1 Flotation Weight 9,513 kg Less Than Inert Weight

		WEIGHT		POST SEPARATION		FLOTATION	
		INERT					
		lb	kg	lb	kg	lb	kg
SRM	CASE	88,810	40,730	88,810	40,730	88,810	40,730
	INSULATION	14,800	6,821	8,780	3,973	8,780	3,973
	NOZZLE	11,500	5,216	7,500	3,401	7,500	3,401
	IGNITION SYSTEM	750	340	575	261	575	261
	THRUST TERMINATION	830	376	830	376	830	376
	GROWTH	2,350	1,068	2,150	975	2,150	975
STAGE	HARDWARE & RECOVERY	(40,535)	(18,383)	(37,385)	(16,988)	(29,775)	(13,503)
	NOSE CONE	1,920	871	1,920	871	0	0
	FORWARD SKIRT	7,570	3,433	7,570	3,433	7,570	3,433
	AFT SKIRT	10,590	4,803	10,590	4,803	10,590	4,803
	AFT SUPPORT STRUCTURE	1,465	660	700	317	700	317
	SEC. ADJARY STRUCTURE	2,145	977	2,155	977	2,155	977
	TVC SYSTEM	3,810	1,728	3,810	1,728	3,810	1,728
	SEPARATION SYSTEM	2,800	1,270	700	317	700	317
	RECOVERY SYSTEM	6,000	2,721	6,000	2,721	1,880	856
	AVIONICS GENERAL	550	248	550	248	550	248
	GROWTH	3,685	1,671	3,400	1,543	2,700	1,224
	SRB INERT	(160,375)	(72,732)	(147,020)	(66,675)	(130,400)	(59,218)
X_{cg}		57.0		56.9		56.6	
Y_{cg}		7.6 (3)		3.8 (1.5)		3.8 (1.5)	
Z_{cg}		0		0		0	
r_{cg}		44.2 m (1741 in.)					

The location and uncertainty of the longitudinal center of gravity is an important factor in predicting the reentry dynamic behavior. Experience has shown that these values improve with program development time, but for early program parametric studies somewhat more conservative estimates are necessary. Figure 2.2-2 shows the sensitivity of X_{cg} to percent changes in major stage hardware weight. Using the allowable growth factor of 10% in these structures does not produce much change in X_{cg} . However, the nozzle extension does have a greater effect on X_{cg} , and, as will be developed later, the change in X_{cg} through nozzle extension jet-tison is in a favorable direction.

2.2.1.2 Reentry Initial Conditions

The initial state vector, separation rates, and their dispersions were provided by NASA. The state vector conditions and expected dispersions are shown in Table 2.2-2. The staging rates--nominal, minimum, and maximum values--are shown in Table 2.2-3.

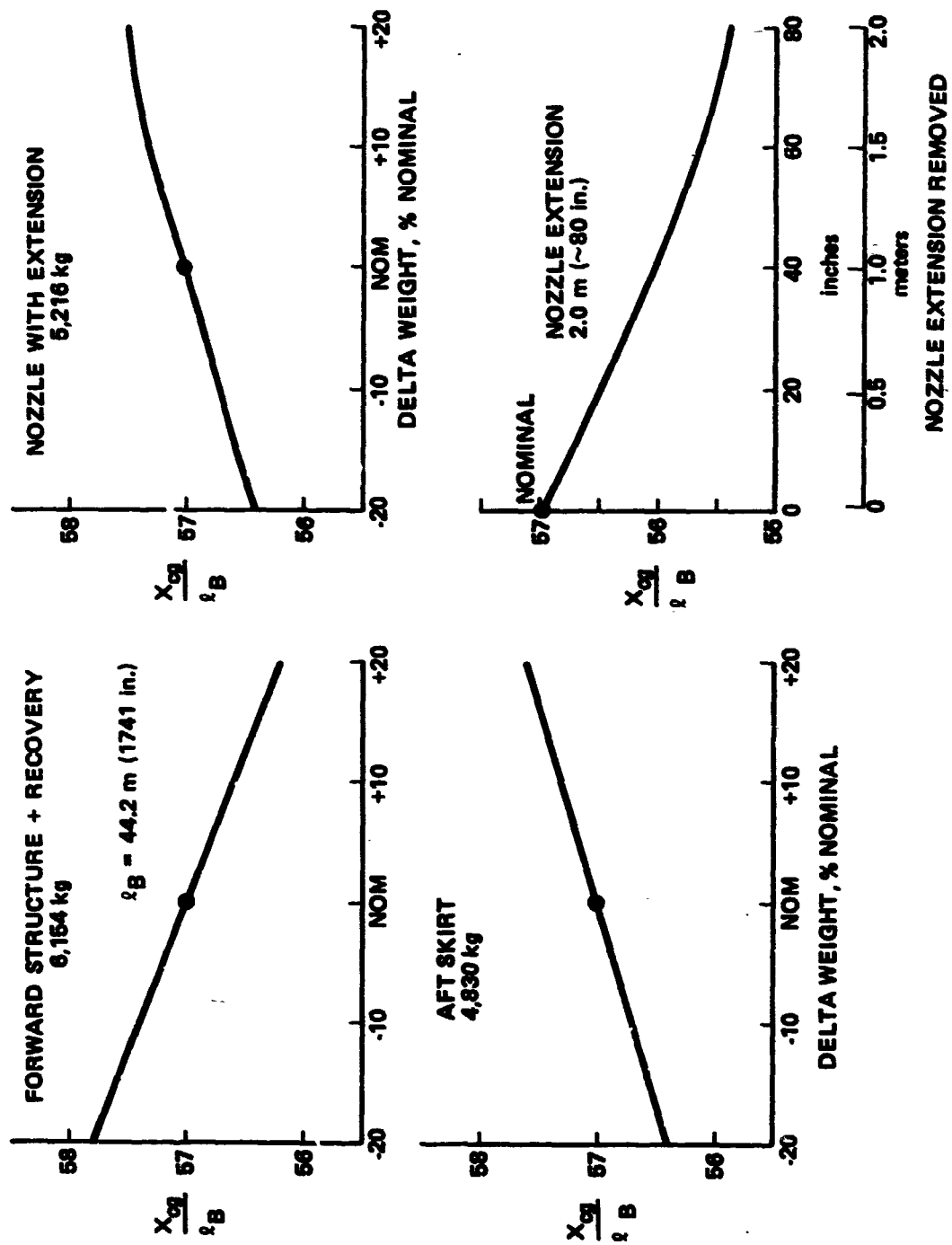


Figure 2.2-2 Longitudinal CG Location Is Most Sensitive to Nozzle Extension Jettison

Table 2.2-2 Initial State Vector for Reentry Analysis

	NOMINAL	+3 σ	-3 σ
ALTITUDE, km (ft)	41.1 (134,721)	2.9 (9,580)	3.4 (11,154)
VELOCITY, m/s (fps)	1,361 (4,466)	53 (174)	38 (124)
FLIGHT PATH ANGLE, rad (deg)	0.5 (29)	0.06 (3.2)	0.06 (3.3)

Table 2.2-3 Staging Rates for Reentry Analysis

	NOMINAL	MINIMUM	MAXIMUM
ROLL, rad/s (deg/s)	0.03 (1.83)	0.02 (1.37)	-0.04 (-2.34)
PITCH, rad/s (deg/s)	-0.17 (-9.76)	-0.005 (-0.30)	-0.31 (-17.54)
YAW, rad/s (deg/s)	-0.21 (-12.25)	-0.05 (-2.85)	-0.29 (-16.55)

2.2.1.3 Aerodynamics

The SRB aerodynamic characteristics provided by NASA received a great deal more evaluation than originally anticipated. Since the reentry dynamic behavior of the SRB is governed by aerodynamic forces and moments, a high degree of confidence in these data was necessary to produce a realistic set of recovery system requirements. The aerodynamic data evaluation involved a review of wind tunnel test procedures, analytically deriving coefficients, comparison of analysis and test results, and coordination of these studies with the appropriate NASA labs.

The aerodynamic characteristics of NASA Memo S&E-Aero-AA-73-27 were used to generate the trajectory results that follow. These data were derived from wind tunnel tests at the MSFC 36 cm (14-in.) transonic facility. Test procedures were modified on this test to account for suspected sting interference identified in previous results. These data were used in the reentry analysis as provided. The following discussion serves only to establish the quantitative uncertainty, not to validate the wind tunnel test results.

The comparison of experimental and theoretical data should be best for supersonic Mach numbers and angles of attack between $0.52 < \alpha < 2.62$ rad ($30 < \alpha < 150$ deg). The comparison of experimental and theoretical predictions is shown in Figure 2.2-3 for Mach number 3.5. These comparisons are only of interest insofar as reasonable uncertainties in the data for parametric analysis of reentry can be established. Bodies of high fineness ratios should have center of pressure uncertainties less than 2% of body length (l_B) at the higher Mach numbers. The shaded areas around the experimental data represent a 2% l_B uncertainty, which also contains the analytic prediction. While this does not absolutely quantify the uncertainty, it does serve to enhance confidence in the prediction techniques.

Comparisons of subsonic Mach number predictions in Figure 2.2-4 reveal a larger disparity in results. This is not surprising because both the experimental and theoretical uncertainties are largest in the transonic Mach number regime. Uncertainties in Reynolds number, sting interference, tunnel wall interference, and modeling inaccuracies all contribute to test result uncertainty. Reynolds number (subcritical or supercritical) is the major contributor to the uncertainty of analytic predictions. Establishing an uncertainty for parametric reentry studies for subsonic data thus favors a much larger bound. While 4% l_B may be conservative, the test model size and facility size tend to justify some conservatism.

The foregoing reasoning was only applied for the purpose of defining logical limits to the parametric reentry dynamics study. As the Shuttle program proceeds and more test data become available, the magnitude of aerodynamic characteristics uncertainties should get smaller. Allowing for large dispersions in this study should bound the reentry dynamics and increase our confidence in the system requirements developed.

2.2.2. 6 DOF Reentry Analysis

The determination of the probable reentry dynamic behavior and expected environment for SRB recovery has a large influence on the recovery system concept choice. Indeed, the natural flow of an integrated system design procedure is first to define the performance requirements to be satisfied. Our approach to the reentry studies has been to define all parameters that affect reentry and then systematically perturb these parameters, via

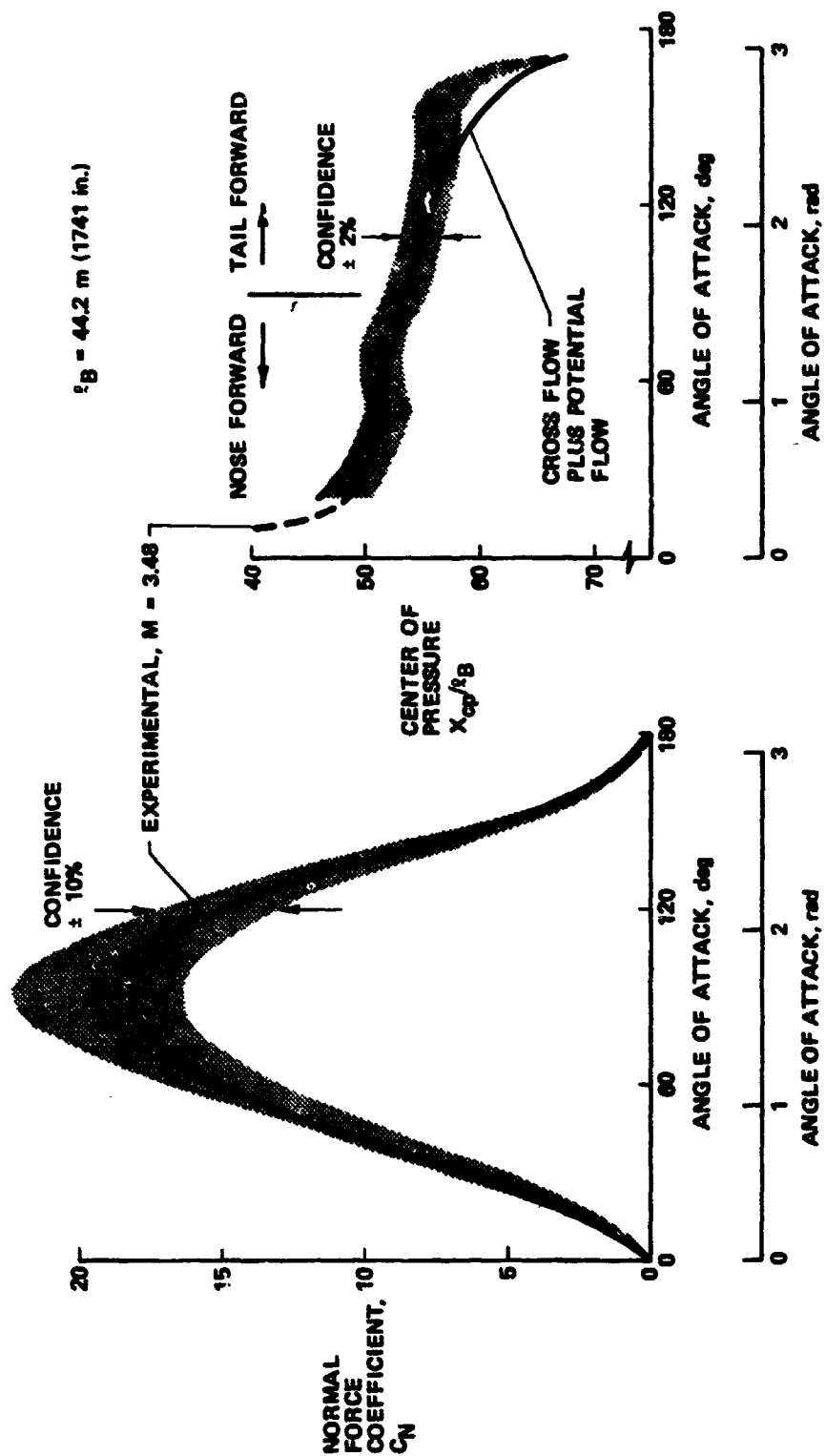


Figure 2.2-3 Supersonic Aerodynamic Uncertainties Are Not Critical

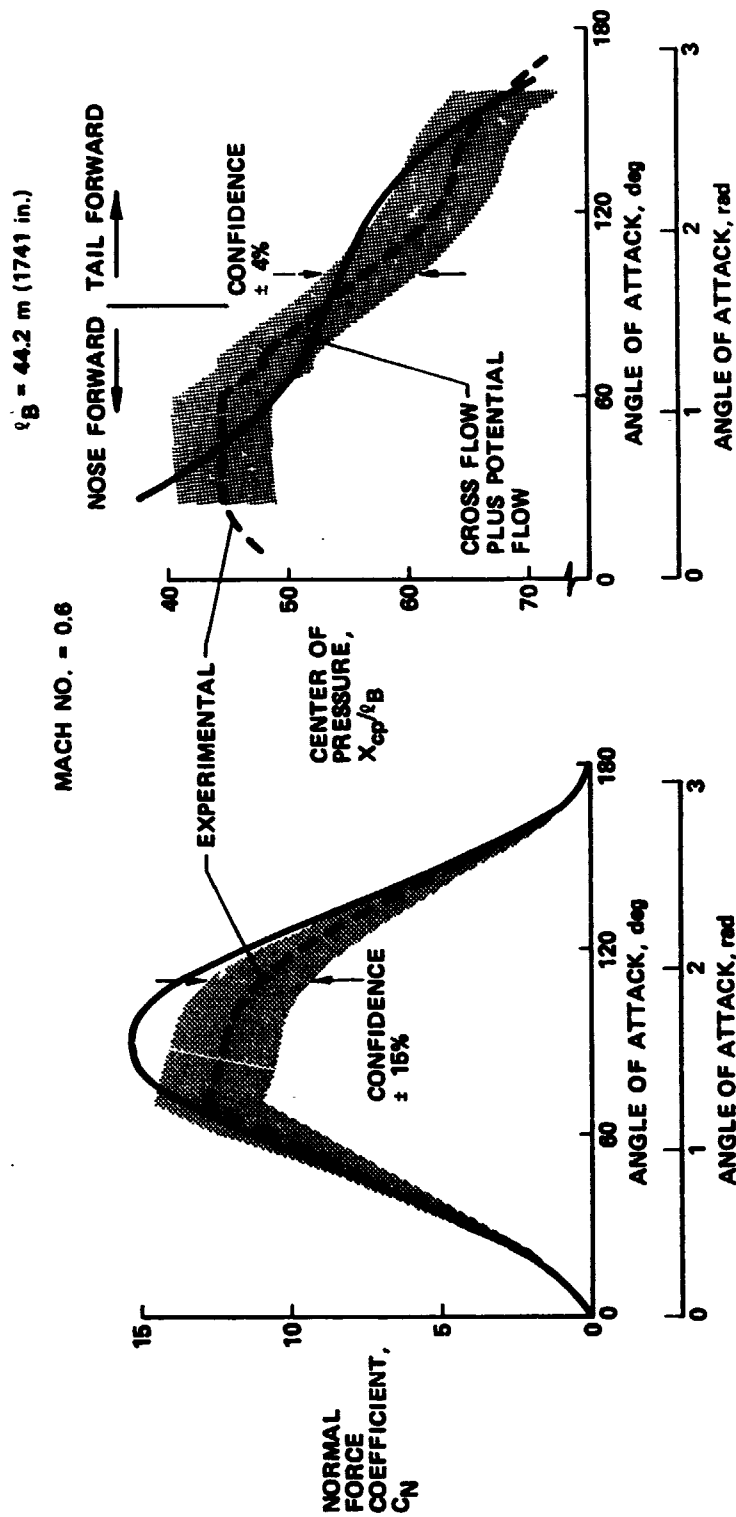


Figure 2.2-4 Subsonic Aerodynamic Uncertainties Define Maximum Reentry Dispersions

linear techniques, to determine their individual and composite effect on the SRB dynamic behavior. The result is a reentry corridor or bound about the nominal profile that limits the requirements on recovery system design to only expected flight conditions.

2.2.2.1 6 DOF Program Description

The UD214 six degree of freedom trajectory program is a modularized N phase digital computer program capable of simulating the trajectories of various types of vehicles operating under the influence of a single attracting body with a generalized atmosphere.

The vehicle being simulated is a rigid body with 6 DOF and complete moments and cross products of inertia, generalized aerodynamic coefficients, generalized center of gravity, and multiple engines per phase.

The attracting body is an oblate, rotating spheroid with gravitational accelerations including zonal and tesseral harmonics. The generalized atmosphere is described by user input in terms of density, temperature, pressure, and speed of sound, or appropriate combinations thereof.

The program has generalized table inputs with no restriction on the size of individual tables. Each table has its own multiplexer and interpolation can be either linear or quadratic. Tables can be input as a constant, monovariant, bivariate, or trivariate function of any internally computed variable.

The 6 DOF reentry simulations have used the aerodynamics provided by NASA. All the coefficients were input as a function of Mach number, angle of attack, and, where applicable, aerodynamic roll angle. All simulations used the 1963 Patrick Air Force Base atmosphere. A nonrotating, spherical earth was used as the attracting body.

2.2.2.2 Reentry Envelope

The reentry analysis was conducted by determining the nominal and the expected uncertainty values of all parameters affecting reentry dynamics and then systematically simulating these conditions via linear perturbation in the 6 DOF computer program. Since our approach is to determine the deviations from nominal, an understanding of the nominal reentry trajectory is in order.

The reentry profile for an undispersed (nominal) SRB is shown in Figure 2.2-5. Following separation from the external tank, both dynamic pressure (q) and Mach number decrease as the altitude increases to an apogee of approximately 62.5 km (205,000 ft). The SRB descends in the coast phase to approximately 45.7 km (150,000 ft) where the q begins to increase, until reaching a maximum value of $31,000 \text{ N/m}^2$ (650 psf) near 16.7 km (55,000 ft) altitude. From a maximum value, q decreases to a steady state value of 6220 N/m^2 (130 psf). During this same period the Mach number has decreased from nearly 4.0 to subsonic conditions. The relationship between Mach number and static trim angle of attack (α), Figure 2.2-6, helps to explain the q and Mach number histories. For high supersonic Mach numbers, the SRB trim angle is between 2.62 rad (150 deg) and 1.92 rad (110 deg). For values in the transonic regime, the trim angle moves closer to $\pi/2$ (90 deg). As the q builds up during reentry, the resulting decelerating forces reduce the Mach number which, in turn, results in α closer to the broadside attitude. The broadside attitude (α near $\pi/2$) is the attitude for maximum total drag. The strong aerodynamic stability of the SRB near $\alpha = \pi/2$ produces maximum drag, resulting in a near steady state dynamic pressure of 6200 N/m^2 (130 psf) below 12.2 km (40,000 ft) altitude. These conditions of low q and dynamic stability are ideal for deployment of aerodynamic decelerators.

The angle of attack from separation through q buildup, Figure 2.2-7, exhibits the characteristics of a damped sinusoidal function. As q builds up to a maximum value, the pressure forces and natural aerodynamic damping of the SRB rapidly diminish the magnitude of α oscillations with convergence toward the static trim conditions associated with supersonic Mach number. As the dynamic pressure drops the tendency for the SRB to diverge from the damped conditions is overcome by the natural aerodynamic stability of the SRB in the transonic Mach number range and the SRB quickly converges to the subsonic trim point. Thus, the α history reflects the reduction in Mach number and associated change in trim stability attitude after achieving maximum q .

The SRB body rates during reentry are shown in Figure 2.2-8. As with the α history, the dynamic pressure buildup changes the coast phase behavior of the body rates. In this case q buildup excites large amplitude rates about the body axes. The rates achieve maximum magnitude near q_{max} and then decline as q and aerodynamic damping combine to reduce the rates. The pitch and yaw rates damp to near zero amplitude soon after q_{max} . However, the roll rate continues with oscillations of $\pm 0.31 \text{ rad/s}$ ($\pm 18 \text{ deg/s}$). The roll behavior will be discussed in more detail later in this section.

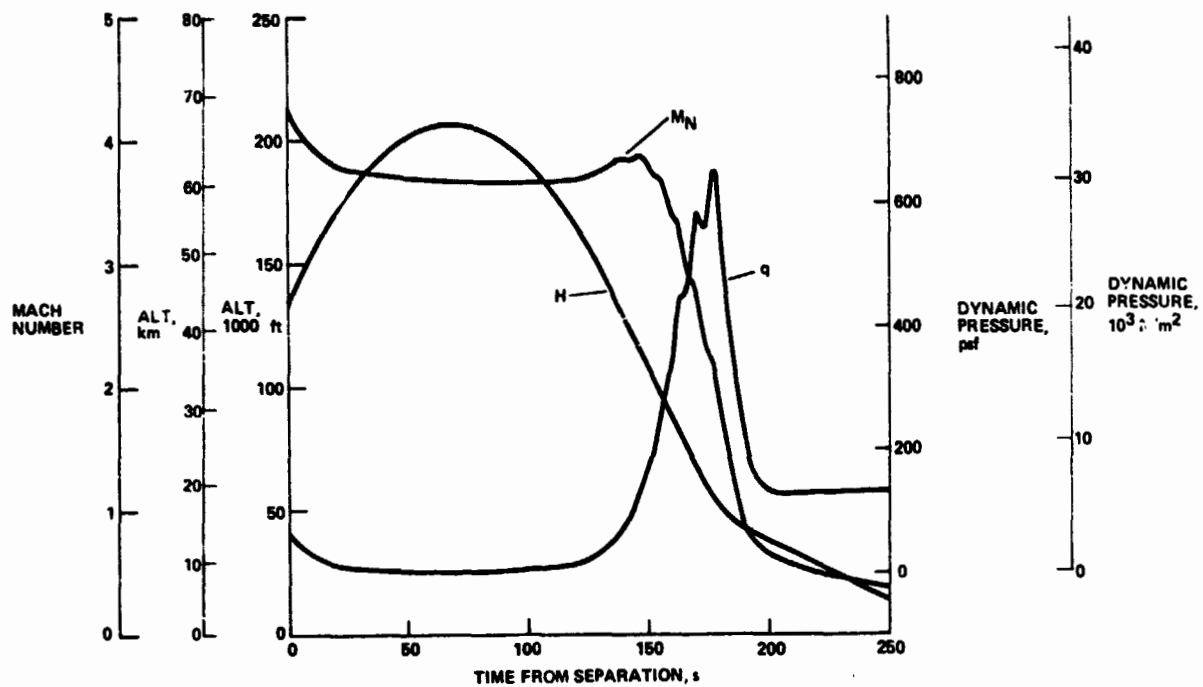


Figure 2.2-5 SRB Baseline Reentry Trajectory

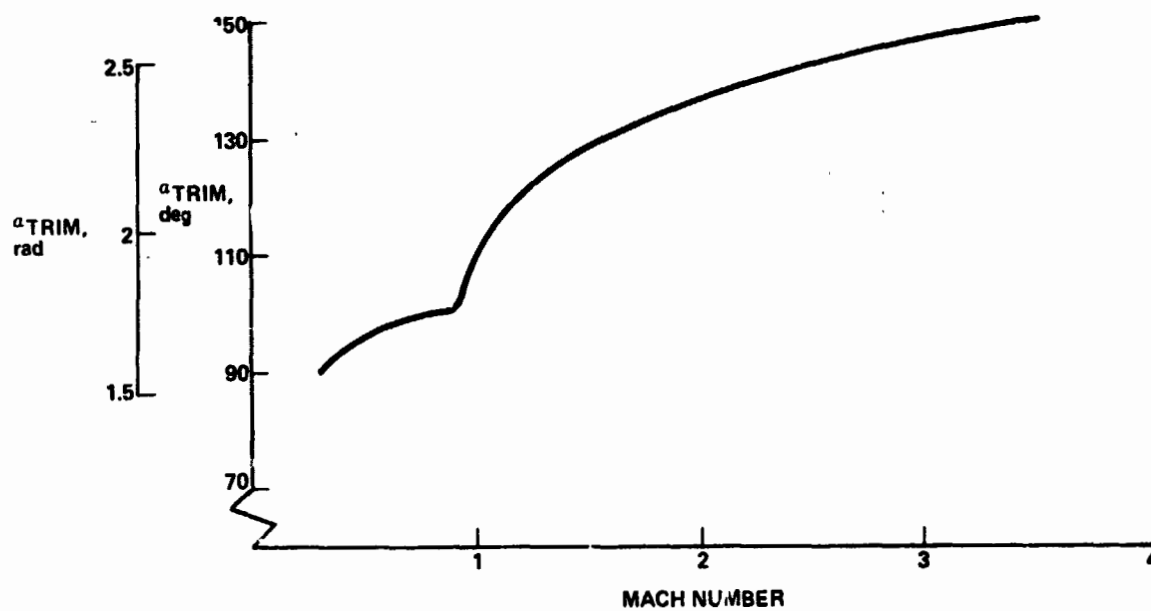


Figure 2.2-6 High α Trim Produces Maximum Total Drag

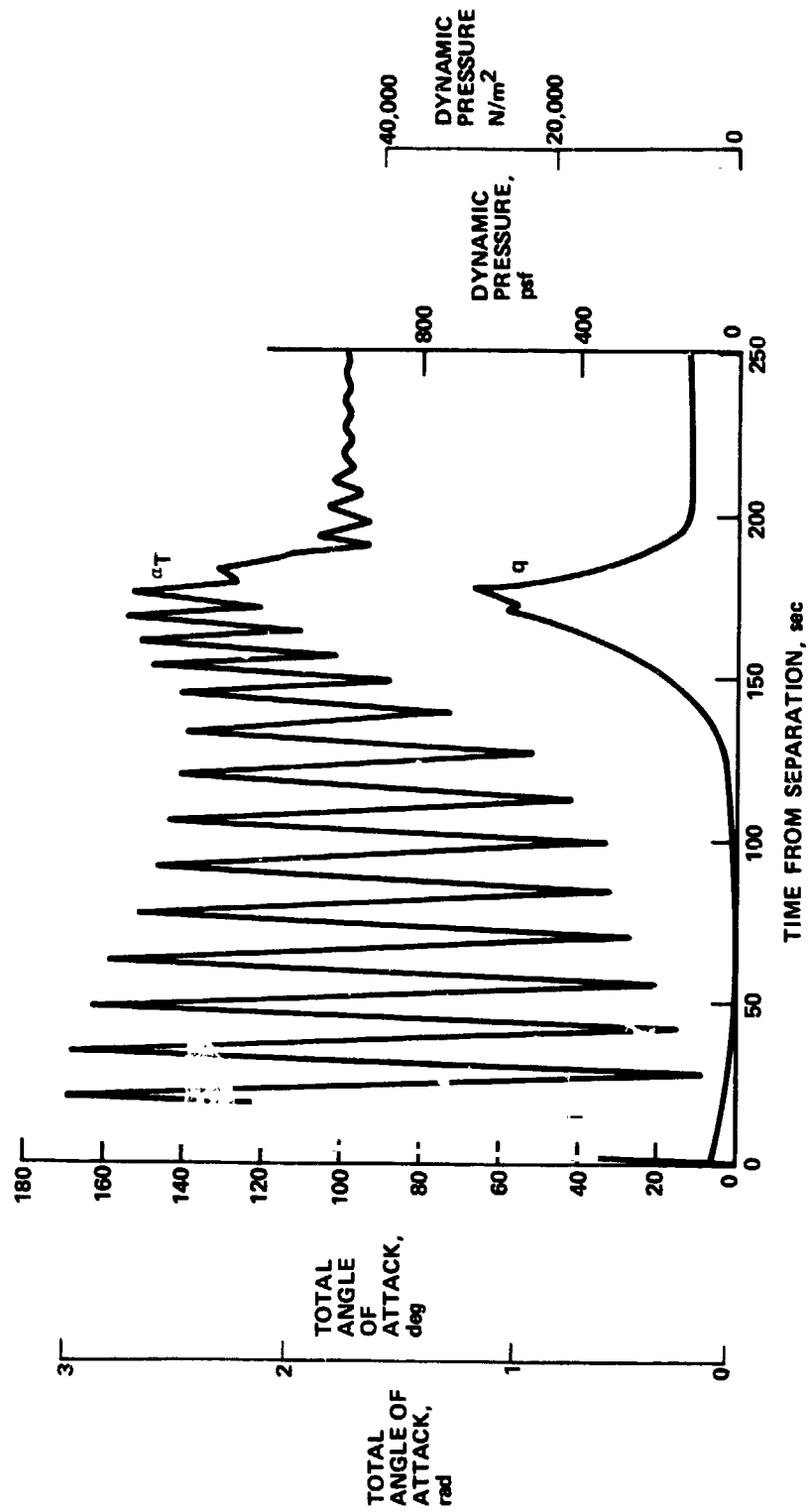


Figure 2.2-7 Dynamic Pressure Buildup Provides Damping Force

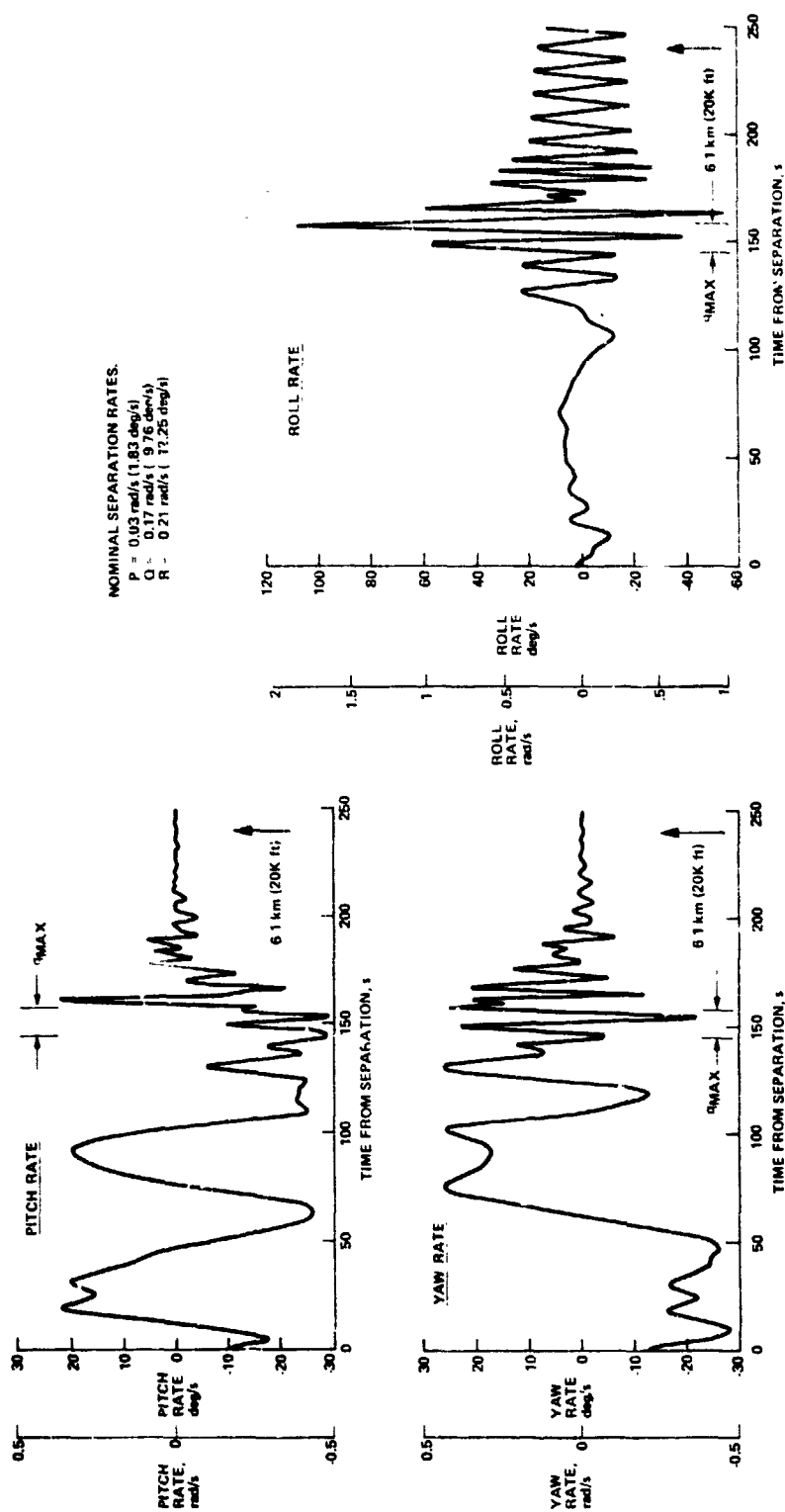


Figure 2.2-8 SRB Experiences Large Attitude Rates at Max q

Even before actually simulating any dispersed conditions it seemed the aerodynamic characteristics would be the key to understanding and predicting reentry behavior. Previous studies earlier in the Shuttle Program had shown that physical and environmental parameters as well as staging rates did not affect the maximum dynamic pressure experienced during reentry.

The major uncertainty affecting the dynamic behavior is the instantaneous relationship of the longitudinal center of gravity (X_{cg}) and center of pressure (X_{cp}). The curves of Figure 2.2-9 show the sensitivity of maximum q and the q at 6.1 km and 3 km altitude to uncertainty in X_{cg} and X_{cp} locations. These results assume either the cg or cp prediction is off by some percentage of body length and that the uncertainty is constant during reentry.

The trend of these data is significant, particularly at parachute deployment altitude. While the maximum q variation with X_{cg} or X_{cp} uncertainty has a steep slope, the sensitivity of q at 3 km (10,000 ft) is nearly flat. Over the range of expected uncertainty previously discussed, $\pm 4\%$ of l_b for cg - cp , the q at 3 km shows only small change from the nominal value of $6,220 \text{ N/m}^2$ (130 psf). At the intermediate altitude of 6.1 km (20,000 ft) the q sensitivity is flat for uncertainty in X_{cg} in the forward direction, but is highly sensitive in the aft direction near the 4% condition. This is of more concern for parachute deployment altitude near 4.6 km (15,000 ft), but as was shown earlier, we feel the minimum altitude for deployment can be as low as 2.3 km (7,500 ft).

The investigation of other reentry dispersions did not reveal another "driver" such as the cg to cp uncertainty. The uncertainties in staging state vector, separation rates, mass properties, and other aerodynamic coefficients produced only small changes in q_{max} and almost no change in the q at 3.0 km.

The q sensitivities of four of these parameters are shown in Figure 2.2-10. Table 2.2-4 presents a summary of all the dispersions simulated for conditions at q_{max} and 6.1 km. While most of these parameter uncertainty simulations resulted in small contributions to variation in q at specific altitudes, their consideration should not be totally eliminated from future reentry studies. Before the requirements for the recovery system are finalized, selected parameters should again be simulated to assure the trend shown here is still valid.

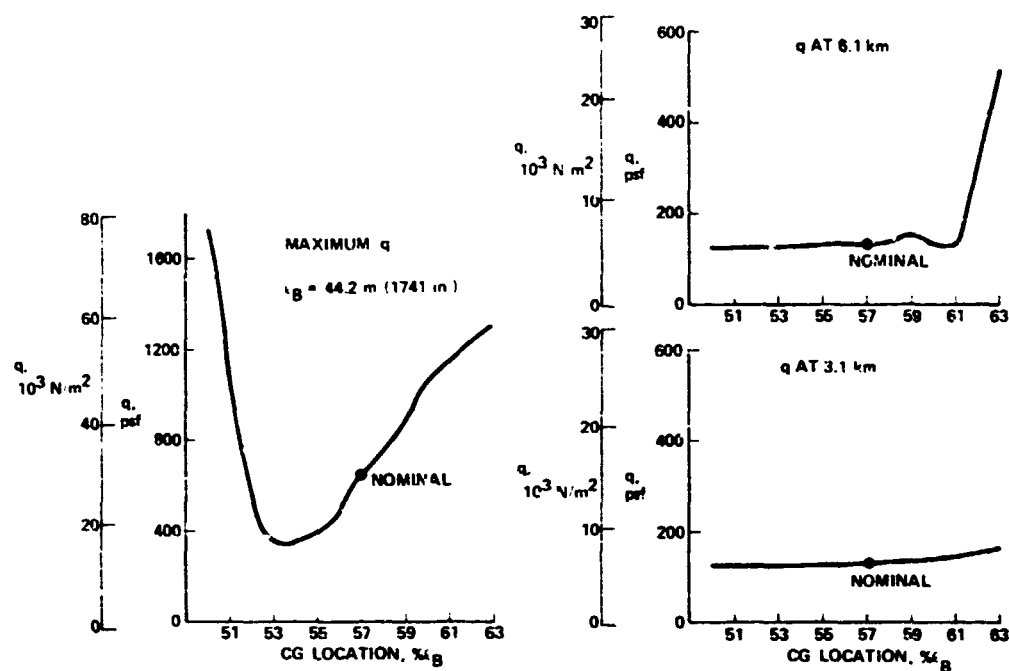


Figure 2.2-9 Longitudinal CG Location Determines Maximum and Deployment q

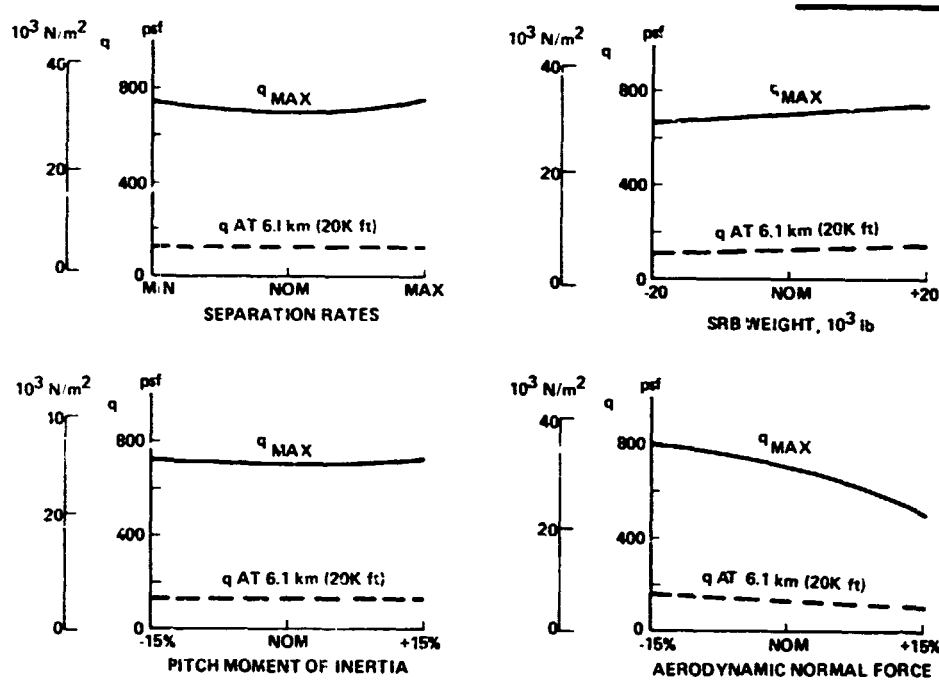


Figure 2.2-10 Maximum Dynamic Pressure Insensitive to Most Dispersions

RUN NO.	DISPERSION	CONDITIONS AT q_{max}						CONDITIONS AT 6.1 km (20K ft)					
		Δq (DISP-NOM)			q			PIROLL			QIPITCH		
		N/m'	lb/ft'	rad	deg	N/m'	lb/ft'	rad	deg	rad/s	deg/s	rad/s	deg/s
1	NOMINAL	(31,122)	(650)	2.60	149	6,368	133	1.73	99	0.31	0.18	0.0	0.0
2	$\Delta_1 = +0.056 \text{ rad (+3.2 deg)}$	2,394	50	2.11	121	5,985	125	1.55	89	0.44	0.25	0.007	0.3
3	$\Delta H = +2.82 \text{ km (+9680 ft)}$	2,873	60	1.78	102	5,985	125	1.55	89	0.79	45.25	0.009	0.5
4	$\Delta V_R = +53 \text{ m/s (+174.5 ft/s)}$	622	13	2.20	126	5,937	124	1.52	87	0.79	45.25	0.006	0.3
5	$\Delta WT = +9080 \text{ kg (+20K lb)}$	3,256	68	1.62	93	6,799	142	1.55	89	0.13	0.65	0.003	15.2
6	$I_{xx} + 15\%$	1,532	32	1.75	100	5,985	125	1.55	89	0.70	0.40	0.007	0.4
7	$I_{yy} + 15\%$	1,245	26	1.82	104	5,985	125	1.66	95	0.46	0.26	0.008	0.4
8	$I_{zz} + 15\%$	1,149	24	1.69	97	5,985	125	1.55	89	0.106	0.80	0.005	0.3
9	$I_{xy} + 15\%$	1,867	39	1.97	113	5,985	125	1.64	94	0.24	0.48	0.006	2.1
10	$I_{yy} + 10\%$	1,772	37	1.97	113	5,985	125	1.66	95	0.77	0.44	0.009	0.5
11	$\Delta Y_{cg} = +7.1 \text{ cm (+2.8 in.)}$	1,245	26	1.71	98	5,985	125	1.55	89	0.36	0.20	0.006	0.3
12	$\Delta Y_{cg} = -8.1 \text{ cm (-3.2 in.)}$	1,772	37	1.78	102	5,985	125	1.54	88	0.09	0.5	0.009	0.24
13	MAX TIPOFF	3,878	81	2.09	120	5,985	125	1.82	93	1.05	60.20	0.009	0.4
14	MIN TIPOFF	3,016	63	1.90	109	5,985	125	1.59	91	0.52	0.30	0.021	0.14
15	REVISED MAX TIPOFF	1,341	28	1.55	89	5,985	125	1.55	89	0.42	0.24	0.005	0.3
16	Q&R DAMPING	-2,155	-45	2.22	127	6,033	126	1.66	95	0.77	0.44	0.007	0.3
17	CG FWD 1%	-622	-13	1.66	95	8,140	170	2.22	127	0.87	50.5	0.033	13.20
18	CG FWD 2%	-8,253	-173	2.32	133	6,512	136	1.89	97	0.87	50.15	0.0	0.0
19	CG FWD 4%	-11,874	-248	1.88	108	6,416	134	1.64	94	1.05	60.15	0.0	0.0
20	CG FWD 6%	-14,556	-304	1.20	89	6,272	131	1.54	88	0.44	0.25	0.0	0.0
21	CG FWD 7%	17,620	368	0.65	37	6,177	129	1.43	82	1.05	60.15	0.0	0.0
22	CG FWD 8%	51,232	1,070	0.48	28	6,081	127	1.40	80	0.70	0.40	0.0	0.0
23	CG AFT 1%	11,108	232	2.68	154	7,517	157	1.85	108	0.87	50.15	0.003	0.15
24	CG AFT 2%	19,583	409	2.72	156	6,177	129	1.57	110	0.87	50.15	0.006	0.2
25	CG AFT 3%	23,892	499	2.74	157	6,177	129	1.95	112	0.81	0.36	0.003	0.25
26	CG AFT 4%	31,314	654	2.79	160	24,562	513	2.50	143	0.105	0.60	0.003	0.15
27	CG AFT 5%	7,230	151	2.51	144	5,508	115	1.73	99	1.31	75.20	0.001	0.05
28	$C_n + 15\%$	7,086	148	2.39	137	7,469	156	1.73	98	-0.79	45.25	0.0	0.0

Table 2.2-4 Summary of Reentry Dispersion Results

A perusal of the body rates at 6.1 km altitude in Table 2.2-4 reveals an interesting trend in roll rates. The pitch and yaw rates have damped to near zero amplitude but the roll behavior is of two distinct types, oscillatory, or continuous roll. Comparing the parameter dispersion with the resulting roll behavior does not provide any immediate clues to explain what causes either condition. However, looking at the conditions near q_{max} for each case does provide some insight to the roll behavior later in the reentry.

As noted earlier in this section, the buildup of dynamic pressure produced large body rate amplitudes but these rates began to damp to zero as the q declined. This damping in pitch and yaw is primarily a result of large aerodynamic damping derivatives. Since the SRB is axisymmetric in roll and has virtually no protuberances the aerodynamic damping is very small. Thus, any large roll rate existing as the dynamic pressure falls off would not have a counteracting force.

The two largest forces acting on the SRB roll behavior are the angular rotation inertia and the instantaneous aerodynamic moment. To represent the aerodynamic induced moment, the aerodynamic roll angle at q_{max} (i.e., the vector projection of the velocity vector into the SRB roll plane, measured from the SRB yaw axis) and the lateral cg moment arm were tabulated for the 28 trajectories tabulated in Table 2.2-4. These data were then plotted versus the roll rate at q_{max} . These results are shown in Figure 2.2-11.

The reentry trajectories that resulted in oscillatory motion with zero mean have roll angles within ± 1.4 rad of the lateral cg (vertical dashed line), and roll rates less than ± 1.0 rad/s at q_{max} .

Those cases not within these limits resulted in a continuous roll. The implication of this correlation is that instantaneous conditions at q_{max} , conditions which are not random cannot be controlled, govern the subsequent roll behavior of the SRB and any recovery system must be capable of successful deployment in the presence of potentially large roll rates. The ability of parachutes to either withstand suspension line twisting, or the roll damping provided by a parachute after deployment require more analysis, and possibly testing, than could be performed under this contract. Our approach has been to incorporate a swivel in the recovery system. This issue certainly deserves more attention before committing to hardware procurement.

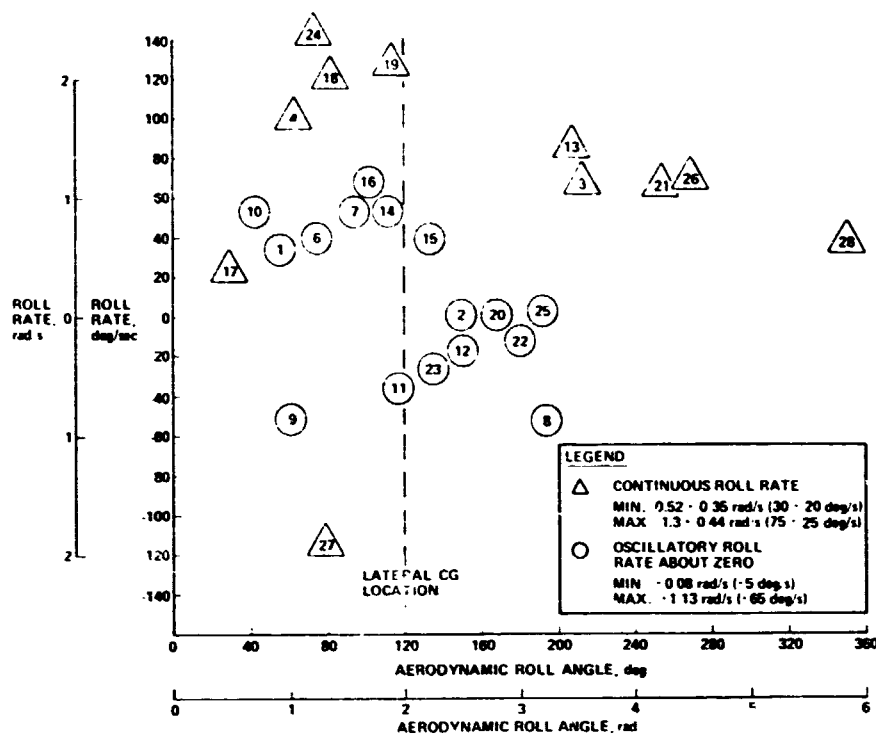


Figure 2.2-11 Roll Rates at Deployment Altitudes Correlated to Conditions at Maximum Dynamic Pressure

Another aspect of SRB reentry affecting recovery system components is the variation of altitude with time from separation. A simple timer would be a desirable method for initiating the recovery sequence. Figure 2.2-12 shows the corridor of altitude uncertainty possible as a function of time. For a specific time to initiate the recovery sequence, say 255 seconds, the altitude uncertainty would be approximately ± 2.7 km (9,000 ft). Obviously this uncertainty of altitude with time is much too large to rely on a simple timer for sequence initiation; therefore an altitude sensing device such as a baroswitch or radar altimeter is required.

The flow of recovery system requirements was previously identified as starting with water entry and flotation and backing up the reentry profile. The TD&D system placed requirements on the ID&S phase to provide conditions compatible with parachute deployment. The results of the reentry study can be summarized by defining a reentry corridor as shown in Figure 2.2-13. The deployment boxes for both a drogue and main system, and the main-only system are superimposed on the high α reentry corridor bounded by the cg-cp uncertainty simulations of $\pm 4\% l_B$ defined earlier.

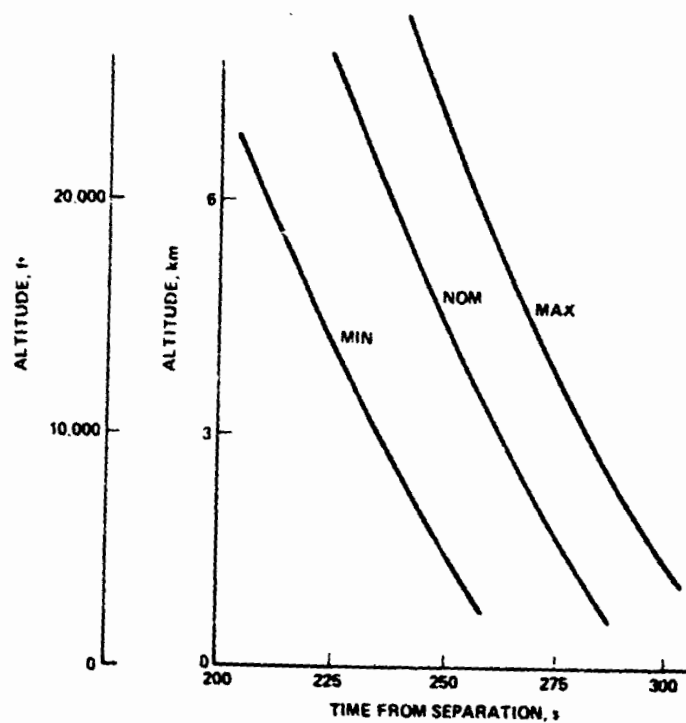


Figure 2.2-12 Parachute Deployment Will Require Active Altitude Sensing Device

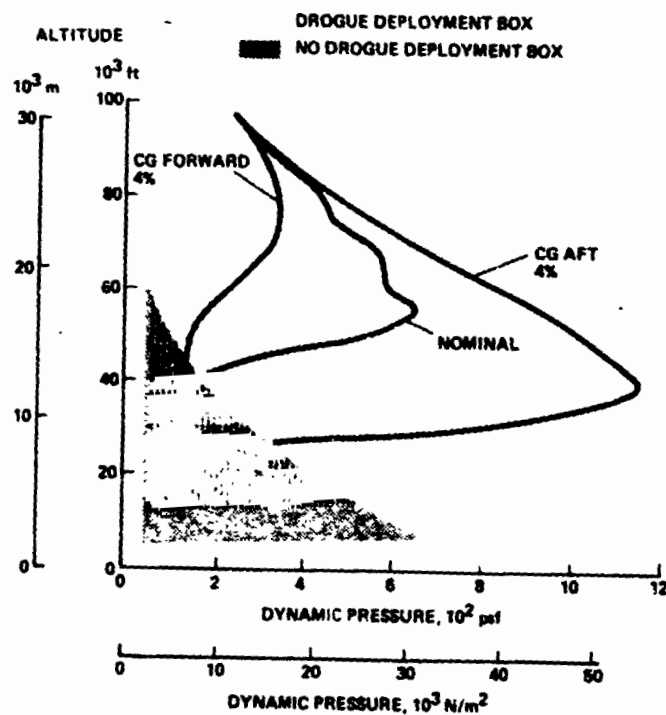


Figure 2.2-13 High α Reentry with Dispersions Meets ID&S Requirements

The plot clearly shows that the natural stability and deceleration of the high α reentry meet the TD&D deployment boxes for either concept. In addition, the low q below 6.1 km (20,000 ft) altitude influences the TD&D concept selection of a main-only recovery system, as previously discussed. Thus, for the present SRB configuration, no ID&S system concept appears to be necessary.

However, the reentry analysis has identified two requirements of the TD&D design: the ability to accommodate significant continuous roll rates, and recovery sequence initiation via an altitude sensing device.

2.2.2.3 Predicted Impact Area Ellipse

The trajectory results discussed in the previous section were also used to make a preliminary estimate of the size of the recovery area. The recovery area size will influence the selection of, or perhaps eliminate the need for, electronic and visual locator aids. These issues are the subject of another current contract and will not be addressed in this report.

Table 2.2-5 lists the contributions to the predicted impact area in three parts: state vector uncertainty at SRB separation, reentry dispersions, and recovery area wind effects. The state vector at separation should be known within minutes of the event and could be used to decrease the recovery area size by trajectory simulation. These data are presented as symmetric along either axis of the ellipse.

Table 2.2-5 Recovery Area Ellipse

DISPERSION	DOWNRANGE		CROSSRANGE	
	km	n mi	km	n mi
STATE VECTOR	12.2	6.6	3.1	1.7
REENTRY	10.4	5.6	6.1	3.3
RECOVERY AREA WIND	8.7	4.7	7.8	4.2
TOTAL RSS	18.3	9.9	10.5	5.7

3.0 SRB IMPACT LOADS ANALYSIS (INCREMENT II)

An amendment to the basic contract defined four additional tasks in the structural analysis of the case. The following four sections present the results of these tasks.

3.1 COMPUTER PROGRAM TO TRANSLATE SLAPDOWN PRESSURE DISTRIBUTIONS TO CONCENTRATED NORMAL LOADS

The basic output of this task was a document titled *Water Impact Loads Program Utilization Instructions* dated October 1973. A FORTRAN IV program deck and tape were also generated. This section presents a summary of the loads program; additional detail is given in the Utilization Instructions.

3.1.1 General Description

The total vertical load, normal concentrated pressure loads, and the center of pressure of typical SRB water impact slapdown pressure distributions are computed in this program, which prepares the concentrated pressure load information in punched card format suitable for input to the STAGS computer program. In addition, the program prepares for STAGS input the inertia reacting loads to the slapdown pressure distributions. The inertial reacting loads are calculated so as to balance the total vertical pressure load at each incremental vehicle station. The net normal and tangential load components are then computed for each mesh point.

The mesh size of this program must be made consistent with the STAGS model mesh size. Because the program uses a linear integration scheme, the accuracy of the load results will generally be a function of the mesh density. The accuracy is improved if the data points used to describe the keel pressure and wetted angle are input at a vehicle station corresponding to a mesh point location.

3.1.2 Program Inputs

The program is written to handle an asymmetric pressure profile. A normalized distribution both longitudinally and circumferentially, as shown in Figures 3.1-1 and 3.1-2, is built into the program. The input consists of data points to describe the normalized curves, peak pressure, vehicle radius, and vehicle length. These data are required for each pressure distribution and/or time point.

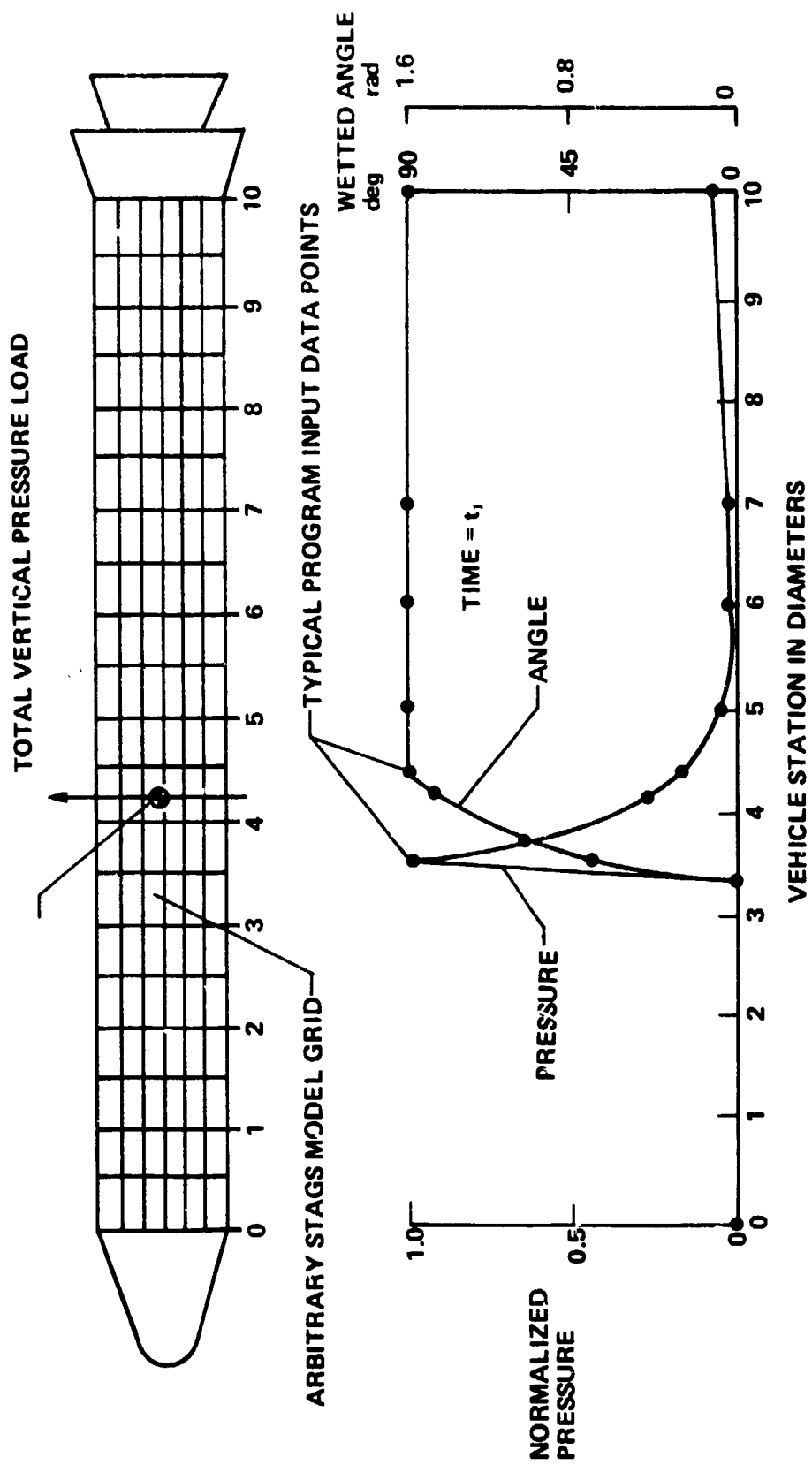


Figure 3.1-1 Normalized Keel Slapdown Pressure Distribution and Wetted Angle Curves

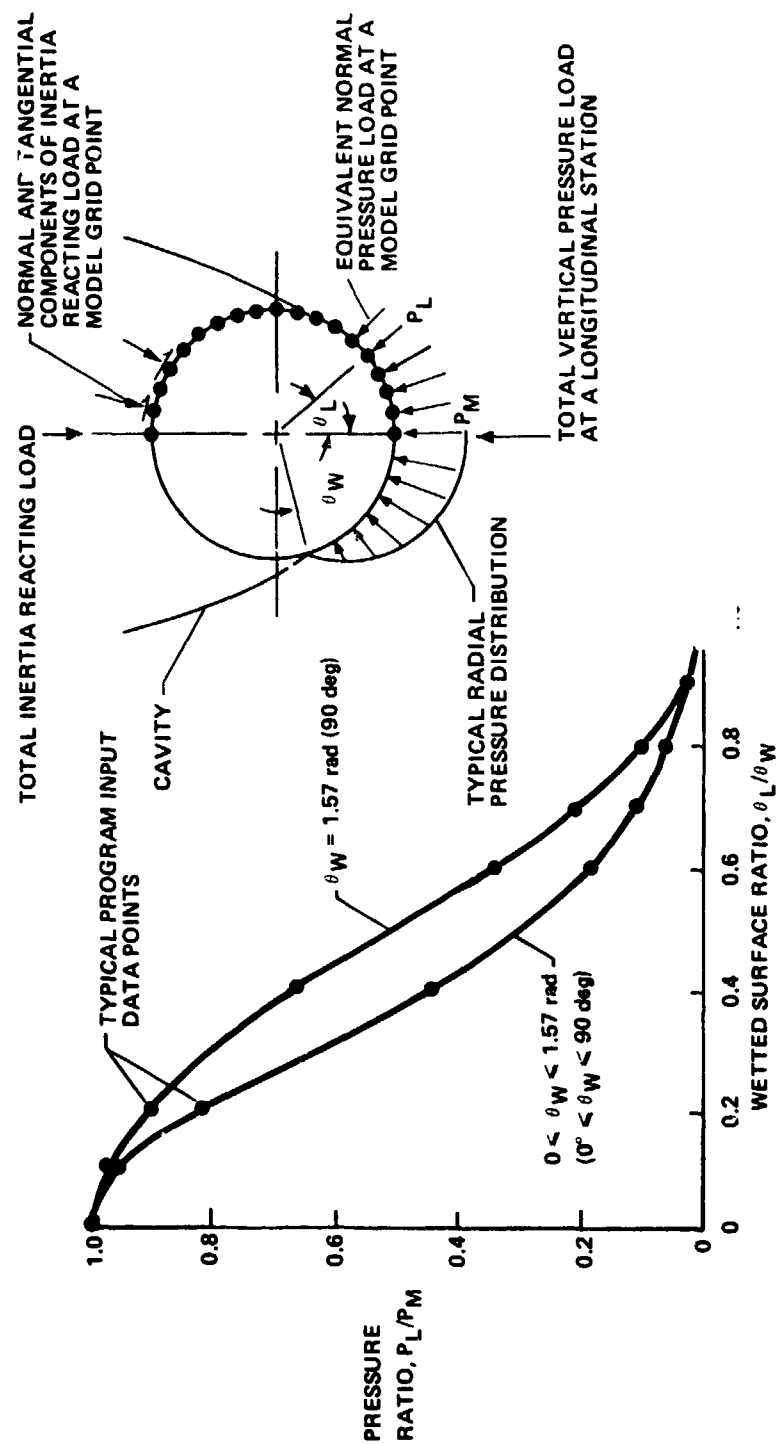


Figure 3.1-2 Normalized Radial Slapdown Pressure Distribution Curve 8

3.1.3 Program Outputs

The output is a set of punched cards listing the net normal and tangential concentrated loads at each mesh point that is loaded either with pressure or inertially. These cards can be used as a direct input to the STAGS computer program. An additional output is the total vertical component of pressure load and its center of pressure.

3.2 WATER IMPACT FAILURE CRITERIA

The Space Shuttle Program requirement that the solid rocket boosters be recovered and refurbished imposes unique requirements on the structural design. The booster must be designed to maintain structural integrity through many cycles of launch, reentry, water impact recovery, handling, shipping, and refurbishment. This document establishes design criteria primarily applicable to the water impact loading condition.

The solid rocket booster (SRB) is comprised of the solid rocket motor (SRM), forward skirt, nose cone, aft skirt and engine thrust chamber. The number of operational flight cycles to be used in the design of the major components is dependent on the recycle time needed for the refurbishment of that component. The additional flight cycles anticipated on components requiring short refurbishment time must be considered in the design, analysis, and testing.

The criteria is separated into two distinct categories identified as failure criteria and design allowables. The section on failure criteria will address the limiting conditions that must be considered to assure structural integrity throughout the multi-mission life of each SRB. The section on design allowables will recommend specific approaches and methods that will satisfy the requirements established in the Failure Criteria.

3.2.1 Failure Criteria

This section covers factor of safety selection, failure modes, special considerations regarding refurbishment and reuse, and retest requirements. Some of the basic requirements are established regarding the acceptance or rejection of the various possible types of structural failure that could result from water impact and recovery.

3.2.1.1 Factor of Safety Selection

The three primary considerations for selection of factors of safety are:

- 1) manned versus unmanned flight conditions;
- 2) structural test requirements;
- 3) statistical probability of loads and allowables.

Manned Versus Unmanned Flight - The launch portion of each mission requires the factors normally associated with a manned vehicle. The water impact loading condition, although unmanned, requires sufficiently high safety factors to provide adequate confidence in the survivability of the structure with minimum refurbishment requirements. To minimize the amount of permanent deformation that might occur during water impact, a factor of safety on yield of 1.10 is specified. For typical SRM case materials, the 1.10 yield factor is achieved by designing to the 1.25 ultimate factor of safety. It is expected that the SRB skirts may require some structural weight penalty in order to obtain the 1.10 yield factor as opposed to the conventional 1.00 factor.

Preliminary studies have indicated that the water impact loads are significantly higher than the loads experienced during manned flight for many structural elements. It is, therefore, probable that the resulting effective factors of safety (including margin of safety) for the manned flight conditions will be higher than the specified design values. Safety factors are presented in Table 3.2-1.

Table 3.2-1 Recommended Factors of Safety

CONDITIONS	SRM				SRB	
	GENERAL STRUCTURE		PRESSURIZED		GENERAL STRUCTURE	
FLIGHT	YIELD	ULT	YIELD	ULT	YIELD	ULT
MANNED	1.1	1.4	1.2	1.4	1.1	1.4
UNMANNED (WATER IMPACT)	1.1	1.25	1.1	1.25	1.1	1.25
TEST	PROOF	ULT	PROOF	ULT	PROOF	ULT
PROOF TESTS* (MANNED CONDITIONS)	1.1	-	1.2	-	1.1	-
ULTIMATE TESTS:						
MANNED	-	1.40		1.40 (BURST TEST)	-	1.40
UNMANNED	-	1.25		1.25	-	1.25

*MINIMUM FACTORS - ACTUAL FACTORS TO BE DETERMINED BY CONTRACTOR'S FRACTURE MECHANICS ANALYSIS.

Structural Test Requirements - The design factors of safety are closely interrelated with the structural test program. Table 3.2-1 specifies the minimum factors of safety to be used in all ultimate and proof tests of SRB structure. The actual proof factors will be determined by the SRB contractors based on requirements resulting from fracture mechanics analysis.

Statistical Probability of Loads and Allowables - The Monte Carlo analysis output includes a set of loads corresponding to a 99% probability of not being exceeded. The Material Properties used in the analysis are to be the "A" values or equivalent of MIL-HDBK-5B within which 99% of the population of values is expected to fall with a 95% confidence level. The resulting probability of failure due to water impact is approximately 0.01% as a result of combining these loads, strengths, and a 1.25 safety factor. This level of structural reliability is consistent with accepted structural analysis practice.

Since the failure of the SRB for the water impact condition does not risk loss of life or mission, a tradeoff is recommended to consider deletion of some structural tests of the SRM for water impact loads, taking into account the magnitude of the analytical margin. This will require a failure probability analysis to confirm the low loss of vehicles caused by water impact loads and must consider the variation of strength between articles. The lowest cost approach between the test and analysis is recommended, giving due consideration to risk.

3.2.1.2 Failure Modes

The SRB structure is loaded primarily by axial compression and pressure caused by water impact, submersion, and slapdown. The structure is to be designed and analyzed using conventional methods of structural analysis, including math models when necessary. All structural elements will be analyzed for their critical loading conditions. Design and analysis shall consider basic strength failure such as tension, compression, bending, shear, and bearing. The compression loads resulting from axial load and bending will require consideration of stability-type failures of both a local and general nature.

Fatigue - The structural loading that occurs during the SRB recovery, transportation, and refurbishment sequence shall be included in the service life analysis of the SRB structure. The number of operational uses required for each component will be consistent with the recycle time needed for refurbishment of that

component. More flight cycles are anticipated on components requiring short refurbishment time. Fatigue life is to be considered for the total load cycles for the anticipated missions, accounting for static and dynamic loads including acoustic and thermal loading. Cumulative fatigue damage effects from the total life are to be considered in the design.

Exposure to Temperature - Various elements of the SRB structure will be exposed to temperature extremes during the launch and descent phases of each flight. Consideration will be given to temperature differentials that may occur during flight and water impact to preclude failure caused by thermally induced stress. The reduction in material properties due to repeated exposure to elevated temperatures will be considered to avoid a reduction in the projected service life.

Stress Corrosion - Special attention will be given to areas of the SRB structure that may be subjected to preloads or other locked-in stresses, especially during the recovery period when direct exposure to salt water occurs. Use of materials having susceptibility to stress corrosion cracking will be avoided (Ref. NASA SP 8082).

3.2.1.3 Problems Associated with Reuse

In addition to structural design safety factors, there are several other considerations that affect the probability of achieving flight certification for each SRB. These considerations are basically tied to the evaluation of structural damage and evaluation of data, which might indicate susceptibility to future damage. The specific items covered in the evaluations include:

- 1) salt water exposure;
- 2) evaluation of structural damage;
- 3) permanent deformation;
- 4) retest criteria.

Salt Water Exposure - The SRB will be exposed to salt water from time of water impact until flushed with fresh water following recovery. Consideration will be given to the cumulative effect of salt water exposure to verify that no premature failure will result. Reduction in material thickness and strength caused by corrosive effects will be accounted for in the analysis.

Evaluation of Structural Damage - Following the recovery of each SRB, it will be necessary to assess any structural damage that may have occurred during the water impact. The water impact load condition does not lend itself to high confidence load predictions. It is, therefore, desirable to obtain additional confidence in the water impact loads by statistical evaluation of actual flight impact data. The first several flights should contain instrumentation to satisfy this requirement. In addition, all SRB flight articles should contain instrumentation to aid in location of any structural damage. Any elements that exhibit evidence of rupture or collapse will be replaced during refurbishment.

Permanent Deformation - Any evidence of damage not in the category of ultimate rupture or collapse will be evaluated with regard to the following guidelines:

SRM Case - Inelastic deformation of the SRM case during water impact will be permitted if the case can be brought back within original tolerance and yielding is not excessive as judged by the cognizant structural engineer.

SRB Skirts - Inelastic deformation of the SRB skirts will be permitted if the skirts can be refurbished so that the tolerances of the original configurations are satisfied. Inelastic buckling of skin panels that results in rupture of stiffening elements will not be permitted. A structure damaged to this extent must be replaced.

All critical SRB dimensions will be verified to be within the required tolerances after each flight so that case and skirt interchangeability will be maintained.

Retest Criteria - As a final verification of flight worthiness, proof tests will be performed on the refurbished SRB. The proof test levels will be determined by fracture mechanics analysis.

In order to minimize cost and refurbishment cycle time, it is desirable to keep the retest operation to a minimum consistent with achieving confidence in structural integrity. It is, therefore, a requirement to evaluate the potential necessity for structural proof test against the water impact load data obtained from the previous flights of the SRB in question.

3.2.2 Design Allowables

This section of the criteria proposes specific approaches and methods of analysis that will supplement the failure criteria presented in the previous section. The material is organized so that it parallels the failure criteria as closely as possible.

3.2.2.1 Use of Safety Factors

The table of safety factors presented in Table 3.2-1 will be used for SRB design. These factors will be applied to 99% probability loads and pressures for the water impact condition. The design yield and design ultimate loads obtained through application of the appropriate factors of safety will be compared to material strength properties having 99% probability such as MIL-HDBK-5B "A" values, or equivalent. Margins of safety will be computed for the critical design yield or design ultimate conditions. It will be a design goal to achieve minimum positive margins of safety consistent with all other structural constraints.

3.2.2.2 Methods of Analysis

The SRM structure will be analyzed for all critical loading conditions by conventional aerospace methods of analysis. The following items will be considered in the analysis:

Use of Plastic Bending Allowables - To minimize structural weight, it is possible to take advantage of the moment carrying capability that certain materials exhibit in the plastic range. It is recommended that no use be made of these increased allowables except in the range between limit and ultimate load. Use of plastic bending allowables below limit load could result in an excessive amount of permanent deformation that would require refurbishment.

For applications where usage of an ultimate plastic bending factor may be appropriate, it is necessary to consider the elongation characteristics of the material in question. Materials having low elongations (less than 4%) are not considered suitable for use of plastic bending allowables. Since there is usually a significant variation in elongation versus material grain direction, close attention to orientation of grain is required.

Use of Pressure Relief and Stabilizing Effects - SRB model test data show that the SRM case internal pressure is increased somewhat during the water impact loading condition. The increase in pressure appears to vary as a function of impact angle with the higher pressures occurring at smaller angles measured from vertical.

The impact velocity does not have a significant effect on pressure buildup. The data indicate that the internal pressure buildup lasts through the time period when the maximum case hoop bending moments occur. It therefore is possible to take advantage of the internal pressure effect when analyzing the SRM case for the water impact loads, assuming the minimum design value can be determined by test.

Buckling and Crippling Analysis - Compression loaded structural elements require analysis for local stability (i.e., buckling of panels, flange crippling, etc). The minimum thickness of the structural element and the mechanical properties anticipated for the last flight are to be used for this analysis.

Designing against SRB structural failure by general instability during the water impact condition is a subject that encompasses interaction equations, nonlinear effects, and choice of correlation factors, as well as the basic consideration of the buckling problem. Recommendations pertaining to these related areas are presented as a part of this section. The analysis to verify the structural integrity for general stability will be based on nominal dimensions and mechanical properties anticipated for the last flight.

The SRB structure will be designed such that any buckling that occurs, due to application of ultimate design loads, will not result in collapse of structural components. For monocoque shell structure, this will include adjacent structural elements such as bulkheads and terminal ring frames. For stiffened shells, this requirement will be extended to mean that any panel buckling that occurs at ultimate load will not cause rupture of the panel or the stiffening elements.

The SRB structure will be designed such that any buckling that occurs because of application of limit design loads will be of an elastic nature only. The deformations produced by such elastic buckling will not be so large as to produce undesirable changes in the loading geometry.

The water impact loading condition produces various types of shell loadings, the most significant of which are the external pressure conditions on the skirts and SRM case. There are various combinations of applied loads that involve external pressure. The initial analysis which has been performed in this area has shown, however, that the longitudinal compression or bending loads that occur in combination with the external pressure are small. The shape of the interaction curve is, therefore, of lesser significance for these loading conditions than for more equally balanced cases.

The literature generally recommends a linear relationship between longitudinal compression and external pressure as indicated by the interaction equation: $R_{comp} + R_{press} = 1$. The linear relationship is believed to be somewhat conservative, but it is expected that very little weight savings could be achieved through use of a less conservative curve.

The buckling analyses performed on the SRB structure for water impact conditions will consider the nonlinear nature of the shell structure's response to external pressure loads. The nonlinear effects will be accounted for by considering the deflected geometry of the shell at each loading increment. Use of a nonlinear shell analysis computer program is necessary to adequately perform the shell buckling analysis.

Fatigue - The requirement for the SRB to be designed for use in many missions requires that special attention be given areas of stress concentrations. It is necessary to provide a design with a minimum of local stress risers and to use appropriate stress concentration factors to prevent initiation of fatigue failures. The total accumulation of load cycles for the number of planned missions for each SRB will be used for the fatigue analysis, including flight, impact, recovery, transportation, refurbishment, and confirmation testing. The use of Miner's equation is recommended.

$$\sum \frac{n_i}{N_i} = \frac{n_1}{N_1} + \frac{n_2}{N_2} + \frac{n_3}{N_3} + \dots = 1.0$$

Thermal Stress Analysis - The exposure of the SRB structure to elevated temperatures during launch and reentry followed immediately by immersion in salt water creates a need to evaluate the structure for thermally induced stresses. The design ultimate thermal stresses will be combined with the ultimate water impact stresses for conditions that are shown to co-exist.

Stress Corrosion - The use of materials having significant susceptibility to stress corrosion is not allowed. The residual stresses due to installations, welding, and assembly of the vehicle shall be used to compare actual stress intensities with allowable threshold stress intensity levels for the material. Protective coatings should be used to avoid exposure to corrosive environments; however, these coatings are susceptible to damage and the integrity of the design should not depend on their being intact.

3.2.2.3 Reuse Considerations

The structural design and analysis will give consideration to SRB reuse, especially with regard to salt water exposure, evaluation of structural damage, permanent deformation, and retest.

Salt Water Exposure - Consideration in the design, analysis, and testing will be given to reduction in mechanical properties and dimensional changes resulting from the anticipated service life of the SRB. This may require designing for reduced properties and increased thicknesses to show structural adequacy for the last flight. Overtesting of the structural qualification test article is required to account for the difference in capability between this article and the reduced capability anticipated for the last flight.

Evaluation of Structural Damage - The SRB design shall provide instrumentation to aid in the evaluation of structural damage. This instrumentation should consist primarily of accelerometers to be located in the forward and aft skirts. Strain and pressure gages and thermocouples may also be desirable in areas of anticipated locally high stresses and temperatures. Following SRB recovery, the article will be disassembled as required for the planned refurbishment. Each structural element will be examined as defined in the inspection procedure.

Permanent Deformation - The SRB design will minimize the amount of permanent deformation that can result from water impact loads. Use of the analysis methods recommended in Section 3.2.2.2 will help to achieve this design requirement.

In the design of the skirt/case interfaces, consideration must be given to interchangeability of the refurbished structural components. It will be a design goal to achieve reassembly of the refurbished components without having to rework the interface holes.

Retest Criteria - Following the refurbishment operation, each SRB must be recertified for the next launch. Any testing of the refurbished SRB will be to verify its structural integrity only for the manned flight environments. The retest conditions will be to proof-test levels determined by fracture mechanics analysis. All major structural assemblies installed as part of the refurbishment must have been previously qualified by ultimate test. This shall include any structural redesigns or beefups that may be required because of a water impact failure during the SRB service life.

3.3 STRUCTURAL RESPONSE OF 120-in. DROP TEST SPECIMEN

The purpose of this task was to review the data from the 120-inch static strength tests and the 120-inch (77%) model drop tests to resolve any differences between the two structural responses. The basic approach taken was to compare measured stresses and deflections from static and drop tests using a common loading parameter. All of the drop test data was taken from *Data Book for 120-inch Diameter (77 %) Solid Rocket Booster Model Water Recovery Drop Test Program*, dated June 1973. The instrumentation locations are depicted in Figure 3.3-1.

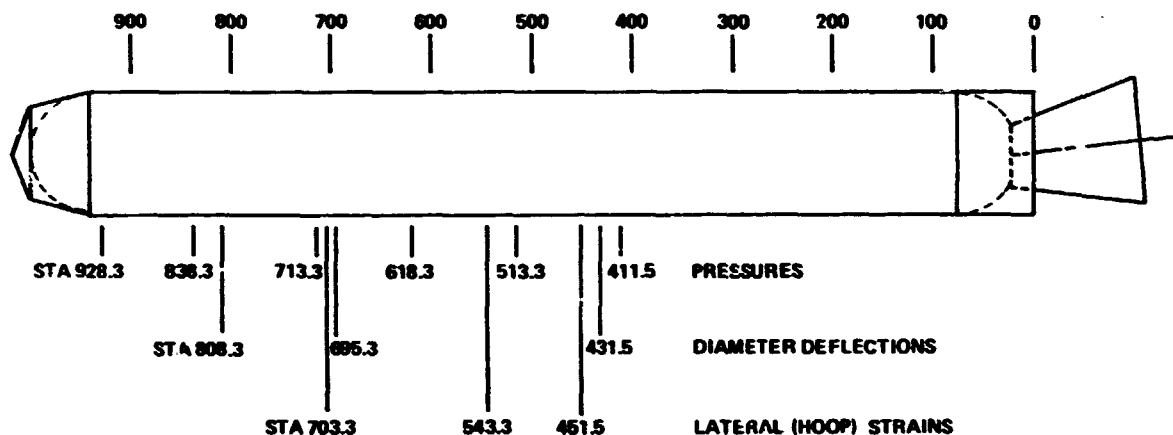


Figure 3.3-1 120-in. Drop Instrumentation Locations

3.3.1 Tabulation of Drop Test Results

Maximum pressure loads, deflections and stresses occurred for the higher value of vertical impact velocity and impact angle θ ; therefore, only the results for θ of 0.35 rad (20 deg) or greater were evaluated (11 drop conditions).

Peak pressure readings were taken at six longitudinal stations along the keel. Because of rolling during the slapdown impact condition, the maximum pressure did not necessarily occur at the keel. Circumferential measurements at Station 928.3 were used for each drop condition to calculate a roll compensation factor. This factor was applied to all of the measured keel pressures at the other stations in order to make a more realistic prediction of maximum pressure. Table 3.3-1 lists the compensated peak pressure at each of the six stations and the associated time of peak pressure for all 11 drop conditions. Note that in some cases measurements were not taken.

Table 3.3-2 lists the maximum diameter deflection at three different stations for the same six times that were shown on Table 3.3-1. The appropriate roll compensation factors were again used to calculate somewhat higher deflections. Conditions 3, 4, and 5 were the only conditions where deflections at stations 431.5 and 695.3 were measured. In all three instances the deflections at Station 431.5 were greater than at 695.3 for the first four times shown. This information was used to calculate average factors that were multiplied times the Station 695.3 deflections for conditions 1, 2, and 13 to approximate station 431.5 deflections. The same factors were used to calculate Station 431.5 deflections for condition 12 to replace instrumentation results that definitely appeared to be in error. All of the listed deflections represent diameter decreases (negative sign) except at Station 808.3 for conditions 13, 14, 17, 18, and 20. The only explanation of this latter data (assuming it is correct) is that a different mode shape was excited in those five drops. This possible discrepancy in the data is not considered important since the deflections at Stations 431.5 and 695.3 are larger and of more interest.

The maximum hoop bending stresses at each of three different stations for the six times of interest are tabulated in Table 3.3-3 for the 11 drop conditions. The sign of the stress is of little concern because it is primarily a bending stress. No Poisson or roll compensation correction was included since the effect of each would be small. The check marks adjacent to some of the stress readings indicate that the strain gage that would have shown the highest reading (at the keel) was not recorded at that station during that particular drop condition. In two cases no strain gage data was recorded at Station 703.3.

FOLDOUT FRAME

Table 3.3-1 120-in. Drop Peak Pressures

KEEL PRESSURE MEASUREMENT NO.	MEASUREMENT LOCATION STATION	TEST RUN DESCRIPTION	TIME OF PEAK PRESSURE, s	PEAK PRESSURE		TEST RUN DESCRIPTION	TIME OF PEAK PRESSURE, s
				UNCOMPENSATED $\frac{N}{m^2}$, (psi) 10^4	ROLL COMPENSATED $\frac{N}{m^2}$, (psi) 10^4		
DO 010	411.5	C145-01	2.14	9.0 (13)	10.4 (15)	C145-05	2.60
DO 009	513.3	$\theta = 0.52$ rad (30°)	2.33	12.4 (18)	13.8 (20)	$\theta = 0.35$ rad (20°)	2.80
DO 008	618.3	$V_v = 2.68$ m/s	2.46	21.4 (31)	24.2 (35)	$V_v = 9.45$ m/s	2.99
DO 007	713.3	(8.8 fps)	2.57	35.9 (52)	40 (58)	(31 fps)	—
DO 005	838.3		2.70	24.8 (36)	27.6 (40)		3.39
DO 003	928.3		2.80	22.7 (33)	25.5 (37)		3.57
		C145-02	—	—	—	C145-12	—
		$\theta = 0.52$ rad (30°)	2.30	12.4 (18)	12.4 (18)	$\theta = 0.52$ rad (30°)	2.90
		$V_v = 5.36$ m/s	2.43	15.9 (23)	15.9 (23)	$V_v = 10.7$ m/s	3.04
		(17.6 fps)	—	—	—	(35.1 fps)	3.18
			2.69	28.3 (41)	28.3 (41)		3.29
			2.80	26.2 (38)	26.2 (38)		3.39
		C145-03	2.10	4.8 (7)	5.5 (8)	C145-13	2.27
		$\theta = 0.35$ rad (20°)	2.59	6.2 (9)	6.9 (10)	$\theta = 0.40$ rad (23°)	2.50
		$V_v = 2.68$ m/s	2.80	8.3 (12)	9.0 (13)	$V_v = 10.7$ m/s	2.60
		(8.8 fps)	2.97	11.7 (17)	13.1 (19)	(35.1 fps)	2.78
			3.18	10.4 (15)	11.1 (16)		2.98
			3.36	6.9 (10)	7.6 (11)		3.11
		C145-04	2.50	6.2 (9)	6.2 (9)	C145-14	—
		$\theta = 0.35$ rad (20°)	2.80	8.3 (12)	8.3 (12)	$\theta = 0.40$ rad (23°)	—
		$V_v = 5.85$ m/s	2.87	8.3 (12)	8.3 (12)	$V_v = 16$ m/s	—
		(19.2 fps)	—	—	—	(52.6 fps)	3.02
			3.28	9.0 (13)	9.0 (13)		3.22
			3.44	5.5 (8)	5.5 (8)		3.35

FOLDOUT FRAME

2

DESCRIPTION	TIME OF PEAK PRESSURE, s	PEAK PRESSURE		TEST RUN DESCRIPTION	TIME OF PEAK PRESSURE, s	PEAK PRESSURE	
		UNCOMPENSATED $\frac{N}{m^2}$, (psi) 10^4	ROLL COMPENSATED $\frac{N}{m^2}$, (psi) 10^4			UNCOMPENSATED $\frac{N}{m^2}$, (psi) 10^4	ROLL COMPENSATED $\frac{N}{m^2}$, (psi) 10^4
05	2.60	6.9 (10)	6.9 (10)	C145-17	—	—	—
35 rad (20°)	2.80	6.9 (10)	6.9 (10)	$\theta = 0.35$ rad (20°)	3.13	7.6 (11)	8.3 (12)
9.45 m/s	2.99	8.3 (12)	8.3 (12)	$V_v = 16.2$ m/s (53.2 fps)	—	—	—
(ps)	—	—	—	3.40	15.2 (22)	15.9 (23)	—
	3.39	9.0 (13)	9.0 (13)	—	—	—	—
	3.57	5.5 (8)	5.5 (8)	3.70	11.7 (17)	12.4 (18)	—
-12	—	—	—	C145-18	—	—	—
52 rad (30°)	2.90	14.5 (21)	15.2 (22)	$\theta = 0.35$ rad (20°)	—	—	—
10.7 m/s	3.04	20.7 (30)	22.1 (32)	$V_v = 2.87$ m/s (9.4 fps)	2.81	10.4 (15)	10.4 (15)
(fps)	3.18	26.9 (39)	28.3 (41)	2.99	13.1 (19)	13.1 (19)	—
	3.29	27.6 (40)	28.0 (42)	—	—	—	—
	3.39	24.2 (35)	25.5 (37)	3.35	9.7 (14)	9.7 (14)	—
-13	2.27	6.9 (10)	6.9 (10)	C145-20	—	—	—
40 rad (23°)	2.50	5.5 (8)	5.5 (8)	$\theta = 0.52$ rad (30°)	2.78	9.7 (14)	9.7 (14)
10.7 m/s	2.60	6.9 (10)	6.9 (10)	$V_v = 15.4$ m/s (50.5 fps)	2.90	24.2 (35)	24.2 (35)
(fps)	2.78	10.4 (15)	10.4 (15)	3.00	31.1 (45)	31.1 (45)	—
	2.98	11.7 (17)	11.7 (17)	3.12	45.5 (66)	45.5 (66)	—
	3.11	9.0 (13)	9.0 (13)	3.22	27.6 (40)	27.6 (40)	—
-14	—	—	—				
40 rad (23°)	—	—	—				
16 m/s	—	—	—				
(fps)	3.02	11.7 (17)	11.7 (17)				
	3.22	16.6 (24)	16.6 (24)				
	3.35	10.4 (15)	10.4 (15)				

FOLDOUT

Table 3.3-2 120-in. Drop Diameter Deflections (Roll Compensated)

TEST RUN NO.	TIME, s	MAXIMUM DEFLECTIONS			TEST RUN NO.	TIME, s	MAXIMUM DE	
		SECTION A-A STATION 808.3 100 m (in.)	SECTION B-B STATION 695.3 100 m (in.)	SECTION C-C STATION 431.5 100 m (in.)			SECTION A-A STATION 808.3 100 m (in.)	SECTIC STATIC 100 m (
C145-01	2.14	-1.14(-.45)	-1.42(-.56)	-2.16(-.85)	C145-05	2.60	-.76(-.3)	-2.03(-
	2.33	-2.29(-.90)	-3.4 (-1.34)	-4.6 (-1.81)		2.80	-1.27(-.5)	-3.05(-
	2.46	-4.27(-1.68)	-6.56(-2.58)	-7.68(-3.02)		2.99	-1.27(-.5)	-4.32(-
	2.57	-5.42(-2.13)	-8.25(-3.25)	-8.75(-3.44)		—	—	—
	2.70	-3.71(-1.46)	-4.55(-1.79)	-2.36(-.93)		3.39	—	-2.03(-
	2.80	-1.7 (-.67)	-1.42(-.56)	—		3.57	1.27(.5)	-.51(-
C145-02	—	—	—	—	C145-12	—	NOT MEASURED	—
	2.30	-3.05(-1.2)	-4.06(-1.6)	-5.48(-2.16)		2.90		-9.4 (-
	2.43	-4.32(-1.7)	-6.85(-2.7)	-8.02(-3.16)		3.04		-10.7 (-
	—	—	—	—		3.18		-13.4 (-
	2.69	-5.84(-1.4)	-5.84(-2.3)	-3.02(-1.19)		3.29		-9.67(-
C145-03	2.80	-2.29(-.9)	-2.54(-1.0)	—	C145-13	3.39	—	-5.36(-
	2.40	-.84(-.33)	-2.24(-.88)	-2.8 (-1.10)		2.27	1.02(.4)	-2.54(-
	2.59	-1.4 (-.55)	-2.8 (-1.10)	-3.91(-1.54)		2.50	2.29(.9)	-3.85(-
	2.80	-2.23(-.88)	-4.47(-1.76)	-5.03(-1.98)		2.60	2.54(1.0)	-5.85(-
	2.97	-2.8 (-1.10)	-5.03(-1.98)	-5.03(-1.98)		2.78	3.05(1.2)	-7.36(-
	3.18	-1.96(-.77)	-2.8 (-1.10)	-1.68(-.66)		2.98	2.29(.9)	-5.08(-
C145-04	3.36	-.28(-.11)	-.84(-.33)	—	C145-14	3.11	—	-1.02(-
	2.50	-.76(-.3)	-1.53(-.6)	-2.8 (-1.1)		—	—	NOT MEASL
	2.80	-1.52(-.6)	-3.3 (-1.3)	-4.32(-1.7)		—	—	
	2.87	-2.03(-.8)	-3.55(-1.4)	-4.32(-1.7)		—	—	
	—	-2.54(-1.0)	—	—		3.02	6.35(2.5)	
	3.28	-1.52(-.6)	-1.52(-.6)	-.51(-.2)		3.22	5.85(2.3)	
	3.44	-.51(-.2)	-.51(-.2)	—		3.35	1.77(.7)	

FOLDOUT FRAME

2

MAXIMUM DEFLECTIONS			TEST RUN NO.	TIME, s	MAXIMUM DEFLECTIONS		
SECTION A-A STATION 808.3 100 m (in.)	SECTION B-B STATION 695.3 100 m (in.)	SECTION C-C STATION 431.5 100 m (in.)			SECTION A-A STATION 808.3 100 m (in.)	SECTION B-B STATION 695.3 100 m (in.)	SECTION C-C STATION 431.5 100 m (in.)
.3)	- 2.03(-.8)	- 3.05(-1.2)	C145-17	—	—	NOT MEASURED	—
.5)	- 3.05(-1.2)	- 4.06(-1.6)		3.13	4.3 (1.69)		- 9.68(-3.81)
.5)	- 4.32(-1.7)	- 5.08(-2.0)		—	—		-12.6 (-4.98)
	—	—		3.40	6.46(2.54)		- 8.34(-3.28)
	- 2.03(-.8)	- 1.27(-.5)	C145-18	—	6.74(2.65)	NOT MEASURED	—
.5)	- .51(-.2)	—		3.70	2.41(.95)		- .81(-.32)
	—	—		—	—		—
RED	- 9.4 (-3.70)	-12.7 (-5.0)		—	—		—
	-10.7 (-4.23)	-12.6 (-4.94)	C145-20	2.81	4.06(1.6)	NOT MEASURED	- 2.8 (-1.1)
	-13.4 (-5.29)	-14.3 (-5.6)		2.99	4.32(1.7)		- 2.29(-.9)
	- 9.67(-3.81)	- 5.0 (-1.97)		—	—		—
	- 5.36(-2.11)	—		3.35	1.78(.7)		—
.4)	- 2.54(-1.0)	- 3.86(-1.52)	C145-20	—	—	NOT MEASURED	—
.9)	- 5.85(-2.3)	- 7.9 (-3.11)		2.78	4.32(1.7)		-10.2 (-4.0)
.0)	- 5.85(-2.3)	- 6.83(-2.62)		2.90	7.62(3.0)		-14.5 (-5.7)
1.2)	- 7.36(-2.9)	- 7.8 (-3.07)		3.00	8.38(3.3)		-13.2 (-5.2)
.9)	- 5.68(-2.0)	- 2.64(-1.04)		3.12	7.62(3.0)		- 7.6 (-3.0)
	- 1.02(-.4)	—		3.22	2.54(1.0)		- .51(-.2)
	NOT MEASURED	—					—
2.5)		-13.7 (-5.4)					- 7.62(-3.0)
2.3)		- 7.62(-3.0)					- 7.62(-3.0)
.7)		.51(.2)					

FOLDOUT FRAME

Table 3.3-3 120-in. Drop Maximum Stresses

TEST RUN NO.	TIME SEC.	MAXIMUM STRESS			TEST RUN NO.	TIME SEC.	MAXIMUM STRESS	
		SECTION A-A STATION 703.3 N/m ² (ksi) 10 ⁷	SECTION B-B STATION 543.3 N/m ² (ksi) 10 ⁷	SECTION C-C STATION 451.5 N/m ² (ksi) 10 ⁷			SECTION A-A STATION 703.3 N/m ² (ksi) 10 ⁷	SECTION B-B STATION 543.3 N/m ² (ksi) 10 ⁷
C-145-01	2.14	.40 (.58)	- 9.03 (-13.1)	- 8.0 (-11.5)	C145-05	2.60	-1.0 (-1.45)	- 6.9
	2.33	.40 (.58)	-15.6 (-22.6)	-14.0 (-20.3)		2.80	-1.1 (-1.59)	10.0
	2.46	.40 (.58)	-22.0 (-31.9)	-18.0 (-26.1)		2.99	-1.2 (-1.74)	-13.0
	2.57	.60 (.87)	-24.0 (-34.8)	-13.0 (-18.8)		—	—	—
	2.70	.60 (.87)	-13.0 (-18.8)	- 6.97 (-10.1)		3.39	2.4 (3.48)	- 4.4
	2.80	.40 (.58)	- 8.0 (-11.6)	3.6 5.22		3.57	2.4 (3.48)	- 2.0
C145-02	—	—	—	—	C145-12	—	—	—
	2.30	- 6.97 (-10.1)	-16.0 (-23.2)	13.0 (18.85)		2.90	-3.2 (-4.64)	-16.4
	2.43	-10.0 (-14.5)	-22.0 (-31.9)	14.6 (21.2)		3.04	-3.4 (-4.93)	-22.0
	—	—	—	—		3.18	-3.8 (-5.51)	-26.0
	2.69	-14.0 (-20.3)	-14.0 (-20.3)	8.0 (11.6)		3.29	-4.0 (-5.8)	-14.0
C145-03	2.40	- 2.0 (- 2.9)	- 5.0 (- 7.25)	- .80 (- 1.16)	C145-13	2.27	- .80 (-1.16)	- 6.0
	2.59	- 3.0 (- 4.35)	- 8.0 (-11.6)	- .80 (- 1.16)		2.50	-1.0 (-1.45)	-10.7
	2.80	- 6.0 (- 8.7)	-10.4 (-15.1)	- .80 (- 1.16)		2.60	-1.2 (-1.74)	-10.6
	2.97	-11.2 (-16.2)	10.0 (14.5)	3.6 (5.22)		2.78	- .60 (- .87)	-11.4
	3.18	- 5.4 (- 7.83)	- 4.4 (- 6.38)	2.6 (3.77)		2.98	- .60 (- .87)	- 6.0
	3.36	- 2.4 (- 3.48)	1.6 (2.32)	1.6 (2.32)		3.11	- .80 (-1.16)	2.0
C145-04	2.50	- .40 (- .58)	- 4.8 (- 6.96)	- 1.2 (- 1.74)	C145-14	—	NOT MEASURED	—
	2.80	- .60 (- .87)	- 9.18 (-13.3)	- 1.2 (- 1.74)		—		—
	2.87	- .60 (- .87)	-10.0 (-14.5)	- 1.0 (- 1.4)		—		—
	—	—	—	—		3.02		-12.0
	3.28	- 2.6 (- 3.77)	3.0 (4.5)	.40 (.58)		3.22		- 6.0
	3.44	- 2.8 (- 4.06)	2.2 (3.19)	.60 (.87)		3.35		- 4.0

FOLDOUT FRAME

2

MAXIMUM STRESS			TEST RUN NO.	TIME SEC.	MAXIMUM STRESS		
SECTION A-A STATION 703.3 N/m ² (ksi) 10 ⁷	SECTION B-B STATION 543.3 N/m ² (ksi) 10 ⁷	SECTION C-C STATION 451.5 N/m ² (ksi) 10 ⁷			SECTION A-A STATION 703.3 N/m ² (ksi) 10 ⁷	SECTION B-B STATION 543.3 N/m ² (ksi) 10 ⁷	SECTION C-C STATION 451.5 N/m ² (ksi) 10 ⁷
1.45)	- 6.97 (-10.1)	- .60 (- .87)	C145-17	--	--	--	--
1.59)	-10.0 (-14.5)	.40 (.58)		3.13	-1.2 (-1.74)	-14.0 (-20.3)	-16.0 (-23.2)
1.74)	-13.0 (-18.8)	.40 (.58)		--	--	--	--
3.48)	--	--		3.40	-2.0 (-2.9)	-16.0 (-23.2)	14.0 (20.3)
3.48)	- 4.4 (- 6.38)	.60 (.87)		--	--	--	--
3.48)	- 2.0 (- 2.9)	1.0 (1.45)	C145-18	3.70	4.0 (5.8)	4.4 (6.38)	- 5.0 (- 7.25)
4.64)	--	--		--	--	--	--
4.93)	-16.4 (-23.8)	- 1.0 (- 1.45)		--	--	--	--
5.51)	-22.0 (-31.9)	- 1.2 (- 1.74)		2.81	-1.2 (-1.74)	9.6 (13.9)	11.6 (16.8)
5.51)	-26.0 (-37.7)	- 1.0 (- 1.45)		2.99	-1.2 (-1.74)	6.0 (8.7)	8.42 (12.2)
5.8)	-14.0 (-20.3)	- 1.0 (- 1.45)	C145-20	--	--	--	--
5.51)	- 8.0 (-11.6)	- 1.0 (- 1.45)		3.35	- .80 (-1.16)	1.80 (2.61)	- .80 (- 1.16)
1.16)	- 6.0 (- 8.7)	-10.0 (-14.5)		--	NOT MEASURED	--	--
1.45)	-10.7 (-15.6)	-12.0 (-17.4)		2.78		-20.0 (-29.0)	- 1.2 (- 1.74)
1.74)	-10.6 (-15.4)	-13.2 (-19.1)		2.90		-30.0 (-43.5)	- 1.8 (- 2.61)
.87)	-11.4 (-16.5)	-13.2 (-19.1)		3.00		-28.0 (-40.6)	- 2.0 (- 2.9)
.87)	- 6.0 (- 8.7)	-10.0 (-14.5)		3.12		-16.0 (-23.2)	- 1.60 (- 2.32)
1.16)	2.0 (2.9)	- 1.6 (-11.0)	C145-20	3.22		-10.0 (-14.5)	- 1.0 (- 1.45)
URED	--	--		--		--	--
URED	--	--		--		--	--
URED	--	--		--		--	--
URED	-12.0 (-17.4)	4.0 (5.8)		--		--	--
URED	- 6.0 (- 8.7)	- 2.0 (- 2.9)		--		--	--
URED	- 4.0 (- 5.8)	- 5.0 (- 7.25)		--		--	--

PRECEDING PAGE BLANK NOT FILLED

3.3.2 Plots of Drop Test Results

Figures 3.3-2 and 3.3-3 present the most significant data points from Tables 3.3-2 and 3.3-3. Different symbols were used to signify the time event when the pressure peaked at the five stations shown. In each instance only maximum deflection and stress were plotted for each time. Enveloping curves were estimated and plotted based on data points shown. The trend shown for the different stations is as expected; i.e., lower stresses and deflections result for any given value of peak pressure as it moves to a more forward location (higher station number). The big spread between data points at any station could be caused by inaccuracy in instrumentation or differences in the dynamic response from one drop to the next. There is good correlation when comparing stresses and deflections for any one drop at the same time frame; i.e., they are either both low or both relatively high.

Figure 3.3-4 shows the longitudinal and circumferential distributions that were derived by NASA-MSFC from the drop test results. These distributions were used to calculate an equivalent unit running hoop moment as explained in Section 4.3.5. These curves for t_1 and t_2 are shown on Figure 3.3-5. A loading length of 3.81 meters (150 in.) was used as being most representative of an average moment loading. Figure 3.3-6 presents stress versus static average hoop moments for various loading lengths. Data shown on Figure 4.3-15 were ratioed down by $(t_{120}/t_{142})^2$ to obtain hoop moments and associated loading lengths at a stress level of 1,245,000,000 N/m² (180,000 psi). Moments at any one loading length for other stress levels were ratioed using results from the 120-inch static test condition D (See Figure 4.3-13).

Figure 3.3-7 shows a plot of diameter deflection versus average running hoop moment using a loading length equal to 3.81 meters (150 in.) for the static load condition B and for the envelope of drop test results that produced the maximum deflection (peak pressure at station 513.3). Note that the static hoop moment corresponding to yield was increased by a 1.15 factor to account for static test deflections being 1.5 times those that would be expected for a VQ/I reaction versus a 1.3 factor between stresses ($1.5/1.3 = 1.15$). The peak pressure values from Figure 3.3-2 were multiplied by 122 (from Figure 3.3-5) to determine the applied average running hoop moment for each drop test condition. Figure 3.3-8 presents the maximum hoop stress versus average running hoop moment for the static test condition (taken from Figure 3.3-6) and also for the drop tests using the Station 513.3 curve from Figure 3.3-3.

PRECEDING PAGE BLANK NOT FILMED

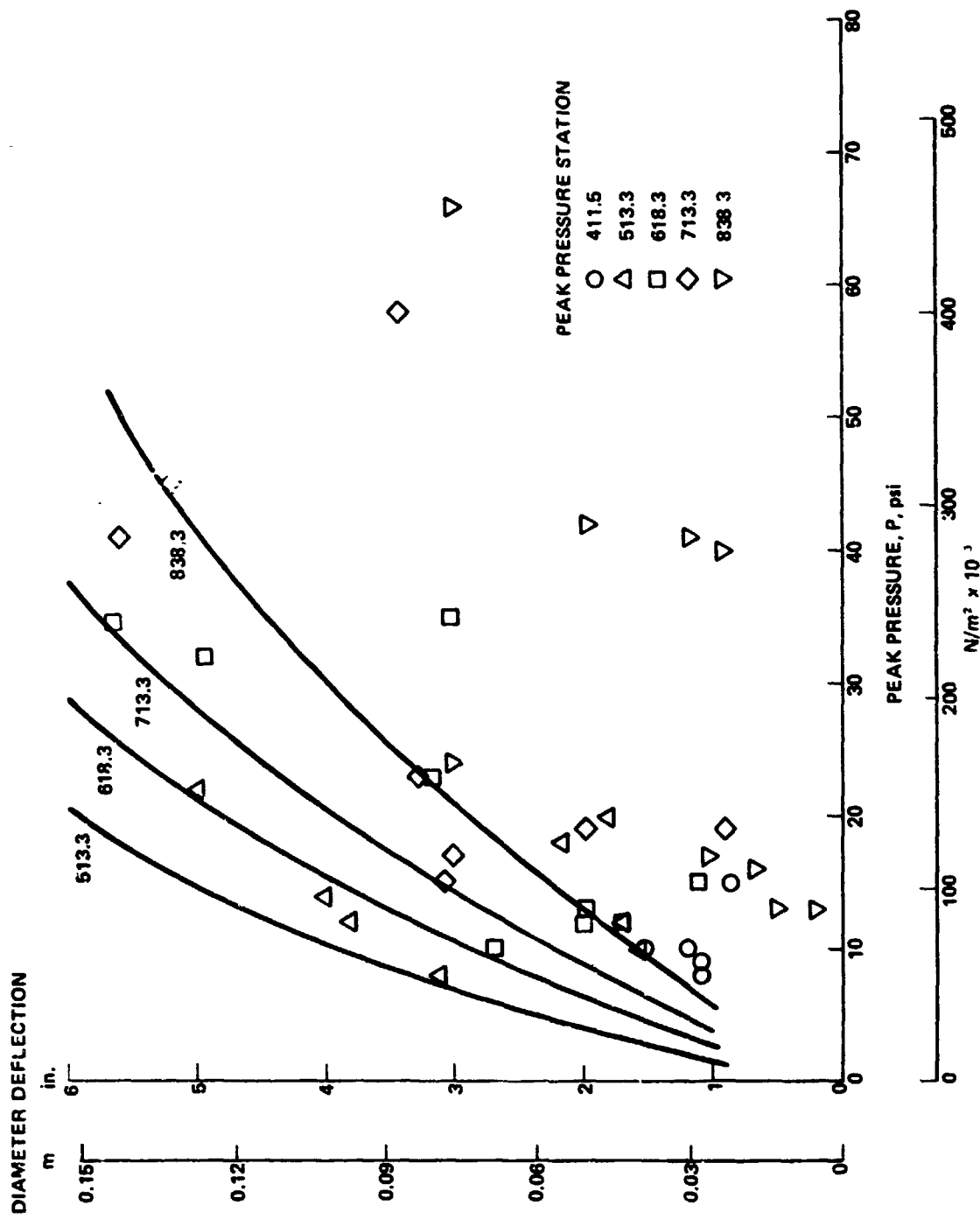


Figure 3.3-2 120-in. Drop Maximum Diameter Deflection

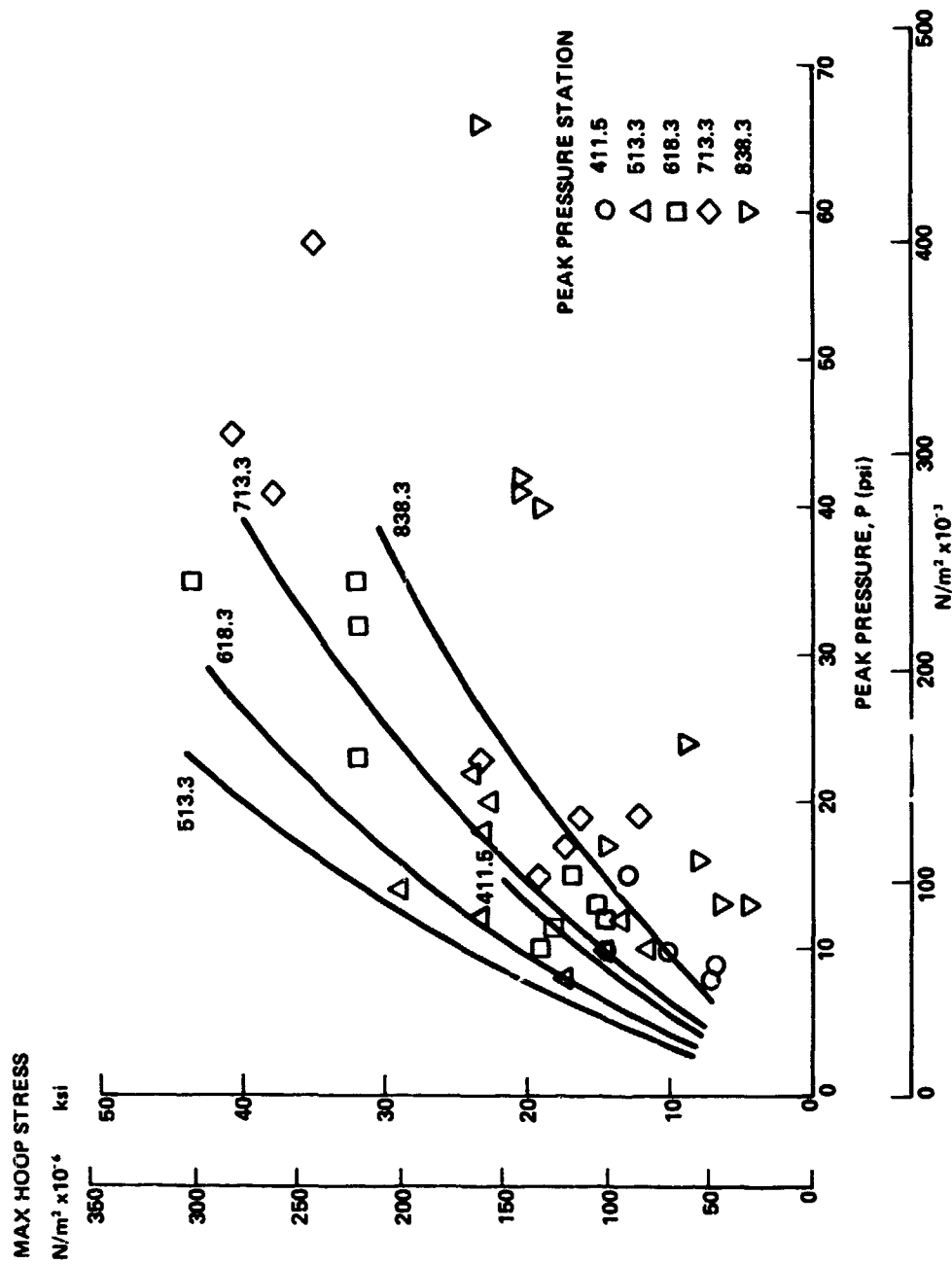


Figure 3.3-3 120-in. Drop Maximum Hoop Bending Stresses

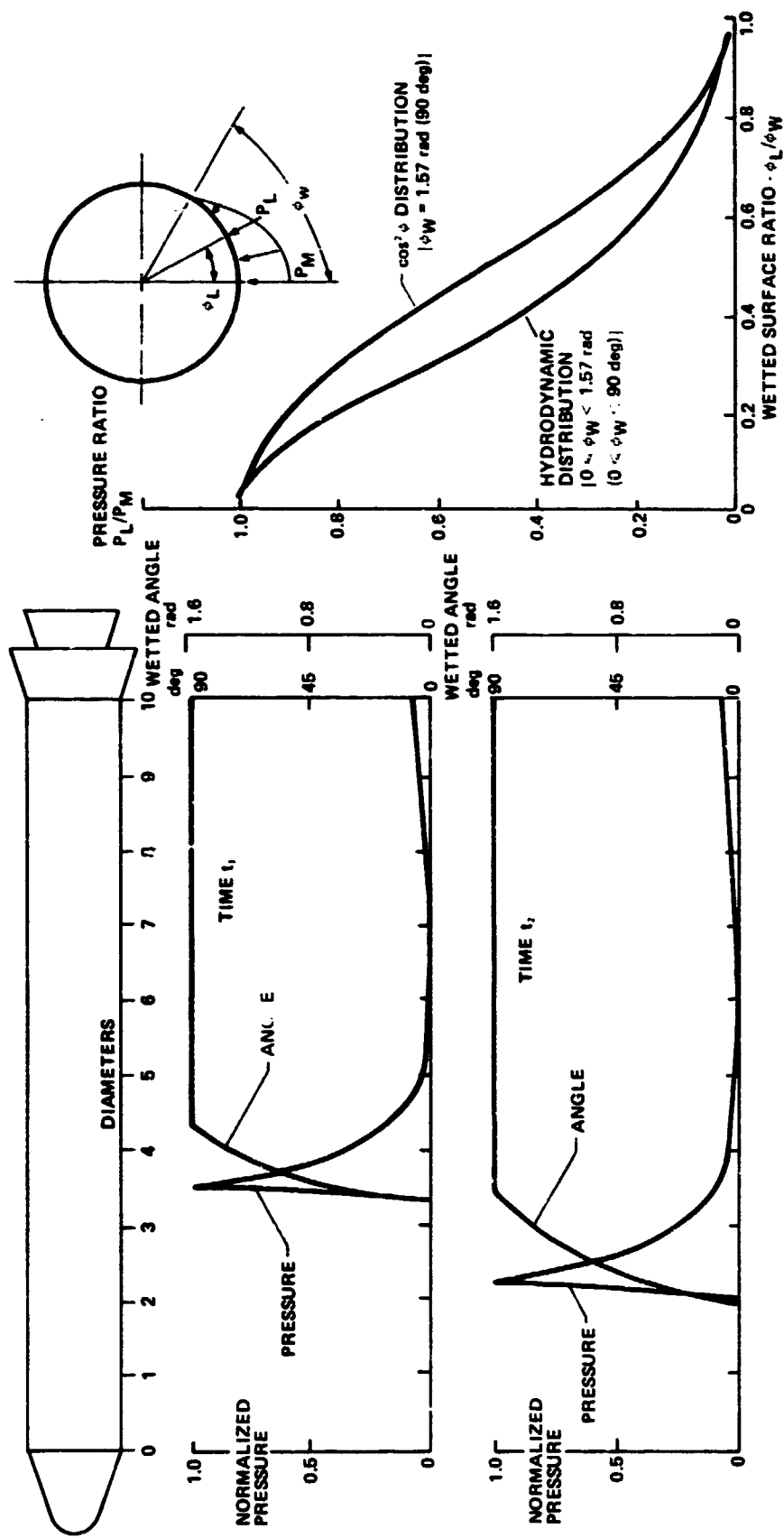


Figure 3.3-4 Slapdown Longitudinal and Circumferential Load Distribution

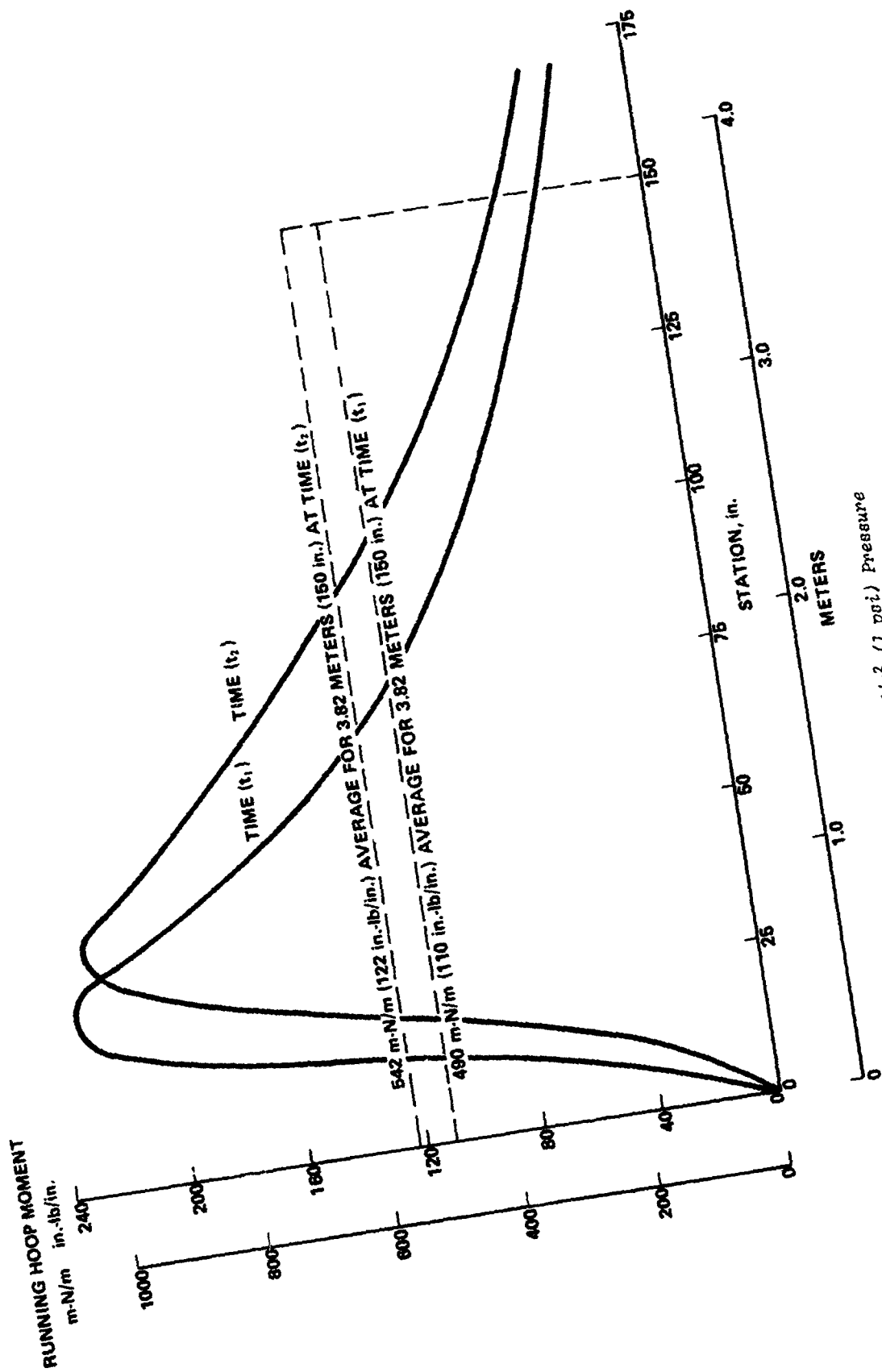


Figure 3.3-5 Average Running Hoop Moment for 6900 N/m^2 (1 psi) Pressure

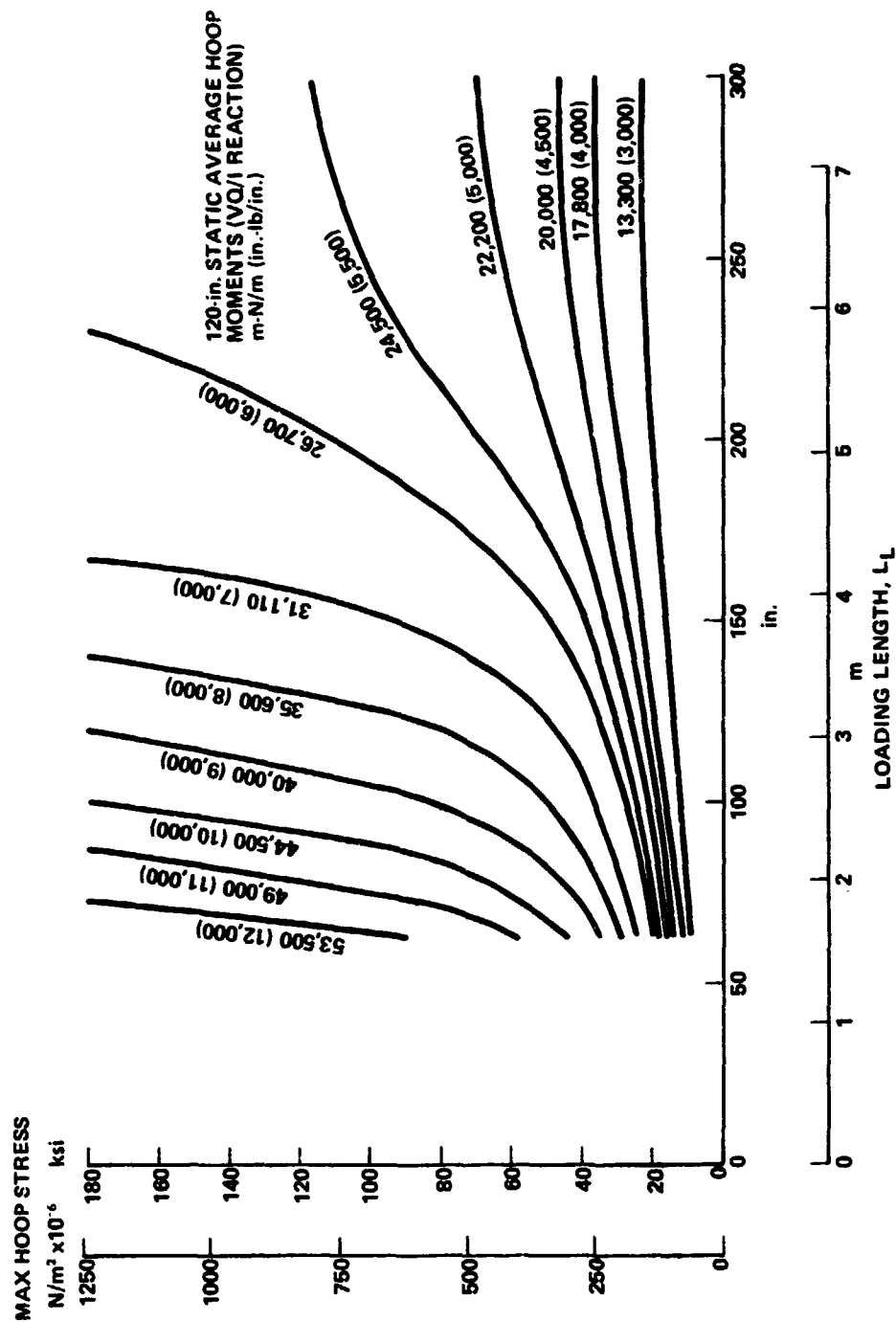


Figure 3.3-6 Maximum Hoop Bending Stress for Static Hoop Moments

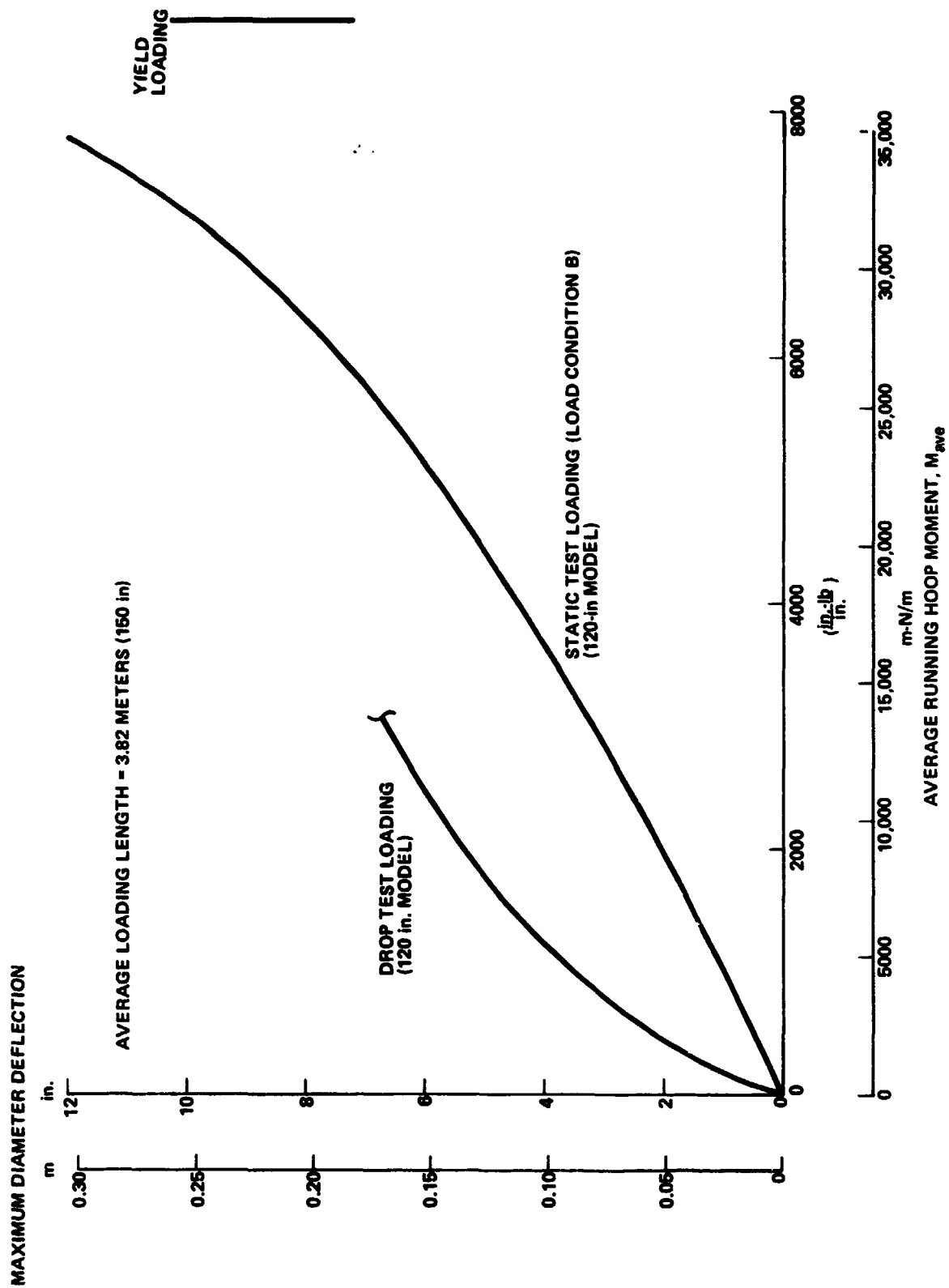


Figure 3.3-7 Comparison of Static and Drop Test Deflections

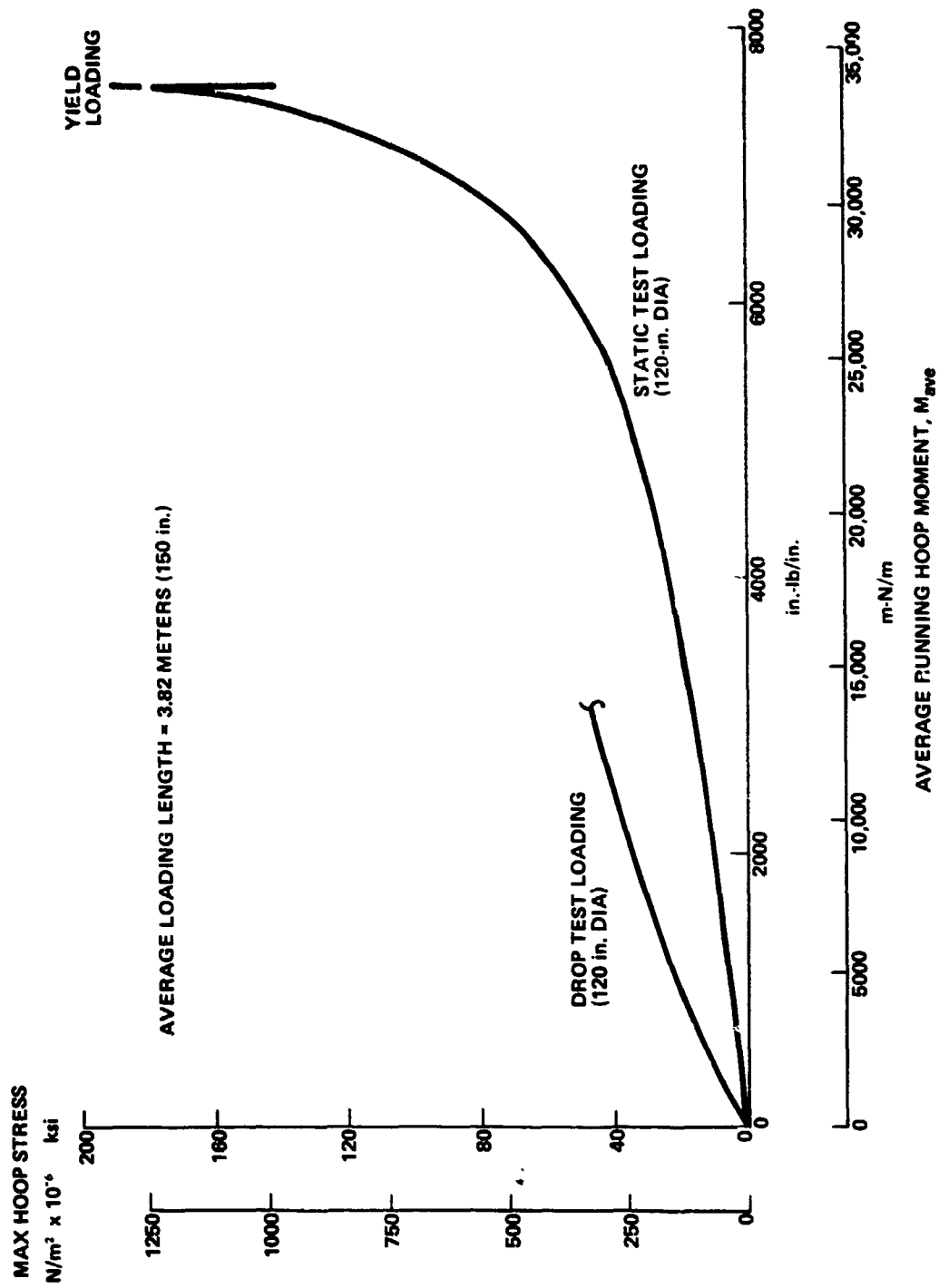


Figure 3.3-8 Comparison of Static and Drop Test Hoop Stresses

3.3.3 Conclusions

The final results plotted in Figures 3.3-7 and 3.3-8 show that there appears to be some dynamic amplification in the load range for which the drop test results are applicable. The trend is for less amplification with increasing peak pressure. This trend makes sense assuming that higher peak pressures occur due to higher impact velocities (less time to peak pressure), and therefore have higher frequencies associated with the applied loads. Assuming that the lower values of pressure correspond to frequencies near that of the structural frequency of the case for a hoop bending vibration mode (approximately 15 Hertz), a resonance of some magnitude would exist. With increasing applied load frequency (and also decreasing structural frequency caused by nonlinear deflections), the resonance would be expected to decrease.

It is our understanding that NASA-MSFC has reduced the predicted slapdown loads for the 3.61 m (142 in.) SRB to account for the dynamic short term nature of the loading. The results from the 120-inch drop tests do not seem to justify this reduction. The resolution of this concern should be a dynamic analysis of the slapdown loading condition combined with additional instrumented drop tests and static tests.

3.4 MONOLITHIC VERSUS SEGMENTED JOINT CASE DESIGN

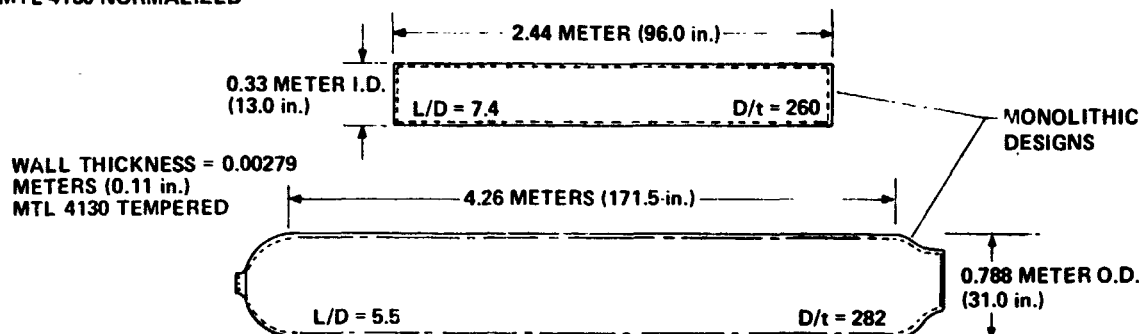
Extensive strength evaluation of the case center segments has been conducted analytically and through static testing. The basic purpose of this task was to evaluate the results of subscale model tests to determine the magnitude of strength increase associated with a segmented case design versus a monolithic design. The results are normalized to a baseline case diameter of 3.61 m (142 in.), 0.0121 meter (0.475 in.) nominal thickness sized for D6AC steel with an $F_{tu} = 1,345,000,000 \text{ N/m}^2$ (195,000 psi) and $F_{ty} = 1,240,000,000 \text{ N/m}^2$ (180,000 psi).

3.4.1 Subscale Model Test Specimens and Loading Conditions

Three SRM scale models were used during the static test program. Two of these models were of a monolithic construction (no internal frames). One model was 0.33 meter (13.0 in.) in diameter, 2.44 meters (96.0 in.) long, and had a skin thickness of 0.00127 meters (0.050 inch). The other model was 0.787 meter (31.0 inches) in diameter, 4.36 meters (171.5 inches) long, and had a skin thickness of 0.0028 meter (0.110 inch). Both monolithic models were manufactured from 4130 steel.

The third model was an actual Air Force missile of a segmented design. It was 3.05 meters (120.0 in.) in diameter, 21.2 meters (835.2 in.) long, had a skin thickness of 0.00952 meter (0.375 in.) and was manufactured from D6AC steel. Sketches of these three specimens are shown in Figure 3.4-1.

WALL THICKNESS = 0.00127 METER (0.05 in.)
MTL 4130 NORMALIZED



WALL THICKNESS = 0.00953 METERS (0.375 in.)
MTL. D6AC

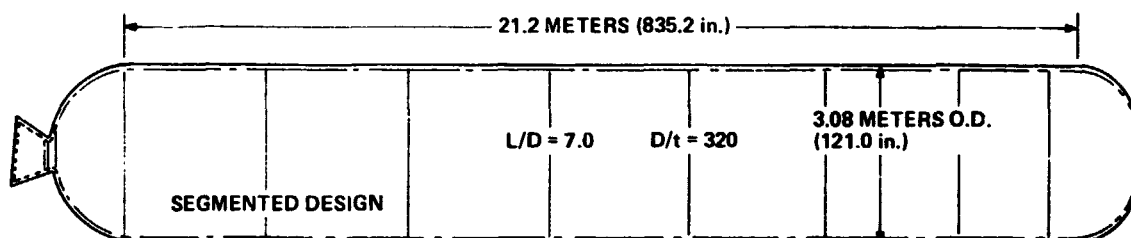


Figure 3.4-1 Three Subscale Models Static Tested

The critical impact loading condition occurs during slapdown and produces a circumferentially varying pressure wave propagating forward along the case with time. All three static test subscale models were loaded with somewhat similar pressure load distributions. Five load conditions, as shown in Figure 3.4-2, were applied to the 13-inch and 31-inch models. Figure 3.4-3 shows the three load conditions that were tested and evaluated for the 120-inch model. The target peak pressure varied from 55,200 N/m² (8 psi) to 310,000 N/m² (45 psi) longitudinally. Circumferentially the target pressures varied as a cosine function from 0 psi to 55,200 N/m² (8 psi) peak over a half radial angle of 1.05 rad (60 deg) and from 0 psi to 310,000 N/m² (45 psi) peak over a half radial angle of 0.26 rad (15 deg). Reactions were accomplished with straps applying

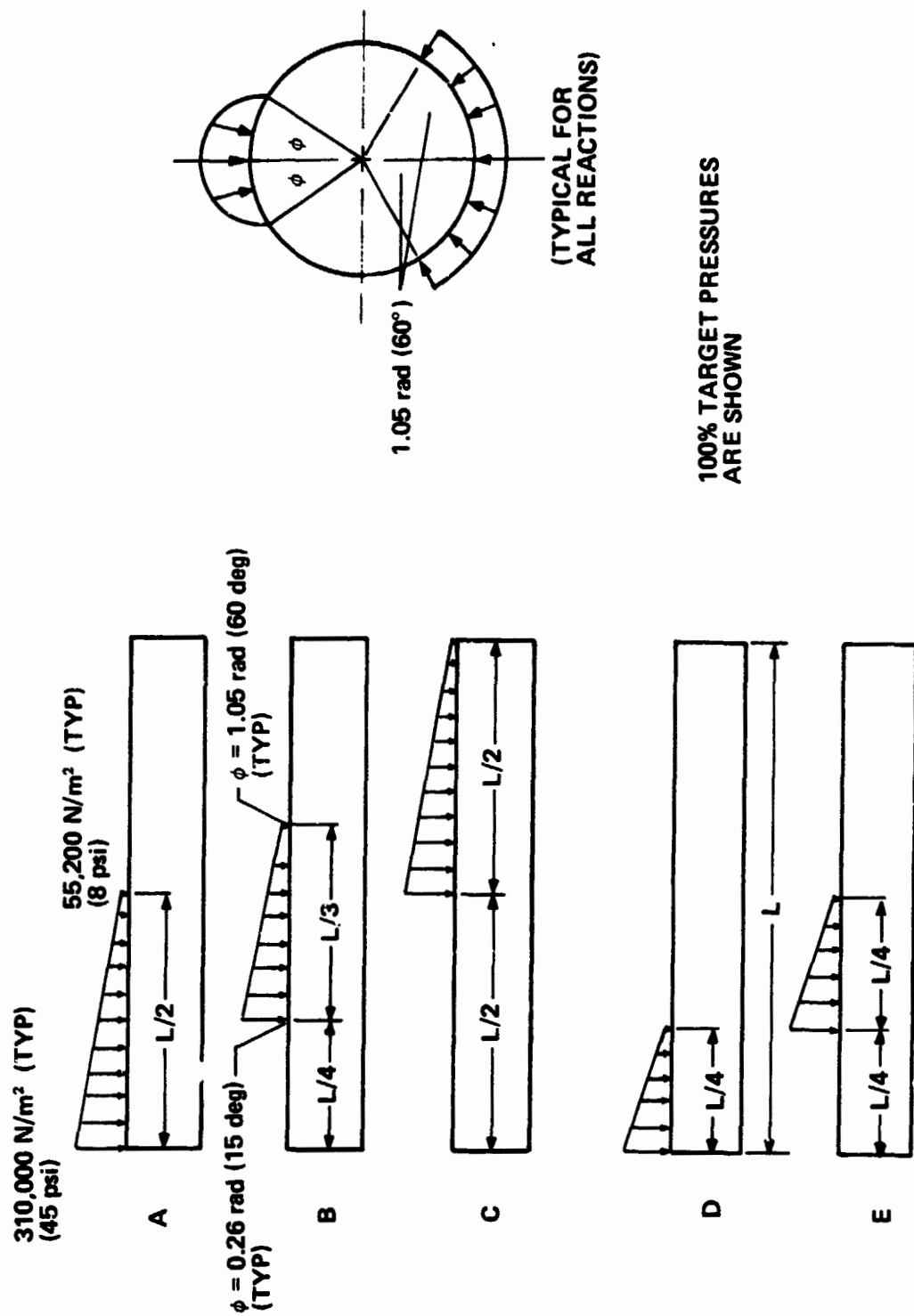


Figure 3.4-2 Five Loading Conditions Applied to 13- and 31-in. Monolithic Specimens

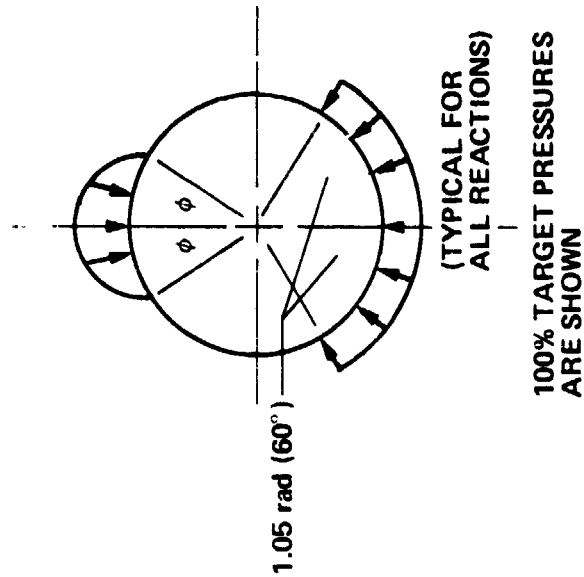
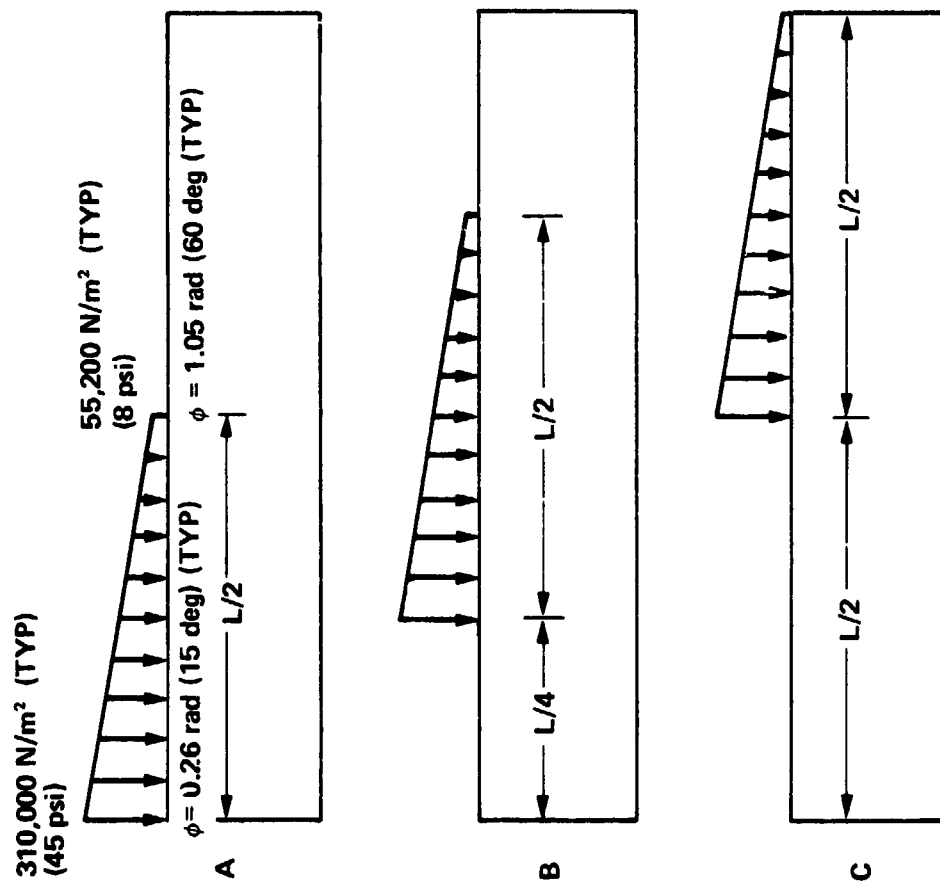


Figure 3.4-3 Three Loading Conditions Evaluated for the 120-in. Specimen

uniform circumferential pressure over a 2.1 rad (120 deg) included angle. Condition A loaded up the forward half length of the case; condition B, the middle one half for the 120-in. model and the middle one third for the 13-in. and 31-in. models; condition C, the aft half length of the case; condition D, the forward one quarter length of the case; and condition E the second quarter length of the case.

3.4.2 Subscale Test Results Extrapolated to Yield Strength

All five static test conditions for each of the monolithic cases were conducted on the same specimen. Loading conditions were cut off at varying percentages of the target loading to preclude yielding during any of the tests. Plots of stresses and deflections showed a definite nonlinear nature in the hoop bending failure mode. The maximum hoop stresses were plotted for the five loading conditions and extrapolated to an F_{ty} of 1,240,000,000 N/m² (180,000 psi) to obtain an allowable yield load for each loading condition (Figures 3.4-4 and 3.4-5).

All three static test conditions on the 120-in. segmented case were also conducted on the same specimen. Loading conditions were cut off at varying percentages of the target loading to preclude yieldings during any of the tests. A calculation of the total load cell readings applying the pressure loading showed that the actual test cutoff percentage values were different than the nominal values. Plots of stresses and deflections showed a definite nonlinear nature in the hoop bending failure model. The maximum hoop stresses were plotted (using corrected test cutoff percentages) for the three loading conditions and extrapolated to an F_{ty} of 1,240,000,000 N/m² (180,000 psi) to obtain an allowable yield load for each loading condition (Figure 3.4-6).

3.4.3 Subscale Yield Allowables Ratioed to 142-in. Diameter

Through the use of proper factors, the results obtained from subscale model tests were ratioed to obtain strengths of the 142-in. case for each particular critical loading condition. The hoop bending moments in the case static tests were higher than would result during an actual slakedown for the same applied pressures because of the method of reacting the load. Analysis showed that if a VQ/I shear reaction could have been used in the static test, approximately 30% greater loads could have been superimposed for the same resultant stress level. This factor of 1.3 was used in ratioing the static test results up to obtain allowables for the 142-in. case.

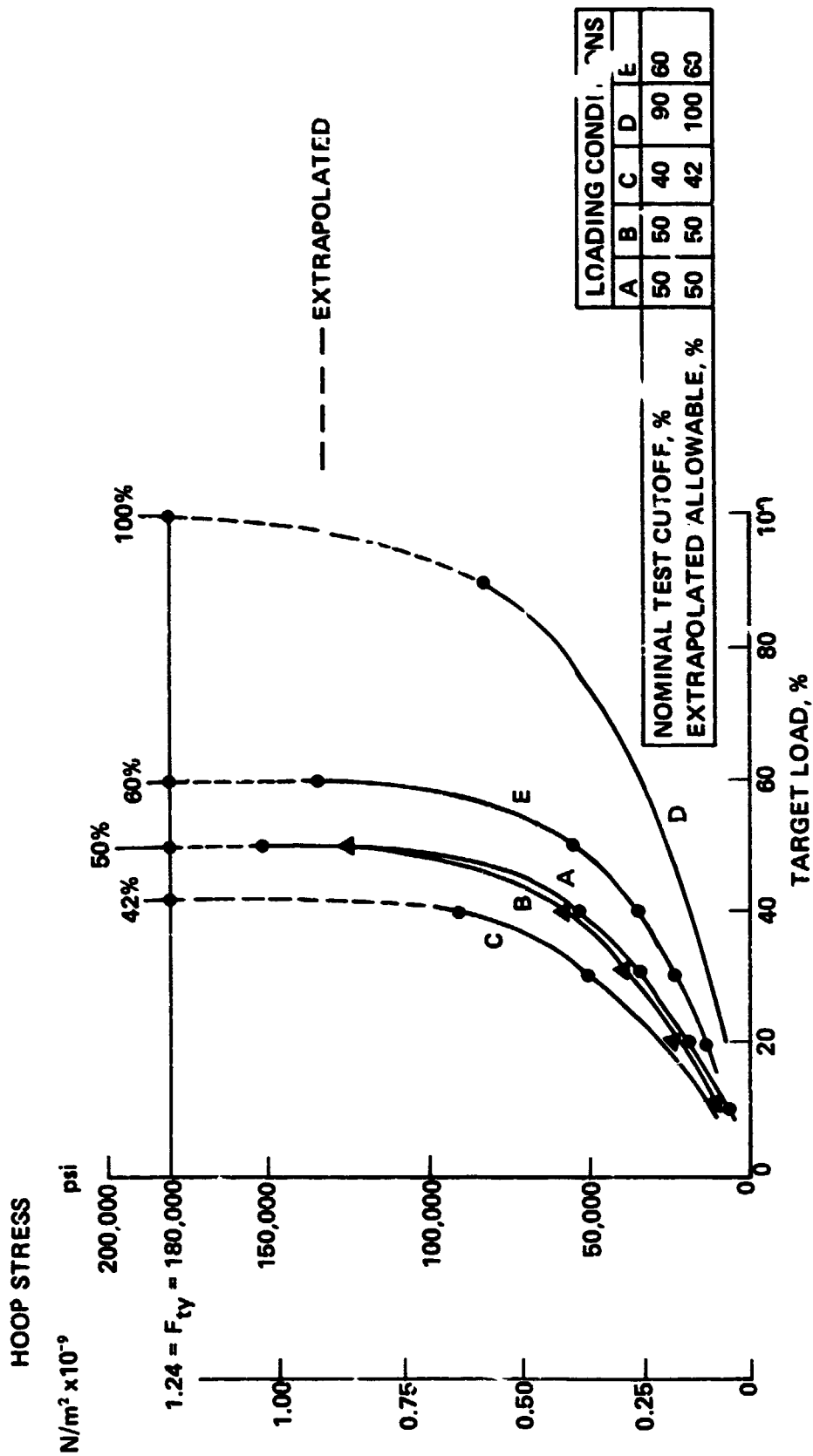


Figure 3.4-5 31-in. Case Center Segment Yield Strength Extrapolated from Static Test Results

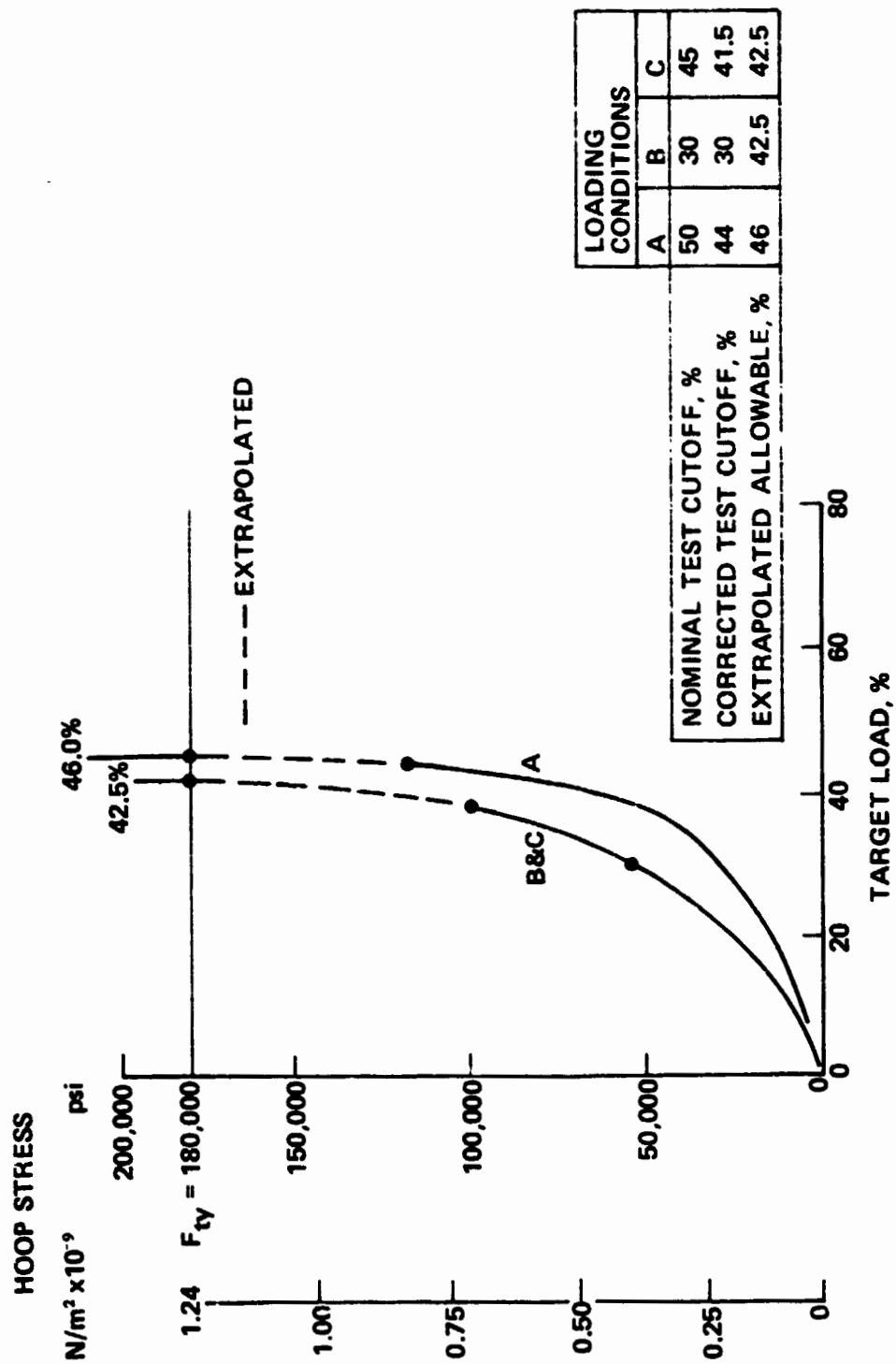


Figure 3.4-6 120-in. Case Center Segment Yield Strength Extrapolated from Static Test Results

The relative hoop bending strength between a 142-in. case and the subscale static test specimens is proportional to the thickness ratio squared and inversely proportional to the radius ratio. The net effect of considering these two ratios is a strength increase factor of 1.35 between the 142-in. case and the 120-in. test specimen. Similarly, a strength increase factor of 4.075 exists between the 142-in. case and the 31-in. test specimen; a strength increase factor of 8.26 exists between the 142-in. case and the 13-in. test specimen. The resultant strength increase factor is a combination of the 1.3 and the other factors listed in this paragraph.

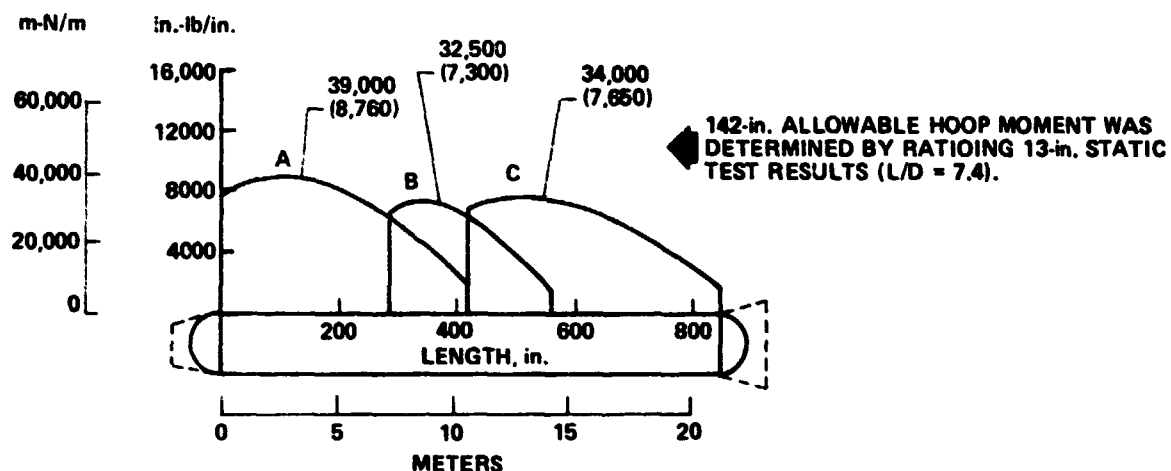
3.4.4 Allowables Converted to Hoop Bending Moments

Since the case static test conditions for all three subscale models tested had a varying included angle for the applied pressure load, a means of evaluating this effect needed to be determined. The method selected was to first plot allowable running load along the loaded length. Then the running load was multiplied by the radius and the moment coefficient corresponding to the included angle at each station to obtain an allowable running hoop moment.

The allowable hoop moment for the 142-in. diameter case of monolithic construction was determined using the factors discussed previously and the results obtained from the 13-in. static test results ($L/D = 7.4$) and the 31-in. static test results ($L/D = 5.5$). These allowables are presented on Figure 3.4-7. The peak allowable hoop moments, based on the 13-in. static test results, are 39,000 meter Newtons/meter (8760 in.-lb/in.) for Test condition A, 32,500 meter Newtons/meter (7,000 in.-lb/in.) for condition B, and 34,000 meter Newtons/meter (7650 in.-lb/in.) for condition C. The peak allowable hoop moments, based on the 31-in. static test results, are 42,500 meter Newtons/meter (9500 in.-lb/in.) for conditions A and B and 35,700 meter Newtons/meter (8020 in.-lb/in.) for condition C.

The allowables based on the 31 in. test specimen are higher than those based on the 12 in. specimen because of the lower value of L/D for the 31 in. specimen. Since the 120 in. specimen had an L/D of 7.0, it was decided to calculate weighted average allowables for a 142 in. monolithic case using the 13 in. and 31 in. values. The results are shown on Figure 3.4-8. The allowable hoop moment for a 142 in. segmented design is shown on the same figure.

ALLOWABLE HOOP MOMENT



ALLOWABLE HOOP MOMENT

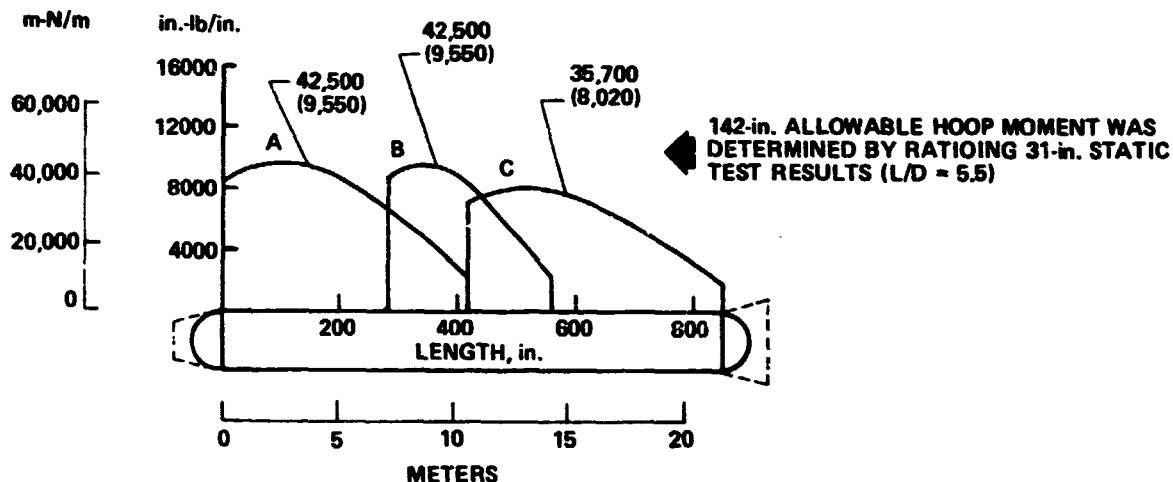
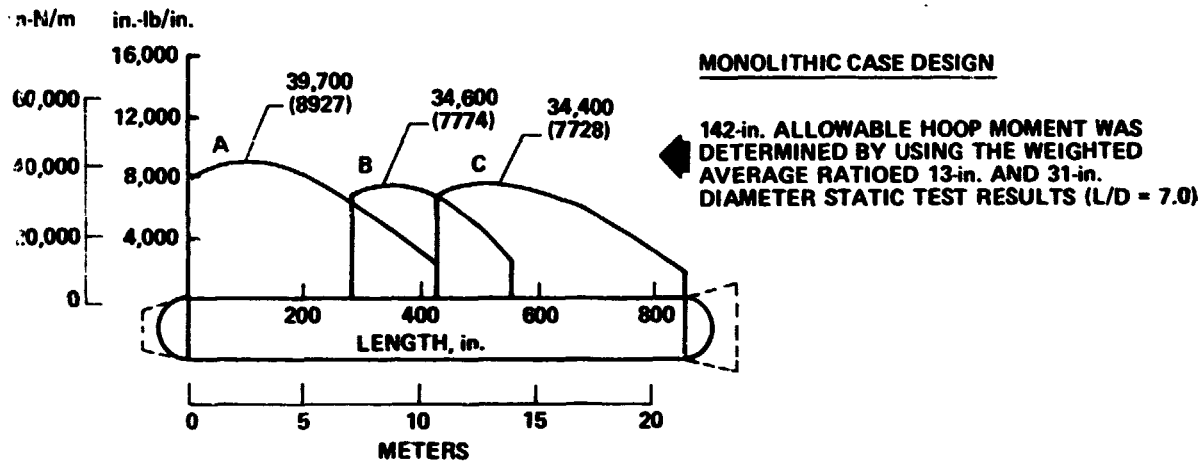


Figure 3.4-7 142-in. Case Hoop Bending Strength Determined for Monolithic Case

ALLOWABLE HOOP MOMENT



ALLOWABLE HOOP MOMENT

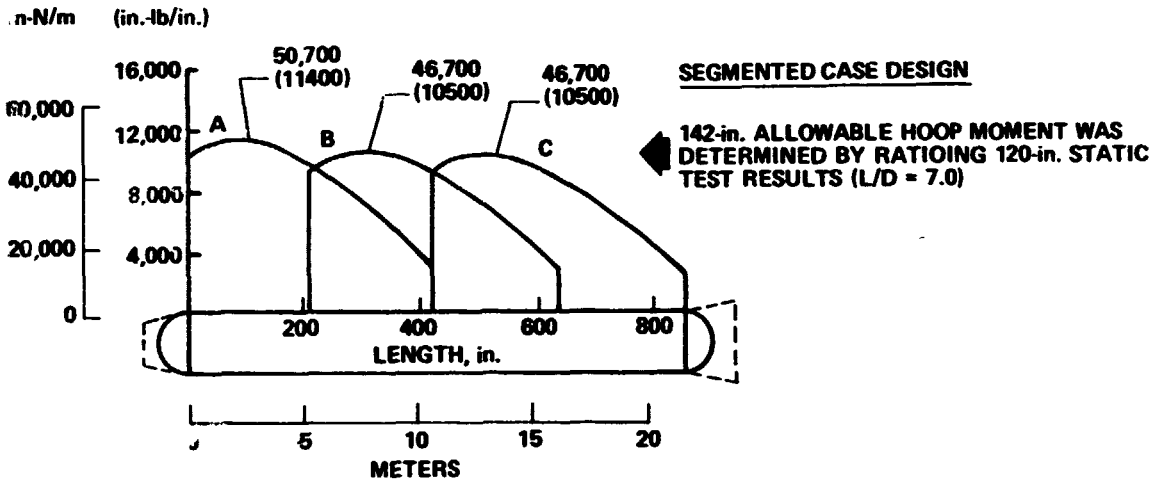


Figure 3.4-8 142-in. Case Hoop Bending Strength for Monolithic and Segmented Case Design

3.4.5 Conclusions

The summary presented in Figure 3.4-9 shows that the larger differences between the segmented and monolithic strengths occur for conditions B and C. This is apparently due to the fact that the help from the end bulkheads is not as great as for condition A. If the loading length for condition B on the monolithic specimens had been $L/2$ rather than $L/3$, the segmented design would have exhibited an even larger strength increase for condition B. The results presented here should be representative of the strength differences between the segmented and monolithic designs, assuming a 142 in. segmented frame strength equivalent to that of the 120 in. specimen. The weight of the segmented design would be somewhat greater than a monolithic case designed to the same MEOP. An approximate delta strength for equal weight designs is 25%. This magnitude of strength differential should be used by the SRM contractor in trading off fabrication methods and optimum design MEOP values.

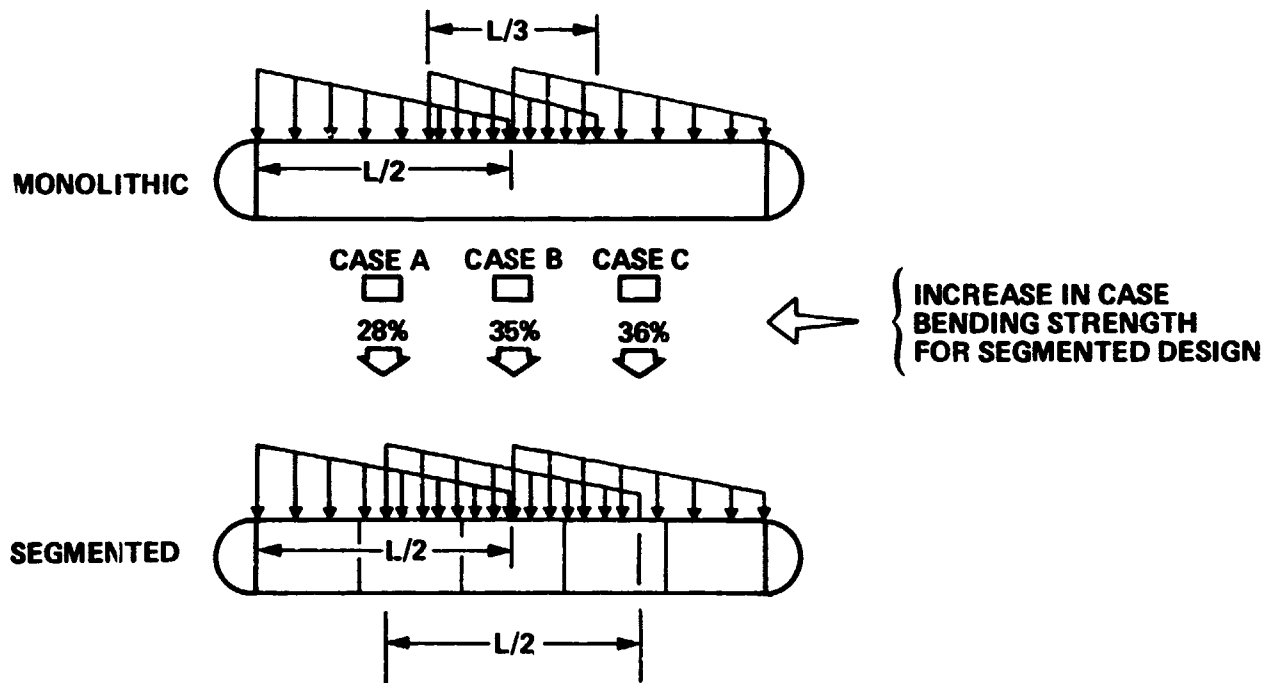


Figure 3.4-9 142-in. Segmented Design Appreciably Stronger Than Monolithic Design for a Given Value of MEOP

4.0 WATER IMPACT REQUIREMENTS DEFINITION

4.1 ATTRITION

A definition of water entry conditions compatible with a high confidence of successful SRB recovery involves modeling of many probabilistic parameters. Some of these parameters have nonlinear probability distribution functions, making simple techniques such as root-sum-square (rss) too conservative. In general, what is needed is a deterministic solution to a nondeterministic problem. The nondeterministic nature of structural strength (e.g., for a given load near the structural design limits sometimes failure will occur) can be accommodated by a random sampling technique like the so-called Monte Carlo method, which can be applied to any method of calculation involving random sampling. Monte Carlo also allows for interdependence of parameters and simultaneous perturbation of all parameters at randomly selected values. Because the technique is effective only for problems formulated in probabilistic terms, the SRB water impact problem must be modeled accordingly. The variables involved in formulating the water entry problem are shown in Figure 4.1-1.

Armed with the appropriate random number generators, the cumulative probability distribution of the input parameters, and functional relationships among the inputs, analysis of the behavior of the SRB for large numbers of water entries may be conducted. The results of the random trials can be tabulated to obtain the resultant probability distributions and these may then be statistically analyzed to determine the SRB damage for numerous impact velocities.

As used in this study, attrition is defined as the sinking of the SRB. This has been assumed to occur when a 20% overload ruptures either of the forward two case segments. Damage is defined as an overload that renders components unsuitable for reuse. No repair beyond nominal refurbishment is considered in this study; thus component damage results in component attrition.

4.1.1 Environmental Parameters

The most critical parameters in the attrition analysis are environmental factors. The water parameter data were obtained primarily from NASA TM-X-64589 and its Addendum *Water Entry and Recovery*

θ_1	IMPACT ATTITUDE ANGLE
\vec{V}_I	IMPACT VELOCITY
V_V	VERTICAL COMPONENT OF V_I
V_H	HORIZONTAL COMPONENT OF V_I
\vec{V}_{TD}	TERMINAL DESCENT VELOCITY
\vec{V}_W	WIND VELOCITY
\vec{V}_{PT}	PARACHUTE TRANSLATION VELOCITY DUE TO LIFT
\vec{V}_{PO}	PARACHUTE ROTATIONAL VELOCITY AT THE NOZZLE
\vec{V}_{WM}	WAVE MASS VELOCITY
\vec{V}_{CUR}	CURRENT VELOCITY
θ_1	OSCILLATION ANGLE OF PARACHUTE
θ_2	OSCILLATION ANGLE OF SRB ABOUT PARACHUTE ϵ
ω_1	ROTATION RATE OF PARACHUTE ABOUT VERTICAL
ω_2	ROTATION RATE OF SRB ABOUT PARACHUTE ϵ
h	WAVE HEIGHT
ψ	WAVE MASS DIRECTION ANGLE
θ_{WM}	WAVE DIRECTION ANGLE
θ_{CUR}	CURRENT DIRECTION ANGLE
ψ_1, ψ_2	AZIMUTH OF PROJECTIONS OF PARACHUTE, SRB ϵ
$\vec{D}\vec{V}_R$	RETROMOTOR ΔV (IF APPLICABLE)
θ_R	RETROTHRUST MISALIGNMENT IN IMPACT PLANE (TO SRB ϵ)

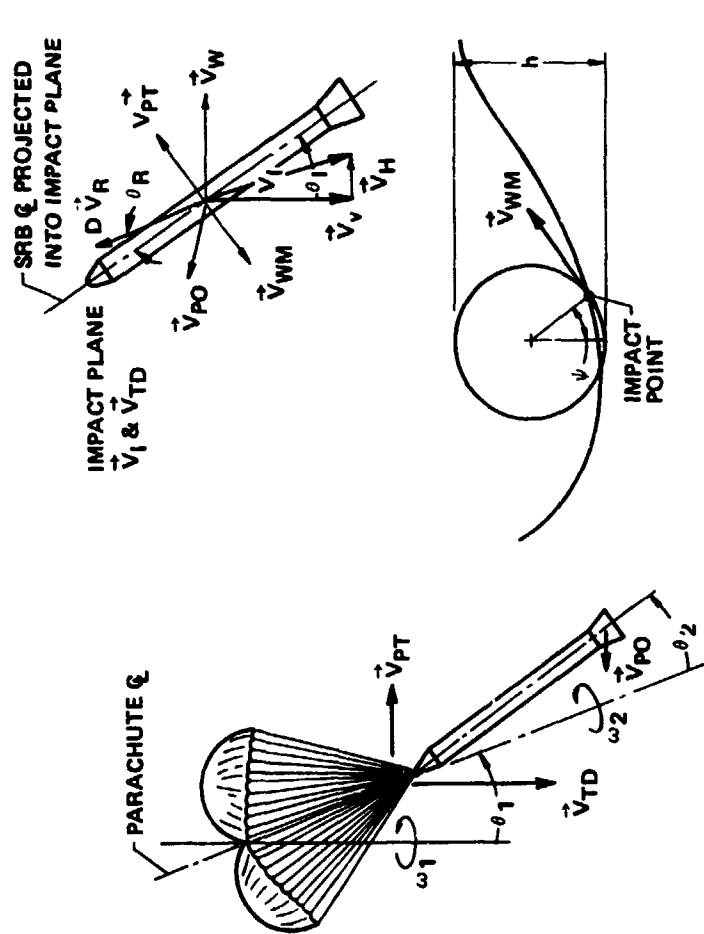


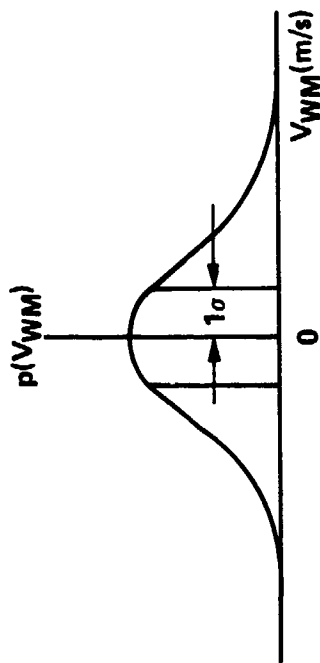
Figure 4.1-1 Impact Related Variables Defined by Environmental and State Vector Uncertainties

Conditions. The water mass velocity distribution (Figure 4.1-2) was derived from the wind wave height power spectrum. The result is a Gaussian distribution for water mass velocity with a zero mean and a standard deviation equal to $0.0646 V_o$, where V_o is the velocity of the reference wind at 19.3-m altitude. The direction of the water mass velocity vector was assumed to be randomly oriented at the impact point. Thus, the angle distribution (Figure 4.1-3) is described by a uniform distribution in the vertical plane. The plane of water movement is oriented in the wave direction which is correlated to the wind direction. No data were available for the shape of the probability distribution for the wave direction angle (azimuth of wave direction). It was assumed triangular (Figure 4.1-4) with the peak in the mean wind direction and with the distribution falling to zero at $\pm\pi/2$ rad from the wind direction.

In addition to the water mass velocity, water current has been simulated. NASA memo YA-25-73 described the current velocity as Gaussian (Figure 4.1-5) with mean of 1.286 m/s and standard deviation of 0.593 m/s. The direction of the current was assumed generally northerly and described by a uniform distribution (Figure 4.1-6) of azimuth angle in the northern quadrants ($\pm\pi/2$ rad from north).

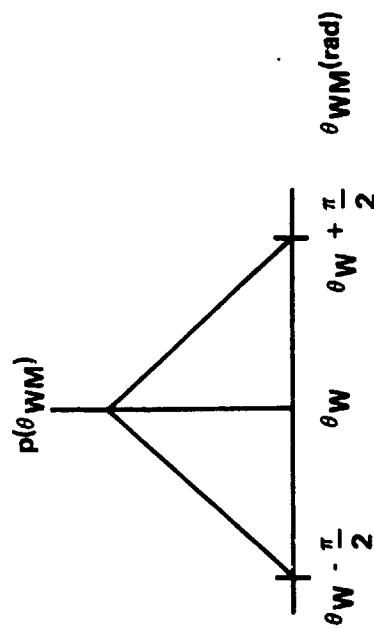
Wave height is calculated from the 19.3-m wind (TMX-64589, Figure 18.2) but is not used presently because its effect is contained within other dispersions. For a retro system, wave height will contribute to ignition altitude uncertainties. Present data are insufficient to quantitatively determine the effect of wave slope on aft end loads. However, we feel this phenomenon will contribute less than a 10% increase in these loads. Further testing in terms of wave height, wave period, and wave slope variation on SRB model drop tests will be required to accurately assess the sea state effect on aft end loads. It is expected that NASA drop tests at the Taylor Model Basin will develop these data on slapdown loads so that wave slope contributions can be incorporated in the attrition analysis.

Wind gust data were obtained primarily from memos written by and personal conversations with Dr. George Fichtl (MSFC-S&E-AERO-YA). These were used to develop TD&D parameters described in Section 4.1.2. Wind statistics for water entry were developed from one kilometer wind velocity statistics described in NASA memo YA-25-73. These statistics give the zonal and meridional wind components (mean and sigma) and the correlation coefficient between them for each month of the year (Table 4.1-1). The wind distributions at one kilometer altitude are thus described as correlated



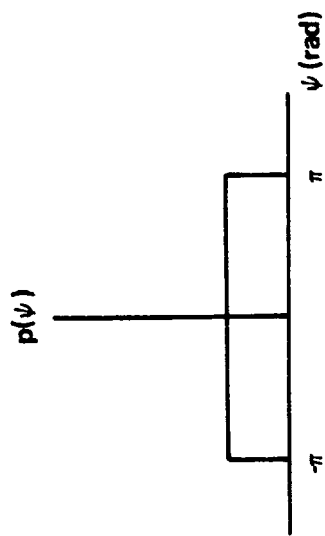
- $\sigma = 0.0646 \times \text{REFERENCE WIND } (V_0)$
AT 19.3 METERS
- MEAN = 0 fps

Figure 4.1-2 Water Mass Velocity



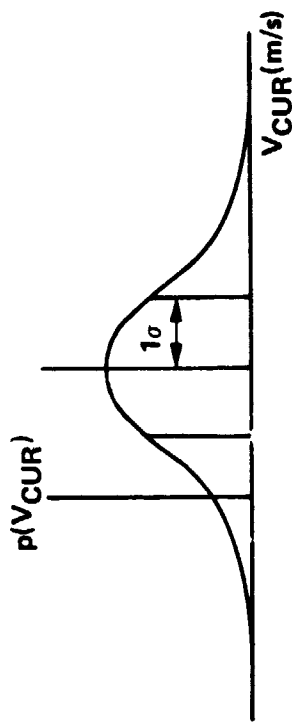
- MEAN IN WIND DIRECTION (θ_W)
- DECREASES LINEARLY TO ZERO AT $\theta_W \pm \frac{\pi}{2}$

Figure 4.1-4 Wave Direction



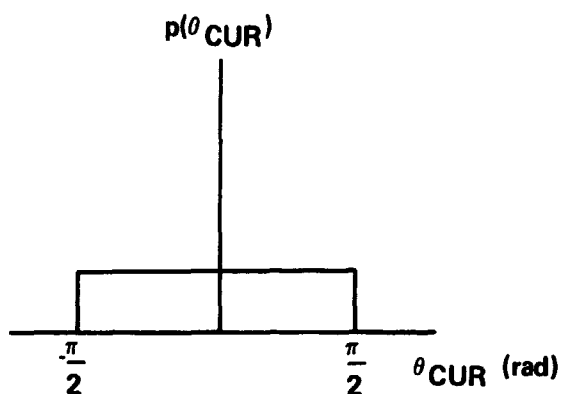
- UNIFORM IN VERTICAL PLANE
- VERTICAL PLANE ALIGNED WITH WAVE DIRECTION (θ_{WM})

Figure 4.1-3 Water Mass Direction



- MEAN AT 1.286 m/s
- $\sigma = 0.593 \text{ m/s}$

Figure 4.1-5 Water Current Velocity



• MEAN IN NORTHERLY DIRECTION

Figure 4.1-6 Water Current Direction

Table 4.1-1 One Kilometer Wind Statistics in SRB Recovery Zone

	\bar{u}	\bar{v}	s_u	s_v	r_{uv}
MONTH	METER SECOND ⁻¹				NONDIMENSIONAL
JANUARY	3.03	0.91	7.01	6.45	0.0080
FEBRUARY	3.65	2.35	7.26	6.54	-0.0520
MARCH	3.22	1.70	6.87	6.12	0.0142
APRIL	0.89	1.20	6.74	5.40	-0.0507
MAY	-0.71	0.90	5.24	4.26	0.1414
JUNE	0.22	1.83	4.97	3.83	0.2453
JULY	0.94	2.84	4.49	3.36	-0.0175
AUGUST	0.19	1.89	4.42	3.46	0.1323
SEPTEMBER	-2.06	0.40	5.87	5.26	0.2784
OCTOBER	-1.56	-1.42	5.89	5.04	0.2349
NOVEMBER	-0.32	-0.78	6.76	5.37	0.1805
DECEMBER	1.11	0.21	6.7	5.79	0.0314

NOTE: STATISTICS ARE FOR ZONAL (u) AND MERIDIONAL (v) WIND COMPONENTS AT 1 km ALTITUDE IN SRB RECOVERY ZONE: \bar{u} AND \bar{v} ARE MEAN VALUES; s_u AND s_v ARE STANDARD DEVIATIONS; r_{uv} IS THE CORRELATION COEFFICIENT BETWEEN u AND v.

bivariate Gaussian functions (Figure 4.1-7). The wind velocity at any lower altitude is calculated using equations in NASA memo YA-62-72. Of particular concern is the wind at parachute canopy height and the reference wind at 19.3 m (used for water mass velocity calculation). The former is used to define the major component of parachute horizontal velocity and is described in Section 4.1.2.

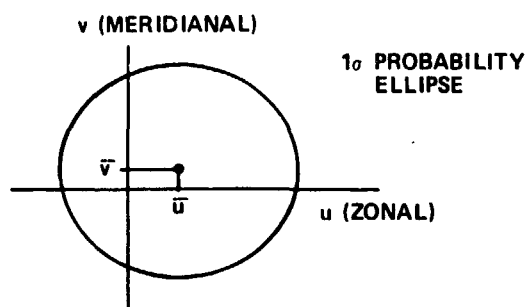
4.1.2 TD&D Parameters

The physical parachute/SRB system parameters used to define water impact conditions for load determination together with the environmental parameters are illustrated in Figure 4.1-1. While not all of these parameters make an equal contribution to the outcome, the mathematical model has been formulated sufficiently general to include their effects. The TD&D system parameter values used in the attrition analysis are all described by probability functions and are summarized in Table 4.1-2.

To define the limits on some of these parameters, a 6 DOF parachute deployment program was exercised. Dispersion data consisted of wind profiles from NASA TMX-64589 and simulated wind gusts as described in NASA memos YA-42-72, YA-62-72, and YA-9-73. From these runs it was determined that rotation rates (ω_1, ω_2) were negligible and that the hang angle, θ_2 , of the SRB has a maximum of 0.14 rad (8 deg). (The other hang angle, θ_1 , was combined with θ_2 .) The SRB motion is basically an harmonic oscillation at the end of the parachute lines. The motion was simulated by assuming as a probability function an arcsine distribution (Figure 4.1-8). The azimuth angles were combined into a single projected angle for the SRB (ψ_2). Because of the random entry orientation, this angle is described by a uniform distribution.

Three additional parachute parameters may be simulated. The prime parameter, which serves as the independent variable in all attrition results, is the terminal descent velocity, V_{TD} . This velocity designs the physical parachute system. It is simulated with a mean velocity and a Gaussian distribution (Figure 4.1-9) whose standard deviation is 5% of the mean. This value was determined from dispersions on parachute $C_D A$ and atmospheric density. Corroboration was obtained from velocity distributions developed in Apollo studies (TMX-2430).

Parachute translation due to lift (V_{PT}) and parachute rotational velocity at the nozzle (V_{p0}) were defined. V_{PT} was negligible in this study because of the use of ribbon chutes that have no trans-

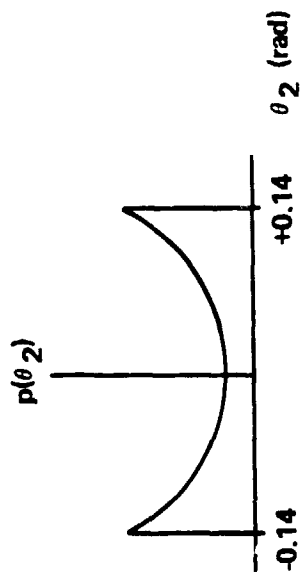


- SAMPLE BIVARIATE GAUSSIAN WIND FOR JANUARY
- MEAN VALUES: $\bar{u} = 3.03 \text{ m/s}$
 $\bar{v} = 0.91 \text{ m/s}$
- $\sigma_u = 7.01 \text{ m/s}$
- $\sigma_v = 6.45 \text{ m/s}$
- $\rho = 0.008$ (CORRELATION COEFFICIENT)

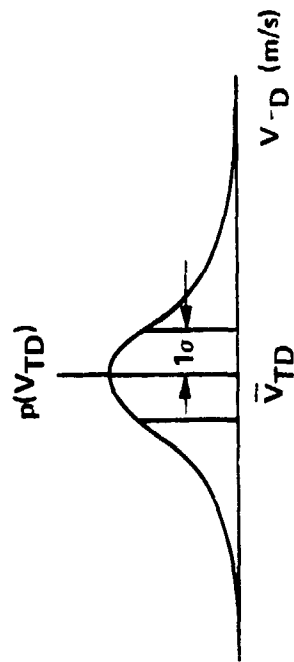
Figure 4.1-7 One Kilometer Wind Velocity Distribution

Table 4.1-2 TD&D Parameter Values Used in Attrition Analysis

SYM-BOL	DEFINITION	DISTRIBUTION AND VALUE
θ_1	HANG ANGLE-PARACHUTE Q_L TO VERTICAL	SET TO ZERO-INCORPORATED IN θ_2
θ_2	HANG ANGLE-SRB Q_L TO PARACHUTE Q_L	$\pm 0.14 \text{ rad } (\pm 8^\circ)$ ARCSINE DISTRIBUTION
ω_1	PARACHUTE ROTATION RATE ABOUT VERTICAL	DAMPS TO ZERO AT IMPACT ($<0.001 \text{ r/s}$)
ω_2	SRB ROTATION RATE ABOUT PARACHUTE Q_L	
ψ_1	PARACHUTE Q_L PROJECTED AZIMUTH	SET TO ZERO - INCORPORATED IN ψ_2
ψ_2	SRB Q_L PROJECTED AZIMUTH	UNIFORM DISTRIBUTION 0 TO $2\pi \text{ rad}$
V_{TD}	MEAN TERMINAL DESCENT (DESIGN) VELOCITY	GAUSSIAN WITH $\sigma = 0.05 \bar{V}_{TD}$
V_{PT}	PARACHUTE TRANSLATION VELOCITY DUE TO LIFT	SET TO ZERO - RIBBON CHUTES
V_{PO}	NOZZLE TANGENTIAL VELOCITY DUE TO ROTATION	SET TO ZERO ($<0.01 \text{ m/s}$ AT IMPACT)
DV_R	RETROMOTOR ΔV (IF APPLICABLE)	GAUSSIAN-MEAN AND SIGMA ARE CONFIGURATION-DEPENDENT
θ_R	RETROTHRUST VECTOR MISALIGNMENT (TO SRB Q_L)	UNIFORM-LIMITS ARE CONFIGURATION-DEPENDENT.



- HARMONIC OSCILLATION ASSUMED
- INTEGRAL OF $p(\theta_2)$ IS ARCSINE FUNCTION



- MEAN AT SELECTED DESCENT VELOCITIES (\bar{V}_{TD})
- $\sigma = 0.05 \bar{V}_{TD}$

Figure 4.1-8 Parachute Hang Angle

Figure 4.1-9 Terminal Descent Velocity

lational lift. The nozzle tangential velocity was negligible because of the negligible rotational rates.

For hybrid systems, parameters must be added to account for retro-motor dispersions. For simplification, retro dispersions are assumed to occur in the impact plane with retrothrust at an angle θ_R (uniform distribution) from the SRB centerline. The delta velocity caused by retrothrust, DV_R , is described as a Gaussian distribution with mean and sigma as inputs. These parameters are both configuration-dependent.

4.1.3 Monte Carlo Computer Model

The Monte Carlo water entry model is defined in terms of the parameters previously described. The Monte Carlo analysis consists of randomly selecting parameters from their respective probability distributions, vectorially combining them at the water entry point, and determining impact velocity and angle distributions that define the entry loading conditions on the SRB. All of the probability distributions described in the previous sections are written into the model but may easily be changed to other distributions if required.

The macrologic for the computer model is illustrated in Figure 4.1-10. Figure 4.1-11 shows the process by which random number generators (seeded by clock time) are used to select environmental and physical parameters from their cumulative probability distributions. Each input parameter is selected using a different random number to assure a realistic unbiased simulation. The parameters are vectorially combined using 3-D kinematic equations to obtain the vertical (V_V) and horizontal (V_H) components of the impact velocity. The impact attitude (θ_I) is the angle between vertical and the projection of the SRB centerline into the impact (V_V, V_H) plane. One output of the simulation is the probability distributions for V_V , V_H , and θ_I . These distributions allow calculation of impact statistics such as the mean and standard deviation for each parameter.

Five structural components are considered in the load analysis: forward skirt, aft skirt, nozzle (with and without extension), SRB case, and the aft dome. Derivation of the loads in terms of V_V , V_H , and θ_I is described in Section 4.2. The model uses linear table lookup to perform trivariate interpolation for the component loads (Figure 4.1-12). The structural strength, a nondetermin-

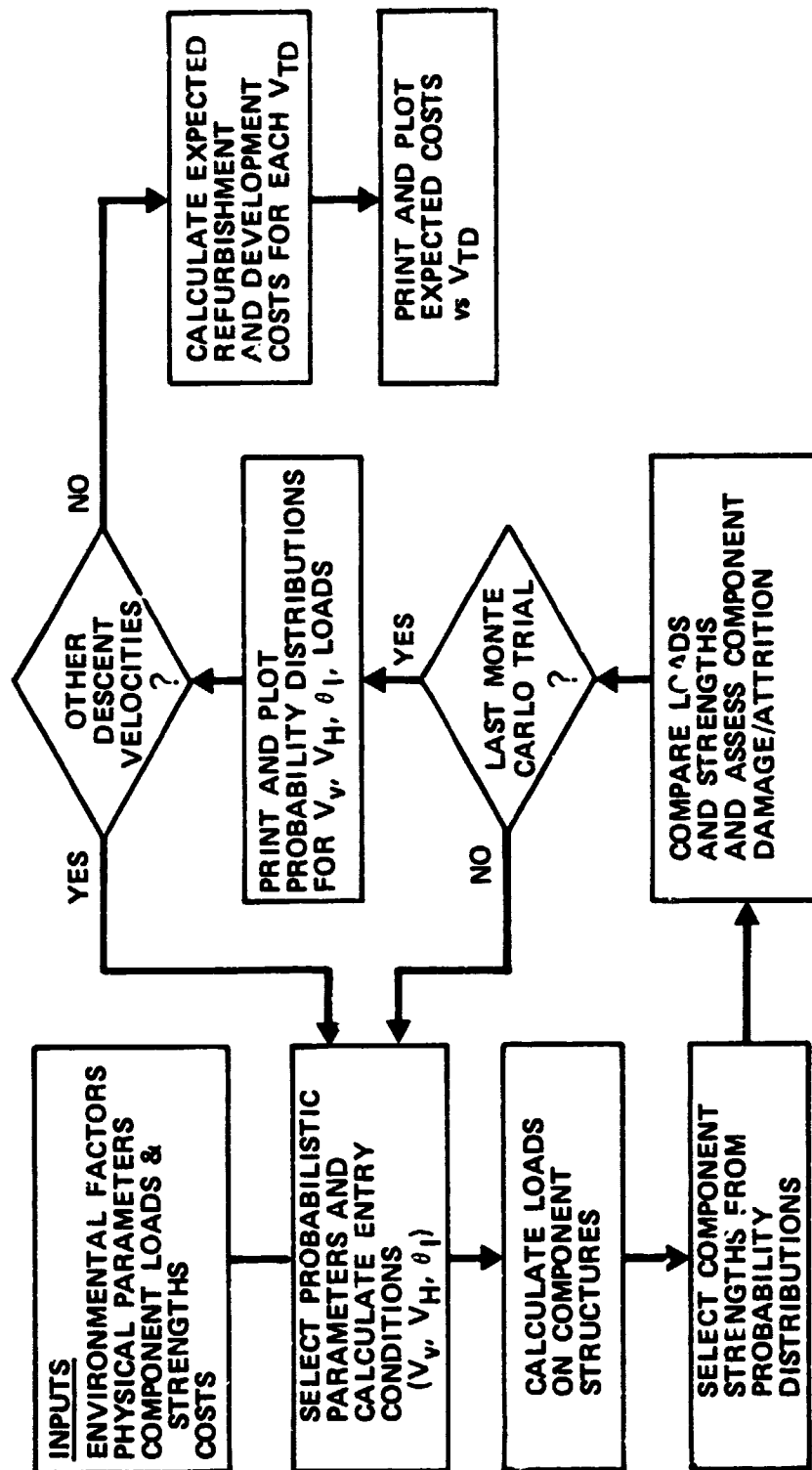


Figure 4.1-10 Monte Carlo Analysis Macrologic

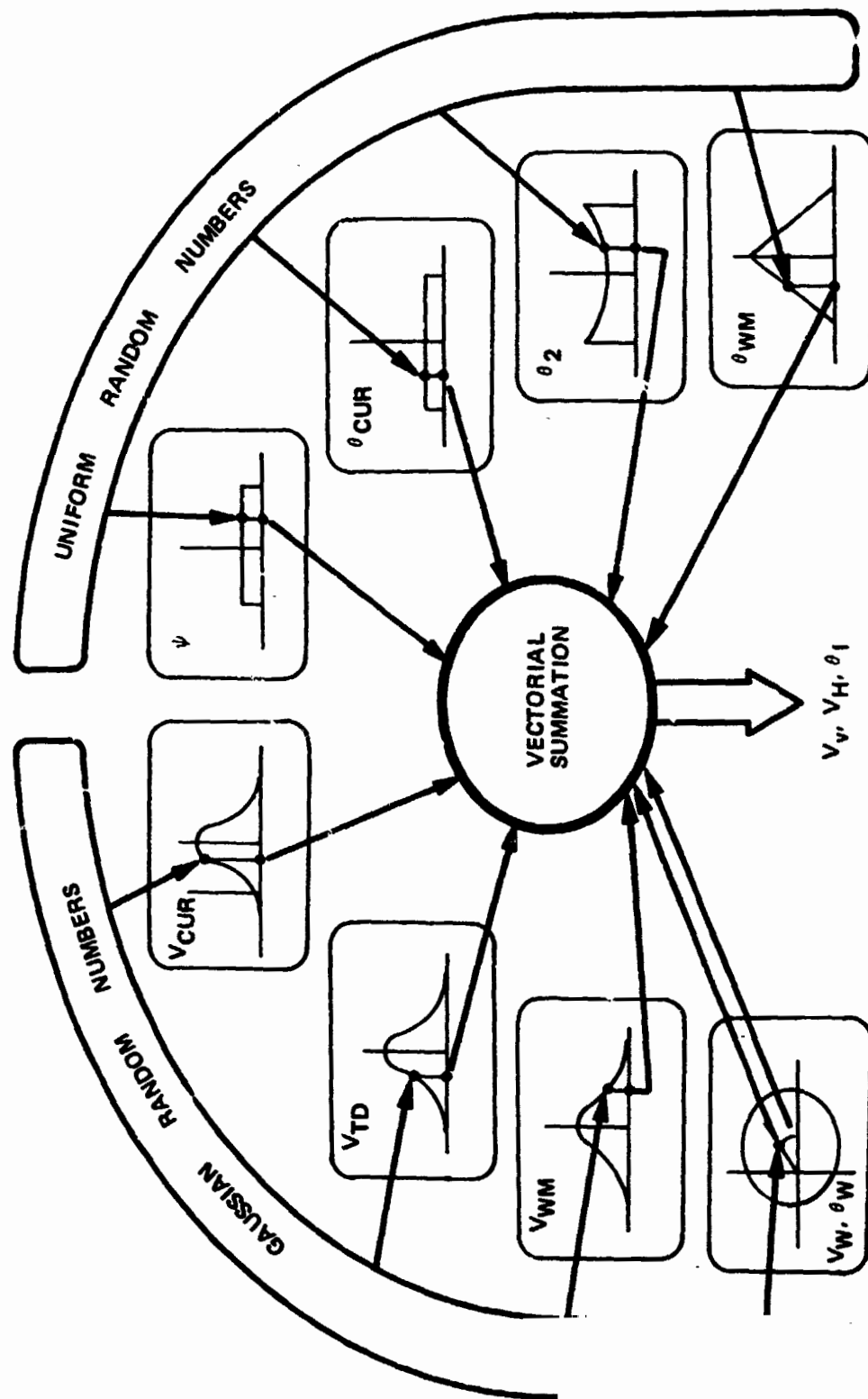


Figure 4.1-11 Independent Random Numbers Generate Impact Conditions

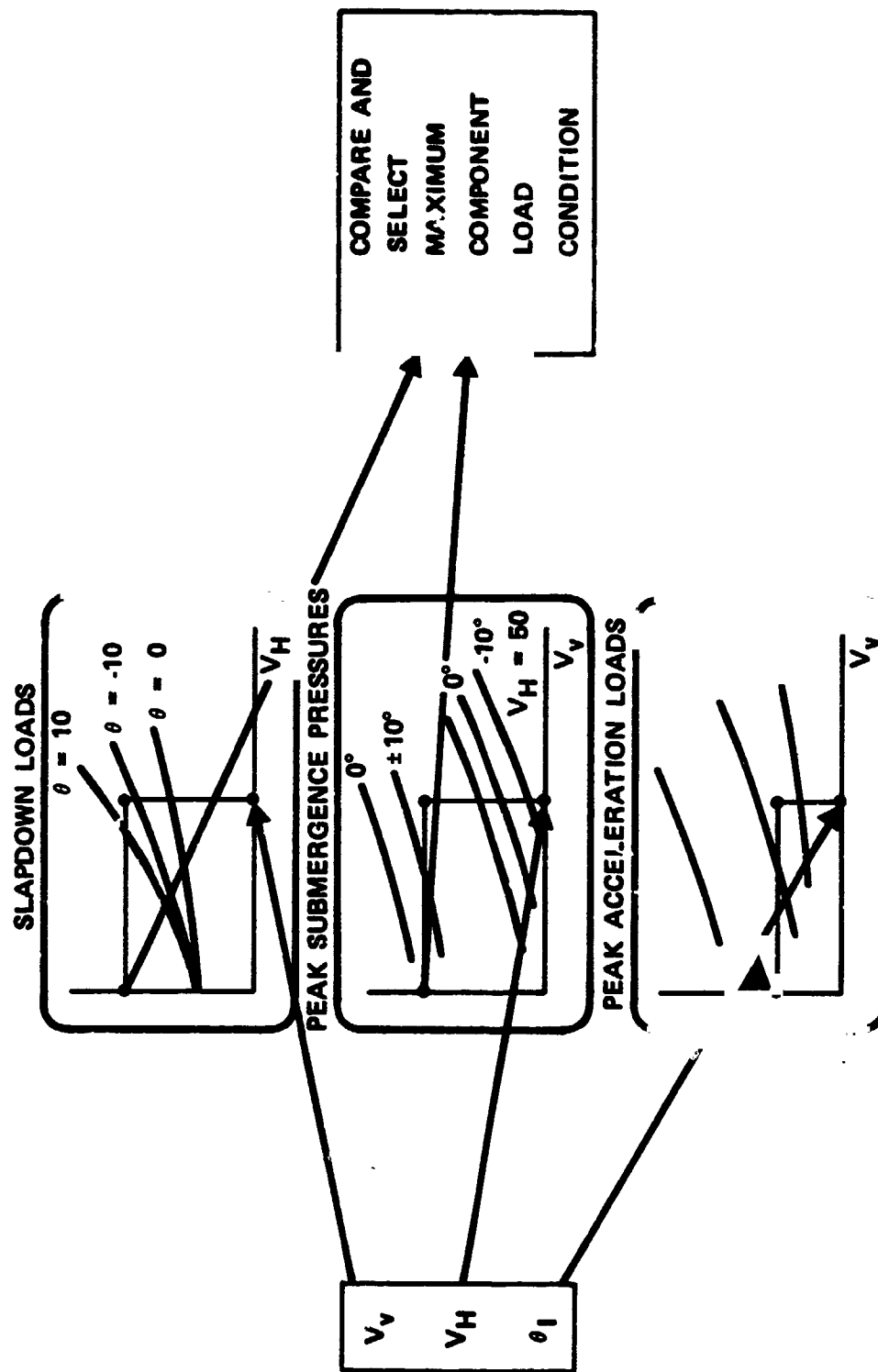


Figure 4.1-12 SRB Component Loads Determined from Impact Conditions

istic quantity, is determined by random selection from the component strength distributions described in Section 4.3. Except for the SRB case, component attrition occurs when the load exceeds the strength. The SRB case is assumed to rupture and sink when a 20% overload occurs in the forward two case segments during SRB slapdown. Attrition of two case segments is assumed for overloads less than 20%. The load to strength comparison is summarized by Figure 4.1-13.

This procedure determines attrition for one randomly selected set of parameters. To obtain reliable statistics, many sets of parameters must be run. The model has storage capability for 2000 Monte Carlo trials and is easily changed if more are desired. Presently, 1000 trials have been found sufficient to create reproducible results. The entire Monte Carlo simulation is run for each terminal descent velocity (V_{TD}) to be examined.

The outcome (attrition) for each component is accumulated over the total number of trials and used to formulate the attrition statistics for each V_{TD} .

Refurbishment and component replacement costs serve as a basis of a simplified cost estimate procedure. When component refurbishment costs are multiplied by attrition probabilities and summed over all components, a resultant SRB refurbishment cost curve is obtained as a function of terminal descent velocity.

4.1.4 Water Entry Conditions

The Monte Carlo water entry computer program has been exercised to determine water entry conditions. The results are presented in terms of cumulative probability distributions for the three impact parameters-- V_V , V_H , and θ_I . These distributions are presented in Figures 4.1-14 through 4.1-16 for terminal descent velocities (V_{TD}) of 12.2, 21.3, 30.5, and 40 m/s (40, 70, 100, and 130 fps). Since horizontal velocity and impact angle are independent of V_{TD} , their distributions will apply to all vertical velocities. The vertical velocity, V_V , is basically the sum of the 5% V_{TD} dispersion and the vertical water mass velocity. The horizontal velocity, V_H , includes the effects of wind, water current, and horizontal water mass velocity. The impact angle distribution results from the harmonic oscillation of the parachute/SRB and is an arcsine function with zero mean and limits of ± 0.14 rad (8 deg). Impact angle distributions were determined from 6 DOF simulations of the parachute/SRB system in the presence of surface winds.

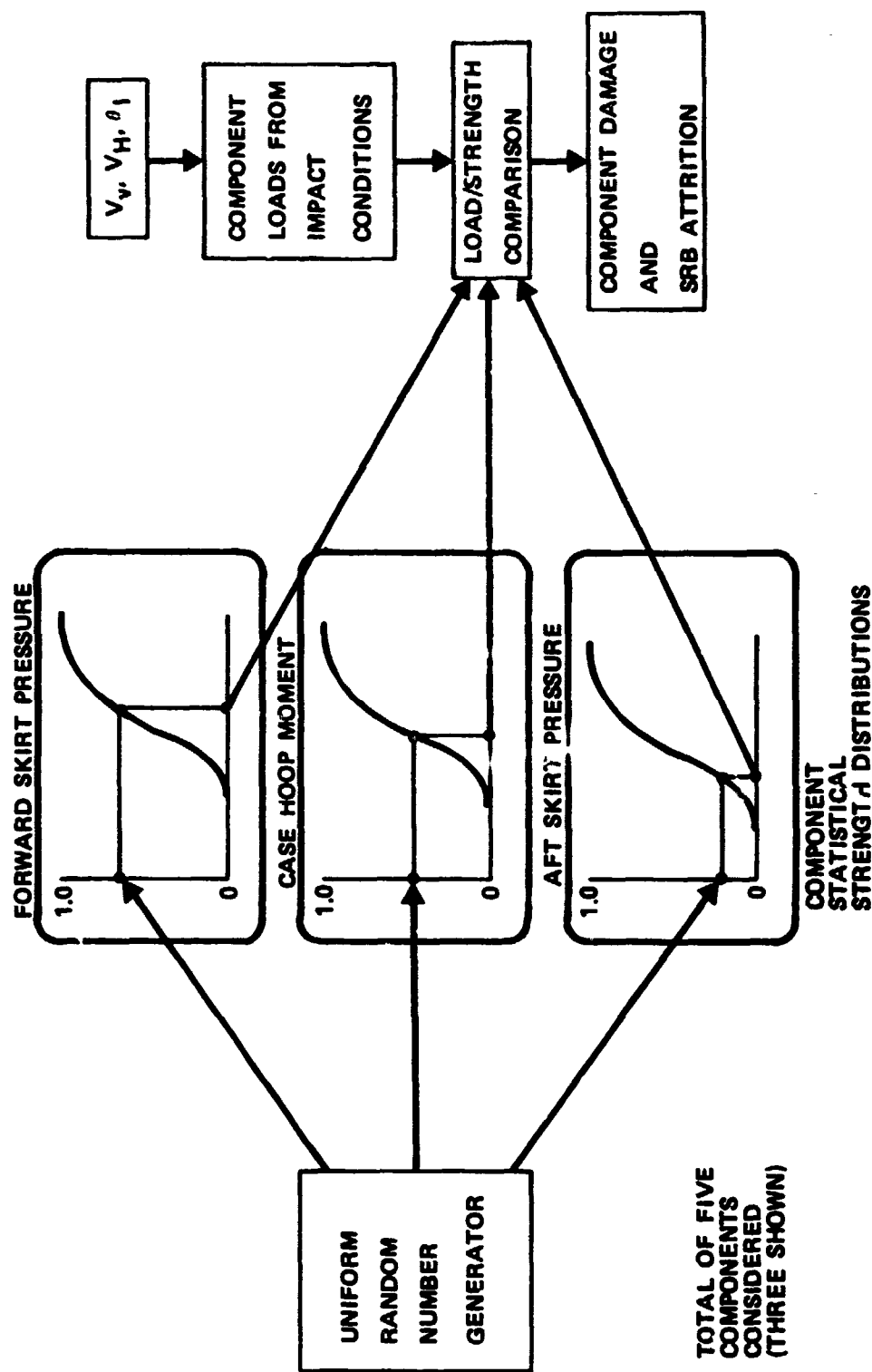


Figure 4.1-13 Damage Assessment Compares Impact Loads with Randomly Selected Component Strengths

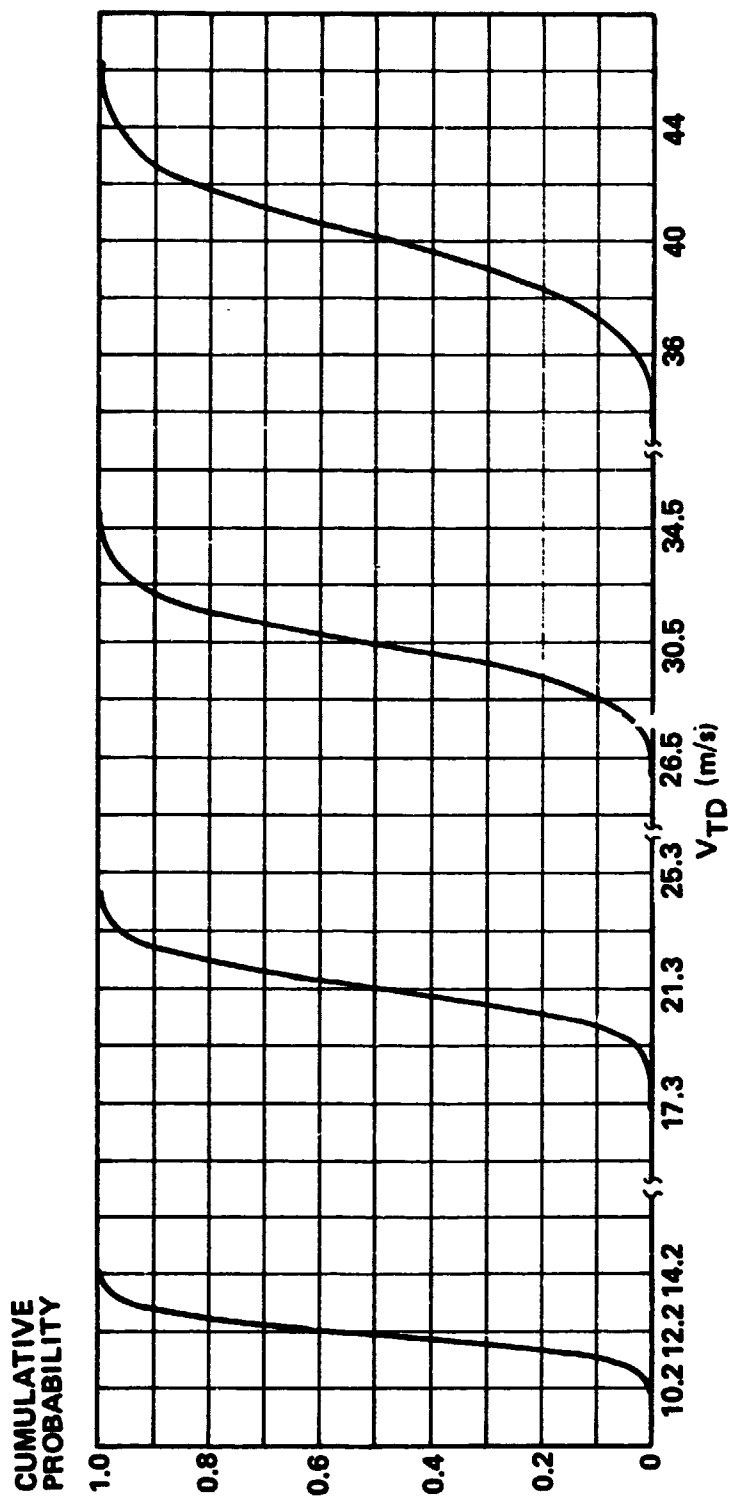


Figure 4.1-14 Cumulative Probability of Vertical Impact Velocity
 V_v (m/s) for $V_{TD} = 12.2, 21.3, 30.5, 40$ m/s

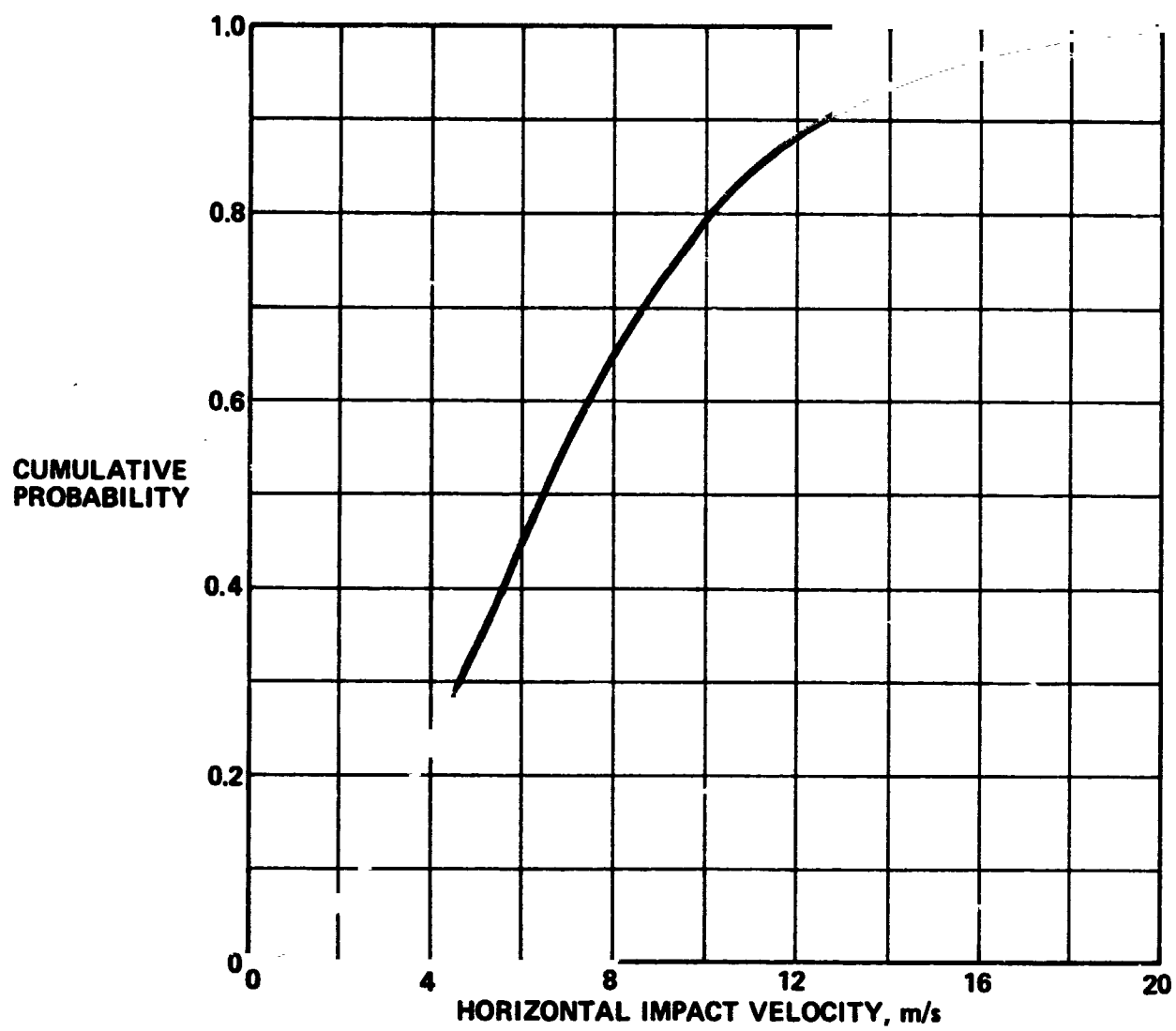


Figure 4.1-15 Cumulative Probability of Horizontal Impact Velocity, V_H

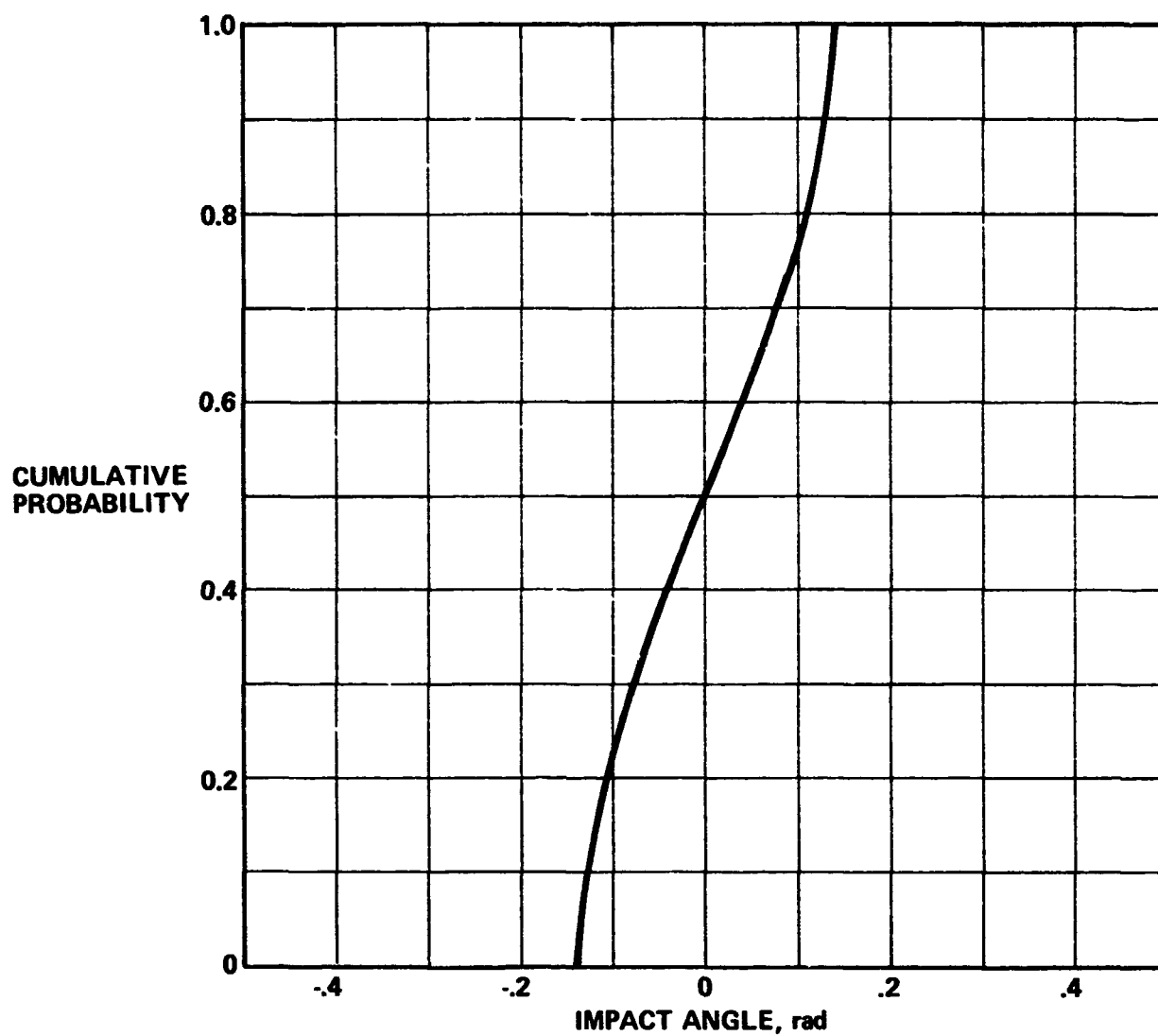


Figure 4.1-16 Cumulative Probability of Impact Angle, θ_I

4.2 WATER IMPACT LOADS ANALYSIS

This section discusses SRB structural loads resulting from a tail-first water impact. The SRB, attached to the parachute recovery system, impacts the water at a specified nominal vertical velocity. Because of existing wind conditions, the SRB also has a horizontal velocity component and an angular position at time of impact. In addition, the water surface may be in any condition from calm to very rough.

The SRB is essentially a cylindrical shell closed at the top, with an open nozzle at the bottom and a skirt structure that extends aft from the cylindrical body. This aft end presents a complicated structure that impacts and penetrates down into the water. After impact, water rushes up into the nozzle and aft skirt enclosure, and through the nozzle throat into the interior of the cylindrical shell.

Analytic tools are not yet available to accurately predict time histories of pressures and resulting loads throughout the structure for such a complex loading phenomena. Prediction of peak loads must rely heavily upon experimental data. Loads presented in this report are based on the latest applicable testing results.

It is important to keep in mind several facts regarding the applicability of the test results to predict SRB loads:

- 1) Tests have not been pressure-scaled or temperature-scaled to give realistic case internal pressure relationships. These factors will affect peak body accelerations as well as peak penetration.
- 2) In the present recovery procedure, the parachute remains attached until three to five seconds after impact to reduce initial slapdown loads. The effect of the parachute on SRB motion and loads after impact has not been considered in the tests to date.
- 3) Testing to date has been in calm waters; effects of waves or wave motion have not been considered.
- 4) Most test data available are in the range of 12.2 to 30.5 m/s (40 to 100 fps) vertical impact velocities. For components whose loads exhibit strong dependence on V_v , results have been extrapolated to 39.6 m/s (130 fps) by assuming that loads are proportional to dynamic pressure, i.e., a function of velocity squared.

The influence of all these factors on peak loads has not been completely assessed at this time. Because loads may change significantly when including these factors, additional testing and analyses including these effects must be accomplished before designs are finalized.

4.2.1 Critical Impact Loading Conditions

The SRB experiences several critical loading events during water entry. Figure 4.2-1 illustrates the four loading events considered. Immediately following initial contact with the water, the SRB experiences peak rigid body axial and lateral accelerations. At this time, only the aft end of the SRB has entered the water. The SRB continues into the water to its maximum submergence position, and then rebounds due to bouyant forces.

Five structural components are studied for survivability during the water impact event. These include the SRB case, the forward skirt, the nozzle, the aft dome, and the aft skirt. The baseline configuration presumes the nozzle extension has been jettisoned before water impact. Loads are presented both with and without the nozzle extension.

The entire aft end (nozzle, dome, skirt) experiences peak loadings at time of peak rigid body accelerations. These loads increase with increasing values of vertical and/or horizontal impact velocities. The case structure loads are not important for low vertical impact velocities, but may become critical for values greater than 30.5 m/s (100 fps). Forward skirt loads are low at this time.

Initial slapdown occurs as a result of appreciable horizontal impact velocities. Following impact, the SRB pitches over as it plows into the water. Peak loads may occur both in the SRB case and on the forward skirt. For low values of horizontal impact velocity, initial slapdown loads are low.

The SRB case may experience critical hydrostatic external pressure loads at maximum submergence for high vertical and very low horizontal impact velocities.

Secondary slapdown occurs during rebound from the maximum submergence position. All tests indicate that in no case does the SRB leave the water during rebound. In general, secondary slapdown loads are significant for low V_H (when initial slapdown loads are low), and are relatively low for high V_H (when initial slapdown loads are high).

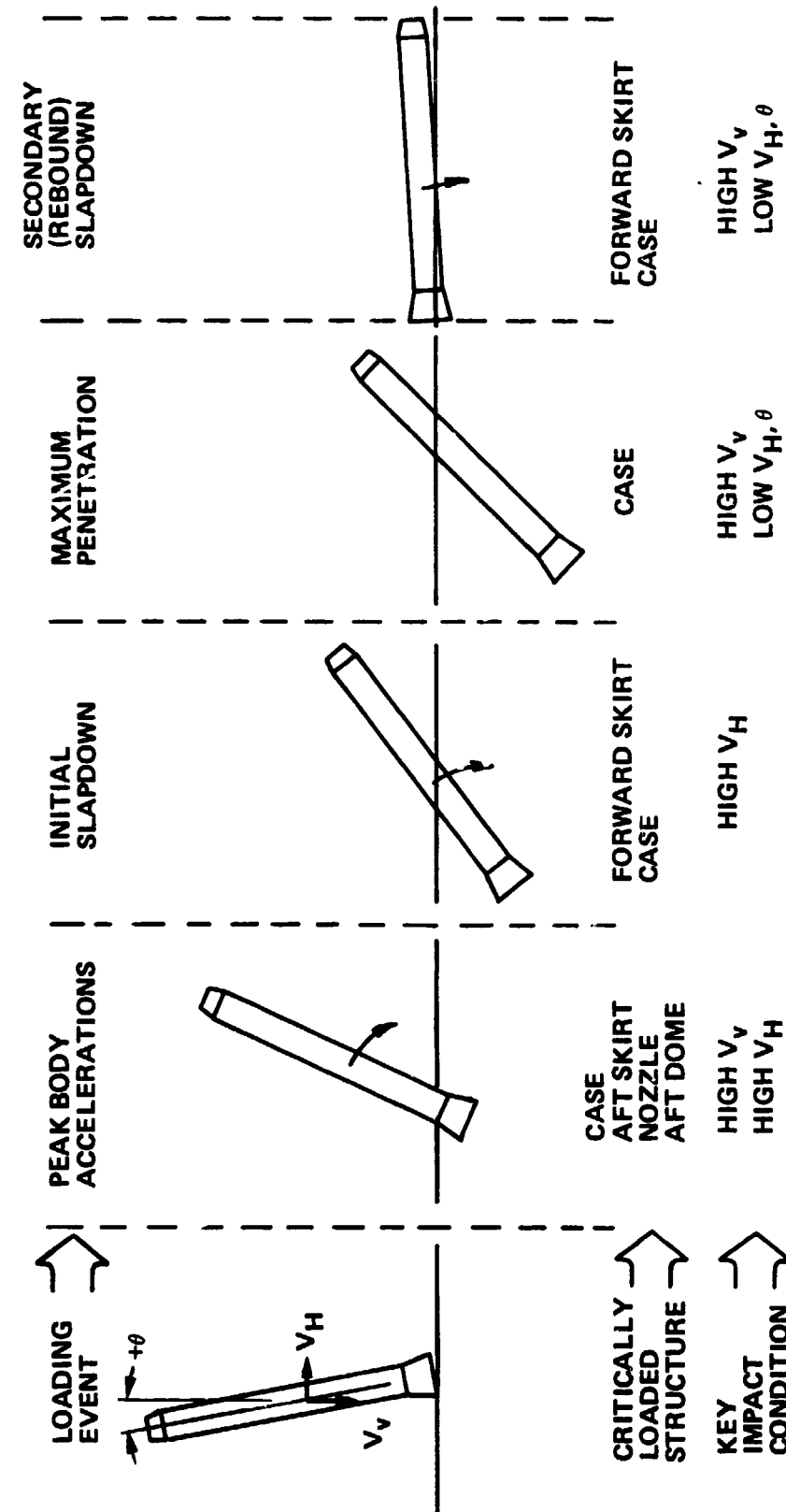


Figure 4.2-1 Critical Loads Vary During Impact Sequence

The effect of impact angle (θ) varies with the resultant velocity vector angle for all loading conditions, and can cause significant changes in peak loadings.

4.2.2 Impact Conditions Using Monte Carlo Analyses

The Monte Carlo analysis described in Section 4.1 combines several input parameters to obtain sets of water impact conditions. One output of this analysis is a probability distribution in terms of vertical impact velocity V_V , horizontal impact velocity V_H , and impact angle θ . A total of 1000 cases of impact conditions are generated by the Monte Carlo attrition analysis for each nominal vertical impact velocity considered.

Results of this analysis are presented in Figure 4.2-2. Significant outputs, which serve as guides in determining values and limits to test impact conditions are:

- 1) the mean horizontal impact velocity is high, about 7 m/s (23 fps); the range is from 0 to 22.9 m/s (75 fps).
- 2) the impact angle is low, with values expected to be less than ± 0.14 rad (± 8 deg); the nominal value is 0 radians.

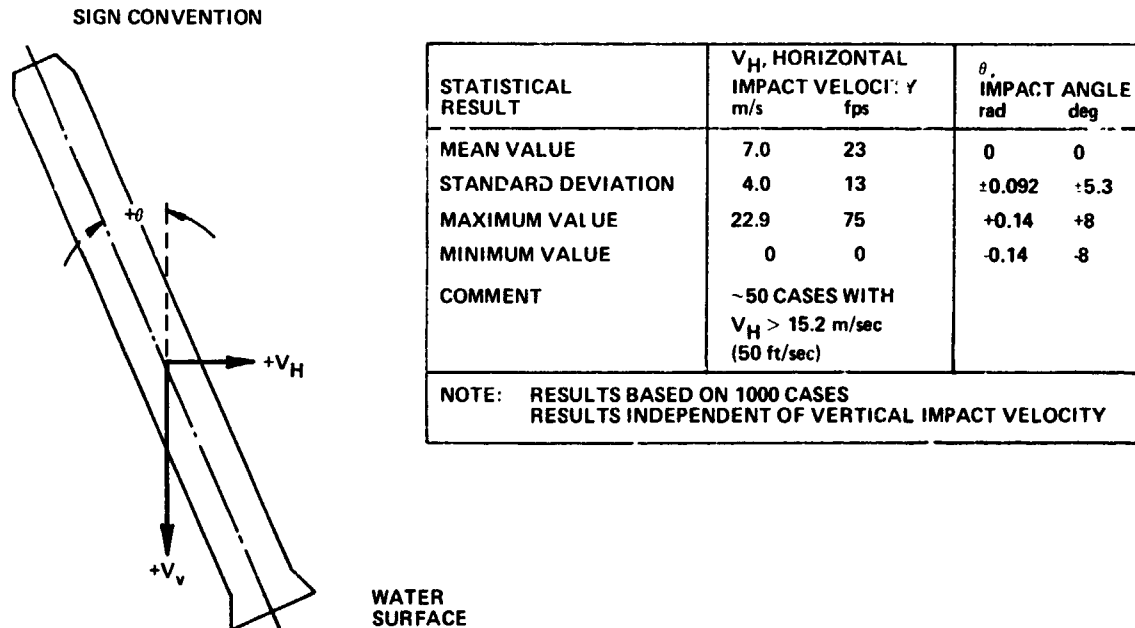


Figure 4.2-2 Monte Carlo Analysis Predicts High V_H and Low Impact θ

The presence of a high mean V_H means that even with a recovery system that could achieve a very low value of V_V , the SRB would still impact the water at nominally 7 m/s (23 fps) horizontally.

4.2.3 Scale Test Models

To predict SRB structural loads during the water impact event, extensive testing programs have been conducted using instrumented scaled models. To construct these models, Froude scaling has been used for mass distributions, moments of inertia, and lengths. Test impact conditions for vertical and horizontal velocities are also based on Froude scaling. Figure 4.2-3 shows these relationships. Scale model tests, as indicated on the same figure, have been performed both by MMC and by NASA to obtain acceleration, pressure, and strain gage time histories. High speed photographic coverage was used to obtain trajectory information, penetration characteristics, and comparisons with instrumented results.

The 8 inch diameter MMC model has tail configurations with straight and canted nozzles. Its aft end configuration closely resembles that of the current SRB baseline. No horizontal velocities were included in these tests.

FROUDE NUMBER $\frac{V^2}{gL}$	
PARAMETER	FROUDE SCALING
LENGTH	$L_M = K L_p$
VELOCITY	$V_M = \sqrt{K} V_p$
WEIGHT	$W_M = K^3 W_p$
PRESSURE	$P_M = K P_p$
FORCE	$F_M = K^3 F_p$
MOMENT	$M_M = K^4 M_p$
TIME	$T_M = \sqrt{K} T_p$
WHERE $K = \frac{\text{MODEL DIAMETER}}{142 \text{ in.}}$ SUBSCRIPT M = MODEL p = FULL SCALE (142 in. SRB)	

SOURCE OF WATER IMPACT LOADS DATA			
A) WATER IMPACT TESTS (BASED UPON NONCURRENT CONFIGURATIONS)			
SOURCE	MODEL DIAMETER	K, SCALE FACTOR	REPORT REFERENCES
MMC	8 in.	0.0563	MMC 880-1001, 6/72
NASA	6.5 in.	0.0468	SB E-ASTN-ADL MEMO SB E-ASTN-ADL (72-76) 8/72 SB E-ASTN-DIR (73-41), 2/73
NASA	12.5 in.	0.0880	SB E-ASTN-DIR (73-113), 4/73
NASA	120 in.	0.845	SB E-ASTN-DIR (73-114), 4/73
B) 142 in. SRB LOADS DATA: NASA SRB QUARTERLY REVIEW, 8/1/73			

Figure 4.2-3 Froude Scaling Relationships Used on Test Models

Extensive NASA tests have been conducted on 16.5, 31.7 and 30.5 cm (6.5, 12.5, and 120-inch diameter) models having a variety of aft end configurations with varying degrees of similarity with the current SRB baseline configuration. The 120-inch test model is actually a Titan III SRM. Test data obtained from this model are especially significant since it is nearly a full scale model.

Horizontal velocity test data is scarce, and recently completed NASA testing emphasized this parameter on 31.7 cm (12.5 inch) models using the current baseline configuration. These data have not been published.

The NASA SRB quarterly review (6/1/73) contains detailed pressure loadings on the aft dome, aft skirt, and nozzle along with slapdown loading information as functions of horizontal impact velocity. Most of these data are not available in any previous test reports, and are the only source for such water impact loads information.

Froude scaling has been assumed to apply when interpreting test results to obtain full scale results. The NASA 12.5-inch model has been tested several times using a variety of aft end conditions. The first 12.5-inch model was constructed by Froude-scaling the 120-inch model. This permitted a direct comparison of test results for models with different scale factors to assess the adequacy of Froude scaling. As reported in the NASA SRB quarterly review (6/1/73), comparison of test data has been found to be quite good for peak body accelerations, slapdown pressures, nozzle pressures, and peak penetration.

SRB loads for the forward skirt, case, and nozzle have been determined by using Froude scaling in conjunction with the 12.5 and 120-inch test results. Aft dome and aft skirt pressure data presented are based upon the NASA quarterly review (6/1/73).

4.2.4 Aft End Configuration Effects

Figure 4.2-4 shows the present baseline aft end configuration. The nozzle extension is jettisoned before water impact but is shown for illustrative purposes. The presence of the nozzle extension greatly increases loads at the nozzle throat. Without the extension, the nozzle loads are significantly lower; however, aft dome and aft skirt loads are increased without the shielding effects of the extension.

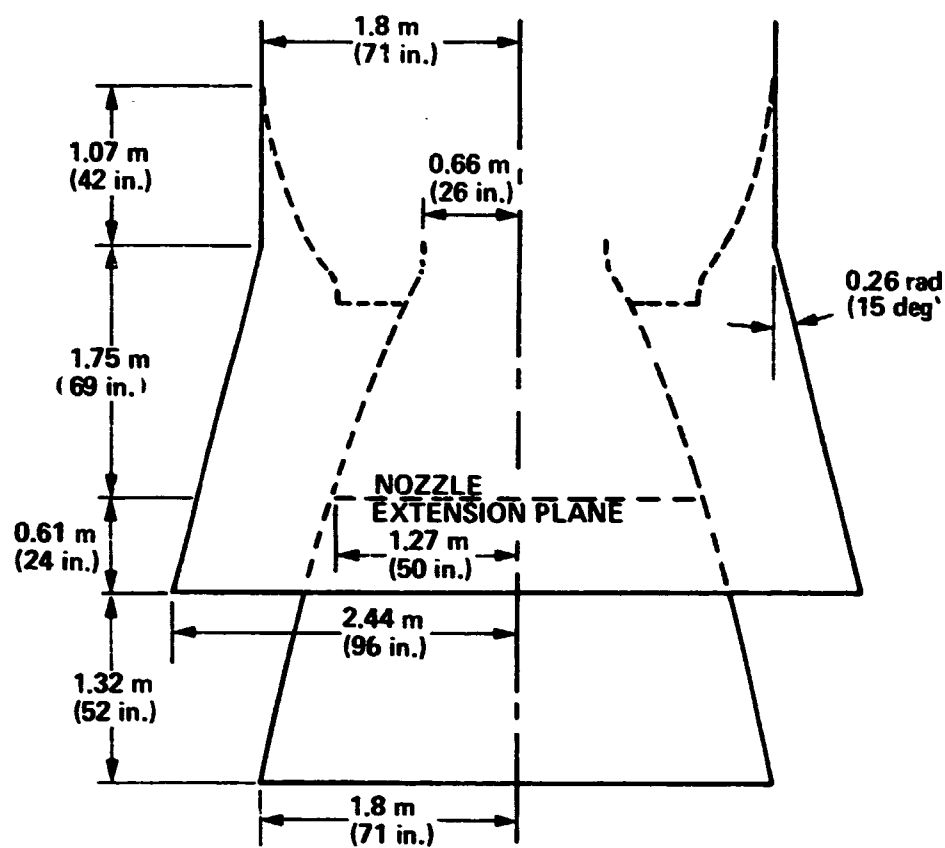


Figure 4.2-4 SRB Aft End Baseline Configuration

A desirable consideration is to keep the SRM aft end (aft dome and nozzle) from being designed by water impact loads. Removal of the nozzle extension before water impact should allow the nozzle to meet this criterion. However, aft dome collapse pressure loads may be critical upon water impact. To reduce these loads, one or more frames of the aft skirt could be enlarged to form a deflector or baffle to absorb energy from water impact and transfer the load to the aft skirt. Section 4.3.3 presents further discussion of this design

The aft skirt will experience collapse pressures if the horizontal impact velocity (V_H) is great enough to cause the water to impinge on the outside of the skirt. As shown in Figure 4.2-4, the aft skirt has a 0.26-rad (15-deg) flare with respect to the SRB centerline. Figure 4.2-5 shows the minimum V_H at which collapse pressures will occur. For increasing V_H values above this minimum, increasing peak collapse pressure will be experienced on the aft skirt. It is seen from the figure that as the vertical impact velocity (V_V) increases, the minimum value of V_H also increases. This indicates that the possibility of existing collapse pressure decreases for increasing V_V .

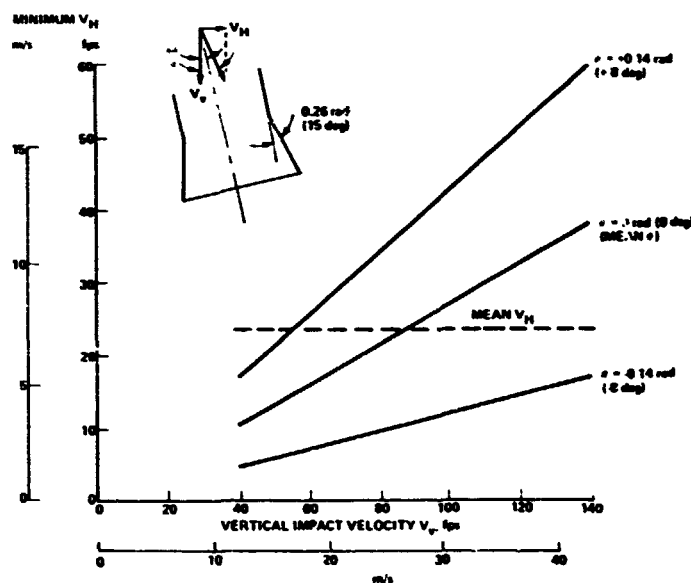


Figure 4.2-5 Minimum V_H for Collapse Pressure on Aft Skirt

4.2.5 Attached Parachute Effect on Slapdown Loads

Test data obtained to date indicates that the SRB tip accelerates downward following SRB initial water impact under high horizontal impact velocity conditions. This results in the high slapdown loads which occur on the forward portion of the case and on the forward skirt. These tests were conducted by dropping the SRB scale model and letting it fall freely to impact with the desired impact conditions. In the current recovery technique, the main parachute system is kept attached to the SRB for approximately 3 seconds after impact. Thus, the actual situation is not a free-falling SRB, but rather an SRB hanging from the parachute as it hits and penetrates the water.

If the SRB tip (parachute attach point) accelerates downward after the SRB tail first impacts the water, the parachute will restrain the downward motion of the tip and reduce its velocity upon slapdown.

Section 2.1.7 describes the effect of an attached parachute system on the SRB motion following initial water impact. Results shown must be considered approximate, but the trend is clear that the parachute indeed does slow down the tip as the SRB plows into the water.

Comparison of tip impact velocities with and without an attached parachute shows that the parachute will slow the tip down by approximately 25% for high values of horizontal impact velocity. If peak slapdown loads are a function of dynamic pressure, loads would be lowered over 40 percent due to the parachute.

These results are for a specific set of impact conditions, for a V_v of 21.4 m/s (70 fps), V_H of 15.2 m/s (50 fps), and $\theta = -0.17$ rad (-10 deg). In general this effect would be more pronounced for higher horizontal impact velocities, since tip slapdown velocities would tend to increase.

Test data giving trajectory information for high V_H conditions are scarce at present, but additional test results as they become available will shed more light on this subject. If peak slapdown loads are a function of the slapdown velocity, and if the slapdown velocity increases with increasing horizontal impact velocity, it is possible that the effect of an attached parachute recovery system will indeed be to reduce peak slapdown loads on both the forward skirt and the SRM case.

More detailed analyses of test data, including correlations of test measurements with photographic coverage, is imperative to more fully understand the trajectory characteristics of the SRB as it penetrates the water.

4.2.6 Sea State Effects on Slapdown Loads

Peak loads contained in this report are based upon interpretations of model test results. All of these tests have been conducted with a calm water surface. Effects of water motion have not been estimated.

Figure 4.2-6 shows the general situation of an SRB impacting a sea state 5 water surface. The probability of occurrence of this sea state is less than 10%. Nominal values and expected variations of wave height, wave shape, wave period, and wave length are listed. The sketch illustrates relative lengths and distances for nominal sea state 5 conditions.

Peak loadings occur for the aft end structures (nozzle, dome, skirt) early in water entry, when only the aft end has been wetted. This is the time of peak rigid body accelerations. These peak loadings were obtained from test data using SRB scale models impacting a water surface with no wave slope. Vertical wave motion effects on initial impact conditions are included in the Monte Carlo attrition analyses and have been considered.

REFERENCE: Paragraph 18.5, Water Entry and Recovery Conditions, Addendum to NASA TM X-64589, Terrestrial Environment (Climatic) Guidelines for Use in Space Vehicle Development, 1971 Revision, 2/8/72

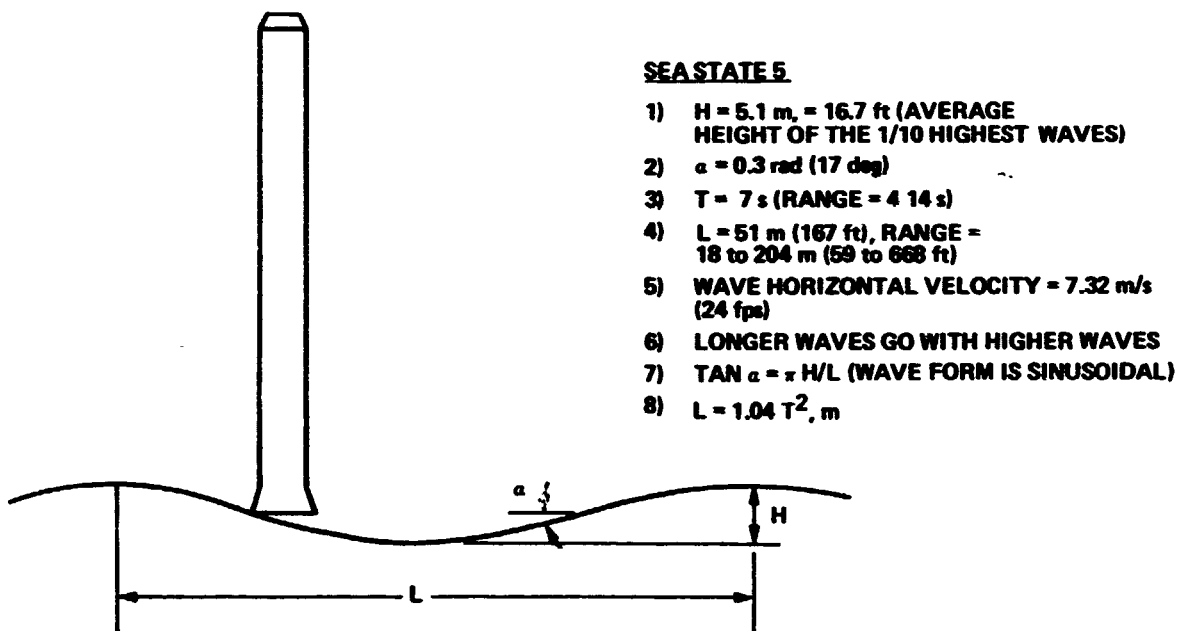


Figure 4.2-6 Sea State 5 Wave Conditions

In a calm sea, the peak aft end loads have occurred by the time the aft end is completely wetted. (See Figure 4.2-4 for the baseline aft end configuration.) The effect of introducing a wave slope at impact is to increase the amount of time to completely immerse the aft end. For a 0.30-rad (17-deg) wave slope, about 30% more time is required. This would probably delay the time of peak loading. Other factors, such as impact angle θ and direction of the resultant impact velocity vector, will affect both the distribution and the time history of the pressure loading on the aft skirt and nozzle. Magnitudes of these changes cannot be estimated because of the complex interaction of water forces with the structure. Intuitively, however, it appears that peak loads would not increase appreciably from calm sea conditions. It is even possible that the peak loading may decrease slightly, since a longer time is required for water to completely fill up the interior volume of the aft skirt.

The change in wave slope with time and the water horizontal motion may be neglected because of the short times associated with peak rigid body accelerations. With a vertical velocity of 21.4 m/s (70 fps), the SRB travels 1.32 m (52 in.) in 0.062 seconds. This compares with a wave period of 7 seconds associated with a sea state 5 condition.

The SRB case and forward skirt experience peak loadings during either initial slapdown or rebound slapdown, as the forward position of the SRB contacts the water surface while pitching over into a horizontal position. Peak loads occur at the leading edge of the case where it plows into the water. In the presence of waves, the SRB tip could essentially fall farther before hitting the water, if SRB initial impact was on a wave crest. This could result in increased slapdown velocities and peak loadings.

Water surface vertical velocity caused by wave motion would also affect slapdown loads on the case and forward skirt.

An upward vertical velocity component of the water surface would effectively increase the relative velocity of the SRB case leading edge with respect to the water surface. For example, the sea state 5 design condition specifies that the water surface rises and falls a total of 5.1 m (16.7 ft) in a sinusoidal motion, with a period of 7 seconds. The maximum vertical velocity under these conditions is about 2.3 m/s (7.5 fps). For a rising water surface with this velocity, the SRB case or forward skirt would feel this additional velocity as it impacts the water surface.

This would tend to increase the loading on the structure. If the case pressures were a function of dynamic pressure, calm sea peak loads would change as a function of the square of the ratio of the velocity including water motion to velocity not including wave motion. Since peak case loads tend to occur with initial slapdown, and increase with increasing horizontal impact velocity, the effect of this wave motion is variable. The relative increase in loads should be less for higher horizontal impact velocities than with lower ones. On the other hand, if the water surface is moving downward, the slapdown loads would be lower, again because the resulting dynamic pressure on the structure is lower.

It should be kept in mind that a sea state 5 condition has a low probability of occurrence (of the order of 10%). Also, the peak wave slope of 0.30 rad (17 deg) occurs only with the top 10% highest waves in a sea state 5 condition. We are thus looking at an extreme water surface condition—one that will seldom occur. The associated increased loads are accordingly loads with a low probability of occurrence.

4.2.7 Aft End Loads

Peak loadings for the aft dome, aft skirt, and nozzle are presented in Figure 4.2-7. The baseline configuration presumes that the nozzle extension has been jettisoned before water impact; however, loads are shown for impacts with and without the nozzle extension.

The aft skirt will feel only bursting pressures for low V_H values, but for certain combinations of V_H and V_V , both bursting and collapse pressures will be felt. At time of these peak loadings, the circumferential distribution is uniform for burst pressures and a cosine distribution over ± 1.57 rad (± 90 deg) for the collapse pressures. Aft dome collapse pressures are considered uniform over the entire dome structure.

The equivalent axial load per unit length of circumference (N), is defined here as the maximum value of $N = \frac{P}{2\pi R} + \frac{M}{\pi R^2}$ where P is the axial load, M is the bending moment, and R is the radius of the structure at the desired location. The envelope of N is shown at two locations: the aft dome/nozzle junction and the nozzle extension joint.

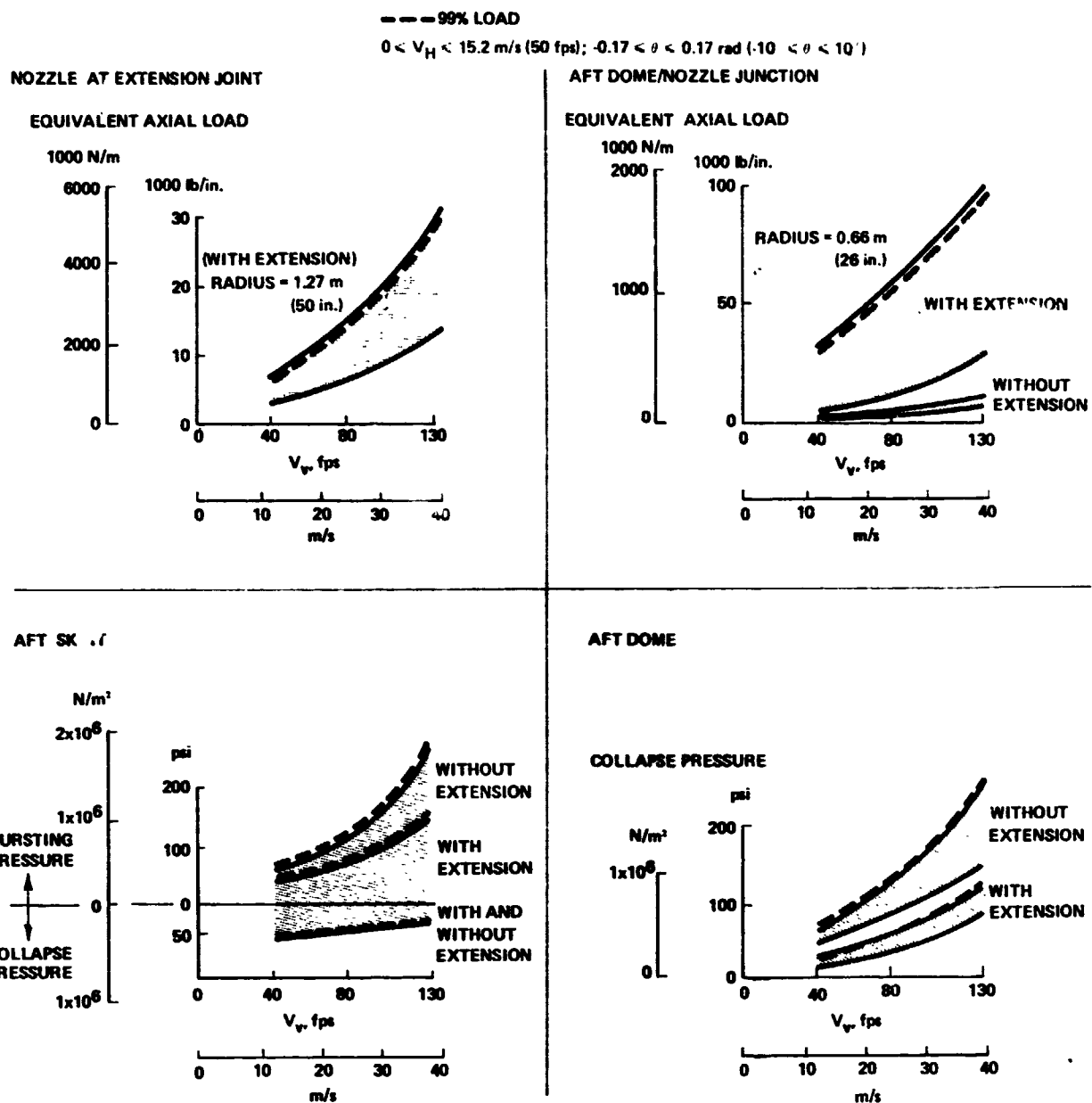


Figure 4.2-7 Aft End Peak Loading Highly Sensitive to Impact Conditions

Aft dome loads are composed of both collapse pressures acting uniformly over its surface, and the edge loads imposed by the nozzle. For the case with no nozzle extension, collapse pressures are high and N values low, while for the case with nozzle extension, collapse pressures are low and N values are high.

Shown with the load envelopes are the 99% load values. There are loads that will not be exceeded more than 1% of the time, based upon 1000 Monte Carlo cases.

4.2.8 SRB Case and Forward Skirt Loads

The SRB case experiences significant loadings at three distinct phases of the water entry: at peak rigid body acceleration, which occurs when only the aft end of the SRB has entered the water; at peak submergence; and at slapdown, which includes both initial slapdown and rebound slapdown. Figure 4.2-8 presents the peak loads for each of these three conditions.

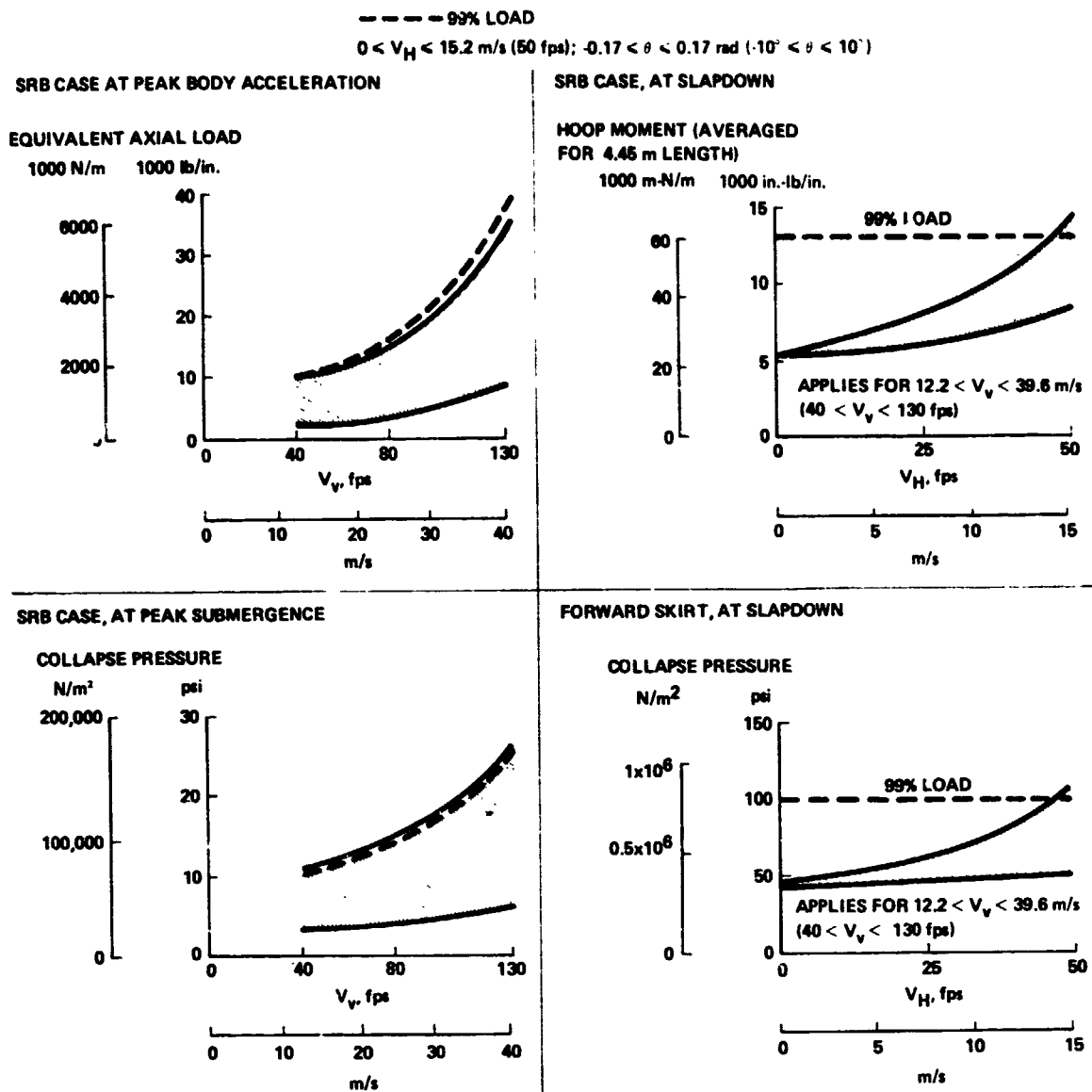


Figure 4.2-8 Critical SRB Case and Forward Skirt Loads Occur at Slapdown

At peak rigid body acceleration, the case experiences only inertial loads in the form of axial loads and bending moments. The equivalent axial load per unit length of circumference is the peak value felt in the case structure. It occurs aft of the center of gravity of the SRB. Loads increase sharply for high V_V values.

The collapse pressure loads given for the maximum submergence condition do not include effects of case internal pressures. The magnitudes of the internal pressure are uncertain; however, presently planned pressure and temperature scaled model tests by NASA will help to assess their absolute values. Case positive internal pressures would lower the net collapse pressures acting at peak submergence.

Case and forward skirt slapdown loads presented are derived from model tests, which imply calm sea conditions and no parachute attached. As discussed in Section 4.2.6 and 4.2.7, wave motions are expected to increase peak slapdown loads, while the presence of an attached parachute should lower the peak slapdown loads. The net effect of these two factors is probably a reduction in peak values. Because of a lack of quantitative data, however, no adjustment in loads is included in this report.

Case slapdown loads are presented in terms of peak hoop moment. This moment is an equivalent frame bending moment tending to distort the SRB cylindrical shape out of round. These moments were computed using test-measured pressure distributions in both the axial and circumferential directions. Section 4.3.5 discusses in greater detail the generation of hoop moments from pressure distributions. Figure 4.2-9 illustrates the pressure distribution buildups with time due to slapdown. Peak loading is concentrated near the intersection of the water surface and the leading edge of the SRB and extends axially over only one or two diameters of SRB length. The peak pressure magnitude increases with time as the SRB pitches over in the water. The circumferential wetted angle θ_M , over which the pressure acts, increases from 0 to ± 1.57 rad (± 90 deg) over the region of high loading, and is about ± 0.7 to ± 0.9 rad (± 40 to ± 50 deg) at the peak pressure location. Loads are presented as a function of horizontal impact velocity since NASA test results to date indicate that slapdown loads do not vary significantly with vertical impact velocity in the range considered.

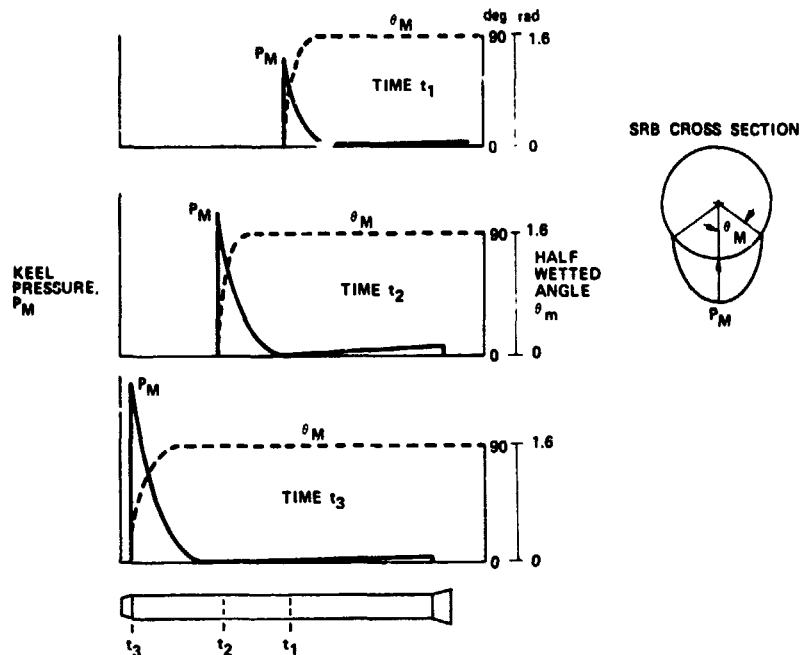


Figure 4.2-9 Slapdown Pressure Peak Moves Forward and Increases with Time

The forward skirt experiences peak loads only during the slapdown condition. These are presented in Figure 4.2-8 as peak collapse pressures. As with the SRB case, these peak pressures are considered independent of vertical impact velocity also, and increase with increasing horizontal impact velocity.

4.2.9 Loads Summary

Water impact loads presented in this report have been generated using data obtained from 6.5-, 8-, 12.5-, and 120-inch diameter Froude scaled models. Tests have been conducted with instrumented models dropped in a free-fall condition into calm water. Instrumented pressure and temperature scaled data are not available at this time, and data on the current aft end configuration are not available. The existing information, although based on aft end configurations that differ from the current SRB baseline, have been sufficiently detailed to predict peak loadings on the forward skirt, case, nozzle, aft dome, and aft skirt. No data for impact velocities greater than 30.5 m/s (100 fps) has been received.

Critical loads are applied to the entire aft end (nozzle, dome, skirt) immediately after initial impact, when only the aft end has entered the water. Loads on all three structural components increase with increasing vertical impact velocity.

Critical loads on the case and forward skirt occur during initial slapdown or during rebound slapdown. These peak loads are highly dependent upon values of horizontal impact velocity. Test data to date has indicated that these peak loads are essentially independent of vertical impact velocity. This means that case and forward skirt slapdown loads are as severe at low vertical impact velocities as at high vertical impact velocities.

4.3 COMPONENT STRENGTH ANALYSIS

The SRB strength analysis considered all of the major structural elements as depicted in Figure 4.3-1. Strength predictions are not presented for the nose cone because it impacts with the pilot chute and no applicable impact loads data are available. The nozzle-first impact condition that has been selected does not produce critical loads on the forward dome, and since the cylindrical section of the forward segment is less critically loaded than the case center segments, neither loads nor strength data is presented for this component.

Statistical distributions are used in all of the strength inputs to the Monte Carlo analysis. The calculated or predicted strength value for each structural component corresponds to the "A" value of MIL-HDBK-5B (99% probability, 95% confidence) unless otherwise noted. A Gaussian (normal) distribution was assumed for all components; however, different coefficients of variation of strength (C_{VS}) were used. C_{VS} is equal to the one sigma strength deviation divided by the mean strength. Based on Martin Marietta reliability work, a coefficient of variation of strength of 0.10 was used for all structures except the case center segments where a value of 0.06 was used. Typical statistical distributions are shown in Figure 4.3-2. It can be seen that failure probabilities are relatively insensitive to the selected value of C_{VS} when failure probabilities are low.

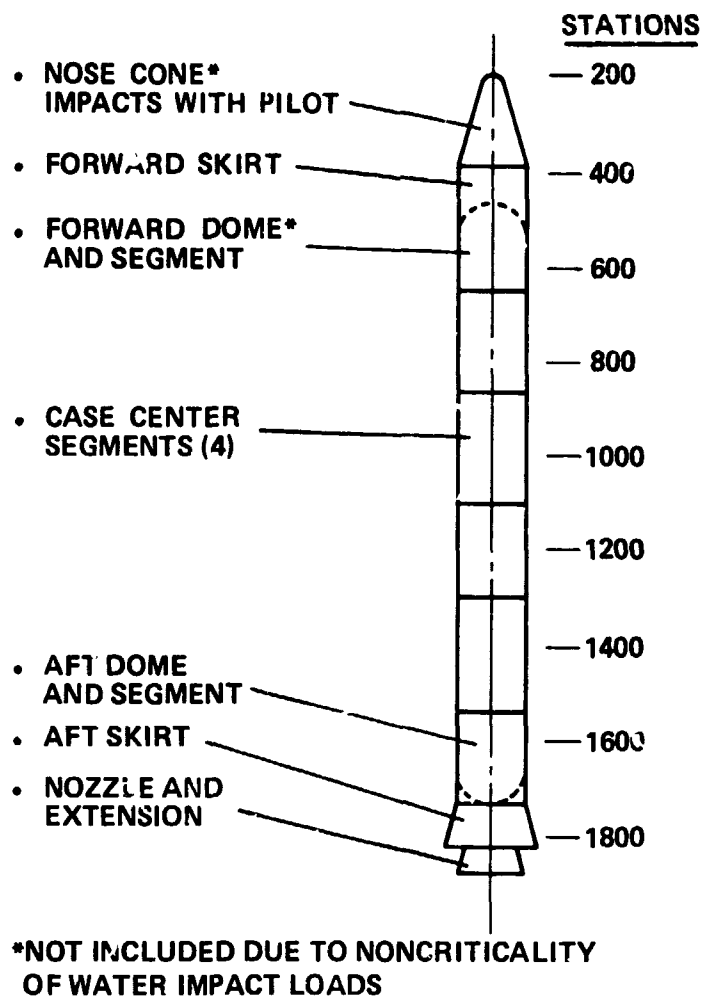


Figure 4.3-1 All Major Structural Elements Included in the Monte Carlo Analysis

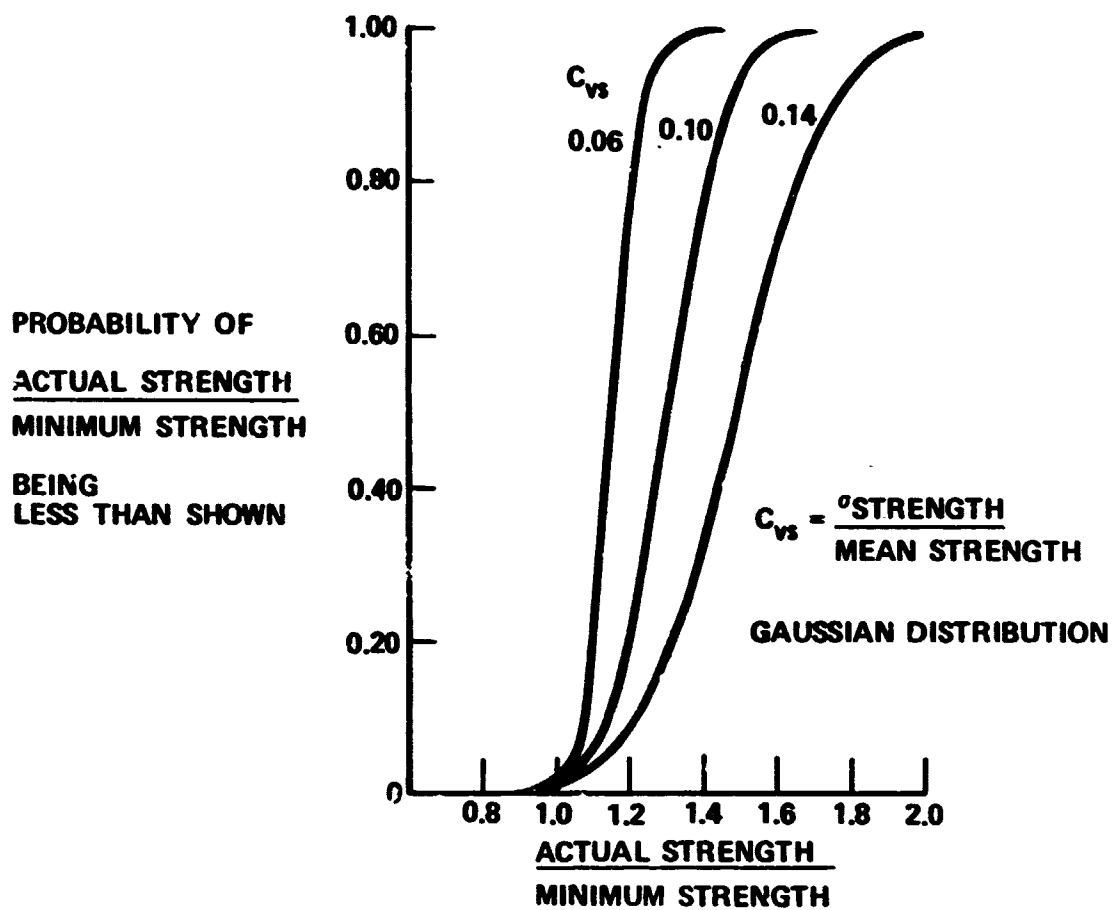


Figure 4.3-2 Statistical Strength Distributions Applied to Each Structural Element

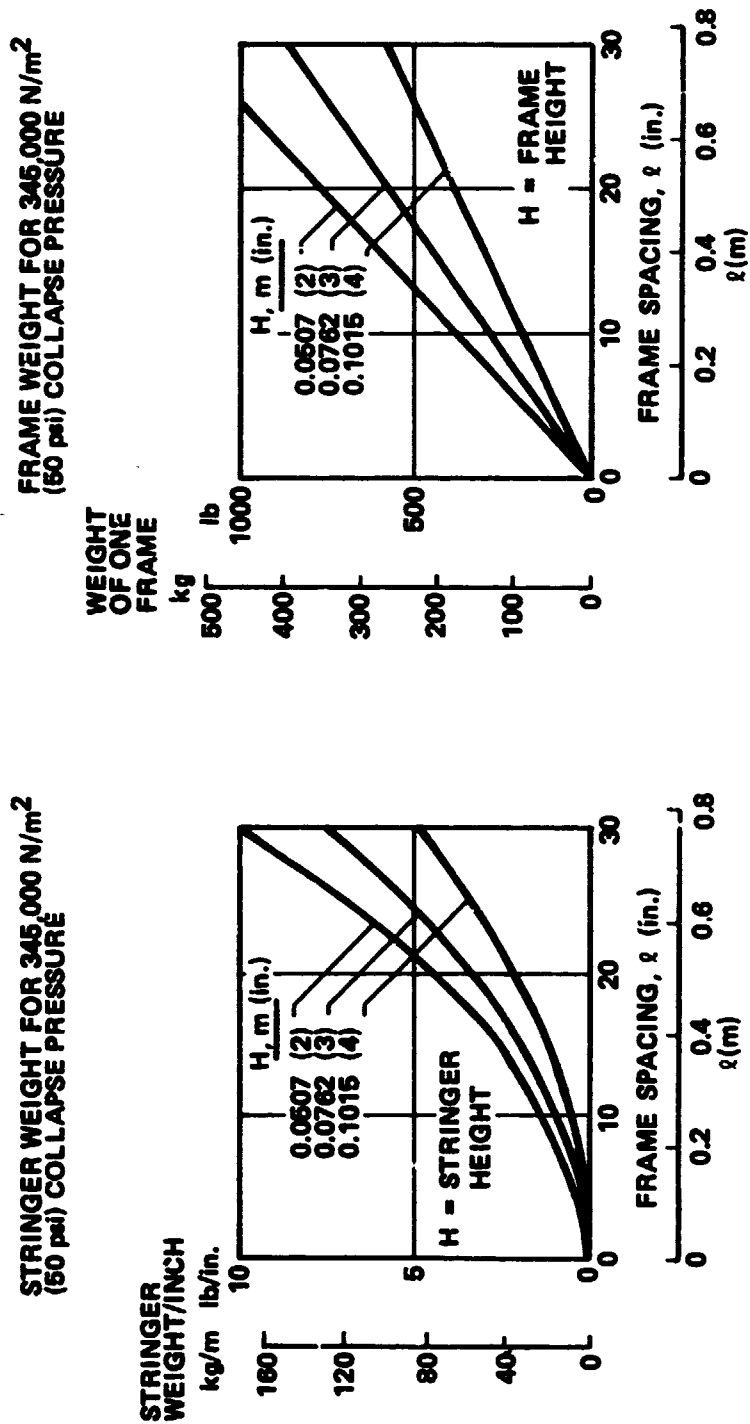
The basis for strength calculations and associated failure probabilities is given in the following paragraphs for the forward skirt, the aft skirt, the aft dome, the nozzle, and the case center segments. When adequate detail was included in the baseline provided by the NASA, these data were used. In other instances previous MMC analysis results were applied.

4.3.1 Forward Skirt

The forward skirt basic structure is designed for boost loads including the forward reaction thrust load to the external tank. Longerons, stepped skin thicknesses, and tapered stringer areas are used to lag the load into the SRB case. Relatively large end bulkheads take out end reactions that result from the thrust load redistribution, and also react the staging motor loads. No significant structural beefup to this skirt is required to react the parachute opening shock loads.

Preliminary design curves (Fig. 4.3-3) were used to evaluate slapdown pressures and determine baseline stringer and frame strength capabilities and weight increases required for other strength levels. The curves are used by entering with the actual frame spacing and reading the stringer or frame weight value for the applicable height. This weight has a strength allowable of $345,000 \text{ N/m}^2$ (50 psi) collapse, and any other weight has a proportionate strength allowable.

During water impact, the forward skirt is critical for slapdown pressures. The circumferential distribution is generally of a cosine shape over a 1.57-rad (90-deg) full included angle. The slapdown pressures are basically independent of vertical impact velocity. The pressure load is beamed by the stringers to the frames and bulkheads where it is circumferentially redistributed and sheared aft along the SRB. The stringers were analyzed as simply supported beams at the frames. The frames were considered as free frames with a VQ/I shearing reaction (same internal moments as using uniform circumferential inertial relief). Stringers designed for basic flight loads show failure probabilities of less than 1% for the slapdown pressures. The critical design load for the intermediate frames occurs during slapdown. The baseline design which was used and the required frame weight to achieve various probabilities of failure are shown in Figure 4.3-4 for two different frame heights. An average frame spacing of 0.635 m (25 in.) was used.



• SIMPLY SUPPORTED STRINGERS

• COSINE PRESSURE LOADING, 1.57 rad (90°) FULL INCLUDED ANGLE

Figure 4.3-3 Forward Skirt: Preliminary Design Curves Used for Stringer and Frame Capabilities

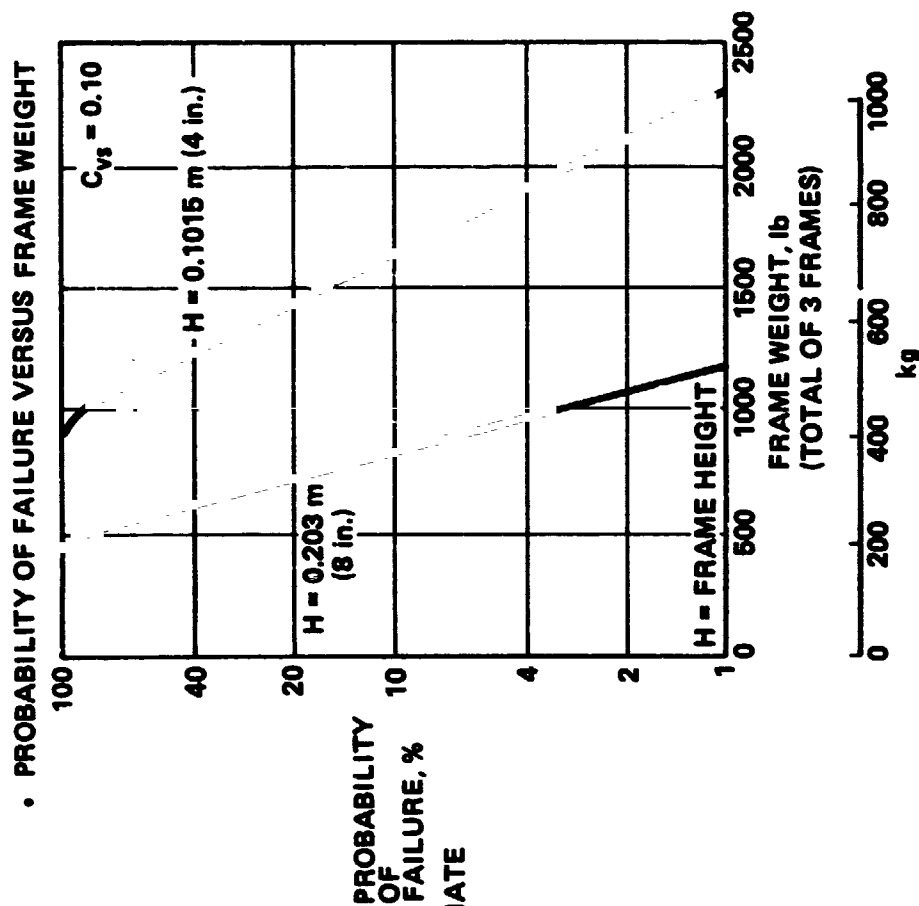
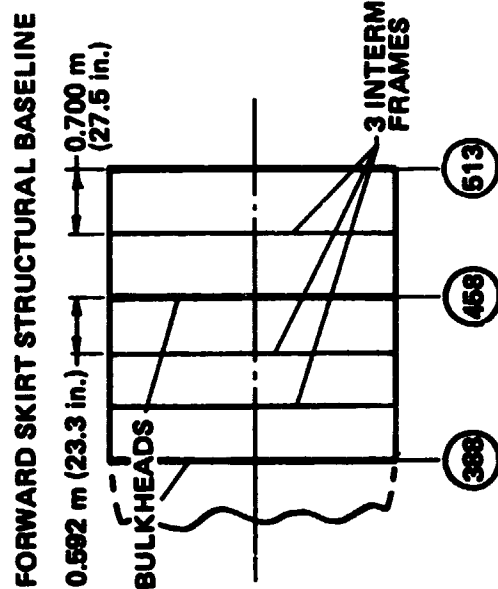


Figure 4.3-4 Forward Skirt: Baseline Frame Design Inadequate For Slapdown Pressure Loads

4.3.2 Aft Skirt

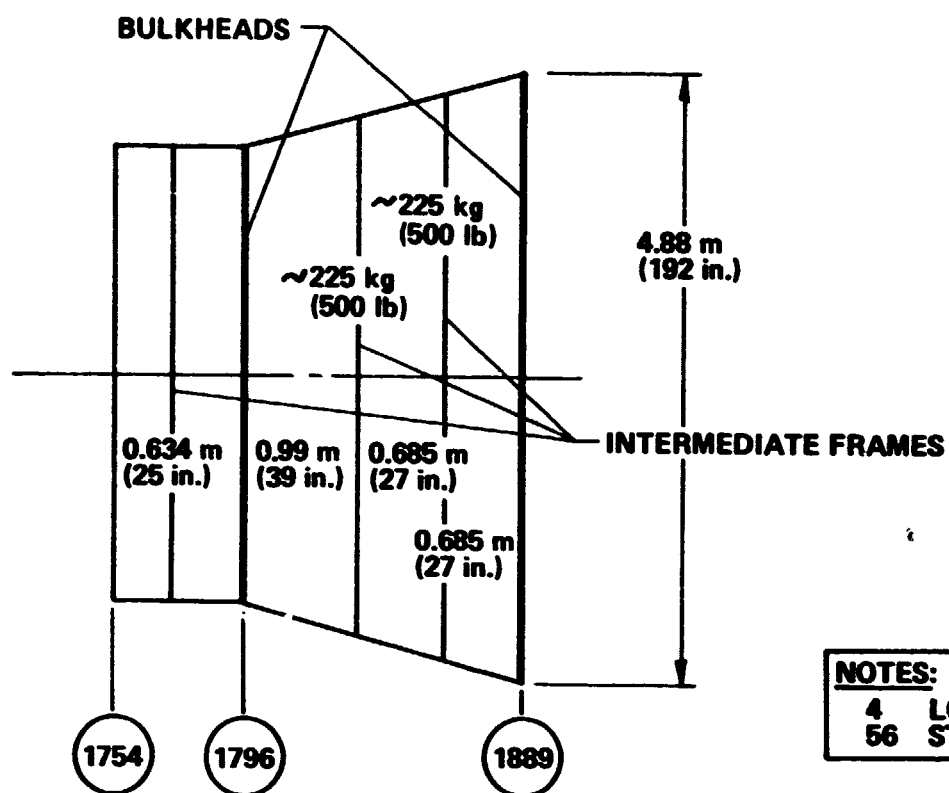
The aft skirt basic structure is designed primarily to support the total Shuttle system in the launch mode on four longerons. Stringers, stepped skin thickness, end bulkheads, and intermediate frames are used to redistribute the concentrated longeron loads. The frames also serve to react staging rocket loads. The baseline design is of steel construction and is shown schematically in Figure 4.3-5.

During initial water impact, the aft skirt can be critically loaded by either burst or collapse pressure, depending on the resultant velocity vector. Since the final skin thickness will vary with location, the probability of failure for burst pressure was evaluated as a function of skin thickness and the results are shown in Figure 4.3-6. For all vertical velocities below 39.6 m/s (130 fps), the failure probability is low if a steel skin thickness of 0.00356 m (0.14 in.) or greater is used. The baseline skin thickness of 0.0051 m (0.2 in.) will therefore result in a failure probability well below 1%. The collapse pressure loading on the frames is of a cosine shape with a 3.14-rad (180-deg) included angle. The weight of intermediate frames to achieve various failure probabilities is also shown in Figure 4.3-6. A 0.152 m (6 in.) frame depth was used for the weight calculations. The baseline frame weight of 456 kg (1000 lb) is adequate to withstand the water impact loads. The stringers designed for prelaunch loads will exhibit failure probabilities of less than 1% for water impact loads; therefore, weight versus failure probability calculations were not performed.

The baseline frame design may require modification to withstand out-of-plane loading on the frame web. Because the frame configuration was not included in the water impact tests, a good pressure definition for this loading is not available. We would expect some pressure increase above values measured for the compartment burst pressure.

4.3.3 Aft Dome

The aft dome is designed for case internal pressures and loads from the nozzle. For the baseline MEOP of 6,210,000 N/m² (900 psi), a dome thickness of 0.00635 m (0.25 in.) is adequate. The critical water impact loads are a function of whether the nozzle extension is on at impact; if it is, the dome is critically loaded by a running axial load from the nozzle around the gimbal joint. If the extension is jettisoned before impact, the dome is critically loaded by collapse pressure. The analysis for these two loadings used applicable NASA-MSFC results for varying R/t values. The recommended values for γ (correlation factor) were used. The resultant allowables are presented in Figure 4.3-7.



NOTES:
 4 LONGERONS
 56 STRINGERS

Figure 4.3-5 Aft Skirt Structural Baseline

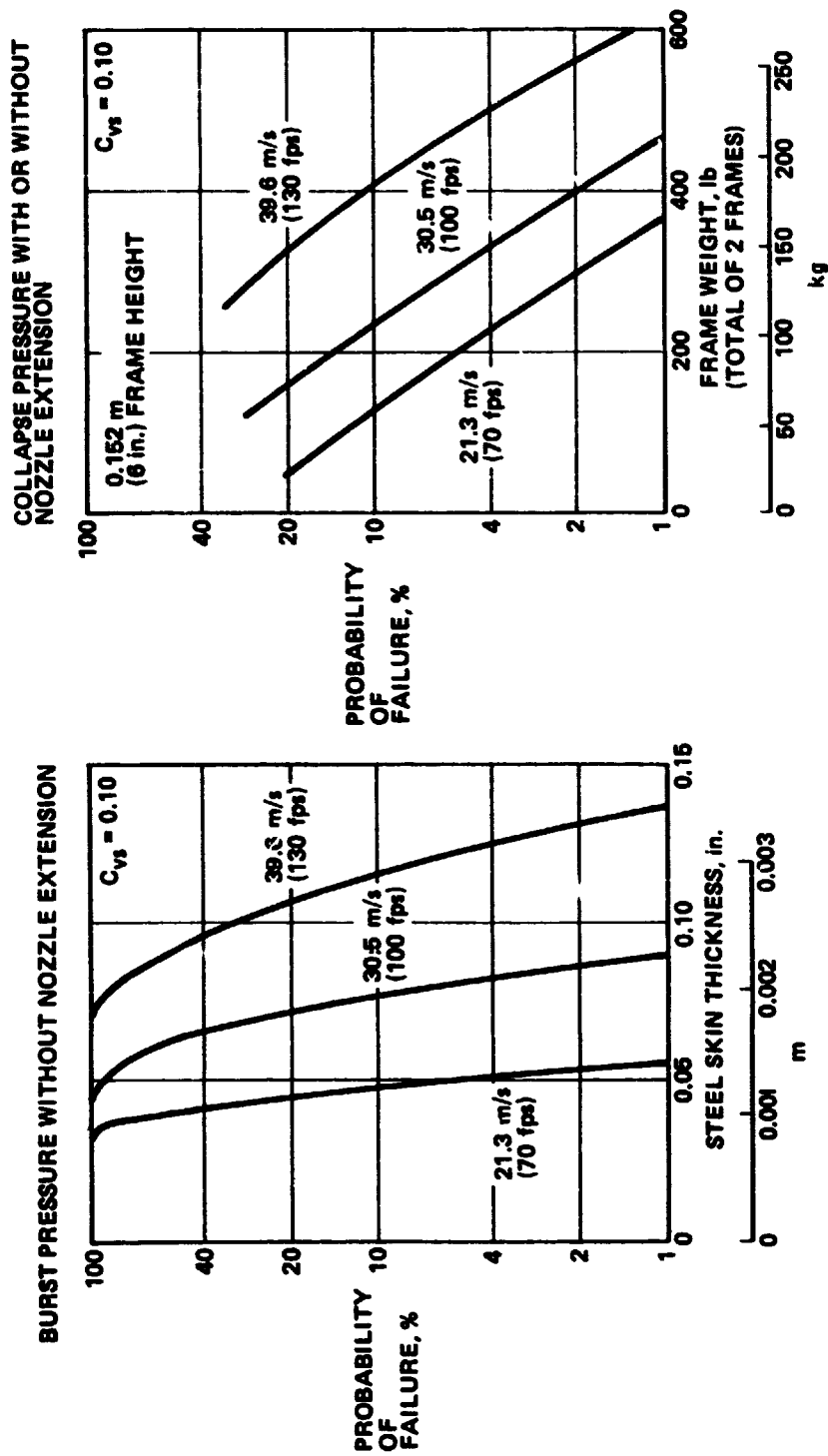


Figure 4.3-6 Aft Skirt: Adequate for Burst and Collapse Pressure Loads

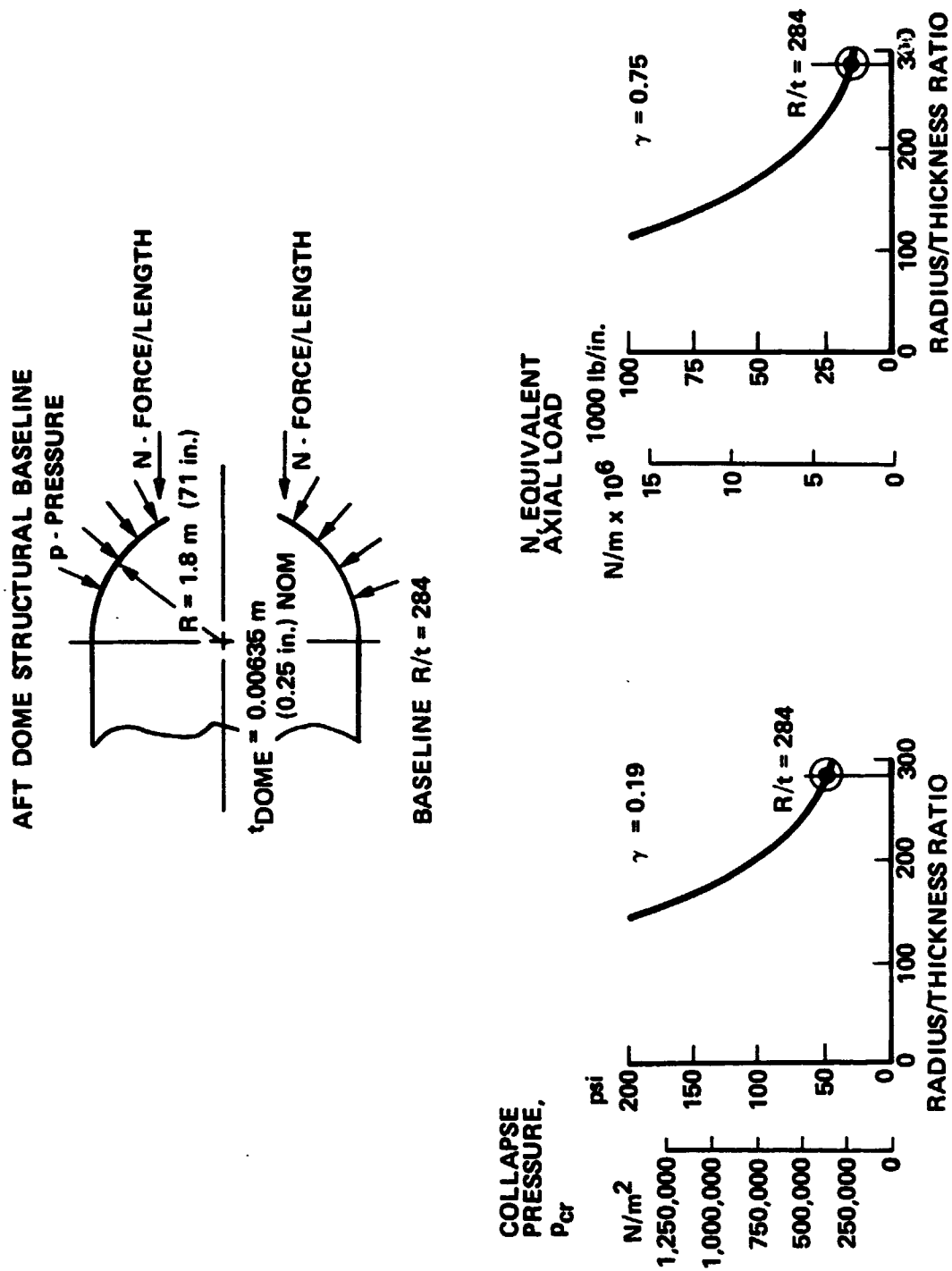


Figure 4.3-7 Aft Dome Strength Capability Based on Analytical Results

The aft dome failure probabilities are shown in Figure 4.3-8 for the critical loading conditions as dictated by the presence or absence of the nozzle extension. The collapse pressure is maximum if the nozzle extension has been jettisoned and results in 100% failure probabilities for the baseline configuration for vertical velocities of approximately 21.3 m/s (70 fps) and greater. The weight penalties to reduce the failure probabilities are shown. With the extension in place at impact, the running axial load, N, becomes the critical loading. The weight penalties to reduce failure probabilities are somewhat greater than those associated with the no-extension impact condition.

A preliminary design concept to protect the aft dome from high collapse pressure is shown in Figure 4.3-9. The weight penalty to the aft skirt associated with this design concept is expected to be less than 227 kg (500 lb) for impact velocities up to 38.1 m/s (125 fps). There is also a built-in advantage in not having to design the motor case aft dome for water impact loads because the aft skirt design details are not as critical from a schedule standpoint.

4.3.4 Nozzle and Extension

The nozzle and extension structure are critically loaded by equivalent axial loads at impact. With the extension in place, the design axial strength level at the separation joint must be increased significantly to reduce failure probabilities for the larger values of vertical impact velocities, as shown in Figure 4.3-10.

The design strengths of the nozzle gimbal joint that must be achieved to minimize the failure probabilities are shown in Figure 4.3-11. With the extension removed, the basic design strength of the gimbal joint appears to be adequate. If the extension were not jettisoned, the loads at the gimbal joint would increase by an order of magnitude and would either require significant structural beefup or result in a failure and a "loose" piece of structure in the aft compartment that could produce uncontrolled damage. The strength requirements for hoop loadings caused by burst pressure were not evaluated, but probably are also critical.

4.3.5 Case Center Segments

Extensive strength evaluation of the case center segments has been conducted, analytically and through static testing. The basic approach of this study was to use the static test results to predict

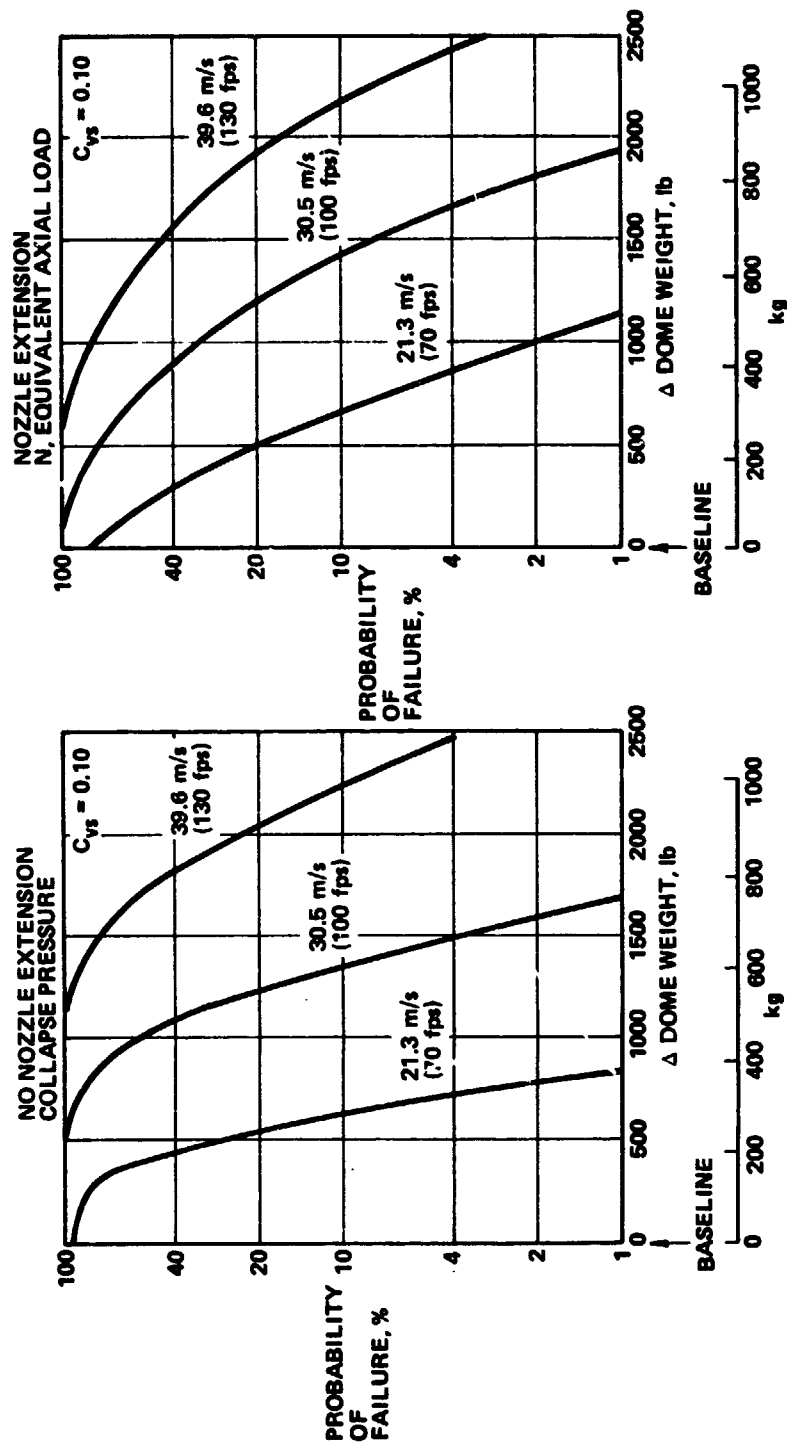


Figure 4.3-8 Aft Dome Probability of Failure High without Increased Structural Strength

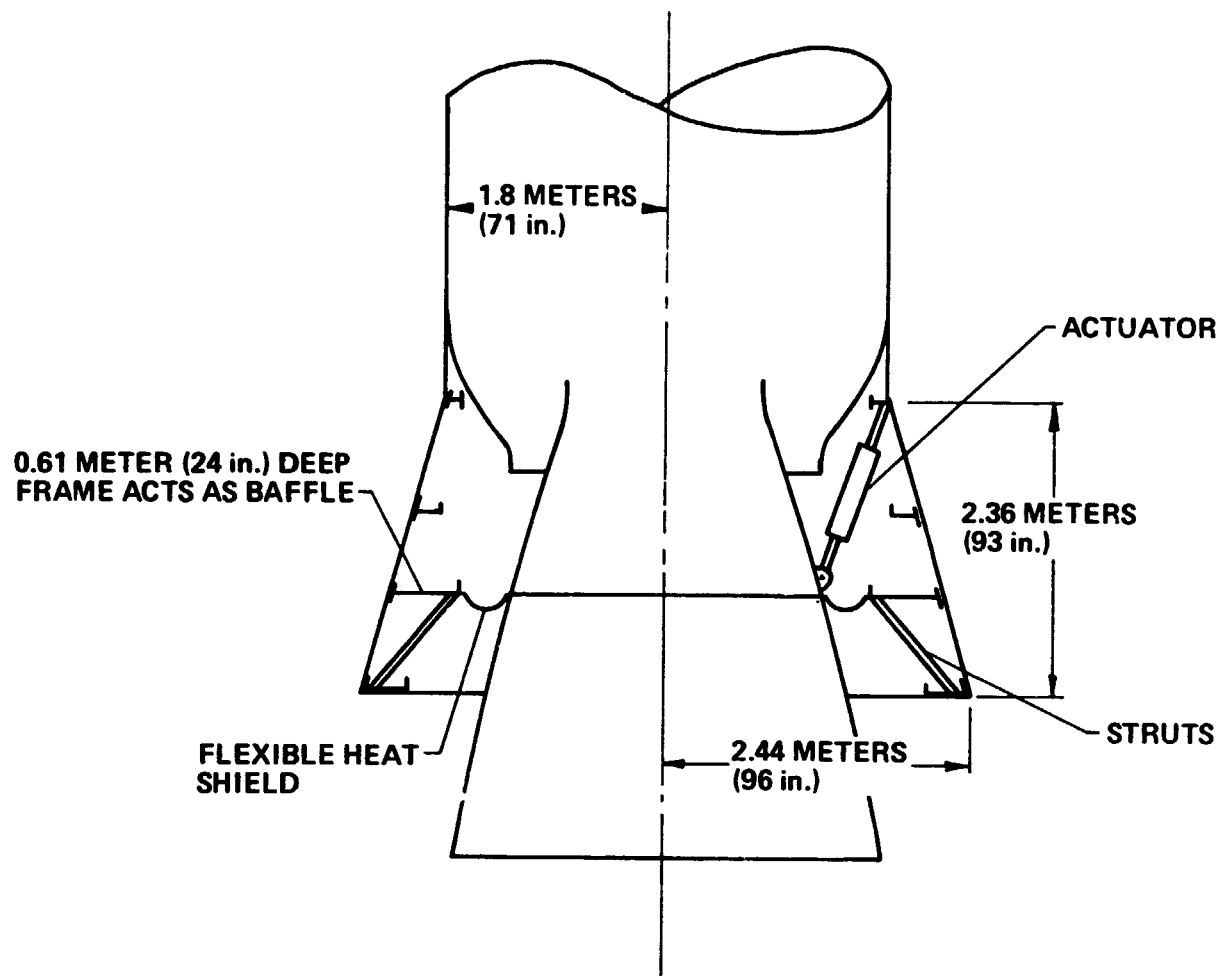


Figure 4.3-9 Aft Dome Protector Baffle Concept

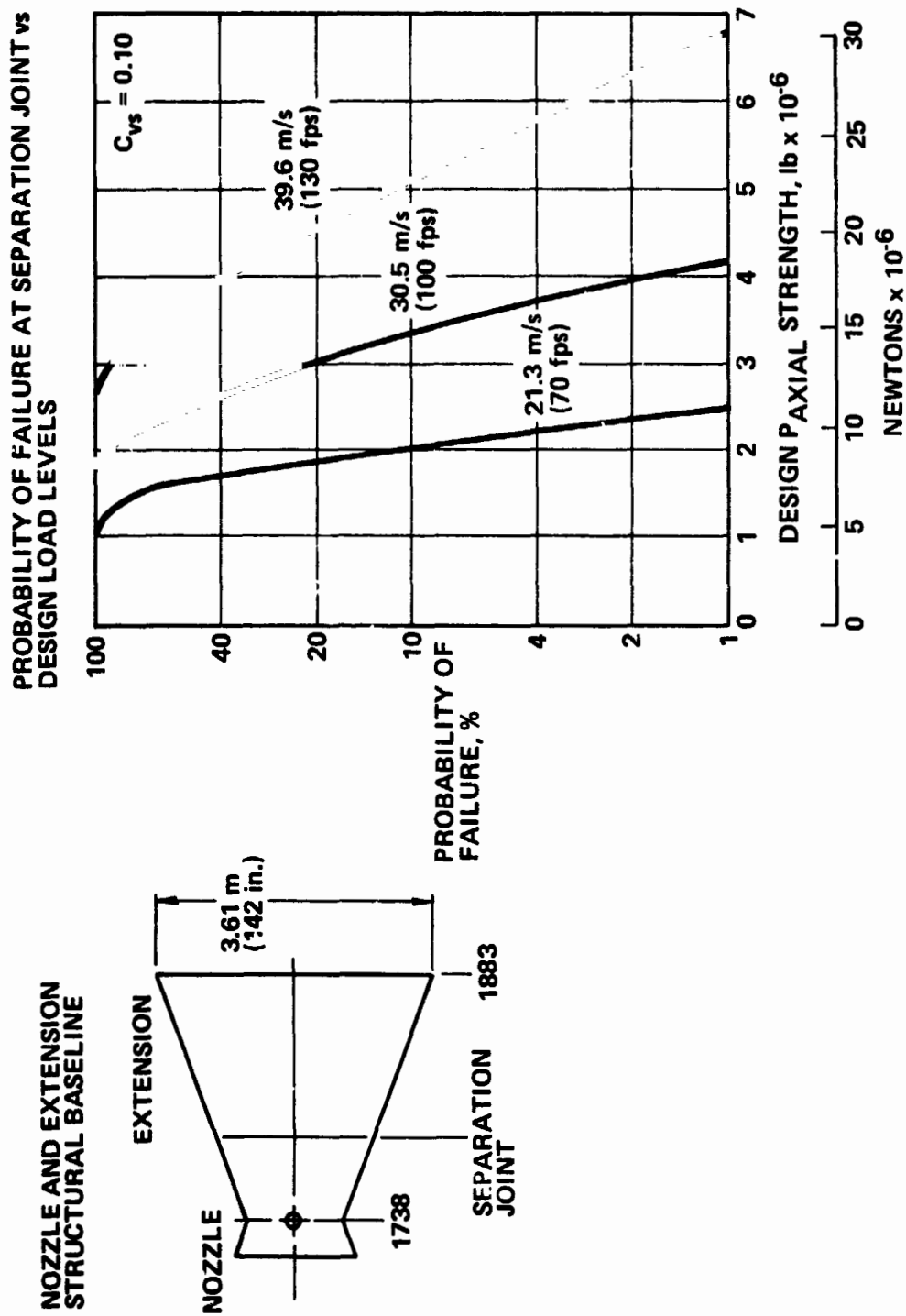


Figure 4.3-10 Nozzle and Extension Design Strength Requirements

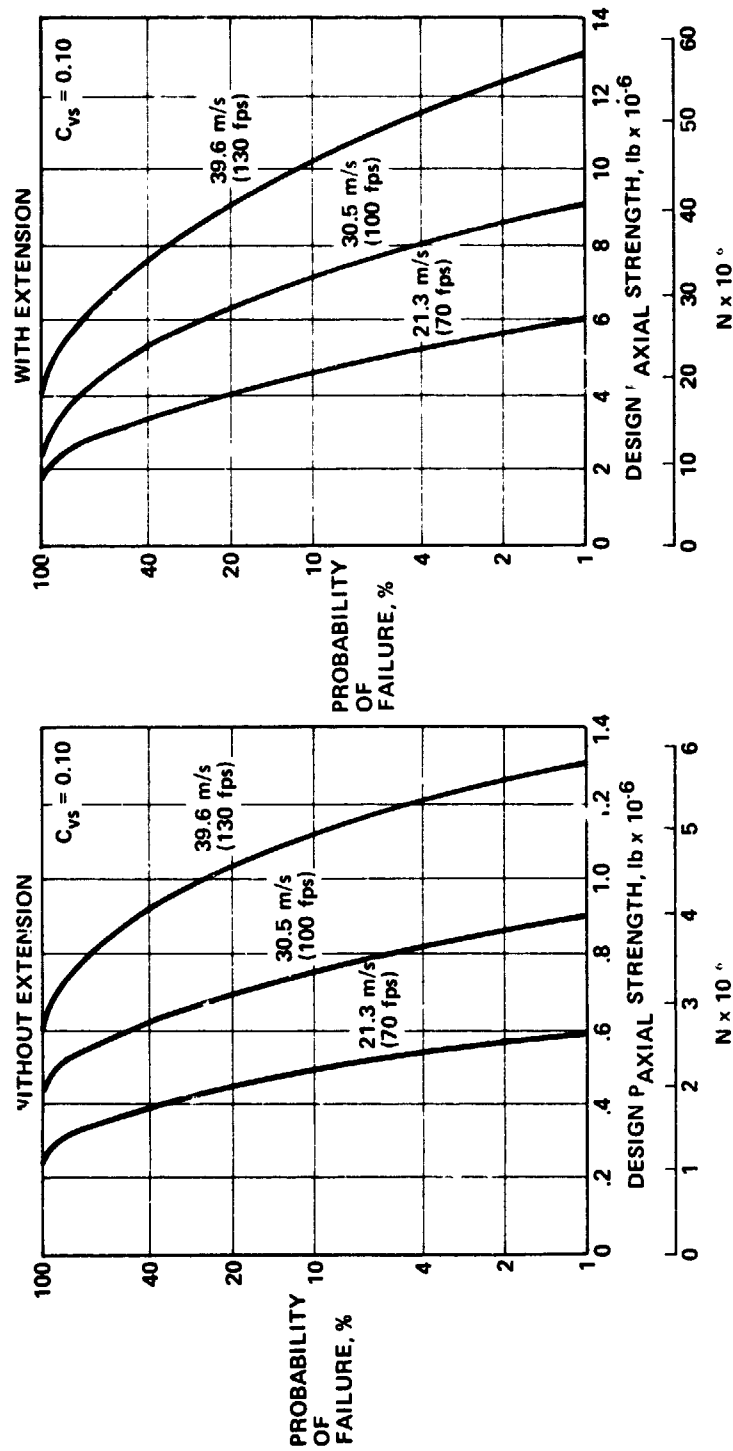


Figure 4.3-11 Gimbal Joint Design Strength Requirement Reduced by Jettisoning Extension

the yield strength of the 120-inch case (static test specimen) for the loads that were applied, and through use of proper factors to ratio these results to obtain strengths for the 142-inch case and its particular critical loading condition.

The critical loading condition occurs during slapdown when a circumferentially varying pressure wave propagates forward along the case. The 120-inch static test case was loaded with somewhat similar pressure load distributions during four load cases (A through D). Cosine varying circumferential distributions were used with an included angle varying from 0.52 to 2.1 rad (30 to 120 deg) in the longitudinal direction (see Fig. 4.3-12). Reactions were accomplished with straps applying uniform circumferential reactions over a 2.1 rad (120-deg) included angle. Condition A loaded up the forward half length of the case; Condition B, the middle one-half; and Condition C, the aft one-half. Condition D was a much more localized loading over a length of 2.22 m (87.5 in.) versus 10.6 m (417.6 in.) for Conditions A, B, and C. The 100% target load for Conditions A, B, and C was 2,050,000 N (460,000 lb) and for Condition D it was 479,000 N (107,500 lb).

All four static test conditions on the case were conducted on the same specimen. Loading conditions were cut off at varying percentages of the target loading to preclude yielding during any of the tests. A calculation of the total load cell readings applying the pressure loading was used to determine the correct test cutoff percentage values since the nominal values were somewhat in error. Stresses and deflections were plotted which showed the definite nonlinear nature of the hoop bending failure mode. The maximum hoop stresses were plotted for the four loading conditions and extrapolated to an F_{ty} of 1,240,000,000 N/m² (180,000 psi) to predict the allowable yield load for each loading condition (Fig. 4.3-13). The static test specimen was most likely of average thickness, and the strength extrapolation was done to a 99% value of F_{ty} . The resulting allowable loads were estimated to be 80% probability values (approximately the average strength minus one sigma deviation).

The hoop bending moments in the case static test were higher than would result during an actual slapdown for the same applied pressures because of the method of reacting the load. Analysis showed that if a VQ/I shear reaction could have been used in the static test, approximately 30% greater loads would have been required to produce the same resultant stress level. This factor of 1.3 was used to ratio the static test results up to obtain allowables for

.. 4 TARGET LOAD CONDITIONS WERE SELECTED

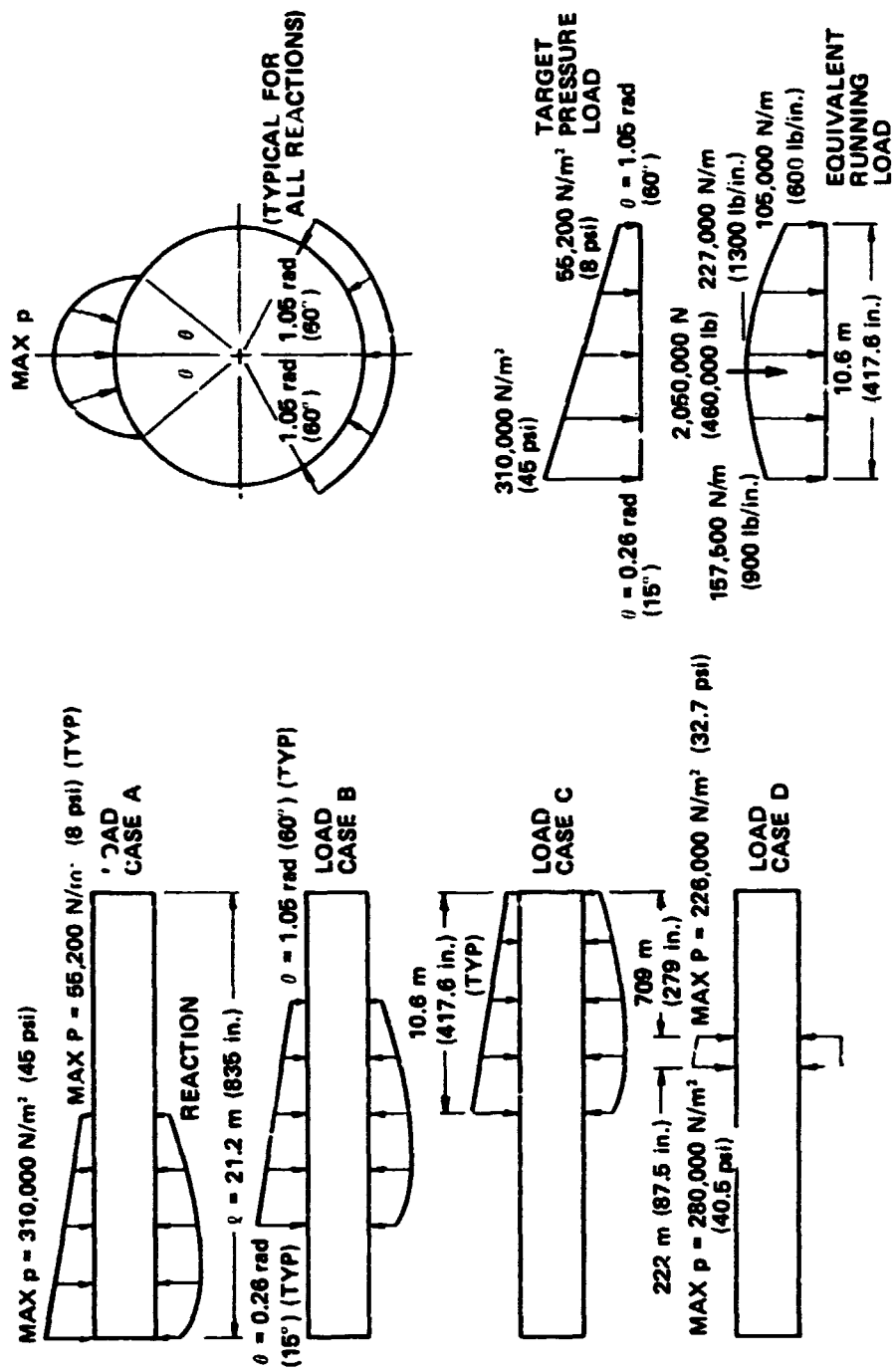


Figure 4.3-12 Case Center Segments: Strength Capability Based on 120-Inch Case Static Tests

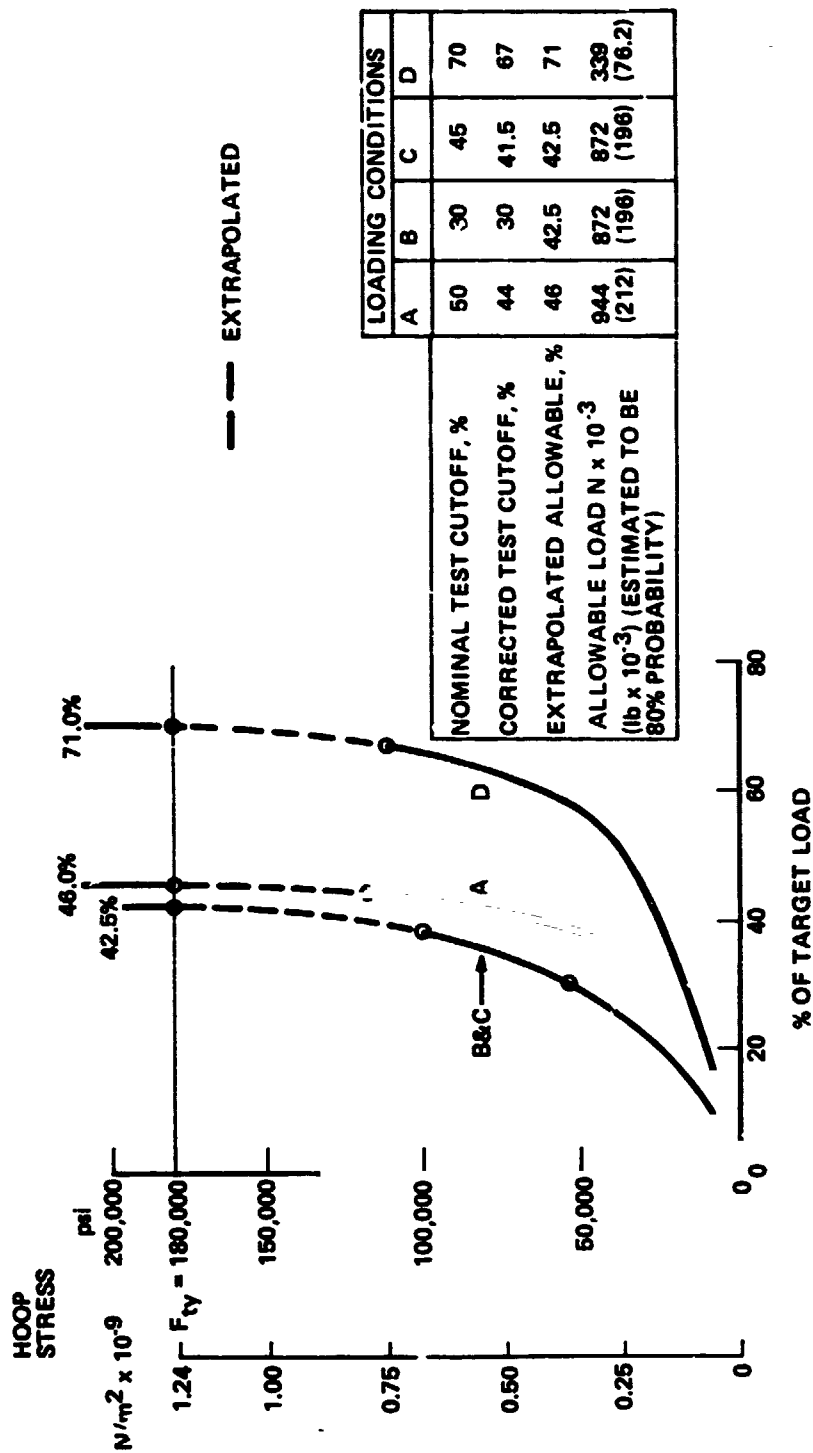


Figure 4.3-13 120-Inch Case Center Segment Yield Strength Extrapolated from Static Test Results

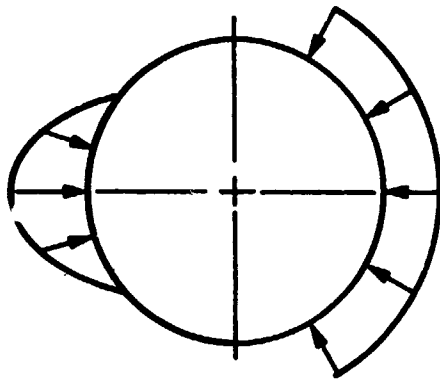
the 142-inch case. The baseline case was sized for D6AC steel with an $F_{tu} = 1,345,000 \text{ N/m}^2$ (195,000 psi) using an MEOP of 6,210,000 N/m^2 (900 psi) and an ultimate factor of safety of 1.4 (see Fig. 4.3-14). A clevis joint strength (for hoop bending loads) equivalent to that of the 120-inch static test specimen was assumed. The relative hoop bending strength between the 142-inch case and the 120-inch static test specimen is proportional to the thickness ratio squared and inversely proportional to the radius ratio. The net effect, considering these two ratios, is a strength increase factor of 1.35 between the 142-inch case and the 120-inch test specimen.

Since the case static test conditions had a varying included angle for the applied pressure load, a means of evaluating the effect needed to be determined. The method selected was to first plot allowable running load along the loaded length; then the running load was multiplied by the radius and the moment coefficient corresponding to the included angle at each station to obtain an allowable running hoop moment. The strength increase factors of 1.3 (reaction) and 1.35 (t^2/R) were included. In order to compare the allowable running hoop moment with the predicted running hoop moment, it was necessary to derive some common loading shape parameter since the longitudinal distributions were significantly different. It was decided that the best comparative method was to use an average running hoop moment for a finite loading length.

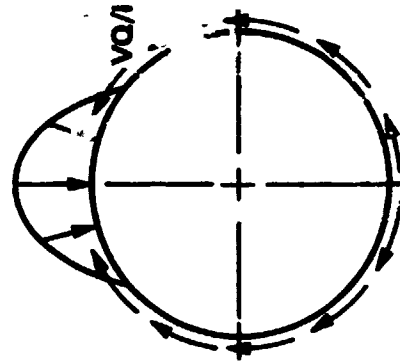
Test Condition D represented one point on the allowable curve 77,500 mN/m (17,400 in.-lb/in.) and a loading length of 2.22 m (87.5 in.). A 5.08 m (200 in.) loading length at the forward end of load Condition C gave an average allowable hoop moment of 44,500 mN/m (10,000 in.-lb/in.); similarly a 7.62 m (300 in.) loading length from Condition B gave an allowable hoop moment of 41,400 mN/m (9300 in.-lb/in.). A curve was drawn through these three points (see Fig. 4.3-15).

The predicted case slapdown pressure loads at three different times were evaluated to determine which was most critical. The running load was converted to running hoop moment by the same method that was used for the allowables, and the critical time was determined to be t_2 . Several different loading lengths and associated average running hoop moments were checked for this condition and a length of 4.45 m (175 in.) gave the largest probability of failure prediction. The average moment for a 4.45 m (175 in.) loading length and 18.3-m/s (60 fps) horizontal velocity is

**STRENGTH INCREASED BY 1.3 FACTOR
TO ACCOUNT FOR CONSERVATIVE METHOD
OF REACTING TEST LOADS**



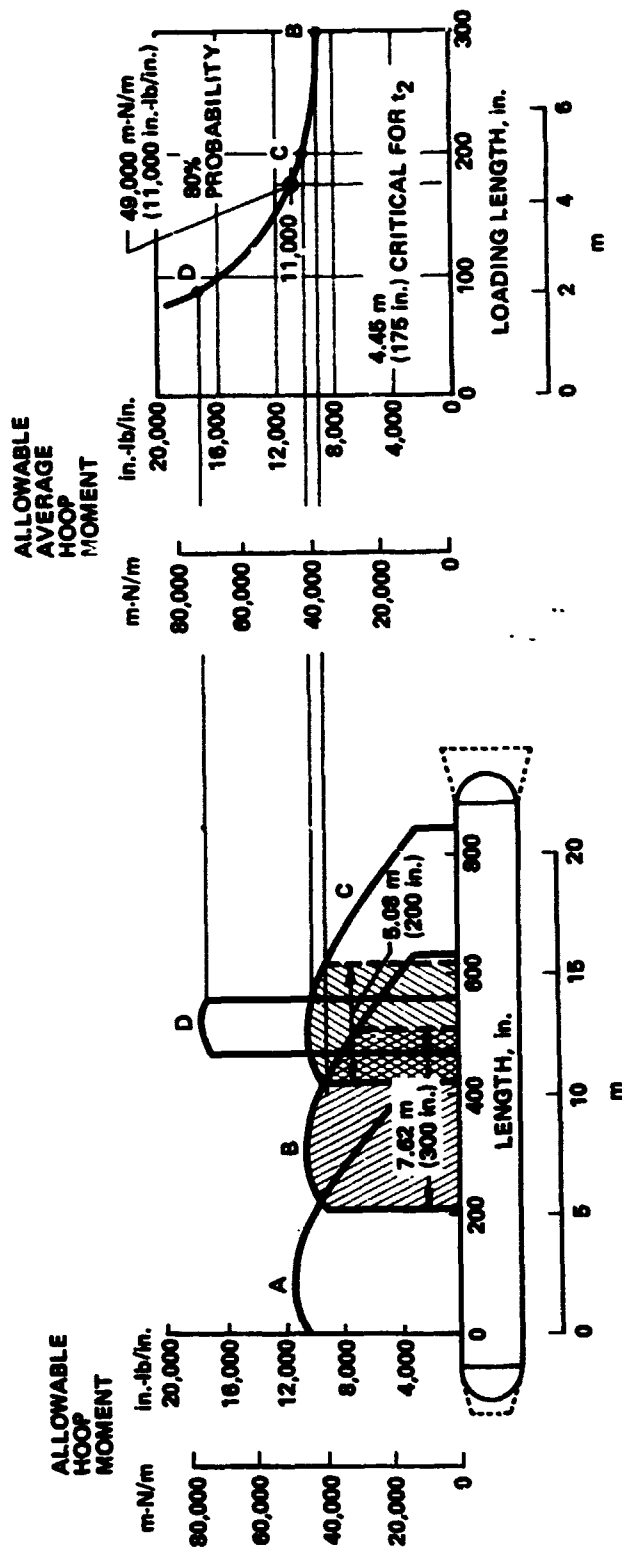
STATIC TEST REACTION



REAL-LIFE REACTION

- 142 in. BASELINE CASE THICKNESS WAS CALCULATED FOR:
- MEOP = 6,210,000 N/m² (900 psi)
- D6AC STEEL · F_{tu} = 1,345,000,000 N/m² (195,000 psi)
- ULTIMATE FACTOR OF SAFETY = 1.4
- $t_{\text{REQUIRED}} = \frac{1.4 \times 6,210 \times 1.8}{1345} = 0.0116 \text{ m (0.457 in.) MINIMUM}$
- ADD TOLERANCE TO GIVE $t = 0.0121 \text{ m (0.475 in.) NOMINAL}$
- 120 in. TEST ALLOWABLES WERE RATIOED BY t^2/R
- 120 in. — $t^2/R = \frac{0.375^2}{60} = 0.00235$
- 142 in. — $t^2/R = \frac{0.475^2}{71} = 0.00318$
- STRENGTH INCREASE FACTOR = $\frac{0.00318}{0.00235} = 1.35$

Figure 4.3-14 Center Segment Strength Increase Factors Used to Adjust Test Results to 142-Inch Case



142 INCH ALLOWABLE HOOP MOMENT
WAS DETERMINED BY RATIOING 120
INCH STATIC TEST RESULTS

Figure 4.3-15 Center Segment Hoop Bending Strength Determined from Static Test Results

59,700 mN/m (13,400 in.-lb/in.) as shown in Figure 4.3-16. The value for other horizontal velocities is proportional to the corresponding peak pressures. The allowable average moment taken from Figure 4.3-15 for a 4.45 m (175 in.) loading length is 49,000 mN/m (11,000 in.-lb/in.).

The case center segment failure mode is quite nonlinear; therefore, it was considered appropriate to reduce the C_{VS} value from 0.10 to 0.06. Using this value of C_{VS} , a 3% failure probability resulted for the 0.01205 m (0.475 in.) baseline case thickness corresponding to an MEOP of 6,210,000 N/m² (900 psi). Increasing the nominal case wall thickness to 0.014 m (0.55 in.) reduces the failure probability to 0.3% and corresponds to an MEOP of 7,200,000 N/m² (1,045 psi). The probability of failure is plotted versus the case thickness in Figure 4.3-17.

The other two loading conditions on the case center segments that were evaluated were peak submergence and peak body acceleration. The allowable hydrostatic buckling pressure was determined using a correlation factor of 0.75 and a segmented allowable pressure equal to 1.2 times a monolithic allowable. The allowable for peak body accelerations was determined neglecting the frame effect of the segmented joints and using a correlation factor of 0.52 for an R/t value of 150. The failure probabilities for peak body acceleration are shown in Figure 4.3-7. The failure probability for peak submergence was approximately 0.3% for a vertical impact velocity of 39.6 m/s (130 fps).

4.3.6 SRB Strength Analysis Uncertainties

Some of the structural elements were found to be considerably understrength for the baseline configuration. Table 4.3-1 gives the weight penalties required to achieve a design corresponding to 1% failure probability, which represents a near minimum cost approach. The weight penalties associated with designing to 1.25 times the 99% probable loads are also presented for comparison. The calculated associated failure probability is approximately 0.01%. The case center segment weight increase permits an increase to 6,650,000 N/m² (965 psi) MEOP and is, therefore, at least partially compensated for by increased performance.

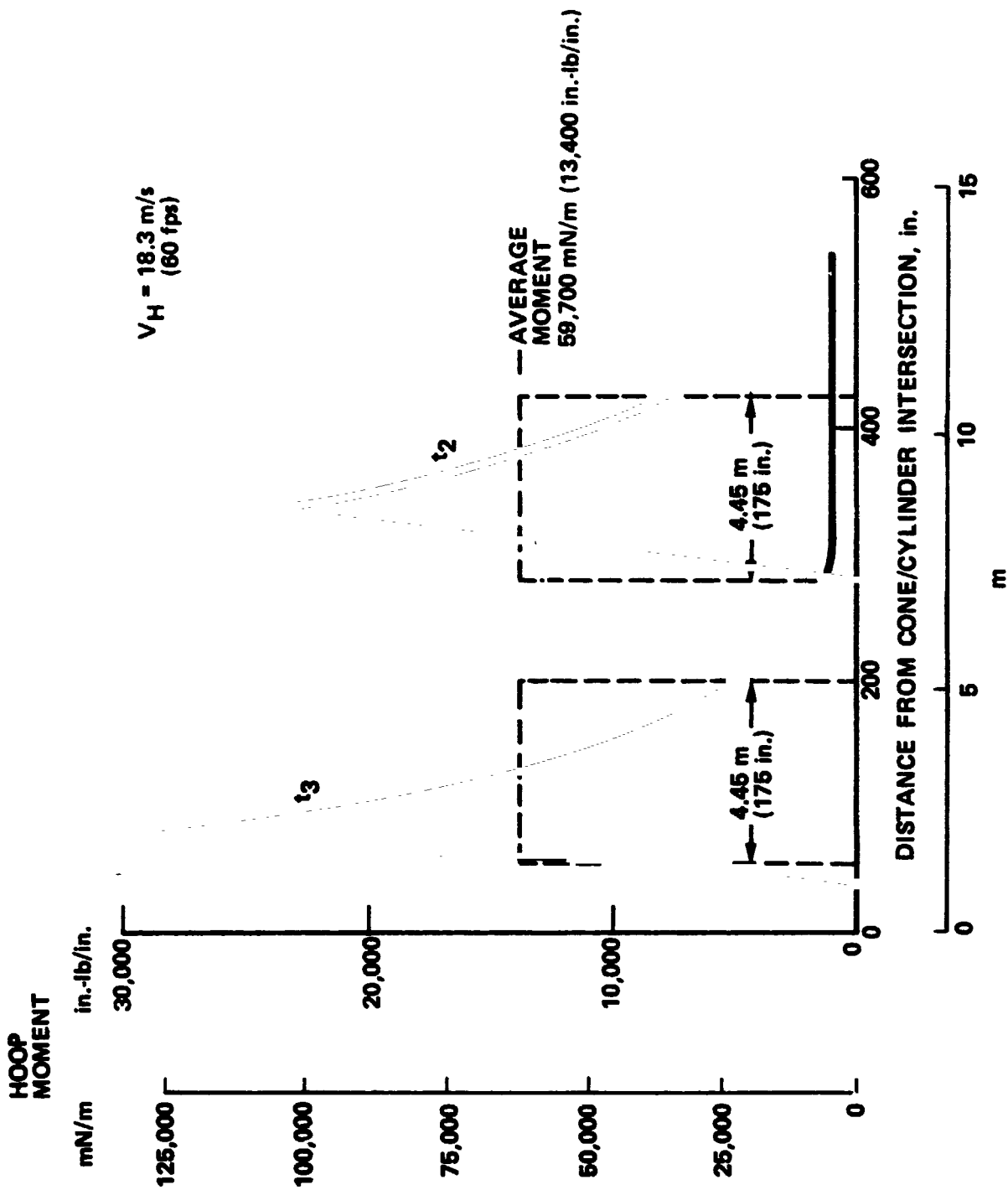


Figure 4.3-16 Slapdown Hoop Moments Averaged for Strength Comparisons

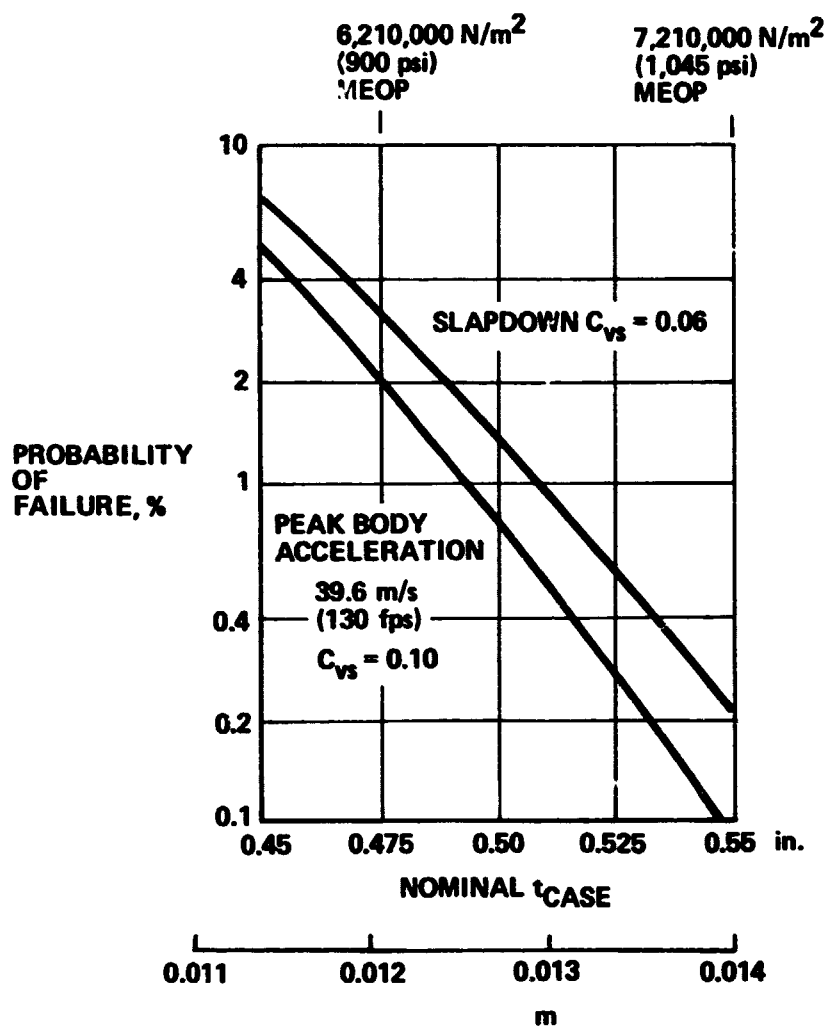


Figure 4.3-17 Center Segment Probability of Failure Sensitive to MEOP

Table 4.3-1 Structural Weight Increases Required to Achieve Low Failure Probability (1%)

SRB STRUCTURAL COMPONENT	UNDERSTRENGTH BASELINE STRUCTURAL ELEMENT	RECOMMENDED CHANGES			WEIGHT PENALTY ASSOCIATED WITH DESIGNING TO 1.25 ULTIMATE SAFETY FACTOR, kg (lb)
		$V_f = m/s$ (fps)	DESCRIPTION	WEIGHT PENALTY, kg (lb)	
FORWARD SKIRT	3 INTERMEDIATE FRAMES AT 45 kg (100 lb) EACH	ALL	USE 0.203 m (8 in.) DEEP FRAMES	385 (870)	697 (1535)
AFT DOME	$t_{BASIC} = 0.00835$ m (0.25 in.)	21.3 (70)	INCREASED DOME t $t = 0.00865$ m (0.34 in.)	418 (920)	604 (1330)
		30.5 (100)	$t = 0.01065$ m (0.42 in.)	790 (1740)	1067 (2350)
		39.6 (130)	$t = 0.0132$ m (0.52 in.)	1271 (2800)	1725 (3800)
		21.3 (70) 30.5 (100) 39.6 (130)	ADD PRESSURE BAFFLE	66 (145) 134 (295) 227 (500)	91 (200) 186 (410) 318 (700)
CASE CENTER SEGMENTS	$t_{CASE} = 0.0121$ m (0.475 in.) MEOP = 6,210,000 N/m ² (900 psi)	ALL	$t_{CASE} = 0.013$ m (0.51 in.) MEOP = 6,660,000 N/m ² (965 psi)	2497 (5500)*	CONSIDER REINFORCING FRAMES
*COMPENSATED FOR BY INCREASED PERFORMANCE					

The three areas that are considered to involve the most uncertainty are:

- 1) The weight penalty that will result when structure is designed to water impact loads can be minimized by considering them during preliminary design. More detailed structural descriptions of the baseline are required to make a good prediction of the additional weight required.
- 2) The effect of the water impact loads on the nozzle and gimbal joint is very sensitive to the SRM contractor design. The failure probability for varying design strength levels should be evaluated further to select the optimum design value.
- 3) Because of the importance of achieving a high case survivability rate, additional comparison of static test results and STAGS analysis results is warranted. The latest slown pressure shapes should be considered together with the possibility of either designing to higher MEOP or adding frames to the case design.

5.0 PRELIMINARY DESIGN CONCEPTS AND CONSIDERATIONS

This section presents the baseline design concept that was selected to satisfy recovery requirements at minimum program cost. It includes description of the sequence of events associated with chute deployment and subsequent water impact, structural arrangement of the baseline, alternative concepts that were considered, and the mass properties that were used in the study. Flotation characteristics are also discussed.

5.1 BASELINE SYSTEM SELECTION AND RATIONALE

The baseline recovery system includes a 7.62-m (25-ft) diameter pilot chute weighing approximately 32 kg (70 lb) and a 40.2-m (132-ft) diameter main chute weighing approximately 908 kg (2000 lb). Both chutes are of 0.35 rad (20 deg) conical ribbon construction with a drag coefficient of 0.58. The system was sized to give a vertical impact velocity (V_{TD}) of 38.1 m/s (125 fps) using an SRB weight of 68,000 kg (150,000 lb). This vertical impact velocity corresponds to minimum total program cost. This relatively high optimum V_{TD} results primarily because the recovery system cost is significantly less for increased V_{TD} values. Minimum cost is also consistent with low component failure probability. It is less expensive to increase the strength of SRB components for higher V_{TD} values than to increase the size and/or number of chutes, providing case redesign is not required.

A single main chute provides a recovery system with good reliability, which is consistent with our premise that the recovery system should be simple to keep costs down and reliable to minimize the number of new SRB components that must be manufactured. The only justification seen at this time for using a more complex system, such as a hybrid, is lack of confidence in the data available or a reluctance to strengthen SRB components.

5.2 BASELINE SEQUENCE OF EVENTS

At time of deployment of the pilot chute, the SRB is trimmed at 1.74 ± 0.17 rad (100 ± 10 deg) and is at an altitude of 2290 m (7500 ft), and a Mach number of 0.35, which results in a dynamic pressure of 6570 N/m^2 (137 lb/ft^2). The nose cap is ejected with three pyro-thrusters that provided sufficient impulse to deploy the pilot chute. The full inflation time of the pilot chute is 3.1 seconds. This event and subsequent steps in the deployment sequence are depicted in Figure 5.2-1.

The explosive separation nuts attaching the forward frustum are fired 2.1 seconds after the nose cap is ejected. At this time, the SRB is at an altitude of 2070 m (6790 ft) and a Mach number of 0.34, which corresponds to a dynamic pressure of 6480 N/m^2 (135 lb/ft^2). The chute reaches its reefed inflated condition 4.15 seconds later and produces a peak loading of 1.85 g on the SRB. At this time the nose cap, frustum, and pilot chute combination moves free of the SRB and main chute because there is no tie between the two combinations. Disreefing occurs 2.95 seconds later at an altitude of 1360 m (4455 ft) and a Mach number of 0.25, which corresponds to a dynamic pressure of 3840 N/m^2 (80 lb/ft^2). The full inflation of the main chute, 4.6 seconds later, produces a peak loading of 1.8 g on the SRB. Water impact of the SRB with main chute attached occurs approximately 26 seconds after full inflation at a vertical velocity of 38.1 m/s (125 fps). The chutes are disconnected 2.9 seconds after impact. The nose cap, pilot chute, and frustum combination impacts the water at 17.2 m/s (56.5 fps) and is recovered separately.

5.3 BASELINE GENERAL ARRANGEMENT

The packaging concept and design details of the recovery system are shown in Figure 5.3-1. The nose cone is fabricated in three sections: nose cap, forward frustum, and aft frustum. The other primary structural components are the swivel and the internal conical structure to which it is attached.

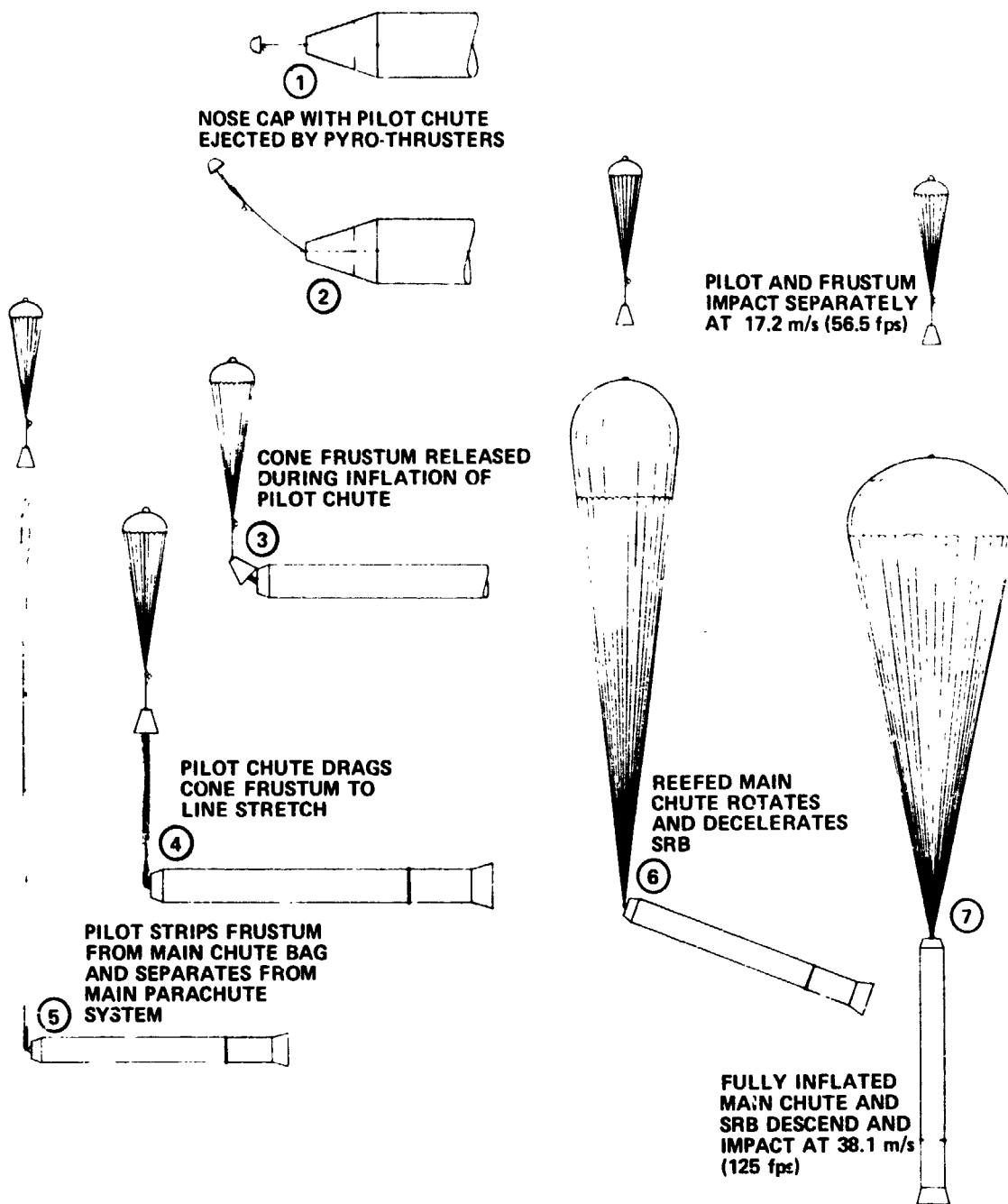
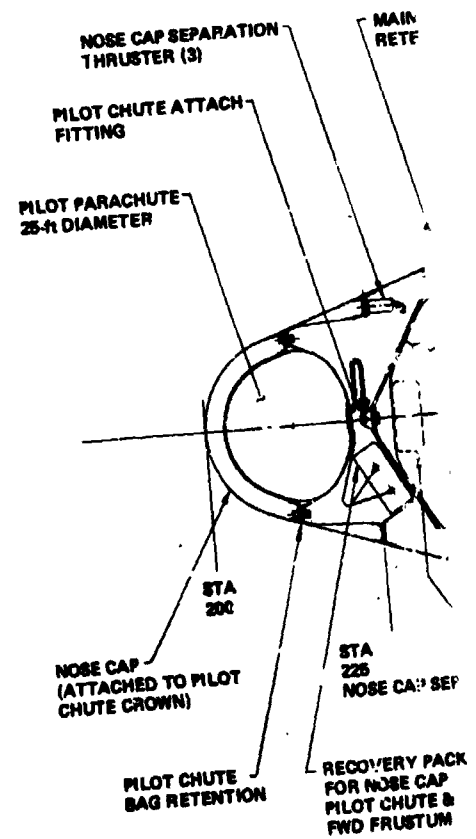
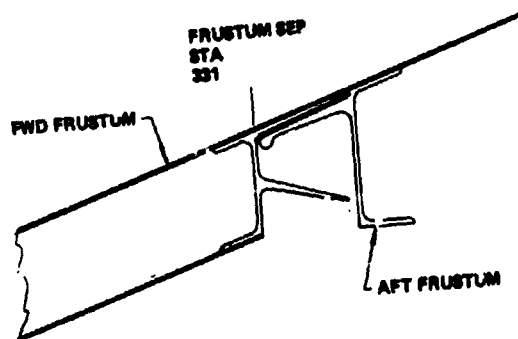
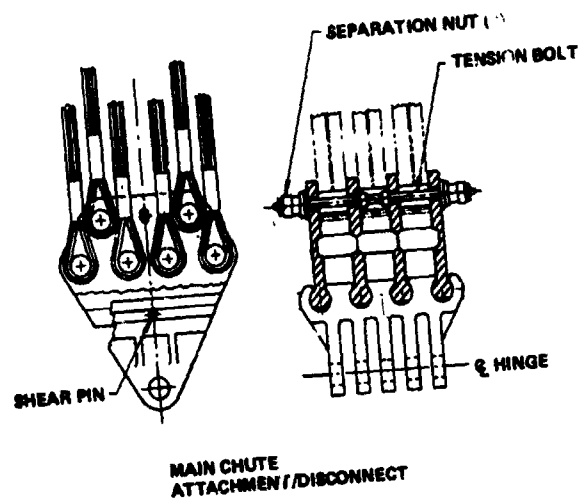


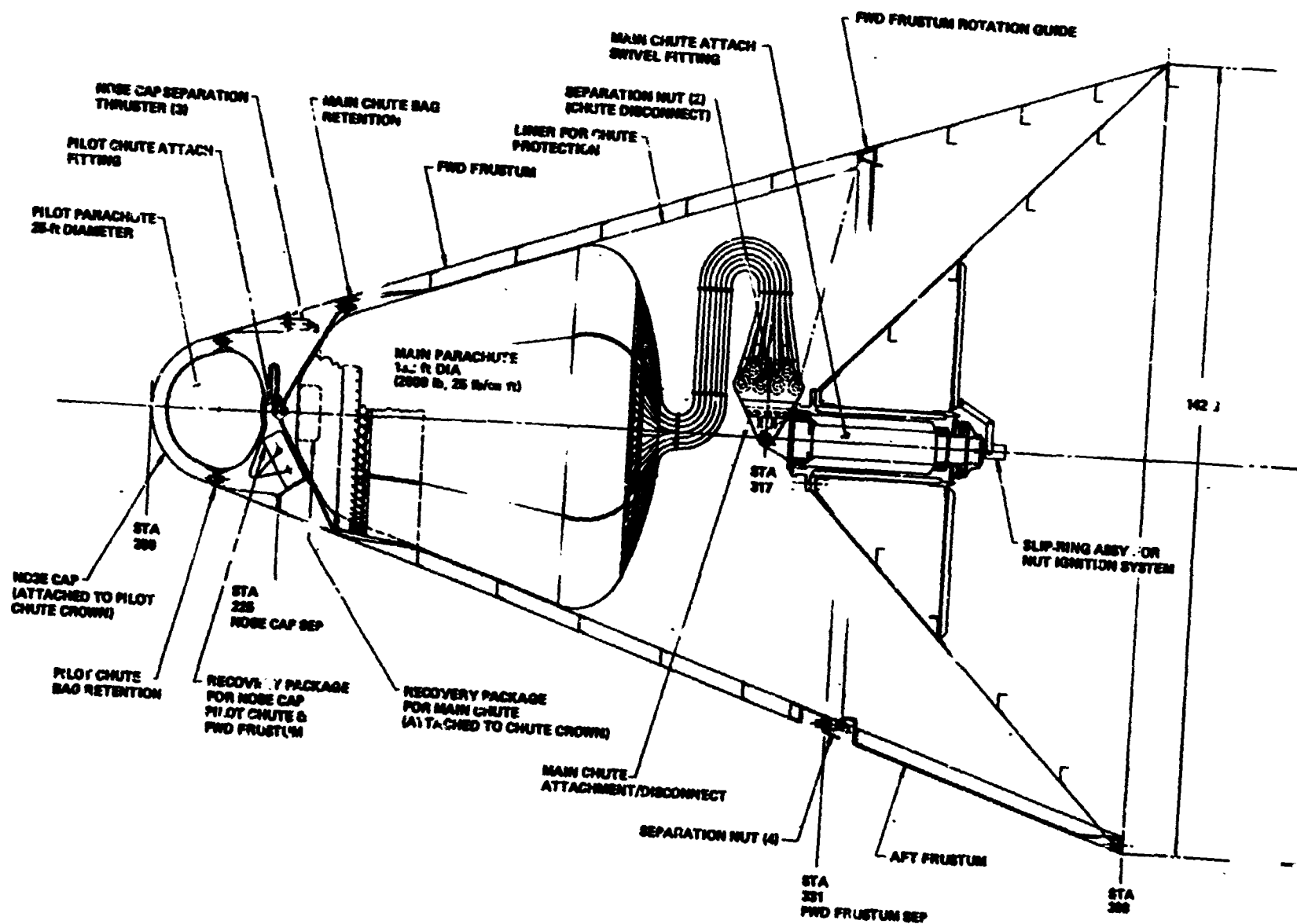
Figure 5.2-1 Deployment Sequence

EJECTOR FRAME



PRECEDING PAGE BLANK NOT FILMED

FOLDOUT FRAME 2



FOLDOUT FRAME

3

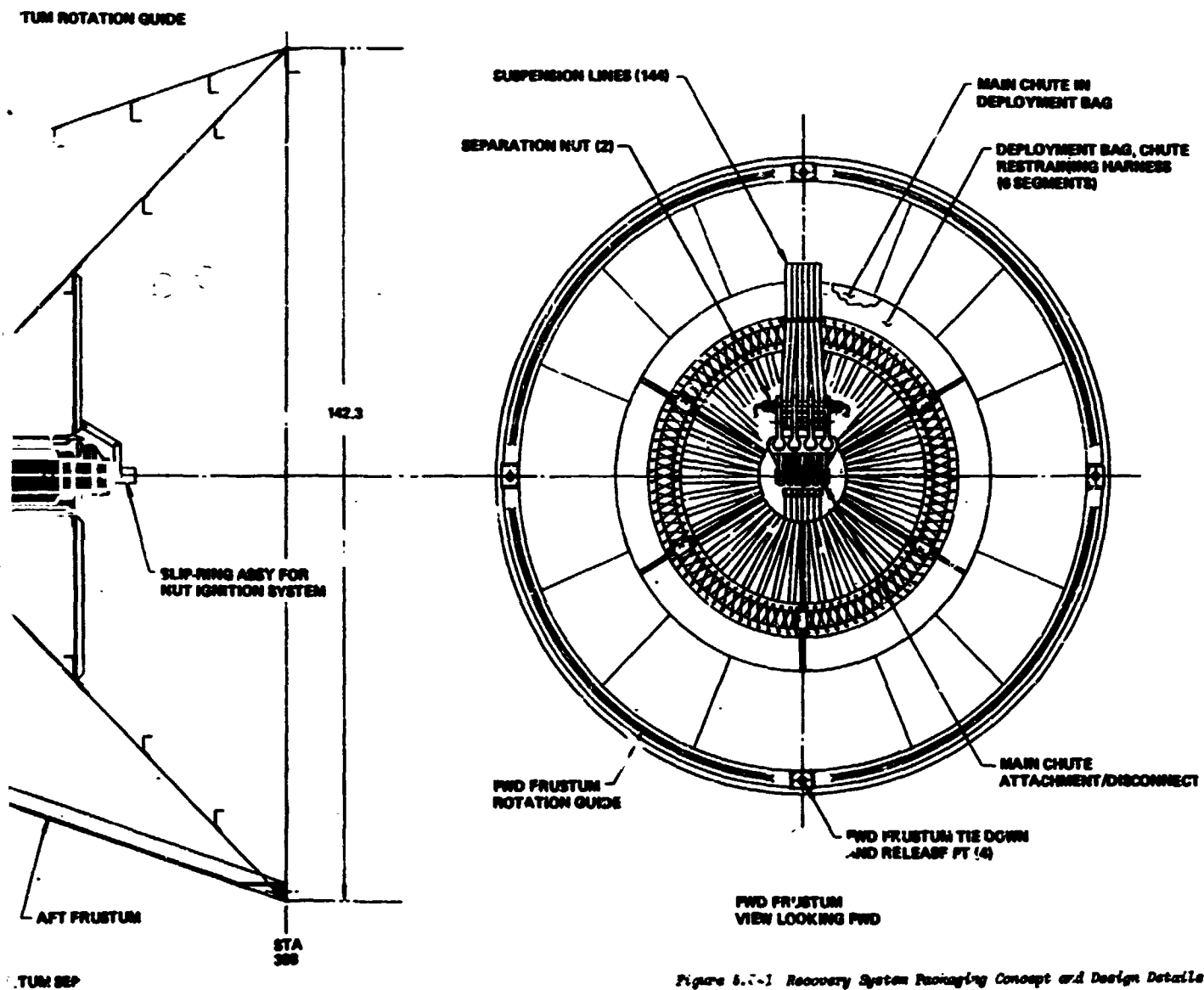


Figure 6.7-1 Recovery System Packaging Concept and Design Details

Our baseline design concept includes a swivel to accept roll rates as high as 1.74 rad/s (100 deg/s) at deployment. With the low deployment altitude and high impact velocity we have selected, the requirement for a swivel to reduce suspension line wrap-up is somewhat weak. With a roll rate of 1.74 rad/s (100 deg/s) and 40-second time span from deployment to impact, a maximum of 11 revolutions between the SRB and the parachute is expected. The opinions of experts in the parachute community are that the suspension lines could easily accommodate a wrap-up of up to 30 revolutions after peak loads have been experienced.

The other function of the swivel, that of assuring the parachute loads are transmitted through the suspension line attachment in the direction for maximum strength, perhaps can be accomplished with a universal joint arrangement as shown in Figure 5.3-2. This approach would not be feasible if maximum loads must be transmitted through a complete 1.57 rad (90 deg) direction change. Examination of deployment dynamic analysis of Section 2, shows that the angle between the parachute force vector and the SRB center line is less than 0.78 rad (45 deg) before the load reaches 1 g. The long time required for the large single main parachute to inflate contributed to this result. If this trend holds for further dynamic analysis for dispersed conditions, the requirement for the swivel may vanish. A weight reduction of approximately 91 kg (200 lb) and a total program cost reduction in the order of one million dollars is estimated. We recommend further evaluation of simpler low-cost alternatives to the swivel, but do not feel the analysis has progressed sufficiently to justify changing the current baseline.

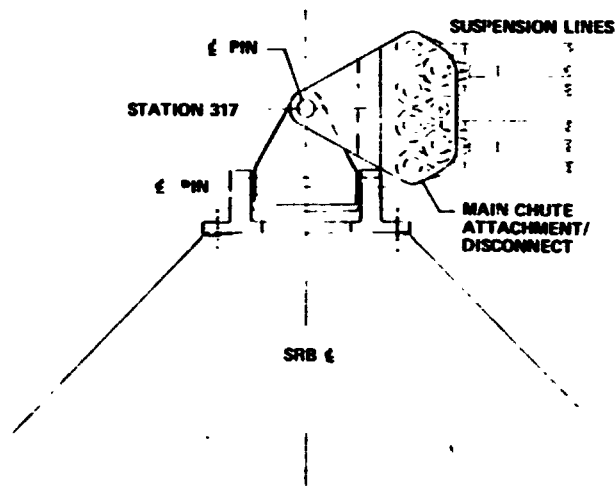


Figure 5.3-2 Possible Universal Joint Attachment

The nose cap separation joint is at Station 225. A retaining bag supports a pilot chute as the suspension lines strip out. The forward frustum is released at Station 331 before the pilot chute opening shock load of 143,000 N (32,000 lb). This load is applied to the forward end of the forward frustum at 1.57 ± 0.17 rad (90 ± 10 deg) to the vehicle reference center line. At Station 331 the separation joint is designed to provide a rotation guide for the forward frustum for 1.57 rad (90 deg) of rotation. The swivel and backup conical structure are designed for 1.85 g limit on the total SRB. The fitting tying the main chute lines to the forward end of the swivel is designed to internally disconnect when the separation nuts on the tension bolt are fired.

Recovery packages are shown for both the pilot chute and main chute systems. These packages include flotation bags and beacon transmitters. A liner is provided in the forward frustum for chute protection. The forward frame of the aft frustum is designed to be smooth to preclude damage to the main chute and/or suspension lines.

5.4 ALTERNATIVE CONCEPTS

The baseline concept described in Section 5.3 has been chosen because it is the most feasible system considering such factors as simplicity, reliability, cost, and applicability. Acceptable alternatives that exist for many operations within the TD&D phase are use of a drogue parachute, an additional pilot parachute, multiple main parachutes, and a hybrid recovery system (parachutes and retrorockets).

5.4.1 Drogue

A drogue chute may be employed to rotate the SRB into a vertical position to simplify the deployment of the main parachute(s). The concept and deployment sequence is similar in systems with and without a drogue chute. If the drogue chute is used, the pilot chute will be much smaller and the minimum altitude to initiate the sequence is higher. The pilot chute is again deployed with the nose cap, using pyro-thrusters. A small cone frustum containing the drogue chute is released. After the drogue inflates, rotating the SRB, the remainder of the frustum (containing the main chutes) is released and deployed by the drogue.

One of the problems of this concept is sizing the drogue to be large enough to rotate the SRB to a near nozzle-first attitude without allowing a large q buildup, but small enough to avoid excessive relative velocity between the chutes and SRB during main deployment. The drogue and cone frustum would be recovered separately from the SRB.

The primary advantages of using a drogue chute are that deployment from high α may be simplified because the components being deployed at this time are smaller, and it offers the potential of higher q deployment. The disadvantages are additional complexity, lower reliability, and increased weight for low q deployment. A small drogue actually increases deployment q for main chutes and the SRB tends to rotate back to high α during the transfer from drogue to main chute operation.

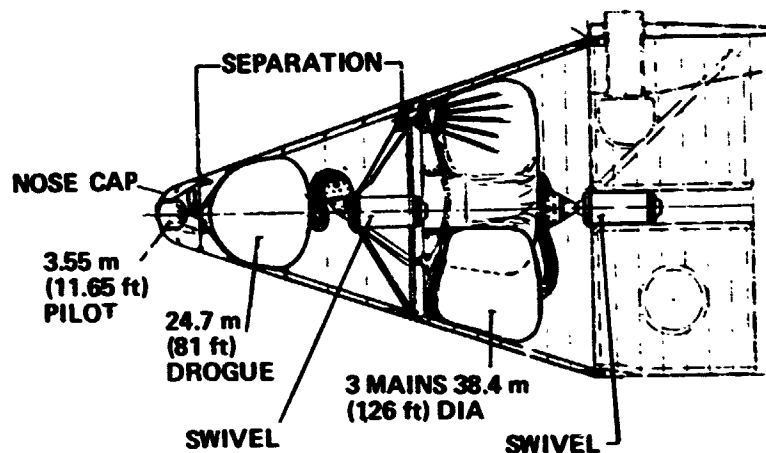
Figure 5.4-1 shows the arrangement of the recovery system in the nose of the SRB both with and without a drogue concept. An alternative concept using three main parachutes is illustrated. Swivels are shown in these designs because analyses have predicted roll rates as high as 1.74 rad/s (100 deg/s) at time of parachute deployment. The system with the drogue required two swivels, both of which are recovered.

5.4.2 Pilot Chute Deployment

Many alternative methods of pilot chute deployment are available. Figure 5.4-2 shows the baseline concept and two typical feasible alternatives. The sketches are shown for direct deployment of the main chutes, but the concepts are similar if a drogue is employed.

The baseline concept, using a pyro-thrusted nose cap, is a simple, lightweight system that allows all components to be recovered with the main chutes (or drogue if used). Axial deployment of the pilot using a mortar makes use of extensive experience in design and application of mortar-deployed systems. A small portion of the nose is expendable when using this system. A more streamwise deployment of the pilot would be achieved by providing roll stability to the SRB and mounting the mortar at an angle. In this case, only a small mortar cover would be expended. The primary concerns with this approach involve the modification of the SRB to provide roll stability, which does not appear to be required for any other reason.

**HIGH α ENTRY; TERMINAL VELOCITY ≈ 24.4 m/s (80 fps)
(3 MAINS CONCEPT SHOWN)**



- ADDITIONAL STAGE ADDS COMPLEXITY, LOWER RELIABILITY
- DROGUE ADDS WEIGHT AT LOW DEPLOYMENT q
- SMALL DROGUE, < 15.2 m (50 ft) INCREASES q FOR MAIN DEPLOYMENT
- SRB TENDS TO RETURN TO HIGH α WHEN DROGUE RELEASED
- DROGUE MAY SIMPLIFY DEPLOYMENT FROM HIGH α
- DROGUE BUYS INSURANCE IF DEPLOYMENT q UNCERTAIN

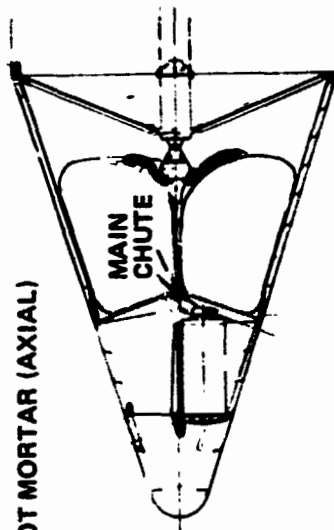
Figure 5.4-1 Concept More Complex If Drogue Needed

PYRO-THRUSTED NOSE CAP



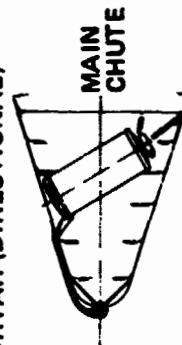
- BASELINE CONCEPT**
- SIMPLE
 - LIGHTWEIGHT
 - ALL PARTS RETRIEVED WITH MAIN CHUTES

PILOT MORTAR (AXIAL)



- ALTERNATIVE CONCEPT**
- EXPENDABLE NOSE CAP
 - EXTENSIVE EXPERIENCE IN MORTAR DESIGN AND APPLICATION

PILOT MORTAR (DIRECTIONAL)



- POOR ALTERNATIVE**
- REQUIRES SRB ROLL STABILITY
 - EXPENDABLE MORTAR COVER

Figure 5.4-2 Alternative Concepts for Pilot Deployment Feasible

5.4.3 Multiple Parachutes

The concept of a single 40.2-m (132-ft) diameter main parachute has been chosen to obtain maximum reliability. This diameter is near the upper limit of present day chute designs. However, the use of multiple chutes, which is equally feasible, reduces the required diameter of the chutes to values well within the state of the art. For example, the use of three main chutes reduces the required chute diameter to 24.1 m (79 ft). Packaging of multiple chutes presents no problem with the existing space envelope of the SRB nose.

5.4.4 Hybrid Recovery System

The most realistic alternative to the baseline recovery concept is a combined parachute/retrorocket recovery system. Figure 5.4-3 shows the sequence of the hybrid system from retrofire to water impact. The TD&D sequence before this point is similar to the all-parachute system described earlier. The typical system shown uses a single 38.4-m (126-ft) main parachute which results in a descent velocity of 41.5 m/s (136 fps). Two retromotors with a thrust-to-weight ratio (T/W) of 3 are fired for 0.8 second when the base of the SRB is 27.4 m (90 ft) above the water. This provides a 15.2 m/s (50 fps) velocity reduction and results in a water impact velocity of 26.2 m/s (86 fps). A variety of combinations of parachute diameters and retrorocket sizes may be employed to give any desired impact velocity.

The hybrid system adds complexity in the form of a radar altimeter, power supply for firing and retromotors, and the addition of a step in the sequence. It does allow lower impact velocities [cost crossover is at 27.4 m/s (90 fps)] and the possibility of using a single main parachute, which tends to improve the system reliability. By allowing higher parachute descent velocities, the retro system tends to reduce the requirement for a drogue. Thus, the retro system allows flexibility to accommodate unforeseen changes in requirements for both impact velocity and deployment dynamic pressure.

**MAIN CHUTE DEPLOYMENT
SAME AS ALL CHUTE SYSTEM**

**ONE 38.4 m (126 ft)
DIAMETER MAIN
CHUTE**

RETRO FIRE

$h = 27.4 \text{ m (90 ft)}$

$v = 41.5 \text{ m/s (136 fps)}$

$T/W = 3$

$\tau_B = 0.8 \text{ sec}$

IMPACT

$v = 26.2 \text{ m/s (86 fps)}$

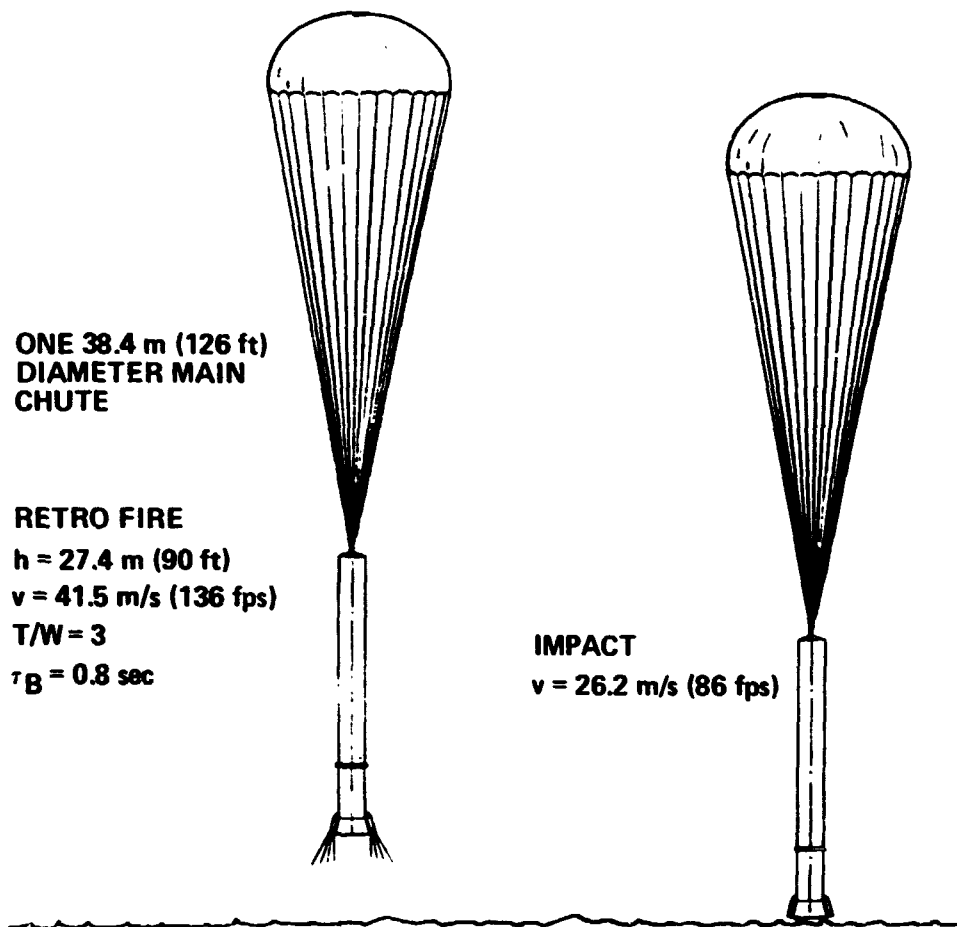


Figure 5.4-3 Hybrid System Sequence Same as All-Parachute System to Retrofire

5.5 RECOVERY SYSTEM WEIGHTS

The baseline recovery system described in Sections 5.1 and 5.3 is lighter than the recovery system which was included in the NASA-provided set of baseline weights, primarily because the baseline terminal descent velocity is now greater than that originally envisioned. Table 5.5-1 presents the weight summary for the 38.1 m/s (125 fps) baseline recovery system.

Table 5.5-1 Baseline Recovery System Weights

	KILOGRAMS	(POUNDS)
AVIONICS	70	(154.4)
ELECTRICAL	45	(98.8)
ORDNANCE	40	(89.0)
PILOT CHUTE INSTALLATION	89	(195.0)
MAIN CHUTE INSTALLATION	1,317	(2,900.0)
RETRIEVAL PACKAGES	52	(114.6)
TOTAL	1,613	(3551.8)

5.6 FLOTATION

The impact/flotation sequence is a complex dynamic and thermal transient problem. A detailed analysis is beyond the scope of this study. The final flotation attitude and the behavior of the SRB between impact and equilibrium are functions of configuration, horizontal and vertical velocity at impact, attitude, and thermal effects. We have postulated various events, performed simplified analysis of parts of the problem, and calculated static stability points to define probable flotation characteristics and trends. Additional scale model testing including thermal effects and wave motion, and more sophisticated analytical analysis combining stage dynamics, thermal, and thermodynamic effects on flotation are required to verify the trends presented.

5.6.1 Basic Flotation Characteristics

The most likely sequence of events is illustrated in Figure 5.6-1. When the stage impacts it will partially submerge and begin to pitch over. The depth of penetration and attitude history are functions of impact velocity, horizontal velocity, and impact angle. At maximum submergence, excess buoyancy will initiate a rebound action. As the stage rebounds and pitches over, the nozzle will move closer to the water surface, and the water that has entered the SRB will move away from the nozzle, permitting part of the contained gas to escape. This reduction of the volume of trapped gas will reduce the internal pressure and will allow additional water to enter. In turn, buoyancy is reduced and the center of buoyancy moves forward, increasing the moments tending to return the stage to the nozzle-down direction. Depending on the remaining gas content, the stage will assume a stable log mode or vertical position.

For the baseline SRB configuration several flotation modes are possible. The flotation height, for the vertical flotation mode, is presented in Figure 5.6-2 as a function of the amount of air trapped in the SRB. This curve shows that if the stage were placed in a calm sea in a vertical attitude and allowed to reach equilibrium with the maximum amount of air [419.5 kg (925 lb)] on board, it would float with 18.3 m (60 ft) submerged, and with 21.3 m (70 ft) of the SRB above water. This is an unstable condition, however, because the center of gravity is slightly above the center of buoyancy. If the air trapped is 2% less than the maximum (because of venting or cooldown), a vertical stable mode exists. It is virtually impossible to reach this condition, however, because the vehicle will pitch over before equilibrium can be realized.

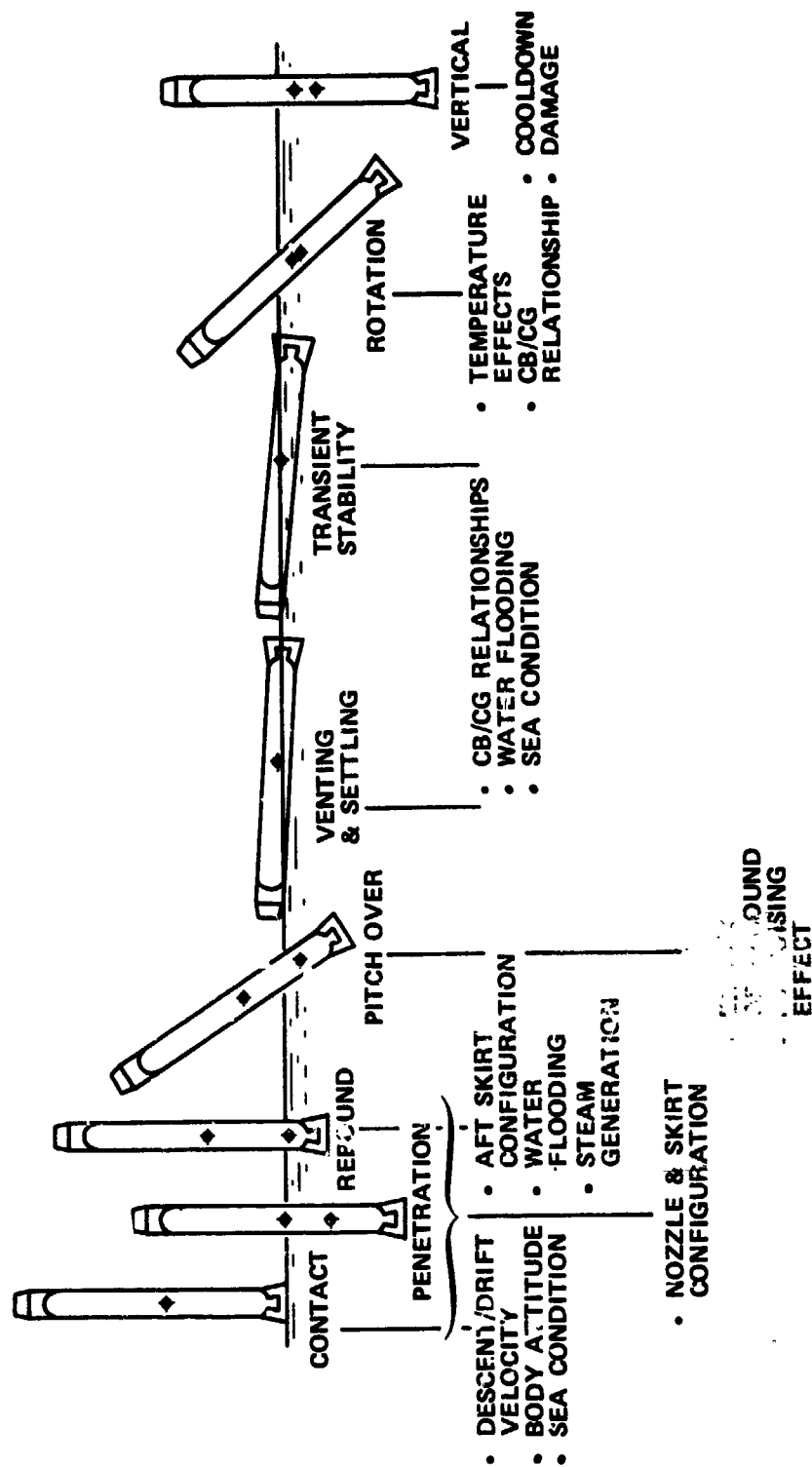


Figure 5.6-1 Typical Impact Sequence Leads to Vertical Flotation

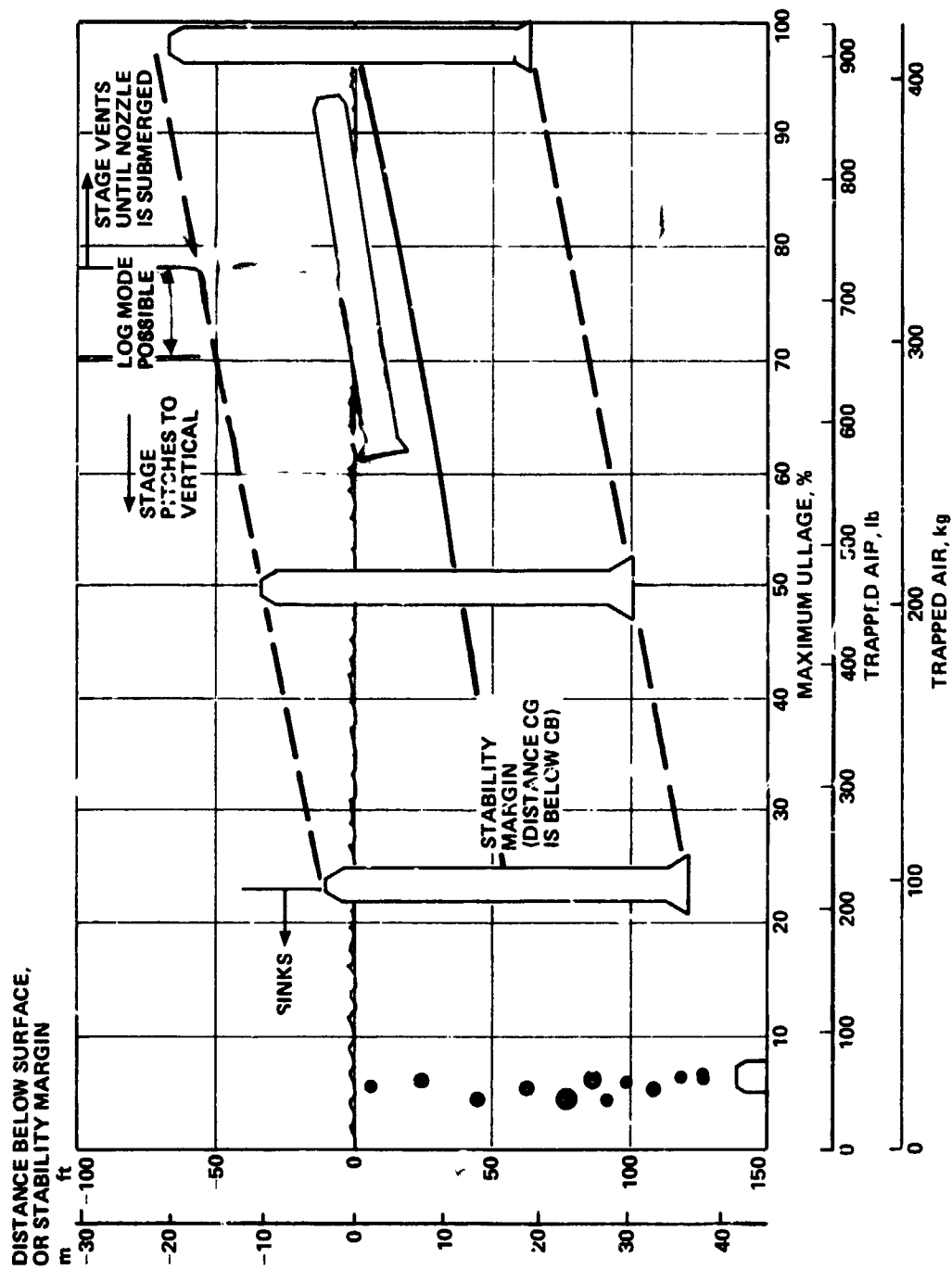


Figure 5.6-2 Flotation Height, a Function of Amount of Air Trapped

If the stage were placed horizontally on a calm sea with no water shipped, it would float with a slightly nozzle-down trim angle with about 0.076 m (3 in.) of freeboard at the nozzle throat. If as much as 2.8 m³ (100 ft³) of water is shipped, the freeboard will disappear, and additional water will enter the stage. Because of the nozzle-down attitude and the location of the center of gravity, the water entry will cause rotation in the nozzle-down direction. This process will continue until approximately 88.5 m³ (3126 ft³) of water has entered, trapping 329.8 kg (727 lb) of air (1 atm at 25°C or 77°F). The stage will then float in a stable log mode attitude with the nozzle submerged, preventing further displacement of the trapped air. If the stage rotates toward the vertical, the internal pressure increases because of the greater submergence of the liquid-gas interface. This results in a compression of the gas, entry of more water, reduction in buoyancy and shifting forward of the center of buoyancy. Thus, for some quantities of trapped air, the stage will be stable in the log mode, but if rotated sufficiently, the center of buoyancy will move past the center of gravity and the stage will go to a stable vertical attitude. When more than 123.5 m³ (4350 ft³) of water has been shipped, (less than 298.5 kg (658 lb) of air trapped) the center of buoyancy is forward of the center of gravity for all attitudes and the log mode is not possible.

After rotation to vertical for this case this SRB will float with about 13.7 m (45 ft) above the surface and 26 m (85 ft) below. More than 18.3 m (60 ft) of the SRB is not likely to be exposed under any circumstances. A minimum trapped gas content of about 98.5 kg (217 lb) of air, or 80.5 m³ (2845 ft³) at 1 atmosphere, is required for flotation. Thus, if more than 291.7 m³ (10,300 ft³) of water is shipped, the SRB will sink.

If at impact 10 m³ (350 ft³) of water enters the SRB and sloshes forward rapidly enough to shift the c.g. ahead of the c.b., a stable nozzle-up attitude is possible. As more water is taken on-board in this manner, the SRB assumes a more nozzle-up attitude until after 158.6 m³ (5600 ft³) of water is shipped, the vehicle is in a vertical attitude. This flotation mode is very unlikely since it would require precise timing of water entry and stage attitude, combined with proper inertia and sea state to create and sustain this attitude. Thus, we have not further considered a nozzle-up attitude as a feasible flotation mode.

5.6.2 Thermal Effects on Flotation

The final gas volume is strongly dependent on the internal temperature at impact. Since the contained air is at 1 atmosphere just before splashdown, its mass will vary inversely with its absolute temperature. The final temperature will be that of the sea water, and this will control the final density and volume of the trapped air. Thus, a higher initial temperature results in a smaller trapped air volume. If the internal surface temperature is above 100°C (212°F), steam will be generated as water enters the SRB case. This will increase the total gas volume and pressure, and result in a greater loss of gas at pitchover. Once the SRB has settled into a stable nozzle-down position, the air and case will come into thermal equilibrium with the sea and the steam will condense. While the quantity of water vaporized directly affects the volume of gas lost, the distribution of the air and steam and the temperature of the mixture are also important factors in determining how much air is lost. Because the air is denser, there will be a tendency for stratification to occur, with the steam above the air. Since the pitchover occurs within about 10 seconds after impact, however, it is more likely that the steam-air distribution will depend on where the steam is generated and on the mixing forces present. The assumption of total stratification would be the worst case, resulting in only air being lost at pitchover.

Generation of steam increases the total gas volume and pressure and acts to resist the entry of water into the stage, thereby increasing buoyancy. This increased buoyancy will affect the submergence and rebound characteristics of the stage. A simplified one-dimensional analysis (without pitchover) was performed to evaluate this effect. Comparison of cases with maximum steam volume and with no steam generated indicated that no significant change in initial submergence depth or frequency resulted from the steam. The initial rebound height was increased less than 10%. Figure 5.6-3 presents a typical result of this analysis. Since the SRB will pitch over during the first cycle, only this portion is applicable for realistic SRB impact.

The SRB internal temperature at impact will be determined by aerodynamic heating or cooling of the outer surface, heat transfer from the interior through the insulation to the case, radiant heat transfer through the nozzle and, by cooling resulting from breathing or circulation of ambient air into the case. Of greater importance, however, are the temperature profiles existing at solid rocket burnout, the amount of insulation that has been eroded, and the thickness of the char. As the remaining insulation thickness is increased, the temperatures and stored heat at splashdown increase because most of the heat to be dissipated must be transferred through the insulation.

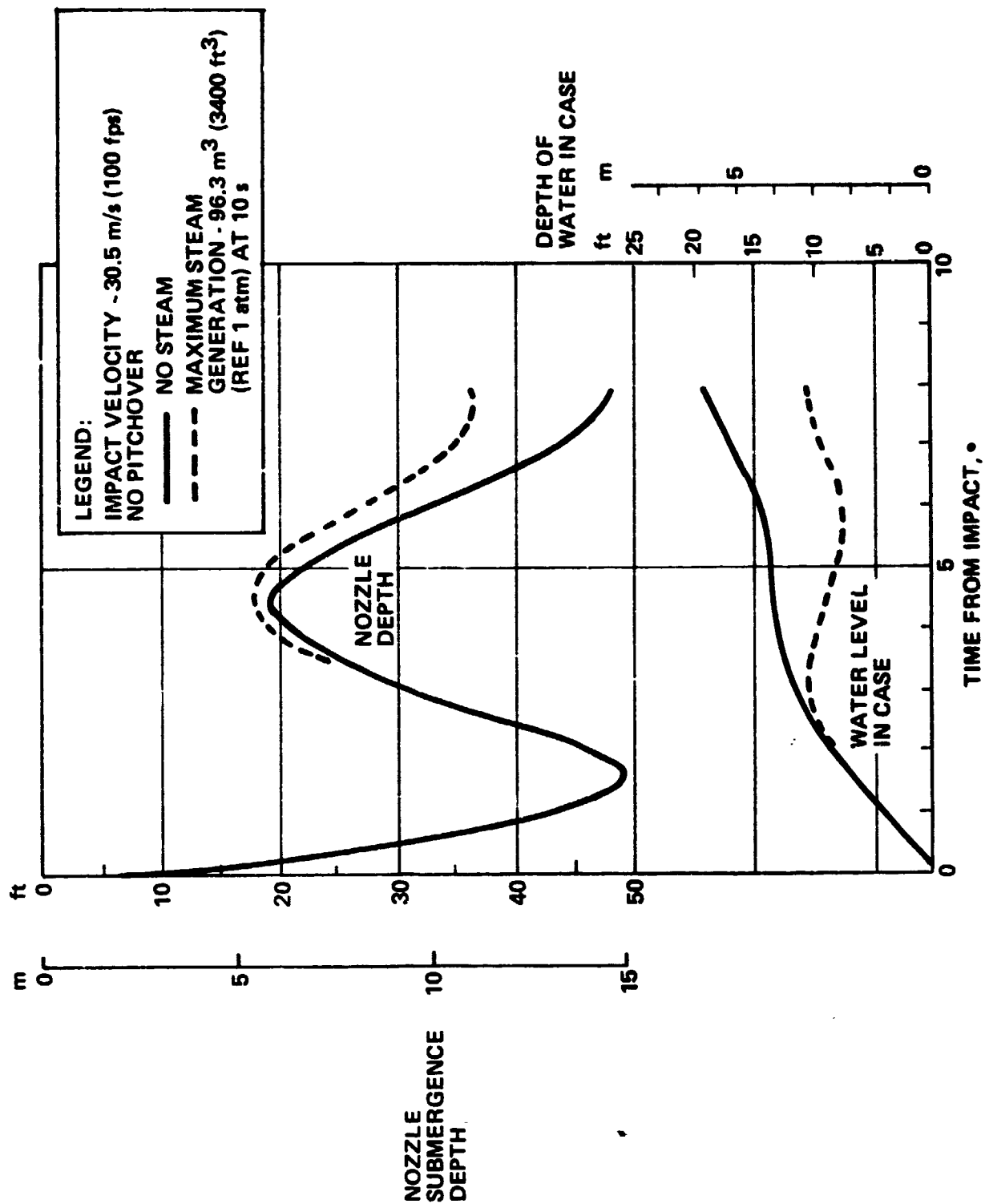


Figure 5.6-3 Small Effect of Steam Generation on Rebound Characteristics

Results of an analysis conducted by Thiokol and reported in an internal memorandum* have been used as the definition of a worst case model of the SRB case and nozzle. The temperature profile predicted for the case cross section in this reference is presented in Figure 5.6-4. It is noted that the interior surface temperature of 293°C (560°F) reflects an original insulation thickness of 35.5 mm (1.4 in.), with approximately 7.6 mm (0.3 in.) eroded. In contrast, a previous Martin Marietta analysis, depicted in Figure 5.6-5 assumed an initial insulation thickness of 6.35 mm (0.25 in.), with a final char depth of 3.37 mm (0.1325 in.) and no erosion. This analysis predicted an internal temperature at impact of approximately 129°C (265°F).

Using the Thiokol model as the worst case temperature distribution, we conducted an analysis to determine the rate of steam generation. Since steam generation is highly dependent on the manner in which the hot insulation surface is wetted, it is first necessary to investigate the mechanisms causing this wetting. On impact, a limited quantity of water may enter through the nozzle at very high velocities to create a water spout effect. We have not analyzed this mechanism in detail to predict water flow rates or distribution; however, simple calculations show that vertical velocities of several hundred feet per second are possible. This value is sufficient to cause wetting within approximately the first one-half second at all levels within the stage interior. NASA movies taken inside a 3-m (120-in.) SRB during drop tests show the occurrence of this phenomenon.

The quantity and distribution of the water entering at impact are very dependent on horizontal velocity, stage attitude, and the vertical impact velocity. Deviation from axial symmetry probably results in nonsymmetric wetting of the interior and some reduction in the rise height of the waterspout and volume of water involved. However, because of the energy available, it is expected that the primary high velocity flow at impact results in the formation of a mist or spray that generally covers areas not otherwise fully wetted.

If the surface is extremely hot and only small droplets of water impinge, it is probable that these droplets will be repelled by steam generated at the instant of contact. For more continuous streams of liquid, the analysis would indicate that the surface would be significantly cooled within the first second, and would be wetted with an unseparated film of water.

7

*Del Mecham, Thiokol/Wasatch Division, Interoffice Memo 2814-72-117; *An Analysis to Determine the Amount of Water Boiled by a Space Shuttle Booster after Water Impact.* October 5, 1972.

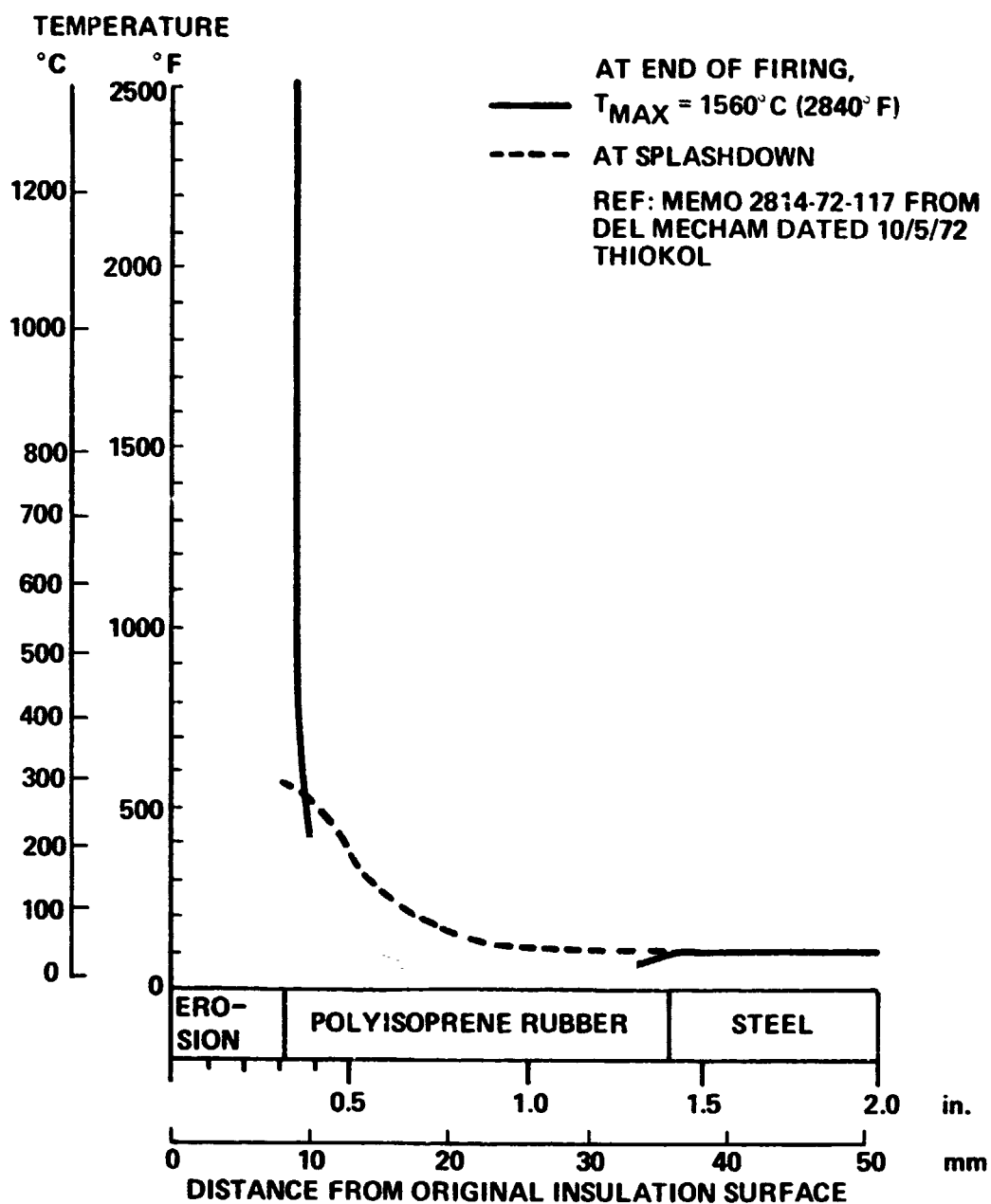


Figure 5.6-4 SRB Case Temperature Profiles

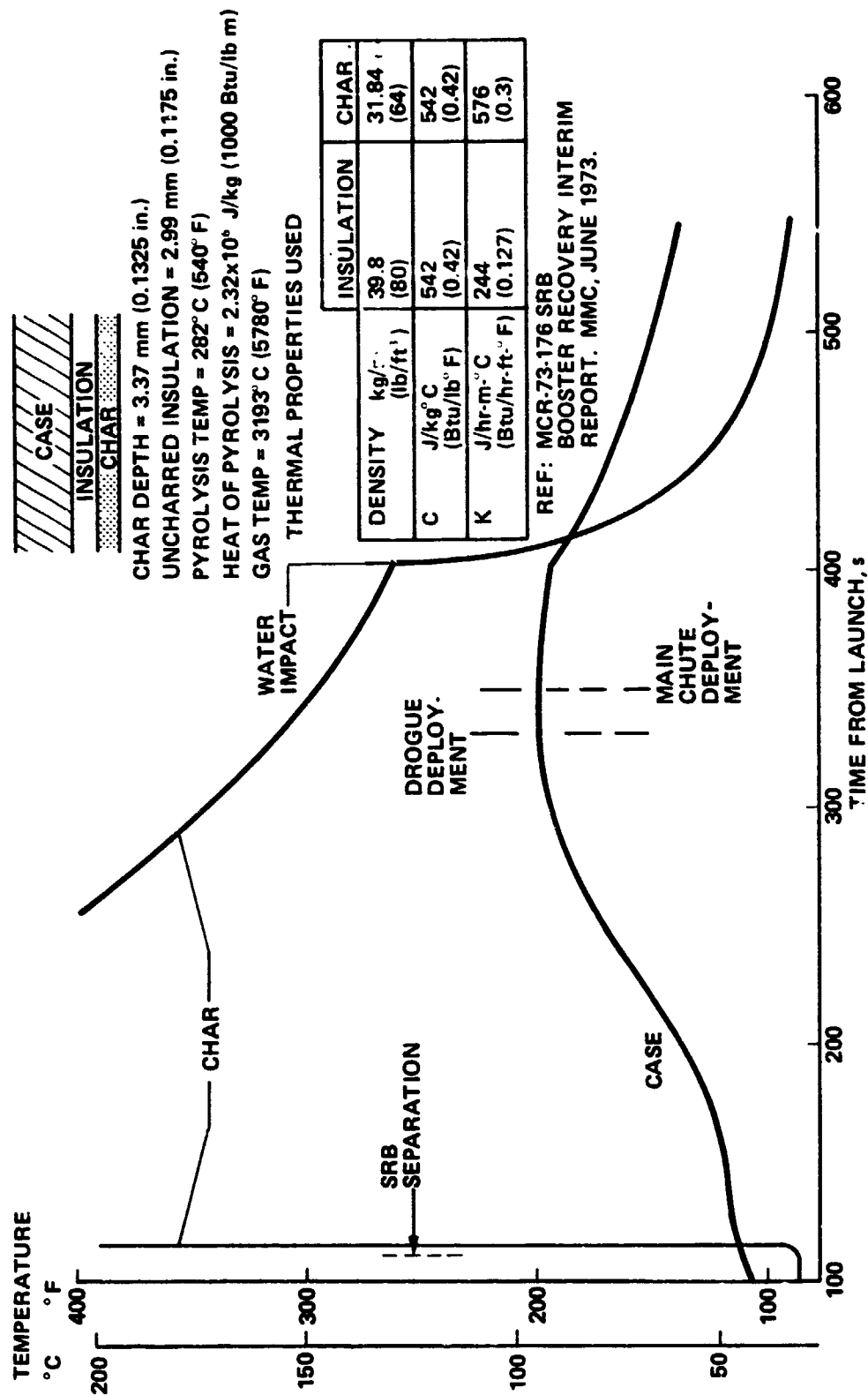


Figure 5.6-5 Temperature Profiles Defined by Aero Heating

Once the upward momentum is dissipated and the water has attached to the wall as a film, it will then begin draining along the surface. Results of an analysis of laminar drainage of a water film on a vertical surface are given in Figure 5.6-6. This analysis shows that at a point 3 m (10 ft) below the top of the wetted area, a thick film 1.6 mm (1/16 in.) or more, drains more rapidly than a much thinner film. A layer of water on the order of 0.15 mm (0.006 in.) thick is stable within the first ten seconds and does not reduce at the comparison point until nearly 17 seconds.

Independently of the initial waterspout mode of wetting at impact, water will flow into the stage as it submerges, flooding and rapidly cooling the lower surface. Steam will be formed in these areas only up to the time of submergence. The lower region will also be well washed by drainage from above.

To predict steam generation rates, we performed one-dimensional transient analyses for various points and conditions. Our model considered as nodes parallel layers of water and insulation (and/or char), backed by the steel case. The node thicknesses were made very small [on the order of 0.025 to 0.075 mm (0.001 to 0.003 in.)] at the boiling interface, and were increased in either direction away from this interface. Heat transfer in the liquid was assumed to be by conduction only with no mixing effects. Means was provided in the computer iteration for decreasing the water film thickness in accordance with predicted draining rates. No prediction of the tendency for steam to carry off water droplets was attempted, and the water remained on the wall until it had either drained away or evaporated. Nucleate or film boiling heat transfer coefficients, depending on the node temperatures, were applied at the boiling interface along with radiant heat transfer. The first water node was constrained to a maximum temperature of 100°C (212°F), and net heat transfer to this node after it reached the boiling point was assumed to result in evaporation.

A typical result is plotted in Figure 5.6-7 for an initial surface temperature of 293°C (560°F) and an initial film thickness of 1.6 mm (1/16 in.) extending 3 m (10 ft) above the point examined. In this case, significant vaporization did not start until the bulk of the water had drained away. For much higher initial surface temperatures, and for materials with a much higher thermal conductivity such as metals, boiling would start almost instantly regardless of the amount of water present. These data also show the result for an initial water film thickness of 0.15 mm (0.006 in.) with a negligible drainage rate. Clearly this condition produces a greater quantity of steam.

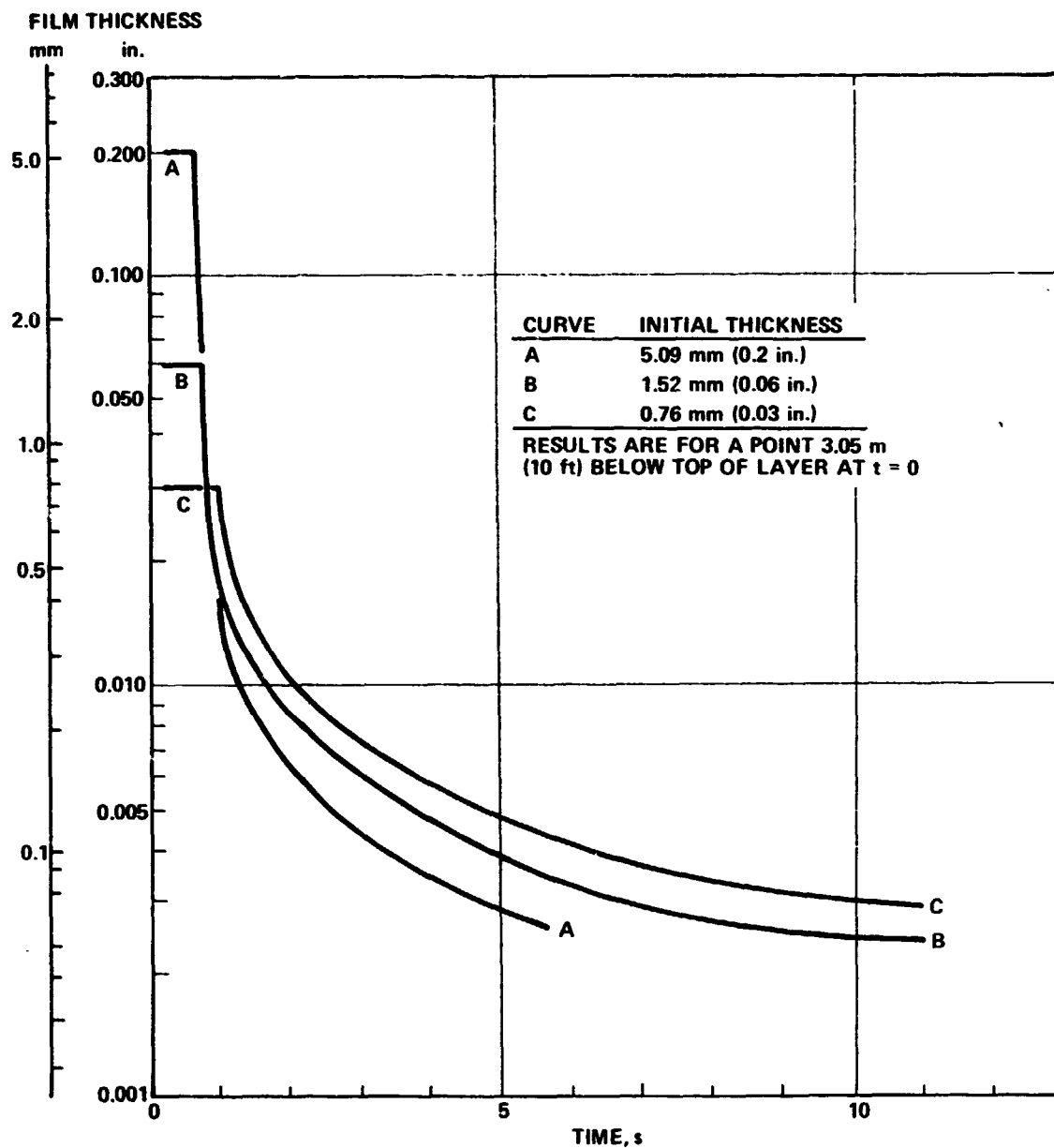


Figure 5.6-6 Increased Initial Water Film Thickness Drains More Rapidly from Flat Plate

**STEAM VOLUME PER
SURFACE AREA**

m^3/m^2 ft^3/ft^2

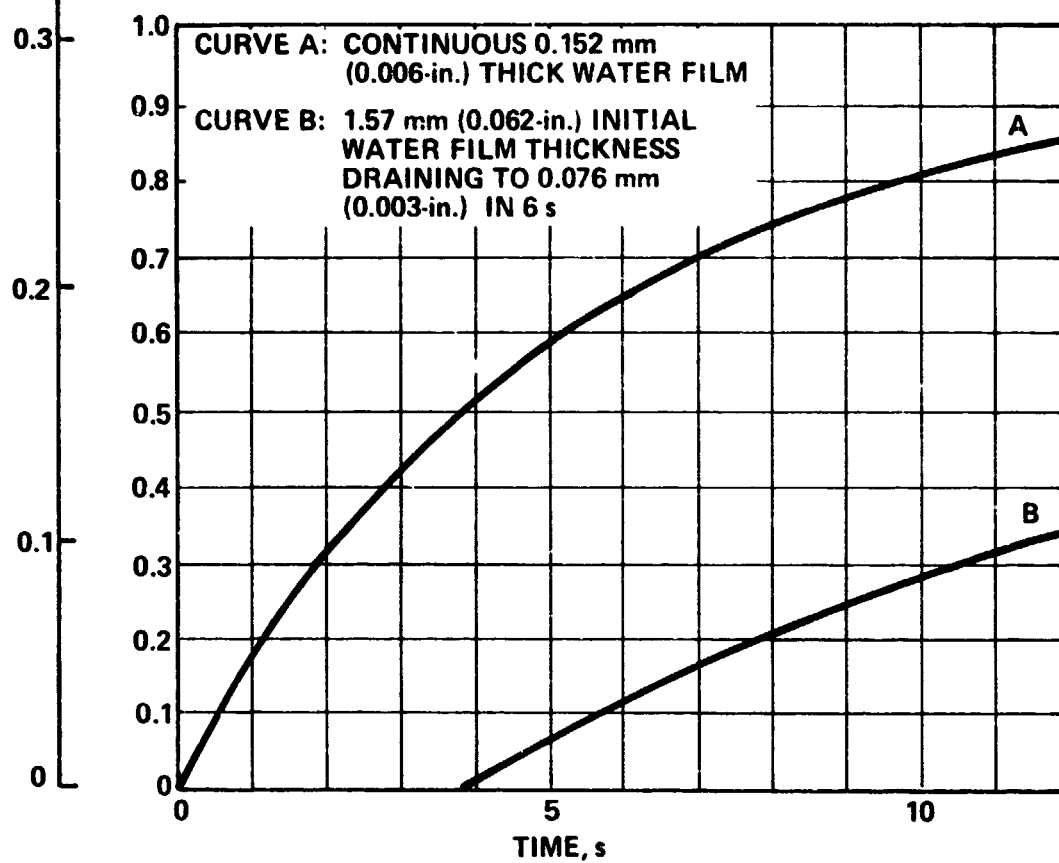


Figure 5.6-7 Thick Water Film Retards Steam Generation

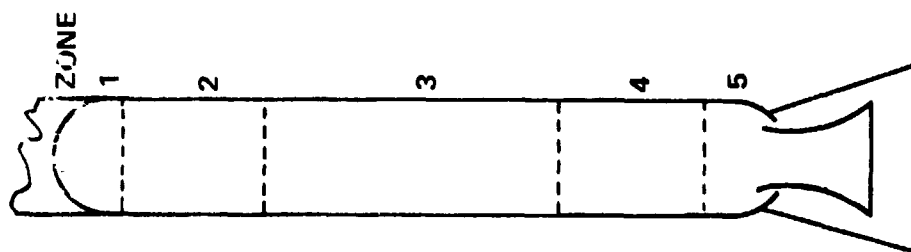
To predict the maximum volume of steam possible with the Thiokol temperature profile, the entire inner surface was assumed to be wetted with a 0.15 mm (0.006 in.) film of water at impact. No drainage was allowed and the flooding of the lower surface of the case was neglected. No steam was assumed to be generated by the nozzle, however, because it is submerged very rapidly. A more probable assumption for water distribution is given in Table 5.6-1. Figure 5.6-8 compares the total steam volumes for these two cases. Clearly, many other wetting assumptions could be made with equal justification. If pitchover is considered, much of zone 3 will be drenched before a significant amount of steam is generated. The purpose of Table 5.6-1 is to postulate a more reasonable, but still conservative, wetting model rather than to assume worst case conditions. Since venting will probably start before 5 seconds, much of the steam generated after this time may escape rather than displace the trapped air.

The nozzle, with predicted temperatures of 870 to 1200°C (1600 to 2200°F) will generate as much as $1.8 \text{ m}^3/\text{m}^2$ ($6 \text{ ft}^3/\text{ft}^2$) of steam during the first 10 seconds. However, the nozzle will be totally submerged for essentially the entire period except briefly at pitchover. The high initial water velocity relative to the nozzle will probably cool the surface more rapidly than predicted by the analysis. To evaluate the contribution of this steam originating under water at 25°C (77°F), an analysis of the survival of steam bubbles was undertaken. It is concluded from this analysis that bubbles of 50-mm (2-in.) diameter or less will have collapsed to less than 0.1% of their original volume before rising 200 mm (8 in.) in 25°C (77°F) water. The heat liberated by this recondensation is only sufficient to raise the temperature of a 0.3-m (1-ft) layer of water about 2.2°C (4°F) during the initial 10-second period. It is, therefore, concluded that the nozzle contribution to total steam volume can be neglected.

Using these final results, air volumes were predicted. The stage was assumed to pitch over and vent sufficient gas to raise the water level to the top of the nozzle and to reduce the internal pressure to approximately 7000 N/m^2 (1 psig). Total stratification of the steam and air was assumed, so that only air was discharged. In addition, the air was assumed to have remained at its original temperature of 293°C (560°F) during venting.

Table 5.6-1 Probable (Assumed) Wetting Conditions

ZONE	TOTAL AREA, %	SURFACE WETTING CONDITION	TOTAL STEAM VOLUME, m ³ (ft ³) AT 1 ATMOSPHERE	
			TO 15 s	TO COOLDOWN
1	10	Remains totally dry	0	0
2	20	0.152 mm (0.006-in.) water layer with- in ½ second, no significant draining	20.8 (736)	21.5 (762)
3	40	Wet by 1.57 mm (0.062-in.) water layer- drains to 0.25 mm (0.010-in.) in 2 seconds 0.076 mm (0.003-in.) in 6 seconds	17.8 (628)	25.0 (884)
4	20	0.152 mm (0.006-in.) mist impingement at impact, drenched after 2 seconds	8.0 (282)	8.0 (282)
5	10	Flooded continuously after impact	0	0
TOTAL			46.6 (1646)	54.6 (1928)



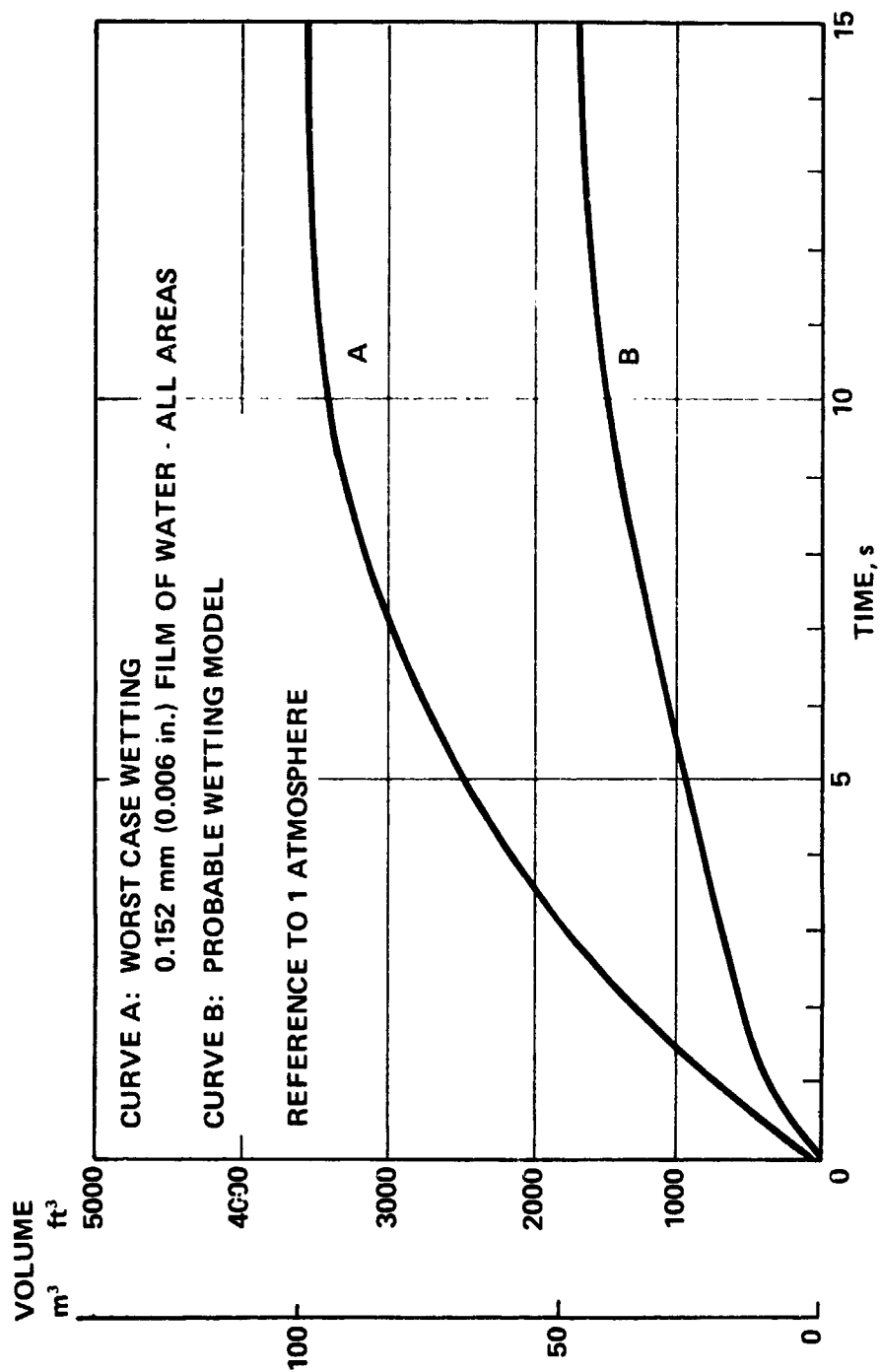


Figure 5.6-8 Predicted Steam Volumes Versus Time

For the maximum steam case, 100.2 kg (221 lb) of air remained, occupying 157.6 m³ (5567 ft³) at 1.07 atm (15.7 psia) or 81.9 m³ (2892 ft³) at 25°C (77°F) and 1 atm. Thus, with compounding of worst case conditions, the trapped air slightly exceeds the 98.5 kg (217 lb) or 80.5 m³ (2845 ft³) at 1 atm required for flotation. Using the more probable wetting assumptions of Table 5.6-1, but applying the conservative air temperature and stratification assumptions for venting, 133.8 kg (295 lb) of air or 109.5 m³ (3867 ft³) at 1 atm remained. This is 36% greater than the minimum required for flotation but substantially below the 298.5 kg (658 lb) needed for log mode. Thus, the SRB is expected to float in the vertical mode, but could have as little as 6.1 m (20 ft) above the water surface and 33.5 m (110 ft) below.

5.7 RECOVERY ENVIRONMENTAL ANALYSIS

The SRB experiences four environmental flight phases during the Space Shuttle mission: liftoff and ascent, separation from external tank, reentry and parachute deployment, and water impact. Considering the total mission, there does not exist a single critical period for all environments (acoustic, vibration, shock, thermal). The peak conditions for the various environments occur in different flight phases.

The component environmental analysis was performed using the equipment list and equipment locations of the NASA/RI baseline recovery system. The shock environment of some components of this layout is considered excessively high because of their proximity to pyrotechnic devices. These high shock areas can be avoided by moving the components a sufficient distance from the shock source (Figure 5.7-1).

The environments presented in Table 5.7-1 were developed for recovery equipment, based on data obtained from the Titan and Viking programs and the external tank proposal effort. The information from 14 Titan flights, consisting of more than 80 data channels, was adjusted to the current SRB baseline design, providing the basis for estimating the vibration and acoustic environments. The shock environment in the area of the forward skirt and nose cone was developed from the Viking pyrotechnic testing, Titan payload separation, and SRM separation tests. To this baseline was added the environmental level developed in the external tank proposal and presented for the SRB in NASA document SP-ET-0002A, Volume I. Finally, the separation vibration predictions were based on results of ground test firing of small solid rocket motors that induce vibration caused by thrust variation.

Table 5.6-1 The Design Environments Within Equipment Capabilities

ENVIRONMENT LOCATIONS	MISSION PHASES			
	LAUNCH	SRB SEPARATION	ID&S/TD&D	IMPACT
ACOUSTICS (DBOAL)				
NOSE CONE	159	---	166	---
FORWARD SKIRT	157	NA	166	1400
AFT SKIRT	166		166	---
NOZZLE	169	---	166	---
VIBRATION (GRMS)				
NOSE CONE	32.0	23.0	47.0	NA
FORWARD SKIRT	21.0	45.0	19.0	
AFT SKIRT	37.0	45.0	28.0	
NOZZLE	33.0	23.0	---	
SHOCK (g)*				
NOSE CONE	NA	2,000 Peak	12,000	25 g amplitude 140 millisec Half sine pulse
FORWARD SKIRT		1,800 Peak	1,800	
AFT SKIRT		12,000 Peak	---	
TEMPERATURE °C (°F)				
NOSE CONE	82(180)	82(180)	127(260)	104(220) 149(300)
FORWARD SKIRT	104(220)	104(220)	121(250)	
AFT SKIRT	177(350)	177(350)	171(340)	
CASE	49(120)	49(120)	104(220)	
INSULATION	27(80)	3193(5780)	---	

*High peak shock loads are dependent on distance from source; these values will decrease dramatically with distance (Figure 5.6-1).

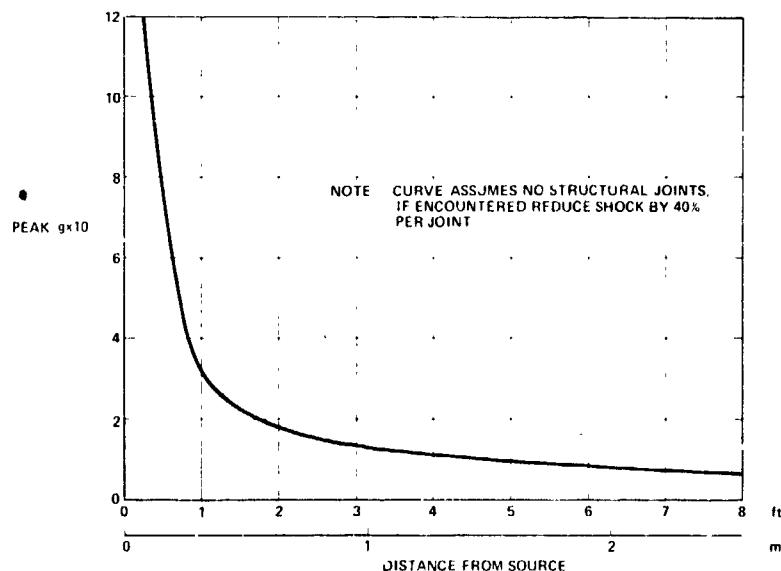


Figure 5.7-1 Shock Attenuation Curve

The effect of these environments on component selection or design is best understood by comparison to previous test levels. Our experience and test levels, as well as that of other aerospace companies, will be used as a reference. The Titan booster uses test vibration levels in the 40 to 50 g rms range for electronics in the equipment trusses and tank domes areas. The external tank study demonstrated that off-the-shelf hardware is available at the 44.5 grms level to meet SRB recovery systems requirements. Viking shock tests in the lab were as high as 12,000 g, with BLDT experiencing a 4000 g shock. The laboratory test values are usually higher than experienced in development or qualification tests. Testing at the 2500 g level for Titan separation shocks and motor firing tests has not resulted in any environmentally induced failures.

The environmental data presented represent maximum expected values for the NASA/RI baseline recovery system. Time did not permit a complete evaluation of component environments for our recovery baseline, but the high shock g identified in Table 5.7-1 was considered when locating electronic components. The analysis seems to confirm ability to use equipment within the current technology for the expected SRB recovery environments.

6.0 CONCEPT EVALUATION AND SELECTION

6.1 APPROACH

The primary ingredient of the concept evaluation and selection studies is the SRB system cost analyses. It is in the cost analyses that the various technically feasible recovery system concepts and SRB modifications are traded one against another to determine the optimum system. In our studies, both DDT&E and production costs have been determined for all significant SRB and recovery system parameters. The optimum recovery system is defined as that system which results in minimum total SRB program cost.

The logical development of the concept evaluation process is shown in Figure 6.1-1, where recovery system variables have been broken down into sets of parameters that can be systematically examined. A baseline set of SRB component designs was selected, and details such as weights, sizes, fabrication techniques, etc were defined to the point that a tops-down cost estimate of all major subsystems could be accomplished. The costs were then systematically varied in the parametric analyses. Parachute sizes were traded with retro-rocket impulses to determine the minimum cost hybrid system at each terminal descent velocity. The hybrid system was then traded with the all-parachute system to determine the minimum cost recovery system at each velocity. The structural parametric studies examined the tradeoff between increased new unit cost caused by strengthening each component to reduce impact failure probability, and the increased cost accrued by allowing some water impact failures, and building replacement units. In this way, the design strength required to provide minimum cost at each velocity was defined.

All parametric trades were then combined to determine the minimum total program cost and the terminal descent velocity associated with that minimum. To test the validity of the parametric analysis, four point design recovery subsystems were defined and investigated. These point designs addressed the sensitivity of the optimization techniques by examining one single parachute recovery system sized to give a terminal descent velocity of 38 m/s (125 fps) and three parachute recovery systems with clusters of three main parachutes sized to provide terminal descent velocities of 24 m/s (80 fps), 30 m/s (100 fps) and 38 m/s (125 fps).

The following discussion will show that both the parametric cost analyses and the point design cost estimates result in minimum total program costs at a terminal descent velocity of 38 m/s (125 fps).

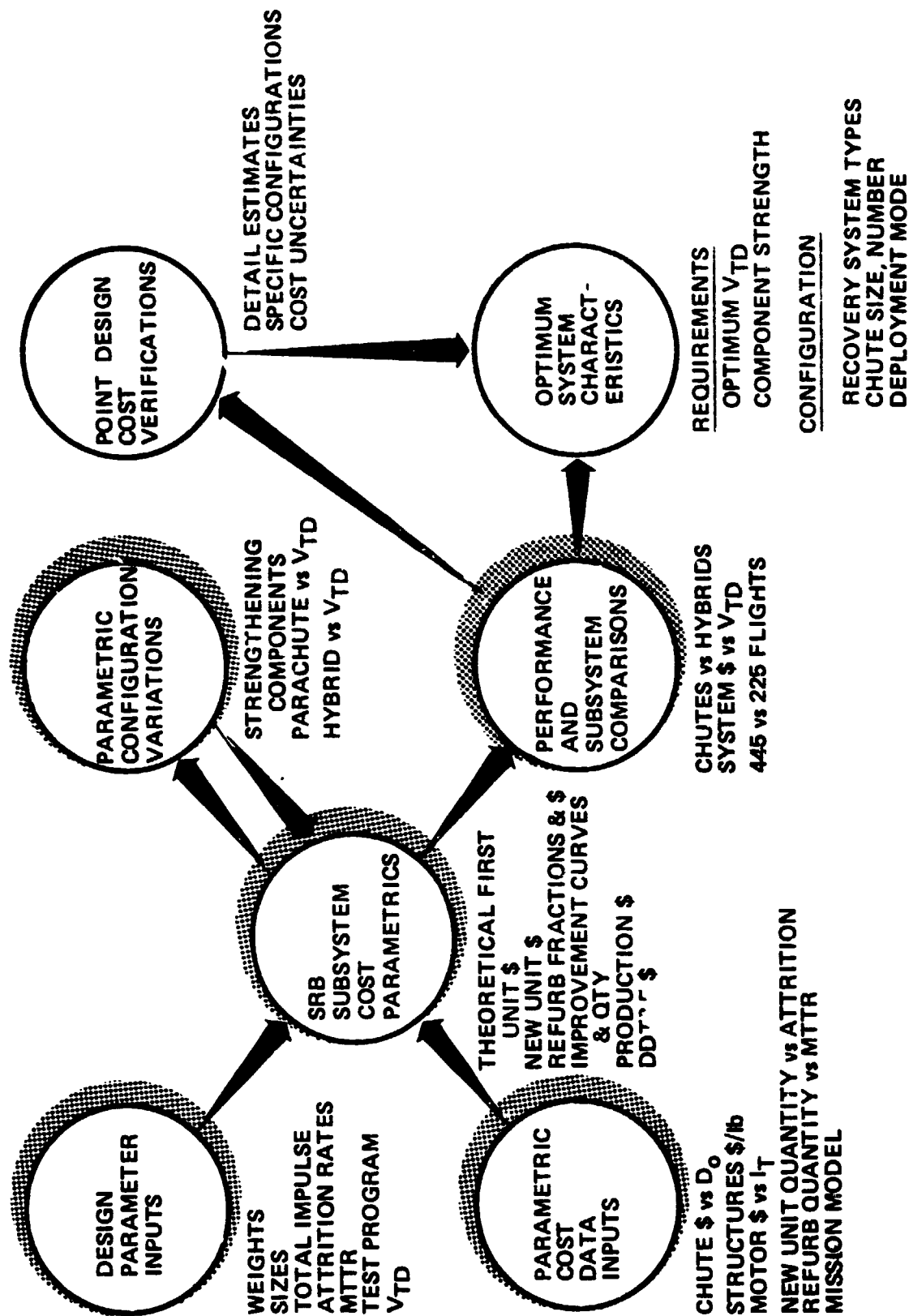


Figure 6.1-1 Requirements and Configuration Evaluations Based on Total SRB Recovery Cost Analysis

6.2 PARAMETRIC COST TRADES

The parametric cost analyses have been conducted using cost factors that allow derivation of final costs independently of component details. Given the number of units manufactured, the number of units refurbished, the new unit cost, and the refurbishment fraction, the recurring (manufacturing and refurbishment) cost is determined. Table 6.2-1 defines the cost terminology used. Total systems costs are obtained by adding to these costs the performance cost and the flight rate independent costs (i.e., DDT&E). From these results, criteria for determining the optimum can be applied.

Table 6.2-1 Cost Analysis Terminology

COSTS	DEFINITION
DDT&E	COSTS FOR SRB SUBSYSTEMS DDT&E INCLUDING NEW UNIT AND REFURBISHMENT COSTS FOR THE SIX FLIGHT TESTS, AND DEVELOPMENT TEST HARDWARE, AND TOOLING FOR FABRICATION OF PRODUCTION ARTICLES.
PRODUCTION	INCLUDES ALL NEW UNIT AND REFURBISHMENT COSTS FROM FLIGHT NO. 7 THROUGH THE REMAINDER OF THE PROGRAM.
NEW UNIT	COSTS TO FABRICATE AND ASSEMBLE AN SRB SUBSYSTEM NEW UNIT EXCLUDING INTEGRATION INTO THE SHUTTLE SYSTEM FLIGHT ASSEMBLY.
REFURBISHMENT	COST TO RECONDITION AND REPAIR A SUBSYSTEM FROM THE POINT OF ON-DOCK WASHDOWN TO RETURNING IT TO INVENTORY READY FOR ASSEMBLY INTO A SHUTTLE FLIGHT SYSTEM.
PERFORMANCE	COST OF TRANSPORTING Δ WEIGHT TO SRB SEPARATION, AT \$3.30/kg (\$1.50/lb).
TOTAL PROGRAM	TOTAL DDT&E, PRODUCTION AND PERFORMANCE COSTS
PARAMETRICS	
THEORETICAL FIRST UNIT (TFU)	THE COST OF THE THEORETICAL FIRST UNIT TO WHICH AN IMPROVEMENT CURVE IS APPLIED TO DETERMINE THE TOTAL OR AVERAGE COST OF ANY DESIRED QUANTITY OR OF A SPECIFIC UNIT.
REFURBISHMENT FRACTION	THE RATIO OF TFU REFURBISHMENT COST TO TFU NEW UNIT COST.
IMPROVEMENT CURVE	UNIT COST REDUCTIONS FOR QUANTITY RESULTING FROM LABOR LEARNING, EXPERIENCE, AND TECHNOLOGICAL IMPROVEMENTS. THE WRIGHT CURVE METHOD, WHICH USES THE STRAIGHT-LINE CUMULATIVE AVERAGE UNIT CURVE FROM THE TFU, HAS BEEN USED IN THIS COST STUDY.

6.2.1 Cost Analysis Methodology

To establish a basis of understanding, a cost summary has been prepared for 96 new operational SRBs and 782 refurbished units. Table 6.2-2 describes the baseline costs and consists of a list of major assemblies within each SRB subsystem and their accompanying DDT&E, new unit and refurbishment costs. The theoretical first unit (TFU) refurbishment fractions and improvement curves used for estimating purposes are also presented for benefit of cost analysts.

The cost estimates shown are based on the structural weights and drawings provided by NASA MSFC at the start of the contract period. Manufacturing costs of the forward skirt and the aft skirt baffle, which is discussed in Section 6.2-3, are included. Performance costs resulting from accelerating additional subsystem weight from liftoff to SRB staging are not included in Table 6.2-2. The recovery system costs are for a recovery system using one pilot chute and one main parachute designed for a terminal velocity of 38 m/s (125 fps).

The methodology used in deriving the cost estimates shown in Table 6.2-2 is as follows:

- 1) Structures - The cost of raceways, aft attach structure, aft skirt, forward skirt, and aft secondary support structure were based upon detail cost estimates for each of these components. Total costs per pound were adjusted for new configurations and weight differences for each baseline subsystem. The nose cap, frustum, and nose internal structure costs were extrapolated from Titan II (aft cone of Stage I fuel tank) actual cost data, adjusted for weight. The cable cutters were estimated from quotations received from three sources in the spring of 1972. The separation motors were estimated from Martin Marietta Orlando curves (cost versus SRM total impulse) that have proven valid in the past.
- 2) Case, Nozzle, SRB Expendables - These items were based upon data received from UTC, Thiokol, LPC, and Aerojet for prior estimates on Shuttle SRBs, and actual cost data on large SRMs.
- 3) Recovery - All of the items in this subsystem were extrapolated from a detailed cost estimate made by Martin Marietta with assistance from parachute manufacturers from a much bigger, more complex 24 m/s (80 fps), three-main parachute system under consideration in the spring of 1972. The detail in this was such that it

Table 6.2-2 Baseline System Cost Data

SRB SUBSYSTEMS	1971 DOLLARS (MILLIONS)**						IMPROVEMENT CURVES (WRIGHT METHOD)		
	DDT&E	PRODUCTION		TOTAL PROGRAM	AVG/FLT (446)	AVG/SRB (890)	TEU REFURBISH FRACTION	NEW UNIT	REFURBISH
		NEW UNITS	REFURBISH						
STRUCTURAL COMPONENTS									
RACEWAYS	1,180	11,432	0	12,612	0.028	0.014	0	85%	0
AFT ATTACH STRUCTURE	2,408	3,088	10,760	16,277	0.037	0.018	85%	85%	85%
*AFT SKIRT	13,651	23,320	25,042	62,013	0.136	0.076	20%	85%	85%
*FORWARD SKIRT	14,871	26,408	27,282	67,969	0.152	0.078	20%	85%	85%
AFT SECONDARY SUPPORT STRUCTURE	4,700	8,029	8,622	21,359	0.048	0.024	20%	85%	85%
NOSE CAP	1,413	2,414	2,592	6,419	0.014	0.007	20%	85%	85%
FRUSTRUM	4,962	8,477	9,102	22,541	0.061	0.025	20%	85%	85%
NOSE INTERNAL STRUCTURE	2,622	4,478	4,809	11,910	0.027	0.013	20%	85%	85%
CABLE CUTTERS	0,110	0,472	0	582	0.002	0.001	0	85%	0
SEPARATION MOTORS	0,689	6,844	1,222	8,535	0.019	0.010	25%	85%	92%
TOTAL STRUCTURAL COMPONENT	46,586	93,761	89,451	229,798	0.516	0.268			
SRM CASE	66,599	106,351	194,366	367,316	0.826	0.413	35%	95%	92%
NOZZLE	29,800	41,773	183,584	235,167	0.528	0.264	76%	95%	92%
SRM EXPENDABLES	34,201	427,369	0	461,570	1.037	0.519	0	95%	0
RECOVERY:									
SRB RECOVERY ORDNANCE	0,571	3,353	0	3,924	0.008	0.006	0	94%	0
MAIN CHUTE RETRIEVAL	0,750	1,272	1,560	3,582	0.008	0.004	30%	94%	89%
NOSE/PILOT RETRIEVAL	0,750	1,272	1,560	3,582	0.008	0.004	30%	94%	89%
MAIN CHUTE (SINGLE CHUTE SYSTEM)	7,084	7,236	3,528	17,858	0.040	0.020	11%	93%	89%
PILOT CHUTE	1,625	1,746	1,308	4,681	0.010	0.005	17%	93%	89%
TOTAL RECOVERY	10,790	14,883	7,594	33,627	0.075	0.038			
AVIONICS:									
SRB ELECTRICAL	5,865	38,781	4,836	49,481	0.111	0.056	13%	94%	90%
SRB INSTRUMENTATION	1,365	2,526	3,206	7,096	0.016	0.008	30%	95%	90%
RECOVERY AVIONICS	1,455	5,955	2,623	10,033	0.023	0.011	22%	94%	90%
TOTAL AVIONICS	8,685	47,262	10,663	66,610	0.150	0.075			
TVC	9,370	10,406	9,544	29,320	0.066	0.033	30%	92%	86%
TOTAL SRB (1971 \$ in millions)	206,031	741,805	475,572	1,423,408	3.197	1.600			

**446 Flight Program

* Optimum subsystem costs sensitive to design for
water impact

permitted extraction of only those items required in the various recovery systems studied with adjustments made for quantity and configuration. Theoretical first unit costs have been modified as described in the recovery system parametric section to account for design reuse numbers.

- 4) Avionics - These costs were based on a detailed estimate from a list of parts for the baseline recovery system. Existing cost data for components were taken from various sources.
- 5) TVC - TVC cost was based upon data from SRM manufacturers such as UTC, Thiokol, LPC, and Aerojet, and from Rockwell International studies.

Some general ground rules for the parametric cost estimates are:

- 1) The Wright curve method for unit cost reductions due to experience, learning, and technology improvements was applied. This method uses the straight-line cumulative average unit curve from the TFU rather than the straight-line unit curve. Some manufacturers, particularly SRM firms, use the straight-line unit curve method; thus differences in curve percentages may be noted when comparing to various manufacturers' data.
- 2) All costs were adjusted to 1971 dollars to maintain compatibility with previous studies and with NASA-MSFC and RI data. In most cases 4% per year escalation or deescalation was used when estimates were based on other than 1971 costs.
- 3) Factors for support, such as management, data, engineering liaison, quality assurance and reliability, etc, were included. Typical contractor general and accounting costs, and profit were included.

6.2.2 Programmatic Parametrics

To make best use of the parametric cost studies, a programmatic rationale for determining the number of various subsystem units required to support a Shuttle flight program was necessary. Figure 6.2-1 graphically shows the relative magnitudes of the various subsystem costs and shows the reduction in total program costs possible if the number of new equivalent SRBs required decreases (with a corresponding increase in number of refurbished units). Such a reduction is considered feasible by increasing system reliability and reducing refurbishment cycle time. The total number of new units is the number required to make up those lost through attrition plus the number in the refurbishment cycle.

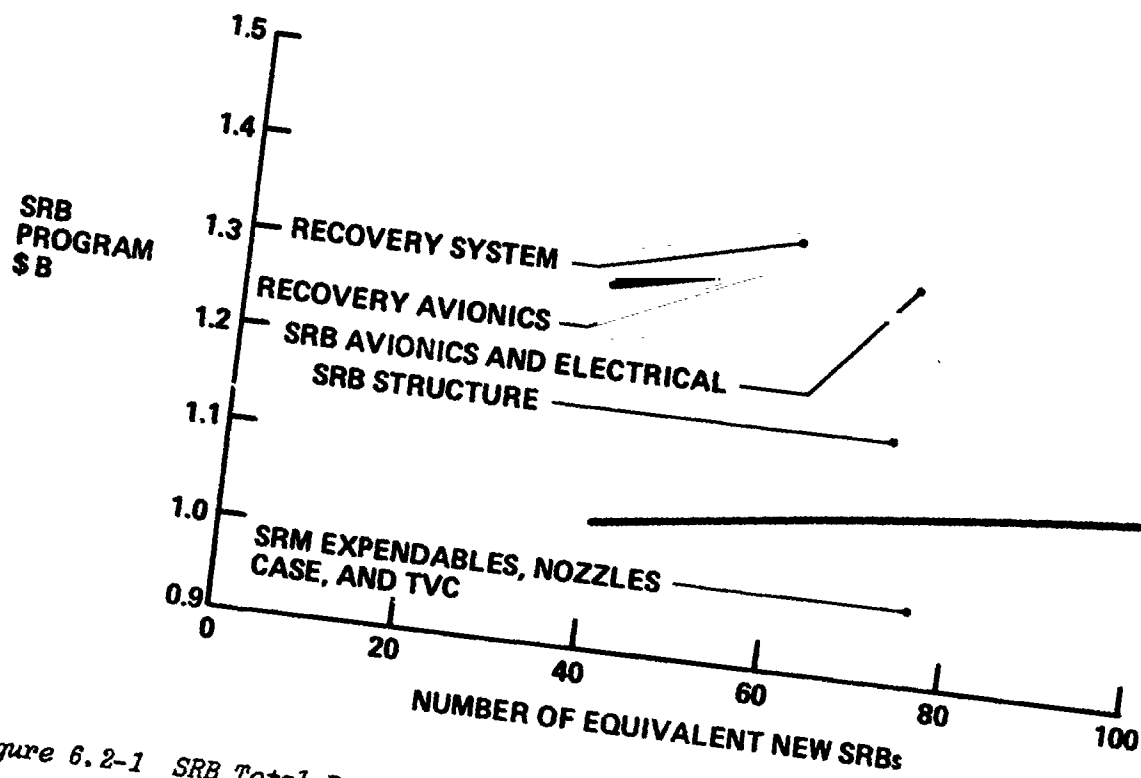


Figure 6.2-1 SRB Total Program Costs Increase with Number of New SRBs

The solid rocket booster has a unique attrition rate that depends on the component failure and wearout rates and on the effectiveness of the retrieval/refurbishment operation. The total number of units required can be calculated as follows:

$$N_T = N_R \left[\frac{MTTR}{MTTF} + F \lambda_R \right]$$

where

N_T = total number of recovery systems required

N_R = number of recovery system required per flight = 2

$\frac{MTTR}{MTTF}$ = $\frac{\text{mean time to refurbish (days)}}{\text{mean time between flights (days)}}$

λ_R = system attrition rate (a function of recovery system reliability, retrieval reliability, and component failure probability)

F = total number of flights.

Figure 6.2-2 parametrically presents the total number of units required for attrition rates of 3 to 7% and for refurbishment times of 30 to 180 days. Since the data in Figure 6.2-2 are based on 445 flights, it represents the total number of units required including DDT&E flights. While it is recognized that the attrition rate will be higher during the DDT&E flights, it is expected that the average value, over the life of the program, will not be significantly altered.

While the idea of designing a unit for a fixed number of reuses has not been considered to be a significant cost impact item (except in parachute refurbishment), the average number of reuses expected is of interest. The number of times a unit can be reused also depends on three factors: attrition rate, refurbishment time, and flight schedule.

Figure 6.2-3 shows that the average number of times a unit can be reused is limited by refurbishment time for low attrition rates, but refurbishment time becomes less important as attrition rate increases, because more new units must be provided to replace those lost through attrition.

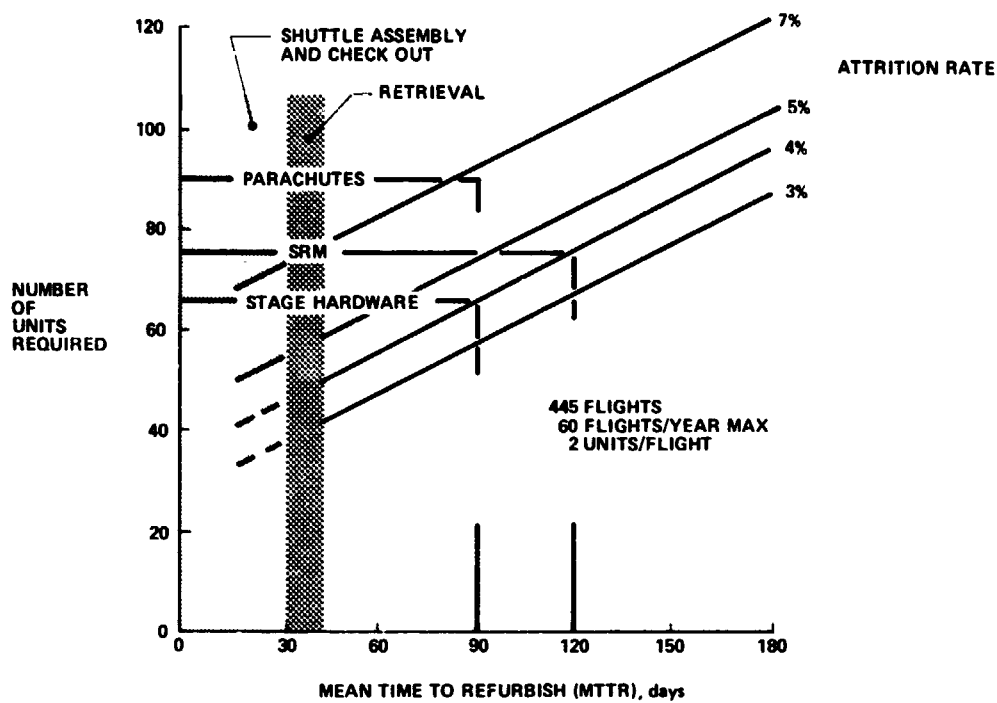


Figure 6.2-2 Attrition Rate and Refurbishment Times Determine Number of Subsystems Required

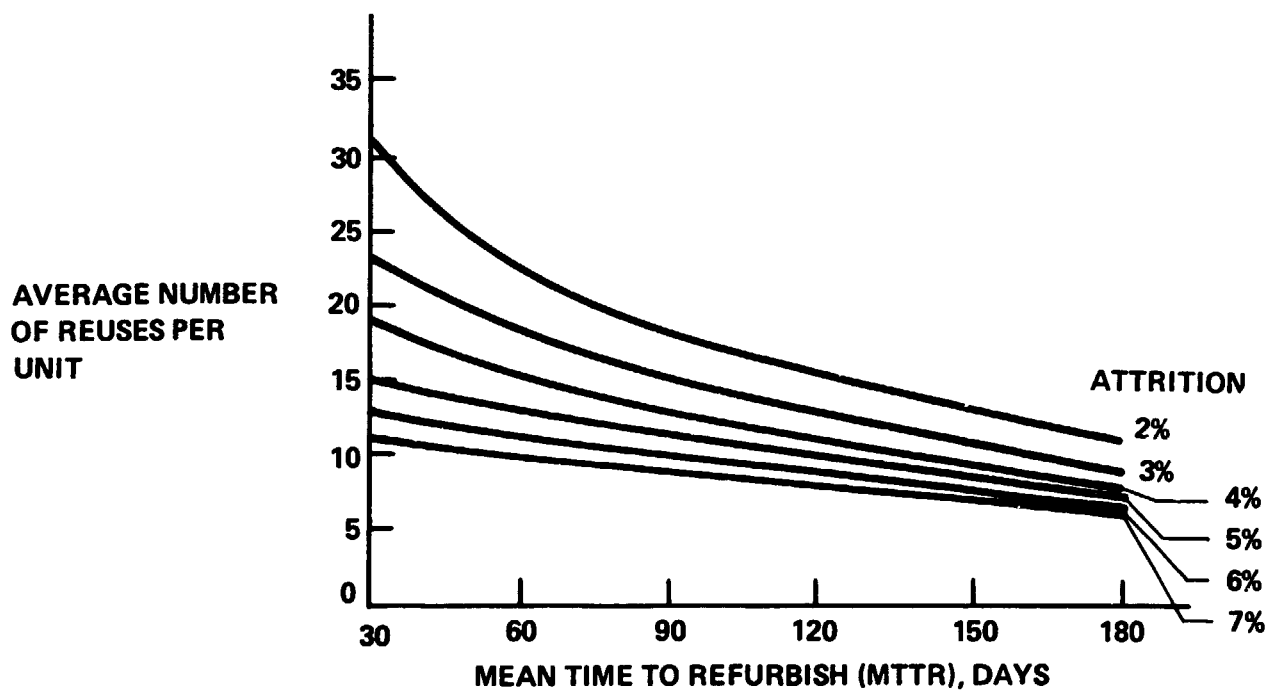


Figure 6.2-3 Average Number of Reuses Per Unit Based on Refurbishment Time and Attrition Rate

Because each subsystem has a unique MTTR, it is not sufficient to describe SRB program costs as a function of numbers of new SRB units. For example, the portion of Figure 6.2-1 marked "recovery system" may be more precisely presented as a function of the recovery subsystem attrition rate as shown in Figure 6.2-4. The number of new units required reflects the SRB attrition rate plus any losses of the recovery subsystem during retrieval and refurbishment, and the recovery subsystem MTTR. Figure 6.2-4 shows that significant system savings can be realized by minimizing the subsystem attrition rate and MTTR. The effect of a 30-day reduction in recovery subsystem refurbishment time saves approximately \$1.2 M, and a reduction of 1% in attrition results in a \$1.0 M savings.

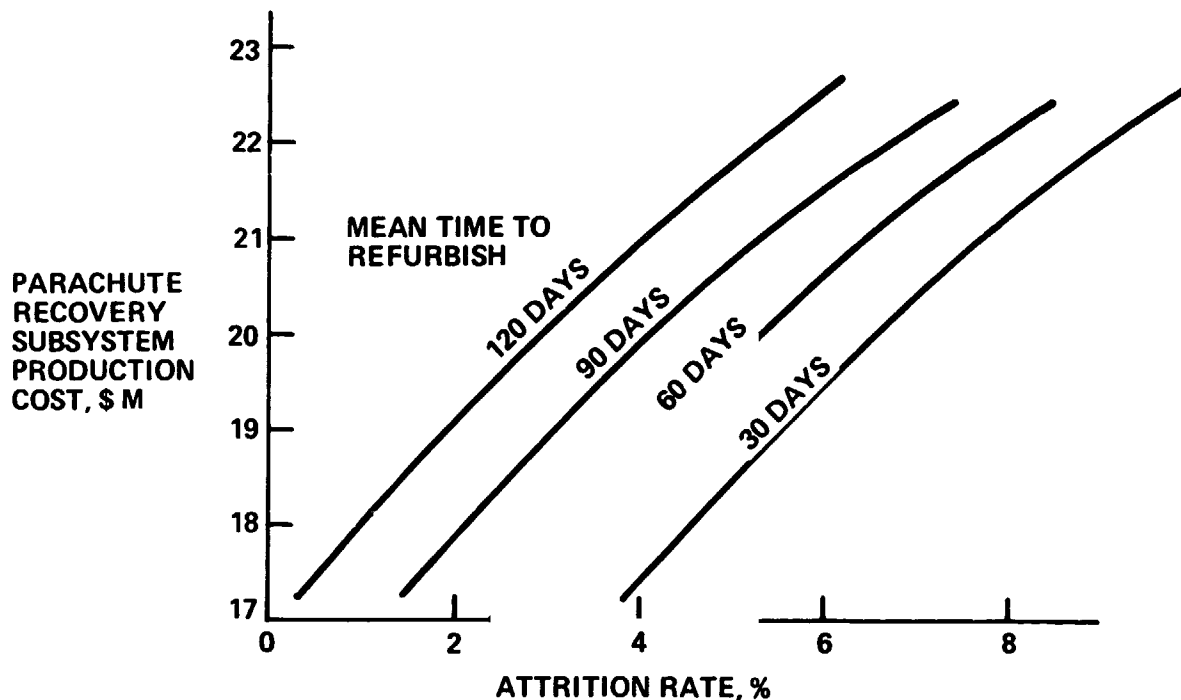


Figure 6.2-4 Recurring Cost Tradeoffs

6.2.3 Structural Component Cost/Failure Parametrics

Concurrent evaluations of water impact loads (via the Monte Carlo program) and strength analyses of the major structural components have defined the relationship between component weight and component failure probability. The results of these studies determined that the critical loads on the lower half of the case and the aft skirt are determined by initial water impact and are sensitive to vertical impact velocity. The loading on the forward skirt was determined to be critical for slapdown and independent of vertical impact velocity. The failure probability for the baseline forward skirt was found to approach 1. The aft skirt appears to have a negligible failure probability for the baseline design.

The SRM case itself is rather complex. Only a case with four center segments and an aft and forward dome has been considered. Segments and domes have been considered to be separate elements. Treated this way, the center segments have failure probabilities of between 3 and 5% depending on the vertical velocity. The baseline aft dome has a failure probability that depends on vertical velocity but approaches 1 for all vertical velocities in the region of interest.

The structural component cost tradeoffs have used baseline cost factors as a starting point. The number of new units required has been determined by considering the mean time to refurbish, the SRB retrieval attrition probability, and the structural failure probability. Table 6.2-3 shows the range of values considered. Manufacturing costs and refurbishments costs are estimated by determining theoretical first unit costs that are varied by cost per unit weight factors. Wright (straight line cumulative average unit) experience curves have been applied to the number of new units to determine total new unit costs, and to the number of refurbished units to determine total refurbishment costs. Performance costs are estimated by using the NASA provided cost/weight sensitivity factor of 3.30 \$/kg (1.50 \$/lb) weight increase.

Table 6.2-3 New Unit Requirements for Low Failure Probabilities

STRUCTURAL COMPONENT FAILURE PROBABILITY	STAGE HARDWARE, NEW UNITS REQUIRED (MTTR = 90 DAYS)	SRM HARDWARE, NEW UNITS REQUIRED (MTTR = 120 DAYS)
0	65	75
0.001	66	76
0.003	68	77
0.010	74	83
0.030	90	100
0.100	149	159

Cost elements that are independent of weight, refurbishment, attrition rate, and launch schedule have not been used in the structural component cost trade studies.

6.2.3.1 Forward Skirt Cost Analysis

The results of a cost analysis determining the increase in theoretical first unit cost of the forward skirt due to weight change, and the subsequent impact on production costs for a 439 operational flight program are shown in Figure 6.2-5. These characteristics are typical of similar trades for all the structural components. It was previously pointed out that as failure probability increases, the number of new units increases, and the number of refurbished units decreases. This fact dominates the curve shapes of the new unit and refurbishment costs. Theoretical first unit costs increase as failure probability decreases, but the increase is not large enough to drive the minimum total program cost above a failure probability of 0.01. The increase in the theoretical first unit cost reflects the increased cost due to increased weight and design complexity. Performance costs have been computed but their magnitude is so small that they scarcely appear on the figure in the scale chosen.

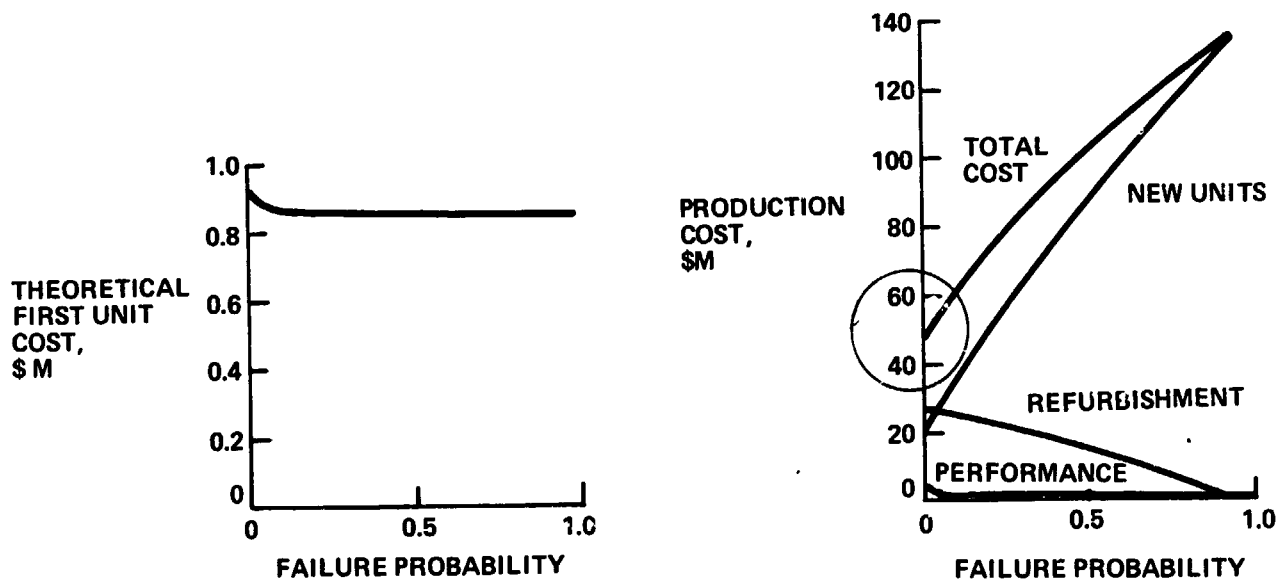


Figure 6.2-5 Structural Strengthening Decreases Forward Skirt Cost

The portion of Figure 6.2-5 that is circled has been expanded and is presented in Figure 6.2-6 which shows that minimum cost occurs at a failure probability of 0.01. This figure also shows that the failure probability at which the minimum component cost occurs is not sensitive to changes in attrition rate. Standard design practice (ultimate safety factor of 1.25) results in a failure probability of approximately 0.0001. Decreasing the failure probability below the optimum value of 0.01 to 0.0001 increases the recurring cost by approximately \$3.1 M, or 8% for this component. This approach results in some margin for uncertainty in case the predicted water impact loads are optimistic.

6.2.3.2 Aft Dome Cost Analysis

The results of cost analyses of the aft dome for both 21.5 m/s (70 fps) and 30.5 m/s (100 fps) presented in Figure 6.2-7 indicate that large program savings are achievable by increasing the strength capability of the aft dome. A weak optimum was found for all vertical velocities in the range of interest at failure probabilities near 0.01.

The preliminary design analyses considered two concepts for protecting the aft dome: a strengthened aft dome and a protective baffle inside the aft skirt. Although added weight in the aft dome is much greater than that required for a baffle in the aft skirt, the associated cost per pound for the aft dome is much less. The net effect, however, is that the lighter baffle has a decided cost advantage at all vertical velocities as shown in Figure 6.2-8. Furthermore a failure probability of 0.01 produces lower costs than those resulting from using a failure probability consistent with a 1.25 ultimate safety factor. The Monte Carlo analysis did not predict any SRB losses due to aft dome failures; thus total SRB attrition was not a factor in this trade.

6.2.3.3 SRM Case Cost Analysis

The cost analysis of the four center segments of the SRM was divided into two parts:

- 1) SRM case production costs were determined considering the effects of increasing case thickness;
- 2) total system costs were evaluated considering the impact of increasing MEOP.

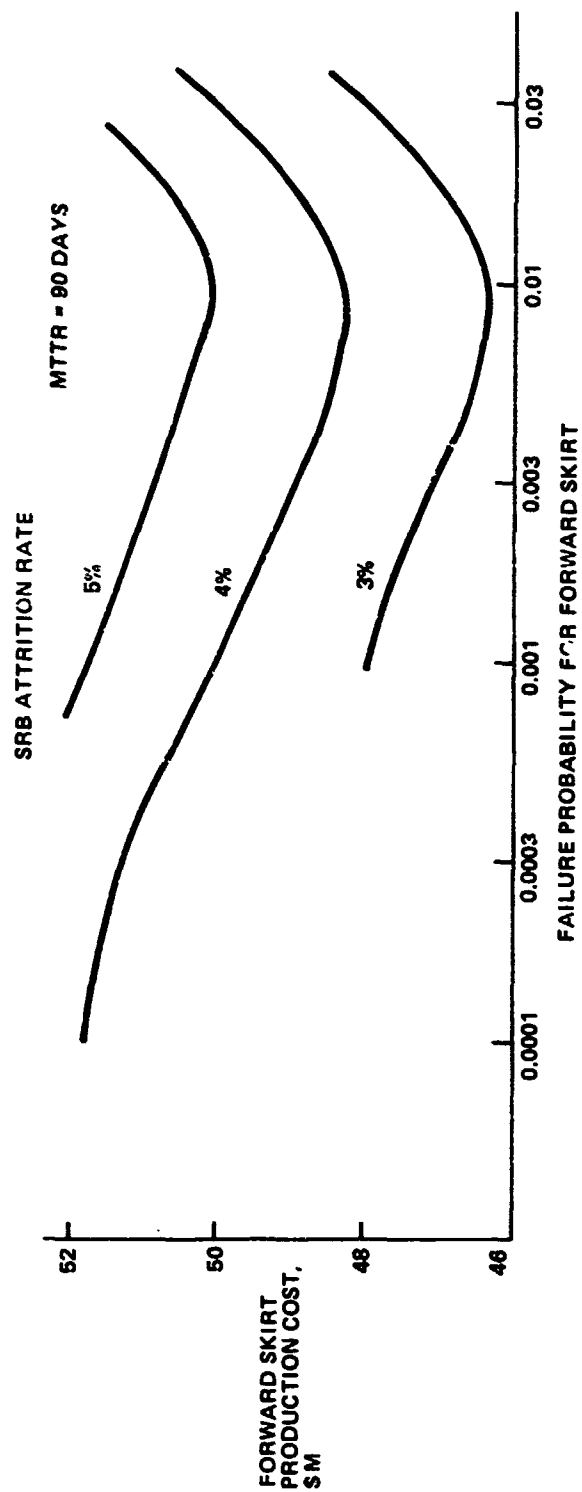


Figure 6.2-6 Optimum Forward Skirt Design Independent of SRB Attrition Rate

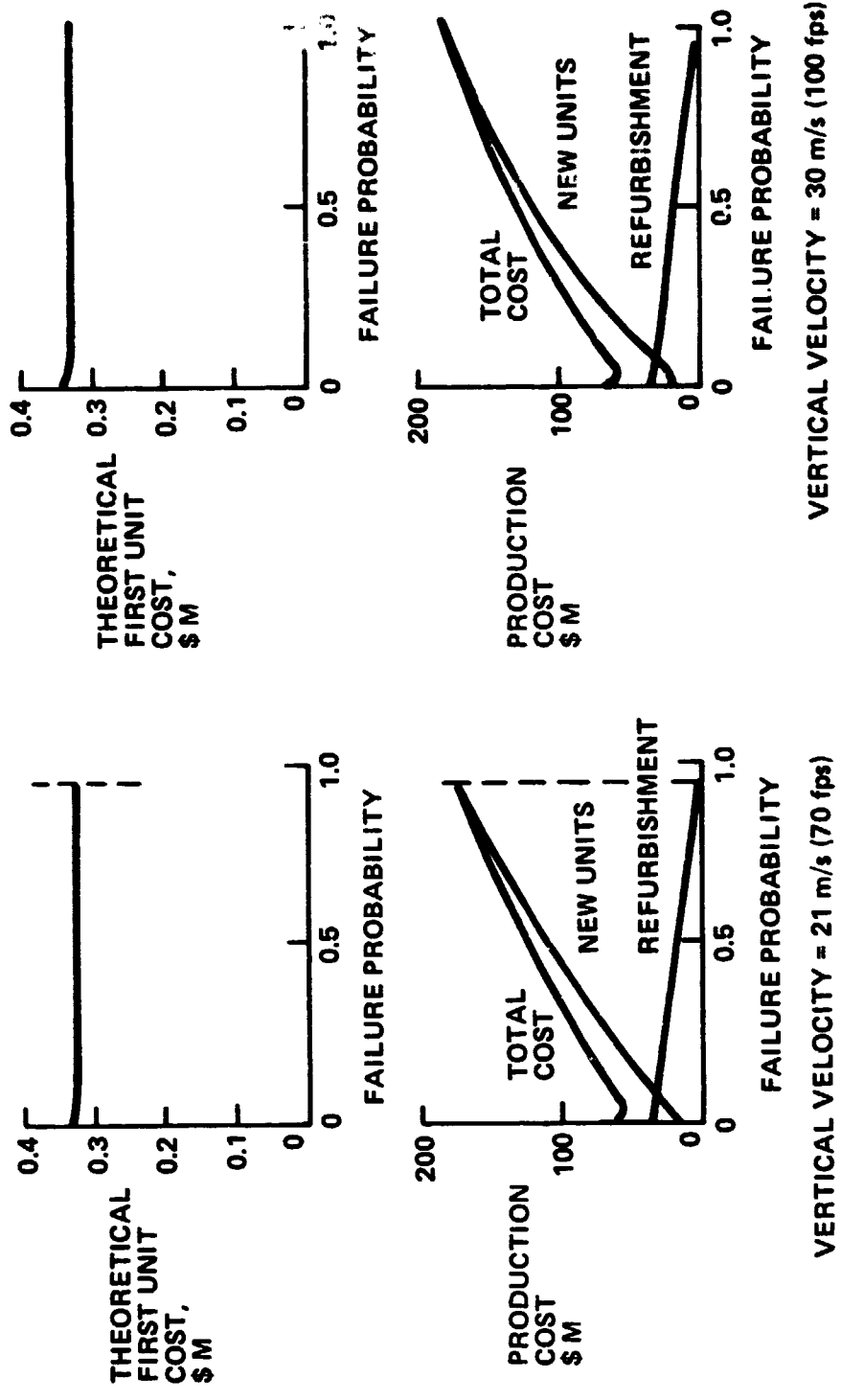


Figure 6.2-7 Structural Strengthening Reduces Aft Dome Cost

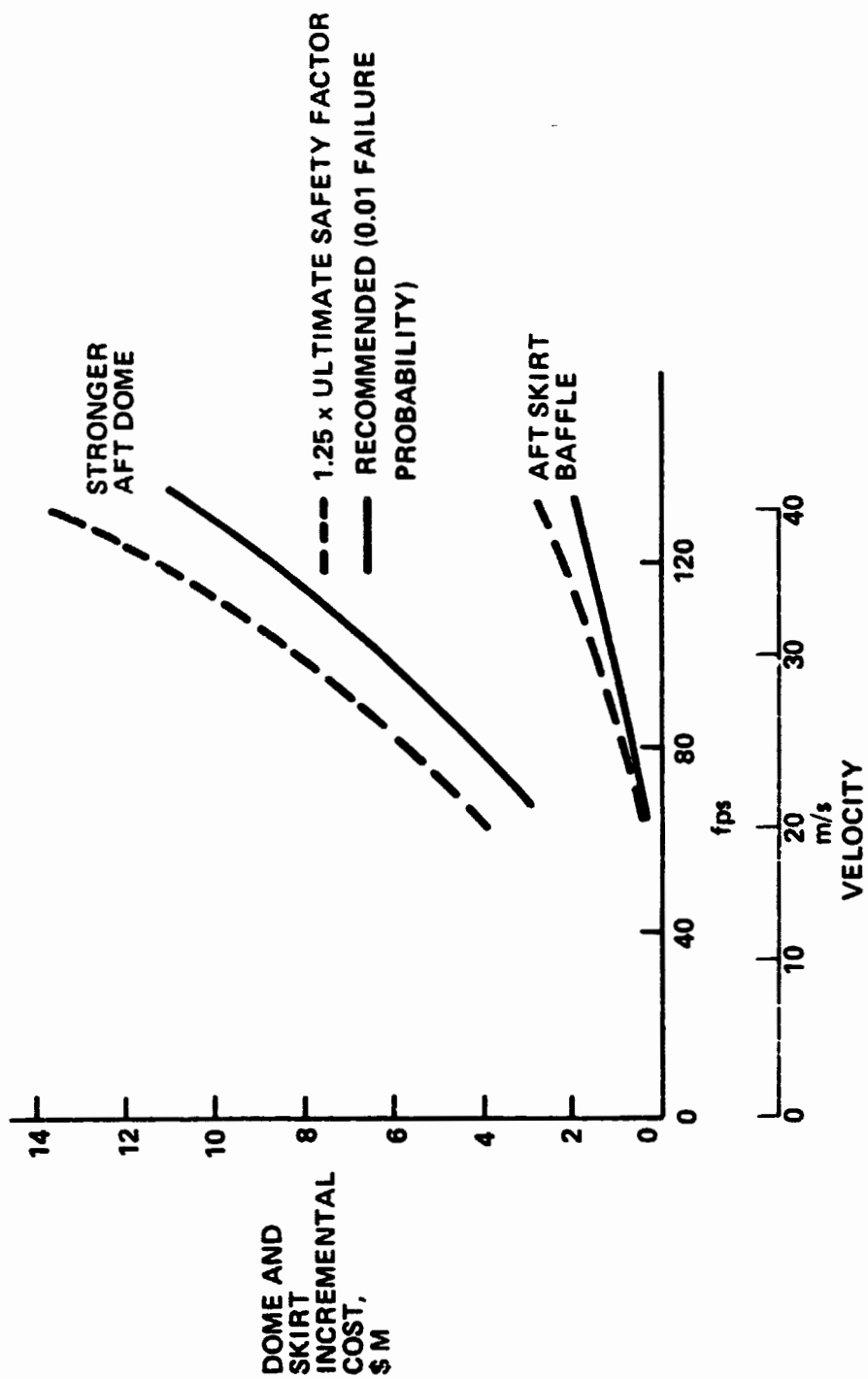


Figure 6-2-8 Aft Skirt Baffle Minimizes Dome and Skirt Costs

The strength analysis of the SRM case indicated that failure caused by slapdown loads would occur only in the forward two segments. Similarly, failures due to axial acceleration, which occur upon water impact, or due to hydrostatic buckling pressures, which occur at peak submergence, occurred only in the aft two segments. These failure modes were treated as being completely independent. Replacement due to case damage was then assumed for the two failing segments. Weight increases for strengthened elements were distributed to all four center segments in order to preserve commonality in design. In determining the effects of the experience curve on costs, the set of four center segments and forward dome was considered to be one unit; thus, the total number of units handled (new plus refurbished) was 878. The results shown in Figure 6.2-9 indicate that reducing failure probability by SRM case strengthening increases production costs.

Several analyses of the effect of increasing the SRM maximum expected operating pressure (MEOP) have been conducted. The latest available results have been obtained from the *Space Shuttle Solid Rocket Booster/Solid Rocket Motor Quarterly Review*, June 1973. This report concluded that the optimum system has a thrust-to-weight ratio of 1.5 and SRM nozzle expansion ratio of 7. The data for this system have been converted from real year dollars to 1971 dollars to make it consistent with the cost analyses presented here. An escalation factor of 4% per year and a production midpoint of 1982 have been used. The delta program production costs are shown in Figure 6.2-10 as a function of MEOP. The baseline point is for a MEOP of $6.2 \times 10^6 \text{ N/m}^2$ (900 psi), expansion ratio of 7, thrust-to-weight ratio of 1.5, and SRM case impact failure probability of zero. Incremental costs due to nonzero SRM case failure probabilities have been taken from Figure 6.2-9 and added to the data from the June review. The results show that for terminal descent velocities less than 30.5 m/s (100 fps), the optimum MEOP is $6.2 \times 10^6 \text{ N/m}^2$. Increasing the descent velocity to 39.6 m/s (130 fps) shifts the optimum MEOP to $6.48 \times 10^6 \text{ N/m}^2$ (940 psi) and increases the case program cost 3 million dollars. Keeping the MEOP at $6.2 \times 10^6 \text{ N/m}^2$ (900 psi) while increasing the velocity to 39.6 m/s (130 fps) penalizes the system by 2 million dollars over the optimum value of $6.48 \times 10^6 \text{ N/m}^2$ (940 psi).

6.2.3.4 Optimally Designed Structural Components

Minimum structural costs at each terminal descent velocity shown in Figure 6.2-11 were determined by combining cost characteristics of the previously discussed SRB components. The buildup shown starts with a fixed cost that is independent of terminal velocity.

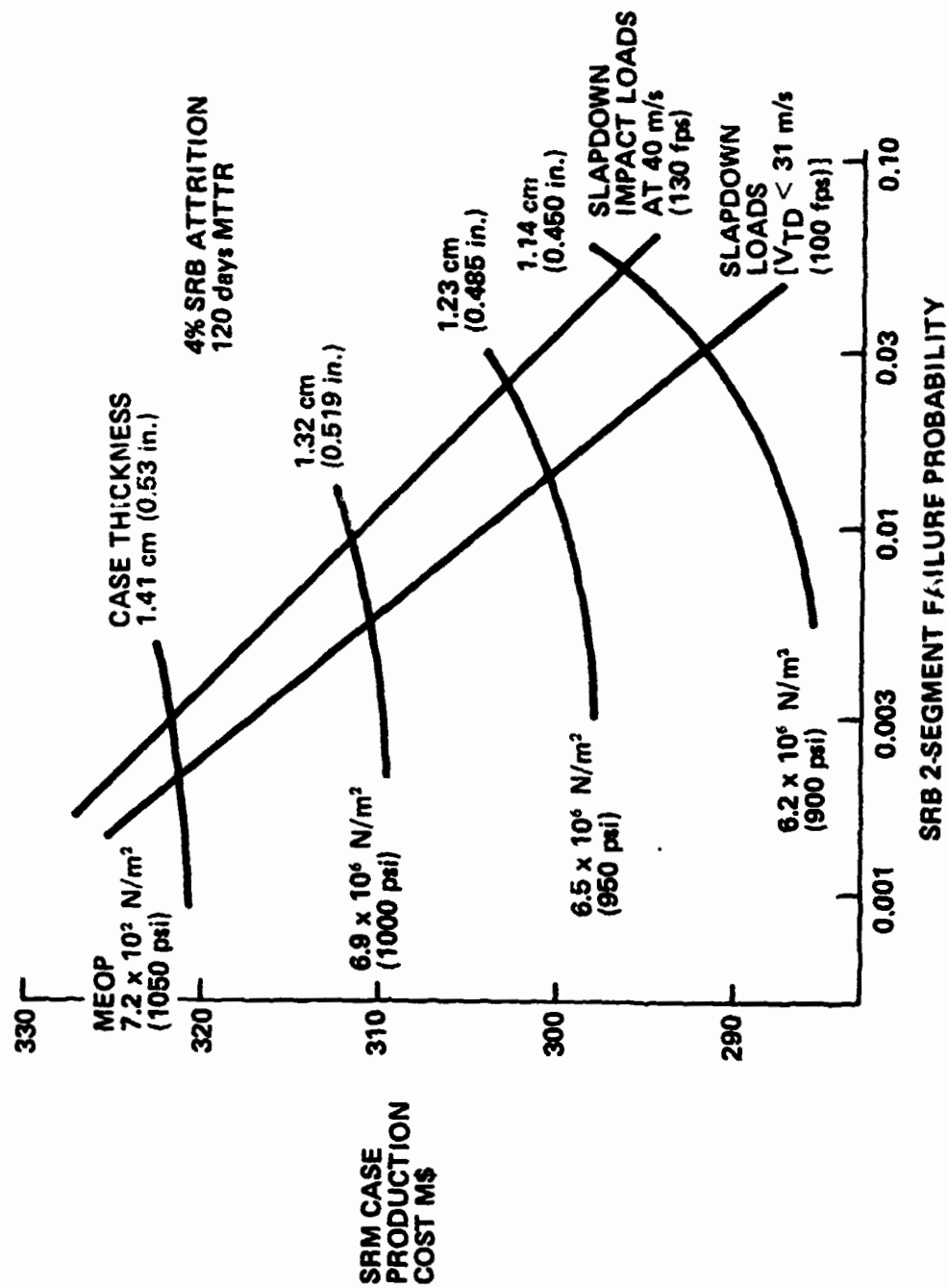


Figure 6.2-9 Strengthening the SRM Case Increases Production Costs

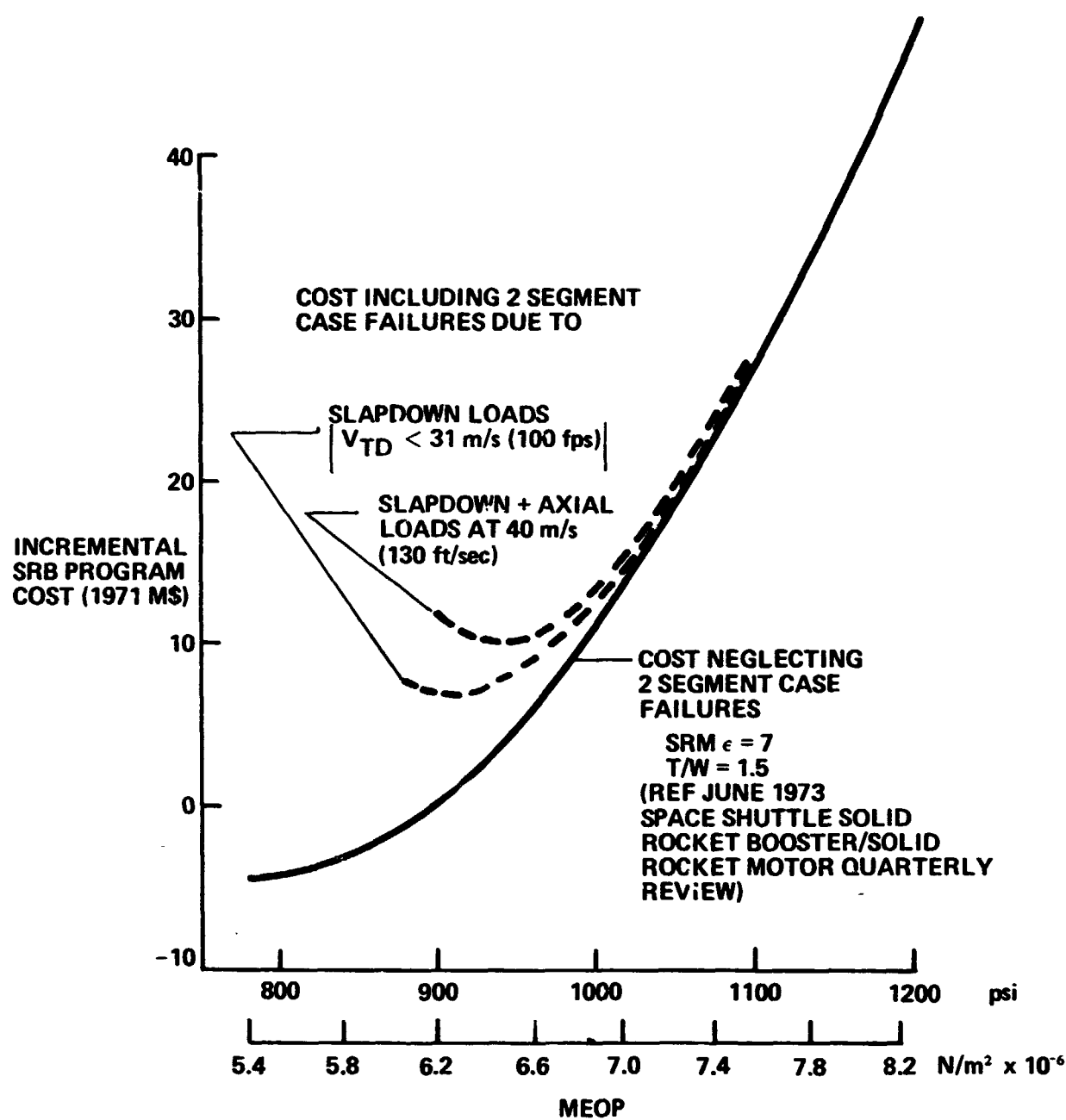


Figure 6.2-10 Effect of MEOP on SRM Case Program Costs

This includes all expendable items such as SRM expendables (propellant, ignitor, insulation, etc), raceways, ordnance, cable cutters, electrical cables, and batteries. Cost of refurbishable items have been included considering new unit and refurbishment costs for 75 SRM cases, nozzles, and TVC subsystems and 65 avionics, recovery, and structural subsystems. Added to the fixed cost is the new unit and refurbishment cost increment for baffles added to the aft skirt. Costs for the baffle increase as the design velocity increases because it is strengthened to maintain a constant failure probability (0.01) as the impact velocity (and loads) increase. The cost increment shown for the SRM case reflects the replacement costs of segments damaged during water impact. Case design has been held constant with the MEOP equal to $6.2 \times 10^6 \text{ N/m}^2$ (900 psi).

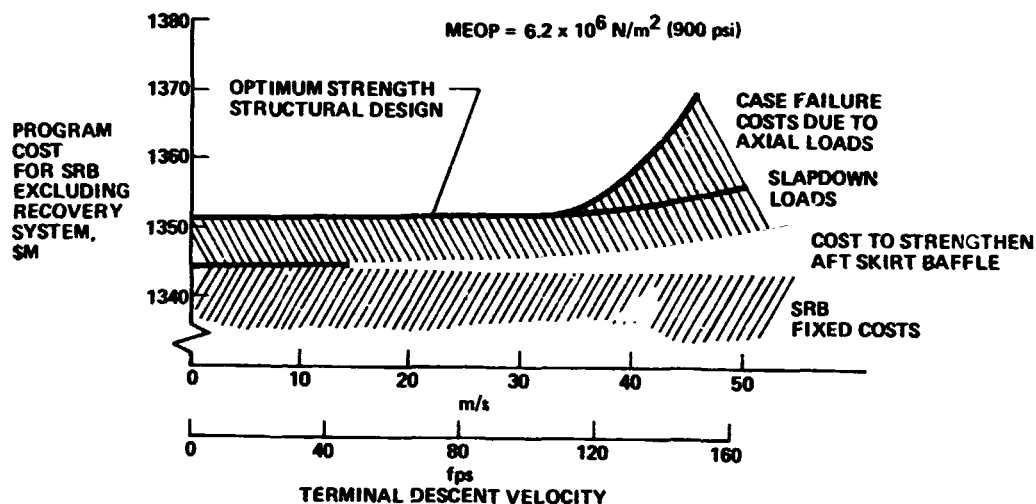


Figure 6.2-11 Optimum SRB Component Costs Increase with Terminal Descent Velocity

6.2.4 Recovery SRB System Cost Parametrics

While the cost of the SRB structural components or the SRM case can be modeled and optimized by considering the effects of failure probability and adding structural weight to strengthen components, the analogous study of recovery system costs is considerably more complex and involves other parameters. A parachute part failure (failure of ribbons, gores, or other minor components) probably does not significantly affect system cost or the survivability of the SRB. This type of failure has not been quantitatively treated in this study. For the purposes of this investigation, catastrophic failures (e.g., failure to deploy, attachment failure, etc) are more influential in selecting an optimum recovery system. Catastrophic failure represents a total failure (attrition) of the SRB and is treated in an overall parachute system reliability estimate. Thus, cost trades on the recovery system do not involve direct consideration of failure probability and therefore depend on cost sensitivities to the basic design parameters.

In order to determine which parameters affect the variation in parachute system costs as a function of parachute terminal velocity, an analysis and correlation of historical data was performed. This analysis showed that parachute costs were primarily a function of diameter (or area) with a second-order cost variation due to weight. We found, however that chute weight tends to define the cost of related recovery system equipment (bags, reefing, flotation, packing labor, etc).

It is widely believed by parachute fabricators that overdesign of chutes to provide for many reuses will substantially reduce refurbishment costs so that an optimum design may be defined.

6.2.4.1 Parachute Costs

Parachute design characteristics and cost estimating data have been correlated and analyzed and are shown in Figure 6.2-12. Correlated cost per unit weight as a function of weight, along with selected point design data for reference are shown. It is of interest to note that the constant diameter data are very nearly negative unity-slope lines on this logarithmic plot. Thus, it would appear that total cost is a much stronger function of diameter than weight. For example, the two point designs at 7.3 m (24 ft) diameter cost \$9430 at 37 kg (82 lb) of weight versus \$10,170 at 102-kg (226 lb) of weight, while the 45 m (148 ft) diameter costs \$33,440 at 700 kg (1548 lb) of weight. The 15.2 m (50 ft) diameter drogue chute does not fit the correlation because it is a high velocity, high dynamic pressure device which involves additional costs that increase its cost per unit weight. Thus the correlation should apply only to parachutes deployed from a 68,000 kg (150,000 lb) vehicle at relatively low velocities.

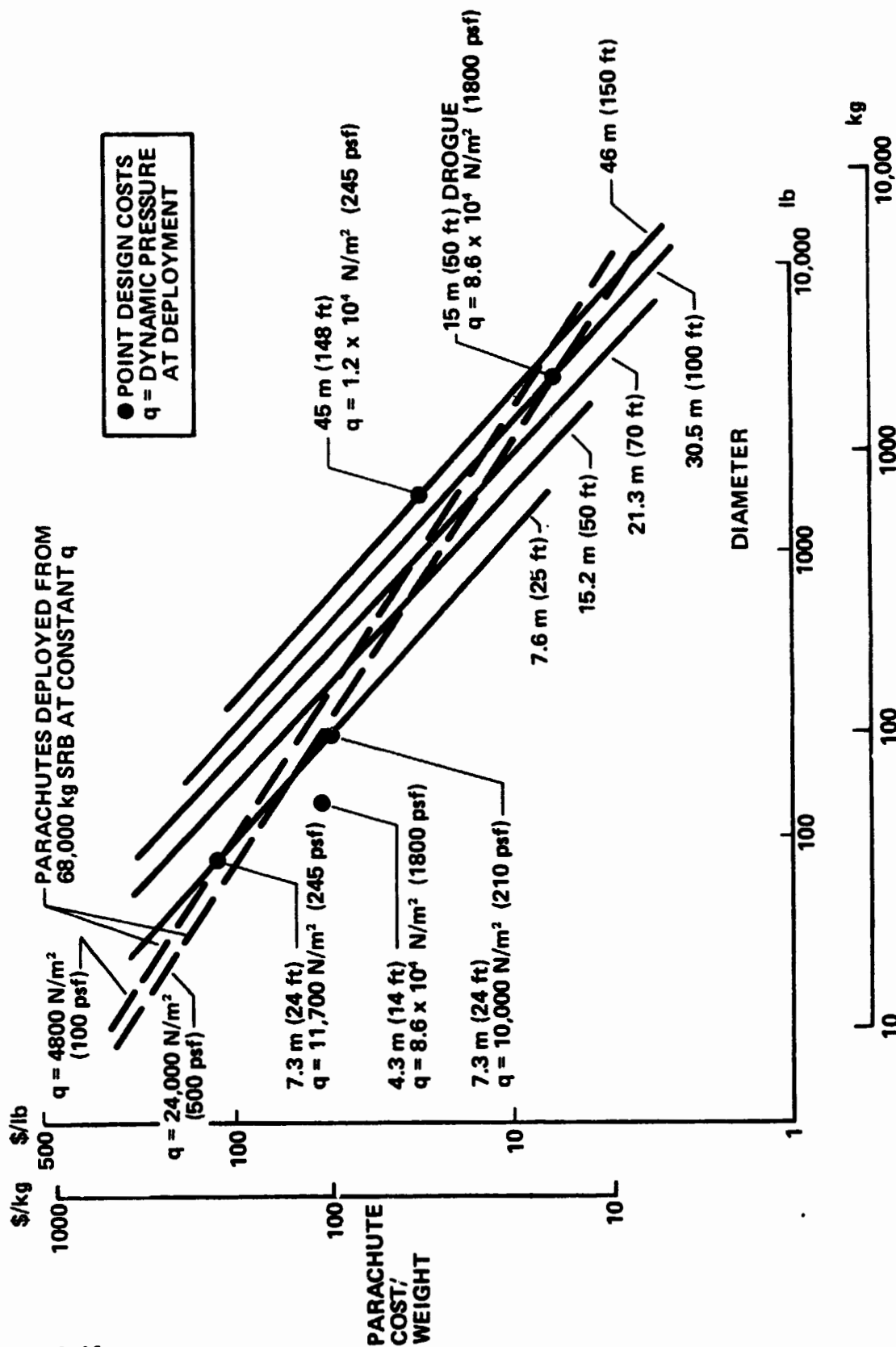


Figure 6.2-12 Parachute Total Cost Is Primarily a Function of Diameter

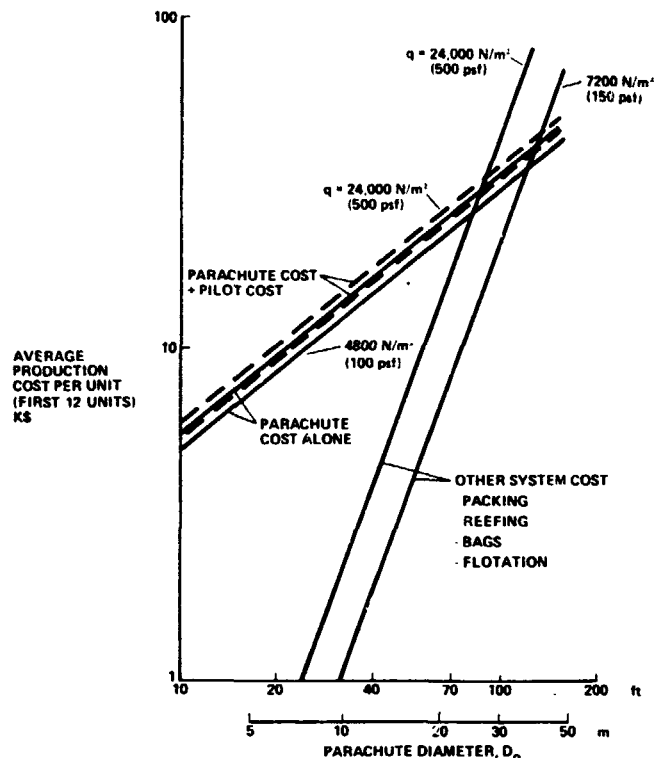


Figure 6.2-13 Diameter Dependent Parachute Costs

In order to provide some design perspective in viewing the figure, lines of constant deployment dynamic pressure have been superimposed. These were obtained by estimating the ultimate load on parachutes deployed from a 68,000 kg (150,000 lb) SRB at the given dynamic pressure, and plotting the corresponding parachute weight for each diameter. Thus, the parachute cost per unit weight versus chute weight for given deployment conditions (dynamic pressure), and varying diameter tends to follow very closely a negative 2/3-slope line on a logarithmic plot.

These parachute costs are plotted against parachute diameter in Figure 6.2-13. Ancillary parachute system equipment costs for packing, reefing, bags, flotation, and miscellaneous equipment required to complete the recovery system tend to vary in proportion to the weight of the parachute. This trend is indicated by the steeper slope of the curves for the "other system costs" in Figure 6.2-13.

The DDT&E costs shown in Figure 6.2-14 were systematically developed by estimating the DDT&E costs versus diameter assuming high confidence and a design process devoid of special problems. Then "complexity factors" were applied as the number of chutes in the system were increased: and progressive "advanced design factors" were applied as the chute diameter increased from standard design practice, to state-of-the-art limit, to extended state-of-the-art values.

6.2.4.2 Parachute Refurbishment Costs

In the structural trade studies for SRB water impact loads it was assumed that any damage sustained by an element would result in replacement of that element with a new manufacture. However, by nature of their construction, parachutes can always be expected to sustain some degree of damage. Thus the refurbishment cost of parachute systems will entail replacement of gores, ribbons, panels, etc. We feel, however, that parachute construction can be designed for such strength that joints, ribbons, panels, and gores are not likely to fail even after many reuses. Further, such construction should not entail large increases in weight or manufacturing cost.

Figure 6.2-15 indicates the decrease in refurbishment fraction expected for parachutes as they are designed and constructed for increasing numbers of uses (straight line). The refurbishment fraction shown is the average refurbishment fraction (without considering the experience curve) for a recovery system in which the average unit is reused 10 times. Thus, a parachute designed for a single use would be totally refurbished each time at a cost equal to replacement, while a parachute designed for 30 reuses would have a refurbishment cost of 7% of replacement cost during its program life of 10 uses. When certain fixed costs such as washing, transportation, handling, etc., are added (about 8%) the upper curve results. The corresponding percentage increases in a first unit manufacturing cost shown in Figure 6.2-16 have been estimated. The solid curve represents a 10% increase in new unit costs at 5 reuses compared to single use, 20% increase at 20 reuses, 30% increase at 75 reuses, etc. We believe this variation is more practical than the dashed curve which assumes a 10% increase in cost each time the number of uses is doubled.

The increase in manufacturing cost and corresponding decrease in refurbishment fraction as the chutes are made more rugged results in an optimum value for refurbishment fraction. This occurs when the rate of reduction in program cost due to refurbishment balances the rate of increase in new unit production cost. Figure 6.2-17 shows that this optimum occurs at a refurbishment fraction of 0.10 and results in a total recovery system cost factor of 0.128 for a program requiring 90 new units covering a total of 878 SRB flights.

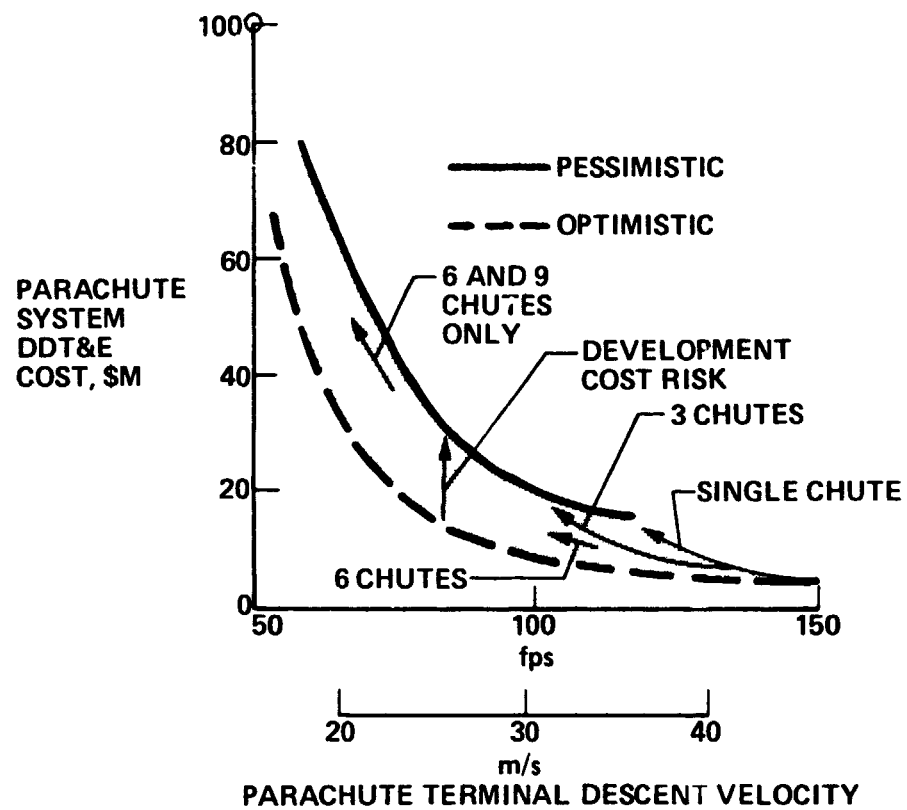


Figure 6.2-14 Velocity Dependence of Parachute System DDT&E

REFURBISHMENT OF PARACHUTE
SYSTEMS DEPENDS ON THE
"REUSABILITY" DESIGNED INTO THEM

- HIGHER STRENGTH RIBBONS
- STRONGER JOINTS
- LOW FAILURE PROBABILITY

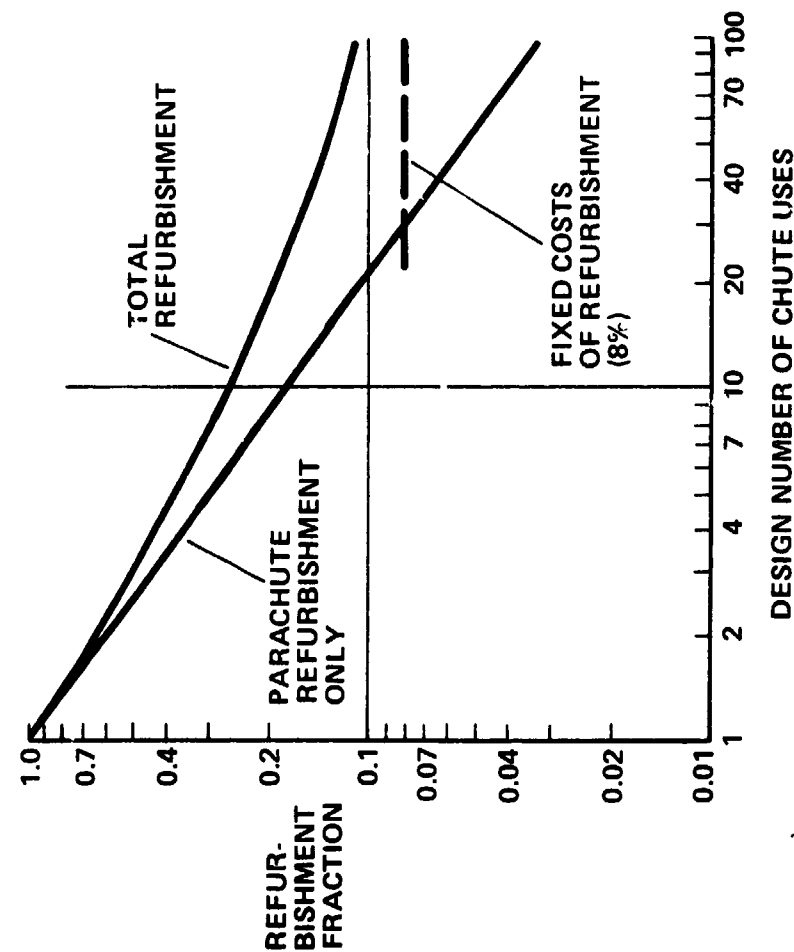


Figure 6.2-15 Parachute Refurbishment Fraction
Depends on Reuses

DESIGN FOR MANY REUSES RESULTS
IN HIGHER UNIT MANUFACTURING
COST AND LOWER REFURBISHMENT
COST

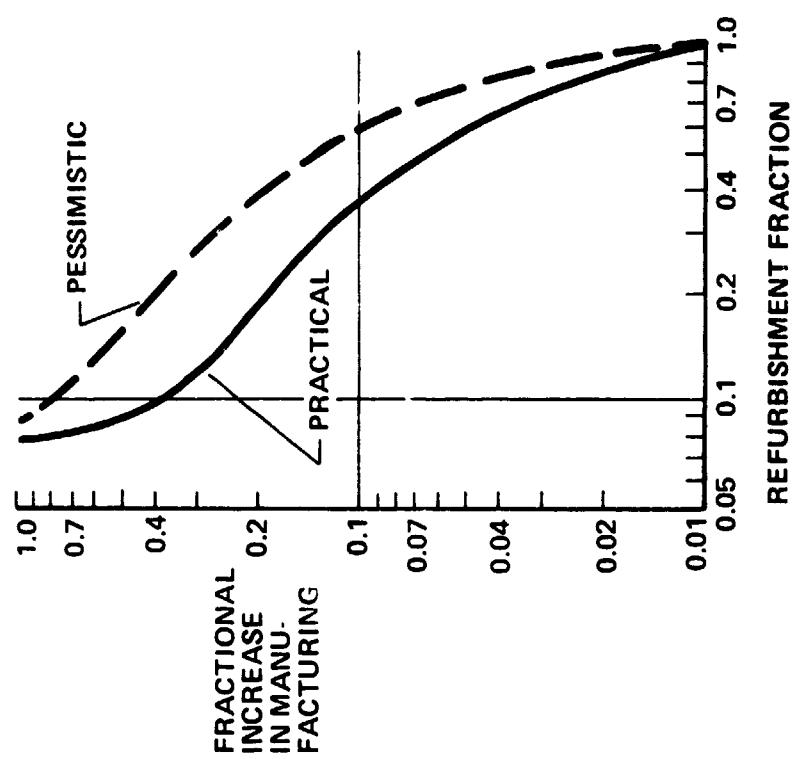


Figure 6.2-16 Parachute Manufacturing Costs
Depend on Refurbishment Fraction

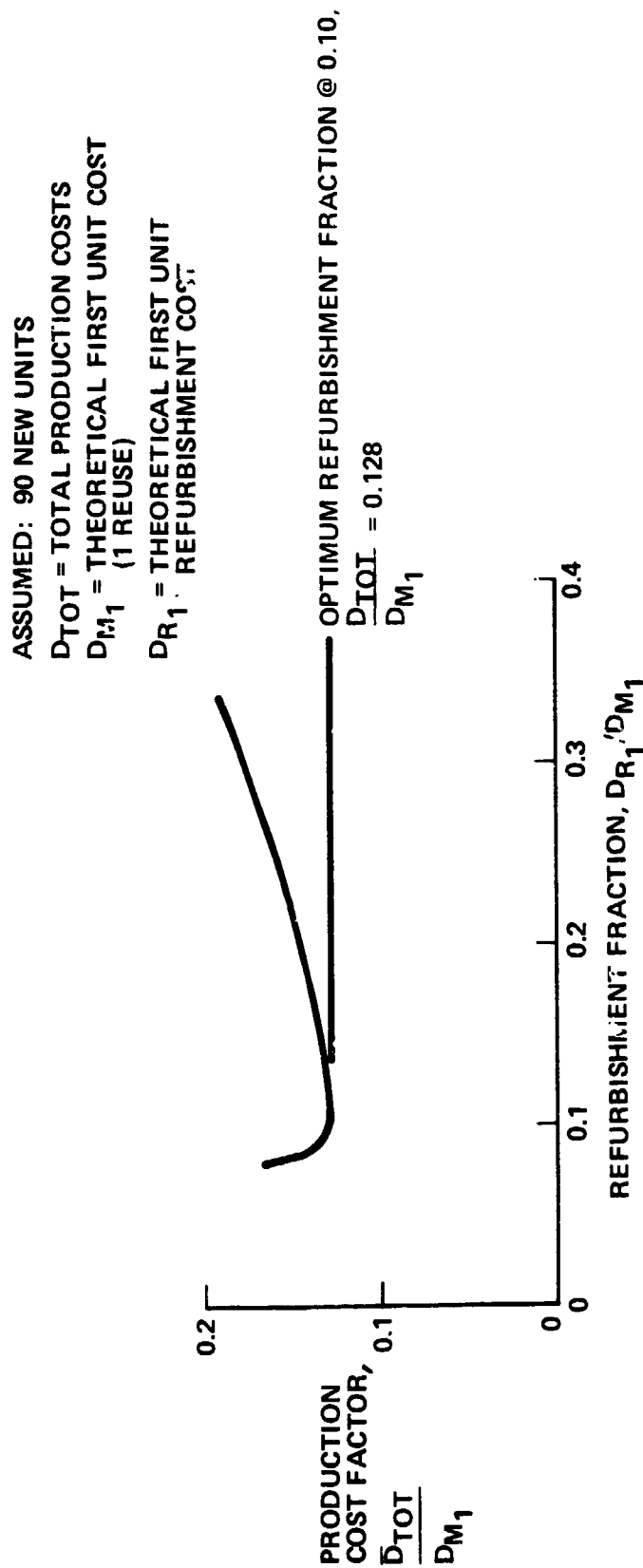


Figure 6.2-17 Manufacturing and Refurbishment Cost Trade Yields Optimum Refurbishment Fraction

That is, the average cost per SRB for the recovery system is 0.128 times the first unit manufacturing cost. We believe that recovery subsystem costs can be minimized if this design/cost approach is taken. While the numerical values are subject to considerable further study, the trends of the present analysis should be considered quite reliable.

Exercising the parametric parachute cost data for an SRB recovery system, the total recovery subsystem program cost estimate presented in Figure 6.2-18 can be determined. Ascent performance costs, i.e., the cost of preserving baseline performance from liftoff to SRB staging, were evaluated at \$3.30/kg (\$1.50 per pound) of recovery system weight per flight. The parachute DDT&E cost uncertainties are reflected in the DDT&E cost band shown. Production costs include the cost of building 90 new units and refurbishing 788 units, which result for a design having an optimum refurbishment fraction of 0.128 as previously discussed.

6.2.5 Hybrid Retrorocket/Parachute Costs

The high cost of an all parachute system to achieve low terminal descent velocities leads to the consideration of a hybrid retrorocket/parachute recovery system. The cost trade for this system is developed by using retrorocket cost parametrics similar to the parachute cost parametrics already presented. The two sets were then systematically combined at different descent velocities to determine the optimum combination of parachute and retrorocket.

The cost of small solid rocket motors is comparatively well known. Total impulse appears to be the governing parameter for preliminary design estimates. Figure 6.2-19 presents the average unit cost for 1756 units (2 units per SRB). An experience percentile of 0.95 was used to develop the average unit cost variation. The retrorocket system costs have been found to be insensitive to the number of retromotors used on an SRB. The DDT&E costs shown in Figure 6.2-20 assume that no special design problems occur. Other costs associated with the hybrid system include a fixed cost consisting of installation, checkout, and handling of the retrorocket system (not required in all-parachute system), and the cost of a radio-altimeter to provide the ignition signal for the retromotors.

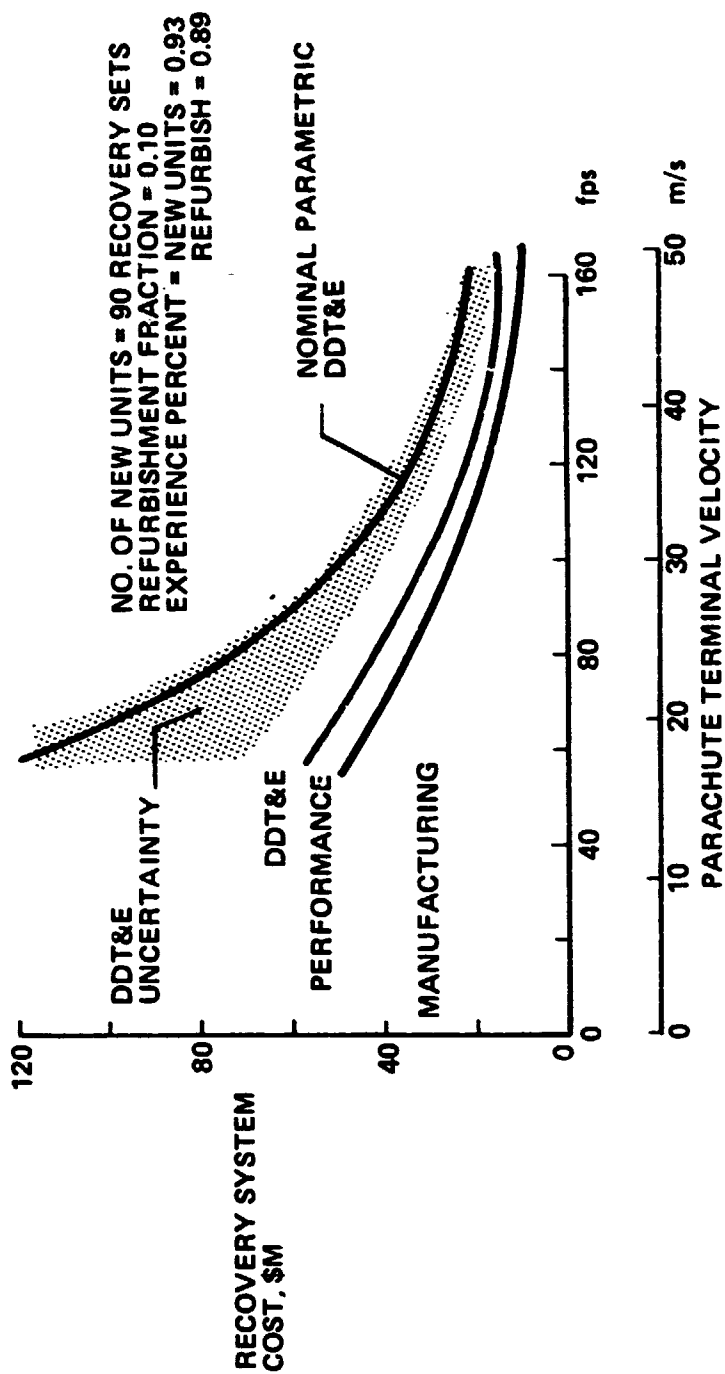


Figure 6.2-18 Cost of All-Parachute Recovery System

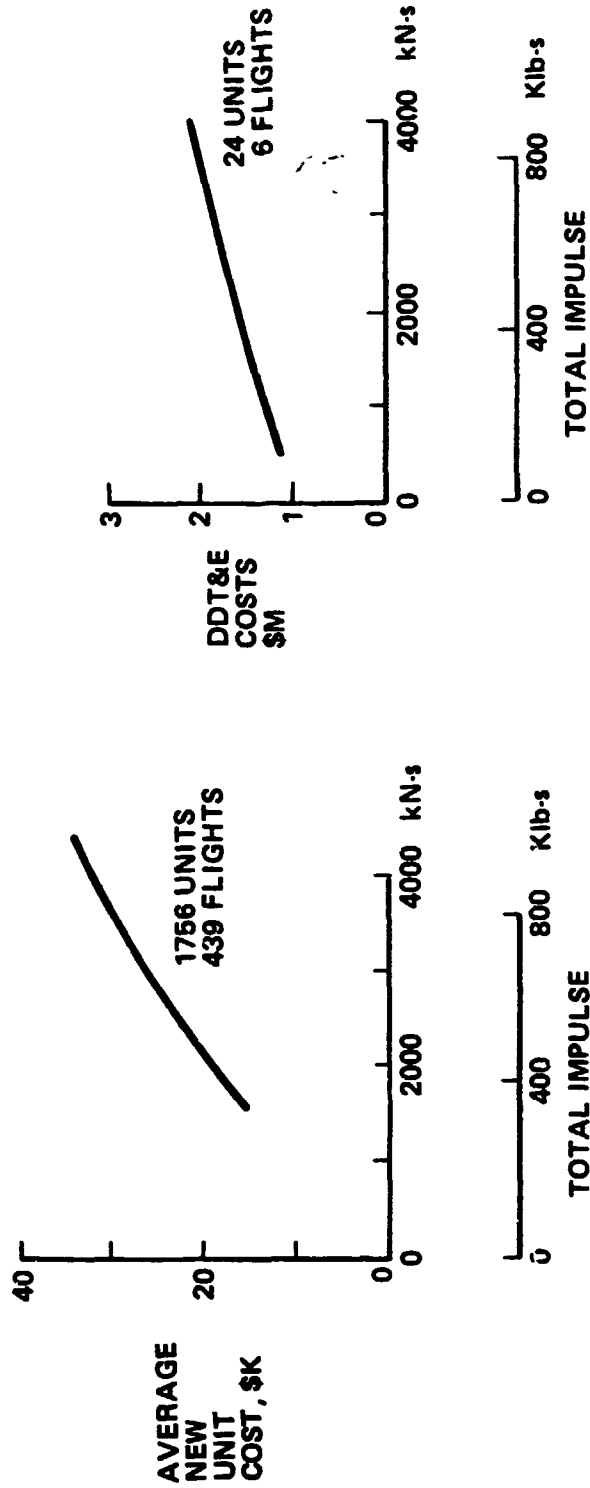


Figure 6.2-19 Retrorocket Motor Costs for Hybrid System Correlate with Total Impulse

Figure 6.2-20 Retrorocket Motor DDT&E Costs

Figure 6.2-21 shows the total cost for the retrorocket portion of the hybrid recovery system as a function of parachute terminal velocity with retrorocket terminal velocity shown as a parameter. The difference between the retrorocket and parachute terminal velocities is the ΔV required of the retromotors. This figure shows that a minimum fixed cost of \$14 M is required to include a retromotor. The \$14 M is made up of the following:

- Retrorocket fixed cost \$5.5 M
- Radio-altimeter \$5.3 M
- DDT&E \$2 M
- Performance cost \$1 M

The minimum total DDT&E costs for a retromotor system of \$2,000,000 is made up of \$1,200,000 for motors and \$800,000 for integration and mounting hardware design. For retrorocket systems providing velocity changes of 49 m/s (160 fps), the motor DDT&E costs increase to \$2,200,000 and the cost for integration with the SRB increases to \$1,500,000. If a dual thrust design is required, the DDT&E cost is increased by \$500,000.

The cost to include a retromotor increases linearly from \$14 M for a minimum ΔV system to \$56 M for a ΔV of 30.5 m/s (100 fps). The cost slope increases above a ΔV of 30.5 m/s (100 fps) because longer burn times are required to remain within the state of the art with consequent increase in gravity loss and an increase in total impulse required per unit ΔV . The cost of incorporating a dual thrust mode also increases with increasing ΔV . It has been assumed that retromotors will not be reused because of their high refurbishment fraction (0.83).

The hybrid recovery system costs are the sum of the parachute and retromotor costs and are presented as a function of parachute velocity in Figure 6.2-22. Because parachute system costs decrease with increasing velocity and retromotor system costs increase with ΔV required, an optimum parachute velocity may be expected for each hybrid system final velocity. This optimum parachute terminal velocity varies from 34 m/s (112 fps) for very low final velocities to 41 m/s (135 fps) for relatively high final velocities (indicated by dashed line).

The optimum cost points for the hybrid system are cross plotted against the SRB final descent velocity in Figure 6.2-23. The contributions of performance, DDT&E and production costs and the corresponding costs for the all-parachute system are shown. The minimum cost recovery system has its highest cost of \$101 M at zero terminal descent velocity (\$113,000 per SRB for hybrid system) and drops to \$60 M (\$67,500 per SRB) at the crossover point of 27.4 m/s (90 fps). Above this velocity, the all-parachute system is optimum and its cost drops until at 49 m/s (160 fps) it is \$20 M or \$22,500 per SRB.

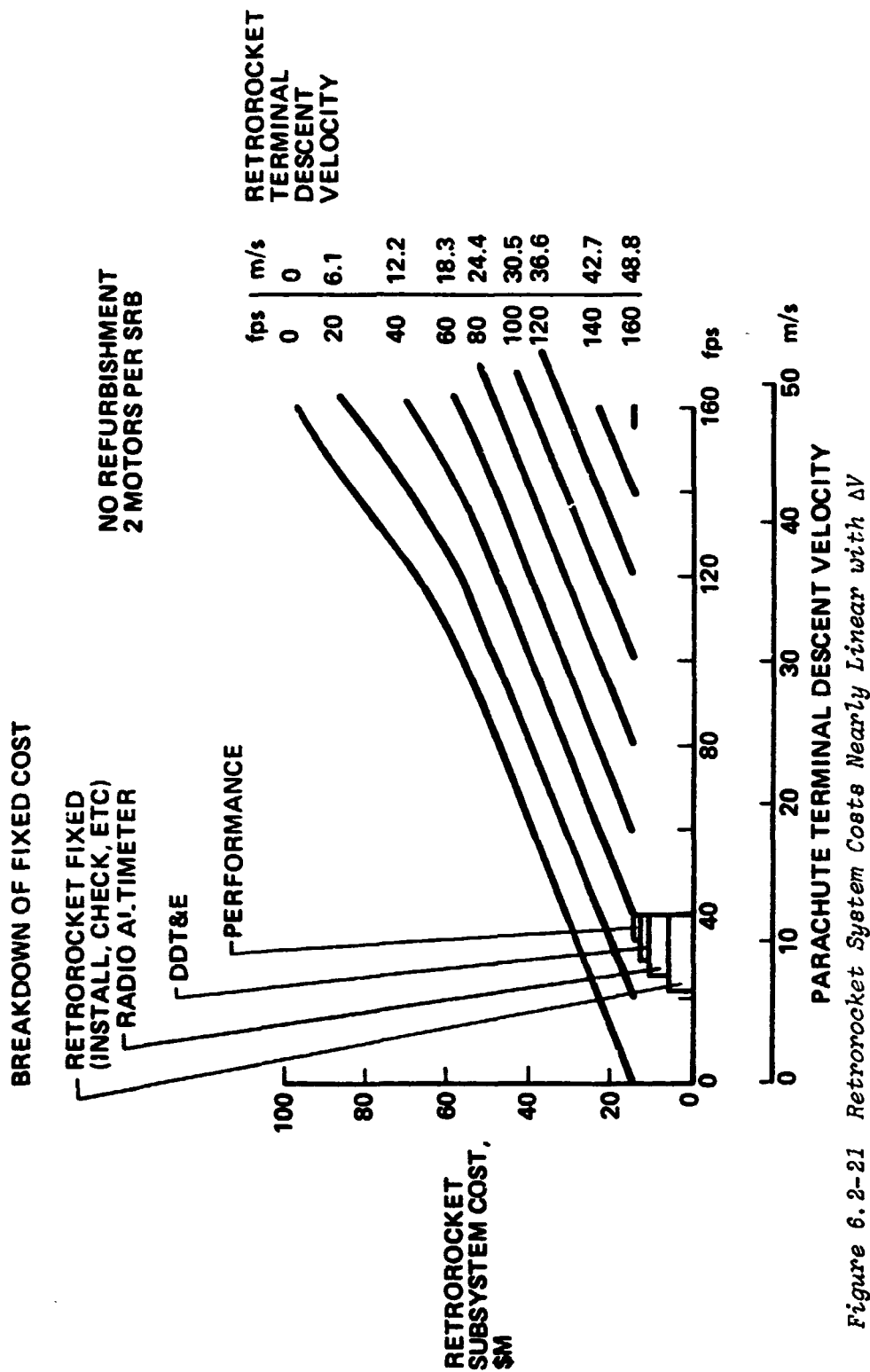


Figure 6.2-21 Retrorocket System Costs Nearly Linear with ΔV

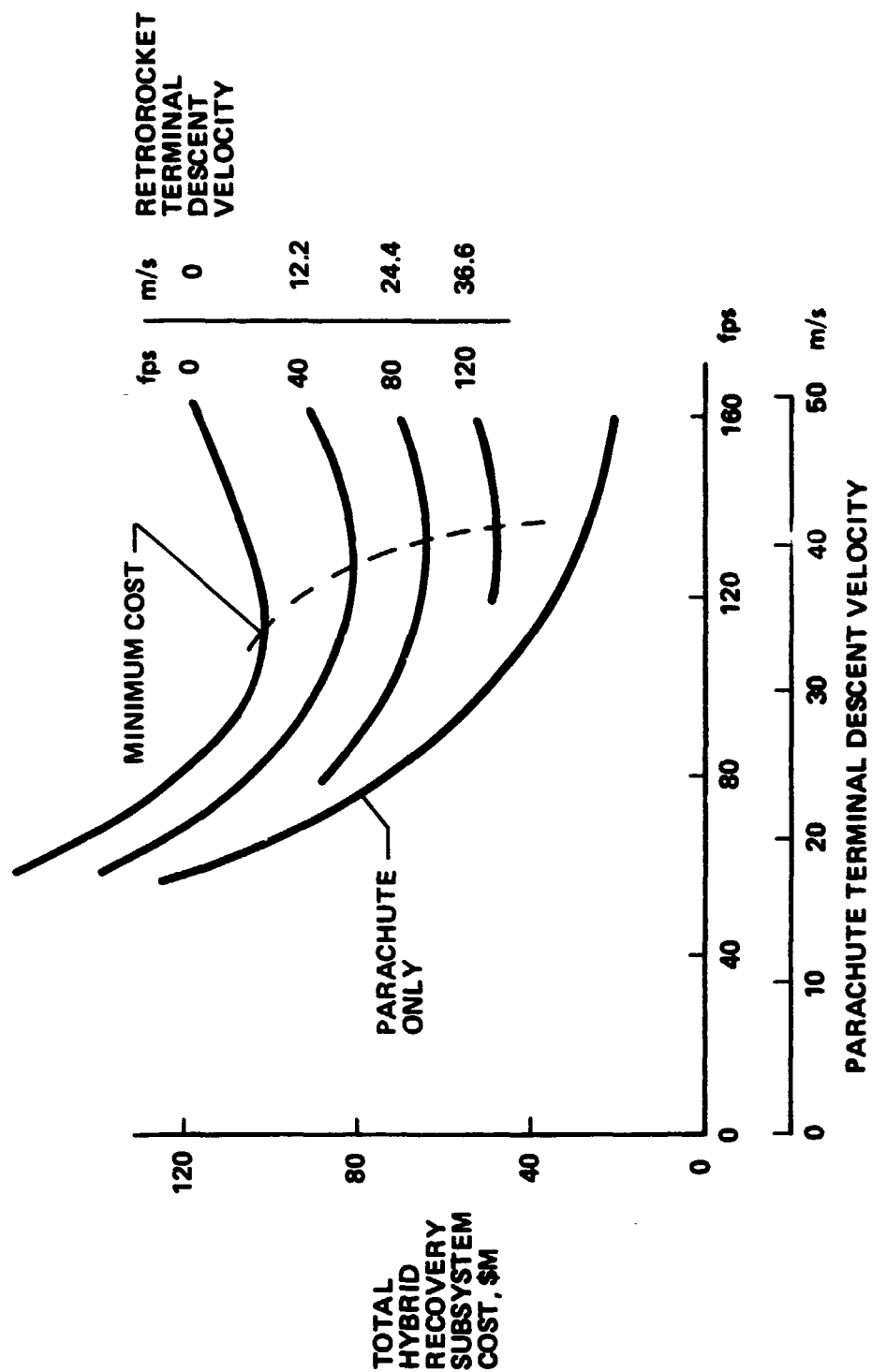


Figure 6.2-22 Optimum Parachute Terminal Velocity for Hybrid System between 33 and 41 m/s

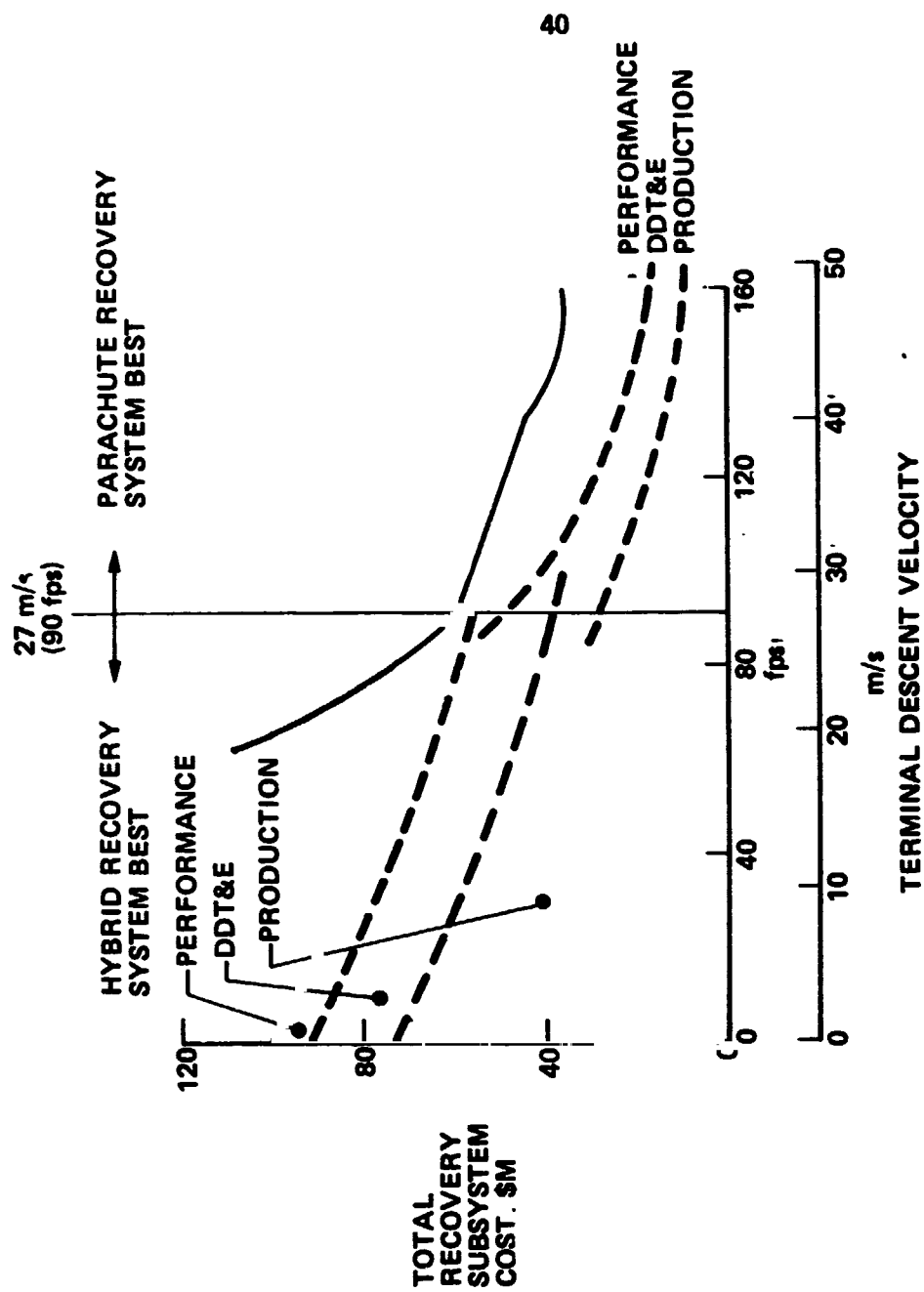


Figure 6.2-23 All-Parachute Systems Cost Less Than Hybrid Above 27.4 m/s (90 fps)

It was pointed out in Section 6.2.4 that considerable uncertainty exists as to the DDT&E costs of large parachutes (i.e., those parachutes associated with low terminal velocities). Figure 6.2-24 shows that the effect of considering these uncertainties is to define a band from 20 m/s (65 fps) to 29 m/s (95 fps) in which there is an uncertainty as to which system is less expensive. Below 20 m/s (65 fps) the hybrid system clearly has a cost advantage, and above 29 m/s (95 fps) the all-parachute system has the advantage.

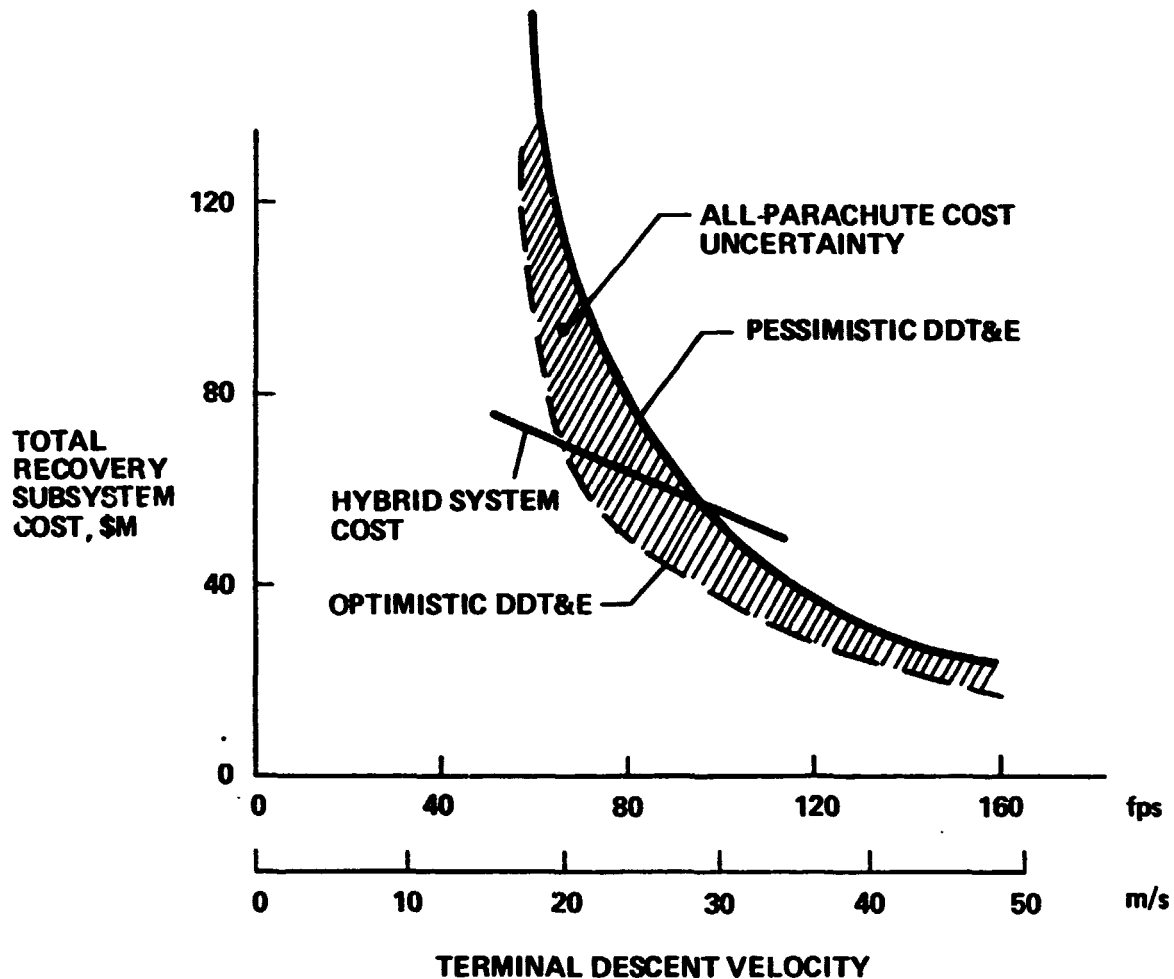


Figure 6.2-24 Pessimistic Parachute Costs Still Show All-Parachute System Cost Advantages

6.2.6 Total SRB Program Parameter Cost Results

Total program cost for optimally designed structural components and recovery subsystems have been determined as a function of terminal descent velocity in the previous discussion. By combining these elements to determine total SRB program costs an optimum terminal descent velocity criteria is defined. This is accomplished by combining the optimally strengthened structural component costs from Figure 6.2-11 with the recovery subsystem cost from Figure 6.2-23. The resultant total SRB program cost, shown on Figure 6.2-25 has a minimum cost of \$1388 M at 38 m/s (125 fps). As parametrically defined, this terminal descent velocity is optimum for a 445-flight program.

A similar calculation for a 225 flight program is shown in Figure 6.2-26. This program has been structured to have a DDT&E phase identical to that of the 445-flight program (i.e., 6 DDT&E flights). The production phase includes systems for 219 flights with a maximum flight rate of 30 flights per year. Cost for the production phase of the 445 flight program have been modified to reflect the changed quantities. For a 225-flight program, the optimum velocity is reduced to 35 m/s (115 fps) and the minimum total program cost is \$840 M.

5.3 POINT DESIGNS COST ESTIMATES

Due to the parametric nature of the previous results, we believe certain complexities within the SRB recovery subsystems are not fully reflected in the cost estimates. During the parametric analysis the effects on DDT&E costs of extending the state of the art in parachute diameter and/or cluster size were estimated in general terms. In order to verify the previous conclusions, four point design recovery systems were sized for the baseline SRB and more detailed cost analyses were conducted. These were:

- 1) A recovery system using one main chute sized to 38 m/s (125 fps) V_{TD} .
- 2) Three other recovery systems each with clusters of three main chutes and sized to different terminal descent velocities.

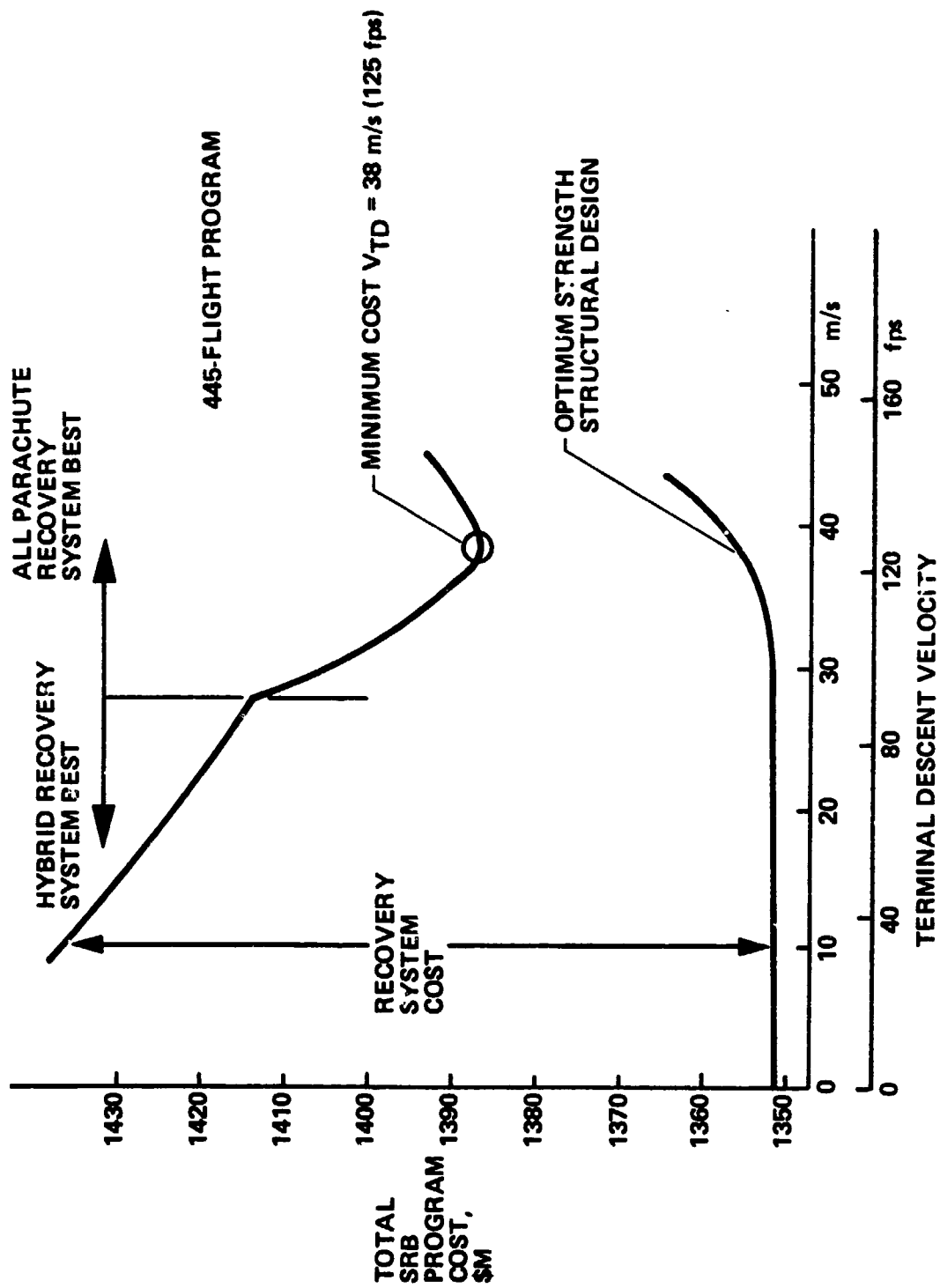


Figure 6.2-25 Optimum Descent Velocity Is 38 m/s (125 fps)

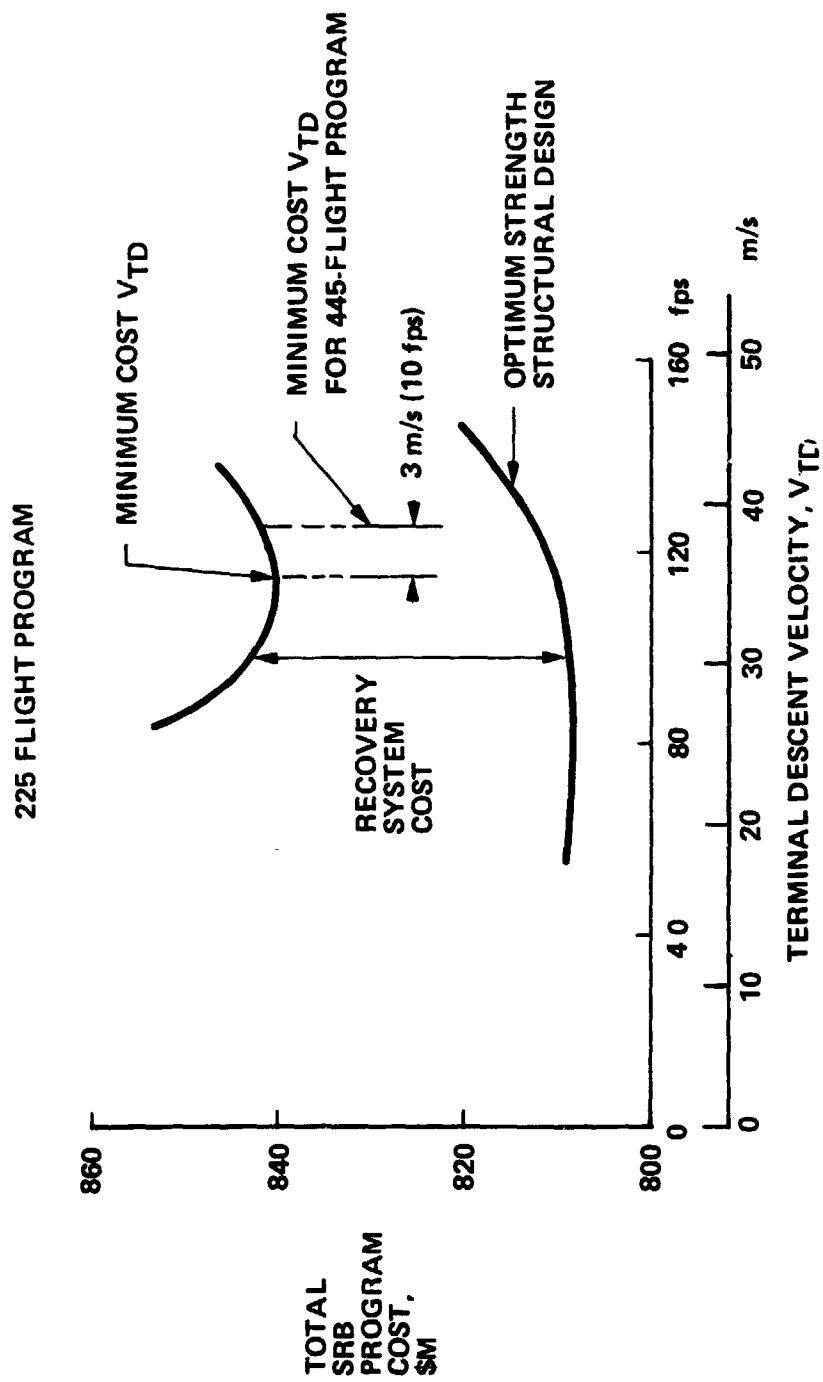


Figure 6.2-26 Reducing Number of Shuttle Flights Lowers Optimum Terminal Descent Velocity 3 m/s (10 fps)

These systems were obvious choices for more detail cost analysis since:

- 1) Single chute systems have the lowest apparent cost (due primarily to reduced quantity) as well as high reliability.
- 2) Three-chute clusters could have competitive costs since individual chute size and weights are reduced for a given velocity and because three-chute system reliabilities are higher when single chute failures are considered.

Table 6.3-1 presents a comparison of recovery subsystem DDT&E and production costs including the basic subsystem components: SRB recovery ordnance, main chute retrieval, nose/pilot retrieval, main chute fabrication and packing, and pilot chute fabrication and packing.

The cost component with the largest variance in this comparison is main chute fabrication and packing. Individual chute costs were varied for both diameter and weight between single and multiple chute systems. DDT&E and production costs were also varied for the additional total quantities in the multiple chute systems. These multiple chute quantity costs were carried down the improvement curve to the total quantity of individual main chutes required rather than the quantity of clusters. This assured a more realistic and lower total chute cost for the multiple chute systems. Only single pilot chutes were considered for the multiple chute systems: however, diameter and unit costs were varied.

SRB recovery ordnance and the nose/pilot/frustum retrieval package have the same component requirements for both single and multiple chute systems, therefore costs do not vary. The main chute retrieval package, however, requires separate flotation equipment, flashing lights, dye markers, and power sources for each individual main chute which causes an increase in multiple chute systems. Only one set of the remaining components of the retrieval package such as beacon, antenna, sonar transmitter, cables, and connectors are required in the multiple chute recovery systems and thus do not cause a cost variance. Comparisons of cost increases relative to the single chute recovery system are as follows:

Table 6.3-1 Single Parachute Recovery Subsystem Has Lowest DDT&E and Production Costs

RECOVERY SUBSYSTEM COSTS*	VTD = 38.2 m/s (125 fps) ONE-132-ft MAIN ONE-25-ft PILOT	VTD = 38.2 m/s (125 fps) THREE-79-ft MAINS ONE-22-ft PILOT	VTD = 30.5 m/s (100 fps) THREE-102-ft MAINS ONE-25-ft PILOT	VTD = 24.4 m/s (80 fps) THREE-130-ft MAINS ONE-28-ft PILOT
SRB RECOVERY ORDNANCE				
DDT&E	0.571	0.571	0.571	0.571
PRODUCTION	3.353	3.353	3.353	3.353
TOTAL	3.924	3.924	3.924	3.924
MAIN CHUTE RETRIEVAL				
DDT&E	0.750	0.978	0.978	0.978
PRODUCTION	2.832	4.839	4.839	4.839
TOTAL	3.582	5.817	5.817	5.817
NOSE/PILOT RETRIEVAL				
DDT&E	0.750	0.750	0.750	0.750
PRODUCTION	2.832	2.832	2.832	2.832
TOTAL	3.582	3.582	3.582	3.582
MAIN FABRICATION & PACKING				
DDT&E	7.094	7.764	8.101	8.442
PRODUCTION	10.764	16.428	19.549	22.740
TOTAL	17.858	24.192	27.650	31.182
PILOT FABRICATION & PACKING				
DDT&E	1.625	1.687	1.723	1.758
PRODUCTION	3.056	2.908	3.210	3.498
TOTAL	4.681	4.595	4.933	5.256
TOTALS				
DDT&E	10.790	11.760	12.123	12.499
PRODUCTION	22.837	30.360	33.783	37.262
TOTAL	33.627	42.110	45.906	49.761
COST/FLIGHT (445)	0.075	0.095	0.103	0.112
COST/SRB (890)	0.038	0.048	0.052	0.056

*COST IN \$M

	<u>DDT&E</u>	<u>Production</u>	<u>Total</u>
One chute system with $V_{TD} =$ 38 m/s (125 fps)	100%	100%	100%
Three chute system with $V_{TD} =$ 38 m/s (125 fps)	109	133	125
Three chute system with $V_{TD} =$ 30 m/s (100 fps)	112	148	137
Three chute system with $V_{TD} =$ 24 m/s (80 fps)	116	163	148

The point design DDT&E cost estimates were basically optimistic in that the DDT&E program presupposed a success-oriented development test program with minimal failures and little or no redesign. Thus the variations in cost from the baseline recovery system to the multiple chute systems and among the different diameter parachutes from 24 m (79 ft) D_0 to 40 m (132 ft) D_0 were reflected

only in additional hardware for cluster tests and in unit cost due to the chute diameter variations. It was felt that a more realistic DDT&E program cost assumption would be somewhere between this lowest cost approach and more pessimistic estimates which add costs due to failures and redesign resulting from potential problems inherent in developing clustered and very large diameter parachutes.

Table 6.3-2 presents a summary of the complexity factors which were applied to the baseline system DDT&E program in order to quantify a more pessimistic DDT&E cost estimate. The rationale for applying the specific factors is itemized below each system. We believe the relative magnitude of the factors closely approximate the potential problems presented for the DDT&E program.

Figure 6.3-1 illustrates the relative DDT&E costs of the optimistic and pessimistic estimates. A prediction of a realistic DDT&E cost trend line between the two extremes indicates the following:

$V_{TD} = 38$ m/s (125 fps)	DDT&E Cost = \$13 M
$= 30$ m/s (100 fps)	$= \$16$ M
$= 24$ m/s (80 fps)	$= \$20$ M

Table 6.3-2 DDT&E Uncertainties Were Systematically Explored

	VTD = 38 m/s (125 fps) ONE 132-ft MAIN	VTD = 38 m/s (125 fps) THREE 79-ft MAINS	VTD = 30 m/s (100 fps) THREE 102-ft MAINS	VTD = 24 m/s (80 fps) THREE 130-ft MAINS
OPTIMISTIC DDT&E COST ASSUMPTION	BASELINE RE- COVERY SYSTEM COST BASED ON SUCCESS ORIENTED TEST PROGRAM WITH NO REDESIGN	COST ESTIMATED BY ADDING CLUSTER TESTS TO DDT&E AND ADJUSTING FOR DIAMETER	(SAME)	(SAME)
DDT&E AREAS OF CONCERN	LARGE DIAMETER INFLATION CHARACTERISTICS ARE UNCERTAIN NEAR UPPER LIMIT OF TEST EXPERIENCE CANOPY STRENGTH REQUIRES NEW MANUFACTURE TECHNIQUES	CLUSTER INFLA- TION INTERFER- ENCE POSSIBLE LEAD PARACHUTE OVERLOADING POSSIBLE	CLUSTER INFLA- TION INTERFER- ENCE POSSIBLE LEAD PARACHUTE OVERLOADING POSSIBLE LIMITED TEST EXPERIENCE	CLUSTER INFLA- TION INTERFER- ENCE POSSIBLE LARGE DIAMETER INFLATION CHARACTERISTICS ARE UNCERTAIN NO TEST EXPERIENCE LEAD PARACHUTE OVERLOADING POSSIBLE CANOPY STRENGTH REQUIRES NEW MANUFACTURE TECHNIQUES
PESSIMISTIC DDT&E COST ASSUMPTIONS	2 x TEST HARD- WARE + 15% OF OTHER DDT&E COSTS	3 x TEST HARD- WARE + 5% OF OTHER DDT&E COSTS	3 x TEST HARD- WARE + 10% OF OTHER DDT&E COSTS	4 x TEST HARD- WARE + 20% OF OTHER DDT&E COSTS

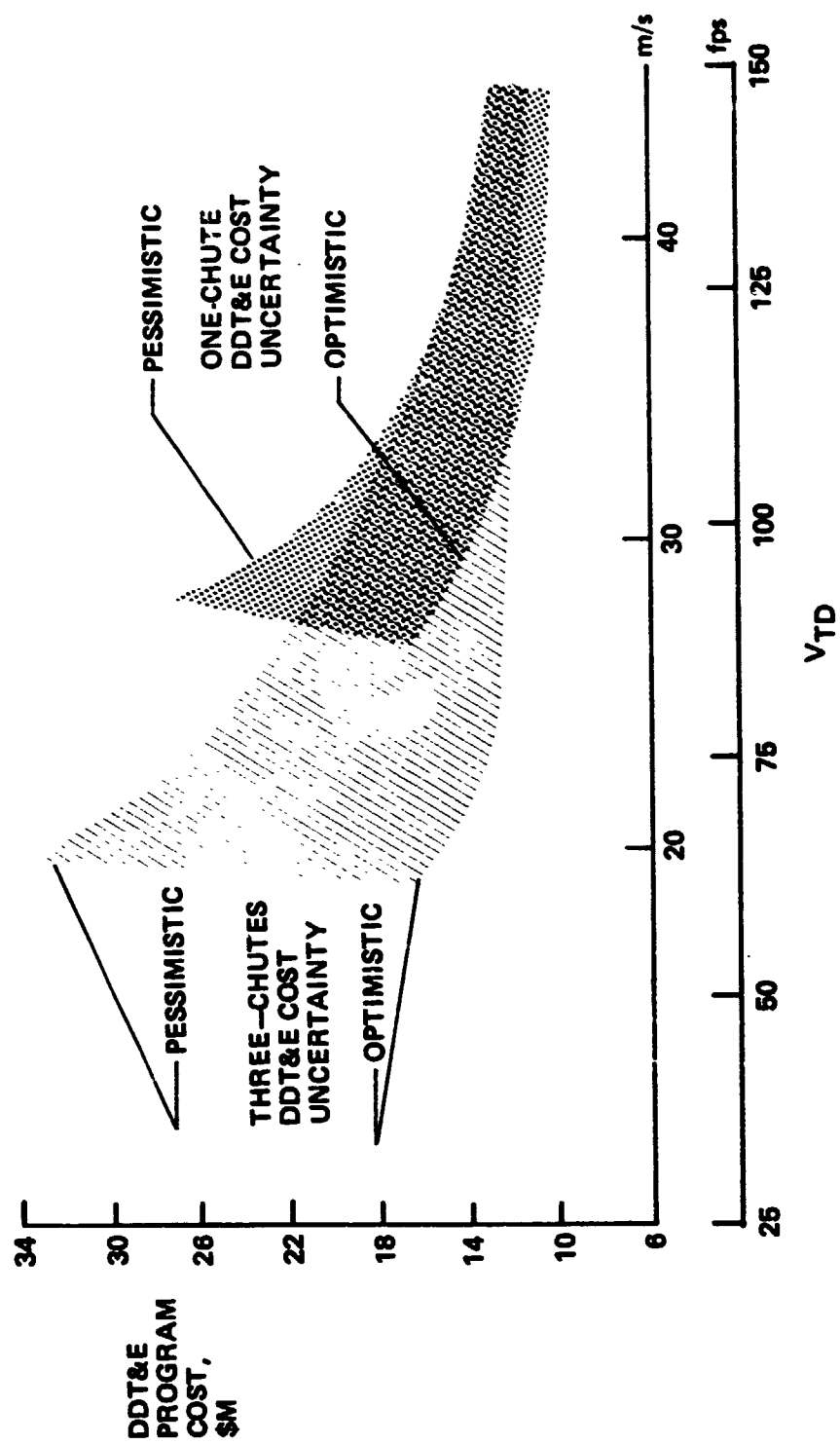


Figure 6.3-1 DDT&E Costs Are Sensitive to State of the Art Uncertainties

In Figure 6.3-2, the point design recovery subsystem cost estimates are combined with the optimally designed structural component cost to obtain total SRB program costs. The recovery DDT&E cost uncertainty band is included. This figure illustrates that regardless of the DDT&E cost uncertainties, a minimum cost still occurs at terminal descent velocities of approximately 38 m/s (125 fps). This optimum V_{TD} is also insensitive to whether a single chute or three chute recovery system is chosen.

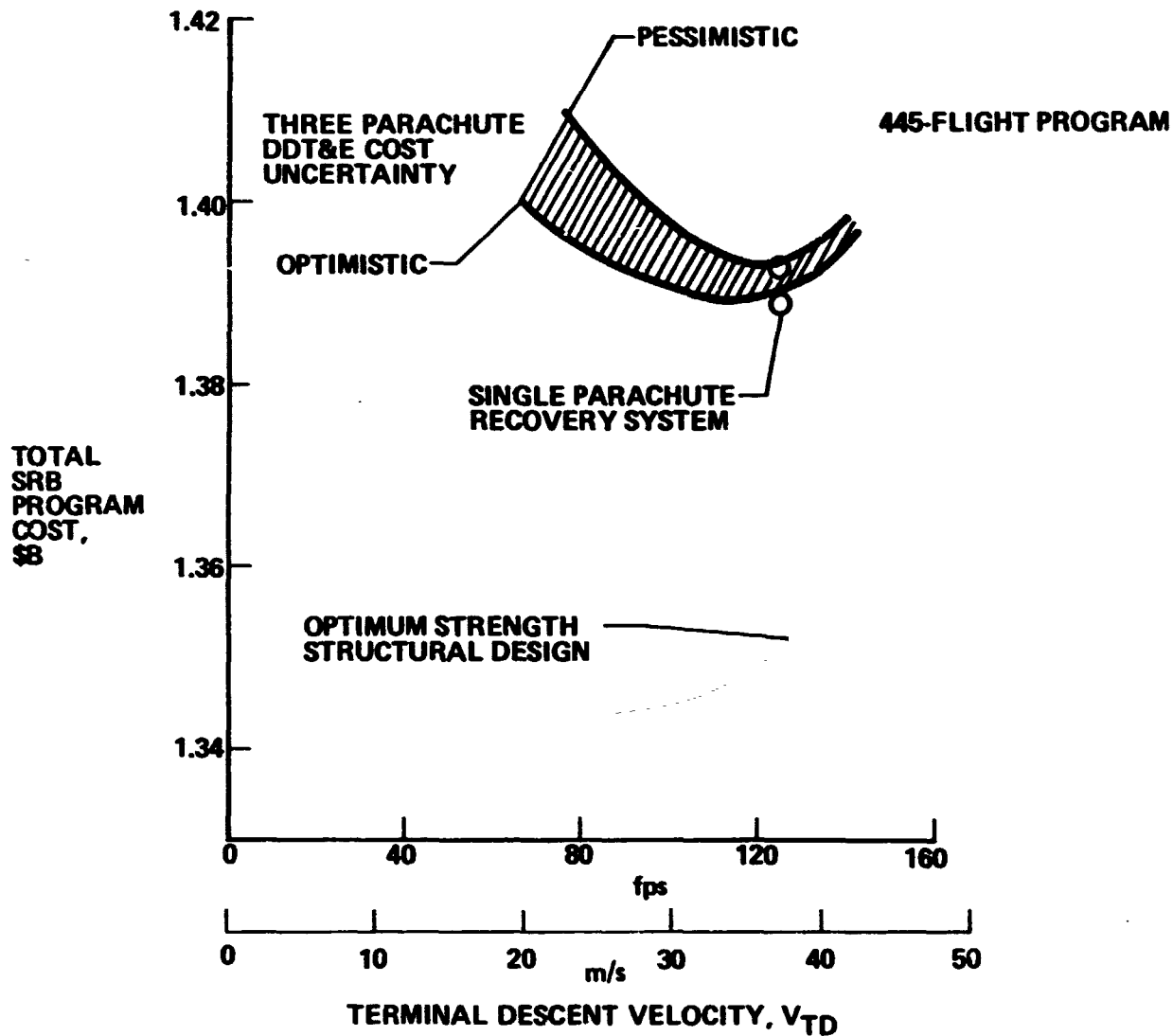


Figure 6.3-2 Optimum Terminal Descent Velocity Is Insensitive to Recovery System DDT&E Cost Uncertainty

Our study was not primarily design-concept oriented, but in the process of defining the Recovery Subsystem requirements, configuration selection considerations other than those that can be quantified became apparent. The fact that an impact velocity of about 38 m/s (125 fps) results in near minimum program costs for several different design options and DDT&E cost assumptions was established in the previous section. A summary of the optimum impact velocity, program cost, and the increment between the minimum cost and the cost at an impact velocity of 24 m/s (80 fps) is presented in Table 6.4-1. These data show that the optimum impact velocity varies between 36 m/s (118 fps) and 38 m/s (125 fps) and that the total program cost savings over a system with an impact velocity of 24 m/s (80 fps) varies from 5 to 30 million dollars. The shape of the DDT&E curve is the major driver in determining the cost advantage for the optimum velocity while the reliability of the recovery system influences the level of the minimum cost point. The probability of at least two parachutes of a three-parachute cluster functioning is predicted to be very high, as shown in Table 6.4-2. If this reliability is assumed for the three parachute system, the total program difference between this system and a single main parachute system is very small. Higher SRB component damage probability is assumed and included in the cost estimate for the flights that experience a single main parachute failure; however, the resulting increased impact velocity does not cause complete loss of the SRB. Thus the increased parachute system cost of the cluster is nearly offset by its increased reliability.

The very high reliability predicted for the three main parachute cluster results from the assumptions that:

- 1) there is no clustering effect on individual parachute deployment and inflation probability;
- 2) failure of one parachute will not cause failure or degradation of the other two.

While these assumptions reflect accepted reliability estimating practice, they intuitively appear optimistic because of the potential of physical and aerodynamic interference effects.

Table 6.4-1 Cost - Optimum V_{TD} Is Insensitive to Design Approach and Cost Assumptions

DESIGN APPROACH	DDT&E COST ASSUMPTION	RECOVERY SUBSYSTEM RELIABILITY	COST OPTIMUM V_{TD} , m/s(fps)	TOTAL PROGRAM COST AT OPT V_{TD} , \$M	TOTAL PROGRAM COST AT 24 m/s(80 fps) \$M	COST Δ FOR 24 m/s(80 fps) V_{TD} , \$M
PARAMETRIC TRADES	TOPS DOWN ESTIMATE	4% ATTRITION ASSUMED	38(125)	1387	1417	30
SINGLE MAIN PARACHUTE	OPTIMISTIC BOTTOMS-UP ESTIMATE	0.9950 4% ATTRITION	38(125)	1388	---	---
THREE MAIN PARACHUTES	OPTIMISTIC BOTTOMS-UP ESTIMATE	0.9996 (2 of 3) 3.4% ATTRITION	36(118)	1389	1394	5
THREE MAIN PARACHUTES	PESSIMISTIC BOTTOMS-UP ESTIMATE	0.9996 (2 of 3) 3.4% ATTRITION	37(122)	1394	1408	14
THREE MAIN PARACHUTES	OPTIMISTIC BOTTOMS-UP ESTIMATE	0.9859 SINGLE FAILURE LOSSES SRB 4.9% ATTRITION	36.5(120)	1412	1418	6

STRENGTHENING OF SRB STRUCTURAL COMPONENTS IS MORE COST EFFECTIVE THAN REDUCING V_{TD} BELOW 38m/s (125 fps)

Table 6.4-2 System Simplicity Improves Reliability

FUNCTION	RECOVERY SYSTEM SUCCESS PROBABILITY				
	OPTION 1 NASA BASELINE 3 MAINS WITH DROGUE	OPTION 2 SINGLE MAIN NO DROGUE	OPTION 3 3-MAIN NO DROGUE	OPTION 4 SINGLE MAIN WITH DROGUE	OPTION 5 SINGLE MAINS, NO DROGUE, HYBRID
DEPLOYMENT SEQUENCE	0.9998	0.9998	0.9998	0.9998	0.9998
DROGUE CHUTE	0.9914	-----	-----	0.9914	-----
MAIN CHUTES	0.9863	0.9954	0.9863	0.9954	0.9954
ELECTRICAL POWER	0.9999	0.9999	0.9999	0.9999	0.9999
STRUCTURAL SUPPORT	0.9999	0.9999	0.9999	0.9999	0.9999
RETROMOTOR	-----	-----	-----	-----	0.9989
SYSTEM RELIABILITY	0.9775*	0.9950	0.9859**	0.9865	0.9939
FAILURE PROBABILITY	0.0225	0.0050	0.0141	0.0135	0.0061

*PROBABILITY AT LEAST 2 MAINS FUNCTION = 0.9910

**PROBABILITY AT LEAST 2 MAINS FUNCTION = 0.9996

1% INCREASE IN RELIABILITY SAVES \$17.3 MILLION PROGRAM COST

The assumptions used in estimating DDT&E costs are discussed in the previous section. The variation in DDT&E cost with impact velocity has only minor influence on the optimum impact velocity, but a major effect on the level of program funding required to deviate from that optimum.

Since differences in total program costs are small, this parameter alone cannot be used to select between single and multiple parachute systems. Subjective reasoning was therefore attempted. Table 6.4-3 lists several issues and the subjective relative ratings for each issue among four configurations providing an impact velocity of 38 m/s (125 fps). These configuration options are:

- 1) Single main parachute;
- 2) A cluster of three main parachutes sized for the design impact velocity;
- 3) A cluster of three main parachutes sized for the design impact velocity with a single parachute failure;
- 4) A cluster of 6 main parachutes.

The single main parachute system rates best in cost, development testing, logistics, refurbishment, and available test data. The cluster systems are favored for reliability (if a single failure does not cause SRB loss), weight, handling, and growth capability. While such an evaluation is admittedly subjective, the total rating score favors the single main parachute.

The primary objective of the SRB Recovery System Requirements Study was to select a recovery system which results in minimum total program costs. We selected the single main parachute recovery system for the baseline design concept because of its: lower DDT&E costs, lower total program costs, and design simplicity.

Table 6.4-3 Parachute Configuration Options - 38 m/s (125 fps) Terminal Descent Velocity

ISSUE	OPTION WEIGHTING FACTOR	A	B	C	D	REMARKS
		ONE 40.3 m (132 ft) CHUTE	THREE 24.1 m (79 ft) CHUTE	THREE 31.1 m (102 ft) CHUTE	SIX 17.7 m (58 ft) CHUTE	
RELIABILITY	10	8	7	9	5	A SINGLE PARACHUTE IS BETTER THAN A CLUSTER UNLESS THE CLUSTER IS DESIGNED FOR A PARACHUTE FAILURE
PROGRAM COST	10	9	8	7	5	SINGLE CHUTE SYSTEM LOWERS COST
WEIGHT	5	3	4	3	2	THIS FUNCTION HAS A MINIMUM AT A CLUSTER OF THREE
DEVELOPMENT TESTING	10	5	4	4	2	CLUSTERED DEPLOYMENT IS COMPLEX. AERIAL DROP TESTS CANNOT BE MADE WITH AN EQUIVALENT SRB WEIGHT
HANDLING	5	2	4	3	5	THIS IS A FUNCTION OF INDIVIDUAL PARACHUTE WEIGHT
LOGISTIC (SPARES)	5	3	2	2	1	PERMANENT SET AFFECTS ACCEPTABLE CLUSTER GROUPINGS
REFURBISHMENT	5	5	3	3	1	NUMBER OF PARACHUTES IN CYCLE
SRB GROWTH	5	3	4	3	4	$D_0 < 49$ m(160 ft) FOR SINGLE PARACHUTE 41 m(135 ft) FOR CLUSTER OF 3, AND 37 m(120 ft) FOR CLUSTER OF 6
AVAILABLE TEST & DESIGN DATA	5	3	2	2	0	T&D DATA AVAILABILITY INVERSELY PROPORTIONAL TO CLUSTER SIZE
SWIVEL REQUIREMENT	5	4	2	2	2	CLUSTERS ARE LESS TOLERANT TO RELATIVE ROTATIONS, ESPECIALLY DURING DEPLOYMENT
TOTAL SCORE		45	40	38	27	
RATING		BEST	GOOD	GOOD	POOR	
*DESIGNED FOR SINGLE PARACHUTE FAILURE						

7.0 RECOVERY SYSTEM PROGRAM PLANS

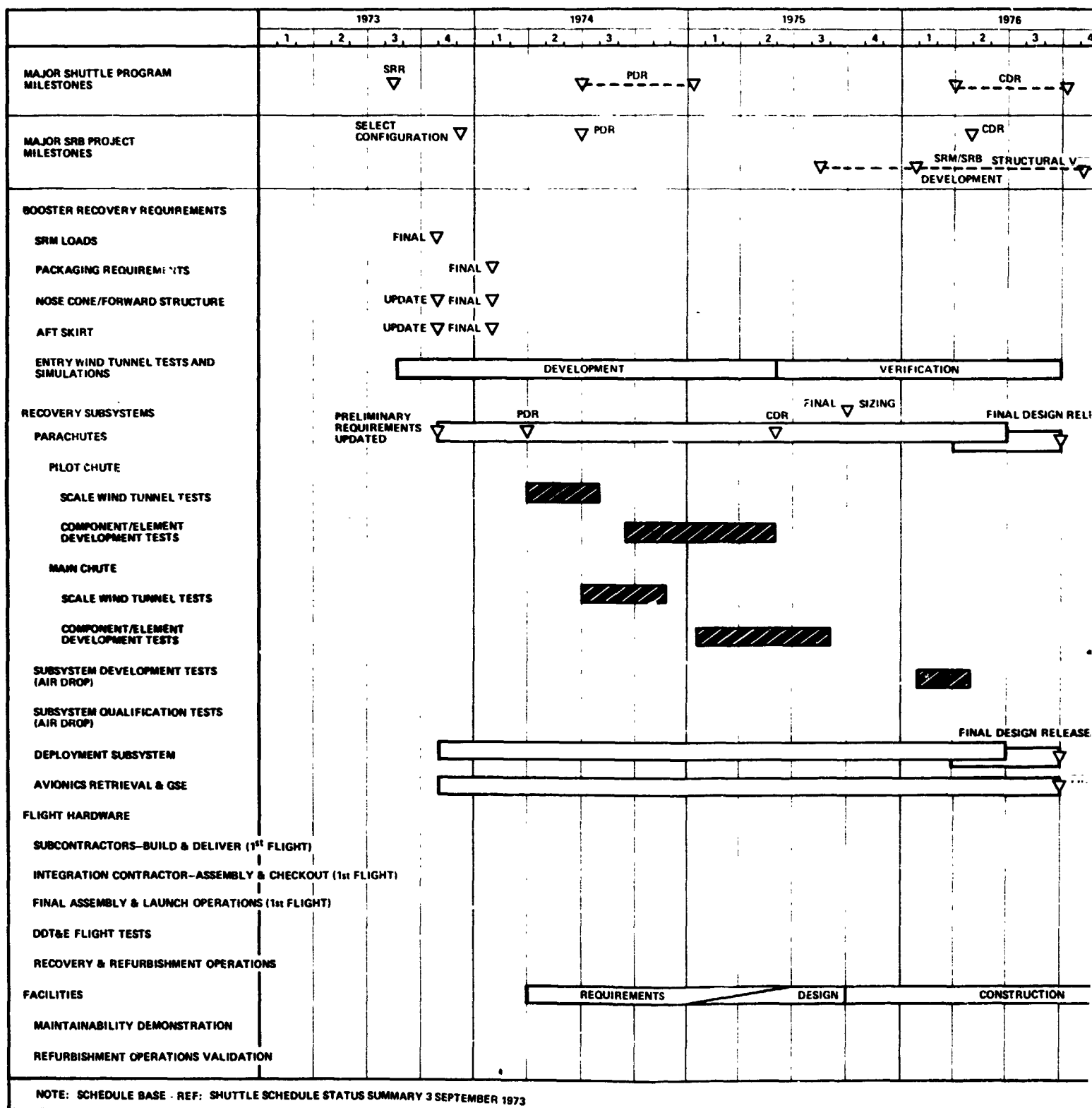
The overall SRB Recovery System Development Plan is presented in Figure 7.0-1. This milestone schedule shows the relationship of the recovery system development, qualification, demonstration, and facilities requirement, with the SRB and Shuttle program milestones. The development plan supports the program milestones in all areas. To support the SRB project PDR milestone, the SRB recovery system definition and stage hardware loads interface must be defined at the earliest possible date.

The top level logic network for developing, demonstrating, and qualifying the defined recovery system is presented in Figure 7.0-2. This network is keyed to the SRB development milestones and indicates that the recovery system development, verification, and demonstration of refurbishment operations can be accomplished well within the milestones to support the first vertical flight test. The decelerator system can only be partially qualified before flight test because of inability to drop test the system at full operational loads. Flight certification for first vertical flight (FVF) will therefore be met by test plus analysis. Full decelerator system qualification will be by flight demonstration during the DDT&E FVF.

7.1 DEVELOPMENT TEST PLAN

Development of the Space Shuttle SRB recovery system will entail increasingly complex testing and evaluation after the initial feasibility tests are complete. A development program goal is to achieve the lowest possible program cost while satisfying the technical objectives. All hardware of new design will be tested to determine suitability for the intended application, while analysis will be used to show correlation between existing hardware and recovery system specification requirements. Essentially, all development testing should be completed before the recovery system CDR to influence critical designs, provide background for review, and achieve preliminary design verification for production design approval.

FOLDOUT FRAME



PRECEDING PAGE BLANK NOT FILMED

2

AUGUST 28, 1973

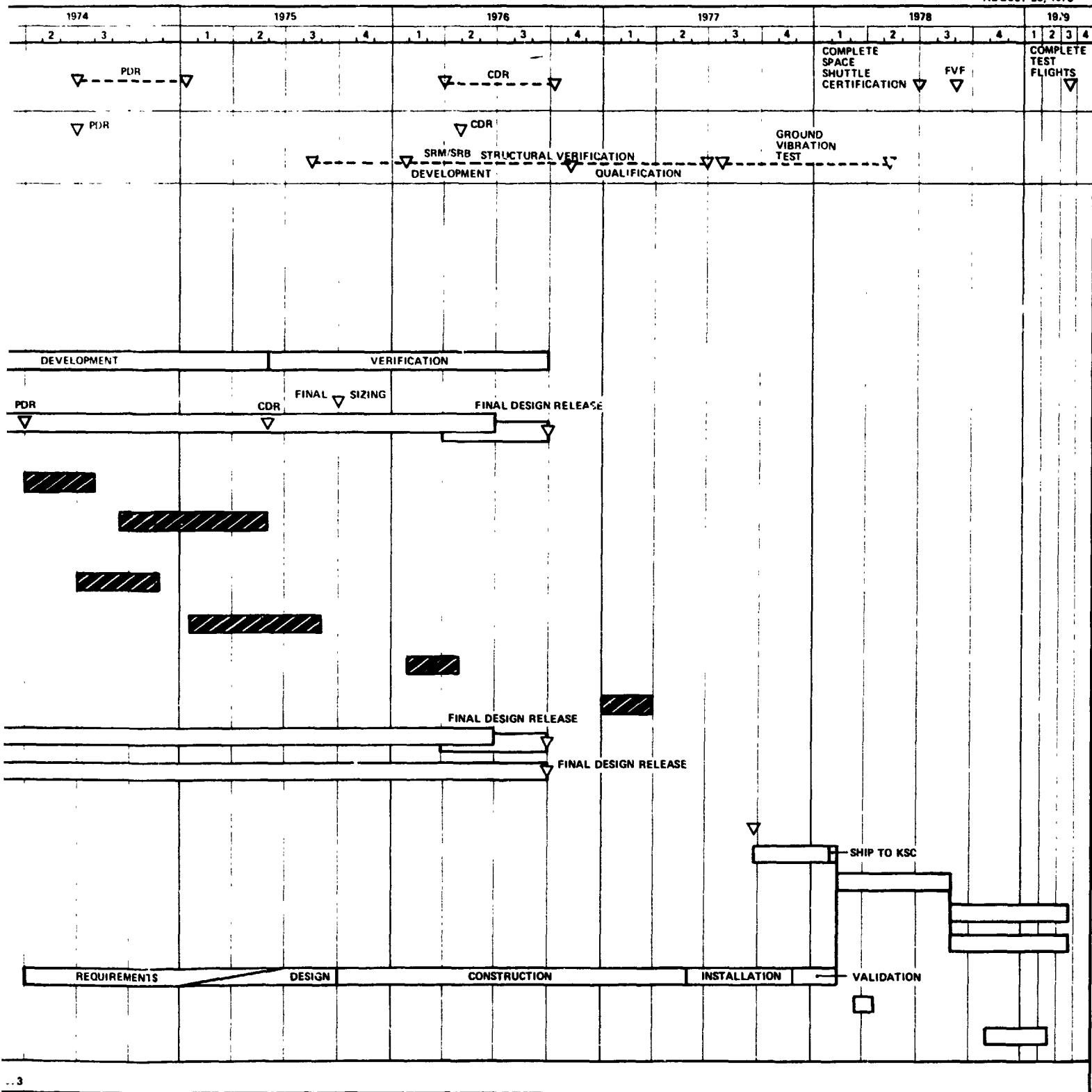
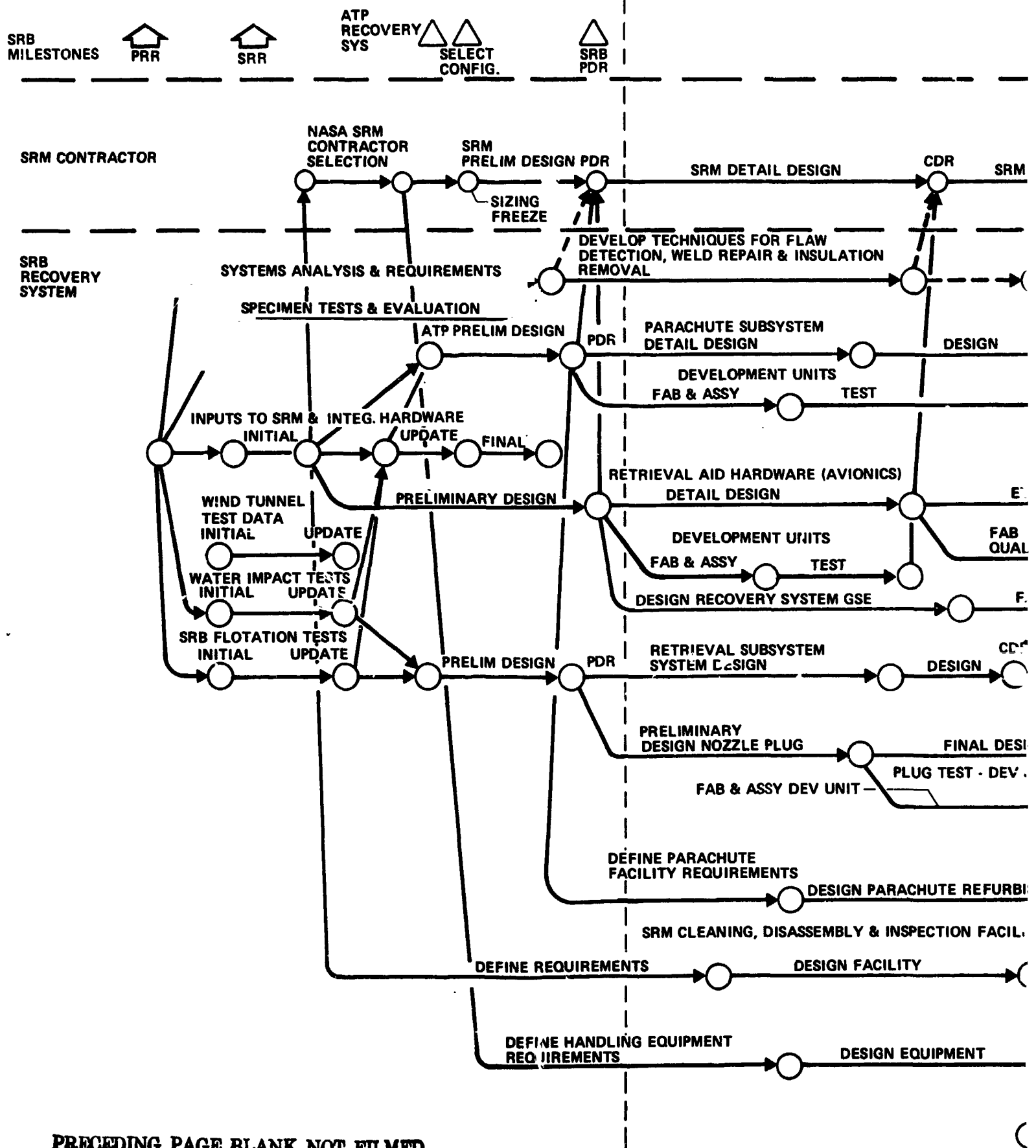


Figure 7.0-1 SRB Recovery System Development Plan

FOLDOUT FRAME



PRECEDING PAGE BLANK NOT FILMED

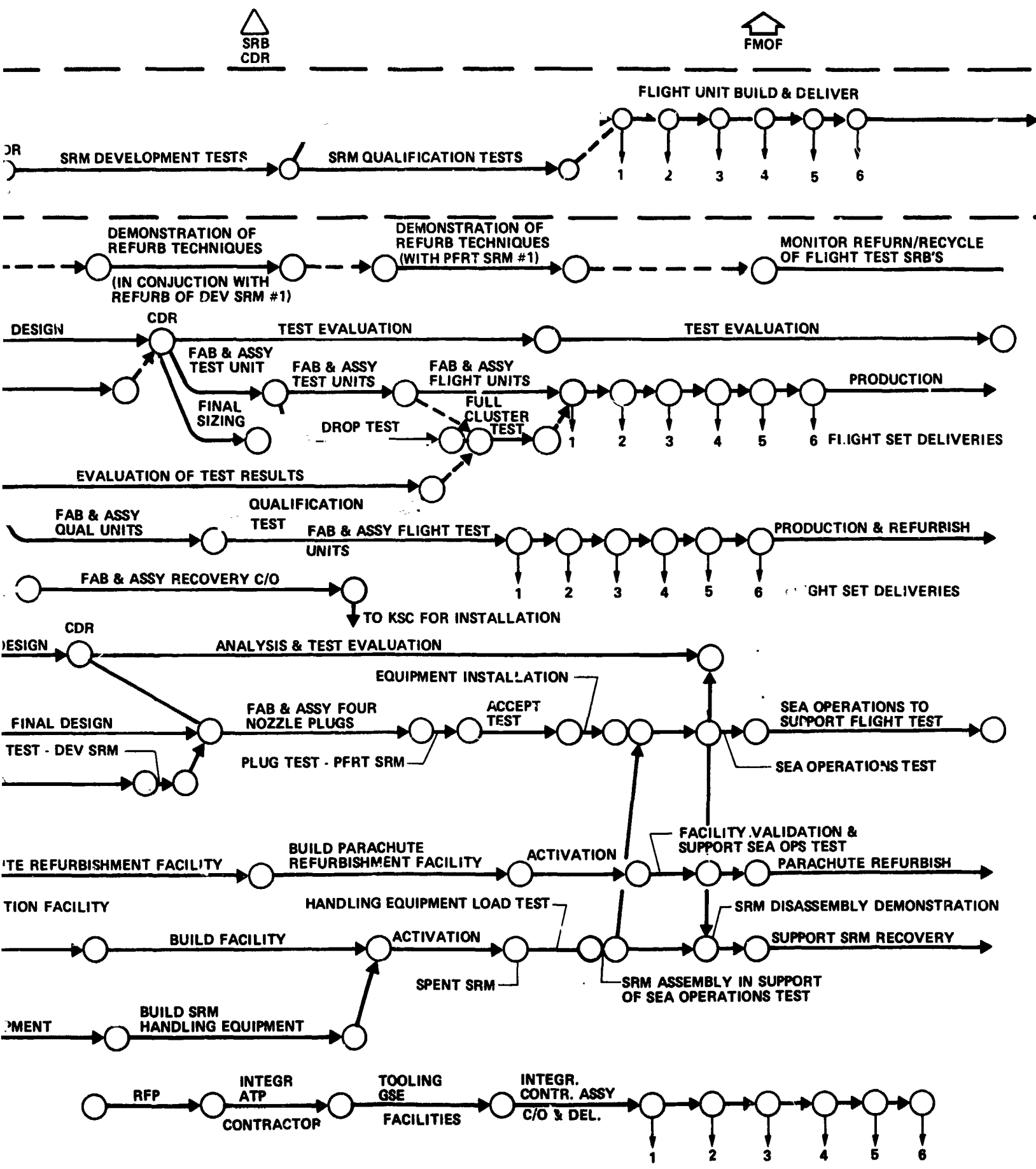


Figure 7.0-2 SRB Recovery System Logic Network

Testing at the component or piece part level will be planned at a low level of activity as many of the electrical, ordnance, and instrumentation components will be off-the-shelf and previously qualified for the intended SRB usage. Components that meet known recovery system functional and environmental requirements will be selected after careful comparison with design specifications, and after reviewing current manufacturing and supplier status information. If these components meet or exceed the required operating performance criteria, no component development tests will be required.

Development of the recovery system must be closely coordinated with development of the other SRB systems as critical interfaces exist with structures, electrical, instrumentation, separation, and SRM systems. Physical, test, and checkout interfaces must be coordinated with the SRB structures system to ensure that proper envelopes are maintained for the recovery system installation, checkout, maintenance, and operational deployment. Significant components of the SRB recovery system should be supplied to the Shuttle Ground Vibration Test at MSFC for installation on the SRB to ensure dynamic compatibility of the test configuration being tested. Tests of SRM nozzle separation, that will probably be performed at the SRM contractor's facility, should be closely scheduled with tests of the avionics subsystem to assure compatibility. Elements of the recovery system will also be supplied for test on the SRB breadboard test and the SRB vibro-acoustic test.

Wind tunnel tests of a small scale SRB are required to determine the orientation of the SRB during reentry. The test results will provide static forces and moments, dynamic forces and moments, and selected surface pressures over the reentry Mach number range for angles of attack from zero to π radians. These data will be used to determine the final SRB trim conditions and will therefore be direct inputs to the recovery system sizing. Care must be taken in the planning and conduction of these tests to maximize the accuracy of the data. The model will be of a small scale, making some of the full scale protuberances difficult to accurately model. This may result in errors in the force, moment, and separated flow data. In addition to the protuberance effect the allowable overall model size may make the duplication of the full scale Reynolds numbers impossible. It will also be necessary to analyze the sting interference, tunnel blockage, and tunnel wall interference to minimize these effects on the data that are obtained.

PRECEDING PAGE BLANK NOT FILMED

The recovery system parachutes will be tested in both wind tunnels and free-fall vertical drops. Potential sting interference and blockage effects will be evaluated. Since the wind tunnel parachute model scale will be relatively large, there should be no appreciable errors introduced into the test results because of the scaling of the model's canopy or suspension lines. However, it will be necessary to consider such factors as local Reynolds number conditions in the parachute material's pores, the porosity of the parachute, canopy pressure coefficient and the tension in the cloth. Tunnel testing can not simulate the dynamic conditions of a parachute descent, so free-fall tests will be used to correlate and augment the wind tunnel results.

A development plan has been formulated to provide a recommended test plan for the selected recovery system configuration and is shown in Figure 7.1-1. The test program proposed will generate data to support design and verification that cannot be accomplished by analysis. A limited number of development tests are planned and most of these tests are related to decelerator development and sequencing for optimum recovery conditions. A limited number of recovery component avionics tests are required, as the major need for verification will be at the system level to show interaction with other systems.

A proposed schedule for the Recovery System development is shown in Figure 7.1-2. SRB milestones have been included to indicate recovery development schedule requirements that are time-phased to support the SRB development.

Development tests must be paced to provide timely data for engineering analysis and design. Preliminary designs of the recovery system will be tested, when necessary, to confirm design concepts. Materials tests will be performed only where existing data is inadequate to verify material suitability for the intended use. Element tests of critical recovery system hardware will be performed to supply empirical data to relate to the analytical models. These tests will include structural attachments, fabrics, joints, and seams.

Drop testing of the recovery system using a 68,040 kg (150,000 lb) SRB or simulated weight is beyond present day capabilities of the test facilities. Loads of up to 22,680 kg (50,000 lb) have been dropped from aircraft and recovered at JPTF, El Centro, California. AIAA Paper No. 43-471 reports that drop tests of a platform weighing up to 18,141 kg (40,000 lb) have been completed to develop drop test techniques for parachute recovered loads up to 31,752 kg

FOLDOUT FRAME

SRB IMPACT, FLOTATION AND WIND TUNNEL TESTS

SRB IMPACT AND FLOTATION FEASIBILITY TESTS
NOL, NSRDC, LONG BEACH

SRB IMPACT & FLOTATION TESTS, FINAL SRB CONFIGURATION
NOL HYDROL TANK

WIND TUNNEL TESTS-SRB DESCENT CHARACTERISTICS
LRC 4-ft & 8-ft UNITARY

WIND TUNNEL TESTS-0.75 SCALE PILOT CHUTE
NASA/ARC 40x80 ft

PILOT CHUTE FULL TEST
PARACHUTE

PIECE PART, ELEMENT, AND MATERIALS TESTS
SUPPLIERS

WIND TUNNEL TESTS, 0.15 SCALE MAIN CHUTE
NASA/ARC 40x80 ft

MAIN CHUTE FULL TEST
PARACHUTE

PILOT AND MAIN PARACHUTE SUBSYSTEMS

RECOVERY STRUCTURE

NOSE CONE MOCKUP

SRB NOSE CAP SEPARATION TESTS
SRB STRUCTURE SUPPLIER

FORWARD SKIRT MOCKUP

SRB FRUSTUM SEPARATION TESTS
SRB STRUCTURE SUPPLIER

AVIONICS SUBSYSTEM

ELECTRICAL COMPONENT FUNCTIONAL DEVELOPMENT TEST
SUPPLIERS

COMPONENT-ENVIRONMENTAL TESTS
SUPPLIERS

CHUTE RETRIEVAL PACKAGE TESTS
AVIONICS SUPPLIER

RECOVERY SYSTEM ELECTRICAL BREADBOARD
AVIONICS SUPPLIER

GROUND SUPPORT EQUIPMENT

GSE-CHECKOUT, HANDLING, AND TRANSPORTATION DEVELOPMENT TESTS

SYSTEM TESTS (OR OTHER TESTS SUPPORTING RECOVERY SYSTEM)

SRM ENGINE NOZZLE SEPARATION TESTS

SRB AVIONICS BREADBOARD TEST

SRB/ET GVT (MASS SIMULATION)
MSFC BLDG

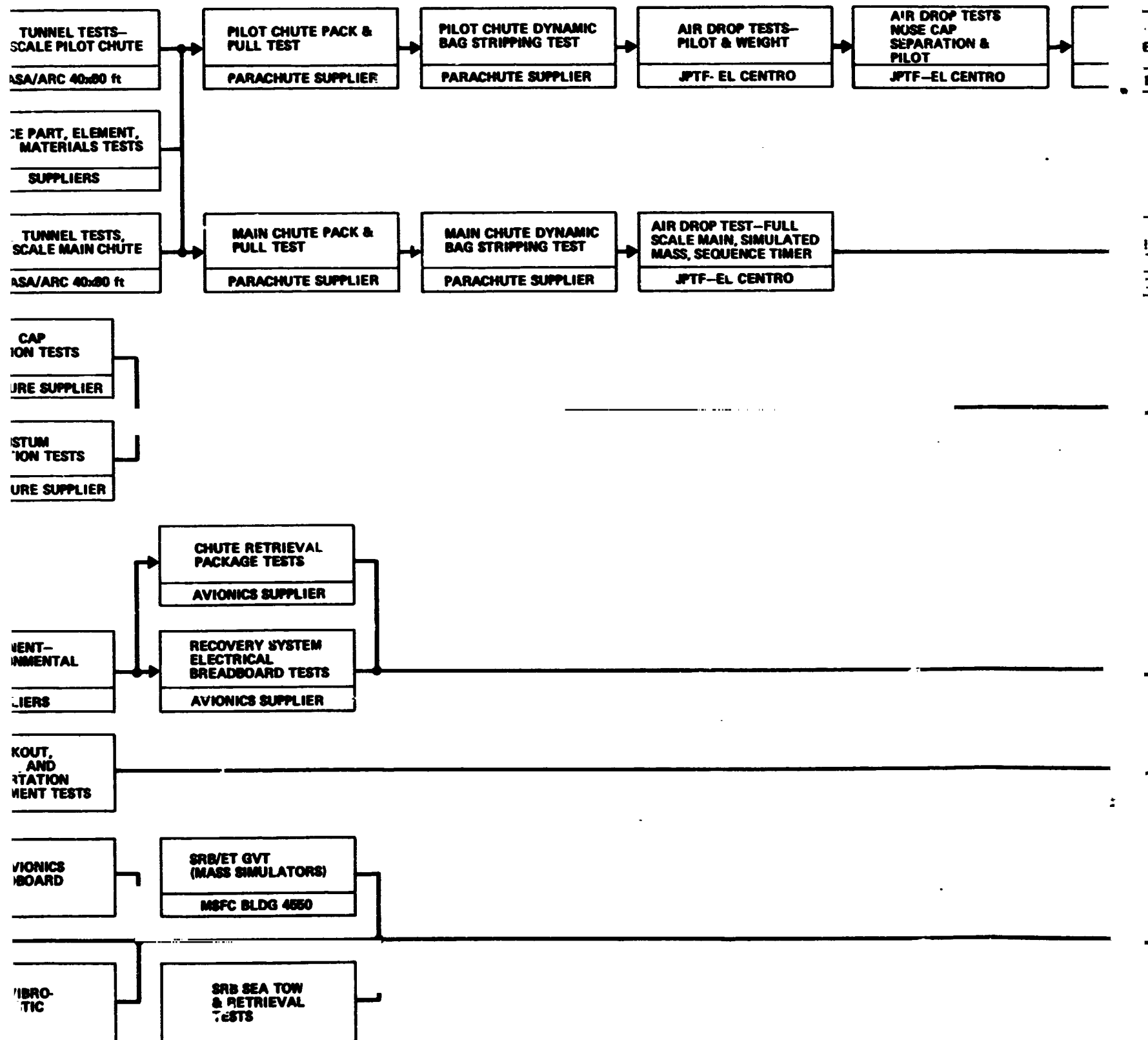
AFT UPPER & LOWER BRACE SEPARATION TESTS

SRB VIBRO-ACOUSTIC TEST

SRB SEA TO & RETRIEVAL TESTS

FOLDOUT FRAME

2



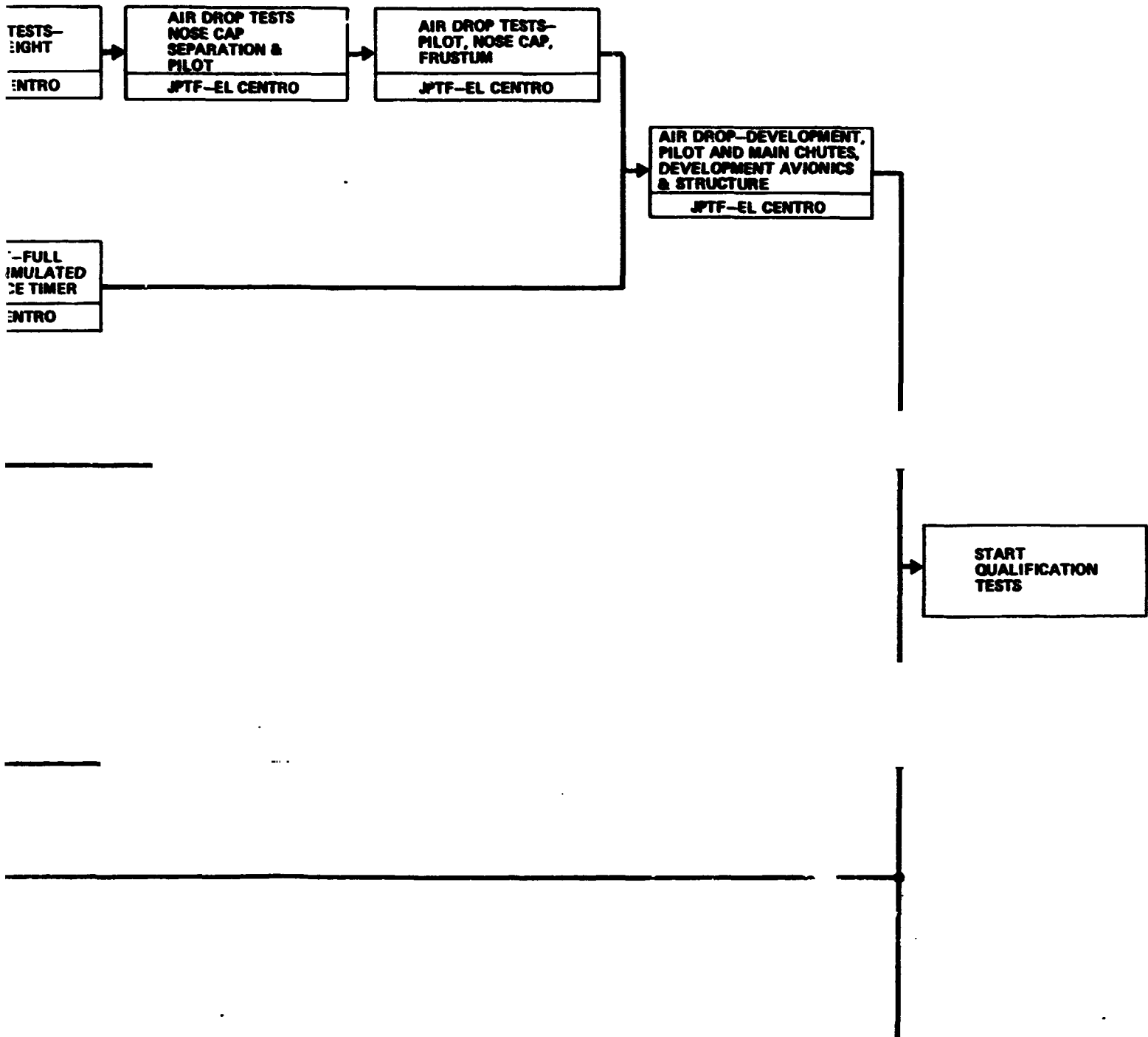
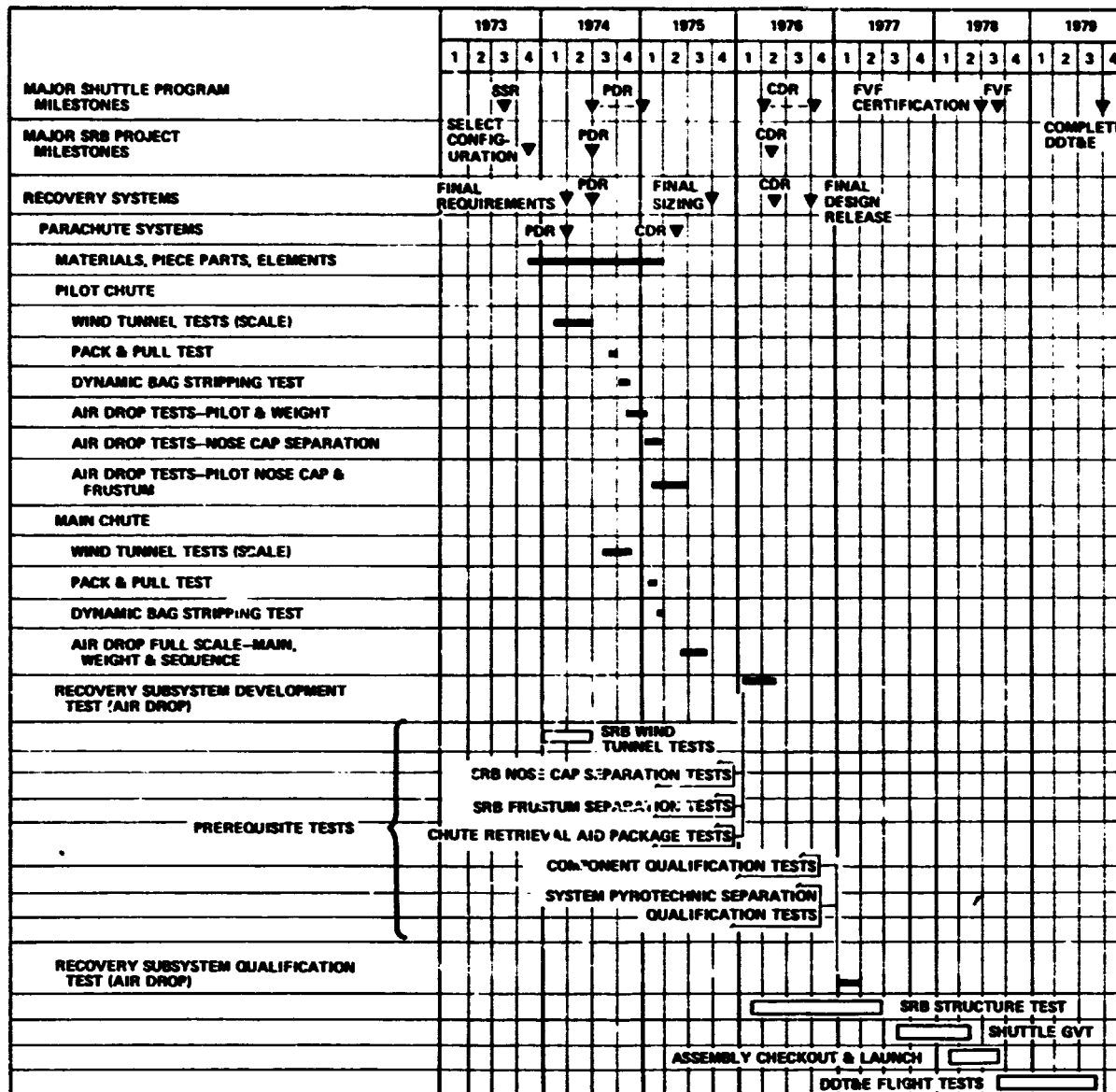


Figure 7.1-1 SRB Recovery System Development Test Summary



(70,000 lb) and possibly up to 40,824 kg (90,000 lb). These techniques use a C-5A as the drop aircraft and require use of a standard platform as the basic test bed upon which a recovery system could be mounted. The only way to test a full weight expended SRB would be to actually launch an SRB and recover it. This approach is inherently too costly, so testing must be done by use of scaled vehicles. Scaled vehicles can accomplish most of the desired test objectives of the recovery system development drop tests, but cannot test ultimate loads on the single large main parachute system. This objective must be accomplished by tests of components, scale models, and ultimately by the DDT&E flights.

The test program outlined in this report uses drop test techniques which are currently in existence at JPTF, El Centro. The program requires development of test vehicles which provide simulation of a broadside SRB descent trim to test the nose cap and frustum separation techniques adequately.

Continuing coordination with the prime test facilities is desirable so that testing of large loads with the SRB recovery system configuration may be further developed.

7.1.1 Decelerator Development

Development of the decelerator system will be characterized by analysis, material tests, wind tunnel tests of both the pilot and main parachutes, a series of bomb drop tests, and finally a system bomb drop test of the simulated frustum and decelerator. These tests, shown in Table 7.1-1, will verify the design, sequencing, and construction before commencing system qualification tests.

Criteria used for selection of test requirements and approaches was to achieve the best practical approximation of operational conditions and to comply with Space Shuttle program philosophy regarding low cost by employing maximum use of existing facilities, test hardware, and resources developed for other space programs.

Table 7.1-1 SRB Decelerator Development Test Summary

TEST CATEGORY	TEST TYPE	PURPOSE	NO. OF TESTS DURATION	TEST ITEM CONFIGURATION/ QUANTITY	FOREBODY	DATA REQUIRED	TEST FACILITY	FACILITY SUPPORT	TEST CONDITIONS
(1) MATERIAL, PIECE PART, AND ELEMENT	LABORATORY EVALUATION	DETERMINE CHARACTERISTICS FOR SINGLE AND MULTIPLE USES. VERIFY DESIGN ANALYSIS	AS REQUIRED CONTINUING	ELECTRICAL, FABRIC, STRUCTURE TEST ITEMS	NOT APPLICABLE	PERFORMANCE DATA, PHOTOS	SUPPLIERS AND LABORATORIES	MATERIALS TEST EQUIPMENT, DATA RECORDING	SIMULATE FLIGHT USAGE AND ENVIRONMENT WITH REPEATED USES
(2) PILOT CHUTE	WIND TUNNEL	OBTAIN SUBSONIC DATA ON PILOT WITH AND WITHOUT SRB. VARY CHUTE CONFIGURATION, ϕ , AND TRAILING DISTANCE	1 SERIES 100 to OCCUPANCY	0.75 PILOT MODEL	NONE	DRAG FORCE STABILITY PHOTO, OPENING LOADS DEPLOYMENT SEQUENCE	NASA/ARC 40-50 N TUNNEL	TUNNEL OPERATIONS, DATA ACQUISITION, DATA REDUCTION, PHOTO	VARY CHUTE CONFIGURATIONS AND ϕ
(3) MAIN CHUTE	WIND TUNNEL	OBTAIN SUBSONIC DATA ON MAIN CHUTE, WITH AND WITHOUT SRB. VARY CHUTE CONFIGURATION, ϕ , AND TRAILING DISTANCE	2 SERIES 100 to OCCUPANCY 100 to OCCUPANCY	0.15 MAIN MODEL	NONE	DRAG FORCE STABILITY PHOTO, OPENING LOADS DEPLOYMENT SEQUENCE	NASA/ARC 40-50 N TUNNEL	TUNNEL OPERATIONS, DATA ACQUISITION, DATA REDUCTION, PHOTO	VARY CHUTE CONFIGURATIONS AND ϕ
(4) PILOT CHUTE	AIR DROP	OBTAIN PILOT CHUTE AERO DRAG, DEPLOYMENT INFLATION CHARACTERISTICS, AND STABILITY WITH SIMULATED WEIGHT OF FRUSTUM AND NOSE CAP	4 2 MONTHS	FULL SCALE PILOT WITH BOMB	3200-lb 5000-lb	GROUND AND CHASE PHOTO, ORBOARD PHOTO, 3-AXIS ACCELEROMETER, STRAIN LINK LOADS	JTF, EL CENTRO	DROP & PHOTO AIRCRAFT, PHOTO SHAPING DATA REDUCTION, FOREBODY HANDLING, CHUTE HANDLING, TELEMETRY, RANGING AREA	JETTISON BALLAST BEFORE IMPACT, VARY MACH NUMBER AND ϕ
(5) NOSE CAP	AIR DROP	DEMONSTRATE NOSE CAP SEPARATION AND PILOT CHUTE DEPLOYMENT	4 2 MONTHS	PROTOTYPE FULL SCALE NOSE CAP, PILOT CHUTE	3200-lb 5000-lb	GROUND AND CHASE PHOTO, ORBOARD PHOTO, 3-AXIS ACCELEROMETER STRAIN LINK LOADS	JTF, EL CENTRO	SAME AS (4)	SEPARATE NOSE CAP IN BRASSIDE APPROACH: TEST TO PILOT CHUTE INFLATION
(6) PILOT CHUTE	AIR DROP	OBTAIN PILOT AND NOSE CAP PERFORMANCE BEFORE AND AFTER SEPARATION FROM SRB. OBTAIN DESCENT CHARACTERISTICS	2 2 MONTHS	FULL SCALE PILOT WITH NOSE CAP & FRUSTUM	FULL SCALE NOSE CAP & FRUSTUM	GROUND AND CHASE PHOTO, ORBOARD PHOTO, 3-AXIS ACCELEROMETER STRAIN LINK LOADS	JTF, EL CENTRO	SAME AS (4)	NOSE CONE WEIGHT, MINIMUM REQUIRED
(7) MAIN CHUTE	AIR DROP	OBTAIN STRUCTURAL DEPLOYMENT, INFLATION, STABILITY, RELIEF CHARACTERISTICS DATA ON MAIN CHUTE	5 3 MONTHS	FULL SCALE MAIN WITH WEIGHT	50,000-lb 5000-lb	GROUND AND CHASE PHOTO, ORBOARD PHOTO, 3-AXIS ACCELEROMETER STRAIN LINK LOADS	JTF, EL CENTRO	SAME AS (4)	USE GPP "PROGRAMMER" CHUTE TO INFLATE MAIN CHUTE AT PROPER ϕ , VARY MACH NUMBER AND ϕ
(8) PILOT CHUTE	PACK & PULL	DETERMINE CHUTE RELEASE PERFORMANCE AND CHARACTERISTICS	AS REQUIRED 2 WEEKS	PROTOTYPE CHUTE WITH BAG AND STRUCTURE	NONE	PHOTO, FORCE MEASUREMENT	PARACHUTE SUPPLIER	SUPPLIER PACK & PULL FACILITIES, PHOTOS, FORCE MEASUREMENT	HORIZONTAL GROUND TEST
(9) PILOT CHUTE	DYNAMIC BAG STRIPPING TEST	DETERMINE REAL TIME BAG AND CHUTE DEPLOYMENT CHARACTERISTICS AND FORCES	2 1 MONTH	PROTOTYPE CONFIGURATION CHUTE AND DEPLOYMENT BAG	NONE	VISUAL, PHOTO, STRAIN LOADS	PARACHUTE SUPPLIER	PHOTO, DATA RECORDING, DYNAMIC PULL FACILITY	SIMULATE DYNAMIC DEPLOYMENT OPERATION
(10) MAIN CHUTE	PACK & PULL	DETERMINE CHUTE RELEASE PERFORMANCE CHARACTERISTICS AND FORCES	AS REQUIRED 2 WEEKS	PROTOTYPE CHUTE WITH BAG AND STRUCTURE	NONE	PHOTO, FORCE MEASUREMENT	PARACHUTE SUPPLIER	SUPPLIER PACK & PULL FACILITIES, PHOTOS, FORCE MEASUREMENT	HORIZONTAL GROUND TEST
(11) MAIN CHUTE	DYNAMIC BAG STRIPPING TEST	DETERMINE REAL TIME BAG AND CHUTE DEPLOYMENT CHARACTERISTICS AND FORCES	2 1 MONTH	PROTOTYPE CONFIGURATION CHUTE AND DEPLOYMENT BAG	NONE	VISUAL, PHOTO, STRAIN LOADS	PARACHUTE SUPPLIER	PHOTO, DATA RECORDING, DYNAMIC PULL FACILITY	SIMULATE DYNAMIC DEPLOYMENT OPERATION
(12) NOSE CAP SEPARATION	GROUND STRUCTURAL DEVELOPMENT	OBTAIN DYNAMIC NOSE CAP TO FRUSTUM SEPARATION PERFORMANCE DATA	2 2 MONTHS	FULL SCALE NOSE CAP WITH THRUSTERS, SIDE AND AXIAL LOADS	NOT APPLICABLE	PHOTOS, ACCELERATION DATA, EVENT RECORDS	SUPPLIER STRUCTURAL TEST LAB	TEST FIXTURES, ORDNANCE HANDLING, ACCELEROMETERS	SIMULATE IMFLIGHT NOSE CAP SEPARATION WITH DYNAMIC LOADS
(13) FRUSTUM SEPARATION	GROUND STRUCTURAL DEVELOPMENT	OBTAIN DYNAMIC FRUSTUM TIP OFF AND SEPARATION DATA	2 3 MONTHS	FULL SCALE FRUSTUM AND FORWARD EQUIPMENT SECTION WITH SIDE AND AXIAL LOADS	NOT APPLICABLE	PHOTOS, ACCELERATION DATA, EVENT RECORDS	SUPPLIER STRUCTURAL TEST LAB	TEST FIXTURES, ORDNANCE HANDLING, ACCELEROMETERS	SIMULATE IMFLIGHT FRUSTUM SEPARATION, TIP OFF AND CLEARANCE FROM SRB
(14) PILOT & MAIN SYSTEM	AIR DROP	OBTAIN INITIAL SEQUENCING DEPLOYMENT AND INFLATION CHARACTERISTICS AND STABILITY DATA OF FULL SCALE PILOT AND MAIN WITH STRUCTURE	2 3 MONTHS	FULL SCALE DEVELOPMENT MAIN, PILOT, NOSE CAP, FRUSTUM, REEFING, WEIGHT, ORDNANCE, BRASSIDE APPROACH	50,000-lb TOTAL WEIGHT	GROUND, CHASE, AND ORBOARD PHOTO, 3-AXIS ACCELEROMETER, STRAIN LINK LOADS, ALTITUDE, RATE GYRO	JTF, EL CENTRO	SAME AS (4)	GROUND RECOVERY
(15) PILOT & MAIN SYSTEM	AIR DROP	OBTAIN OPERATIONAL SEQUENCING DEPLOYMENT AND INFLATION CHARACTERISTICS AND STABILITY WITH COMPLETE RECOVERY CONFIGURATION; RETRIEVAL AIDS AND FLOTATION UNITS FLIGHT DEMONSTRATION & QUALIFICATION OF SRB DECELERATOR SYSTEM AND RECOVERY	2 3 MONTHS	FULL SCALE PROTOTYPE CHUTES, FRUSTUM, NOSE CAP, ORDNANCE, BRASSIDE APPROACH	50,000-lb TOTAL WEIGHT SPECIAL EQUIPMENT SECTION	GROUND, CHASE, AND ORBOARD PHOTO, 3-AXIS ACCELEROMETER, STRAIN LINK LOADS, ALTITUDE, RATE GYRO	JTF, EL CENTRO	SAME AS (4)	WATER IMPACT: FINAL MARRIAGE TEST BEFORE LAUNCH
(16) OPERATIONAL FLIGHT TEST	DOT&E FLIGHT TEST		8 12 MONTHS	TWO COMPLETE SRB RECOVERY SYSTEMS PER LAUNCH	FLIGHT SRB	COMPLETE LAUNCH COVERAGE, CHASE PHOTO, GROUND TRACK, TRACKING AND PHOTO	KSC	RECOVERY VESSELS, REFURBISHMENT FACILITY, RANGE DATA COVERAGE, DATA REDUCTION, PHOTO	

Evaluation of the baseline design was performed to determine if the decelerator concept proposed was a fully testable concept. Several different testing techniques were considered for evaluating each design requirement. Capabilities and limitations of various test facilities were reviewed and the test plan evolved. The plan is a compromise of factors that were considered, including cost, state-of-the-art test capabilities, scaling credibility, future test capabilities, and test article design.

Three areas exist that will dictate less testing than would be desirable before the final configuration tests of the six DDT&E flights. These are:

- 1) ultimate load testing of the full scale main parachute, including reefing;
- 2) nose cap and frustum separation with a full burnout weight SRB, including separation normal to the line of descent;
- 3) full scale SRB water impact behavior and parachute release.

These difficulties all result from inability to perform testing of a full scale SRB from simulated separation to impact. These limitations can be overcome by a rigorous test program, and adequate verification can be accomplished by use of scale vehicles, bomb drops, wind tunnel tests, and proven analytical methods to allow commitment of the SRB recovery system to the DDT&E flights.

The development wind tunnel tests involving scaled parachutes at simulated Mach number and dynamic pressure are required to determine pilot and main parachute efficiency and stability. The tests will provide data on line lengths, drag, stability, loads, and overall decelerator efficiency. The forebody will be a scaled model of the SRB. Predicted and actual results will be carefully analyzed and adjustments made to the configuration before subsequent tests, if required.

Materials tests will be performed to determine physical properties of seams, joints, attachments, and effects of environments on materials. Special emphasis should be placed on cyclic effects of sea recovery and exposure to salt water. These tests will serve to identify the extent of refurbishment required on selected materials.

Parachute drop tests will be made using full scale parachute test configurations dropped from aircraft at JPTF, El Centro, California. The pilot and main parachutes will be tested individually during bomb drop tests. Test conditions will include low, nominal, and high q tests with equivalent altitude and Mach number compatible with existing test facilities. The test forebodies for the individual parachute tests will be existing equipment bombs modified for this use. Separation tests of the nose cap and pilot chute from the forward frustum must include a bomb configuration in which the nose cap is separated on a broadside approach. The full scale recovery system tests will require a new configuration bomb drop vehicle including the nose cap and frustum. Since the broadside approach of the SRB must be duplicated to provide meaningful data, this vehicle must reliably provide a broadside approach at the proper q. General objectives of the drop test program to be attained in progressive steps are:

- 1) Demonstrate the deployment system and sequence. Dynamically stress the parachute system canopies, suspension lines and fittings and provide data on deployment dynamics of each parachute.
- 2) Verify deployment to line stretch.
- 3) Verify initial inflation and full inflation, including reefing.
- 4) Demonstrate stabilization of the system and steady state performance.
- 5) Demonstrate functional performance of the entire deceleration system before qualification tests.

The drop tests are required to substantiate specific design features of the baseline system. Two significant design features of the baseline system that require substantiation are pilot parachute ejection normal to the relative velocity, and large main parachute inflation under SRB loads.

The pilot parachute full scale deployment tests will demonstrate the baseline concept of ejecting the pilot parachute contained in the SRB nose cap normal to the relative velocity. These test data will be used to evaluate:

- 1) suspension line "fish hooking" effects during bag stripping;
- 2) SRB wake interference;
- 3) nonsymmetric canopy filling caused by a relatively high angle of attack.

The main parachute size and weight approach the state of the art for parachute design. Large parachutes present a design problem in assuring uniform, complete, and stable inflation. The following test data will be needed for inflation verification:

- 1) inflation rates for initial and disreef openings;
- 2) initial and disreef opening loads;
- 3) canopy porosity sufficient to prevent squidding under SRB deployment loads and velocities.

The pilot parachute may be full scale drop tested at nearly actual deployment conditions. The main parachute drop tests encounter limitations that evolve from inability to air drop a payload the size and weight of the SRB. The SRB weight is 68,040 kg (150,000 lb) and the maximum feasible payload weight that may be air dropped is approximately 22,680 kg (50,000 lb).

The weight scaling of the main parachute payload affects the dynamic pressure gradient during both initial and disreef inflations. The dynamic pressure predicted for .3 recovery drops during initial reefed inflation from 6,500 to 4,300 N/m² (135 to 90 lb/ft²) and then during disreef from 3,840 to 1,440 N/m² (80 to 30 lb/ft²) (Figure 2.1-14). If the drop test deployment is initiated at a dynamic pressure of 6,500 N/m² (135 lb/ft²) with a scaled 22,680 kg (50,000-lb) payload, the system will decelerate significantly below the 4,300 N/m² (90 lb/ft²) opening load dynamic pressure. Otherwise, if the drop test deployment is designed to achieve the 4,300 N/m² (90 lb/ft²) full open (reefed) dynamic pressure and match the opening loads, the initial velocity will be greater causing a faster filling. This situation becomes even more pronounced for disreefing tests.

It is recommended that the needed inflation verification data be obtained by designing the main parachute drop tests to match opening loads, and differential pressure and strain measurements be made on the canopy. These measurements will be used to analytically predict the filling times. Drop tests matching opening loads may be made with varying degrees of reefing (minimal reefed area to unreefed deployment) to evaluate the disreefing performance.

Functional parachute development tests will be performed at the parachute suppliers facility (or other suitable location) as part of the routine development of parachutes, and will include pack and pull tests and dynamic bag stripping tests.

Ground tests that will complement the parachute tests are the nose cap separation tests and nose frustum separation tests, which must be completed before the final systems air drop tests are performed. These tests must demonstrate satisfactory separation of the nose cap from the nose frustum and the frustum from the SRB forward skirt under simulated SRB descent conditions, which will include axial and side loads, and roll.

Test results will be used to update the preliminary design data, verify analysis, and support any system modifications that are required during the test phases.

7.1.2 Avionics Systems

Development testing of the recovery avionics will be required only where necessary to ensure that component design will meet the required environments and functional requirements. Most of the electrical and instrumentation components selected for the baseline recovery system will be items that are currently in use on space program applications. Other items of equipment may have to be modified to be adapted to recovery requirements, and this hardware will be subjected to development tests at the component level. These tests will verify analysis and prove design or manufacturing concepts before being incorporated in qualification tests on production hardware.

The component test program will include development tests at full qualification levels, including extended stress or off-limits tests. Since most of the hardware will be of mature design, these tests will be limited.

Trade studies will be completed to arrive at optimum approaches to implementing the avionics requirements, such as whether to qualify electrical equipment to higher vibration or acoustic levels, or to provide shockmounting to reduce the environmental levels.

After the required component development tests are complete, electrical systems breadboard (or mockup) of the recovery systems hardware will be set up to verify systems compatibility. This test will evaluate parametric voltage performance, transients, EMC, redundant circuitry, operating performance, and sequencing. This test will provide a basis for confidence in completion of a successful qualification program.

Areas that will receive special attention during avionics development tests are ordnance circuitry, SRB to recovery system electrical and instrumentation interfaces, ground checkout methods, and checkout of redundant circuitry. Results of this development testing will provide requirements for design of electrical ground support equipment.

The testing will progress from lower level piece part and component tests to use of the avionics system on the low altitude bomb drop tests of the full systems configuration. These tests will verify the system represented by simulated or partial configurations before the qualification bomb drop tests in which the entire avionics system will be proven.

A portion of the development tests will be devoted to determining reuse capabilities and refurbish requirements to support the program recovery concepts and low cost requirements.

7.1.3 Interface Tests

Development of the recovery system must be closely coordinated with development of the SRB systems as physical and electrical interfaces exist with the structure, electrical, instrumentation, SRM, and separation systems. Beginning with systems development tests of the SRB, the prototype recovery system components should be integrated with the SRB for static and dynamic testing, functional tests of the active systems, and maintenance, accessibility and refurbishment demonstrations. The parachute packages in the nose cap and nose frustum must be carefully integrated for space allocation and proper operation during the recovery sequence. The instrumentation and electrical interfaces must be proven compatible during the checkout activities, although these interfaces will not be active during the ascent phase until SRB/ET separation.

Emphasis should be placed on thorough testing of both electrical and mechanical interfaces of the SRB and recovery system at various phases of development. Sufficient testing should be performed on the initial assembled flight hardware to assure that the prime and redundant systems of the recovery system are compatible with other systems of the SRB. Interface separation testing of the nose cap to frustum and frustum to forward skirt interfaces should receive special attention.

Recovery system simulators will be furnished to the SRB forward skirt, frustum, and nose cone contractors for their development and interface verification. Up to four sets of recovery system mass simulated hardware should be furnished for the SRB dynamic GVT at MSFC. Complete interface and envelope information must be exchanged early in the program to enable finalization of structure and recovery system design.

To verify retrieval and recovery interfaces, the recovery system contractor should actively participate in the SRB sea recovery and towing tests that will be conducted before the first manned orbital flight.

7.2 QUALIFICATION TEST PLAN

Qualification of the SRB recovery system--that part of the verification of design and construction that will be performed on flight hardware--will result in certification of the recovery system hardware for operational use.

To provide the greatest economy, test will be used only when analysis is not feasible, and, in some cases, selected tests will be run to support required analysis. These tests will be performed after finalization of a preferred recovery system configuration and the feasibility and development tests are complete. Qualification tests will not be performed on alternative configurations; qualification will be performed initially on piece parts and components.

System level tests will be used whenever feasible. Final qualification drop tests on the flight type hardware will be performed at JPTF, El Centro, California before the Space Shuttle launches. Final qualification and certification for operational use of the SRB recovery system will be accomplished during the six DDT&E launches from KSC.

Qualification of the SRB recovery system will be limited to thorough tests of components and assemblies of components, but will stop short of full scale flight tests of the booster. Confidence in reliable full system operation will be gained during the verification program, which precedes the DDT&E Space Shuttle launches.

Hardware used for qualification testing will be of flight configuration and must be subjected to flight acceptance tests before and after qualification tests. Qualification test levels (environmental and functional) must be sufficiently higher or longer in duration than acceptance test and flight levels to provide confidence that the flight equipment will perform within specification after exposure to repeated acceptance testing and flight mission environments.

7.2.1 Component Qualification

Environmental qualification tests will verify that flight type hardware meets performance and design requirements under anticipated operating environments plus margin as defined in applicable specifications.

Components and assemblies should be qualified at the highest assembly level identified as a remove and replace item from the flight vehicle. All new designs must be qualified by test. Existing designs may be qualified by test data, together with detailed analysis of any design modifications or changes in manufacturing techniques.

Some of the recovery system hardware will be used for one flight only; however, the majority of equipment and structure will be reusable. Reusable hardware used for the Space Shuttle recovery system has a relatively difficult to analyze requirement for repeated cycles of acceptance, checkout, operational use, recovery, and refurbishment. Therefore, the requirement for cycle life qualification is an important consideration in setting up the test program. For example, some components that are currently in use on space applications may be selected for the SRB recovery system and may be qualified for the anticipated SRB environments for one use, but have not been proven for repeated use and refurbishment. A partial qualification will be required for these components.

Table 7.2-1 shows the major components of the recovery system and indicates the natural and induced environments that are applicable for the usage. Most of the recovery system components will be located within the nose cone and forward skirt forward of the SRB propellant segments. The recovery system environmental requirements will be determined by requirements in this area. This report has not selected specific components by part numbers; therefore complete qualification test requirements for individual components cannot be determined at this time. Hardware, when selected, will be reviewed to determine if requalification is required as a result of any changes, or a more severe environment or operating condition exists than that for which the hardware was originally qualified.

Table 7.2-1 SRB Recovery Component Qualification Test Requirements

COMPONENT	FUNCTIONAL	PROOF PRESS	BURST PRESS	SEAL	STATIC LOAD	SELECTED NATURAL ENVIRONMENTS	ACCELERATION	ACOUSTIC	RANDOM/SINE VIBRATION	TEMPERATURE	SHOCK	EMC	EXPLOSIVE ATMOSPHERE	OPER. LIFE	MARGIN
SRB RECOVERY AVIONICS															
TIMER	X			X		X	X		X	X	X	X		X	
BAROMETRIC SWITCH	X			X		X	X		X	X	X	X		X	
IMPACT SWITCH	X			X		X	X		X	X	X	X		X	
SQUIB FIRING CIRCUIT	X			X		X			X	X	X	X		X	
CURRENT LIMITING RESISTOR	X			X		X			X	X	X	X		X	
ORDNANCE CHECKOUT CIRCUIT	X			X		X			X	X	X	X		X	
FLASHING LIGHT	X			X		X			X	X	X	X		X	
RECOVERY BEACON	X			X		X			X	X	X	X		X	
BEACON ANTENNA	X			X		X			X	X	X	X		X	
CONNECTORS	X			X		X			X	X				X	
CABLING	X			X		X				X					
SRB RECOVERY ORDNANCE															
SRB NOZZLE SHAPED CHARGE	X							X	X	X		X			
NOSE CAP THRUSTERS	X	X		X	X	X			X	X	X	X			X
AFT UPPER BRACE EXPLOSIVE BOLTS	X	X			X	X			X	X		X			X
AFT LOWER BRACE EXPLOSIVE BOLTS	X	X			X	X			X	X		X			X
FORWARD FRUSTUM EXPLOSIVE NUTS	X	X			X	X			X	X	X	X			X
MAIN CHUTE RELEASE EXPLOSIVE NUTS	X	X	X		X	X			X	X	X	X			X
PARACHUTE RETRACTION PACKAGE															
FLOTATION SPHERE				X		X								X	X
PRESSURE BOTTLE		X	X	X		X								X	X
PRESSURE RELEASE VALVE (PYRO)	X	X	X			X				X	X	X		X	X
PRESSURE SWITCH	X			X		X			X	X	X	X		X	X
EQUIPMENT BATTERY	X			X		X			X	X	X	X		X	X
SALT WATER SWITCH	X			X		X			X	X	X	X		X	X
RECOVERY BEACON	X			X		X			X	X	X	X		X	X
BEACON ANTENNA	X			X		X			X	X		X		X	X
FLASHING LIGHT	X			X		X			X	X	X	X		X	X
SONAR TRANSMITTER	X			X		X			X	X	X	X		X	X
DYE MARKER	X			X		X			X					X	
BEACON ANTENNA EXPLOSIVE BOLTS	X			X		X			X	X	X	X			X
CONNECTORS	X			X		X			X	X				X	
CABLING	X			X		X				X					
PILOT CHUTE INSTALLATION															
PILOT PARACHUTE ASSEMBLY	X				X	X	X		X					X	X
BRIDLE & RISER					X	X								X	X
RETAINER BAG					X	X								X	
FORWARD FRUSTUM ATTACH FITTING					X	X			X					X	X
RETAINER BAG ATTACH FITTING					X	X			X					X	X
PILOT CHUTE ATTACH FITTING					X	X			X					X	X
MAIN CHUTE INSTALLATION															
MAIN PARACHUTE ASSEMBLY	X				X	X	X		X					X	X
RETAINER BAG					X	X								X	
RETAINER BAG ATTACH FITTINGS	X				X	X			X					X	
REEFING CLIPPERS	X	X	X	X					X	X	X	X		X	X
ATTACH & DISCONNECT FITTING					X	X			X					X	X
SWIVEL FITTING	X				X	X			X	X				X	X

A minimum of one flight-type component will be subjected to all qualification tests after completion of factory acceptance tests. The tests will be accomplished in the sequence that parallels the mission exposure sequence.

7.2.2 System Qualification

Qualification tests that are best accomplished at the system level are shown in Figure 7.2-1. These tests will use flight-type hardware that has been factory acceptance tested. Satisfactory completion of these proposed tests will, with the component qualification tests, enable testing of the complete flight systems during the DDT&E flights. These tests are briefly described.

7.2.2.1 Recovery/SRB Interface Verification Tests

These tests will verify that the SRB recovery system interface with the other SRB and Orbiter systems are compatible. Simulators will be used to check interfaces. These tests will also serve to provide verification of the electrical and instrumentation cabling, which will not receive component qualification testing. Structural interfaces will be checked using master gages and tooling, and by actual fit checks of interfacing hardware.

7.2.2.2 System Pyrotechnic Separation Tests

A complete nose cap, frustum and forward equipment skirt will be tested to demonstrate capability of the systems to survive the pyro-shock environments created by the various active ordnance devices in the recovery system. Physical separation of the mating interfaces and clearances will be verified. Special test instrumentation such as triaxial accelerometers will be required.

7.2.2.3 Air Drop - Production Recovery System

A full production recovery system will be installed in sufficient production supporting structure to adequately test the entire recovery sequence at JPTF, El Centro, California. The weight of the test bomb will be 22,680 kg (50,000 lb) or the maximum feasible at the time of the test. The configuration will include batteries, ordnance, pilot and main parachutes, timers, cabling, swivel and flight type separation interfaces. The entire SRB recovery descent sequence will be simulated within the limits allowed by the test setup and will end with retrieval from the Salton Sea. This test series will provide valuable information on actual recovery system performance before the manned launches. Additional contributions to refurbishment capabilities and requirements will be obtained on the parachutes and components.

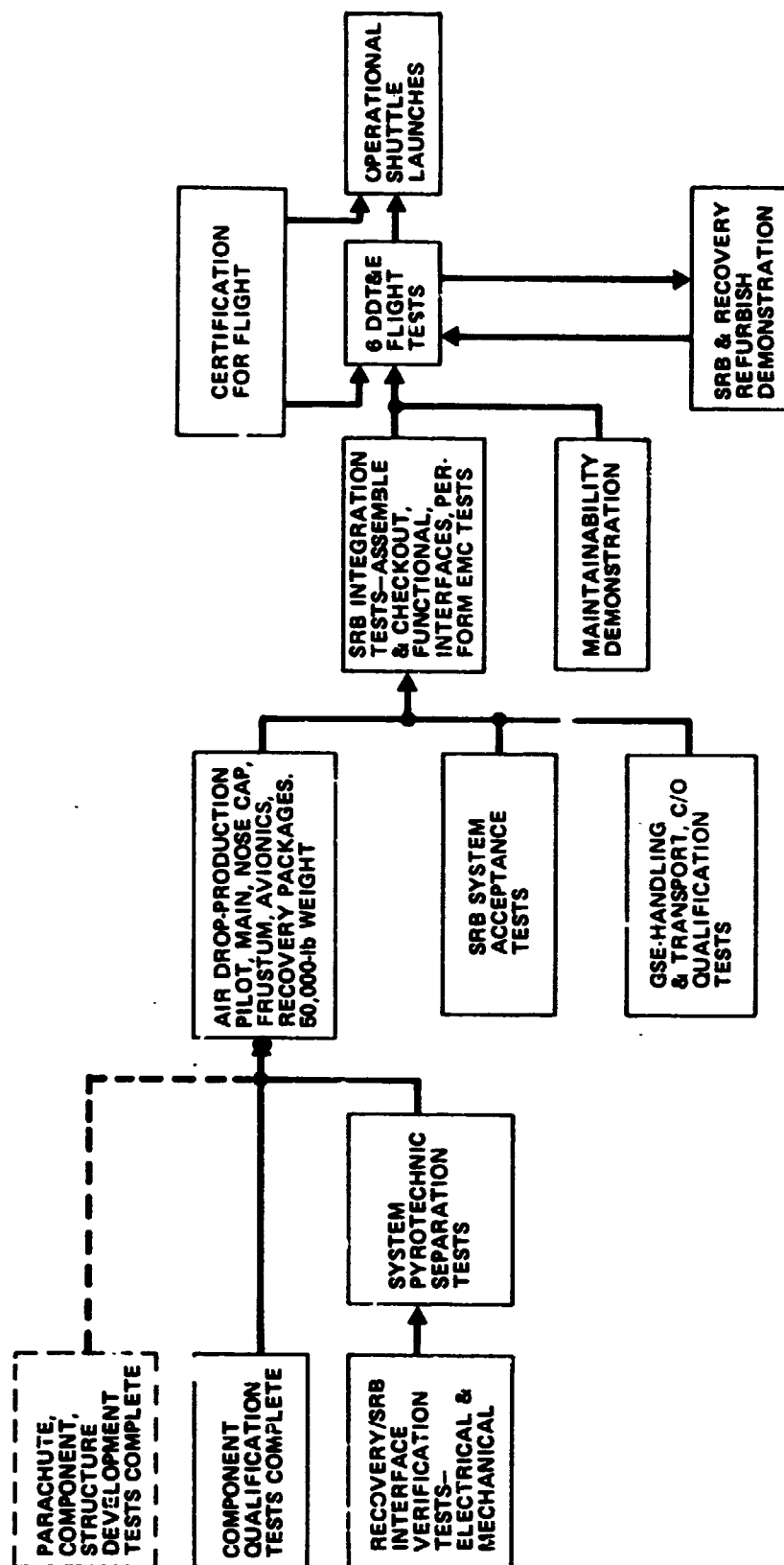


Figure 7.2-1 SRB Recovery Qualification Summary

7.2.3 Maintainability Demonstration

Maintainability of the recovery system after installation in the forward skirt, frustum, and nose cap will be demonstrated at the SRB assembly facility at KSC. Compliance with maintainability and serviceability design criteria will be demonstrated on one of the first flight SRBs, and recommendations for modifications will be made when required. The maintainability demonstration should be made using flight-type hardware, using provisioned ground handling equipment when required. The maintenance demonstration must support the program milestones for final qualification, and provide timely resolution of all factors adverse to achievement of launch-on-time and low cost program goals.

Several features to be evaluated are handling capability, easy accessibility to components and cables, installation and removal of large volume and weight components, easy access for installation and removal of ordnance and pressurized components, and access for postinstallation checkout. All maintenance will probably be performed with the SRB major assemblies in the vertical position, both in the SRB Final Assembly Facility and in the VAB. Time events for performing maintenance will be monitored to ensure that turnaround times for refurbishment and launch can be met.

The maintenance demonstrations will be performed using procedures that have been developed during the development phase and continually refined as the design changes or new techniques are implemented. Early definition of operational GSE capabilities is required to ensure that the maintainability baseline is realistic, maintainability inputs to trade studies are complete, and test plans and test procedures are accurate.

The test procedures and GSE will be validated during the demonstration test activity for subsequent use at any repair area using specified GSE in comparable facilities.

7.2.4 DDT&E Flight Test

The final verification of the SRB recovery system before the operational flight phase will be accomplished by recovery of the 12 SRBs used on the six DDT&E flights from KSC. These flights will use both new and refurbished recovery systems.

At least three sets of the SRBs will be new manufacture and up to three will be refurbished. Special ground and seaborne instrumentation and photo coverage will be required to gather performance data for the SRB recovery sequences. Optical coverage of the SRB descent attitude and parachute deployment of both pilot and main will be very desirable. Extensive evaluation of the recovered SRB systems will be performed to determine performance of the systems and to evaluate hardware capability for reuse. Components such as timers and switches must be disassembled, inspected and retested after initial recoveries to adequately establish suitability for reuse. After reliability and confidence is established in the reusability and survivability of the hardware, these tests can be reduced or eliminated except for retest. Trend data should be recorded on the component performance to establish presence of gradual parametric degradation and to gather statistical data on expected component lifetimes.

Major recovery systems objectives of the six flights are:

- 1) verification of recovery system and SRB compatibility in the checkout, launch, and recovery environments;
- 2) demonstration of nose cap and frustum mechanical separation;
- 3) demonstration of parachute performance and capability of attaining an SRB water impact within specified conditions;
- 4) qualification of the recovery system for operational use by demonstrations in actual use;
- 5) verification of retrieval systems operations;
- 6) demonstration of refurbishing capability and operational use of refurbished SRB recovery components;

Unless flight testing reveals the necessity to modify the parachutes, equipment, or time sequence of recovery, all six flights from the SRB recovery system standpoint will be nearly identical. A great deal of confidence will be gained concerning the operational suitability, recovery, and refurbishment of the recovery system after successful completion of the six DDT&E flights, and the system will be certified for operational use.

7.3 MANUFACTURING PLAN

SRB recovery system elements will be manufactured using a plan that encompasses simplified tooling, state-of-the-art processes, maximum usage of existing facilities, and proven manufacturing techniques to provide lowest program cost. This manufacturing plan is described in this section.

The SRB recovery system manufacture will involve fabrication of sheet metal structure, parachutes, electronic timers, beacons, cables, lights, batteries, ordnance, and similar items. It will also include major repair and refurbishment of these elements. Insofar as possible the goal will be to use existing facilities, existing equipment, existing processes, proven techniques, and a minimum of special tooling.

The most cost-effective and producible design can be attained by coordinated efforts by Manufacturing and Engineering to identify the process and techniques that will result in high quality, minimum cost hardware. Design reviews are to be held periodically to interchange manufacturing and design know-how and plans. Manufacturing, Quality, and Tooling will review plans, designs, and schedules, analyze alternative approaches, and make recommendations to reduce cost, schedule, and technical risk.

Structural parts and subassemblies will be fabricated at a facility familiar with design and fabricating of this type of hardware. The same philosophy holds true for the avionics and parachutes. The ordnance will be supplied by an ordnance manufacturer. In production, testing will be accomplished at each stage of manufacture and each hardware assembly will be acceptance tested using simulators, gages, and interface dimensional verifications before delivery to final assembly site. The test plan will be designed to provide environmental tests, with each subsequent test building on the results of the past, for positive assurance of acceptable workmanship.

Figures 7.3-1 and 7.3-2 show the general manufacture of the major SRB recovery system elements and system final assembly and check-out, launch, recovery, disassembly, refurbishment, and repair. The typical flow is described in the following paragraph.

The structural, avionics, parachutes, and ordnance elements will be received at the final assembly area. Ordnance will be routed to an ordnance storage area. The remaining hardware will be assembled into a SRB recovery system and a system test and check-out performed. This system will then be moved to SRB assembly facility and mated with the solid rocket booster. The ordnance may either be installed at this time or just before mating. A final complete system test will be run with the ordnance installed.

Following the recovery of the solid rocket booster and the recovery system, the components of the recovery system will be received at the recovery/refurbishment facility. The parachutes, nose cone, and forward frustum will be brought in from the recovery ship while the forward skirt, swivel, avionics, cabling, and the components attached to the SRB will be received from the SRB disassembly area.

The recovery system will be disassembled and the parachutes washed and dried to an acceptable salt level. The parachutes, after drying, will be examined and, if repairable, will be routed to the parachute refurbishment facility where the chutes will be repaired, then reassembled, tested, and packed by the same methods used in the manufacture, assembly, test, and packing of a new chute. The refurbished parachutes then return to the same assembly flow as a new chute. The avionics will be disassembled to black-box level, and if a sealed assembly, a complete functional test run after the exterior has undergone a complete cleaning. If repair of this assembly is required, it will be routed to the manufacturing facility where it will be disassembled and repaired under the same conditions and tests given the original assembly.

The structural subassemblies will be cleaned disassembled, and inspected. This inspection will include dimensioned inspection, visual and, if required, x-ray and magnetic particle inspection. If only minor repair and refinishing is required, this could be accomplished at the refurbishment facility; any major repair will be accomplished at the manufacturing facility. The swivel will require complete disassembly to remove all salt water contamination, cleaning, lubrication, and reassembly. This will probably be accomplished at the refurbishment facility.

All the handling and test equipment, etc used at the refurbishment facility will be ground support equipment, most of which will be designed and fabricated for its specialized function. However, whenever that commercial equipment will accomplish the function, it will be specified and used.

REPRODUCIBILITY OF THE ORIGINAL PAGE IS POOR

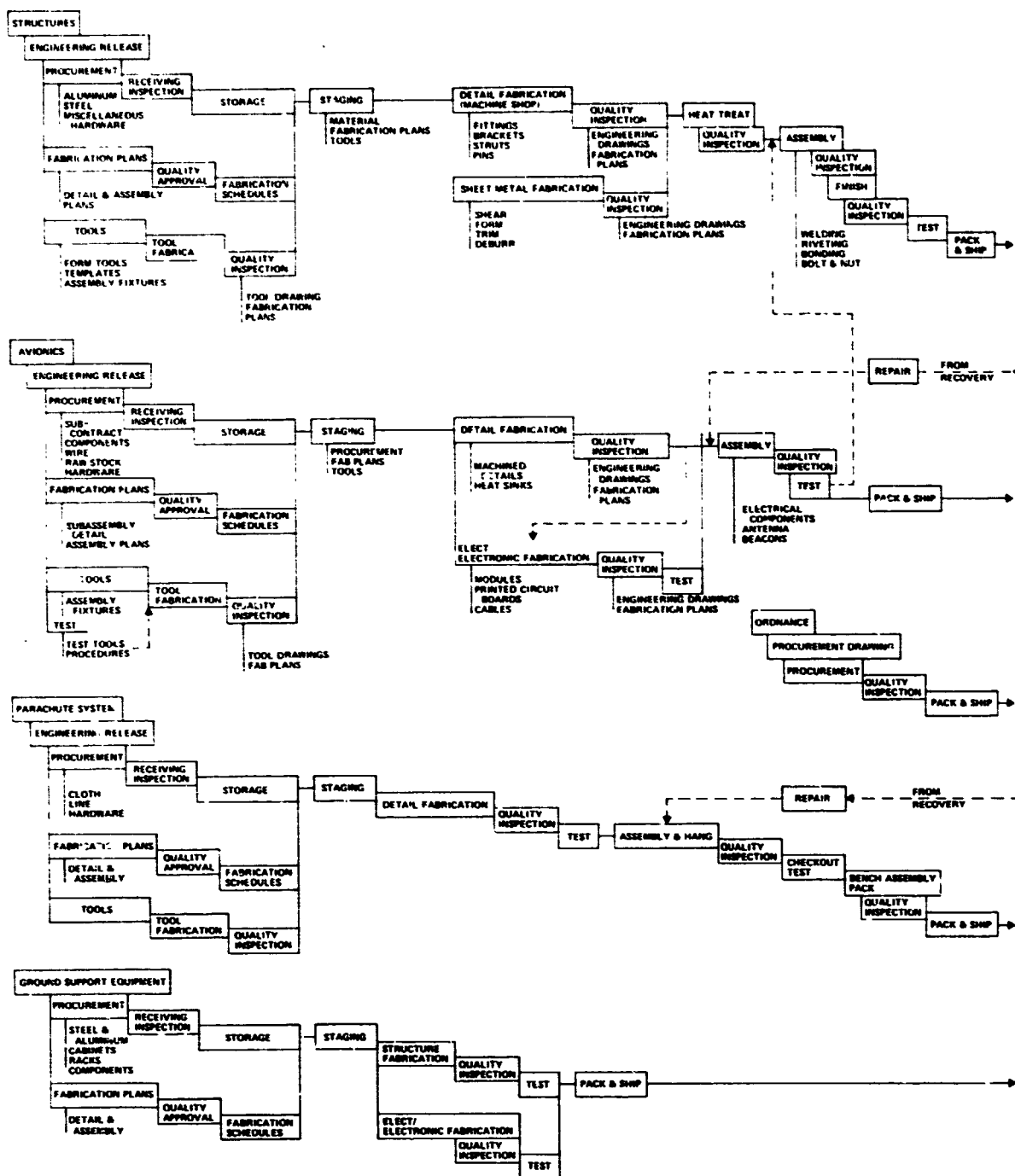


Figure 7.3-1 Manufacturing Flow - Factory

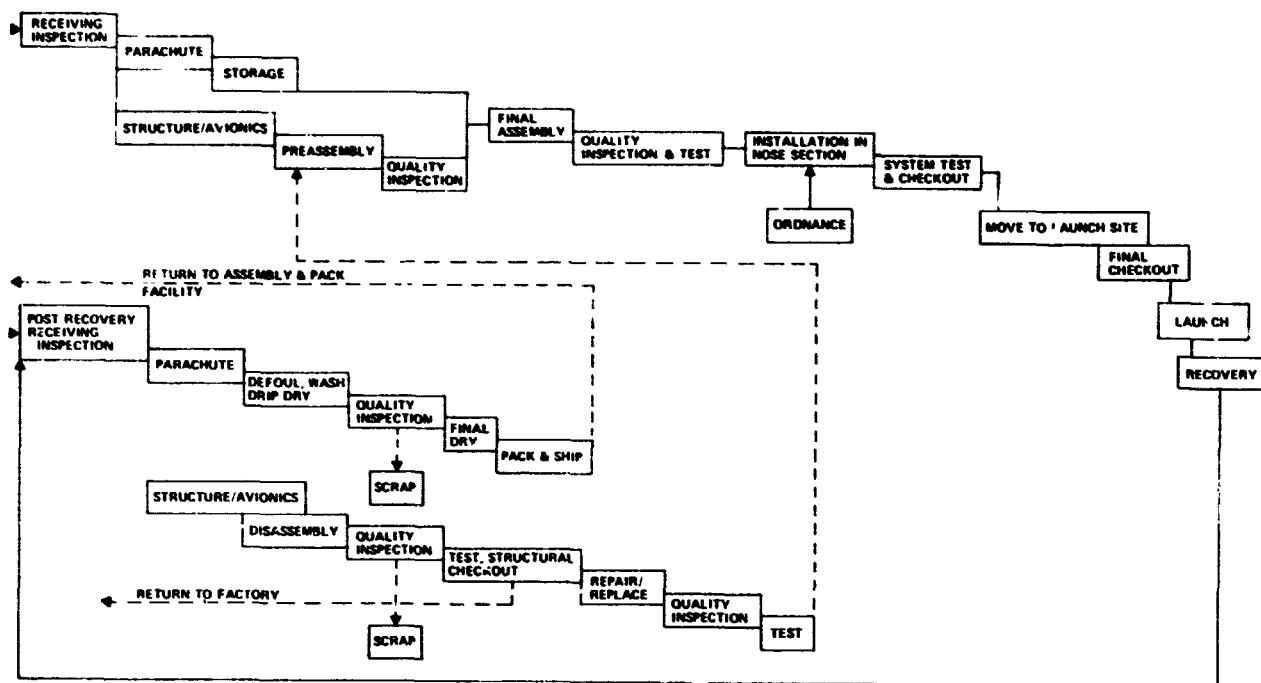


Figure 7.3-2 Manufacturing Flow - Launch and Refurbishment

In general, as can be seen from the flow charts in Figure 7.3-1, the refurbishment/repair will be accomplished by the manufacturer with the exception of those units requiring only cleaning, testing, and refinishing. To maintain uniformity between new and refurbished hardware, it would be desirable to use the same facility for repair, assembly, testing, and packing of the refurbished chutes, and the assembly, testing, and packing, of new chutes. Thus, after repair and acceptance, all recycled elements of the recovery system flow into the normal production/assembly cycle and go through the same acceptance tests, assembly, and system checkout as new hardware.

7.3.1 Fabrication

Structural parts will be of two main types: (1) sheet metal test assemblies such as the nose cone, frustum, and forward skirt, and (2) machined parts such as the swivel, and component housings. These will be fabricated in a facility equipped for mechanical fabrication and assembly. At assembly, laying surfaces and fasteners will receive a sealant to prevent corrosion and after assembly the entire assembly will receive corrosion protection.

Tooling Approach - Production tooling for SRB recovery system elements will generally be "hard" tooling due to the large number of units to be fabricated, product complexity, and materials. Tooling will be as simple as possible and innovations will be incorporated that will reduce production costs through more efficient fabrication techniques. Development tooling will be designed for minimal conversion for production use. Interchangeable interfaces will be controlled by numerical control, gages, and positional tolerance where considered cost effective. Tooling multiples will be held to a minimum for startup and introduced as program requirements dictate. Handling equipment will provide for in-process handling. Test tooling for interface and integration elements will generally be hard tooling for reasons of quantity. "Soft" test tooling, i.e., commercial equipment with tool adapters, will be used to test items of limited quantity, complexity, and program or mission impact.

7.4 OPERATIONS PLAN

Final assembly and checkout of the SRB recovery system will be accomplished at a central integration facility. The recovery system will be checked out and tested at both the module segment and assembled SRB level before mating to the external tank (ET). The system will again be verified on the launch pad before launch. After recovery, the SRB recovery system will be disassembled and refurbished for the next usage.

7.4.1 Assembly and Checkout

The structure, avionics, parachute system, and ordnance will be received from the manufacturing or refurbishment site in the SRB Assembly and Checkout Facility. These subsystems will have undergone acceptance testing before shipment to the launch site. The nose cap, parachute system, forward and aft frustum, forward skirt, and recovery avionics, along with the remainder of the SRB system, will be installed or assembled into the various segments of the SRB. Ordnance will not be installed at this time. System functional checks will be performed on the segments as shown in Figure 7.4-1.

The built up SRB segments will then be moved to the VAB Integration Cell for vertical stacking and final assembly of the SRB. At this point, final installations, alignment, leak checks, electrical checkout and power-on tests will be performed. After interface verification, the ET is mated to the SRB and aligned. The Orbiter is then mated and after power-on interface tests and ordnance installation, the total assembly is ready to be transported to the launch pad (Fig. 7.4-2).

7.4.2 Launch

As can be seen in Figure 7.4-2, launch operations at the launch pad for the SRB recovery system are minimal. Electrical checks of the recovery system will be performed during the final launch readiness verification. A final power check will be made during the countdown.

7.4.3 Refurbish and Repair

After water retrieval and return to the launch site by ship, the recovered SRB will be transported with the parachute assembly to the Disassembly Area. At this Facility the SRB will be disassembled as shown in Figure 7.4-3.

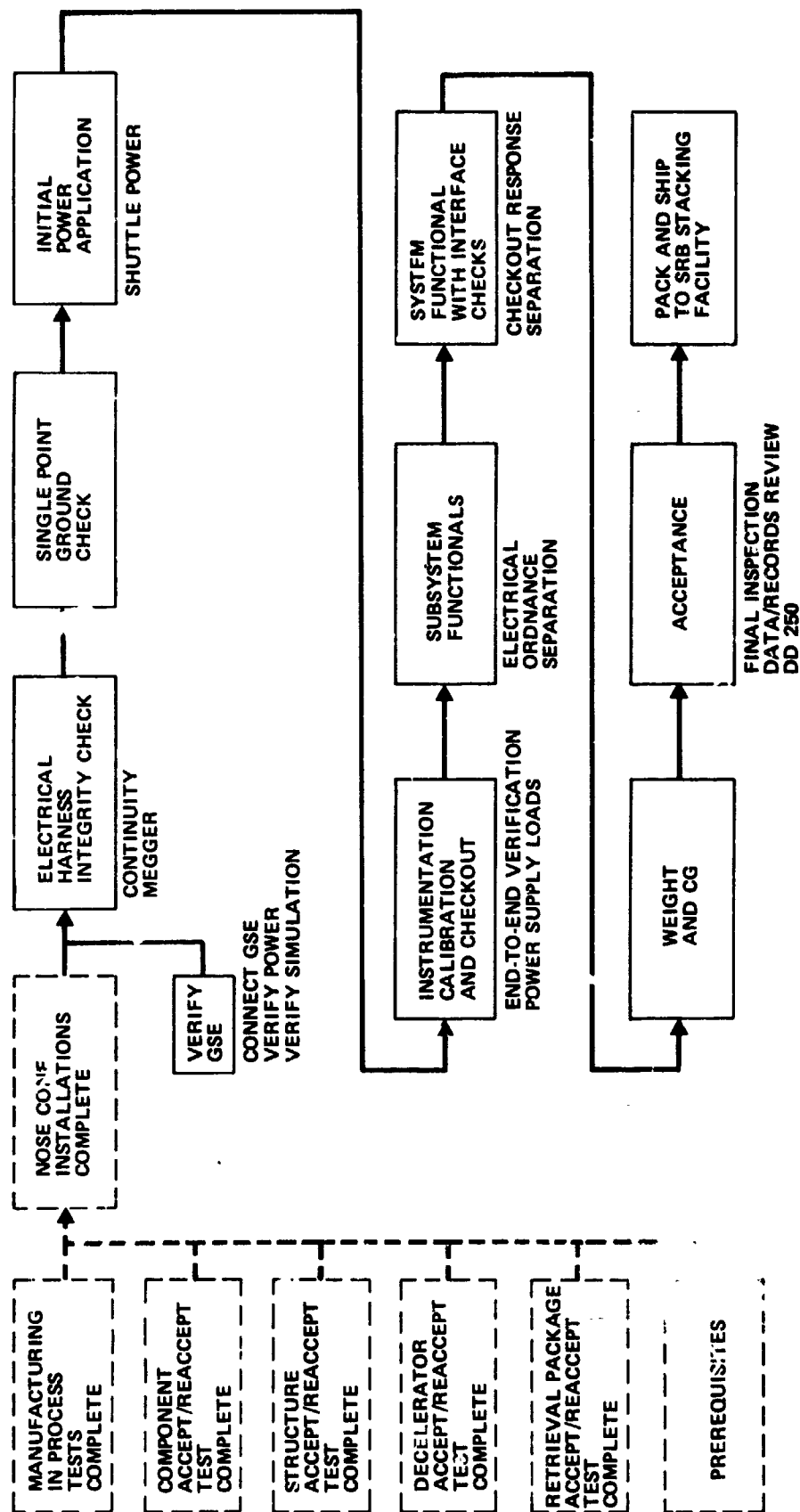
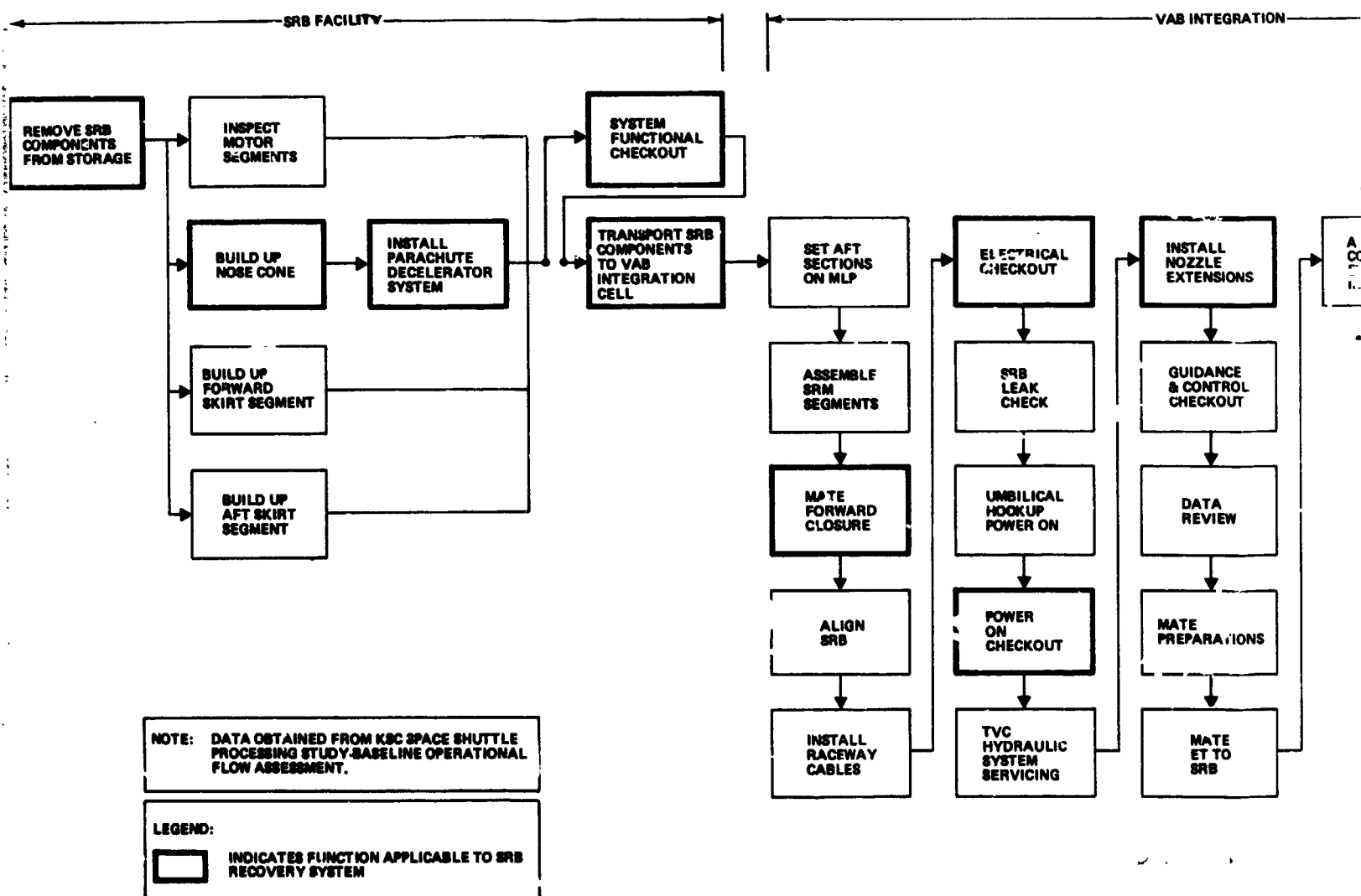


Figure 7.4-1 Recovery Subsystems Postassembly Functional Checkout

FOLDOUT FRAME

1



WOLDOUT FRAME

2

VAB INTEGRATION

INSTALL
NOZZLE
EXTENSIONS

GUIDANCE
& CONTROL
CHECKOUT

DATA
REVIEW

MATE
PREPARATIONS

MATE
ET TO
SRB

ALIGN AND
CONNECT
ET-SRB
INTERFACES

MATE
ORBITER TO
ET

INSTALL
ACCESS

REMOVE
ORBITER
FORWARD
ERECTION
SLING

CONNECT AND
VERIFY
ORBITER-ET
INTERFACES

CONNECT AND
VERIFY
ORBITER-MLP
INTERFACES

POWER ON
SHUTTLE
INTERFACE
TEST

INSTALL AND
CONNECT
ORDNANCE

PREPARE
FOR
ROLLOUT

TRANSFER
TO PAD

MATE MLP
& VEHICLE TO
PAD & VERIFY
INTERFACES

POWER ON -
LAUNCH
READINESS
VERIFICATION

HYGL HE
LOADING
PREP

INSTALL GSE,
OPEN PAYLOAD
DOORS, INSTALL
ACCESS

DATA
REVIEW

CLEAR
PAD

INSTALL
PAYLOAD

COUNTDOWN
PREP

ORBITER PAYLOAD
INTERFACE
CONNECT
VERIFICATION

PAYLOAD
PRELIMINARY
CLOSEOUT

LAUNCH
READINESS
VERIFICATION
FINAL

DATA
REVIEW

CLOSEOUT FRAME

3

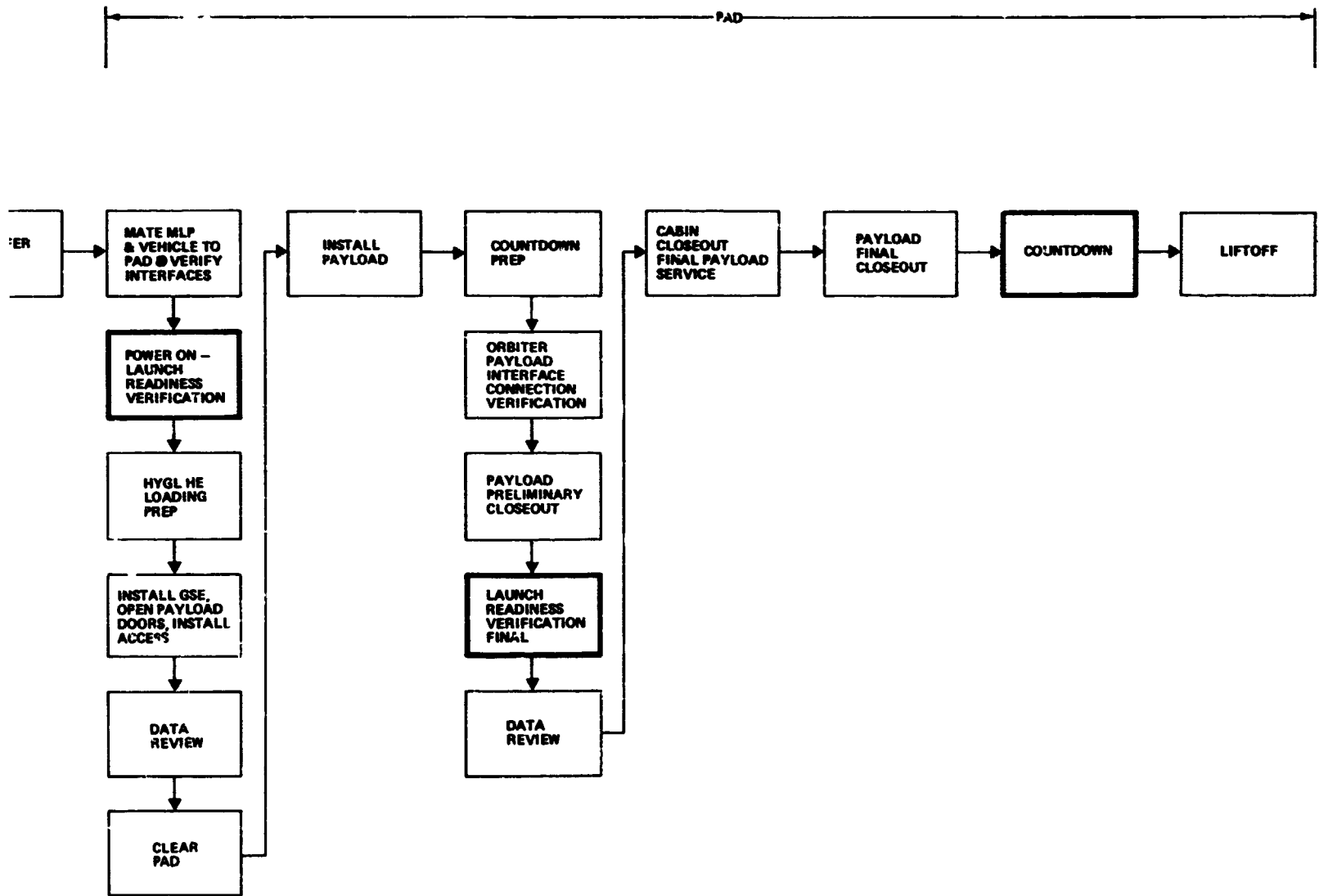


Figure 7.4-2 SRB Launch Site Operations

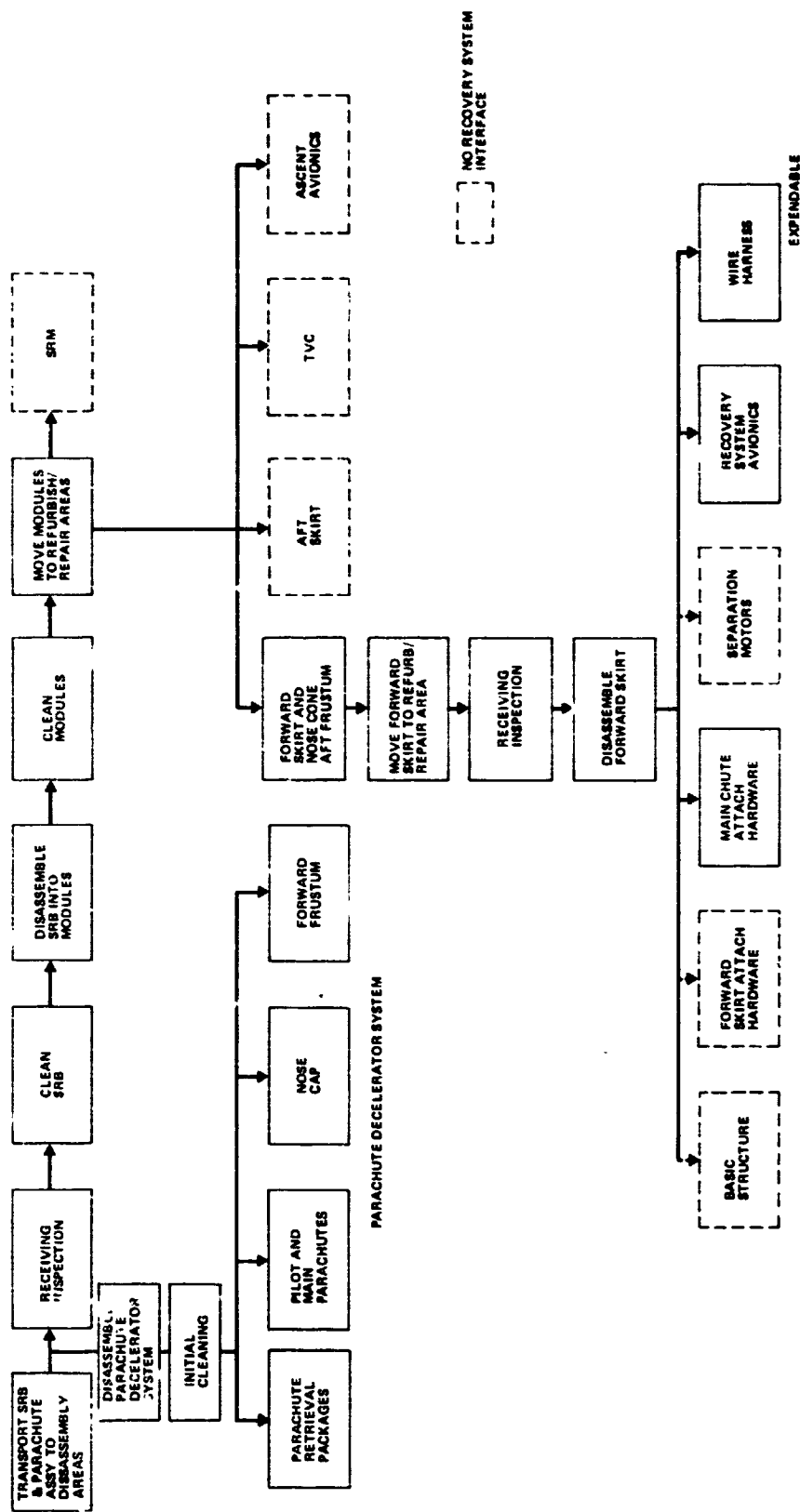


Figure 7.4-3 SRB Refurbishment Disassembly

The parachutes will then be transported to the Parachute Refurbishment Facility where they will be defouled, washed, dried, and inspected to determine the refurbishment requirements. Following repair and refurbishment (Fig. 7.4-4), the parachutes will enter the pack and rig area, where they will be rigged and packed in their deployment bags to the same procedures and processes used for new build parachutes. After final inspection, the packed parachutes are either stored in an environmental controlled area or transported to the launch site for use.

The structural and avionics components will be disassembled. The avionics will be disassembled to component, module and cable level, and structure to assembly level. The swivel and other moveable components will be disassembled to make sure all salt water residue is removed. Structure, swivel, and components will be inspected for damage, distortion or fracture, to determine suitability for repair. Minor repair and rework will be accomplished in the refurbishment area. Major rebuild will be accomplished at the manufacturing location. A functional flow is presented in Figures 7.4-5, -6, and -7.

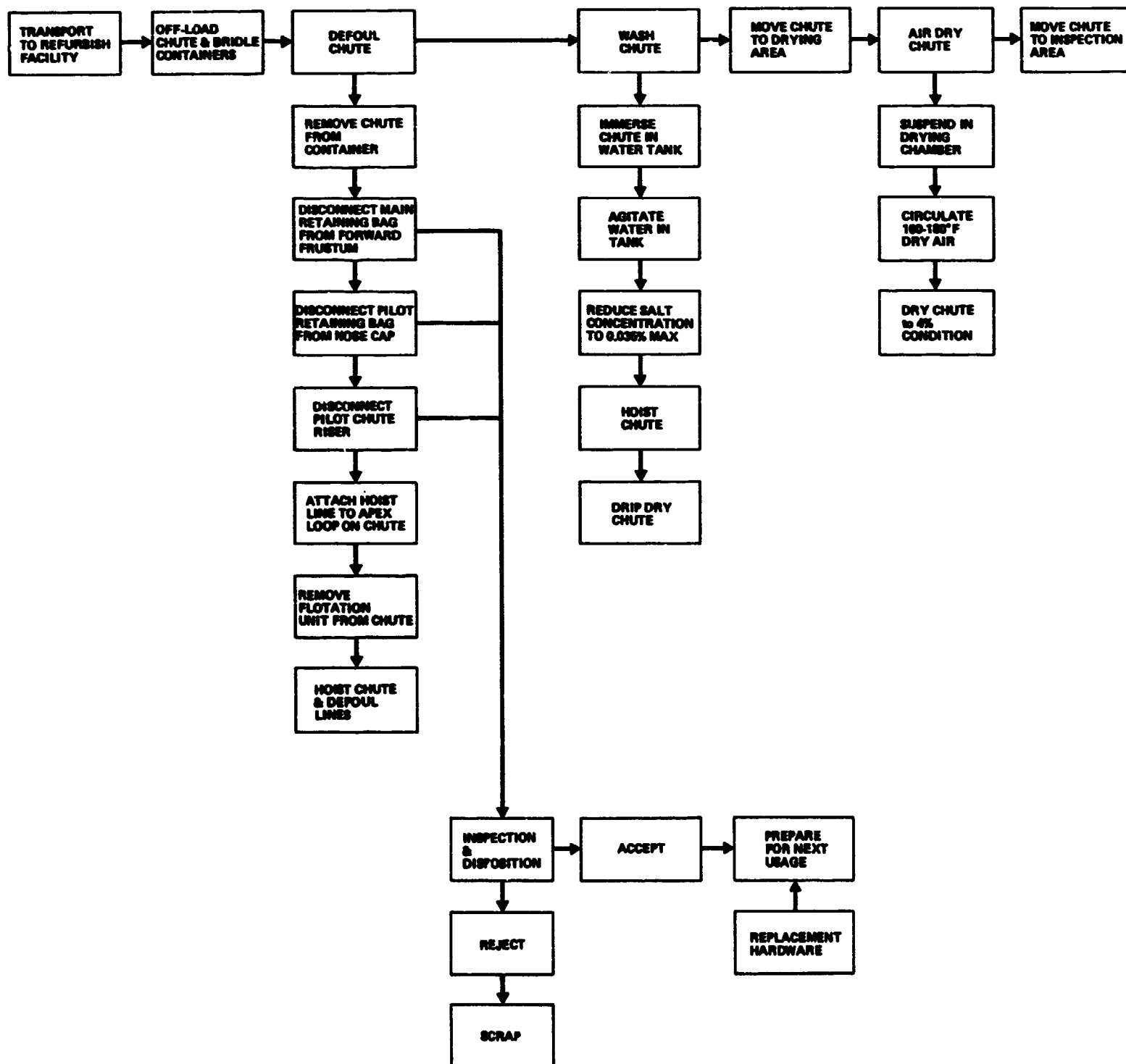
Avionics components will be subjected to appropriate checkout (vibration, functional, continuity, temperature cycling) to determine need for repair. Again major rework of a black box will take place at the manufacturing location.

As a part of refurbishment, all components and assemblies will return to the final assembly and checkout area and go through the same assembly and checkout as a new system.

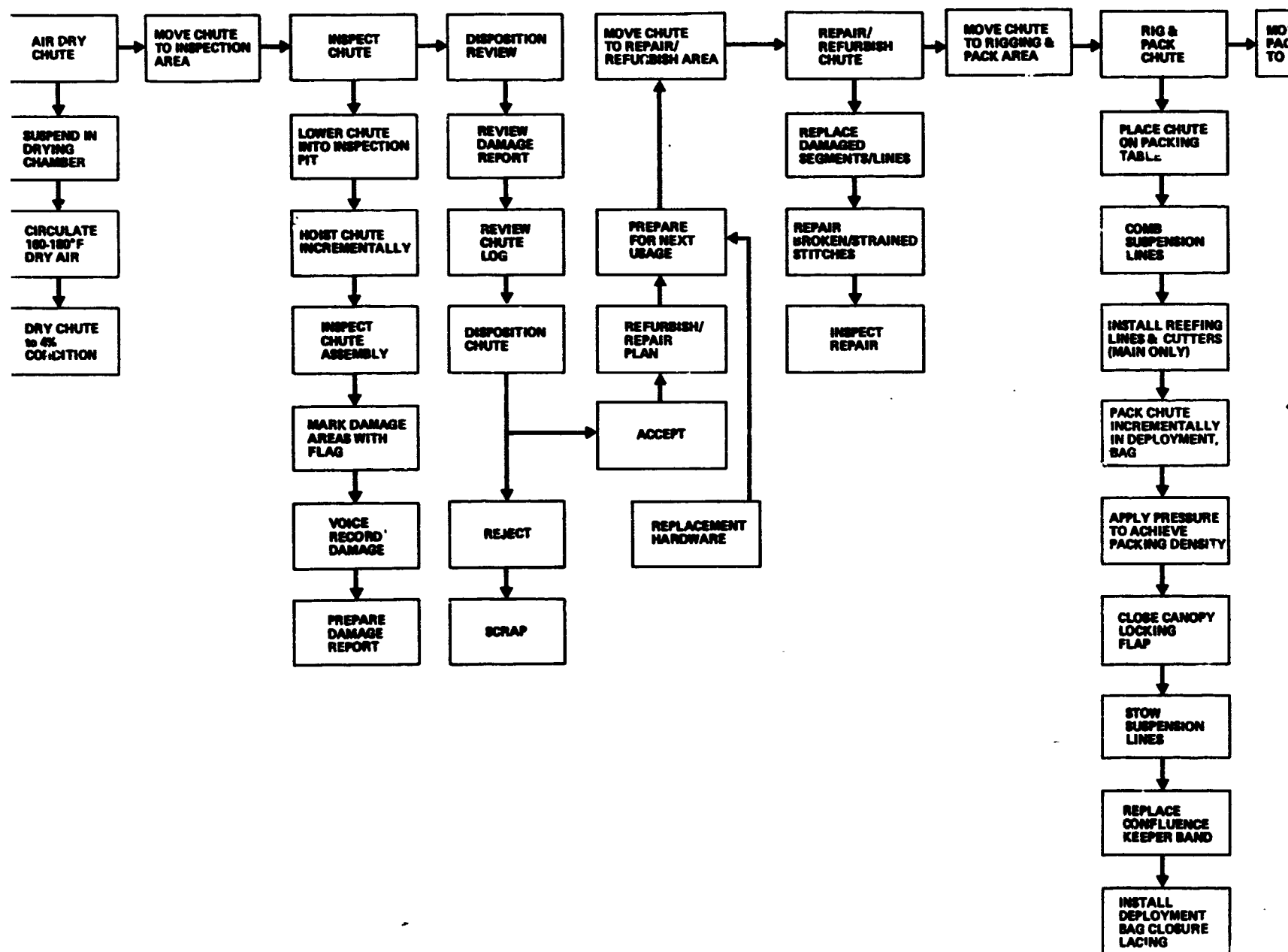
7.5 LOGISTICS PLAN

The sole purpose for the SRB Recovery System is to reuse expended SRB hardware and reduce Shuttle costs. The recovery system logistics task is to minimize the ownership costs required for support and contribute toward realization of a cost-effective recovery system. The Space Shuttle Program *Integrated Logistics Requirements* document (JSC 07700 Volume XII) establishes Level II program definition and requirements and has been used as the basis for our logistics planning effort. It is envisioned that MSFC will implement the Level II requirements through a SRB Integrated Logistics Support Plan that will apply to all elements of the SRB system, including the recovery system. Figure 7.5-1 is a logistics requirements tree which is provided to illustrate two points regarding SRB logistics management.

FOLDOUT FRAME



FOLDOUT FRAME 2



FOLDOUT FRAME 3

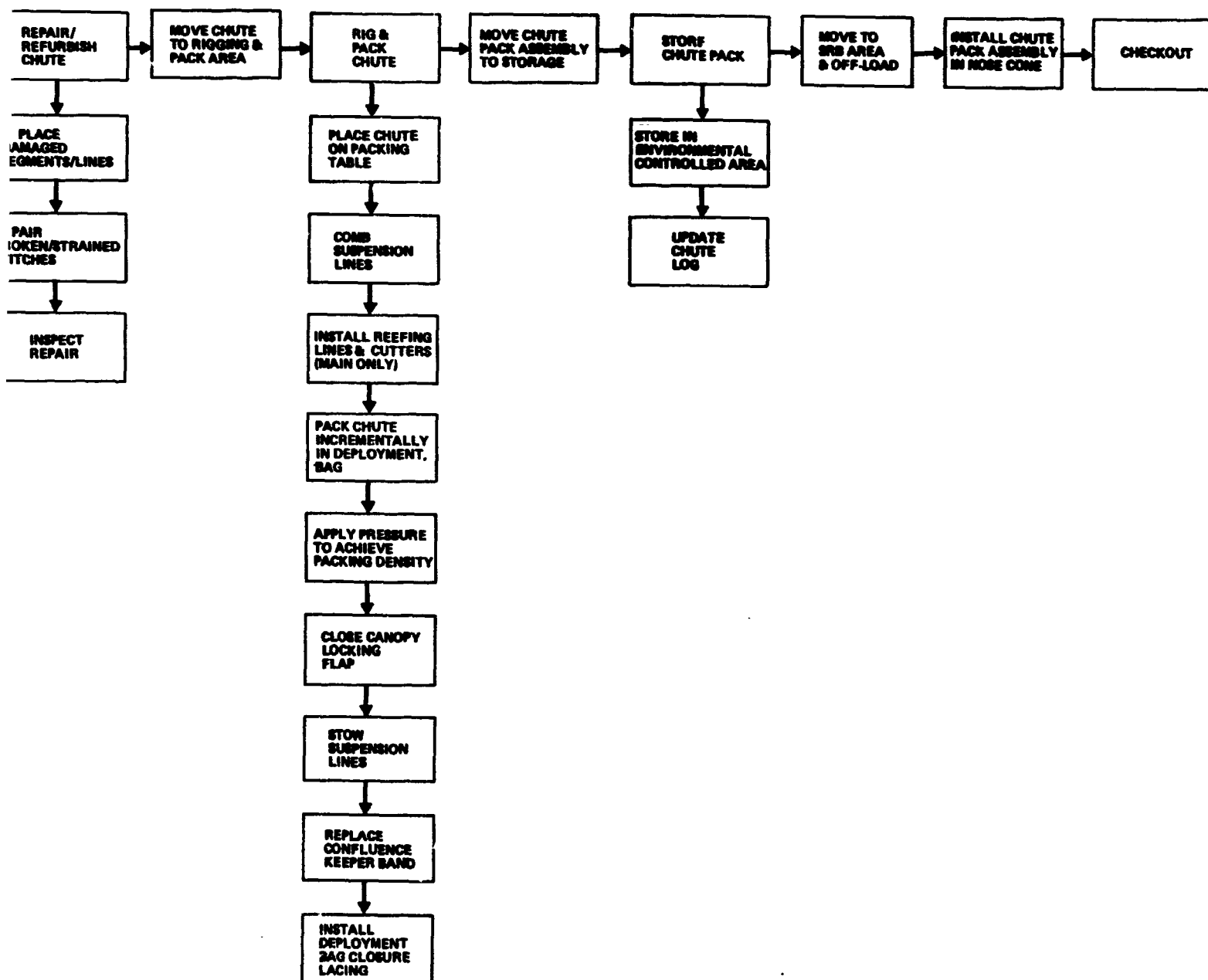
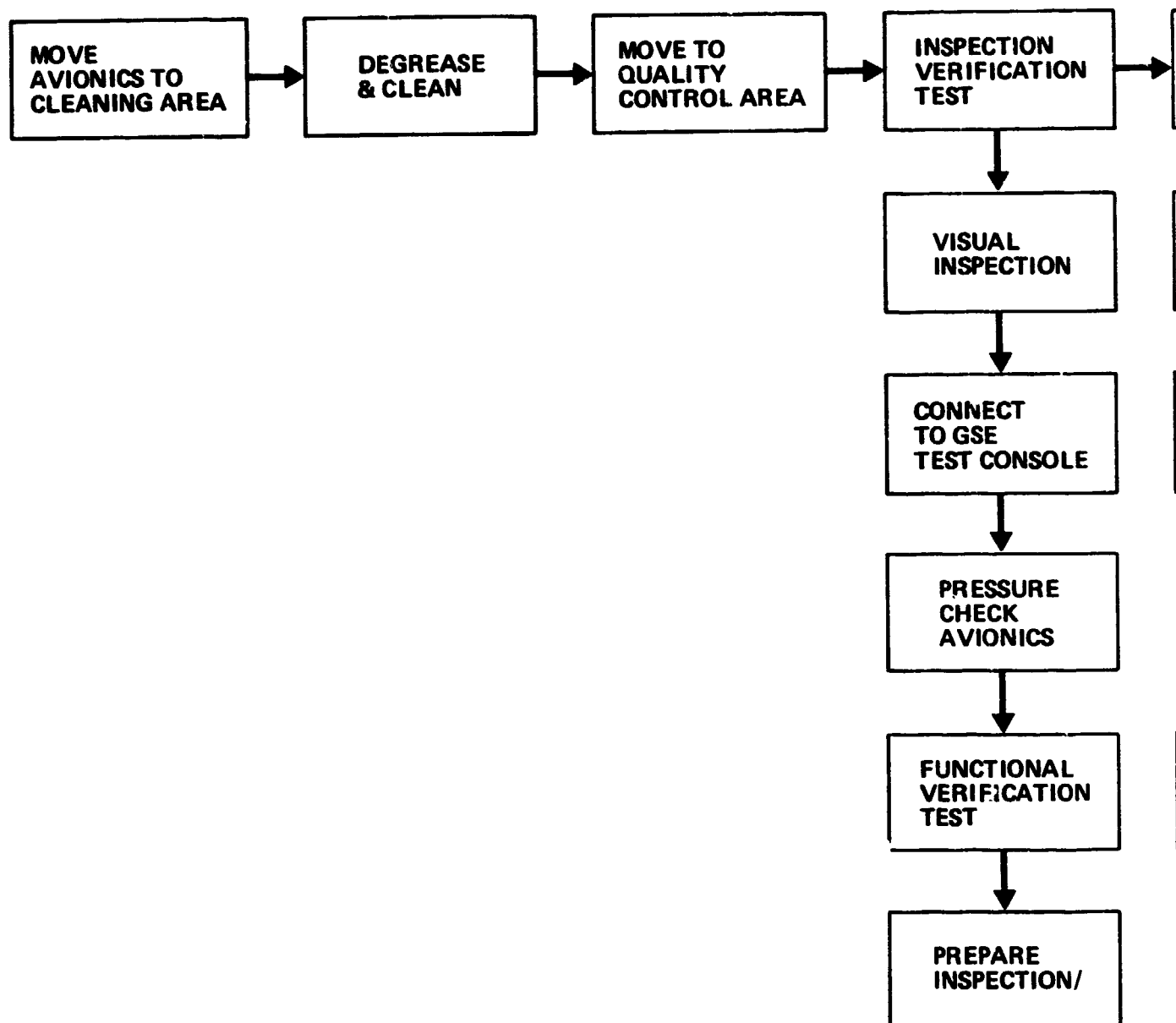


Figure 7.4-4 Parachute System Refurbishment Functional Flow

FOLDOUT FRAME



RECORDING PAGE BLANK NOT FILMED

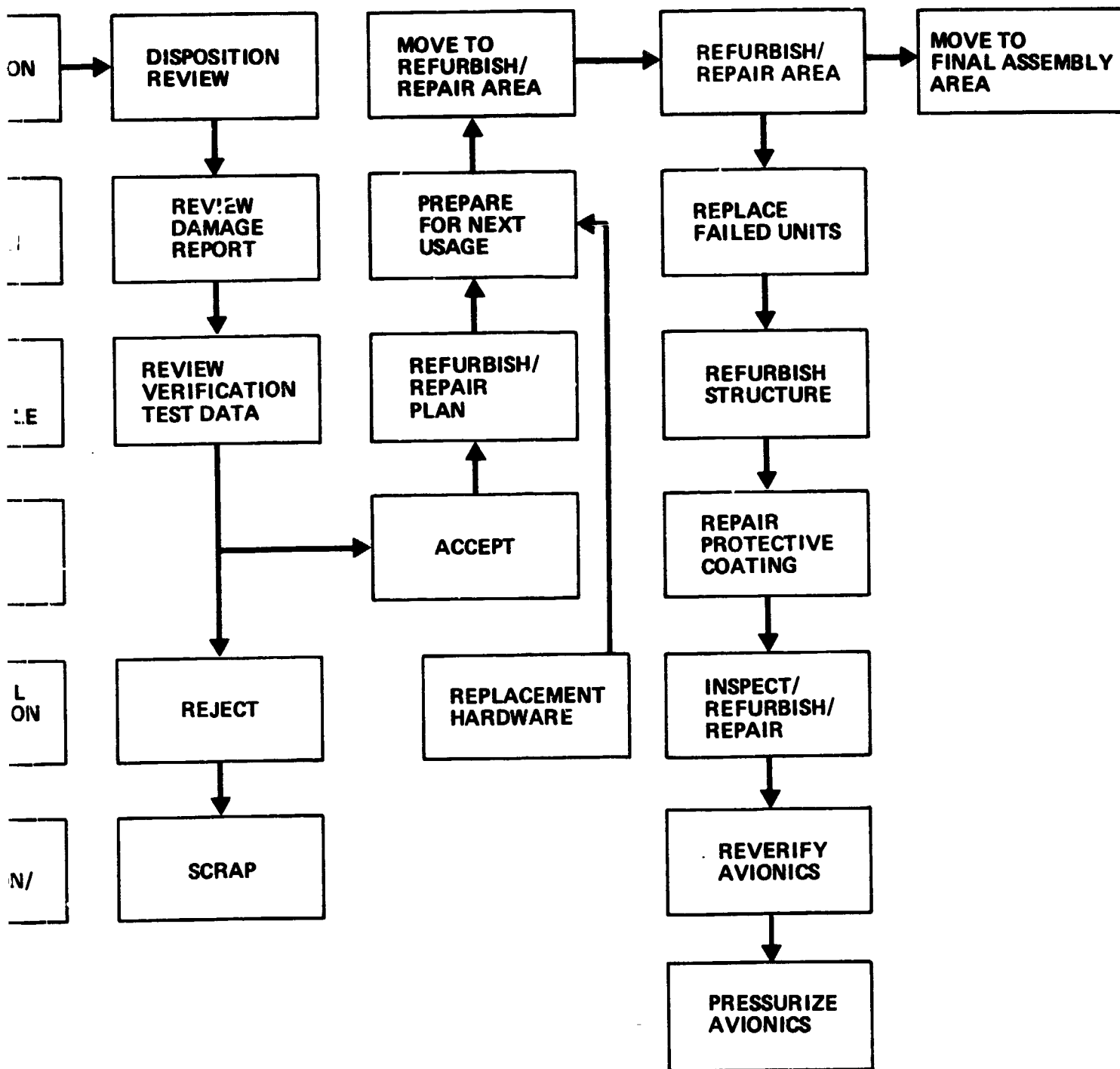
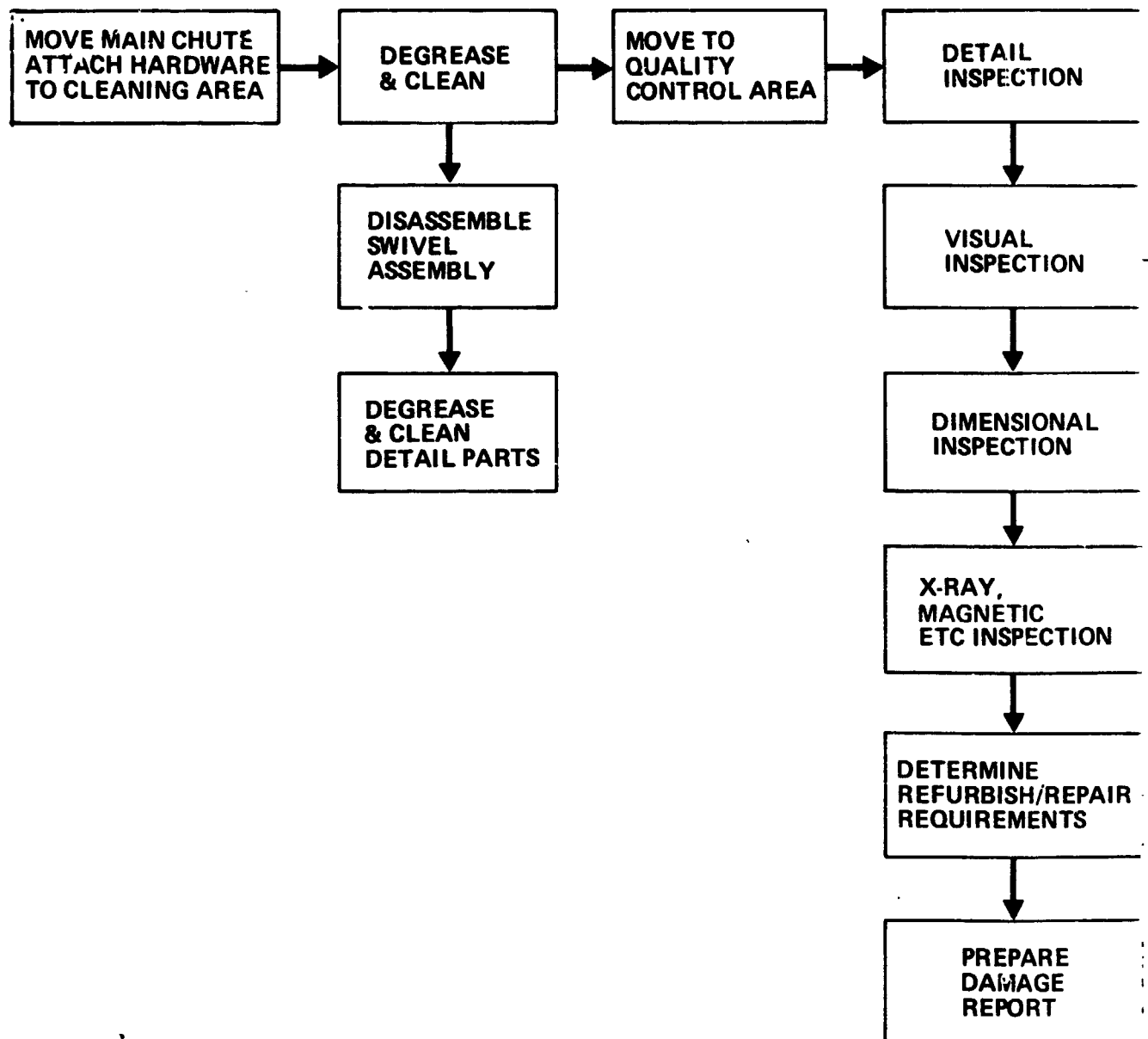


Figure 7.4-5 Recovery System Avionics Refurbishment Functional Flow

FOLDOUT FRAME



PRECEDING PAGE BLANK NOT FILMED

FOLDOUT FRAME

2

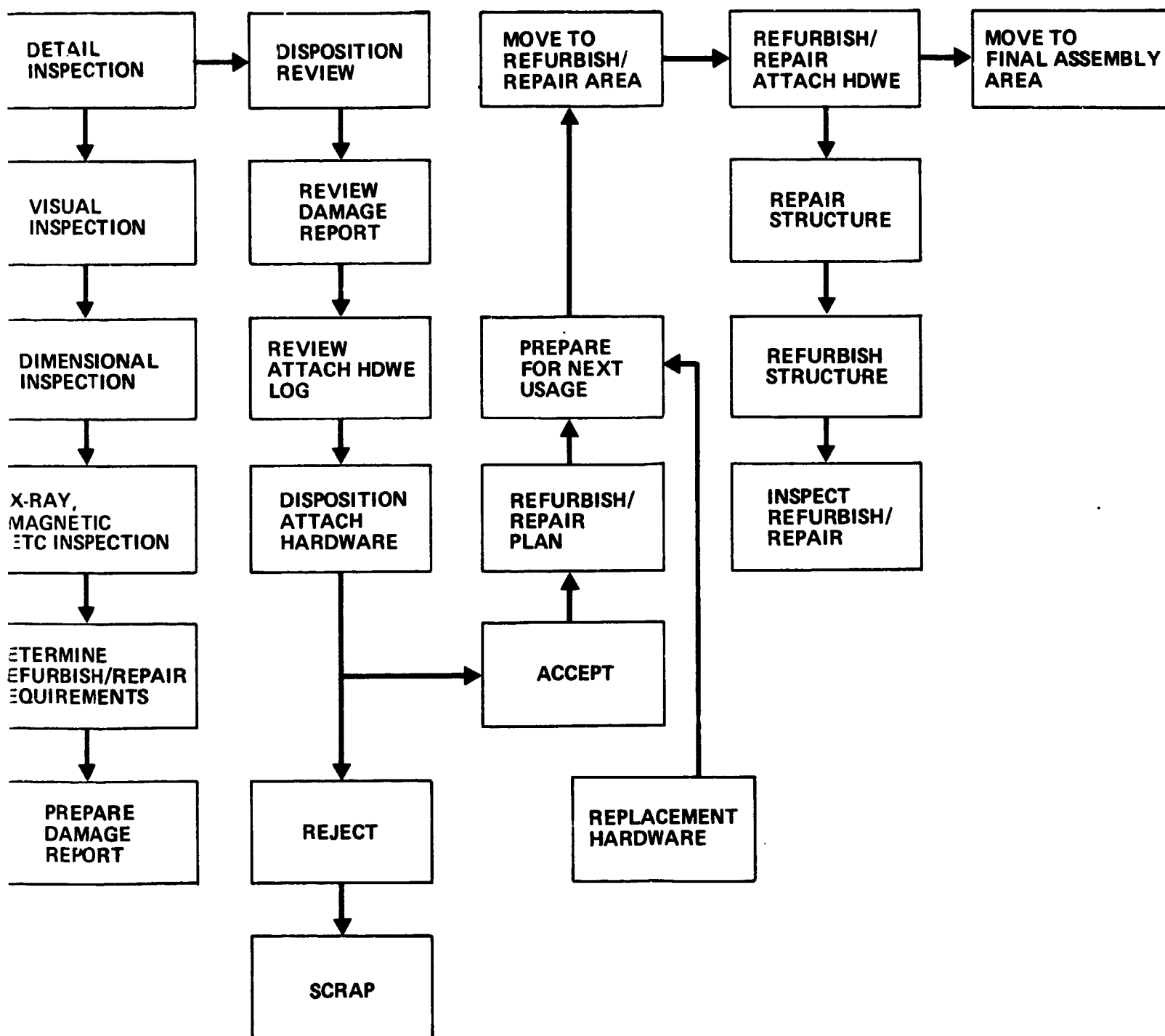


Figure 7.4-6 Main Chute Attach Hardware Refurbishment Functional Flow

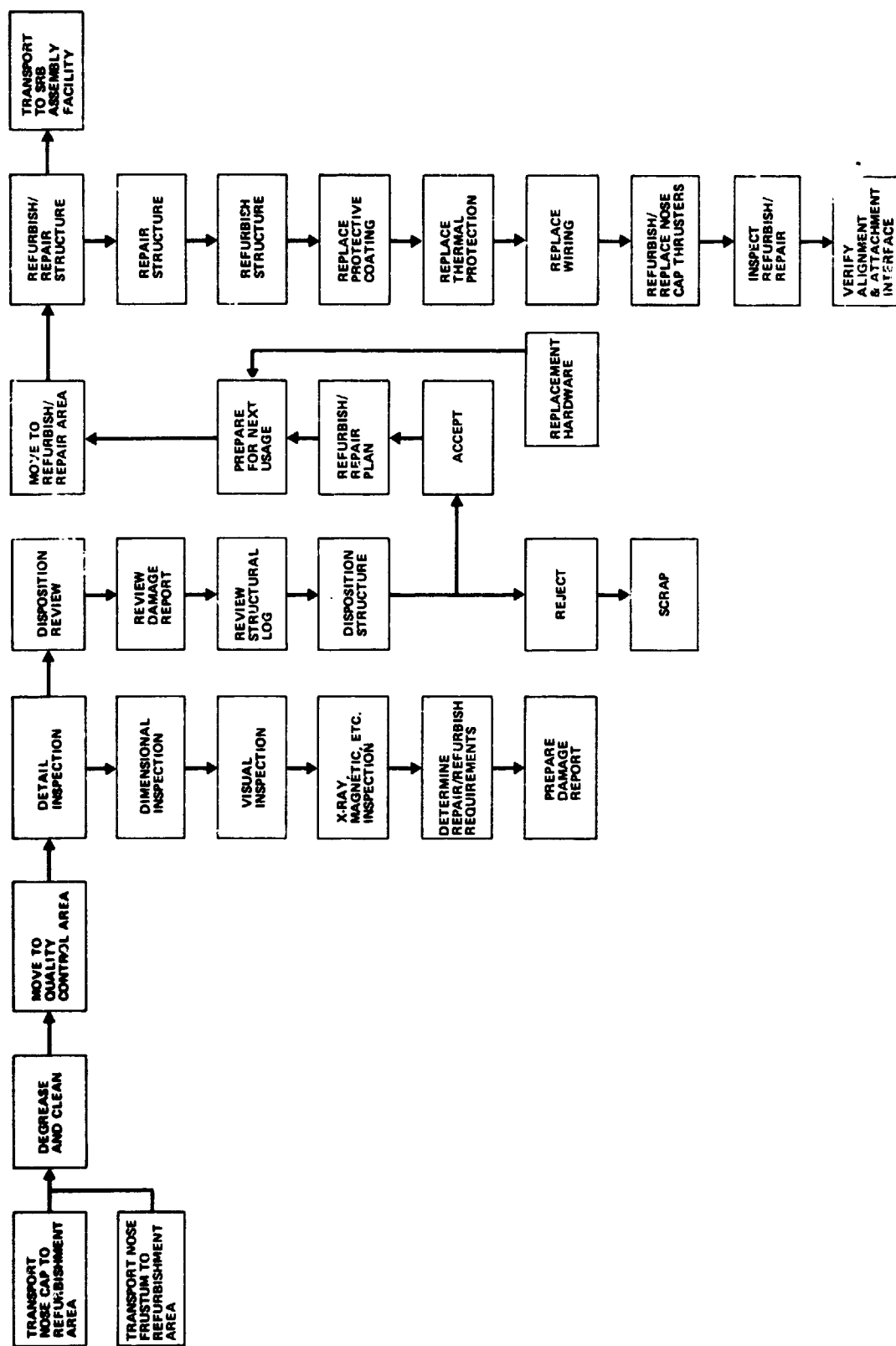
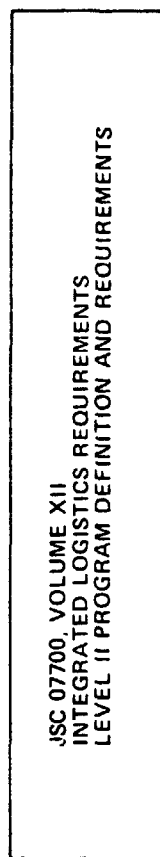


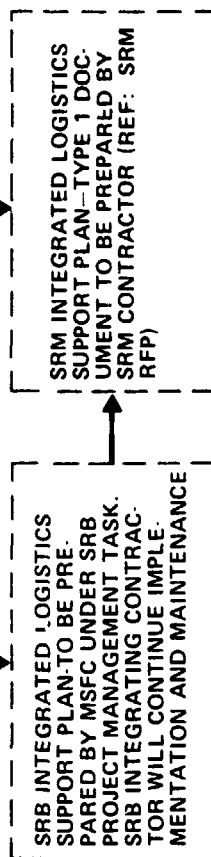
Figure 7.4-7 Nose Cone Structure Refurbishment Functional Flow

PRECEDING PAGE BLANK NOT FILMED

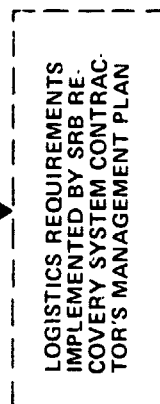
SPACE SHUTTLE PROGRAM



SOLID ROCKET BOOSTER PROJECT



SRB RECOVERY SYSTEM



SRB RECOVERY SYSTEM COMPONENTS
(PARACHUTES, AVIONICS, ETC)

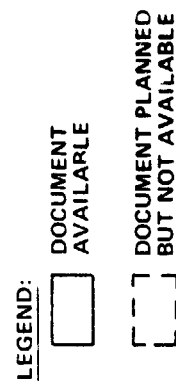


Figure 7.5-1 Logistics requirements Trace--SRB Recovery System

1) The SRB Integrated Logistics Support Plan is the keystone in establishment and implementation of a cost-effective support system. This plan should ensure that all SRB element contractors are providing support features in their hardware and developing support plans that are compatible with one another and the overall SRB support concept.

2) Except for the SRM, individual logistics plans are not recommended for each SRB element; i.e., structures, avionics, TVC, and recovery. Logistics requirements can be effectively implemented as a part of each contractor's management plan and thereby reduce documentation costs.

The remaining paragraphs of this section identify the significant logistics support considerations for the recovery system and present our plans for the selected system.

7.5.1 Logistics Support Considerations

Based upon analysis of an SRB recovery system functional flow, refurbishment is the most significant activity from a logistics viewpoint. Refurbishment is a recurring task with a known frequency of occurrence, as opposed to the requirement for corrective maintenance in support of receipt-to-launch operations which is based on anticipated failures. This fact makes refurbishment the driver for establishment of maintenance and repair concepts and support resources. We have, therefore, concentrated our logistics planning effort during this study on support of refurbishment. A disciplined approach to establishment of refurbishment requirements and resources is shown in Figure 7.5-2.

The first step in the process is establishment of basic maintenance concepts including initial identification of line replaceable units (LRU). This task should be initiated in parallel with the system definition and preliminary design effort in order to influence the design with supportability features.

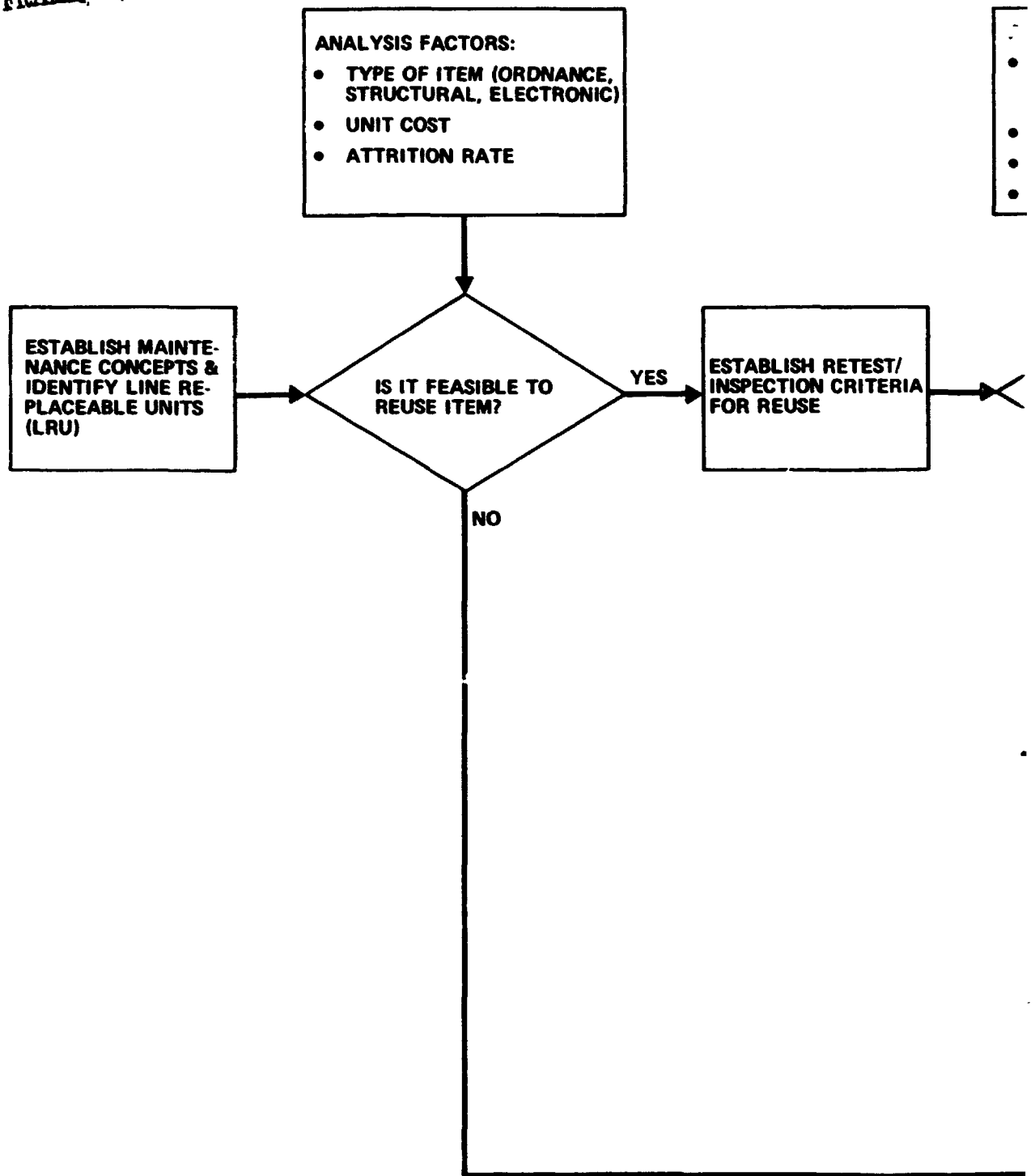
After initial identification of LRUs, a reusability decision is required on each item based upon unit cost, type of item involved, and anticipated attrition rate. This is a feasibility decision that is made without benefit of detailed design information or maintenance engineering data. Questionable items should be selected for reuse and further analysis rather than elimination for consideration at this point. Planning for replacement parts for items identified as not reusable should consider launch rate, life limitations, economical lot sizes, and stability of design. Items identified for reuse must be analyzed to establish retest and inspection criteria to establish serviceability.

After the retest and inspection criteria has been established, a decision is required on where this function will be performed-- launch site or the supplier's factory. The extent of new facilities and special test equipment will be the driver on this decision. This is a prime example of the importance of integration of SRB recovery system requirements with other SRB and Space Shuttle elements; a decision based solely on recovery system requirements may indicate that site retest is not cost effective, whereas an integrated decision may identify enough common requirements to justify site retest and reduce overall program costs. The retest location decision is closely related to the refurbishment location decision, further downstream in the flow, and requires iteration to select the best approach.

The next decision is to establish the disposition of items that fail retest--either refurbishment or scrap. The comparison of refurbishment cost to replacement cost is the driver for this decision; our current planning is that items with an average estimated refurbishment cost of 65% or more will not be considered for refurbishment.

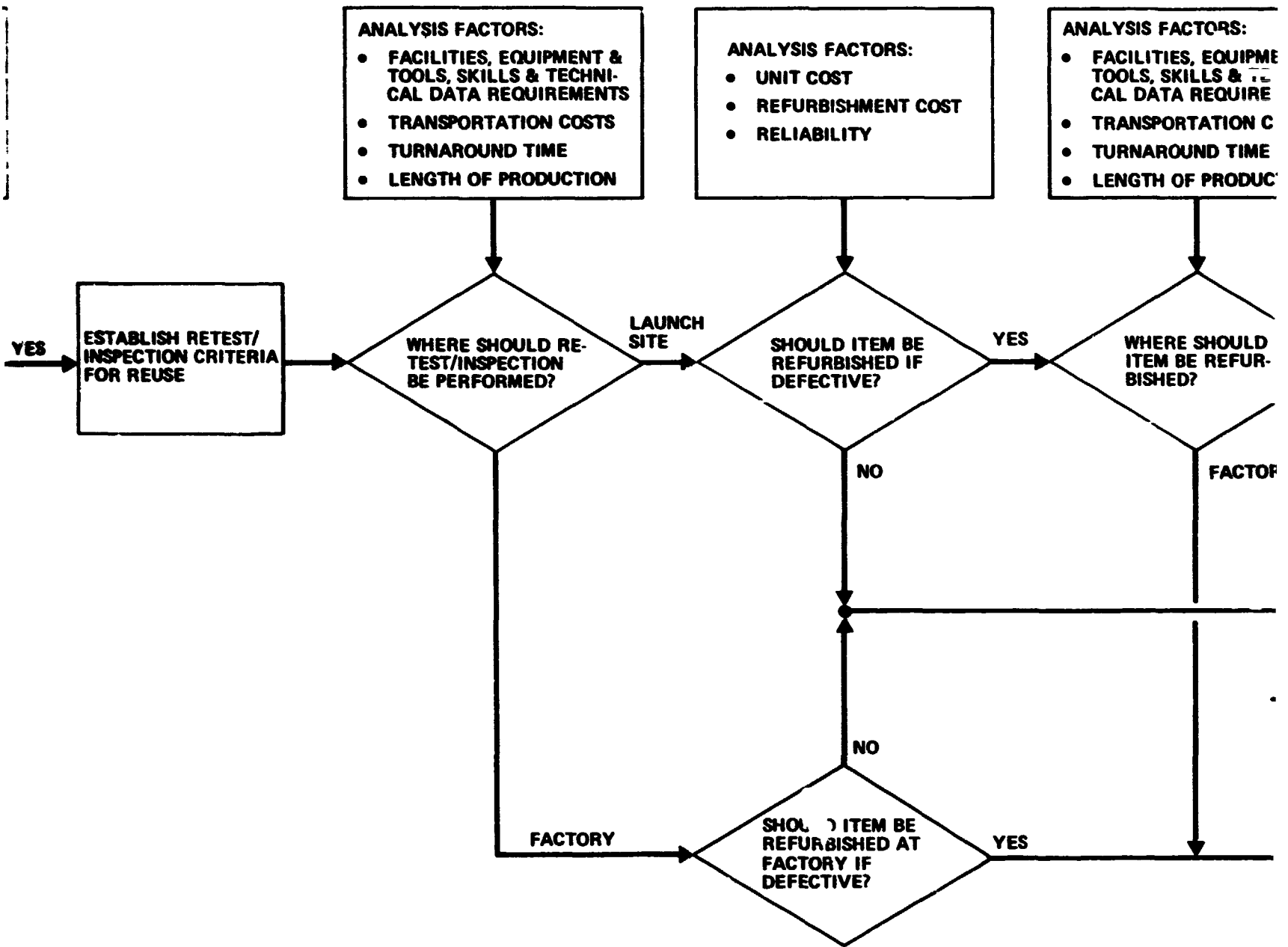
Items selected for factory retest and subsequent refurbishment will not be considered for refurbishment at site because it would require duplication of facilities and equipment for retest to establish condition and acceptance testing after refurbishment. Items selected for site retest and subsequent refurbishment present the final decision in the process in order to determine where the refurbishment should be accomplished. This is a critical decision and requires a comprehensive maintenance engineering analysis and a tradeoff of alternatives based on cost. There are essentially two alternative locations available--launch site or supplier; however, a decision for launch site refurbishment can be deferred until after the DDT&E flights in order to obtain field test data. In this case, options should be negotiated with the supplier for tooling availability, technical data, additional units or repair parts and overhaul capability (short and long term). A final decision should be made and implemented before the end of the scheduled production run in order to exercise the necessary options and prevent excessive implementation costs.

FOLDOUT FRAME



DEFINITION

FOLDOUT FRAME 2



ANALYSIS AND TRADEOFF

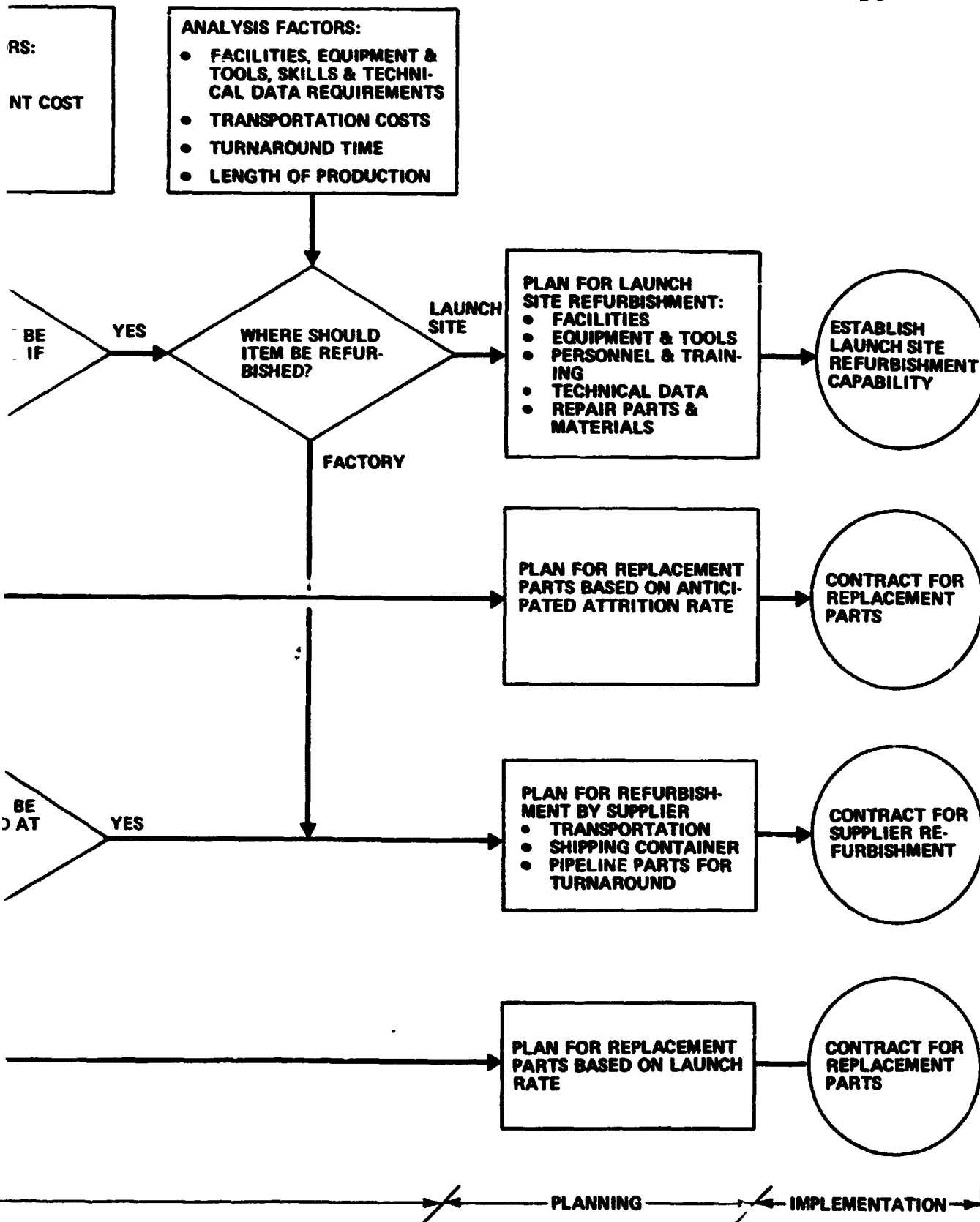


Figure 7.6-2 Refurbishment Planning Process

7.5.2 Spares and Supply Support

Replacement parts and materials will be required to support maintenance and refurbishment operations. For purposes of identification, these items are categorized as spares, refurbishment parts, and bulk items.

Spares consist of line replaceable units (LRU), shop replaceable units (SRU), and repair parts that are required to support preventive and corrective maintenance operations at organizational, intermediate and depot maintenance levels. Spares will be provided by separate provisioning action in addition to production and refurbishment parts.

Refurbishment parts consist of those items required at the launch site or a supplier's factory in direct support of refurbishment operations. Refurbishment parts will be provided as a part of a production or refurbishment contract based upon the number of anticipated refurbishments.

Bulk items consist of those standard parts and raw materials (i.e., bolts, nuts, washers, wire, tape, paint) that are required in support of maintenance and refurbishment operations. Bulk items required at the launch site will be supplied by NASA from a centralized common inventory.

A maintenance engineering analysis (MEA) will be performed to identify the type, level, and location of maintenance and the requirements for the necessary supporting resources, i.e., spares, maintenance facilities and equipment, technical data, and personnel skills. Based upon MEA requirements, spares quantities and stocking locations will be determined and the provisioning process initiated. Whenever feasible, production and refurbishment items will be used to defer the procurement of spares and thereby reduce the cost of providing and maintaining spares.

A limited quantity of selected LRUs are planned to support organizational maintenance with backup provided by the "next vehicles" hardware for spares depth and insurance items.

Intermediate and depot level maintenance will be accomplished using the same turnaround cycle and resources established for component refurbishment. This approach prevents establishment of dual inventories (one for repair and one for refurbishment) and allows for provisioning SRUs and repair parts on an as-used basis.

7.6 FACILITIES PLAN

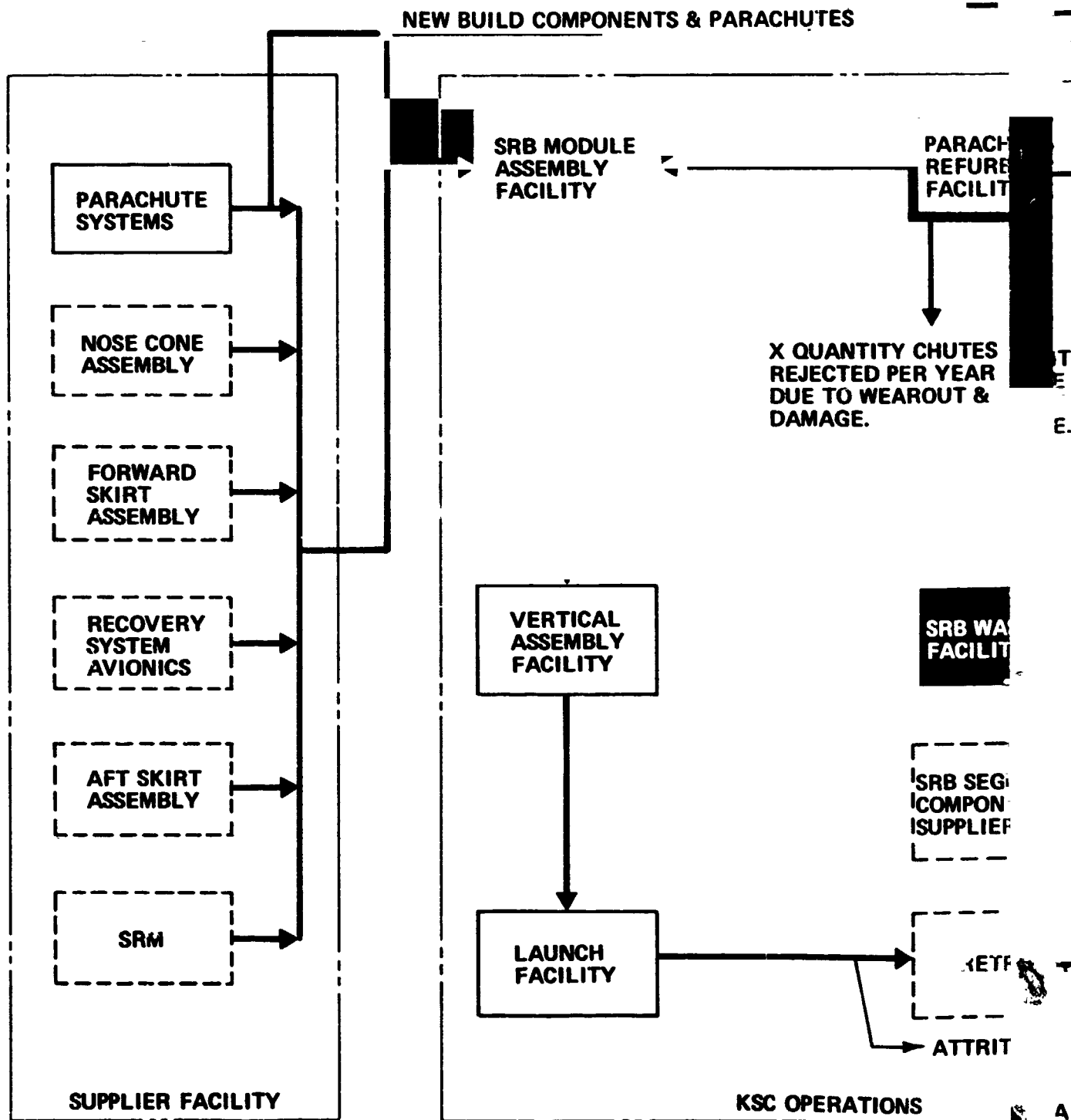
A significant factor in the selection of the baseline approach is the use of existing facilities and identification of new facilities that can effectively support the recovery system during the development and qualification testing phases of the Shuttle SRB Program and the operational SRB refurbishment phases. Since the baseline recovery system configuration employs the use of a single pilot and a single main chute, the logistics and the facility impact aspects are minimal when compared to decelerator concepts requiring additional chutes or solid motor decelerator systems. In any event, facility costs will have a significant impact on the attributes of the recovery system selected. In the operational and refurbishment phase, major emphasis must be focused on optimizing the capabilities of the facility to meet operational and refurbishment demands imposed by the presently defined launch rate of 60 launches maximum per year.

Cost and time associated with hardware recycle are dependent upon the selection of processing locations and Figure 7.6-1 is provided as a facility functional flow of SRB recovery subsystem and an approach to optimize the recovery facilities required for support of the WTR and KSC operational plan.

The key to optimization of facilities is a central processing facility for parachute refurbishment. Further study is required to equate the transportation costs and the logistics involved in processing parachutes from WTR launches; however, preliminary indicators show that a significant cost savings can be realized by providing a single facility for this purpose.

In the interest of parachute rig and pack accountability, it would be desirable to have all the parachutes, new and refurbished, processed at a single facility. Because the delivery rate of new parachutes per year is low (5 to 10 sets per year) and the refurbishment quantity is of the order of 115 sets per year, this would indicate that it would be desirable to have these operations performed at the same facility.

FOLDOUT FRAME



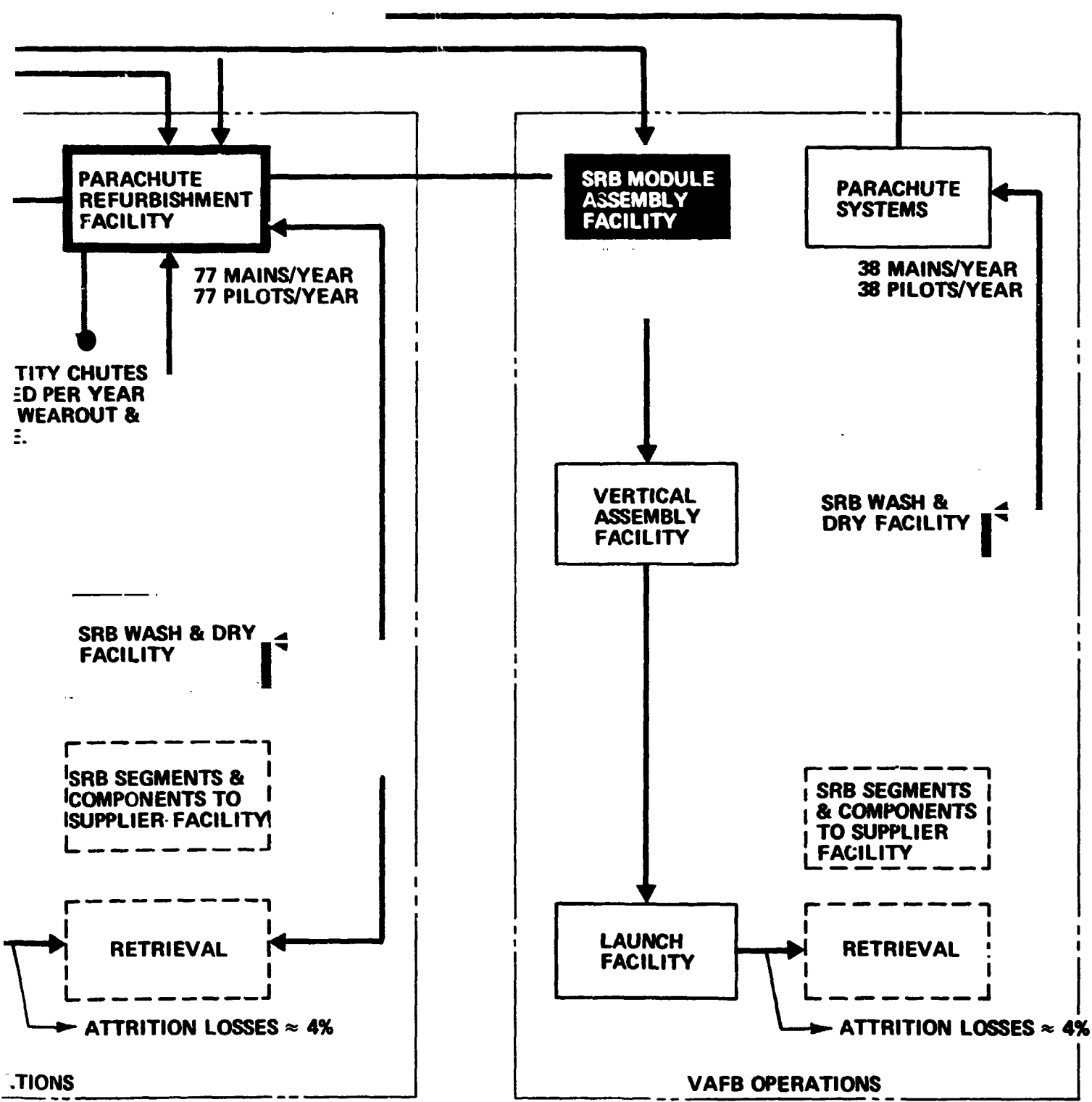


Figure 7.6-1 SRB Facilities Recovery System Subassembly Flow

7.6.1 Test Facilities

Supplier facilities and equipment will be used to the maximum extent possible to develop and to provide acceptance tests on SRB recovery components. Determination of what equipment is required at each supplier facility to comply with development testing and acceptance testing should be undertaken in a cost-effective approach to provide like GSE for similar functions at the operational sites during refurbish activity. The objective is to minimize the variety of test equipment required at the supplier's facility and at the operational site for maintenance and check-out of the SRB recovery components and subassemblies.

Table 7.6-1 indicates the facilities that will be used during the development and qualification testing of the recovery system. All of these facilities are in existence. Some facilities, however, may require modification or outfitting with new equipment.

7.6.2 Refurbish and Repair Facility

A parachute refurbishment facility is required to prepare the recovered SRB parachutes for reuse. The parachute facility must be of adequate proportions and equipped to support the baseline of 40 Shuttle launches per year at Kennedy Space Center and pending the results of further trade studies, the facility should have the increased capability to support 20 Shuttle launches per year at WTR. The number of parachutes to be processed at this facility will be a maximum of 120 main chutes and 120 pilot chutes per year, including 40 main chutes and 40 pilot chutes from WTR. These numbers represent the baselined SRM recovery system, and it must be pointed out that facility costs will increase with the number of additional chutes to be processed should a decelerator system using multichutes be chosen.

If a parachute facility is sited at KSC, it would be necessary to build a new facility since no existing facilities are available for this case (KSC document TR-1177).

The sequence of refurbishment operations to be performed is shown in Figure 7.4-4, *Parachute System Refurbishment Functional Flow* and Figure 7.4-6, *Main Chute Attach Hardware Refurbishment Functional Flow*.

Table 7.6-1 SRB Decelerator Development and Qualification Test Facility Requirements

FACILITY	OPERATIONS	STATUS		UTILIZATION		
		E	M	D	Q	A
SUPPLIER LABORATORIES	MATERIAL TESTS	●		●		
NASA/ARC 40x80 FT WIND TUNNEL	PILOT CHUTE MODEL TESTS	●		●		
NASA/ARC 40x80 FT WIND TUNNEL	MAIN CHUTE MODEL TESTS	●		●		
JPTF, EL CENTRO	PILOT CHUTE AIR DROP	●		●		
JPTF, EL CENTRO	MAIN CHUTE AIR DROP	●		●		
JPTF, EL CENTRO	DECELERATOR SYSTEM AIR DROP TESTS	●		●	●	●
PARACHUTE SUPPLIER	PILOT CHUTE TESTS	●		●		
PARACHUTE SUPPLIER	MAIN CHUTE TESTS	●		●		
SUPPLIER STRUCTURAL TEST LAB	NOSE CAP/NOSE FRUSTUM SEPARATION TEST	●		●		
SUPPLIER STRUCTURAL TEST LAB	NOSE FRUSTUM TIPOFF & SEPARATION TEST	●		●		
SUPPLIER STRUCTURAL TEST LAB	SRB SWIVEL STRUCTURAL TESTS	●		●	●	●
SUPPLIER STRUCTURAL TEST LAB	STAGING HARDWARE STRUCTURAL TEST	●		●	●	●
SUPPLIER TEST LABS	ELECTRONIC COMPONENT TESTS	●		●	●	●
SUPPLIER TEST LABS	RECOVERY SYSTEM ELECTRICAL BREADBOARD	●		●		
SUPPLIER TEST LABS	ORDNANCE SYSTEM SEPARATION TESTS	●		●	●	●
KSC	MAINTAINABILITY DEMONSTRATION	●		●	●	●
KSC	DDT&E FLIGHT TEST	●	●		●	●
KSC OR VENDOR SITE	REFURBISH DEMONSTRATION		N		●	●
LEGEND:						
E	EXISTING FACILITY					
M	MODIFIED FACILITY					
N	NEW					
D	DEVELOPMENT					
O	QUALIFICATION					
A	ACCEPTANCE					

A refurbishment work plan is presented in Figure 7.6-2. Based on a 2-shift/5-day week this plan indicates a 10-day processing cycle per chute. Note that the repair and rig and pack tasks are the major limiting factors in the scheduling of chute refurbishment. To process an expected maximum of 240 chutes per year on a 2-shift/5-work day week will require a minimum of four rig and pack stations and three repair stations.

A conceptual facility to meet the parachute system refurbishment requirements is shown in Figure 7.6-3. Estimated costs for such a facility are shown in Table 7.6-2.

Table 7.6-2 Estimated Costs for Parachute Facility

SIZE, FT ²	TRAFFIC, SETS/YR	MEN/SHIFT	NO. SHIFTS	FACILITY COST
40,400	40	26	1	\$2,925,000
40,400	80	26	2	\$2,925,000
54,600	120	36	2	\$3,969,000

7.6.3 Storage

Only a small environmentally controlled area will be needed for storage of the parachute system. This storage area would be approximately the same whether the parachutes were stored in the packed or unpacked condition. Flow schedule should be adjusted to minimize packed storage time.

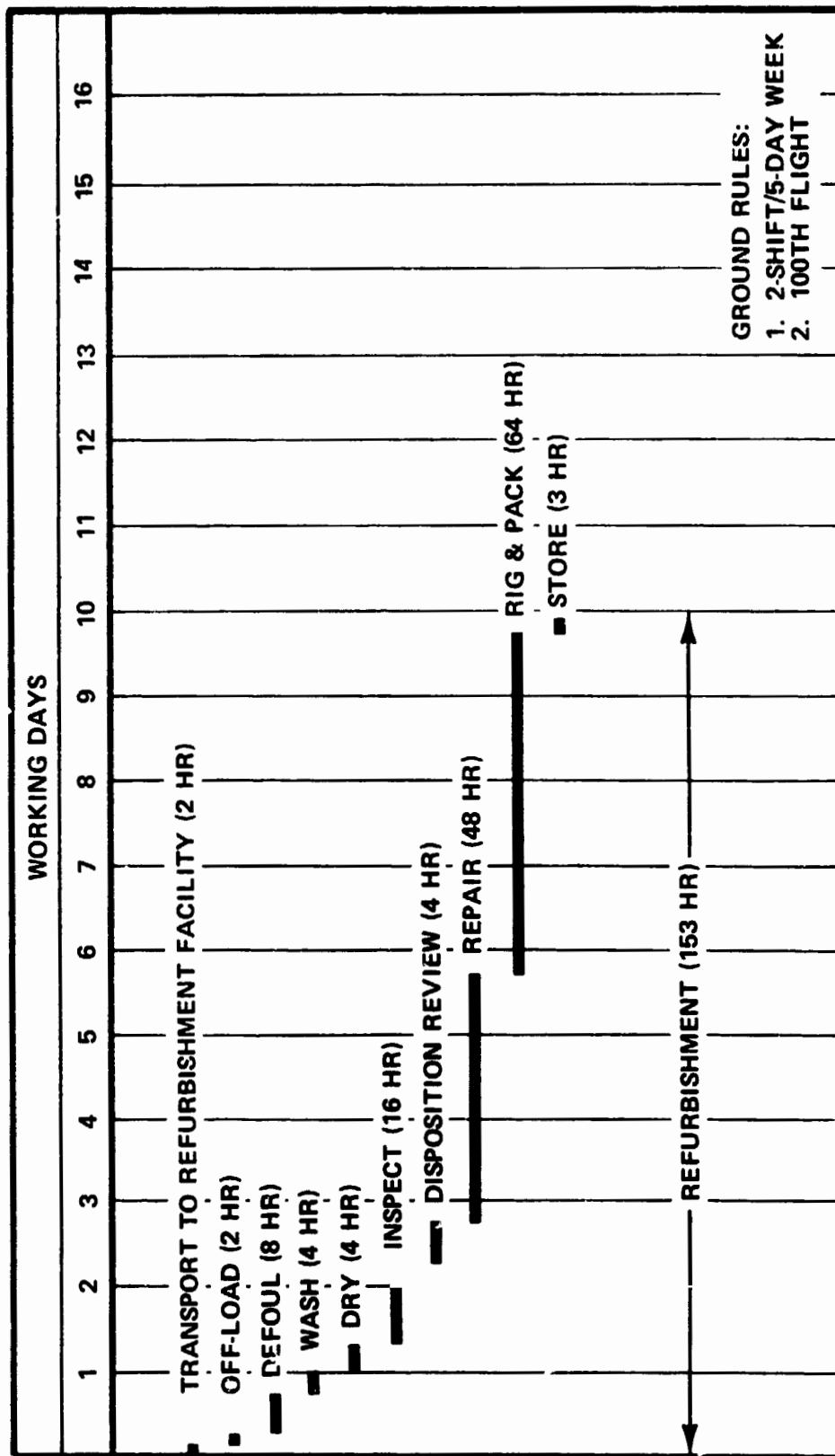
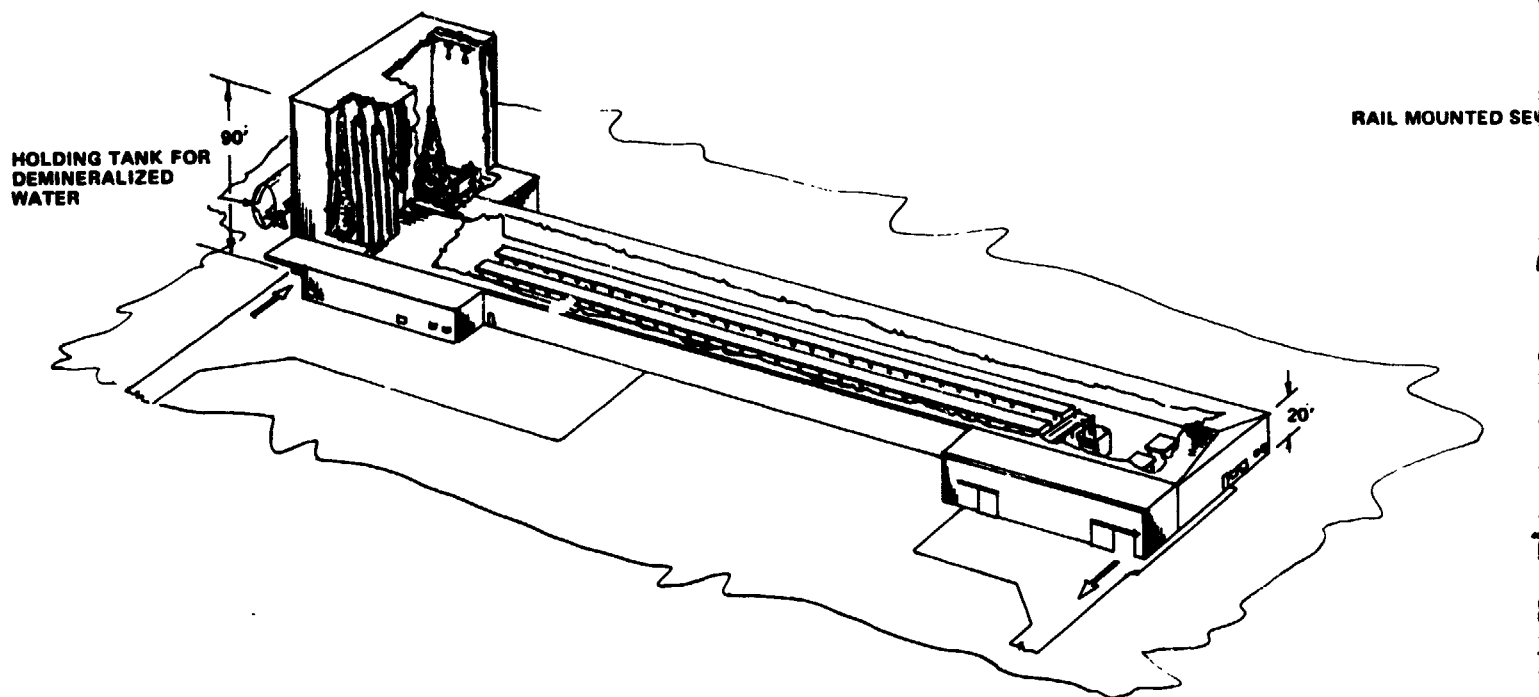
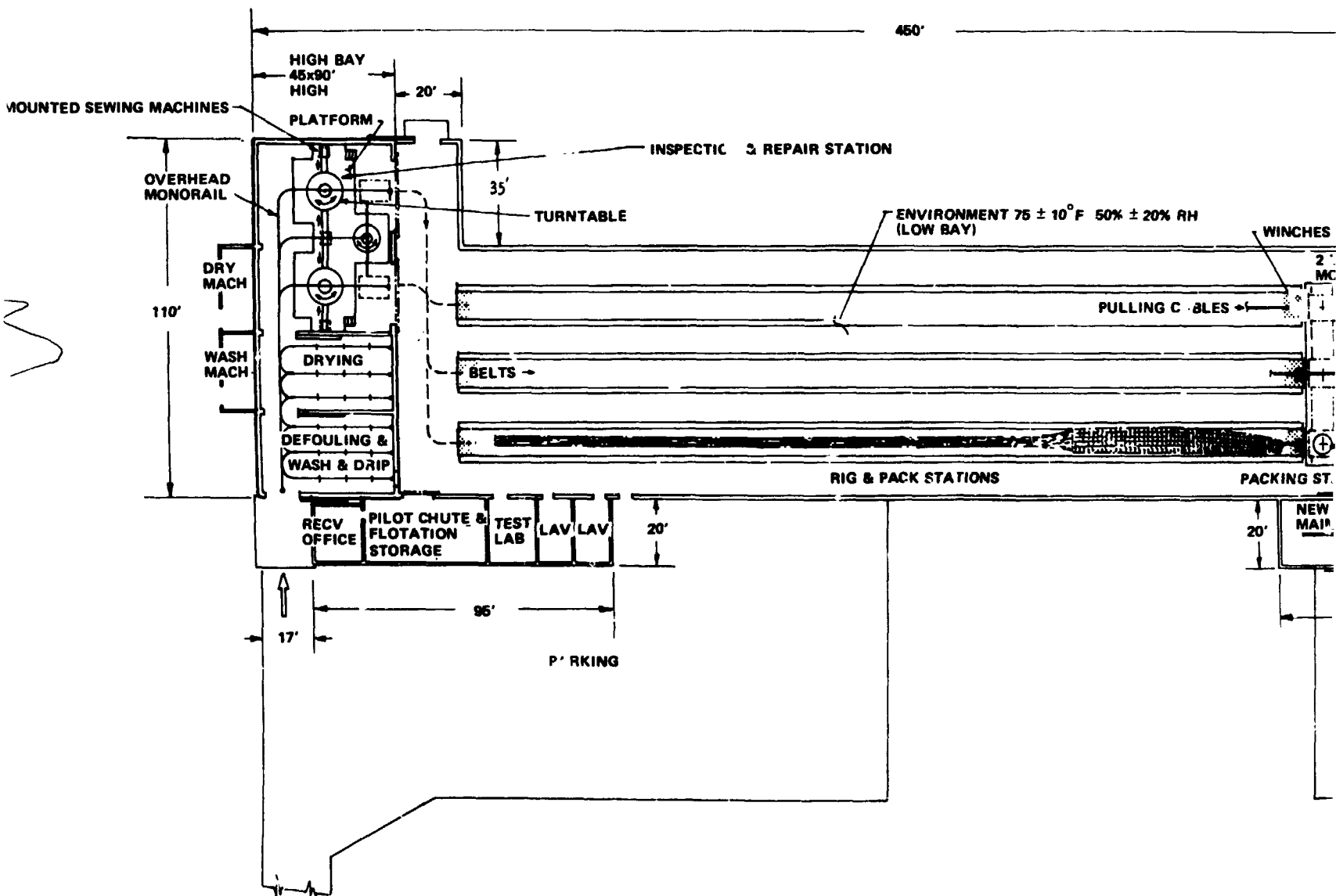


Figure 7.6-2 Main Chute Refurbishment Work Plan

FOLDOUT FRAME



FOLDOUT FRAME 2



FOLDOUT FRAME 3

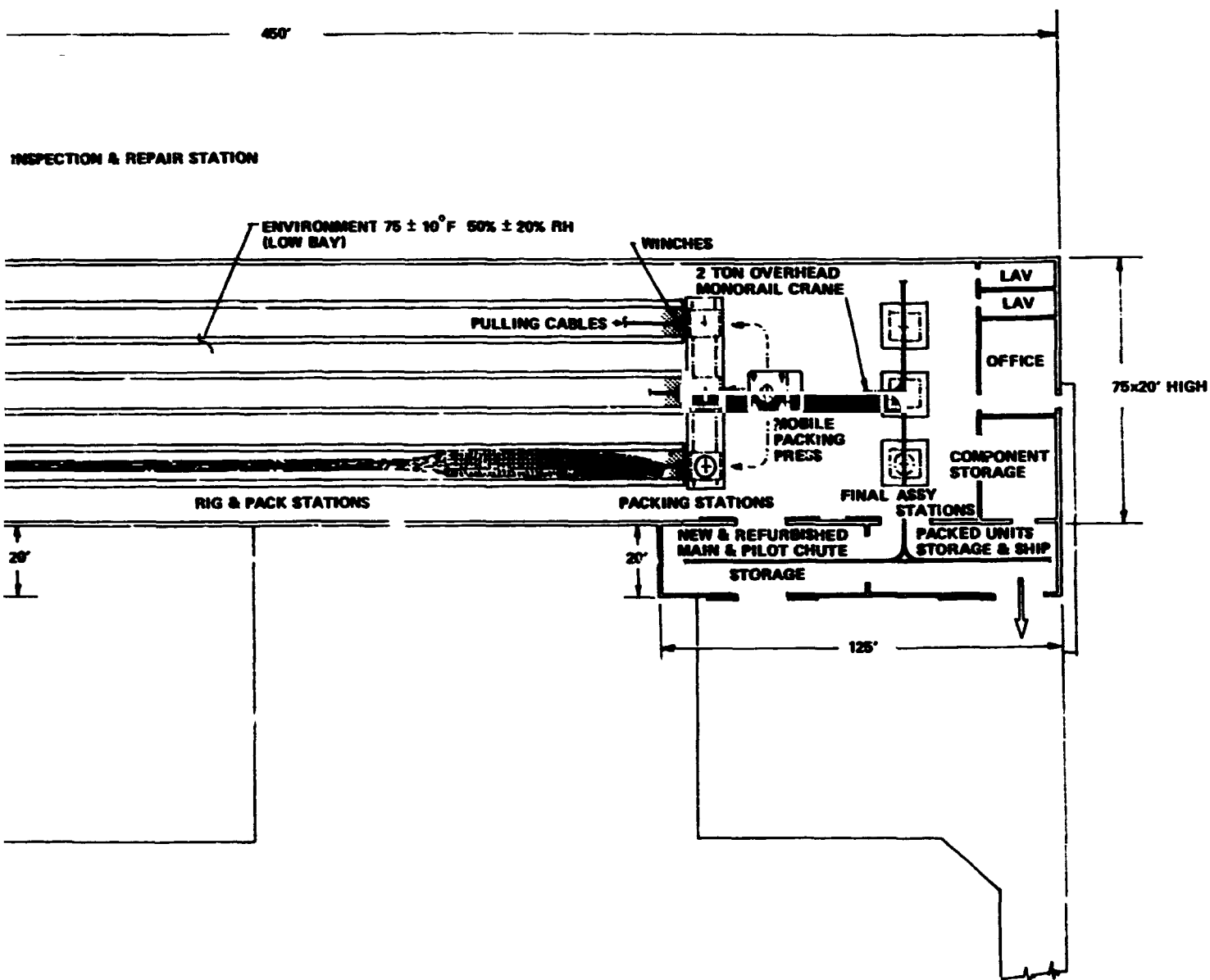


Figure 7.6-3 Parachute Processing Facility

8.0 CONCLUSIONS AND RECOMMENDATIONS

8.1 CONCLUSIONS

The principal objectives of this study were to determine the underlying requirements for an SRB recovery subsystem, and to formulate preliminary design concepts satisfying those requirements. Since the single most important criterion in both of these tasks was to achieve the lowest total program costs, we attempted to isolate, insofar as possible, the subjective and contingency aspects of these tasks from the baseline design approach. In this manner, we established a cost baseline for a minimum cost recovery subsystem based on the best available data for SRB aerodynamic characteristics and water impact loads, including no contingency factors to offset uncertainties in these data. This approach allows evaluation of the program cost increments arising from each contingency or subjective requirement and design decision.

The minimum cost baseline resulting from this approach is subject to two types of uncertainties, or design risks:

- 1) the quality of environmental data upon which requirements are based;
- 2) subjective uncertainties relating to the state of the art and design risk associated with the various decelerator elements of the recovery subsystem.

We have identified concerns regarding the completeness, accuracy, and applicability of the data used for the requirements analyses, suggested methods for resolving these concerns, and estimated the impacts these uncertainties could have on recovery system design and program costs. In those areas of concern relating to state of the art or design risk of an element in the selected preliminary design (such as main chute size, requirement for a drogue chute, etc), we have assessed the design impacts and program costs related to a contingency approach. Parametric cost results and design alternatives are provided to permit evaluation, from a reliability and cost basis, of recovery subsystems encompassing a range of requirements and design uncertainties.

Through the approach described above, this report provides the NASA with a minimum cost baseline and a data base for evaluating contingencies, design conservatism, and subjective value judgments in light of the associated program cost growth.

An immediate conclusion from this approach is that it is much more cost-effective to minimize the remaining uncertainties in requirements (i.e., deployment and water impact conditions) through additional testing and analyses, than to select a baseline recovery subsystem design incorporating additional elements or capability to accommodate these uncertainties.

The principal criteria for reducing total system costs are achieved by designing for low SRB component failure probability (1%) and high recovery system reliability. These goals are enhanced by simplicity and rugged design. The SRB structural design approach is intimately related to recovery system requirements because it has proved to be more cost effective to design SRB structural components for higher water impact loads than to reduce impact velocity via a larger, more costly recovery system.

Analysis of existing data predicts an optimum impact velocity of 38 m/s (125 fps). The difference in total program cost between the optimum impact velocity and 24.4 m/s (80 fps) varies from \$5 million to \$30 million, depending upon DDT&E cost assumptions. The 38 m/s (125 fps) impact velocity was selected for our preliminary design concept because of minimum predicted cost, and to preserve the option of a single main parachute with its simplicity and reliability.

The forward case segments and forward skirt are designed by initial slapdown loads which are independent of vertical impact velocity, according to existing test data. Preliminary analyses indicate that slapdown loads on SRB forward structure can be significantly reduced by leaving the parachutes attached for about three seconds after impact.

The initial deceleration and stabilization phase analyses show that the SRB will trim at a nominal angle of attack of 1.75 rad (100 deg) with a variation from 1.4 to 2 rad (80 to 115 deg) over a 4% body length variation of relative cg and cp location. This feature results in a recovery system deployment dynamic pressure less than 9600 N/m^2 (200 psf). These deployment conditions eliminate the requirement for a drogue chute. The reentry analyses also predict continuous roll rates of up to 1.75 rad/s (100 deg/s) at deployment, possibly requiring the addition of a swivel to the recovery system/SRB structural interface.

The minimum cost impact velocity can be achieved by a single main parachute of 40 m (132-ft) nominal diameter, which is below the size limitation for low risk design guidelines established for the study. A single reefing stage is adequate for this system. Initiation of deployment at 2.3 km (7500 ft) allows adequate time to reach equilibrium velocity before impact. The hybrid system (parachute plus retrorocket) was found to be less cost effective than an all-parachute system for impact velocities above 27.5 m/s (90 fps).

Vertical flotation of the SRB arising from natural buoyancy is predicted with from 6.1 to 18.3 m (20 to 60 ft) of the SRB above the surface of the water.

Comparison between static test results of the 120 in. SRM case and the deflections experienced during drop tests of a similar specimen indicate a dynamic amplification of loads over the range of loads tested. These data do not approach failure conditions and the trend is not conclusive; however, it may indicate that the use of knock-down factors for dynamic loads is optimistic.

The segmented case has approximately 25% greater strength to resist slapdown loads than an equal weight monolithic case. This results from the stiffening effect of the segmented case clevis joints.

8.2 RECOMMENDATION

We feel that continued testing and analysis is required to improve confidence in existing data, resolve uncertainties in some results, and provide data where none currently exists. Specific recommendations for this effort are discussed briefly in this section.

The water impact dynamics and resulting loads applied to the SRB must be better understood, particularly at higher impact velocities. This should be achieved by conducting additional tests simulating vertical impact velocities up to 40 m/s (130 fps), wave action, winds, parachute forces, thermal transient effects, and pressure scaling effects. Computer simulation capability should be increased concurrently so that the test results can be included in the simulation, creating a good semi-empirical computer model(s) for analyzing water impact and flotation dynamics. This capability is needed to accurately evaluate the effects of configuration modification without retesting, the effect of parachute loads on slapdown, and the effects of wave action and thermal transients on flotation.

Additional wind tunnel testing of larger scale SRB models are needed to improve confidence in the aerodynamic characteristics in subsonic and transonic speed ranges. The observation and analysis of a Titan III SRM during reentry is recommended to improve confidence in our ability to predict reentry dynamics using the technique developed for Shuttle SRB simulation. These data may also identify the significance of unsteady aerodynamic forces on reentry dynamics.

Tests should be initiated to provide data on the problems of parachute deployment near 1.57 rad (90-deg) angle of attack, such as fish-hooking, uneven inflation of the pilot chute, aerodynamic interference, etc. Existing parachute deployment simulation models should be improved to allow analysis of this approach.

The computer program generated under Increment II of this contract should be expanded to provide inertial reaction along the entire SRB case. This will allow more accurate analysis of dynamic structural response during slapdown loading. The results of our comparison between static stress and dynamic deflection of the 120-in. case were not conclusive. This issue should be resolved by performing more dynamic analysis of the slapdown loading in conjunction with additional drop tests and static tests.

Water impact loads data from all tests conducted to date have not been available in time for incorporation into the analyses in this report. Analysis of these data must continue in order to substantiate our conclusions and define requirements for future tests.

Recommendations for SRB component design criteria based on current results are also included. We feel that the stage hardware components critical to vertical impact velocity should be designed for a 1% failure probability for an impact velocity of 38 m/s (125 fps). These components are the aft skirt and baffle. The SRM case should be isolated from water impact loads as much as possible by dropping the nozzle extension before impact and using a baffle in the aft skirt to protect the aft dome. The forward skirt should be designed for a 1% failure probability for initial slapdown loads. Techniques for reducing slapdown loads should be developed to minimize case failures without increasing MEOP.

The rationale for these recommendations is that 38 m/s (125 fps) is currently predicted to yield minimum costs. If the structure is designed for these loads, the recovery system designer preserves several options for minimizing costs; such as single main parachute, clusters of main parachutes, or multiple main parachutes designed to accomplish recovery with a single chute failure. This approach also provides some strength margin for the stage hardware design. If load predictions prove to be low, the impact velocity can be reduced without extending the state of the art parachute design.